THE PHYSICAL REVIEW

VOLUME 96 Second Series NUMBER 3

NOVEMBER 1, 1954

Published for the

AMERICAN PHYSICAL SOCIETY

by the

AMERICAN INSTITUTE OF PHYSICS

Lancaster, Pa., and New York, N. Y.

THE
PHYSICAL REVIEW

A journal of experimental and theoretical physics established by E. L. Nichols in 1893

SECOND SERIES, VOL. 96, NO. 3 NOVEMBER 1, 1954

Orthobaric Densities of He^3 1.3°K to 3.2°K*

EUGENE C. KERR
University of California, Los Alamos Scientific Laboratory, Los Alamos, New Mexico
(Received July 19, 1954)

Saturated liquid and vapor densities of He^3 have been measured by a direct method in the temperature range of 1.3°K to 3.2°K. The experimental data are represented by an empirical equation to probable errors of 0.1 percent for the liquid phase and of 1.3 percent for the vapor phase.

I. INTRODUCTION

THE only previous measurements of the orthobaric† densities of He^3 are those of Grilly, Hammel, and Sydoriak.[1] They measured directly the difference between the liquid and vapor densities and then derived the component densities by distributing one-half of each measured density difference above and below a derived rectilinear diameter. This mean density line was obtained by drawing a straight line between a low temperature point, at which the vapor density was assumed to be ideal, and a critical density point which was located at the same fractional distance between the calculated Dieterici and van der Waals densities as was the corresponding value for He^4. Their reported uncertainties in terms of liquid density range from 2 percent at 1.27°K to 5 percent at 2.79°K.

The purpose of the present investigation was to measure the liquid and vapor densities directly and independently and in such a way that the above uncertainties in the densities could be reduced by a factor of at least ten.

II. APPARATUS AND MATERIALS

The section of the apparatus external to the cryostat was the same as that used for an earlier investigation on deuterium and tritium.[2] It contained a calibrated constant volume gas pipette of approximately 50-cm^3 capacity for measuring the gas at room temperature, a small Toeppler pump for controlling the transfer of gas to the low-temperature part of the system, and the necessary manometers to determine gas pressures in the various parts of the system.

The gas measuring system was connected to the pycnometer by means of a Monel metal capillary tube, 0.013 inch i.d. This capillary was also connected to a Wallace and Tiernan differential pressure gauge used to read the pressure in the He^3 system. This gauge was used as a null instrument by adjusting the case pressure until the indicating needle was brought to the same scale reading as was used when the gauge volume was calibrated. The case pressure of the gauge was then observed on a mercury manometer.

In order to avoid serious fluctuations in the amount of gas contained in the capillary tube where it passed through severe temperature gradients, it was vacuum jacketed from a point one inch above the lid of the helium bath Dewar to a point just above the density bulb. In addition, 30 cm of the 33 cm jacketed length was plated rather heavily with copper to insure nearly uniform temperature throughout this length. With one end of this section immersed in liquid nitrogen, which completely covered the helium bath Dewar, and the other end in the helium bath, it was estimated that the temperature gradient in the plated section was 0.1°K/cm, whereas in the 3-cm unplated portion the gradient was 24°K/cm. This arrangement minimized *variations* in the amount of gas in the dead space from run to run. The additional conductivity of the copper plating vaporized about 4 cm^3 of bath helium per hour.

The Pyrex glass bulbs for liquid or vapor densities were attached to the Monel metal capillary by means of a small Kovar metal to Pyrex glass joint. A butt-

* This paper is based on work performed under University of California contract with the U. S. Atomic Energy Commission.
† Orthobaric density: the density of a liquid when in equilibrium with its own vapor, or of a vapor in equilibrium with its own liquid phase, at a specified temperature.
[1] Grilly, Hammel, and Sydoriak, Phys. Rev. 75, 1103 (1949).
[2] Eugene C. Kerr, J. Am. Chem. Soc. 74, 824 (1952).

joint and sleeve arrangement was used between the Monel capillary and the Kovar metal tube so that the separate sections could be calibrated independently and then assembled without change in volume at the joint. The bulb used for liquid density measurements had a neck drawn down to a fine capillary (3.93×10^{-4} cm³/mm) on which a calibration line was etched and filled. It was calibrated to this mark and also between the mark and the tip of the Kovar tubing by weighing it empty and when filled with mercury. The volume obtained was corrected to He bath temperatures by use of the extrapolated expansion data of Buffington and Latimer.[3] It was further checked in place by filling it with He^4 at 4.0°K using the same techniques as for the He^3 density measurements. The volume obtained with He^4 was 0.07 percent higher than that obtained by the mercury weighing with expansion correction. Using 0.1298 g/cm³ for the density of He^4 at 3.955°K, the average of six measurements gave 0.11148 ± 0.00006 cm³ for the volume of this bulb.

A larger bulb (0.7465 ± 0.0003 cm³) was used for the vapor density measurements in order to minimize the ratio of dead space volume to bulb volume for these smaller densities.

The helium bath temperature was controlled by an electrical heater balanced against the pumping rate on the bath by means of the signal generated in a carbon resistance thermometer in one arm of a bridge circuit. This bath control system has been described by Sommers.[4] The temperatures are observed, in terms of the vapor pressure of the bath helium, on mercury or on butyl sebacate manometers.

Liquid density measurements were made by transferring known amounts of gas, measured in the calibrated pipette, to the small density bulb until the liquid meniscus was brought close to the etched mark on the neck of the bulb. The distance between the meniscus and the mark was measured with a small cathetometer. If several measurements were to be made in the same series, the temperature was then lowered, an additional small amount of gas was added to bring the meniscus back to the vicinity of the mark, and the measurement was repeated. With each measurement, the bath pressure and the He^3 pressure were recorded. After completion of all of the liquid density measurements, the apparatus was disassembled and the density bulb was sealed off at the etched calibration mark. After reassembly, the amount of gas required to fill the dead space with dew point pressure gas was measured as a function of bath temperature.

Vapor densities were obtained from the measurement of isotherms of the number of moles of He^3 required to fill the density bulb (plus dead space) as a function of the He^3 pressure. Extrapolation of each isotherm to the saturation pressure gave the number of moles of gas required to fill the system at saturation. Five to six points were obtained on each isotherm, most of them being at pressures above 0.75 of the saturation pressure, so that extrapolation could be made unambiguously. Calibration of the dead space was made subsequently in the same manner as was used for the liquid density dead space measurements.

The purity of the He^3 used was determined by analysis with a Consolidated Nier type isotope ratio mass spectrometer. The only detectable impurities were 0.28 percent He^4 and 0.02 percent nitrogen. The atomic weight of He^3 was taken as 3.0162 on the chemical scale.[5]

All observed manometer readings, except those of the helium bath, were corrected to mm of Hg at 0°C and standard acceleration of gravity. The helium bath manometer readings were corrected to 20°C in order to coincide with the "agreed" temperature scale for He^4 vapor pressures.[6] Temperatures so obtained were corrected to the Kistemaker temperature scale T_K[7] by use of the smoothed data given by Abraham, Osborne, and Weinstock.[8]

The saturation pressures of He^3 used for dead space corrections and for extrapolation of the vapor density isotherms were obtained from the helium bath temperature and the data on He^3 vapor pressures given by Abraham, Osborne, and Weinstock.[8] Observed vapor pressures read from the null Wallace and Tiernan gauge and backing manometer agreed with the calculated pressures to within 0.5 mm on the average.

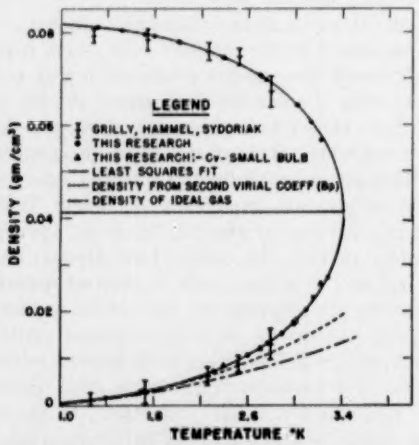

FIG. 1. Orthobaric densities of He^3.

III. EXPERIMENTAL RESULTS

The results of fifteen measurements of the density of saturated liquid He^3 in the temperature range 1.30°K

[3] R. M. Buffington and W. M. Latimer, J. Am. Chem. Soc. 48, 2305 (1926).
[4] H. S. Sommers, Jr., Rev. Sci. Instr. 25, 793 (1954).
[5] J. Mattauch and A. Flammerfeld, "Isotopic Report," Z. Naturforsch. (1949).
[6] H. van Dijk and D. Shoenberg, Nature 164, 151 (1949).
[7] J. Kistemaker, Physica 12, 272, 281 (1946).
[8] Abraham, Osborne, and Weinstock, Phys. Rev. 80, 366 (1950).

TABLE I. He^3: Orthobaric liquid densities.

T_K °K	Density (obs) g/cm³	Density (calc) g/cm³	Deviation (%)
1.304	0.08121	0.08121	0.00
1.516	0.08051	0.08053	+0.02
1.709	0.07964	0.07971	+0.09
1.787	0.07935	0.07931	−0.05
1.998	0.07803	0.07803	0.00
2.013	0.07792	0.07792	0.00
2.378	0.07470	0.07472	+0.03
2.393	0.07444	0.07456	+0.16
2.698	0.07072	0.07054	−0.26
2.710	0.07040	0.07035	−0.07
2.748	0.06971	0.06973	+0.03
3.010	0.06434	0.06437	+0.05
3.020	0.06423	0.06412	−0.17
3.135	0.06067	0.06086	+0.31
3.223	0.05681	0.05775	+1.62

to 3.22°K are given in Table I. Here, the first column is the temperature in degrees Kelvin on the Kistemaker scale, the second is the liquid density in g/cm³, the third is the liquid density calculated from Eq. (4) below, and the fourth is the deviation in percent between the observed and calculated values.

The results of twelve measurements of the orthobaric vapor density are given in Table II in which the columns have the same significance as in Table I.

Several attempts were made to fit the data into equations related to modified van der Waals equations such as those given by Haggenmacher,[9] in which the molar volume is expressed as a function of (T/P) and of the critical constants. Within any reasonable assignment of the critical constants, these equations did not give results consistent with the precision of the experimental data. Consequently, a completely empirical method, based on the symmetry properties of the density *vs* temperature curves, was adopted.

The density of either of the co-existing phases can be represented by the identity

$$\rho=\tfrac{1}{2}(\rho_L+\rho_v)\pm\tfrac{1}{2}(\rho_L-\rho_v). \quad (1)$$

In this case, the first term on the right, which represents the mean density or rectilinear diameter, can be expressed with sufficient precision:

$$\rho_m=0.04117_3+4.14\times10^{-5}T. \quad (2)$$

The remaining portion of Eq. (1) can best be represented by

$$\tfrac{1}{2}(\rho_L-\rho_v)=(A_0^2+YT^2)^{\frac{1}{2}}. \quad (3)$$

The variable Y was fitted to several simple polynomial expansions in T, the best of which was a linear form. Thus the vapor and liquid densities can be represented by:

$$\rho=A_0+BT\pm(A_0^2+CT^2+DT^3)^{\frac{1}{2}}, \quad (4)$$

[9] John E. Haggenmacher, J. Am. Chem. Soc. **68**, 1123–26 (1946).

where $A_0=0.04117_3$, $B=4.14\times10^{-5}$, $C=-3.3015\times10^{-6}$, and $D=-4.1876\times10^{-5}$.

Densities obtained from Eq. (4) are shown in Tables I and II as ρ_{calc}. The deviations between the observed and calculated densities give for the probable error of a single measurement: 0.00006 g/cm³ or 0.09 percent for the liquid phase measurements and 0.00016 g/cm³ or 1.13 percent for the vapor phase measurements.

The liquid density point at 3.223°K was not included in the equation fitting since preliminary least squares solutions showed that the deviation of this point was more than five times the probable error. However, an examination of Fig. 1 will show that, had only the liquid density data been considered, the best curve could well have come much closer to the plotted points at 3.135°K and 3.223°K. Such a fit would also have had an apex nearer the accepted critical temperature of 33.35 ±0.02°K than that given by Eq. (4) of 3.416°K.

Extrapolation by means of Eq. (4) gives the liquid density at 0°K as 0.08235 g/cm³ which is almost equal to twice the critical density of 0.04131 g/cm³. This is the only case, within the author's knowledge where such a relationship occurs.

Liquid and vapor densities according to this equation are shown by the solid curve in Fig. 1 on which are superimposed the observed densities and the densities as given by Grilly, Hammel, and Sydoriak.[1] Included as triangles along the vapor density curve are five points obtained by the use of the small liquid density bulb. Because of the relatively greater uncertainty in the dead space corrections for these measurements, as compared to those obtained with the larger bulb, these points were not included in Table II nor in the least squares summations.

The dashed curves in the figure represent the vapor densities as calculated from the perfect gas law and those calculated from the pressure expansion form of the virial equation of state in closed form involving only the second virial coefficient. Densities derived from the virial equation in the inverse volume expansion, actually give a much better fit with respect to the experimental data below 2.6°K than do those obtained from the pressure expansion. However, in the closed

TABLE II. He^3: Orthobaric vapor densities.

T_K °K	Density (obs) g/cm³	Density (calc) g/cm³	Deviation (%)
1.395	0.00146	0.00152	+3.94
1.689	0.00269	0.00268	−0.37
2.305	0.00713	0.00706	−0.99
2.596	0.01059	0.01051	−0.76
2.767	0.01315	0.01317	+0.15
2.890	0.01529	0.01550	+1.35
2.991	0.01756	0.01776	+1.13
2.994	0.01774	0.01783	+0.50
3.097	0.02030	0.02058	+1.36
3.157	0.02293	0.02247	−2.04
3.160	0.02297	0.02257	−1.77
3.282	0.02727	0.02752	+0.91

form used, the inverse volume form gives imaginary densities above about 2.8°K. This indicates that, when the data are available, the vapor densities will most probably be best represented by the inverse volume virial equation with at least the third virial coefficient included.

The values used for the second virial coefficient in the calculations were obtained from the calculations of Kilpatrick, Keller, Hammel, and Metropolis.[10]

Since Eq. (4) is somewhat cumbersome to use, the densities have been evaluated at even temperatures (Kistemaker scale) and are given in Table III. If estimated contributions of possible systematic errors are combined with the precision indices given above, the results in this table should be reliable to about 0.3 percent for the liquid phase up to 3.1°K and to about 2 percent for the vapor phase between 1.6°K and 3.1°K. At low vapor densities, it appears that the nature of Eq. (4) and the method of evaluation of its constants tend to give values which are too high and that vapor densities calculated from the second virial coefficients (in $1/v$ form) will give more reliable values below about 1.6°K. The present experimental method does not have enough inherent accuracy at low densities to decide this point.

TABLE III. Calculated liquid and vapor densities at even temperatures.

T_E °K	Liquid density g/cm³	Vapor density g/cm³	ΔH_{vap} cal/mole
1.0	0.08185	0.00058	9.10
1.2	0.08147	0.00098	9.76
1.4	0.08093	0.00154	10.32
1.6	0.08020	0.00228	10.71
1.8	0.07924	0.00325	11.02
2.0	0.07801	0.00450	11.15
2.2	0.07645	0.00608	11.05
2.4	0.07448	0.00806	10.71
2.6	0.07200	0.01056	10.11
2.8	0.06882	0.01376	9.19
3.0	0.06462	0.01798	7.88
3.1	0.06193	0.02067	7.01
3.2	0.05861	0.02400	5.91
3.3	0.05416	0.02845	3.36

[10] Kilpatrick, Keller, Hammel, and Metropolis, Phys. Rev. 94, 1103 (1954).

The last column of Table III gives the heat of vaporization in calories per mole as calculated from the thermodynamic relation

$$\Delta H_{vap} = T(V_{gas} - V_{liq}) dP/dT. \quad (5)$$

The molal volume of the gas was obtained from the gas densities given in the third column of the table at temperatures of 2.0°K and above. Below 1.2°K molar volumes given by the density virial equation were used. In the intervening region, a graphical interpolation between the densities given by Eq. (4) and those given by the density virial equation was used. Since the two curves agree to within 0.00030 g/cm³ over most of this region, little uncertainty is introduced by this method. Values of dP/dT were obtained from the vapor pressure data of Abraham, Osborne, and Weinstock.[8]

Entropy of Radiation*

PHILIP ROSEN†
Applied Physics Laboratory, The Johns Hopkins University, Silver Spring, Maryland
(Received May 20, 1954)

An expression for the entropy flux of linearly polarized electromagnetic radiation of any specific intensity, K_ν, is obtained. The latter expression is then generalized to include radiation of any type of polarization.

IF one has linearly polarized light passing through a surface element, $d\sigma$, the total radiation energy passing through in time, dt, can be written as[1]

$$d\sigma dt\int K_\nu\cos\theta d\Omega d\nu = Jd\sigma dt.$$

K_ν is the specific radiation intensity of frequency ν which passes through the surface in the solid angle $d\Omega$; θ is the angle between the direction of propagation and the normal to surface, and J is the net flux. In a similar manner Planck[1] has defined the specific entropy intensity, L_ν, by

$$d\sigma dt\int L_\nu\cos\theta d\Omega d\nu = Hd\sigma dt,$$

where H is the net entropy flux.

Our problem is to find a relationship for L_ν in terms of K_ν. Planck has derived a functional relation, $L_\nu = \nu^2 f(K_\nu/\nu^3)$. However, no explicit expression was given for $f(K_\nu/\nu^3)$. If one knows the exact dependence on K_ν, the flux of entropy through a surface may be computed for any radiation field.

Let us consider a surface element, $d\sigma$, through which pass linearly polarized photons of momenta p_x, p_y, p_z and which lie in the momentum volume element $dp_x dp_y dp_z$. If the direction of propagation makes an angle θ with the surface normal, all photons with the above momenta which lie in the space volume element $dV = d\sigma c\cos\theta dt$ will pass through in time dt. If $N(\mathbf{r},\mathbf{p})$ is the average number of photons with position $\mathbf{r}$ and momentum $\mathbf{p}$ in a phase space element of volume h^3, then $Ndp_x dp_y dp_z dV/h^3$ is the number of photons in the phase space volume under consideration. Thus the entropy of these photons (bosons)[2] is

$$dS = -k[N\ln N-(N+1)\ln(N+1)]dp_x dp_y dp_z dV/h^3.$$

Consequently the entropy flux for linear polarized light of any momentum distribution is

$$H = -k\int[N\ln N-(N+1)\ln(N+1)]c\cos\theta\frac{dp_x dp_y dp_z}{h^3}.$$

It can be easily seen by computing the energy flux that

$$N = c^2K_\nu/h\nu^3.$$

In terms of K_ν we have

$$H = -\frac{k}{c^2}\int\left[\frac{c^2K_\nu}{h\nu^3}\ln\left(\frac{c^2K_\nu}{h\nu^3}\right) - \frac{h\nu^3+c^2K_\nu}{h\nu^3}\ln\left(\frac{h\nu^3+c^2K_\nu}{h\nu^3}\right)\right]\nu^2\cos\theta d\Omega d\nu.$$

For a general type of polarization we have two independent states of polarization with specific intensities in the principal directions (directions of maximum and minimum intensities) K_ν and K_ν'. For such a case we take the sum of the separate entropy fluxes for each polarization state to obtain the total entropy flux. The intensities in the principal directions of polarization must be used if the entropy flux is to be invariant to a rotation about the direction of propagation.

Note that information about the phase difference between two polarization states and information on the directions of the principal axes does not enter into the expression for the entropy. The photon field is described only by the occupation numbers in the momentum states and the two polarization states. The phase difference and the polarization directions have no thermodynamic significance, but lie in the domain of information theory. Both the phase difference and direction of the polarization can theoretically be measured with infinite precision since no uncertainty principle exists for these. The limits on a measurement of these quantities are solely determined by experimental apparatus, and thus these quantities would not affect the thermodynamic entropy.

* Supported by the Bureau of Ordnance, Department of the Navy.
† Now at University of Connecticut, Storrs, Connecticut.
[1] M. Planck, *The Theory of Heat* (MacMillan Company, New York, 1949).
[2] J. Slater, *Introduction to Chemical Physics* (McGraw-Hill Book Company, Inc., New York, 1939).

Vacuum Fluctuation Noise and Dissipation*

J. WEBER
Glenn L. Martin College of Engineering and Aeronautical Sciences, University of Maryland, College Park, Maryland
(Received June 14, 1954)

An electron beam interacting with the fields in an enclosed region is considered. The induced noise caused by the vacuum fluctuations and the thermal fluctuations is calculated in terms of the dissipation function $R(\omega)$ and the electron transit time τ. The observable mean squared electromotive force is given by

$$\langle V^2\rangle_{Av}=\frac{2}{\pi}\int_0^{\omega_{max}}R(\omega)\left[\frac{\hbar\omega}{2}+\frac{\hbar\omega}{\exp(\hbar\omega/kT)-1}\right]\left[\frac{\sin\frac{1}{2}\omega\tau}{\frac{1}{2}\omega\tau}\right]^2d\omega+\frac{1}{\pi}\int_{\omega_{max}}^{\infty}\left[\frac{R(\omega)\hbar\omega}{\exp(\hbar\omega/kT)-1}\right]\left[\frac{\sin\frac{1}{2}\omega\tau}{\frac{1}{2}\omega\tau}\right]^2d\omega.$$

ω_{max} is defined by $\hbar\omega_{max}=U$, where U is the energy of the incident electrons. The effect of the fluctuations of the vacuum is given by the temperature-independent part of the first integral.

The above expression is employed to calculate the fluctuations induced in an electron beam which interacts with a damped electrical oscillator. The results are valid even if the oscillator is heavily damped. As the damping becomes very large the fluctuations are shown to approach zero. For a weakly damped oscillator the fluctuations reduce to those already given in an earlier paper.

The differential form of the fluctuation dissipation theorem is shown to be very useful for the evaluation of matrix elements.

INTRODUCTION

A PREVIOUS paper[1] considered the interaction of an electron beam with a damped electrical oscillator. The fluctuations of the vacuum were shown to contribute to the electron-beam noise. This observable zero point noise contribution is important because it is one effect of field quantization which is finite in the first nonvanishing approximation.

In order to calculate the noise, the assumption had to be made that the oscillator is very weakly damped. The dissipation was assumed to have no effect on the wave functions for the fields. The coupling to the internal degrees of freedom was considered to have only the effect of establishing thermal equilibrium, between individual electron interactions. Also the electron was assumed to be highly localized. In this paper we consider interaction of a system which may be heavily damped with an electron which is not necessarily highly localized. The fluctuations are shown to depend on the degree of damping, unless the damping is very small. For large damping the fluctuations approach zero.

FLUCTUATIONS MEASURED BY AN ELECTRON BEAM INTERACTING WITH FIELDS IN AN ENCLOSED REGION

For the Hamiltonian of the system of Fig. 1 we take

$$\mathcal{H}=H_0+\frac{P^2}{2m}-\frac{e}{mc}\mathbf{A}\cdot\mathbf{P}. \tag{1}$$

(1) is the Hamiltonian of the system, with one electron in the interaction gap. H_0 is the Hamiltonian for the fields of the enclosed region, $\mathbf{P}$ is the operator corresponding to the momentum of an electron in the beam, m is the mass of the electron, c is the velocity of light, e is the charge on the electron, and $\mathbf{A}$ is the magnetic vector potential for the interaction gap. We assume, at first, that the region is in an eigenstate of its unperturbed Hamiltonian H_0. The electron is to some extent localized and its energy is not known precisely while it is in the interaction gap. A linear combination of free-electron wave functions will therefore be used to represent the electron during the entire interaction time. For the wave functions of the electron and interaction region we assume the expression.

$$\Psi=\sum_{K,M}a_K(t)b_M(t)\psi_K\varphi_M\exp\left(-\frac{i}{\hbar}(E_K+E_M')t\right). \tag{2}$$

In (2) ψ_K is an unperturbed wave function for the fields of the enclosed region. E_K is the Kth eigenvalue of H_0 and E_M' has the corresponding meaning for the electron. φ_M is given[2] by

$$\varphi_M=(1/\sqrt{l})\exp(2\pi iMx/l). \tag{3}$$

(3) is the wave function for a free particle moving in the X direction with momentum given by

$$P_M=2\pi Mh/l. \tag{4}$$

M is an integer. The wave function (3) satisfies periodic boundary conditions with period equal to the length l of the interaction gap, and is normalized within the region of the gap. At the beginning of the interaction time, we have: $a_N=1$, $a_K=0$, $K\neq N$. At this time (2) is a summation only over M. At any time after interaction has begun, we have, from perturbation theory,

$$\frac{d}{dt}[a_K(t)b_L(t)]=\frac{e}{mc}(ih)^{-1}\sum_M b_M\exp\left[\frac{i(E_K+E_L'-E_N-E_M')t}{\hbar}\right]\times\int_0^l\psi_K^*\varphi_L^*(\mathbf{A}\cdot\mathbf{P})\varphi_M\psi_N d\tau_\varphi d\tau_\psi. \tag{5}$$

* Supported by the U. S. Office of Naval Research.

[1] J. Weber, Phys. Rev. 94, 214 (1954).

[2] L. I. Schiff, *Quantum Mechanics* (McGraw-Hill Book Company, Inc., New York, 1949), p. 49.

We let $\mathbf{A}=\mathbf{A}_0 q(t)$, and assume that the fields have no spacial variation over the interaction gap. $\mathbf{A}_0$ is then a constant. Making use of (3) and the operator for $\mathbf{P}$ we can carry out one integration required by (5) to obtain

$$\int_0^l \varphi_L^*(\mathbf{A}_0\cdot\mathbf{P})\varphi_M dx=\frac{A_{0x}}{l}\int_0^l \exp\left(-\frac{2\pi iLx}{l}\right)\left[-ih\frac{d}{dx}\right]\times\exp\left(\frac{2\pi iMx}{l}\right)dx=A_{0x}P_M\delta_{LM}. \quad (6)$$

We assume the interaction gap to be so oriented that $\mathbf{A}_0$ is parallel to $\mathbf{P}$. Making use of (6), we can write (5) in the form

$$\frac{d}{dt}[a_K(t)b_L(t)]=\frac{e}{mc}(ih)^{-1}\langle E_K|q|E_N\rangle b_L(t)|\mathbf{A}_0|P_L\times\exp\left(\frac{i(E_K-E_N)t}{h}\right). \quad (7)$$

Let $\omega_{KN}=(E_K-E_N)/h$. We assume that the momentum of the electron while in the interaction gap is approximately known to be P_E. The value of L corresponding to P_E can be obtained from (4) and is given by $L=lP_E/2\pi h$. b_L for this value of L will be large and can therefore be considered to remain approximately constant during a not too long interaction time. Under these conditions we can integrate (7) to obtain

$$a_K(t)b_L(t)\approx\frac{e(ih)^{-1}\langle E_K|q|E_N\rangle b_L(t)|\mathbf{A}_0|P_E[\exp(i\omega_{KN}t)-1]}{imc\omega_{KN}}. \quad (8)$$

From (8) we can obtain an expression for $|a_K(t)|^2$ and from this we can calculate the induced noise, since energy is conserved in these transitions. $|a_K(t)|^2$ is given by

$$|a_K(t)|^2=\frac{4e^2|\mathbf{A}_0|^2P_E^2|\langle E_K|q|E_N\rangle|^2\sin^2(\frac{1}{2}\omega_{KN}t)}{m^2c^2h^2\omega_{KN}^2}. \quad (9)$$

In (9) $\langle E_K|q|E_N\rangle$ is the matrix element of q over the quantum states of the fields with eigenvalues E_K and E_N. We now proceed to calculate the matrix elements of q.

We assume that the magnetic vector potential and the scalar potential are not functions of the x coordinate, within the interaction gap, and that the electric field intensity is therefore uniform over the interaction gap. We express the electric field intensity in the interaction region in terms of q and a canonically conjugate variable p following the procedure outlined by Schiff.[3] Using Maxwell's equations, we obtain for the electric field intensity:

$$\mathbf{E}=-\frac{1}{c}\frac{\partial\mathbf{A}}{\partial t}=-\frac{1}{c}\mathbf{A}_0\dot{q}=-\frac{1}{c}\mathbf{A}_0 p. \quad (10)$$

The electromotive force V is given by $\int_c \mathbf{E}\cdot d\mathbf{l}$, where the contour is over the interaction gap. For a uniform field over an interaction region of length l, we have

$$V=El=-(1/c)A_0 pl. \quad (11)$$

Consider the matrix elements of the operator p. We can write

$$p_{KN}=\frac{dq_{KN}}{dt}=\frac{[H_0q-qH_0]_{KN}}{ih}=\frac{(E_K-E_N)}{ih}\langle E_K|q|E_N\rangle. \quad (12)$$

We substitute (12) in (11) to obtain

$$\langle E_K|V|E_N\rangle=(i/c)A_0\omega_{KN}\langle E_K|q|E_N\rangle l. \quad (13)$$

Let the total time of interaction be τ. Now τ is approximately given by $\tau=ml/P_E$. Evaluating (9) at time $t=\tau$, and making use of (13), we obtain

$$|a_K(\tau)|^2=\frac{e^2|\langle E_K|V|E_N\rangle|^2}{h^2\omega_{KN}^2}\left[\frac{\sin(\frac{1}{2}\omega_{KN}\tau)}{\frac{1}{2}\omega_{KN}\tau}\right]^2. \quad (14)$$

If an electron undergoes a transition such that the region goes to a state E_K, we say the measured electromotive force is V_K, where $eV_K=h\omega_{KN}$. If no transition occurs, the electromotive force is taken to be zero. The mean squared electromotive force measured by a large number M electrons as a result of transitions to the state K is

$$(|V_K|^2)_{Av}=\frac{[M|a_K(\tau)|^2]|V_K|^2}{M}=\frac{|a_K(\tau)|^2h^2\omega_{KN}^2}{e^2}. \quad (15)$$

Making use of (14), we can write (15) as

$$(|V_K|^2)_{Av}=|\langle E_K|V|E_N\rangle|^2\left[\frac{\sin(\frac{1}{2}\omega_{KN}\tau)}{\frac{1}{2}\omega_{KN}\tau}\right]^2. \quad (16)$$

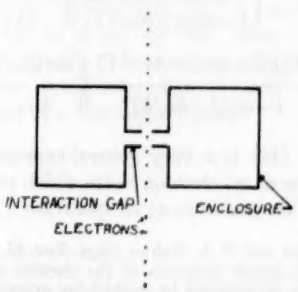

FIG. 1. Electron beam interacting with the fields of an enclosure.

[3] L. I. Schiff, *Quantum Mechanics* (McGraw-Hill Book Company, Inc., New York, 1949), p. 362.

The region with which the electrons interact is only partially specified, but its temperature will be known. Also, since dissipation is present ω_{KN} will have a continuous range of values. In order to obtain the total noise contribution (16) has to be summed over all states K and an ensemble average taken. This procedure can be carried out, using the methods of Callen and Welton,[4] in the following way. From the rules for matrix multiplication

$$\langle E_N|V^2|E_N\rangle=\sum_K|\langle E_K|V|E_N\rangle|^2. \quad (17)$$

We can average both sides of (17) over an ensemble, at temperature T. We denote by $[\langle E_N|V^2|E_N\rangle]_{\text{Av, }d\omega_{KN}}$ the ensemble average of the contribution of the group of matrix elements $\langle E_N|V|E_K\rangle$ in the vicinity of $\pm\omega_{KN}$ within a range $d\omega_{KN}$ to the ensemble average of the operator corresponding to V^2.

A study of Callen and Welton's paper[4] shows that we can write the fluctuation dissipation theorem in differential form as

$$[\langle E_N|V^2|E_N\rangle]_{\text{Av, }d\omega_{KN}}=\Big[\sum_{d\omega_{KN}}|\langle E_N|V|E_K\rangle|^2\Big]_{h\omega}$$
$$=\frac{R(\omega_{KN})\hbar\omega_{KN}}{\pi}\Big[\frac{1}{1-\exp(-\hbar\omega_{KN}/kT)}+\frac{\exp(-\hbar\omega_{KN}/kT)}{1-\exp(-\hbar\omega_{KN}/kT)}\Big]d\omega_{KN}. \quad (18)$$

In (18), the first term of the expression within the brackets represents the contribution of matrix elements $\langle E_N|V|E_N+\hbar\omega\rangle$ and the second term represents the contribution of matrix elements $\langle E_N|V|E_N-\hbar\omega\rangle$. $R(\omega_{KN})$ is the real part of the impedance function, which would be seen between the points at which electrons enter and leave the enclosure. We can make use of (16) and (18) to write an expression for the mean squared electromotive force measured by the electron beam. If the energy of all of the electrons before interaction is almost the same and equal to $U=\hbar\omega_{\max}$, then the mean squared electromotive force measured by the electron beam is

$$\langle V^2\rangle_{h\omega}=\frac{1}{\pi}\int_0^{\omega_{\max}}\Big[\frac{R(\omega)\hbar\omega}{1-\exp(-\hbar\omega/kT)}\Big]\Big[\frac{\sin(\frac{1}{2}\omega\tau)}{\frac{1}{2}\omega\tau}\Big]^2d\omega$$
$$+\frac{1}{\pi}\int_0^{\infty}\Big[\frac{R(\omega)\hbar\omega\exp(-\hbar\omega/kT)}{1-\exp(-\hbar\omega/kT)}\Big]\Big[\frac{\sin(\frac{1}{2}\omega\tau)}{\frac{1}{2}\omega\tau}\Big]^2d\omega. \quad (19)$$

Equation (19) is a very general expression† for the induced noise on an electron beam which interacts with the fields of an enclosure at temperature T, in terms of the dissipation function $R(\omega)$, and the electron transit time τ.

In (19) the first term represents the effect of transitions in which the electrons give up energy to the fields and the second term represents the effect of transitions in which the electrons gain energy. We can write Eq. (19) in the form

$$\langle V^2\rangle_{h\omega}$$
$$=\frac{2}{\pi}\int_0^{\omega_{\max}}R(\omega)\Big[\frac{\hbar\omega}{2}+\frac{\hbar\omega}{\exp(\hbar\omega/kT)-1}\Big]\Big[\frac{\sin(\frac{1}{2}\omega\tau)}{\frac{1}{2}\omega\tau}\Big]^2d\omega$$
$$+\frac{1}{\pi}\int_{\omega_{\max}}^{\infty}\Big[\frac{R(\omega)\hbar\omega}{\exp(\hbar\omega/kT)-1}\Big]\Big[\frac{\sin(\frac{1}{2}\omega\tau)}{\frac{1}{2}\omega\tau}\Big]^2d\omega. \quad (20)$$

In (20) the term,

$$\frac{2}{\pi}\int_0^{\omega_{\max}}R(\omega)\Big[\frac{\hbar\omega}{2}\Big]\Big[\frac{\sin(\frac{1}{2}\omega\tau)}{\frac{1}{2}\omega\tau}\Big]^2d\omega,$$

represents the observable effect of the fluctuations of the vacuum fields.[5]

For the damped oscillator of Fig. 2, $R(\omega)$ can be expressed in terms of the conductance G, the capacity C, and the inductance L as

$$R(\omega)=\frac{\omega^2L^2G}{(1-\omega^2LC)^2+(\omega LG)^2}. \quad (21)$$

Employing (21) in (20), we obtain

$$\langle V^2\rangle_{h\omega}=\frac{2}{\pi}\int_0^{\omega_{\max}}\Big[\frac{\omega^2L^2G}{(1-\omega^2LC)^2+(\omega LG)^2}\Big]\times\Big[\frac{\hbar\omega}{2}+\frac{\hbar\omega}{\exp(\hbar\omega/kT)-1}\Big]\Big[\frac{\sin(\frac{1}{2}\omega\tau)}{\frac{1}{2}\omega\tau}\Big]^2d\omega$$
$$+\frac{1}{\pi}\int_{\omega_{\max}}^{\infty}\Big[\frac{\omega^2L^2G}{(1-\omega^2LC)^2+(\omega LG)^2}\Big]\times\Big[\frac{\hbar\omega}{\exp(\hbar\omega/kT)-1}\Big]\Big[\frac{\sin(\frac{1}{2}\omega\tau)}{\frac{1}{2}\omega\tau}\Big]^2d\omega. \quad (22)$$

If G is very small then the integrand will be large only in the vicinity of $\omega=\omega_0$, where ω_0 is the natural frequency of the oscillator, given by $\omega_0^2LC=1$. For $\omega_{\max}\gg\omega_0$, (22) is approximately equal to

$$\langle V^2\rangle_{h\omega}\approx\frac{2}{\pi}\Big[\frac{\hbar\omega_0}{2}+\frac{\hbar\omega_0}{\exp(\hbar\omega_0/kT)-1}\Big]\Big[\frac{\sin(\frac{1}{2}\omega_0\tau)}{\frac{1}{2}\omega_0\tau}\Big]^2\times\int_0^{\infty}\frac{\omega^2L^2Gd\omega}{(1-\omega^2LC)^2+(\omega LG)^2}$$
$$=\frac{1}{C}\Big[\frac{\hbar\omega_0}{2}+\frac{\hbar\omega_0}{\exp(\hbar\omega_0/kT)-1}\Big]\Big[\frac{\sin(\frac{1}{2}\omega_0\tau)}{\frac{1}{2}\omega_0\tau}\Big]^2. \quad (23)$$

[4] H. B. Callen and T. A. Welton, Phys. Rev. **83**, 35 (1951).

† The mean square deviation of the electron velocities after interaction can be obtained by multiplying expressions (19) and (20) by $(e/P)^2$, where e and P are the charge and momentum of the electrons, respectively.

[5] J. Weber, Phys. Rev. **90**, 977 (1953).

Equation (23) is the expression for the mean squared electromotive force measured by an electron beam interacting with a weakly damped oscillator, and agrees with expression (16) of the earlier[1] paper. To discuss the case where the oscillator is very heavily damped we employ (21) in (19) and obtain

$$\langle V^2\rangle_{\omega}=\frac{1}{\pi}\int_0^{\omega_{\max}}\left[\frac{\omega^2L^2G\hbar\omega}{(1-\omega^2LC)^2+(\omega LG)^2}\right]\times\left[\frac{\sin(\frac{1}{2}\omega\tau)}{\frac{1}{2}\omega\tau}\right]^2\left[\frac{1}{1-\exp(-\hbar\omega/kT)}\right]d\omega+\frac{1}{\pi}\int_0^{\infty}\left[\frac{\omega^2L^2G\hbar\omega}{(1-\omega^2LC)^2+(\omega LG)^2}\right]\times\left[\frac{\sin(\frac{1}{2}\omega\tau)}{\frac{1}{2}\omega\tau}\right]^2\left[\frac{\exp(-\hbar\omega/kT)}{1-\exp(-\hbar\omega/kT)}\right]d\omega. \quad (24)$$

The first term of (24) tends to zero as $G\to\infty$ because the range of integration is finite and the integrand tends to zero. The second term of (24) can be shown to also tend to zero, in the following way:

$$\frac{1}{\pi}\int_0^{\infty}\left[\frac{\omega^2L^2G\hbar\omega}{(1-\omega^2LC)^2+(\omega LG)^2}\right]\times\left[\frac{\sin(\frac{1}{2}\omega\tau)}{\frac{1}{2}\omega\tau}\right]^2\left[\frac{\exp(-\hbar\omega/kT)}{1-\exp(-\hbar\omega/kT)}\right]d\omega=\frac{1}{\pi}\int_0^{\omega_1}\left[\frac{\omega^2L^2G\hbar\omega}{(1-\omega^2LC)^2+(\omega LG)^2}\right]\times\left[\frac{\sin(\frac{1}{2}\omega\tau)}{\frac{1}{2}\omega\tau}\right]^2\left[\frac{1}{\exp(\hbar\omega/kT)-1}\right]d\omega+\frac{1}{\pi}\int_{\omega_1}^{\infty}\left[\frac{\omega^2L^2G\hbar\omega}{(1-\omega^2LC)^2+(\omega LG)^2}\right]\times\left[\frac{\sin(\frac{1}{2}\omega\tau)}{\frac{1}{2}\omega\tau}\right]^2\left[\frac{1}{\exp(\hbar\omega/kT)-1}\right]d\omega. \quad (25)$$

As $G\to\infty$ the first term on the right side of (25) tends to zero because the range of integration is finite and the integrand approaches zero. Consider the second term of (25). In the range $\omega_1<\omega<\infty$, $[\sin(\frac{1}{2}\omega\tau)/\frac{1}{2}\omega\tau]^2$

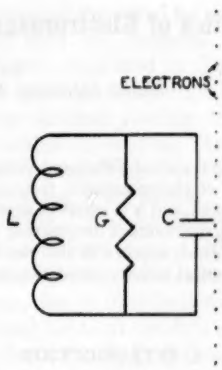

FIG. 2. Electron beam interacting with an oscillator which may be heavily damped.

<1; we can choose two numbers a and b such that

$$(1-\omega^2LC)^2+(\omega LG)^2>a(\omega LG)^2, \quad (26)$$

$$\exp(\hbar\omega/kT)-1>b\exp(\hbar\omega/kT). \quad (27)$$

Using the inequalities (26) and (27), we can write

$$\frac{1}{\pi}\int_{\omega_1}^{\infty}\left[\frac{\omega^2L^2G\hbar\omega}{(1-\omega^2LC)^2+(\omega LG)^2}\right]\left[\frac{\sin(\frac{1}{2}\omega\tau)}{\frac{1}{2}\omega\tau}\right]^2\times\left[\frac{1}{\exp(\hbar\omega/kT)-1}\right]d\omega<\frac{\omega_1kT}{\pi abG}\exp-\left(\frac{\hbar\omega_1}{kT}\right)\times\left[1+\frac{kT}{\hbar\omega_1}\right]. \quad (28)$$

Equation (28) tends to zero as G becomes large. We therefore conclude that the observed electron beam noise caused by both the thermal fluctuations and the vacuum fluctuations tends to zero as the damping becomes very large.

CONCLUSION

We have studied the interaction of an electron beam with the fields in an enclosed region. It is believed that this model is a good representation for low-temperature noise measurement experiments in which the random changes in velocity of the electrons are measured after interaction. The first term of (20) represents the effect of the vacuum fluctuations. For a weakly damped oscillator this is given by the term $(1/C)(\hbar\omega_0/2)\times[\sin(\frac{1}{2}\omega_0\tau)/\frac{1}{2}\omega_0\tau]^2$ of expression (23). This term represents an observable effect of field quantization which is finite in a first-order theory.

Statistics of Electromagnetic Radiation Scattered by a Turbulent Medium*

RICHARD A. SILVERMAN AND MARTIN BALSER
Lincoln Laboratory, Massachusetts Institute of Technology, Cambridge, Massachusetts
(Received March 18, 1954)

The theory of Villars and Weisskopf is used to calculate the univariate and bivariate amplitude distributions of electromagnetic radiation scattered from turbulent fluctuations. The univariate distribution is Rayleigh, and is in excellent agreement with measurements made on a 49.6-Mc/sec ionospheric scatter link. Using the bivariate distribution, we relate the amplitude correlation function to a velocity correlation function which appears in the von Weizsäcker-Heisenberg statistical theory of turbulence. In this way the theoretical velocity correlation can be compared with experiment.

I. INTRODUCTION

FOR some time both vhf ionospheric propagation and anomalous beyond-the-horizon propagation of uhf and microwaves have been attributed to scattering by refractive index fluctuations associated with turbulence.[1,2] A detailed model of the origin of these fluctuations has only recently been made available in the work of Villars and Weisskopf.[3] These authors have applied to the electromagnetic problem results of the statistical theory of homogeneous turbulence developed by von Weizsäcker[4] and Heisenberg.[5] According to this theory, pressure fluctuations in a compressible medium produce corresponding density fluctuations, which in turn produce fluctuations in refractive index and hence a scattered field. Under steady-state conditions, the distribution of turbulent energy in wave number can be derived from similarity considerations[4,5] and leads to a corresponding wave number dependence of the scattered field. The average scattered field is found to involve only one parameter pertaining to the turbulence, namely the amount of turbulent energy dissipated per unit volume and time [see Eq. (48) of reference 3].

In this paper we use the theory of Villars and Weisskopf to derive the amplitude distribution of the scattered radiation, which we then compare with experiment. We also derive a relation between the amplitude correlation function and a velocity correlation function appearing in the Heisenberg theory.

II. THEORETICAL AMPLITUDE DISTRIBUTION

Villars and Weisskopf have shown that the scattered power is proportional to the quantity

$$c(\mathbf{k},t)=\sum_{\mathbf{k}',\mathbf{k}''}(\mathbf{k}\cdot\mathbf{v}_{\mathbf{k}'}{}^{t})(\mathbf{k}\cdot\mathbf{v}_{\mathbf{k}-\mathbf{k}'}{}^{t})(\mathbf{k}\cdot\mathbf{v}_{-\mathbf{k}''}{}^{t})(\mathbf{k}\cdot\mathbf{v}_{\mathbf{k}''-\mathbf{k}}{}^{t}), \quad (1)$$

where $\mathbf{v}_{\mathbf{k}'}{}^{t}$ is the Fourier coefficient in the $\mathbf{k}'$ direction of the turbulent velocity field $\mathbf{v}(\mathbf{r},t)$. $\mathbf{k}$ is the difference between the incident and scattered propagation vectors. The time dependence of $\mathbf{v}_{\mathbf{k}'}{}^{t}$ is here indicated explicitly by a superscript. The allowed values of $\mathbf{k}'$ and $\mathbf{k}''$ are those corresponding to expansion in a cube of side L_0, the linear dimension of the largest eddy. To calculate the average received power, Villars and Weisskopf find the time average of Eq. (1) and obtain

$$\langle c(\mathbf{k},t)\rangle_{Av}=2\sum_{\mathbf{k}'}\langle|\mathbf{k}\cdot\mathbf{v}_{\mathbf{k}'}{}^{t}|^2\rangle_{Av}\langle|\mathbf{k}\cdot\mathbf{v}_{\mathbf{k}-\mathbf{k}'}{}^{t}|^2\rangle_{Av}. \quad (2)$$

They use the basic assumption of Heisenberg[5] that the different Fourier coefficients are independent, in particular that

$$\langle\mathbf{v}_{\mathbf{k}'}{}^{t}\cdot\mathbf{v}_{-\mathbf{k}'+\mathbf{k}''}{}^{t}\rangle_{Av}=\delta_{0\mathbf{k}''}\langle\mathbf{v}_{\mathbf{k}'}{}^{t}\cdot\mathbf{v}_{-\mathbf{k}'}{}^{t}\rangle_{Av}=\delta_{0\mathbf{k}''}\langle|\mathbf{v}_{\mathbf{k}'}{}^{t}|^2\rangle_{Av}. \quad (3)$$

They then proceed to evaluate Eq. (2) [see Eq. (45) of reference 3].

The univariate distribution of the random process $c(\mathbf{k},t)$ (assumed stationary) is easily found. For example, the second moment of $c(\mathbf{k},t)$ is

$$\begin{aligned}\langle c^2(\mathbf{k},t)\rangle_{Av}=&\sum_{\mathbf{k}',\mathbf{k}'',\mathbf{k}''',\mathbf{k}''''}\langle(\mathbf{k}\cdot\mathbf{v}_{\mathbf{k}'}{}^{t})\\&\times(\mathbf{k}\cdot\mathbf{v}_{\mathbf{k}-\mathbf{k}'}{}^{t})(\mathbf{k}\cdot\mathbf{v}_{-\mathbf{k}''}{}^{t})(\mathbf{k}\cdot\mathbf{v}_{\mathbf{k}''-\mathbf{k}}{}^{t})\\&\times(\mathbf{k}\cdot\mathbf{v}_{\mathbf{k}'''}{}^{t})(\mathbf{k}\cdot\mathbf{v}_{\mathbf{k}-\mathbf{k}'''}{}^{t})\\&\times(\mathbf{k}\cdot\mathbf{v}_{-\mathbf{k}''''}{}^{t})(\mathbf{k}\cdot\mathbf{v}_{\mathbf{k}''''-\mathbf{k}}{}^{t})\rangle_{Av}. \quad (4)\end{aligned}$$

Applying Eq. (3), we see that

$$\begin{aligned}\langle c^2(\mathbf{k},t)\rangle_{Av}=&8\sum_{\mathbf{k}',\mathbf{k}''}\langle|\mathbf{k}\cdot\mathbf{v}_{\mathbf{k}'}{}^{t}|^2\rangle_{Av}\langle|\mathbf{k}\cdot\mathbf{v}_{\mathbf{k}-\mathbf{k}'}{}^{t}|^2\rangle_{Av}\\&\times\langle|\mathbf{k}\cdot\mathbf{v}_{\mathbf{k}''}{}^{t}|^2\rangle_{Av}\langle|\mathbf{k}\cdot\mathbf{v}_{\mathbf{k}-\mathbf{k}''}{}^{t}|^2\rangle_{Av}\\=&8[\sum_{\mathbf{k}'}\langle|\mathbf{k}\cdot\mathbf{v}_{\mathbf{k}'}{}^{t}|^2\rangle_{Av}\langle|\mathbf{k}\cdot\mathbf{v}_{\mathbf{k}-\mathbf{k}'}{}^{t}|^2\rangle_{Av}]^2\\=&2\langle c(\mathbf{k},t)\rangle_{Av}^2. \quad (5)\end{aligned}$$

The numerical coefficient in Eq. (5) is obtained by noting the number of combinations of the $\mathbf{k}''$s that are compatible with condition (3). Thus, for example, $\mathbf{k}''$ can equal $\mathbf{k}'$ or $\mathbf{k}-\mathbf{k}'$, but if $\mathbf{k}''=-\mathbf{k}''''$ we get a term which averages to zero. Similarly, we get for the general

* The research in this document was supported jointly by the U. S. Army, Navy, and Air Force under contract with the Massachusetts Institute of Technology.
[1] H. G. Booker and W. E. Gordon, Proc. Inst. Radio Engrs. 38, 401 (1950).
[2] Bailey, Bateman Berkner, Booker, Montgomery, Purcell, Salisbury, and Wiesner, Phys. Rev. 86, 141 (1952).
[3] F. Villars and V. F. Weisskopf, Phys. Rev. 94, 232 (1954).
[4] C. F. v. Weizsäcker, Z. Physik 124, 614 (1948).
[5] W. Heisenberg, Z. Physik 124, 628 (1948).

moment

$$\langle c^n(\mathbf{k},t)\rangle_{Av}=2^n n![\sum_{\mathbf{k}'}\langle|\mathbf{k}\cdot\mathbf{v}_{\mathbf{k}',t}|^2\rangle_{Av}$$

$$\times\langle|\mathbf{k}\cdot\mathbf{v}_{\mathbf{k}-\mathbf{k}',t}|^2\rangle_{Av}]^n=n!\langle c(\mathbf{k},t)\rangle_{Av}{}^n. \quad (6)$$

These moments are identical with the moments of the χ^2 distribution with two degrees of freedom (i.e., the distribution of the sum of the squares of two independent Gaussian variables),[6] with the frequency function

$$f(x)=\frac{1}{2\sigma^2}\exp(-x/2\sigma^2), \quad x>0 \quad (7)$$

and moments

$$\langle x^n\rangle_{Av}=\int_0^\infty x^n f(x)dx=n!(2\sigma^2)^n. \quad (8)$$

Thus, to the extent that Eq. (3) is valid, we have inferred the power distribution of the scattered radiation from the form of Eq. (1), which in turn can be traced back to the nonlinear term of the Navier-Stokes equation [see Eqs. (27) and (29) of reference 3]. The distribution of the signal amplitude (envelope) is that of $\sqrt{x}$, i.e., the Rayleigh distribution.

It is interesting to note that crude (nonhydrodynamical) models of the scattering mechanism, e.g., a cloud of "independent scatterers" with a Maxwell velocity distribution,[7,8] can also lead to a Rayleigh distribution of the received amplitude.

III. EXPERIMENTAL AMPLITUDE DISTRIBUTION

It has already been observed[2] that the fading of the received amplitude in a long-distance vhf transmission seems to follow a Rayleigh distribution. In that experiment, an averaging circuit with a time constant of 12 seconds (much greater than the average fading time[9]) was used.

We have measured the received amplitude distribution of a 49.6-Mc/sec continuous wave transmission from Cedar Rapids, Iowa, to South Dartmouth, Massachusetts (a distance of 1716 km), using a totalizer which records correctly varying signals with frequencies up to about 15 cps. The totalizer gives the amount of time the signal exceeds ten preset levels. These figures, when normalized, give directly ten points on a distribution curve.

The apparatus was run for one-minute intervals in a series of tests conducted in December, 1953. During the tests, the mean signal level was about 20 db above noise. Intervals during which a strong meteoric burst caused enhancement of the signal far out of the range of the distribution were not accepted. (Such meteoric enhancement is not considered in the above theory.) Figure 1 shows a Rayleigh distribution (solid curve) and the means of the totalizer readings from four typical runs, all taken within 15 minutes. Shown also at each point is a segment representing the unbiased estimate of the standard deviation of the sample.

It is clear from Fig. 1 that the observed sample fits a Rayleigh distribution very closely. Other samples give similar fittings. On the other hand, other simple positive distributions (e.g., the χ^2 distributions of one or three degrees of freedom) fail to fit the data satisfactorily.

We wish to thank Dr. J. T. deBettencourt and his associates for making available to us the facilities at South Dartmouth, and Mr. C. A. Wagner for his assistance in conducting the experiment.

IV. THE AMPLITUDE CORRELATION FUNCTION

We obtain the joint distribution of the pair of random variables $\xi=c(\mathbf{k},t)$ and $\eta=c(\mathbf{k},t+\tau)$ by considerations entirely analogous to those used above to obtain the univariate distribution of ξ. As a first step, we calculate the moments $\langle\xi^r\eta^s\rangle_{Av}$ by time-averaging products of the form of Eq. (1), some taken at time $t+\tau$. Using the independence of Fourier coefficients belonging to different wave numbers and the following generalization of Eq. (3),

$$\langle\mathbf{v}_{\mathbf{k}',t}\cdot\mathbf{v}_{-\mathbf{k}'+\mathbf{k}'',t+\tau}\rangle_{Av}=\delta_{0\mathbf{k}''}\langle\mathbf{v}_{\mathbf{k}',t}\cdot\mathbf{v}_{-\mathbf{k}',t+\tau}\rangle_{Av}, \quad (9)$$

we find after considerable manipulation that

$$\alpha_{rs}\equiv\langle\xi^r\eta^s\rangle_{Av}=2^{r+s}r!s!\sum_{l=0}^{\min(r,s)}\binom{r}{l}\binom{s}{l}\sigma_0{}^{r+s-2l}\sigma_\tau{}^{2l}, \quad (10)$$

where

$$\sigma_0=\sum_{\mathbf{k}'}\langle|\mathbf{k}\cdot\mathbf{v}_{\mathbf{k}',t}|^2\rangle_{Av}\langle|\mathbf{k}\cdot\mathbf{v}_{\mathbf{k}-\mathbf{k}',t}|^2\rangle_{Av},$$

$$\sigma_\tau=\sum_{\mathbf{k}'}\langle(\mathbf{k}\cdot\mathbf{v}_{\mathbf{k}',t})(\mathbf{k}\cdot\mathbf{v}_{-\mathbf{k}',t+\tau})\rangle_{Av} \quad (11)$$

$$\times\langle(\mathbf{k}\cdot\mathbf{v}_{\mathbf{k}-\mathbf{k}',t})(\mathbf{k}\cdot\mathbf{v}_{\mathbf{k}'-\mathbf{k},t+\tau})\rangle_{Av}.$$

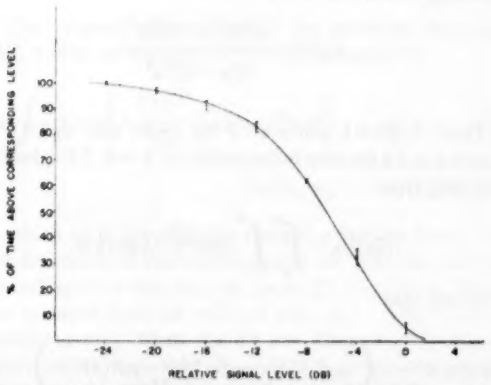

FIG. 1. Rayleigh distribution (solid curve) and experimental distribution points, showing the standard deviations of the latter.

[6] H. Cramér, *Mathematical Methods of Statistics* (Princeton University Press, Princeton, 1951), pp. 233–237.

[7] Booker, Ratcliffe, and Shinn, Trans. Roy Soc. (London) **242**, 579 (1950).

[8] S. O. Rice, Proc. Inst. Radio Engrs. **41**, 274 (1953).

[9] The simple consideration that an eddy is significantly changed in form after "moving its own length" (see reference 4) leads to correlation times of the order of one second.

The characteristic function[10] $\varphi(t,u)$ of the joint distribution is defined as the Fourier transform of the joint frequency function, i.e.,

$$\varphi(t,u)=\langle e^{i(\xi t+\eta u)}\rangle_{Av}=\int\int_{-\infty}^{\infty} e^{i(\xi t+\eta u)}W_2(\xi,\eta)d\xi d\eta. \quad (12)$$

$W_2(\xi,\eta)d\xi d\eta$ is the probability that the received power at any time t is between ξ and $\xi+d\xi$ and that τ seconds later it is between η and $\eta+d\eta$. By comparing the expansion of $\varphi(t,u)$ in Taylor series with its expansion in moments [obtained from Eq. (12)], we find that

$$\alpha_{rs}=(-i)^{r+s}\left[\frac{\partial^r}{\partial t^r}\frac{\partial^s}{\partial u^s}\varphi(t,u)\right]_{t=u=0}. \quad (13)$$

It can be shown that

$$\varphi(t,u)=[1-2i\sigma_0 t-2i\sigma_0 u-4(\sigma_0^2-\sigma_\tau^2)tu]^{-1} \quad (14)$$

is the solution of Eqs. (10) and (13). Finally, $W_2(\xi,\eta)$ is obtained as the Fourier transform of Eq. (14), and is found to be (see Appendix)

$$W_2(\xi,\eta)=\frac{1}{4\sigma_0^2(1-\rho^2)}e^{-(\xi'+\eta')}I_0(2\rho(\xi'\eta')^{\frac{1}{2}}), \quad (15)$$

where $I_0(x)$ is the Bessel function of order zero and imaginary argument, and

$$\rho\equiv\rho_k(\tau)=\sigma_\tau/\sigma_0,$$

$$\xi'=\frac{\xi}{2\sigma_0(1-\rho^2)}, \quad \eta'=\frac{\eta}{2\sigma_0(1-\rho^2)}.$$

The amplitude correlation function $A_k(\tau)$ is appropriately defined as

$$A_k(\tau)\equiv\frac{\langle(\xi\eta)^{\frac{1}{2}}\rangle_{Av}-\langle\xi^{\frac{1}{2}}\rangle_{Av}^2}{\langle\xi\rangle_{Av}-\langle\xi^{\frac{1}{2}}\rangle_{Av}^2}. \quad (16)$$

[Thus $A_k(0)=1$, since $\eta=\xi$ for $\tau=0$; and $A_k(\infty)=0$, since ξ and η become independent as $\tau\to\infty$.] Evaluating $\langle(\xi\eta)^{\frac{1}{2}}\rangle_{Av}$ from

$$\langle(\xi\eta)^{\frac{1}{2}}\rangle_{Av}=\int_0^\infty\int_0^\infty(\xi\eta)^{\frac{1}{2}}W_2(\xi,\eta)d\xi d\eta,$$

we find that

$$A_k(\tau)=\frac{\pi}{4-\pi}\left(\frac{1}{4}\rho_k^2(\tau)+\frac{1}{64}\rho_k^4(\tau)+\frac{1}{256}\rho_k^6(\tau)\cdots\right). \quad (17)$$

[10] H. Cramer, reference 6, pp. 265–6.

As in the case of the univariate distribution, Eq. (17) is the result predicted by the assumption of "independent scatterers."[11]

Heisenberg[5] calculates the quantity

$$\langle\mathbf{v}_{\mathbf{k}}{}^t\cdot\mathbf{v}_{-\mathbf{k}}{}^{t+\tau}\rangle_{Av}/\langle\mathbf{v}_{\mathbf{k}}{}^t\cdot\mathbf{v}_{-\mathbf{k}}{}^t\rangle_{Av}$$

and finds it to be a universal function $g(y)$ of the dimensionless variable $y=\frac{1}{6}v_0k_0^{\frac{1}{2}}k^{\frac{1}{2}}\tau$. As we have defined it, $\rho_k(\tau)$ is simply

$$\rho_k(\tau)=\frac{\sum_{\mathbf{k}'}\langle|\mathbf{k}\cdot\mathbf{v}_{\mathbf{k}'}{}^t|^2\rangle_{Av}\langle|\mathbf{k}\cdot\mathbf{v}_{\mathbf{k}-\mathbf{k}'}{}^t|^2\rangle_{Av}\times g(\frac{1}{6}v_0k_0^{\frac{1}{2}}k'^{\frac{1}{2}}\tau)g(\frac{1}{6}v_0k_0^{\frac{1}{2}}|\mathbf{k}-\mathbf{k}'|^{\frac{1}{2}}\tau)}{\sum_{\mathbf{k}'}\langle|\mathbf{k}\cdot\mathbf{v}_{\mathbf{k}'}{}^t|^2\rangle_{Av}\langle|\mathbf{k}\cdot\mathbf{v}_{\mathbf{k}-\mathbf{k}'}{}^t|^2\rangle_{Av}} \quad (18)$$

(k_0 is the wave number of the largest eddy, v_0 its mean velocity.) The denominator (aside from multiplicative constants) is just the mean power calculated by Villars and Weisskopf by an integration in bipolar coordinates. Given $g(y)$, the numerator can be calculated in exactly the same way. Heisenberg gives only a very approximate solution to the equations determining $g(y)$.[5] The authors hope to improve this approximation and then compare the $\rho_k(\tau)$ calculated from a suitable $g(y)$ with experiment.

APPENDIX

If we substitute

$$2\sigma_0 t=t'/(1-\rho^2), \quad 2\sigma_0 u=u'/(1-\rho^2), \quad \text{(A-1)}$$

into the characteristic function [Eq. (14)], we get

$$\varphi(t,u)=\frac{1-\rho^2}{(1-it')(1-iu')-\rho^2}. \quad \text{(A-2)}$$

The joint probability density is then

$$W_2(\xi,\eta)=\frac{1}{(2\pi)^2}\int_{-\infty}^{\infty}\int_{-\infty}^{\infty}e^{-i(\xi t+\eta u)}\varphi(t,u)dtdu$$

$$=\frac{1}{(2\pi)^2 4\sigma_0^2(1-\rho^2)}\times\int_{-\infty}^{\infty}\int_{-\infty}^{\infty}\frac{e^{-i(\xi' t'+\eta' u')}}{(1-it')(1-iu')-\rho^2}dt'du', \quad \text{(A-3)}$$

where

$$\xi'=\frac{\xi}{2\sigma_0(1-\rho^2)}, \quad \eta'=\frac{\eta}{2\sigma_0(1-\rho^2)}.$$

[11] D. E. Kerr, *Propagation of Short Radio Waves* (McGraw-Hill Book Company, Inc., New York, 1951), pp. 553–557.

Now,

$$\int_{-\infty}^{\infty}\frac{e^{-i\eta' u'}}{1-iu'-\rho^2/(1-it')}du'$$

$$=2\pi\exp\left[-\eta'+\eta'\frac{\rho^2}{1-it'}\right],\quad \eta'>0$$

$$=0,\quad \eta'<0 \text{ (since } \rho^2/(1+t^2)<1). \quad \text{(A-4)}$$

Therefore,

$$W_2(\xi,\eta)=\frac{e^{-\eta'}}{8\pi\sigma_0^2(1-\rho^2)}$$

$$\times\int_{-\infty}^{\infty}\frac{dt'}{1-it'}\exp\left[-i\xi' t'+\eta'\frac{\rho^2}{1-it'}\right]. \quad \text{(A-5)}$$

If $x=1-it'$,

$$\int_{-\infty}^{\infty}\frac{dt'}{1-it'}\exp\left[-i\xi' t'+\eta'\frac{\rho^2}{1-it'}\right]$$

$$=-ie^{-t'}\int_{1-i\infty}^{1+i\infty}\frac{dx}{x}\exp\left(\xi' x+\frac{\eta'\rho^2}{x}\right)$$

$$=2\pi e^{-t'}\sum_{m=0}^{\infty}\frac{1}{(m!)^2}(\xi'\eta'\rho^2)^m,$$

($\xi'>0$, by the Residue Theorem)

$$=2\pi e^{-t'}I_0(2\rho(\xi'\eta')^{\frac{1}{2}}), \quad \text{(A-6)}$$

which when substituted into (A-5) gives the probability density, Eq. (15).

PHYSICAL REVIEW VOLUME 96, NUMBER 3 NOVEMBER 1, 1954

λ Transition of Liquid Helium

RYOICHI KIKUCHI
Institute for the Study of Metals, The University of Chicago, Chicago, Illinois

(Received July 12, 1954)

The partition function of liquid helium proposed by Feynman, $q=\Sigma g(L)\exp(-aTL)$, is calculated for a simple cubic lattice using an approximation corresponding to Bethe's method for the Ising model. It is shown that a second-order transition occurs at $aT_\lambda=\ln 4$, or $T_\lambda=2.9m/m'$ °K (m and m' representing the true and the effective masses of a helium atom). The nature of the approximation is discussed.

I. INTRODUCTION

THE series of papers on liquid helium which Feynman has recently published[1–3] explained many of the so far unsolved properties of this substance. However, the problem of the nature of the λ transformation still does not seem to have been settled. In his papers[1,2] Feynman proposed an expression for the partition function and solved it approximately to obtain a transition of a third order. As it is commonly accepted that the λ transformation of liquid helium is of a second order, Feynman[2] ascribed the disagreement between his results and experiment to the fact that he neglected the correlation among atoms, both in the same cyclic change and in different cyclic changes. Though Chester[4] agreed with Feynman with regard to this interpretation of the discrepancy, Rice,[5] Matsubara,[6] and ter Haar[7] expressed the view that the above neglect of the correlation is not the origin of the discrepancy.

The purpose of the present paper is to show that a technique developed in the order-disorder theories can be applied to this problem to take into account the geometrical correlation, and, though the conclusion is not completely convincing (due to the approximate nature of the technique), that Feynman's partition function does give a second-order transition.

II. FREE ENERGY

The original expression for the partition function with which we begin is Eq. (7) of reference 2:

$$q=\int\sum_P\exp\left[-\frac{m'kT}{2\hbar^2}\sum_i(\mathbf{z}_i-P\mathbf{z}_i)^2\right]$$

$$\times\rho(\mathbf{z}_1,\mathbf{z}_2,\cdots,\mathbf{z}_N)d^N\mathbf{z}_i \quad (1)$$

in which m' is the effective mass of a helium atom. For the derivation of this equation and the notation, readers are referred to the original paper by Feynman. When one assumes that the value of $\rho(\mathbf{z}_1,\mathbf{z}_2,\cdots,\mathbf{z}_N)$ is non-vanishing only when the $\mathbf{z}$'s are located on a simple cubic lattice and that $(\mathbf{z}_i-P\mathbf{z}_i)^2$ is neglected except when its value is equal to d^2, d being the lattice constant of the hypothetical lattice, Eq. (1) reduces to Eq. (4)

[1] R. P. Feynman, Phys. Rev. **90**, 1116 (1953).
[2] R. P. Feynman, Phys. Rev. **91**, 1291 (1953).
[3] R. P. Feynman, Phys. Rev. **91**, 1301 (1953); Phys. Rev. **94**, 262 (1954).
[4] G. V. Chester, Phys. Rev. **93**, 1412 (1954).
[5] O. K. Rice, Phys. Rev. **93**, 1161 (1954).
[6] T. Matsubara, Busseiron Kenkyu **72**, 78 (1954).
[7] D. ter Haar, Phys. Rev. **95**, 895 (1954).

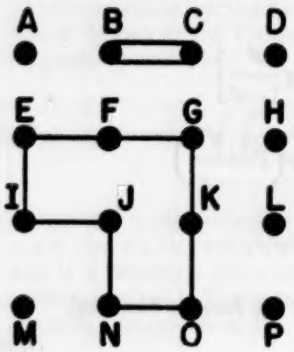

FIG. 1. Examples of allowed polygons for $g(L)$. BC is a two-sided polygon. Each of EF, FG, GK, KO, ON, etc., is called a "side," and each of E, F, G, K, etc., is a "vertex" of the polygon.

of reference 1, namely

$$q=\sum_L g(L)\exp(-aTL), \tag{2}$$

where

$$a=m'd^2k/2h^2.$$

$g(L)$ is the total number of ways that polygons can be drawn by connecting nearest neighbor points of a simple cubic lattice so that the total number of "sides" of all the polygons together is L. Here, by a "side" of a polygon we mean a bond between nearest neighbor lattice points. From the meaning of Eq. (1), the polygons are drawn under the following restrictions: (i) between two adjacent lattice points only one side is drawn, except for two-sided polygons, (ii) polygons must not come into contact, and (iii) polygons except for the two-sided ones are counted twice, corresponding to the two directions of cyclic change.

The terminology is explained in Fig. 1. BC is an example of a two-sided polygon. The polygon $EGONJIE$ has eight "sides" by our definition because, for example, EG contributes two "sides," EF and FG, though this is contrary to the ordinary usage of the word. In Fig. 2 some of the examples are shown which are not allowed. (a) is a pair of two-sided polygons in contact at the point A, (b) two polygons in contact at B, (c) two polygons crossed each other, and (d) two polygons sharing a bond.

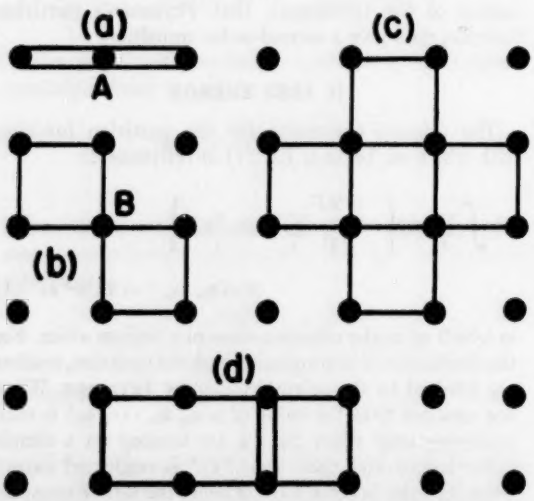

FIG. 2. Examples of polygons not allowed for $g(L)$.

The problem we are concerned with in this paper is to evaluate Eq. (2). For that purpose we follow closely the method used by the author in a treatment of the Ising model.[8] We express L and $g(L)$ as functions of a certain number of parameters and replace q of Eq. (2) by its maximum term; in other words, we minimize the free energy,

$$F=-kT\ln[g(L)\exp(-aTL)], \tag{3}[9]$$

with respect to these parameters.

Under the restrictions mentioned above concerning polygons, the possible configurations of a lattice point and of a bond are as shown in Tables I and II. The symbols in the tables are to be interpreted as follows: A dot is a lattice point which does not belong to any polygon (like the point A in Fig. 1). The double line of y_4 indicates a two-sided polygon (BC in Fig. 1), and the lattice point of x_2 a vertex of this polygon (the point B or C in Fig. 1). The angle for x_3 means that this lattice point is a vertex of a multisided polygon (e.g., the point G in Fig. 1). This symbol also includes a point like K in Fig. 1.[10] The arrows indicate the directions of cyclic change. The x's and y's are the probabilities of finding one of the respective configurations and the values of α's and β's are the number of different configurations having the same probability on the basis of symmetry requirement. For instance, α_2 is six because there are six different directions that a two-sided polygon can be drawn with a given point as its vertex. α_3 is equal to the number of ways of selecting two out of six, multiplied by two, corresponding to the two cyclic directions. The β's are calculated as follows: $\beta_2=2\times{}_6C_1$, $\beta_3=({}_6C_1)^2$, $\beta_5=2\times{}_6C_2\times2$, $\beta_6=2\times{}_6C_1\times{}_6C_2\times2$, $\beta_7=({}_6C_2\times2)^2$, and $\beta_8=({}_6C_1)^2\times2$.

As is seen in these drawings, every point is either a vertex[10] of a polygon or does not belong to any polygon. In other words, we always have closed polygons. Therefore the figures in Tables I and II satisfy the three requirements mentioned above.

When the number of lattice points in the lattice is N, the total number L of "sides" of polygons can be written as

$$L=3N(2y_4+50y_8). \tag{4}$$

[8] R. Kikuchi, Phys. Rev. **81**, 988 (1951). This paper will be referred to as TCP I.

[9] Although F has the form of $F=E^*-TS^*$ when one puts $E^*=akT^2L$ and $S^*=k\ln(L)$, E^* and S^* do not have the meaning of energy and entropy, respectively, because E^* contains T. See Eqs. (7) and (18) below.

[10] A point like F or K in Fig. 1 is called a vertex, too, because EF and FG are each considered separately to be a side.

This is a rigorous relationship. For $g(L)$ one has to be satisfied with an approximate functional form. The best approximation using the parameters defined in Tables I and II is the one corresponding to that of Bethe, and the form of $g(L)$ for that case is given by the last equation of Section B of TCP I, that is

$$g(L)=X_N^{2\omega-1}Y_N^{-\omega}N!^{-\omega+1}, \tag{5}$$

where 2ω is the coordination number of the lattice, and, as defined in Eq. (A.5) of TCP I,

$$X_N=\prod_{i=1}^{\lambda}(x_iN)!^{\alpha_i},$$
$$Y_N=\prod_{i=1}^{8}(y_iN)!^{\beta_i}. \tag{6}$$

Inserting Eqs. (4), (5), and (6) into (3) and using Stirling's formula, the free energy of the system becomes

TABLE I. Configuration of a point.

CONFIGURATION	PROBABILITY	α_i
•	X_1	1
⊃•	X_2	6
⌐•	X_3	30

$$F=3akT^2N(2y_4+50y_8)$$
$$-kTN(5\sum_{i=1}^{3}\alpha_ix_i\ln x_i-3\sum_{i=1}^{3}\beta_iy_i\ln y_i) \tag{7}$$

for $\omega=3$. The next procedure is to minimize F with respect to independent parameters, keeping T constant.

III. REGION FOR He II

One can derive from Tables I and II the following geometrical relations among x's and y's:

$$1=x_1+6x_2+30x_3, \tag{8}$$
$$x_1=y_1+5y_2+20y_5,$$
$$x_2=y_2+5y_3+20y_6=y_4, \tag{9}$$
$$x_3=y_5+5y_6+20y_7=5y_8.$$

If one chooses y_3, y_4, y_6, y_7, and y_8 as independent variables, the other variables can be expressed as linear combinations of these, as shown in Table III.

Minimizing F of Eq. (7) with respect to the independent variables, one obtains the following five fundamental equations:

TABLE II. Configuration of a bond.

CONFIGURATION	PROBABILITY	β_i
• •	y_1	1
• ⊂	y_2	10
⊃ ∪	y_3	25
⊂⊃	y_4	1
• ⌐	y_5	40
⊃ ⌐	y_6	200
⌐ ⌐	y_7	400
⌐ ∪	y_8	50

$$y_1y_3=y_2^2, \tag{10}$$
$$y_1y_6=y_2y_5, \tag{11}$$
$$y_1y_7=y_5^2, \tag{12}$$
$$e^{2aT}y_2^{10}y_4/y_1^{11}=(x_2/x_1)^{10}, \tag{13}$$
$$e^{aT}y_5^4y_8/y_1^5=(x_3/x_1)^5. \tag{14}$$

These equations together with relations in Table III can be solved without much difficulty when one puts

$$y_2/y_1=v,$$
$$y_5/y_1=w, \tag{15}$$

yielding

$$v=\tfrac{1}{5}e^{-aT},$$
$$w=(4e^{-aT}-1)/20. \tag{16}$$

The other variable can be written as functions of v and w.

As y_5 and y_1 are positive, w of (15) should be positive. Then Eq. (16) shows that this solution is valid only when the temperature is lower than the critical temperature T_λ defined by

$$aT_\lambda=\ln 4=1.386. \tag{17}$$

When Eqs. (10) to (14) are satisfied, or when F of Eq. (7) is a minimum with respect to the parameters, the free energy F, the entropy S, and the energy E of

TABLE III. Relations between the dependent and the independent variables. The meaning of this table is, for example, $x_1=1-6y_4-150y_8$.

	1	y_3	y_4	y_5	y_7	y_8
x_1	1		−6			−150
x_2			1			
x_3						5
y_1	1	25	−11	200	400	−250
y_2		−5	1	−20		
y_3				−5	−20	5

the system can be written as

$$F=-kTN(5\ln x_1-3\ln y_1),$$
$$S=-3akTN(2y_4+50y_8)+kN(5\ln x_1-3\ln y_1), \quad (18)$$
$$E=-3akT^2N(2y_4+50y_8).$$

From these relations one can see that if the x's and y's are continuous functions of temperature, then so are S and E.

The specific heat c_{II} per atom can be derived from E of Eq. (18):

$$\frac{c_{II}}{k}=\frac{28.8\theta^2e^\theta}{(14.4-e^\theta)^2}-\frac{2\theta(14.4-3e^\theta)}{14.4-e^\theta}, \quad (19)$$

where we put $\theta=aT$. At the critical temperature, $\theta_\lambda=\ln 4$, Eq. (19) gives

$$\frac{c_{II\lambda}}{k}=\frac{\ln 4}{169}(180\ln 4-78)=1.407. \quad (20)$$

IV. REGION FOR He I

When w is zero, one can see that x_3 and y_6 to y_8 also vanish. As may be seen from Tables I and II, this is a state in which only two-sided polygons exist. Then, of the five equations, (10) to (14), all but (10) and (13) become trivial identities. We can still use v as defined in Eq. (15) for this case, but the results are different, namely

$$v=(r-1)/10, \quad (21)$$

where

$$r^2=1+20e^{-2\theta}.$$

One can use the same expressions (18) for S and E, and the specific heat is given by the temperature derivative of

$$\frac{a}{k}\frac{E}{N}=\frac{4\theta^2e^{-2\theta}}{r}\left[\frac{2(5+6r)}{r+1+12e^{-2\theta}}-\frac{25}{r+1}\right]. \quad (22)$$

At the λ point, the specific heat becomes

$$\frac{c_{I\lambda}}{k}=\frac{\ln 4}{169}(50\ln 4-78)=-0.071. \quad (23)$$

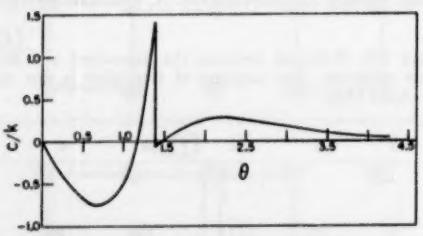

FIG. 3. The specific heat c per atom *versus* $\theta=aT$. The values at the transition point are: $\theta_\lambda=1.386$, $c_{II\lambda}=1.407k$, and $c_{I\lambda}=-0.071k$.

Comparing this with $c_{II\lambda}$ of Eq. (20) and considering that E is continuous at T_λ, one concludes that this temperature corresponds to a second-order transformation.

When one calculates a of Eq. (2) using $d=3.4$ A, which is the average distance between atoms in liquid helium, T_λ of Eq. (17) is equal to

$$T_\lambda=2.9(m/m')\ ^\circ\text{K}, \quad (24)$$

where m and m' are the true and the effective masses of a liquid helium atom, respectively. If one equates the expression for T_λ with the observed λ point, 2.2°K, one obtains $m'/m=1.3$ which is not too unreasonable, though slightly smaller than Feynman's estimate.[2]

The curve of specific heat *versus* $\theta(=aT)$ is plotted in Fig. 3. Since q of Eq. (1) is not the total partition function of the system, but is to be multiplied by a function of temperature as is seen in Feynman's paper,[2] it is to be expected that the negative value of the specific heat in Fig. 3 should be increased to a positive value when the remaining factor of the partition function is taken into account; thermodynamics is therefore not contradicted.

From this and the foregoing section and from some other evidence, one can interpret the transition as follows. Above T_λ the main contribution to the partition function comes from polygons of finite size, their sizes increasing as the temperature is lowered. At T_λ or below, polygons of infinite size predominate. In order to verify this picture, a better approximation which uses a square as the basic figure, as was done in TCP I, is desirable. In that approximation we expect that not only two sided polygons but also squares exist in the He I region. The minimum of the specific heat just above T_λ, which we attribute to the nature of the approximation, is expected to disappear or to be reduced by the improved approximation.

As is the case in the approximate treatment of the Ising model, the actual value of $c_{II\lambda}-c_{I\lambda}$ does not have any physical meaning. Also it should be emphasized again that the present approximation fails near the absolute zero, because we neglected values of $(\mathbf{z}_i-P\mathbf{z}_i)^2$ larger than d^2. However, it seems worthwhile to investigate how good the present approximation is at somewhat higher temperatures. This we shall do in the next section by comparison with the Ising model.

V. COMPARISON WITH ISING MODEL

One of the specific features of the results in the previous sections is that a second-order transition is obtained without recourse to any long-range order parameters. Although in the ordinary order-disorder theories, the concept of long-range order helps one to understand the physical nature of order-disorder to such an extent that it may be looked upon as the central feature of the phenomenon, a moment's reflection will indicate that there are treatments of order-

disorder problems that do not use the concept of long-range order.

To make the presentation simpler, let us consider in this section a two-dimensional square lattice. The partition function of the Ising model can be written as

$$f=2^N(\cosh K)^{2N}\sum\Omega_n \tanh^n K, \qquad (25)^{11}$$

where Ω_n is the number of configurations of polygons when the total number of "sides" of polygons is n. The difference between Ω_n and $g(L)$ of Eq. (2) is that for Ω_n all three restrictions (i), (ii), and (iii) of Sec. II do not hold, and instead the requirements are: (i') between two adjacent lattice points only one side is drawn, and the two-sided polygons are not allowed, (ii') polygons may intersect or touch, but a given bond must be used once only, and (iii') each polygon is counted once. For example, in Fig. 2, (b) and (c) are allowed, but (a) and (d) are not: BC of Fig. 1 is not allowed.

Although Eq. (25) was used to evaluate f rigorously,[11] it seems worthwhile, for the present discussion of the nature of the approximations, to show a method of evaluating f approximately. We shall apply the pair approximation which is analogous to the one used in

TABLE IV. Configuration of a point for the Ising model.

CONFIGURATION	PROBABILITY	α_i
•	X_1	1
⌐	X_2	6
+	X_3	1

previous sections, and shall show that it gives a result identical to the ordinary Bethe approximation which is the pair approximation applied to the partition function including the long-range order parameter.

The different configurations of a lattice point and of a bond, together with the notation for the probability of finding one of them, are listed in Tables IV and V. One can see from Table V that the number n of "sides" of polygons is

$$n=2N(9y_4+6y_5+y_6). \qquad (26)$$

For the pair approximation, we use Eqs. (5) and (6) with $\omega=2$ for Ω_n. Hence from Eq. (25) the free energy contributed from the summation part becomes

$$\begin{aligned}F&=-kT\ln[\Omega_n\tanh^n K]\\&=2kTN\Theta(9y_4+6y_5+y_6)\\&\quad -kTN[3\textstyle\sum\alpha_i x_i\ln x_i-2\sum\beta_i y_i\ln y_i],\end{aligned} \qquad (27)$$

where

$$\Theta=\ln(\coth K).$$

[11] See, for instance, G. F. Newell and E. W. Montroll, Revs. Modern Phys. 25, 353 (1953); Kurata, Kikuchi, and Watari, J. Chem. Phys. 21, 434 (1953).

TABLE V. Configuration of a bond for the Ising model.

CONFIGURATION	PROBABILITY	β_i
• •	y_1	1
• ⌐	y_2	6
⌟ ⌐	y_3	9
⌙⌝	y_4	9
⊣⌟	y_5	6
⊣⊢	y_6	1

Making F a minimum with respect to the independent variables, one obtains

$$y_2/y_1=(3-e^{\Theta})/(3e^{\Theta}-1). \qquad (28)$$

Since this quantity must always be positive, the transition point Θ_c is given by

$$\Theta_c=\ln 3. \qquad (29)^{12}$$

Above T_c, all of the x's and y's vanish except x_1 and y_1, which means that above T_c, Ω_n are all zero except $\Omega_0=1$, giving

$$f=2^N(\cosh K)^{2N}. \qquad (30)$$

This equation is exactly the partition function of the disordered state calculated from the ordinary Bethe approximation. It is just a matter of mathematical manipulation to obtain the solution for the ordered state under Bethe's approximation from Eqs. (27) and (28) when $y_2\neq 0$.

This analysis makes it legitimate to say that the method used in the previous sections corresponds to Bethe's approximation as far as the relation to the rigorous evaluation of the partition function is concerned.

Although we have different restrictions on $g(L)$ of Sec. II and on Ω_n of this section, the difference does not seem to affect appreciably the cooperative nature of the problem. For instance, if we replaced the restrictions on $g(L)$ by those on Ω_n and used the ordinary theories of order-disorder for calculating q, the transition point for the simple cubic lattice would be

$$aT_\lambda=1.5, \qquad (31)^{13,14}$$

which is very close to the value of Eq. (17).

It is desirable to apply the method developed in TCP I in obtaining an improved approximation to

[12] Using the definition of Θ in Eq. (26) and $K=\epsilon/kT$, the value of Θ_c, Eq. (29), corresponds to $2\epsilon/kT_c=\ln 2$, which is the well-known result obtained when Bethe's approximation is applied to the square lattice.

[13] Comparing Eqs. (3) and (27), Θ_c is equated to aT_λ. Actually, the value of aT_λ would be 1.57 by Bethe's approximation and 1.52 by Wakefield's estimate of the true transition point. See reference 14.

[14] A. J. Wakefield, Proc. Cambridge Phil. Soc. 47, 799 (1951).

estimate q of Eq. (2). However, in the next approximation, with a square as the basic figure, the number of independent variables increases to about twenty. But we may take advantage of the close similarity between our q and the ordinary order-disorder partition function, and may predict from a knowledge of the Ising model what would happen if one improved the approximation for q.

With improvement in the approximation, T_λ would change slightly, but the real transition point would not be too far from the value of Eq. (17).[15] $c_{\mathrm{II}\lambda}$ and $c_{\mathrm{I}\lambda}$ would both increase, the former moving higher more rapidly than the latter, increasing the discontinuity $c_{\mathrm{II}\lambda}-c_{\mathrm{I}\lambda}$. Although the three-dimensional case of the Ising model has not yet been worked out, it is probable that $c_{\mathrm{II}\lambda}$, and also $c_{\mathrm{I}\lambda}$, becomes infinite in the rigorous solution.[14] As $c_{\mathrm{I}\lambda}$ increases, the part of the specific heat curve just above T_λ naturally increases, and could give the shape which Feynman obtained using a different approximation.[2]

In short, the relationship between the various approximate and the rigorous solutions of this problem might be similar to that between the approximate solutions and Onsager's rigorous solution[16] of the problem of the two-dimensional Ising model.

VI. DISCUSSION

The present calculation is based on the assumption that atoms are localized on lattice points. This may not be too unsatisfactory for discussing the qualitative nature of the transition, in view of the success of the lattice model for solid-liquid-gas phase changes.[17] It is probable that, using the lattice model, one can reproduce the qualitative nature of the amorphous phases correctly if one does not take advantage of the long-range regularity of the lattice but only of its local nature.[18] The type of lattice one uses would not affect the result very much. Of course it is desirable to extend the calculation to a continuum model.[19]

As Chester pointed out, Matsubara[20] obtained a second-order transition starting from an approximation quite similar to Feynman's. The difference between the treatment of Matsubara and that of Feynman seems to be that the former assumed a positive constant potential for atoms in cyclic rings. This assumption should be justified before we can accept his theory.

From evidence in the treatment of the ideal Bose-Einstein gas and from Feynman's discussion, it seems likely that the dominance of infinitely large polygons below T_λ corresponds to the condensation to the lowest energy level, though we have not succeeded in showing it clearly.

Summarizing, the present paper indicates, following Feynman's ideas, that the λ transition of liquid helium is essentially a Bose-Einstein condensation of hard-sphere Bose particles.

Thanks are due Professor R. P. Feynman for helpful discussions.

[15] If the relation between Bethe's approximation and Wakefield's estimate mentioned in reference 13 is transplanted to the present problem, the value of Eq. (17) would have to be lowered less than 0.1 to coincide with the true transition point.

[16] L. Onsager, Phys. Rev. **65**, 117 (1944).

[17] See, for instance, F. Cernushi and H. Eyring, J. Chem. Phys. **7**, 547 (1939); J. E. Lennard-Jones and A. F. Devonshire, Proc. Roy. Soc. (London) **A163**, 53 (1937); R. Kikuchi, J. Chem. Phys. **19**, 1230 (1951).

[18] For instance, the division into sublattices is a kind of long-range regularity and should not be considered in a model for a liquid.

[19] Although a paper by the author (reference 17) shows how to extend this calculation to a continuum, the method is highly impracticable.

[20] T. Matsubara, Progr. Theoret. Phys. **6**, 714 (1951).

Scintillation Response of Phosphors at Low Particle Energies

G. T. WRIGHT
Department of Physics, Rhodes University, Grahamstown, South Africa
(Received July 26, 1954)

The results of a detailed statistical analysis of the scintillation counter are used to correct previously published data for the response to low-energy photoelectrons of NaI(Tl) and anthracene. The nature of the true response curves is discussed.

INTRODUCTION

DEVELOPMENT of the scintillation counter has for the first time permitted quantitative investigation of the luminescence excited in crystals because of individual nuclear particles. Much useful information has been gained in this way about a fundamental aspect of the interaction between nuclear particles and solids.

In this connection it is essential that the characteristics of the scintillation counter are accurately known in order that the observed pulse-height distribution may be satisfactorily related to the scintillation intensity. At moderate and high particle energies the distribution for monoenergetic particles is essentially Gaussian[1] and it is permissible to identify the position of the mean with that of the maximum as generally done. At low particle energies however, the statistical processes of photoelectron production and cascade multiplication of these in the photomultiplier tube result in a distribution which is markedly asymmetrical. A detailed calculation[2] of these processes has shown that the position of the maximum always lies below that of the mean; for the anthracene scintillation counter this difference becomes significant at electron energies below about 100 kev. It is the purpose of this communication to apply this correction to the previously published data of West, Meyerhof, and Hofstadter[3] and Birks and Brooks[4] for the NaI(Tl) and anthracene counter, respectively.

METHOD

A statistical analysis was made of the experimental distributions in order to convert mean pulse-height measurements $\bar{V}$, into mean photocathode electrons $\bar{n}\bar{p}$. The general expression for the fractional variance of the observed distribution[5] is:

$$\frac{\mathrm{var}(V)}{\bar{V}^2}=\frac{1}{\bar{n}\bar{p}}\left(1+\frac{\epsilon}{\bar{r}}\frac{\delta}{\delta-1}+\frac{\sigma_r^2}{\bar{r}^2}\right)+\text{constant},$$

where $\bar{r}$ is the mean gain of the first dynode stage, δ is the mean gain per stage of the remaining stages, and $\sigma_r^2/\bar{r}^2$ is the fractional variance of the gain of the first stage being due to nonuniform sensitivity over its surface. The quantity ϵ is a statistical enhancement factor, similar to that used by Morton, and is caused by nonnormal variance of the dynode gain; under normal operating conditions it may be taken as unity.[5] The constant is determined by a variety of factors and in a well-designed counter is zero. The fractional variance was derived from the fractional half-width (using only the distributions of Gaussian profile from the higher-energy particles) and plotted in terms of the reciprocal mean pulse height. In each case the resulting curve was linear and passed through the origin. From the slope of this line the original results were interpreted in terms of mean photocathode electrons.

The position of the mean of the distribution differs from that of the maximum np_m. In terms of photocathode electrons we have[2]:

$$\bar{n}\bar{p}=np_m+\delta,$$

where δ is a constant which is slightly dependent upon multiplier gain but whose average value is about 0.7.

The true response curves are shown in Fig. 1 and Fig. 2 for NaI(Tl) and anthracene, respectively; the original experimental results are also shown in these diagrams to illustrate the appreciable magnitude of the correction. The true response curve for NaI(Tl) indicates that for this material the conversion efficiency increases at very low energies while for anthracene the response is exactly proportional to electron energy.

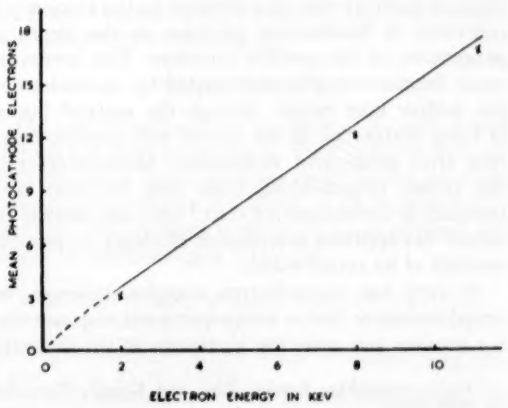

FIG. 1. Response of NaI(Tl) to internally produced photoelectrons. × experimental; — true response.

[1] G. F. J. Garlick and G. T. Wright, Proc. Phys. Soc. (London) B65, 415 (1952).
[2] G. T. Wright, J. Sci. Instr. (to be published).
[3] Mest, Weyerhof, and Hofstadter, Phys. Rev. 81, 141 (1951).
[4] J. B. Birks and T. D. Brooks, Phys. Rev. 94, 1800 (1954).
[5] G. T. Wright, J. Sci. Instr. (to be published).

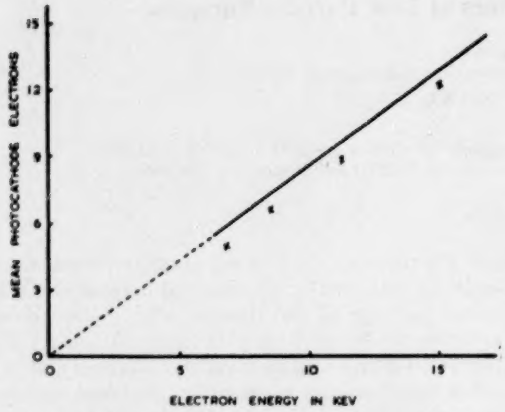

FIG. 2. Response of anthracene to internally produced photoelectrons. ✕ experimental; — true response.

DISCUSSION

Anthracene is typical of the organic phosphors and these will be discussed as a class.

The nature of the response to internally produced photoelectrons as illustrated in Fig. 2 is of considerable fundamental importance unlike the response curves to external electrons for which surface effects may be appreciable. The true fluorescence intensity is proportional to the total energy dissipated in the crystal over the measured energy range. It is of significance that there appear to be no quenching processes dependent upon nonradiative interaction between ionized or excited molecules for, if present, such mechanisms would produce a nonlinear response. The nonlinear response to external electrons[6] must consequently be caused wholly by surface effects such as reflection of primary electrons and escape of secondary electrons and soft x-rays (or possibly far ultraviolet photons, see Birks[7]). In addition, overlap of absorption and fluorescence spectra produces considerable variations in scintillation intensity due to a decrease in the efficiency of collection of fluorescence photons as the depth of penetration of the particle decreases. This occurs because fluorescence photons emitted by molecules near the surface may escape through the surface[8] instead of being reabsorbed in the crystal with possible collection after subsequent re-emission. Measurements by the author (unpublished) show that for short range particles in anthracene ($R<10^{-3}$ cm) this process can reduce the apparent scintillation efficiency to less than one-half of its actual value.

At very low photoelectron energies, however, one would expect to find a nonproportional response since for energies less than the maximum in the ionization curve ionization is no longer the predominant mechanism of energy loss and there is probably an associated change in fluorescence efficiency. Measurements in this region would be made most readily by the techniques of vacuum spectroscopy and are likely to yield results of much interest. It is in this region that scintillation decay times become longer than photofluorescence decay times and constant quantum efficiency of response to absorbed photons changes to constant energy response.

Although the response to heavy particles is nonlinear,[6] the conditions which exist for these are quite different from those for external electrons. For the same initial velocity (which together with charge mainly determines the rate of energy loss), these penetrate many times further through the crystal than electrons and in any event do not suffer the multiple scattering experienced by electrons, which keeps a large proportion near the surface; it is unlikely therefore that surface effects are appreciable for the heavy particles except at very low energies.[9] The quenching processes operative are consequently to be sought in conditions which are not produced by electrons.

It is known that the heavy particles are proficient in producing damage of the crystal lattice. Each absorbed particle produces a large number of permanently damaged molecules and it is almost certainly the case that many more molecules are temporarily damaged or dissociate but recombine on the Franck-Rabinovitch principle before this damage can become permanent. If we accept the effectiveness of the particle for producing radiation damage as a measure of the extent of this latter process it is negligible for electrons as compared with the heavy particles.[10] It is feasible then that the bimolecular quenching mechanisms[11] for the heavy particles are connected with the production of temporary chemical entities in the excitation column which, although recombining rapidly, nevertheless exist for a sufficient period (10^{-11} to 10^{-10} sec) for quenching to occur.

CONCLUSION

The linear response to internally produced electrons shows that quenching by nonradiative interaction of ionized and excited molecules in the excitation column is not the mechanism responsible for the nonlinear response of the organic phosphors to ionizing radiations.

In the case of external electrons this is attributed to surface effects, and for the heavy particles to bimolecular processes connected with the production of temporarily damaged molecules in the excitation column.

ACKNOWLEDGMENTS

The author wishes to thank his colleagues Professor J. B. Birks and Mr. T. D. Brooks for access to their original results.

[6] Taylor, Jentschke, Remley, Eby, and Kruger, Phys. Rev. 84, 1034 (1951).
[7] J. B. Birks, *Scintillation Counters* (Pergamon Press, London; McGraw-Hill Book Company, Inc., New York, 1953).
[8] This is not escape of "primary" photons as envisaged by Birks (reference 7).
[9] G. T. Wright and G. F. J. Garlick, Brit. J. Appl. Phys. 5, 13 (1954).
[10] F. A. Black, Phil Mag. 44, 263 (1953).
[11] G. T. Wright, Phys. Rev. 91, 1282 (1953).

Electrical and Optical Properties of Intermetallic Compounds. I. Indium Antimonide*

R. G. Breckenridge, R. F. Blunt, W. R. Hosler, H. P. R. Frederikse, J. H. Becker, and W. Oshinsky†
National Bureau of Standards, Washington, D. C.

(Received July 19, 1954)

The conductivity and Hall coefficient of InSb have been measured over the temperature range 78°K to 750°K. At low temperatures an electron mobility of 30 000 cm²/volt-sec and a mobility ratio of 29 are observed. The effective mass of electrons is $0.04m$ and the width of the forbidden energy gap is 0.23 ev at $T=0$°K.

Optical absorption studies have been made at temperatures between 13°K and 300°K. The position of the absorption edge of degenerate n-type samples depends on the impurity content and is in good agreement with Burstein's predictions.

INTRODUCTION

INDIUM antimonide is one of a series of semiconducting compounds formed between elements of the B-subgroups of the third and fifth columns of the periodic table. In 1952 Welker[1] focused attention on this family of materials (antimonides, arsenides, and phosphides) and reported briefly on their properties. These compounds possess the zincblende structure; the nearest neighbor distance in InSb is 2.80 A, equal to that of grey tin. The melting point of the compound is 523°C. An earlier publication[2] indicated some of the interesting features of this compound, namely, the small forbidden energy gap and the high electron mobility. Measurements of resistivity and Hall effect have now been made on a number of samples; the optical absorption of the compound has also been studied in detail.

EXPERIMENTAL PROCEDURES AND RESULTS

Samples

The compound is prepared by melting the components together in stoichiometric proportions. The starting materials used were antimony obtained from the Bradley Mining Company and indium from the Anaconda Copper Mining Company. The antimony has a purity of 99.95 percent and contains small amounts of Pb, As, Cu, and Fe. The purity of the indium is 99.954 percent, the major impurities being Zn, Sn, Ni, Cd, Fe, Cu, and a trace of Pb. The melting process is done in an induction furnace with helium or argon as a protecting atmosphere. The melt is contained in a grade A carbon crucible. Further purification of the compound was achieved by repeated zone melting. Ingots were drawn from the melt by the Kyropoulos technique starting with a small seed. In some cases the compound was prepared by melting together antimony and indium in an evacuated vycor tube. The antimony used was chemically purified, following the method of Groschuff.[3] All ingots showed p-type conductivity and were slightly polycrystalline. The samples cut from ingot SC-5 are, however, single crystals. The n-type specimens were prepared by adding tellurium to the melt.

X-ray analysis confirmed the zincblende structure with a lattice constant[4] of 6.4782 A at 25°C in reasonable agreement with the values reported by Goldschmidt.[5]

Electrical Properties

The measurements of resistivity and Hall effect were made with the conventional dc method.[6] For the low-temperature experiments the probes were soldered to the sample with indium metal; pressure contacts were used at high temperatures. Measurements were made in the range 78°K to 700°K with results given in Figs. 1 and 2. These results are in good agreement with data of other investigators.[1,7,8]

The striking feature of these results is that the Hall coefficient of the p-type samples reaches much higher values in the intrinsic range than in the extrinsic region. The Hall and resistivity curves are practically flat in the extrinsic range, indicating very small activation energies for imperfections.

Optical Properties

The optical absorption of several n- and p-type samples has been investigated. These samples were cut from the same ingots as those used for the electrical measurements, except $P4$ which is an impure n-type specimen. The samples were ground and polished, and ranged in thickness from 3 to 5 mil.

* Supported in part by the Office of Ordnance Research.

† Now at Army Engineering Laboratories, Fort Belvoir, Virginia.

[1] H. Welker, Z. Naturforsch. **7a**, 744 (1952); **8a**, 248 (1953).

[2] R. G. Breckenridge, Phys. Rev. **90**, 488 (1953).

[3] E. Groschuff, Z. anorg. u. allgem. Chem. **103**, 164 (1918).

[4] These measurements were made by the Microstructure Section of the National Bureau of Standards.

[5] V. M. Goldschmidt, Skrifter Norske Videnskaps-Akad, Oslo. I. Mat.-Natur. Kl. No. 2 (1926).

[6] R. G. Breckenridge and W. R. Hosler, Phys. Rev. **91**, 793 (1952).

[7] H. Weiss, Z. Naturforsch. **8a**, 463 (1953).

[8] M. Tanenbaum and J. P. Maita, Phys. Rev. **91**, 1009 (1953).

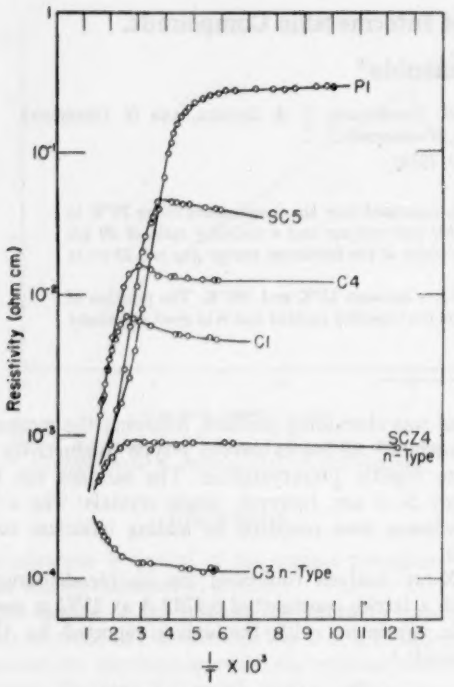

FIG. 1. Resistivity of various InSb samples.

The determination of the optical transmission follows closely the conventional method. The radiation from a source is focused on the sample by means of mirrors. An incandescent lamp is used as a source up to 2 μ and a globar for wavelengths between 1 and 15 μ. The transmitted radiation is refocused on the entrance slit of a Perkin-Elmer model 83 monochromator (NaCl prism) which is used to analyze the transmitted radiation. The light beam is chopped at 10 cps near the source and the analyzed radiation measured with a Perkin-Elmer vacuum thermocouple and a tuned amplifier. The effect of stray radiation on the apparent transmissivity is reduced and checked by means of appropriate transmission filters. Measurements are made at wavelength intervals of 0.5 μ over most of the range and 0.1 μ at the absorption edge.

For measurements at liquid nitrogen temperature, the samples are mounted in a small metal Dewar while data near liquid helium temperature are obtained with a cryostat similar to the one designed by Duehrig and Mador.[9] However, the absorbed radiation heats the samples to a temperature somewhat higher than that of the refrigerant. An Ag-Au thermocouple[10] indicated that the actual temperatures of the sample obtained for liquid nitrogen and helium cooling were about 85°K and about 15°K, respectively.

Several runs were made using a slightly different experimental procedure. In this case monochromatic light from the spectrometer was focused onto the sample and then collected by the detector. The results are essentially the same as those obtained with the previous method.

One very thin p-type sample (1 mil) showed regular maxima and minima of the absorption coefficient in the long wavelength tail (7–15 μ). This interference pattern is caused by multiple reflections inside the sample. The refractive index κ can now be calculated from the well-known interference relation and yields an average value for κ of 3.5 over the range 7 to 15 μ. This value is in good agreement with the one reported by Briggs *et al.*[11] This enables us to correct the transmission for reflection losses and plot the spectra in terms of the absorption coefficient.[12] Absorption spectra for several samples at room temperature are given in Fig. 3. One notices that the location of the absorption edge changes from sample to sample between 3 and 7 μ. This anomaly has been reported also by Tanenbaum and Briggs.[13] Figure 4 shows the temperature variation of the absorption coefficient for a pure p-type sample (*SC*-5) and for an impure n-type specimen (*P*4). The shift of the absorption edge with temperature (expressed in ev/deg) appears to be much larger for the n-type sample than for the p-type specimen.

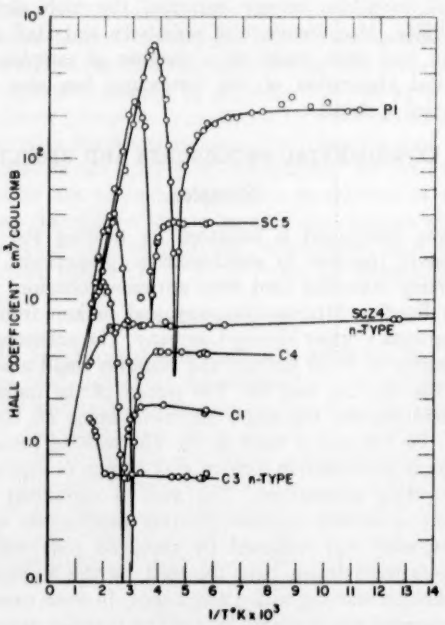

FIG. 2. Hall coefficient of various InSb samples.

[9] W. H. Duehrig and I. L. Mador, Rev. Sci. Instr. **23**, 421 (1952).
[10] Sigmund Cohen, New York, New York.
[11] Briggs, Cummings, Hrostowski, and Tanenbaum, Phys. Rev. **93**, 912 (1954).
[12] H. Y. Fan and M. Becker, *Semiconducting Materials* (Butterworths Publications, London, 1951).
[13] M. Tanenbaum and H. B. Briggs, Phys. Rev. **91**, 1561 (1953).

DISCUSSION

In order to calculate the different parameters, such as charge carrier concentration, carrier mobility, and forbidden band width, we use a procedure slightly different from that of Pearson and Bardeen.[14] We will apply this analysis to the results for sample *SC*-5 (*p* type).

The Hall coefficient (in cm³/coulomb) is given by

$$R=-\frac{3\pi}{8e}\frac{n\mu_n^2-p\mu_p^2}{(n\mu_n+p\mu_p)^2}=-\frac{3\pi}{8e}\frac{nb^2-p}{(nb+p)^2}, \quad (1)$$

where n = concentration of electrons in the conduction band, p = concentration of holes in the valence band, μ_n = electron mobility, μ_p = hole mobility, $b=\mu_n/\mu_p$, and e = electronic charge in coulombs. Furthermore,

$$p=n+N, \quad (2)$$

in which N = number of acceptor impurities per cm³, which are all ionized over the temperature range studied. We want to determine the value of R at its maximum, R_{max}. Now in the case of a *p*-type semiconductor, n is a function only of T and further a monotonic increasing function of T such that R_{max} can be determined from the condition

$$\delta R/\delta n=0. \quad (3)$$

The value for n for which R reaches its maximum is

$$n_{max}=N/(b-1) \quad (4)$$

and

$$R_{max}=\frac{-3\pi}{8eN}\frac{(b-1)^2}{4b}. \quad (5)$$

N is related to the Hall coefficient in the exhaustion range,

$$R_{ex}=3\pi/8eN. \quad (6)$$

Hence,

$$R_{max}/R_{ex}=(b-1)^2/4b. \quad (7)$$

Substituting the numerical values from Fig. 2, we find a mobility ratio $b=29$ for sample *SC*5.[15]

The number of electrons n in the intrinsic range can then be calculated from the Hall coefficient

$$n=-\frac{3\pi}{8Re}\frac{b-1}{b+1}, \quad (8)$$

and the number of holes p follows from Eq. (2). These numbers have been plotted in Fig. 5. One can now compute the product np, which is given by the expression[16]:

$$np=4(2\pi mkT/h^2)^3(m_nm_p/m^2)^{\frac{3}{2}}e^{-E/kT}, \quad (9)$$

where m_n = effective mass of electrons, m_p = effective mass of holes, and E = width of the forbidden energy gap. This last quantity depends, however, on temperature; assuming a linear temperature dependence as found in other semiconductors,[12] we can replace E by

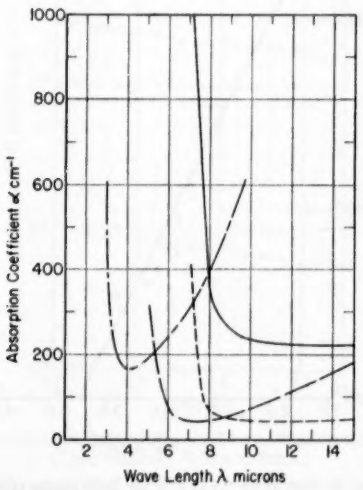

FIG. 3. Absorption spectra of several *n*- and *p*-type samples of InSb at 305°K. —— *SC*-5, — — *Z*4, - - - - *P*4-*A*, — — — — *P*4.

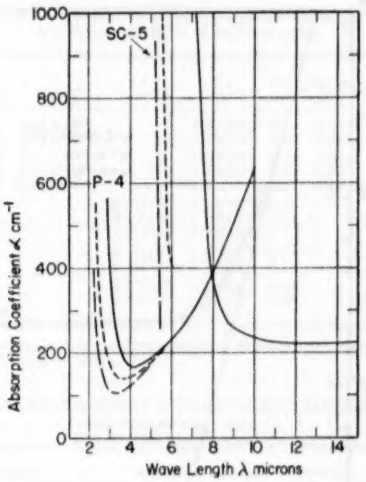

FIG. 4. Temperature dependence of the absorption edge of two InSb samples.

SC-5 (*p* type)	*P*-4 (*n* type)
—— 307°K	—— 303°K
- - - - 86°K	- - - - 83°K
— — 15°K	— — 13°K.

[14] G. L. Pearson and J. Bardeen, Phys. Rev. **75**, 865 (1949).

[15] This ratio depends not only on the total impurity concentration, but also on the number of grain boundaries, and varies widely from sample to sample. Tanenbaum and Maita (see reference 8), report a mobility ratio of 85.

[16] This relation is accurate for completely nondegenerate samples but gives a value of the product np which is too large by about 5 percent for $n=0.4N_c$ and four times too large for $n=20N_c$. The degeneracy temperature of sample *SC*5 is 99°K. N_c = effective density of states in the conduction band $=2(2\pi mkT/h^2)^{\frac{3}{2}}$ [see W. Shockley, *Electrons and Holes in Semiconductors* (D. Van Nostrand and Company, Inc., New York, 1950), p. 240].

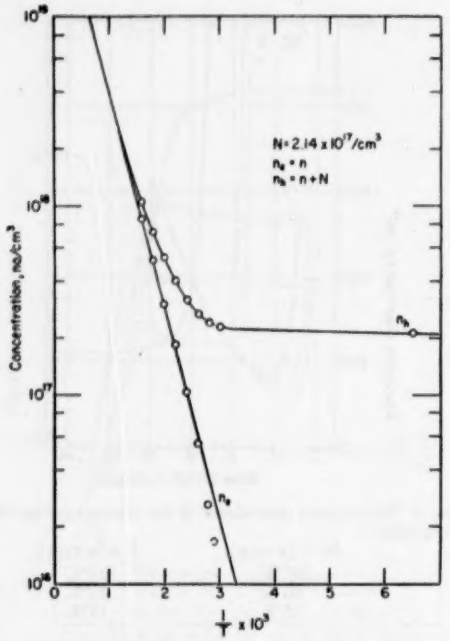

FIG. 5. Charge carrier concentrations of InSb single crystal.

$E_0+\beta T$. Equation (9) can then be written

$$np=4\left(\frac{2\pi mkT}{h^2}\right)^3\cdot\left(\frac{m_n m_p}{m^2}\right)^{\frac{3}{2}}\cdot e^{-\beta/k}\cdot e^{-E_0/kT}. \quad (9a)$$

The slope of the plot of $\ln[np/T^3]$ *vs* $1/T$ will therefore give the quantity E_0 (see Fig. 6). This value appears to be 0.23 ev. The intercept in this plot determines the coefficient before the exponential $e^{-E_0/kT}$ in Eq. (9a). This coefficient contains two unknown parameters: β and $(m_n m_p/m^2)$. The quantity β can be calculated from optical absorption measurements (see Table I). Substituting this value we find for the intercept 2.9×10^{29} and, subsequently,

$$(m_p m_n/m^2)^{\frac{3}{2}}=0.077, \quad (10)$$

in good agreement with the value given by Tannenbaum and Maita.[8] The effective masses are also related to the mobilities[17]:

$$b=\mu_n/\mu_p=(m_p/m_n)^{5/2}. \quad (11)$$

A combination of Eqs. (10) and (11) yields the following values for the effective masses of electrons and holes:

$$m_n=0.04m \quad \text{and} \quad m_p=0.15m.$$

At high temperatures in the intrinsic range the effect of electrons is predominant and R_H should give a value which is approximately equal to the mobility of electrons. In the low-temperature region where the conductivity is mainly by holes, this product should give the hole mobility. Assuming a constant mobility ratio $b=29$, one finds mobility curves for electrons (top) and holes (bottom) as presented in Fig. 7.

Similar calculations have been made for the other samples. Electron and hole concentrations are listed in Table I.

The forbidden band width is also related to the steep rise observed in the absorption spectrum. The exact location of this edge is rather arbitrary. We have chosen the value where the straight line portion of the edge intersects with the extrapolated long-wavelength tail. These values are given in the column marked E_{obs} in Table I and appear to be in good agreement with results reported by other investigators.[13,18]

Burstein[19] has recently offered an explanation for the anomalous behavior of *n*-type InSb based on the very small effective mass m_n observed for conduction electrons. The consequences of this small value of m_n will be a very small density of states in the lower part of the conduction band and also a relatively small degeneracy concentration (10^{17} per cm^3 at room temperature). The Fermi level of degenerate samples will therefore be located at a considerable distance from the bottom of the conduction band, depending on the impurity content. Hence, the energy necessary to excite electrons optically from the valence band into the con-

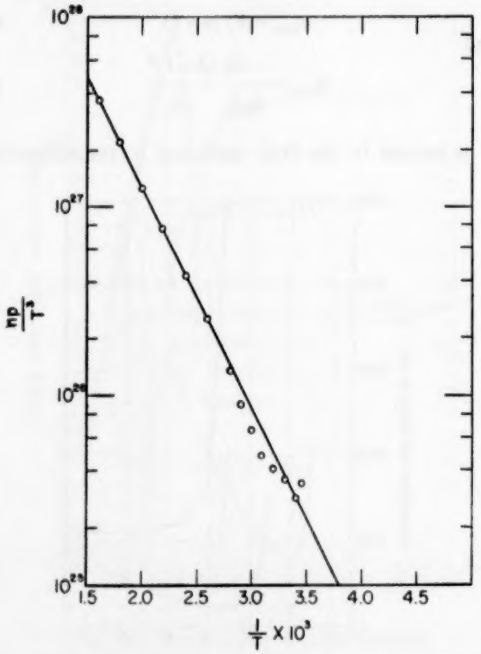

FIG. 6. Plot of np/T^3 *vs* $1/T$ for InSb single crystal.

[17] W. Shockley, *Electrons and Holes in Semiconductors* (D. Van Nostrand and Company, Inc., New York, 1950), p. 287.

[19] W. Kaiser and H. Y. Fan, Phys. Rev. **95**, 1431 (1954).

[19] E. Burstein, Phys. Rev. **93**, 632 (1954). See also: Beer, Willardson, and Middleton, Phys. Rev. **93**, 912 (1954).

duction band will be larger than the width of the forbidden energy gap.

Assuming spherical energy surfaces, Burstein calculates the following expression for the optical activation energy in degenerate n-type samples ($n>6.5N_c$):

$$E_{\text{calc}}{}^{n}=E+(1+m_n/m_p)(E_F-E_c-4kT), \quad (12)$$

where

$$E_F-E_c=\frac{h^2}{2m_n}\left(\frac{3n}{8\pi}\right)^{\frac{2}{3}}, \quad (13)$$

E_F = Fermi level, and E_c = bottom of conduction band.

It has been assumed in the derivation of this expression that the lowest unfilled level lies approximately $4kT$ below the Fermi level. In order to calculate $E_{\text{calc}}{}^{n}$ we have used the following parameters. The energy gap E is taken from the values obtained on the nondegenerate p-type samples. For the effective masses we have used $m_n=0.04$ and $m_p=0.15$ (see above). The results of this calculation are given in column 7 of Table I.

A comparison of the observed and calculated values of the activation energy shows a fair agreement; our measurements seem to substantiate Burstein's explanation of degenerate behavior in InSb.

It is clear that the temperature variation of the forbidden energy gap E can only be derived from the data on the p-type samples. The values of $\beta(=dE/dt)$ are listed in Table I.

It has been shown[20] that transitions of free carriers within the allowed energy bands will also contribute to the absorption. The absorption coefficient α due to this mechanism is given by

$$\alpha=5.06\times10^{-17}\lambda^2N/\kappa\mu(m^*/m)^2, \quad (14)$$

where N = carrier concentration and m^* = effective mass of carrier. We have evaluated the absorption coefficient at a number of wavelengths using the measured values of the parameters N, κ, μ, and m^*. The results of this calculation together with the observed values of α are listed in Table II. It is apparent from the data on the n-type samples that α is indeed proportional to λ^2. The absolute magnitude, however, is not too well predicted by the theory. (Even larger discrepancies have been found in the cases of germanium and silicon.) The absorption of the p-type samples is, within experimental error, independent of wavelength; the observed discrepancies can presumably be attributed to unaccounted reflection losses.

Equation (14) shows that α is very sensitively dependent on the effective mass m^* and the mobility μ. The values of μ taken from the electrical measurements are very low, presumably due to the polycrystalline nature of the samples. It seems reasonable to assume that the mobility within the grains is considerably higher. This in turn would decrease the calculated values of α.

TABLE I. Carrier concentrations, effective densities of states, and activation energies of InSb samples.

Sample	T (°K)	n (cm^{-3})	p (cm^{-3})	N_c (cm^{-3})	E_{calc} (ev)	$E_{\text{calc}}{}^{n}$ (ev)	β (ev/deg)
Z-4	307	1.35×10^{18}[a]		2.0×10^{17}	0.22	0.17	
n type	85	1.35×10^{18}[a]		2.8×10^{18}	0.30	0.32	
P-4	307	5.1×10^{18}[a]		2.0×10^{17}	0.36	0.38	
n type	85	5.1×10^{18}[a]		2.8×10^{18}	0.46	0.54	
	13	5.1×10^{18}[a]		1.7×10^{18}	0.51	0.59	
SC-5	307		2.1×10^{17}	1.2×10^{19}	0.16		-2.5×10^{-4}
p type	85		2.1×10^{17}	1.7×10^{17}	0.21		
	15		2.1×10^{17}	1.4×10^{16}	0.23		
P4-A	307		1×10^{17}	1.2×10^{19}	0.16		-2.3×10^{-4}
p type	85		1×10^{17}	1.7×10^{17}	0.21		
P-1	307		3.4×10^{16}	1.2×10^{19}	0.16		-1.6×10^{-4}
p type	85		3.4×10^{16}	1.7×10^{17}	0.20		

[a] These values are calculated from electrical measurements on the samples used in the optical investigations.

TABLE II. Absorption coefficient of InSb samples at room temperature (cm^{-1}).

	Sample		$\lambda=4\mu$	$\lambda=6\mu$	$\lambda=8\mu$	$\lambda=12\mu$
p-type	*SC-5*	calc	4.5	10	18	39
		obs	···	220	220	220
	P4-A	calc	2.5	5.7	10	22
		obs	···	50	50	50
	P-1	calc	2.4	5.4	10.0	21
		obs	···	180	180	180
n-type	*Z-4*	calc	39	87	150	340
		obs	···	25	40	110
	P-4	calc	720	1600	2900	6500
		obs	150	230	360	···

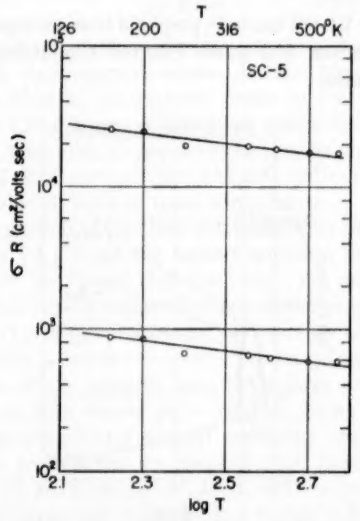

FIG. 7. Temperature dependence of σR for a single crystal of InSb. (Top: electrons. Bottom: holes.)

[20] See reference 12, p. 139.

Electrical and Optical Properties of Intermetallic Compounds. II. Gallium Antimonide*

R. F. Blunt, W. R. Hosler, and H. P. R. Frederikse
National Bureau of Standards, Washington, D. C.

(Received July 19, 1954)

The Hall effect and resistivity of GaSb have been investigated over the temperature range 78° to 750°K. Hole mobilities as high as 400 cm²/volt-sec and a forbidden energy gap of 0.775 ev at absolute zero were found. Optical absorption studies at temperatures between 10° and 300°K confirm this value of the band separation.

INTRODUCTION

GALLIUM antimonide is a semiconductor of the group of IIIB–VB compounds with properties similar to those of Ge and Si. Its lattice has the zinc-blende structure; the melting point of the compound is 702°C.[1]

We report here on measurements of resistivity and Hall effect as well as optical absorption. Results are in general agreement with data reported by others.[1–3]

EXPERIMENTAL PROCEDURE AND RESULTS

Procedures for crystal growing and sample preparation are identical to those used for InSb.[4] The antimony was obtained from the Bradley Mining Company. The first shipment had a purity of 99.957 percent and contained Al, Cu, Fe, Mg, and Si as impurities; later on antimony of 99.994 percent purity was received, the major impurities being As, Cu, Fe, and Pb. Gallium was procured both from the Eagle Picher Company and the Aluminum Company of America. The purity of this metal was about 99.95 percent and the material contained the following impurities: Ag, Al, Ca, Cu, Ni, Pb, and traces of Fe, Mg, and Si. Zone melting improves the purity of the compound considerably. The grain structure of grown ingots can be made visible by etching with HF and HNO_3.

X-ray analysis showed the lattice to be of the zinc-blende type; the lattice constant is 6.1347 A at 26°C,[5] from which the nearest neighbor distance is calculated to be 2.65 A.

The equipment for measuring Hall coefficient and resistivity has been described elsewhere.[6] Measurements cover the temperature range from 78°K to 750°K. Results are given in Figs. 1 and 2.

Sample X-111 (p type) has been cut from an ingot containing excess Ga. This ingot was annealed at 500°C for 24 hours and then slowly cooled to room temperature.

Sample X-117 is a single crystal showing p-type conductivity.

Sample VI-170 is taken from the pure end of an ingot which has been zone-melted 7 times; this specimen is p type.

Sample VI-185 has been prepared from an ingot doped with tellurium and shows electron conduction at all temperatures.

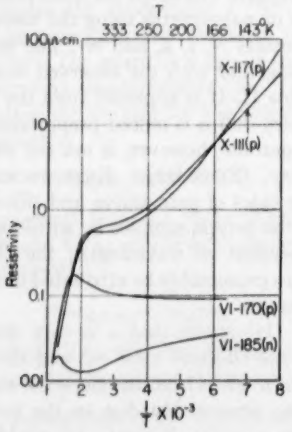

FIG. 1. Resistivity of n- and p-type GaSb.

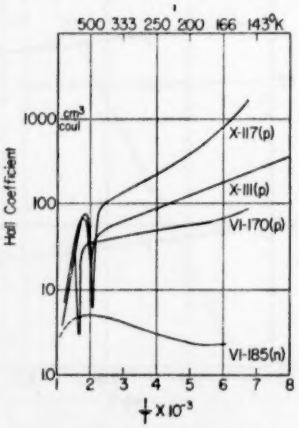

FIG. 2. Hall coefficient of n- and p-type GaSb.

* Supported in part by the Office of Ordnance Research.

[1] H. Welker, Z. Naturforsch. **7a**, 744 (1952); **8a**, 248 (1953).
[2] D. P. Detwiler, Phys. Rev. **94**, 1431 (1954).
[3] H. N. Leifer and W. C. Dunlap, Phys. Rev. **94**, 1431 (1954).
[4] Breckenridge, Blunt, Hosler, Frederikse, Becker, and Ashinsky, preceding paper [Phys. Rev. **96**, 571 (1954)].
[5] These measurements were carried out by the Microstructure Section of the National Bureau of Standards.
[6] R. G. Breckenridge and W. R. Hosler, Phys. Rev. **91**, 793 (1953).

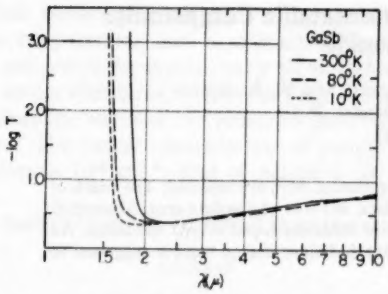

FIG. 3. Absorption spectrum of p-type GaSb at three different temperatures.

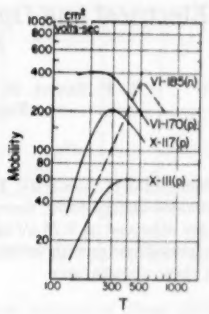

FIG. 4. Charge carrier mobilities of GaSb.

The absorption spectra of several GaSb samples were investigated with a Perkin-Elmer monochromator using procedures described previously.[4] Figure 3 shows the absorption spectrum (minus log transmission *vs* wavelength) of a specimen cut from the ingot labeled VI-170 (impure end); this specimen was ground and polished to a thickness of 0.13 mm. Other samples show similar results; the position of the absorption edge of p- and n-type samples is the same. Measurements taken at three different temperatures (300°K, 80°K, and 10°K) show clearly the shift of the absorption edge; the long-wavelength tail changes very little with temperature.

DISCUSSION

The carrier mobility has been calculated from the Hall coefficient R and the conductivity σ by using the expression

$$\mu = R\sigma/r. \tag{1}$$

r is a factor which depends on the scattering mechanism. At high temperature where lattice predominates $r=1.18$, while in the impurity region at low temperatures $r=1.93$.[7] Figure 4 shows the results for the four samples presented. Other investigators have reported values of 2000 cm²/volt-sec[2] and 800 cm²/volt-sec[3] for the mobility of holes at room temperature.

A comparison of the three p-type samples shows that specimen VI-170 has the highest mobility, but at the same time the lowest Hall coefficient; the mobility of this sample is even higher than that of the single crystal X-117. This suggests that the low mobility of most of our samples is due to two causes: (a) the polycrystalline structure of the samples, and (b) a large amount of impurities, both donors and acceptors, giving rise to a high concentration of ionized scattering centers, but very few carriers due to compensation. Zone melting of ingot VI-170 has apparently removed a larger number of donor impurities, resulting in a higher hole concentration and also higher mobility.

We have used the data of sample VI-170 to calculate the mobility ratio b at the temperature where the Hall coefficient reverses sign.[8]

The conductivity is given by

$$\sigma = e\mu_p(nb+p), \tag{2}$$

where n is the concentration of electrons and p is the concentration of holes. The expression for the Hall coefficient R is

$$R=(3\pi/8e)[(nb^2-p)/(nb+p)^2]. \tag{3}$$

The Hall coefficient reverses sign at $T=617$°K; hence at this temperature,

$$R=0, \quad \text{and} \quad nb^2=p=n+N, \tag{4}$$

where N is the effective concentration of impurities. Substituting n in Eq. (2) and using the values for σ and μ_p from Figs. 1 and 4, we obtain $b=5.5$ for the mobility ratio.

The width of the forbidden energy band can be derived from the relation

$$np=4(2\pi mkT/h^2)^3(m_nm_p/m^2)^{\frac{3}{2}}\exp-(E_0+\beta T)/kT \tag{5}$$

where

$$\beta=dE/dT,$$

and m_n, m_p=effective mass of electrons and holes, respectively. The slope of ln (np/T^3) against $1/T$ determines therefore the energy gap at absolute zero. Calculation yields a value of $E_0=0.77$ ev.

The band separation can also be identified with the optical absorption edge. From Fig. 3 we derive an energy gap $E=0.67$ ev at room temperature. The temperature dependence of E in the range 10–300°K appears to be -3.5×10^{-4} ev/deg. These values are in good agreement with the result from electrical data.

Beyond 2.5μ the absorption curve rises slowly with increasing wavelength; this absorption can be attributed to free carrier transitions. Several samples show at room temperature a slightly higher absorption in the region 4 to 8μ, suggesting a small but broad band.

[7] W. Shockley, *Electrons and Holes in Semiconductors* (D. van Nostrand Company, Inc., New York, 1950), pp. 278–279.

[8] The procedure used in the case of InSb is not applicable here due to the uncertainty of R_{ex} at the temperature of the Hall maximum.

Electrical and Optical Properties of Intermetallic Compounds. III. Aluminum Antimonide*

R. F. Blunt, H. P. R. Frederikse, J. H. Becker, and W. R. Hosler
National Bureau of Standards, Washington, D. C.

(Received July 19, 1954)

Measurements of resistivity, Hall coefficient, and optical absorption of AlSb are reported. The width of the forbidden energy band, derived from electrical and optical data, is 1.6 ev at absolute zero. Absorption bands are observed at 0.75 ev in p-type samples and at 0.31 ev in tellurium-doped n-type specimens. An energy level diagram with several acceptor and donor levels in the forbidden energy band is suggested to explain these observations.

INTRODUCTION

ALUMINUM antimonide is one of a series of semiconducting compounds formed between elements from the columns IIIB and VB of the periodic table. The lattice has the zincblende structure, which is equivalent to the diamond structure when the two components are the same.

This paper presents measurements of Hall effect and resistivity as well as optical absorption of AlSb. The values obtained for the width of the forbidden energy gap and mobility agree reasonably well with those reported previously in the literature.[1-3] Activation energies related to defects in the crystal are also observed. It seems possible to interpret the optical and electrical data with several acceptor and donor levels in the forbidden band.

SAMPLE PREPARATION

The compound (melting point[1] 1060°C) is prepared by melting the components together in stoichiometric proportions. The aluminum is the standard metal used for melting point calibrations supplied by the Chemistry Division of the National Bureau of Standards. The purity of this material is 99.98 percent, the major impurities being As, Fe, Mn, P, Si, and traces of Cu and Mg. The antimony (purchased from Bradley Mining Company) is 99.95 percent pure and contains small amounts of Pb, As, Cu, and Fe. For details of the melting process, crystal pulling and sample preparation we refer to a paper on InSb.[4] The ingots obtained always contained several crystals, but it was usually possible to cut out single-crystal samples of sufficient size for electrical and optical measurements. Zone melting does not seem to improve the resistivity of this compound. The reason might be that defects are more effective than chemical impurities in AlSb as a source of carriers.

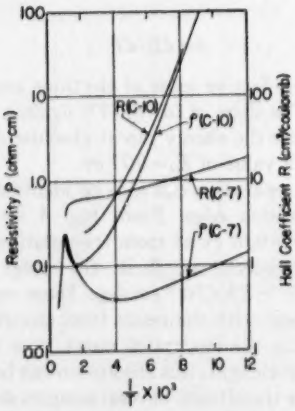

FIG. 1. Resistivity and Hall coefficients of AlSb.

We have noticed that the compound decomposes in a humid atmosphere. Ingots become covered with a black film in a very short time, ultimately crumbling into a black powder. A desiccator affords ample protection from moisture. Pure samples are more corrosion-resistant than samples of higher impurity content. Justi[3] has made these same observations; he has shown that the aluminum reacts with water forming the hydroxide.

X-ray analysis of an AlSb sample indicated a lattice of the zincblende type with a lattice constant[5] of 6.0959 A at 26°C and a nearest neighbor distance of 2.64 A.

ELECTRICAL PROPERTIES

The apparatus used for measurements of Hall coefficient and resistivity has been described previously.[6] The sample holder for the high-temperature range was made of stainless steel; the leads were in pressure contact with the crystal.

Two samples have been investigated. One is a p-type single crystal (C-7); the other was cut from an ingot doped with 9×10^{-3} atomic percent of Te and shows n-type conductivity (C-10). The temperature dependence of resistivity and Hall coefficient is given in Fig. 1.

The intrinsic range for these samples lies above 750°C.

* Supported in part by the Office of Ordnance Research.

[1] H. Welker, Z. Naturforsch. **7a**, 744 (1952); **8a**, 248 (1953).

[2] Willardson, Beer, and Middleton, Phys. Rev. **91**, 243 (1953).

[3] E. Justi and G. Lautz, Abhandl. Braunschweig. wiss. Ges. **5**, 36 (1953).

[4] Breckenridge, Blunt, Hosler, Frederikse, Becker, and Ashinsky, this issue [Phys. Rev. **96**, 571 (1954)].

[5] These measurements were carried out by the Microstructure Section of the National Bureau of Standards.

[6] R. G. Breckenridge and W. R. Hosler, Phys. Rev. **91**, 793 (1953).

The Hall coefficient could not be measured at the highest temperatures due to contact difficulties. At 750°C and above we expect nearly all scattering to be due to lattice vibrations, so that the slope of $\ln\rho$ *vs* $1/T$ determines the width of the forbidden gap; this value is 1.6 ev. The carrier concentration of sample *C*-7 at exhaustion is 10^{18} cm^{-3}; that of sample *C*-10, 3×10^{18} cm^{-3}.

The mobility may be evaluated from the expression

$$\mu = R\sigma/r, \qquad (1)$$

where r is a factor which depends on the scattering mechanism.[7] From the data of sample *C*-7 we calculate a hole mobility of 150 cm²/volt-sec at room temperature. The electron mobility as deduced from the results for sample *C*-10 is about 35 cm²/volt-sec at 300°K. The latter figure is very low, presumably due to the high concentration of both donor and acceptor impurities.

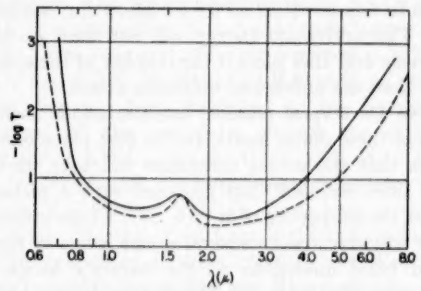

FIG. 2. Absorption spectrum of *p*-type AlSb (sample *C*-7). —— 300°K, - - - - - 85°K, 14°K.

OPTICAL PROPERTIES

The optical absorption spectrum of small samples, ranging in thickness from 5 to 10 mils, has been investigated at wavelengths between 0.6 and 15.0μ. The apparatus and measuring techniques have been described in an earlier publication.[4]

Five different specimens have been investigated. The first sample, *C*-7 (thickness 8 mils), is a *p*-type single crystal. Two other samples, *C*-8 and *C*-9 (both 10 mils thick), were cut from ingots doped with, respectively, 2×10^{-3} and 3×10^{-3} atomic percent of tellurium. Another two samples, *C*-10-1 (10 mils) and *C*-10-2 (5 mils), were cut from an ingot containing 9×10^{-3} atomic percent of tellurium and appeared to be *n*-type.

The spectrum of sample *C*-7 at three different temperatures is given in Fig. 2. Figure 3 compares the room temperature spectra of samples *C*-8, *C*-9, and *C*-10-2; the temperature dependence of the absorption of samples *C*-10-1 and *C*-10-2 is shown in Figs. 4 and 5.

The results of our measurements can be summarized as follows. For all samples a sharp absorption edge is observed at 0.82 μ corresponding to a forbidden energy

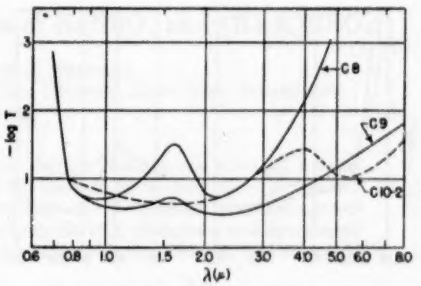

FIG. 3. Absorption spectra of three AlSb samples. Atomic percent Te added to melt

{sample *C*-8: 2×10^{-3},
sample *C*-9: 3×10^{-3},
sample *C*-10-2: 9×10^{-3}.

gap of 1.52 ev at room temperature. This result is in good agreement with the value deduced from the conductivity measurements. The temperature dependence of the energy gap has an average value of -3.5×10^{-4} ev/deg over the temperature range studied.

In all *p*-type samples an absorption band is observed at 1.6 μ (0.75 ev). Hall effect and resistivity data show, however, no corresponding slope. Adding tellurium to the compound converts the conductivity to *n*-type. The band at 1.6 μ has then disappeared and a new band is observed at 4.0 μ (0.31 ev). Plotting $\ln RT^{\frac{1}{2}}$ or $\ln\rho T^{\frac{3}{2}}$ *vs* $1/T$ we find, however, an activation energy of 0.14 ev.

In order to account for these observations we wish to suggest a picture which is rather similar to one proposed by James and Lark-Horovitz[8] to explain the behavior of bombarded Ge and Si.

The AlSb crystal will probably acquire a slight excess of aluminum over the stoichiometric amount due to the larger evaporation of the antimony from the melt. Consequently the compound will tend to contain a number of Sb vacancies. Considering the predominantly covalent character of AlSb,[1] such vacancies will presumably act as acceptors. The omission of an antimony atom leaves 5 unsaturated bonds at that site in the crystal. It is therefore to be expected that several

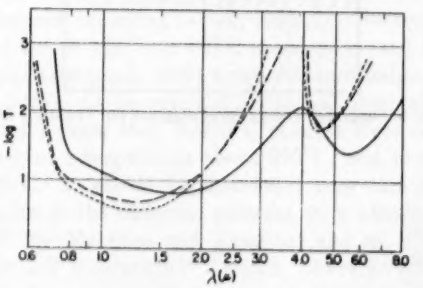

FIG. 4. Absorption spectrum of *n*-type AlSb (Sample *C*-10-1). —— 300°K, — — 85°K, - - - - - 14°K.

[7] W. Shockley, *Electrons and Holes in Semiconductors* (D. van Nostrand Company, Inc., New York, 1950), pp. 278–279.

[8] H. M. James and K. Lark-Horovitz, Z. physik. Chem. **198**, 107 (1951).

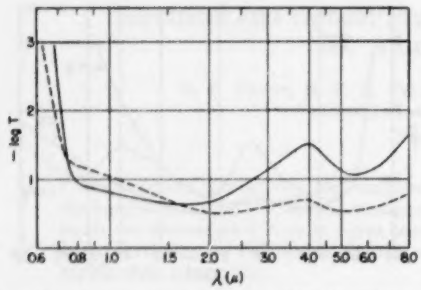

FIG. 5. Absorption spectrum of *n*-type AlSb (Sample *C*-10-2). —— 300°K, - - - - - 85°K.

localized levels will be split off from the valence band as indicated on the left of Fig. 6. The first level will lie close to the filled band, the second, third, etc. levels at a considerable distance from the band edge.

We identify the second activation energy with the value of 0.75 ev observed in the *p*-type samples. The first level will already be occupied at rather low temperatures, while the second level will be essentially empty up to temperatures much higher than 300°K.

It is possible that donor centers in a smaller number than acceptors will be present at the same time. The fact that only the 0.75-ev band has been observed in the *p*-type samples indicates that these levels are lying higher than the second acceptor level (and will therefore be empty) or lower than the edge of the filled band.

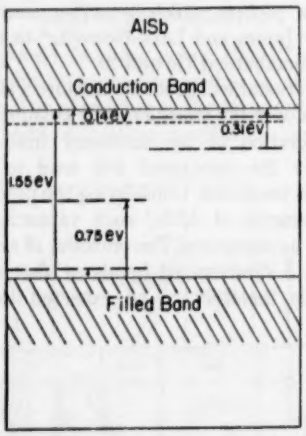

FIG. 6. Suggested energy level diagram for Te-doped AlSb.

It is now readily seen what the result of the addition of tellurium will be. The tellurium atom has approximately the same radius ($r=1.32$ A) as the antimony atom ($r=1.36$ A)[9]; the outer shell contains, however, one electron more. It might be expected therefore that it can replace the antimony in the crystal and act as a donor. The donor centers introduced by the addition of tellurium will then compensate the acceptors normally present. The conductivity of the *p*-type crystal will thus decrease until sufficient tellurium is added to convert the crystal to *n*-type. The activation energy of the tellurium donor levels can be estimated on the basis of the hydrogenic model. With a dielectric constant $\epsilon'=10.8$,[10] this value is calculated to be 0.125 ev. We can identify this activation energy with the value calculated from resistivity and Hall plots.

The absorption band in the *n*-type sample at 0.3 ev is not too well understood. Since this band is only observed in the *n*-type samples, the absorption band might be due to a donor level at 0.3 ev below the conduction band. This activation energy will not show up in the resistivity and Hall plots if the number of these donors is less than the number of tellurium atoms.

There are several possible interpretations as to the origin of these donor levels. In the first place one may assume that the excess aluminum will take up interstitial sites. Kendall[11] has proposed such a picture to explain the properties of *n*-type SiC. These interstitial atoms will give rise to several donor levels in the forbidden band analogous to the vacancy levels. The open structure of the zincblende-type lattice and the geometrical equivalence of intersititial and lattice sites[12] could account for the rather small second activation energy of such donors.

Another possibility is the presence of tellurium in interstitial as well as substitutional positions. One could also explain these donor levels as being due to other chemical substitutions. From spectroscopic analyses of the Al and Sb used there is no indication of any impurity expected to produce *n*-type conductivity with such a large activation energy.

[9] L. Pauling, *The Nature of the Chemical Bond and the Structure of Molecules and Crystals* (Cornell Univeristy Press, Ithaca, 1945).
[10] Briggs, Cummings, Hrostowski, and Tanenbaum, Phys. Rev. **93**, 912 (1954).
[11] J. T. Kendall, J. Chem. Phys. **21**, 821 (1953).
[12] H. W. Leverenz, *An Introduction to Luminescence in Solids* (John Wiley and Sons, Inc., New York, 1950), p. 94.

Dielectric Properties and Phase Transitions of $NaNbO_3$ and $(Na,K)NbO_3$†

G. SHIRANE,* R. NEWNHAM, AND R. PEPINSKY
X-Ray and Crystal Analysis Laboratory, The Pennsylvania State University, State College, Pennsylvania
(Received May 12, 1954)

An optical, dielectric, and structural study has been carried out on $NaNbO_3$ and the solid solution $(Na, K)NbO_3$, both single crystals and ceramics being used. No evidence for ferroelectricity in $NaNbO_3$ was found, and the crystal seems to be antiferroelectric in accordance with the nonpolar structure reported by Vousden. It is shown that a small addition of $KNbO_3$ to pure $NaNbO_3$ produces a new ferroelectric phase, the existence of which suggests a possible explanation of the conflicting dielectric and structural properties previously reported.

The phase diagram of $NaNbO_3$-$KNbO_3$ is given. This, together with the optical and x-ray studies of pure $NaNbO_3$, shows that the three phase transitions in $NaNbO_3$ are quite different in nature from the $BaTiO_3$-type transitions in $KNbO_3$.

I. INTRODUCTION

IN 1949 Matthias[1] reported the perovskite-type niobates and tantalates of sodium and potassium to be ferroelectric. The lattice parameters of $NaTaO_3$ and $KTaO_3$ were reported by Vousden[2] at room temperature, and the Curie temperatures were reported as 13°K for $KTaO_3$[3] and 475°C for $NaTaO_3$.[1] However, no detailed investigation has been published on the ferroelectric transitions of the tantalates except the dielectric properties[3] of $KTaO_3$ near the Curie point at 13°K.

On the other hand, the ferroelectric transitions in the niobates, $KNbO_3$ and $NaNbO_3$, have been studied in some detail. Matthias and Remeika[4] have studied the dielectric properties of these crystals, and Wood[5] has reported on both the optical and structural properties. The crystals show the following transitions, according to these workers:

$$KNbO_3: \text{Orthorhombic} \overset{225°C}{\longleftrightarrow} \text{tetragonal} \overset{435°C}{\longleftrightarrow} \text{cubic};$$

$$NaNbO_3: \text{Orthorhombic} \overset{370°C}{\longleftrightarrow} \text{tetragonal} \overset{480°C}{\longleftrightarrow} \text{cubic}.$$

The ferroelectricity of $KNbO_3$ below 435°C has been well demonstrated. The structural changes at the two transitions are quite similar to those of $BaTiO_3$ at 0°C and 125°C.[6] Moreover, a recent study at our laboratory has revealed the existence of an additional phase change at −10°C, below which the crystal symmetry is rhombohedral.[7] Hence the transitions in $KNbO_3$ are analogous to those of $BaTiO_3$.

In contrast to this, the situation with $NaNbO_3$ is rather confusing. Consider first the x-ray powder photographs obtained with $NaNbO_3$ and $KNbO_3$. In both the orthorhombic and tetragonal phases, superlattice lines were observed on the powder photographs of $NaNbO_3$.[6] $KNbO_3$, on the other hand, shows a simple unit cell, so that the phases in $KNbO_3$ do not correspond crystallographically to those in $NaNbO_3$. A second point of confusion arises from the structural study of $NaNbO_3$ at room temperature. Vousden[8] reported the structure to be nonpolar, which necessarily rejects the existence of ferroelectricity in the crystal.[9] However, he also observed domain movement under a large dc field, which is usually indicative of ferroelectric behavior, as were the hysteresis loops reported by Matthias and Remeika.[4] In defense of his space group assignment, Vousden[10] indicated a possible explanation of this conflicting data by proposing the existence of a less stable, closely related polar structure which may be produced under a strong electric field yielding the observed ferroelectric phenomena. Since no new experimental results either confirming or disproving this hypothesis have been reported, the whole question still remains open to conjecture.

Thirdly, there are discrepancies between the x-ray and optical observations. Optical observations[5] indicate that $NaNbO_3$ crystals are still birefringent above 480°C, and do not become isotropic until 640°C. To add to the confusion, Wood reports that at 300°C $NaNbO_3$ is orthorhombic by optical measurement, while it should be tetragonal according to x-ray evidence. Observations carried out at 425° and 490°C show the crystal to be optically tetragonal, while x-ray evidence indicates a cubic lattice. As the result of his optical observations, Vousden reports that $NaNbO_3$ changes from orthorhombic to tetragonal at about 300°C, and to cubic at 600°C.[2] It should be mentioned here that small anomalies in the dielectric constant were observed at −80°C by Matthias and Remeika[4] and at 0°C by Wainer and Wentworth.[11] Vousden, however, failed to

† Investigation supported by contracts with the U. S. Office of Naval Research, and with the Wright Air Development Center.
* On leave from Tokyo Institute of Technology, Tokyo, Japan.
[1] B. T. Matthias, Phys. Rev. **75**, 1771 (1949).
[2] P. Vousden, Acta Cryst. **4**, 373 (1951).
[3] Hulm, Matthias, and Long, Phys. Rev. **79**, 885 (1950).
[4] B. T. Matthias and J. Remeika, Phys. Rev. **82**, 727 (1951).
[5] E. A. Wood, Acta Cryst. **4**, 353 (1951).
[6] A. von Hippel, Revs. Modern Phys. **22**, 221 (1950).
[7] Shirane, Danner, Pavlovic, and Pepinsky, Phys. Rev. **93**, 672 (1954).
[8] P. Vousden, Acta Cryst. **4**, 545 (1951).
[9] R. Pepinsky, Acta Cryst. **5**, 228 (1952).
[10] P. Vousden, Acta Cryst. **5**, 690 (1952).
[11] E. Wainer and C. Wentworth, J. Am. Ceram. Soc. **35**, 207 (1952).

observe any structure changes optically down to −175°C.[3]

In order to resolve these questions concerning the phase transitions and possible existence of ferroelectricity in pure $NaNbO_3$, detailed optical, x-ray, and dielectric measurements on single crystals and ceramic specimens have been undertaken in this laboratory. A study has also been made of the $NaNbO_3$-$KNbO_3$ system in order to show the relationship between the various phases in the two crystals.

II. OPTICAL STUDY OF THE PHASE TRANSITIONS IN $NaNbO_3$

$NaNbO_3$ single crystals were prepared by the method suggested by Wood.[5] A mixture of 5.3 g of Na_2CO_3, 13.3 g of Nb_2O_5, and 8.9 g of NaF was heated to 1500°C in a platinum crucible, and then cooled to 900°C in 7 hours. This method generally gave rectangular plates which were yellow in color. Well-shaped, thin plates up to 3×3×1 mm in size were often produced. A spectroscopic analysis, kindly carried out by Dr. Lovell of the Mineral Science Department of The Pennsylvania State University, showed the following impurities: K: ≈0.005 percent, Li: <0.001 percent, Rb: ≪0.001 percent, Ta: no trace.

Powder photographs were taken of these crystals by means of a Norelco powder camera (11.4-cm diam) with CuKα radiation filtered through a nickel foil. The photographs taken at room temperature showed well-resolved line splitting due to an orthorhombic distortion of the ordinarily cubic perovskite structure. Monoclinic axes were taken,[12] and the lattice parameters were calculated from the (422) and (332) groups, with the results

$$a'=c'=3.915\text{ A},\quad b=3.881\text{ A},\quad \text{and}\quad \beta=90°\,40'.$$

These values are in good agreement with earlier measurements, particularly those of Vousden.[2]

Extra lines were observed in $NaNbO_3$ powder photographs by Wood,[5] who gave the multimolecular unit cell dimensions. A multiple cell structure was also reported by Vousden in his analysis.[6] A comparison of the extra lines observed by Wood (see Fig. 5 of reference 5) with our own showed the two sets of lines to be identical.

When the larger $NaNbO_3$ crystals were viewed under a polarizing microscope, multidomains in complicated patterns were observed. However, several thin plates, approximately 1 mm² in area, showed only a few domains[13] and very sharp extinction positions. These crystals were used in an optical study of the phase transitions in $NaNbO_3$. Measurements were carried out with a high-temperature optical stage of simple design, which permitted observation under a polarizing microscope at temperatures as high as 700°C.

At room temperature the crystals showed two types of domains. In some domains extinction occurred at positions making an angle of 45° with the crystal edges, while the remaining domains showed parallel extinction. This behavior is quite characteristic of orthorhombic crystals with pseudocubic habit. At 360°C a sudden change was noted in the optical properties of the crystals; above 360°C only parallel extinction was observed. A less pronounced domain-boundary movement was observed to occur at 480°C. The crystals continued to show parallel extinction even above these transitions. A third transition took place at 640°C, above which no extinction was observed; thus it may be safely assumed that the crystal becomes isotropic there.

Although these results are in good agreement with the three optical transitions observed by Wood,[5] the following points of interest should be noted. The optical change at 360°C is much more violent in nature than the phase transitions at 480° and 640°C. Furthermore, it was relatively easy to recognize an optical transition at 640°C, since a change from anisotropy to isotropy is involved; but the transition at 480°C was observed only in exceptionally clear, well-shaped specimens.

In the two phases of $NaNbO_3$ between 360° and 640°C, each crystal showed parallel extinction. In tetragonal crystals, parallel extinction is observed when the c axis lies in the plane of the plate, and optical isotropy is found when the c axis is perpendicular to the plate. The latter case was not observed in the ten or more $NaNbO_3$ crystals we examined. Since the crystals were all primarily thin plates, this optical peculiarity is probably due to some special orientation of the crystal habit.

Color changes were observed between 360° and 480°C as the crystals were heated. Constantly shifting spectra were observed with white light; and when the crystals were illuminated with sodium light, a series of black strips transversed the crystals, one by one. Although there is a possibility that the phenomenon is due to a thickness change, the exact origin of the effect is not known.

Thus optical study clearly shows three phase transitions in $NaNbO_3$. Moreover, the symmetry is definitely orthorhombic below 360°C and cubic above 640°C; but the supposedly tetragonal phases between the two leave some doubt as to their true nature. The three phase transitions in $NaNbO_3$ were recently observed in a differential thermal analysis performed by Dr. Rustum Roy *et al.* of the School of Mineral Industries, The Pennsylvania State University.[14] The transition temperatures are in good agreement with those given above.

[12] Throughout the paper, the monoclinic parameters $a'=c'$, b, and β have been substituted for the orthorhombic unit cell distances a, b, and c so that the lattice parameters can be more conveniently compared with those of the cubic and tetragonal phases. The monoclinic and orthorhombic lattice parameters are related as follows: $a=2a'\sin\frac{1}{2}\beta$, $b=b'$, $c=2a'\cos\frac{1}{2}\beta$. The wavelength of CuK$\alpha_1$ radiation was taken as 1.5405 A in all calculations.

[13] "Domain" is to be understood as "twin" if these crystals are not ferroelectric.

[14] Roy, deVries, Rase, Shafer, and Osborn, Second Annual Report to the U. S. Army Signal Corps, July 15, 1953 (unpublished).

III. X-RAY STUDY OF THE PHASE TRANSITIONS IN $NaNbO_3$

A series of powder photographs were taken of $NaNbO_3$ over a wide temperature range by means of a Unicam 19-cm high-temperature camera with CuKα radiation filtered through nickel. A sample consisting of powdered $NaNbO_3$ crystals was sealed in a glass capillary having an outside diameter of 0.3 mm and a wall thickness of 0.01 mm. The diffraction patterns showed very sharp line splitting, permitting resolution of the CuKα_1, α_2 doublet at an angle $\theta=40°$. The lattice parameters were calculated from the line groups $N=h^2+k^2+l^2=25$, 24, and 22. The results are tabulated as a function of temperature in Table I and plotted in Fig. 1.

Below 360°C the symmetry is obviously orthorhombic, in agreement with optical observation. Although the parameters listed are those corresponding to a simple unit cell, the extra lines present in the photographs may well indicate a multiple cell. The intensity of these extra lines rapidly decreases as the temperature is raised above room temperature.

At the transition temperature near 360°C the diffraction patterns change quite abruptly, so that the line splitting is greatly reduced. For example, at 375°C only the (510), (431), and (422) line groups are well resolved. The line splitting above 360°C appears to be typical tetragonal splitting, in agreement with the optical measurements. It is difficult, however, positively to exclude other possible lattice forms, since the distortion is so slight.

If the crystal is assumed to be tetragonal, the calculated c/a ratio shows a very small deviation from unity, c/a being 1.0023 at 375°C. Moreover, this distortion continues to decrease with increasing temperature, and at temperatures above 430°C no definite line splitting can be observed. Thus if a tetragonal distortion from the cubic perovskite lattice exists above this temperature, the axial deviation is certainly less than 0.1 percent. No structure changes were observed with x-rays at the transition temperatures of 480° and 640°C. Extra lines were again observed above 360° (as first reported by Wood[5]), but no definite conclusions could be drawn as to their character.

TABLE I. Lattice parameters of $NaNbO_3$ as a function of temperature.

T(°C)	$a'=c'$(A)	b(A)	a'/b	β	v(A³)
20	3.915	3.880	1.009	90° 41′	59.45
175	3.918	3.898	1.005	90° 32′	59.82
300	3.921	3.910	1.003	90° 25′	60.11
350	3.922	3.913	1.002	90° 23′	60.18
	$a=b$	c	c/a		
375	3.918	3.927	1.0023		60.28
390	3.919	3.927	1.0020		60.33
410	3.921	3.926	1.0014		60.35
420	3.921	3.927	1.0014		60.38
430	3.925				60.44
460	3.926				60.52
480	3.928				60.61
670	3.942				61.27

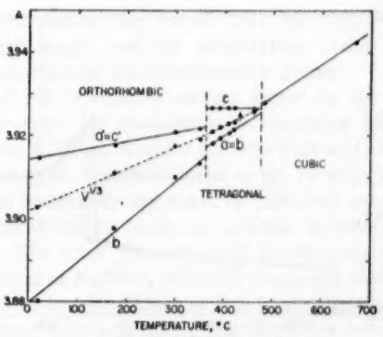

FIG. 1. Lattice parameters of $NaNbO_3$.

Some of the discrepancies observed by Wood between the optical and x-ray measurements on $NaNbO_3$ have been removed by our measurements. Our x-ray powder photographs taken at 300°C indicate an orthorhombic, not a tetragonal lattice, so there is no disagreement between x-ray and optical observation. Wood also reported cubic diffraction lines above 370°C, whereas optical measurements indicated tetragonal symmetry. We were able to observe tetragonal line splitting at temperatures well above 370°C although this distortion became negligible at about 430°C.

Wood hypothesized that the x-ray photographs gave the symmetry of the niobium array, whereas the optical properties were determined principally by the combined oxygen-sodium array. In this way she was able to account for obvious differences between the x-ray and optical observations. However, since the principal differences between these results have been removed by our measurements, it seems more natural to conclude that the optical measurements are simply more sensitive to slight lattice distortions than the x-ray technique.

IV. DIELECTRIC PROPERTIES OF $NaNbO_3$

Dielectric measurements were made on $NaNbO_3$ single crystals using rectangular plates 2–3 mm on edge and having a thickness of approximately 0.5 mm. The dielectric constant ϵ is plotted as a function of temperature in Fig. 2. The measurements were made at a frequency of 10 kc/sec with an alternating electric field of 5 v/cm. The sharp change in the dielectric constant was observed at 355°C, as reported by Matthias and Remeika.[5] This anomaly undoubtedly corresponds to the orthorhombic-tetragonal phase transformation observed in our optical and x-ray measurements at 360°C.

An effort was made to measure the dielectric constant in the vicinity of the second optical transition at 480°C. No dielectric anomaly could be detected in this region. However, since the loss becomes quite appreciable above

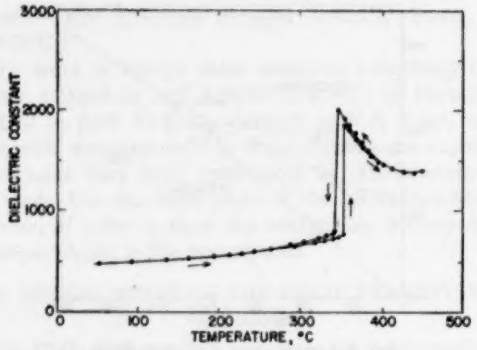

FIG. 2. Dielectric constant of $NaNbO_3$ single crystal.

400°C, a small anomaly could have easily been obscured by the inaccuracy of our measurements.

No dielectric anomalies were detected between room temperature and −185°C, in agreement with Vousden's optical observations[8] but in contradiction with previous dielectric measurements.[4,11]

Several measurements employing various techniques were made in an effort to detect ferroelectricity in $NaNbO_3$. First of all, the relation between polarization and electric field was investigated using a modified Sawyer-Tower's circuit. The $P-E$ relation proved to be quite linear even in fields as high as 15 kv/cm. No hysteresis loops were observed. The relationship was studied over a temperature range extending from 20°C to 420°C and at a frequency of 60 cycles/sec.

Pyroelectric tests were also carried out to detect any spontaneous polarization. First, a dc field of 10 kv/cm was applied across the specimen for five minutes at 300°C, to enable the domains at least partially to align themselves in one direction. The electrodes were then connected across a sensitive galvanometer and the specimen heated to a temperature above the transition at 355°C. A change in the spontaneous polarization should give a current through the galvanometer on passing through the transition, but no discharge current could be detected with $NaNbO_3$. When a similar test is performed on $KNbO_3$, large discharge currents are observed at both the 225° and 435°C transitions.

The effect of a dc biasing field on the dielectric constant has also been studied. In all known ferroelectrics (including Rochelle salt, KH_2PO_4,[15] and $BaTiO_3$)[16] the application of such a field drastically reduces the dielectric constant. With $NaNbO_3$ crystals, however, the application of a dc field of 8 kv/cm does not affect the value of the dielectric constant at room temperature. The application of a similar field at a temperature slightly below the transition at 355°C even resulted in a slight increase in the dielectric constant.

The experiments described above gave no evidence for ferroelectricity in $NaNbO_3$. Recently Cross[17] studied the dielectric properties of pure $NaNbO_3$ and found no evidence for ferroelectricity. Only by assuming the crystal to possess an extremely high coercive field, even in the vicinity of the transition at 355°C, can we justify the existence of ferroelectricity in $NaNbO_3$. A more likely hypothesis is that $NaNbO_3$ is not ferroelectric but is actually antiferroelectric, in accordance with the antiparallel niobium displacement reported by Vousden.[8]

V. PHASE DIAGRAM OF $NaNbO_3$-$KNbO_3$

In contrast with the peculiar properties of $NaNbO_3$ just described, $KNbO_3$ shows typical ferroelectric behavior closely similar to that of $BaTiO_3$. To account for the differences in $NaNbO_3$ and $KNbO_3$, the phase diagram of their solid solution has been studied in some detail. Both ceramics and mixed crystals were used in the investigation.

(a) Dielectric Measurements on Ceramics

Ceramic specimens were prepared in the desired percentages from appropriate mixtures of K_2CO_3, Na_2CO_3, and Nb_2O_5. The firing temperatures ranged from 1050°C for pure $KNbO_3$ to 1200°C for pure $NaNbO_3$. Only by adjusting the firing temperature of pure $KNbO_3$ to just below its melting point could a suitable ceramic be obtained. Silver paste electrodes were applied to the ceramics for dielectric measurements.

The temperature dependence of the dielectric constant was investigated for an ac field of 5 v/cm at a frequency of 10 kc/sec. Some of the results are shown in Fig. 3. The dielectric behavior of pure $NaNbO_3$ and pure $KNbO_3$ ceramics proved to be quite similar to

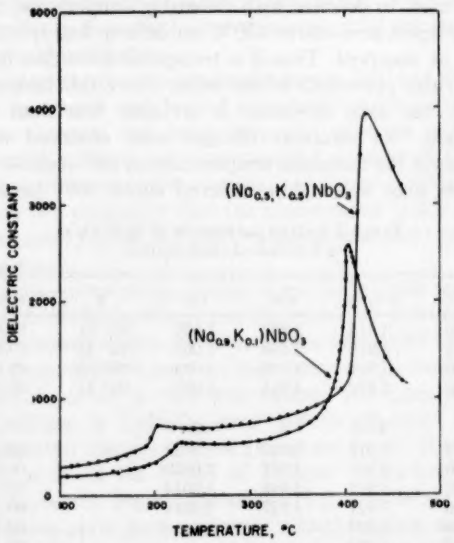

FIG. 3. Dielectric constant of (Na, K)NbO_3 solid solution.

[15] H. Baumgartner, Helv. Phys. Acta 23, 651 (1950).
[16] S. Roberts, Phys. Rev. 71, 890 (1947).
[17] L. E. Cross, Paper read before British Physical Society Spring Meeting, Leeds. Abstract in Nature 171, 1057 (1953).

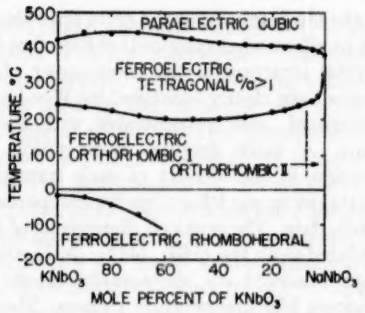

FIG. 4. Phase diagram of $NaNbO_3$-$KNbO_3$ system.

that obtained with single crystals, except that the changes in the dielectric constant accompanying the structural transitions were much sharper for single crystals. No anomaly was observed in the pure $NaNbO_3$ ceramic near the temperature of the second optical transition at 480°C.

One particularly important result came out of the dielectric study of the $KNbO_3$-$NaNbO_3$ solid solutions. When a small amount of $KNbO_3$ is added to pure $NaNbO_3$, a second small anomaly appears in the dielectric constant near 200°C, in addition to the usual dielectric transition observed around 400°C. The result for $(Na_{0.9}K_{0.1})NbO_3$ is shown in Fig. 3. With increasing $KNbO_3$ concentration the two dielectric anomalies continue to appear near 200° and 400°C, so that the lines joining these transition temperatures for various compositions extend continuously to the transitions observed in pure $KNbO_3$. The third and lowest phase transition in pure $KNbO_3$, below which the crystal symmetry is rhombohedral, occurs at −10°C for pure $KNbO_3$, but decreases in temperature with increasing $NaNbO_3$ concentration.

The phase diagram[18] shown in Fig. 4 was drawn from the data gathered with the dielectric measurements on the mixed $KNbO_3$-$NaNbO_3$ ceramics. A standard procedure was used to check each phase in the diagram for ferroelectricity. The hysteresis loops of a number of different compositions were examined at various temperatures by using an ac field of 10–20 kv/cm at a frequency of 60 cycles/sec. As expected, the $P-E$ relationship is always linear above the upper phase line near 400°C. Well defined hysteresis loops were observed in the intermediate phase for all compositions. Hysteresis loops were also found in the orthorhombic phase for all compositions from $KNbO_3$ to $(Na_{0.9}K_{0.1})NbO_3$. By comparing the hysteresis loops of a single specimen in both the orthorhombic and tetragonal phases, we found that the coercive field was much larger and the polarization much further from saturation in the orthorhombic phase.

The $P-E$ relation is almost linear in the orthorhombic phase for compositions containing less than 10 percent $KNbO_3$, even for fields as high as 15 kv/cm. The absence of hysteresis loops might be explained by a sudden increase in the coercive field; but no reasonable explanation for such an increase is immediately obvious. The extra lines observed in the x-ray powder photographs of $NaNbO_3$ indicated structural differences in the orthorhombic phases of this crystal and $KNbO_3$; hence there must be a separating phase line somewhere in the $KNbO_3$-$NaNbO_3$ solid solution. Such a phase line could well be the dividing line between ferroelectric and nonferroelectric phases, explaining the absence of hysteresis loops on the $NaNbO_3$ side. According to our dielectric measurements, the phase line lies somewhere between $(Na_{0.90}K_{0.10})NbO_3$ and $(Na_{0.95}K_{0.05})NbO_3$, as tentatively indicated in Fig. 4.

When measured as a function of increasing temperature, the dielectric constant for the various solid solutions shows a high peak at the upper transition temperature. This peak is followed by a sharp decrease, thereby obeying the Curie-Weiss law $\epsilon=C/(T-\theta)$ which is typical of ferroelectrics above their Curie point. It should be pointed out that even ceramics made up almost entirely of $NaNbO_3$, such as $(Na_{0.95}K_{0.05})NbO_3$, obey the Curie-Weiss law quite closely. In pure $NaNbO_3$ the peak dielectric constant is low even for single crystals, but the behavior of the dielectric constant above the Curie point closely approximates a Curie-Weiss relation until well above 400°C, where the dielectric loss becomes troublesome. For the compositions from $KNbO_3$ to $(Na_{0.9}K_{0.1})NbO_3$, θ is about 300°C and C is the order of 1 to 2×10^5°C. In pure $NaNbO_3$,

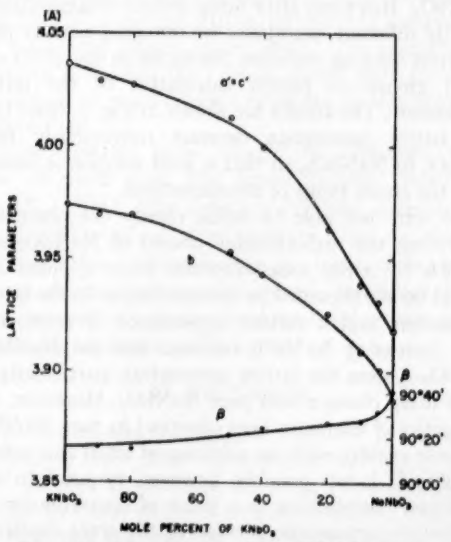

FIG. 5. Lattice parameters of (Na, K)NbO_3 system.

[18] Strictly speaking, each phase line shown in Fig. 4 should be drawn as two slightly separated lines between which both the phases above and below the phase line coexist as a mixture. However these double lines are never observed experimentally, principally because the neighboring phases in this type of compound are so closely related that the line separation is very small and a long time interval is required for the mixed phase to appear.

The authors wish to thank Dr. Rustum Roy and Professor A. J. C. Wilson for illuminating discussions concerning this point.

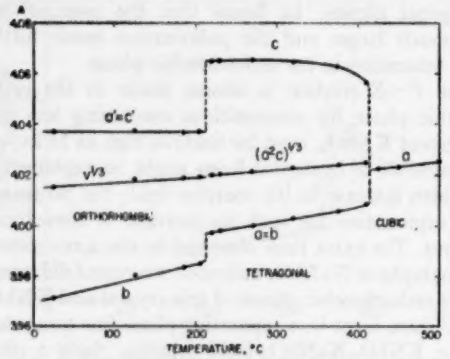

FIG. 6. Lattice parameters of $KNbO_3$.

C varies quite appreciably from specimen to specimen, being of the order of 2 to 4×10^{5}°C. θ, on the other hand, changes little in comparison, generally having values between 60° and 80°C.

The optical and x-ray measurements previously described showed $NaNbO_3$ to be tetragonal above 360°C, not cubic. Moreover, it will be subsequently demonstrated that the mixed crystal $(Na_{0.95}K_{0.05})NbO_3$ also is tetragonal above the transition. It is therefore possible that the validity of the Curie-Weiss law for these particular compounds is only accidental; but it may also mean that the tetragonal phases of $NaNbO_3$ above 360°C are actually paraelectric.

(b) X-Ray Study of the Phase Diagram

The lattice parameters of the $NaNbO_3$-$KNbO_3$ system were determined from powder photographs taken with a Unicam 9-cm powder camera and CuKα radiation. It was difficult to obtain clearly resolved lines, particularly with ceramics consisting principally of $NaNbO_3$. However, after firing several ceramics under slightly different conditions we obtained powder photographs showing sufficient resolution in the (422) and (400) groups to permit calculation of the lattice parameters. The results are shown in Fig. 5. Note that the lattice parameters decrease continuously from $KNbO_3$ to $NaNbO_3$, so that a solid solution is formed over the entire range of concentrations.

We were not able to define clearly the phase line separating the orthorhombic phases of $NaNbO_3$ and $KNbO_3$ by x-ray measurements. Such a phase line should be accompanied by discontinuities in the lattice parameters and a sudden appearance of extra lines with increasing $NaNbO_3$ content. For the $NaNbO_3$-$KNbO_3$ system the lattice parameters, particularly β, show sharp changes near pure $NaNbO_3$. Moreover, the intensities of the extra lines observed in pure $NaNbO_3$ decrease rapidly with the addition of small amounts of $KNbO_3$. It is not possible, however, to point to any particular composition as a point of discontinuity for the lattice parameters, because of the great similarity between the orthorhombic cells of $KNbO_3$ and $NaNbO_3$. Similarly the low intensity of the extra lines also makes it difficult to tell at what composition they first appear.

The crystal structure of the three upper phases of $KNbO_3$ have been clearly identified by Wood as being cubic, tetragonal, and orthorhombic with decreasing temperature. A more detailed investigation of the lattice changes in the vicinity of each transition has been undertaken in our laboratory for comparison with the $NaNbO_3$ data. The unit cell dimensions of $KNbO_3$ were calculated from the (510), (431), (422), and (332) line groups observed on photographs taken with a 19-cm Unicam high-temperature camera. The results are given in Fig. 6 and in Table II. It is obvious from these graphs that the temperature variation of the $KNbO_3$ cell dimensions is quite similar to that observed with $BaTiO_3$.[19]

A comparison of Fig. 6 with Fig. 1 reveals the following important differences between $KNbO_3$ and $NaNbO_3$. The axial ratio observed in the tetragonal phase is much larger for $KNbO_3$ ($c/a=1.016$) than for $NaNbO_3$ ($c/a=1.002$). Moreover, the axial ratio of $KNbO_3$ shows very little temperature dependence in the tetragonal region, and an abrupt discontinuity at the cubic-tetragonal transition. $NaNbO_3$, on the other hand, shows a marked temperature dependence and an extremely small discontinuity at the transition. Similar differences occur in the pseudomonoclinic parameters a'/b and β, used to describe the crystal in the orthorhombic phase.

By way of comparison, $(Na_{0.9}K_{0.1})NbO_3$ shows orthorhombic symmetry at room temperature, which changes to tetragonal ($c/a=1.010$) at 240°C. The tetragonal-cubic transition takes place at 400°C. In general, the behavior of this mixed crystal is much more similar to $KNbO_3$ than to $NaNbO_3$.

(c) Specific Heat Measurements

The specific heats of $NaNbO_3$ and $(Na_{0.9}K_{0.1})NbO_3$ were measured as a function of temperature with a

TABLE II. Lattice parameters of $KNbO_3$ as a function of temperature.

Temp (°C)	$a'=c'$(A)	b(A)	b/a	β	v(A^3)
25	4.0375	3.9711	1.0167	90° 15′	64.73
125	4.0374	3.9797	1.0145	90° 15′	64.87
185	4.0363	3.9830	1.0134	90° 13′	64.89
205	4.0369	3.9839	1.0133	90° 14′	64.93
	$a=b$	c	c/a		
220	3.9972	4.0636	1.0166		64.92
230	3.9978	4.0640	1.0166		64.95
270	3.9992	4.0647	1.0164		65.01
320	4.0023	4.0639	1.0154		65.10
375	4.0048	4.0620	1.0143		65.15
410	4.0080	4.0567	1.0122		65.18
425	4.0214				65.03
450	4.0225				65.09
510	4.0252				65.22

[19] H. F. Kay and P. Vousden, Phil. Mag. (7) 40, 1019 (1949).

Nagasaki-Takagi adiabatic calorimeter,[20] which is a modification of Sykes' calorimeter.[21] The specific heat specimens were prepared by powdering ceramics of the same type used in the dielectric and x-ray studies. About 15 grams of the powdered ceramic was placed in a platinum vessel and heated at a rate of approximately 1°C/min. The heat content of the empty calorimeter was calibrated using SiO_2 as a standard substance.

The specific heat anomalies observed in $NaNbO_3$ and $(Na_{0.9}K_{0.1})NbO_3$ are small in comparison with those observed in $KNbO_3$.[7] This result was to be expected, since the structural anomaly is much more pronounced in $KNbO_3$. The integrated transition energies are listed in Table III.

(d) Further Study of the Phase Diagram of Mixed Crystals

The optical study of $NaNbO_3$ crystals showed three phase transitions at 360°, 480°, and 640°C, while dielectric measurements carried out on $NaNbO_3$ ceramics up to temperatures as high as 500°C showed only the lowest transition. To complete the phase diagram of the (K-Na)NbO_3 system, mixed crystals were prepared from the appropriate mixtures of $NaNbO_3$ and $KNbO_3$, NaF being used as a flux. The compositions of the mixed crystals are not exactly in proportion to the percentages of $KNbO_3$ and $NaNbO_3$ because additional Na is introduced by the flux.

Crystals were prepared of several compositions between $(K_{0.5}Na_{0.5})NbO_3$ and pure $NaNbO_3$. Small rectangular plates, yellow or brown in color, were obtained from the melt. The crystals gave excellent powder diffraction photographs, showing lines which clearly indicated an orthorhombic lattice of the perovskite type at room temperature. Approximate composition values were assigned to the crystals by comparing the unit cell dimensions of the mixed crystals with those obtained with ceramics of various compositions (see Fig. 5). In this manner it was found that crystals of $(Na_{0.9}K_{0.1})NbO_3$ could be obtained by melting a mixture of equal parts of $NaNbO_3$ and $KNbO_3$ along with a NaF flux. It should be emphasized, however, that the estimated compositions shown in Fig. 7 are only approximate, so that the results are only semiquantitative.

Optical observations of the mixed crystals under a polarizing microscope led to the phase diagram shown in Fig. 7. Again we found that the addition of a small amount of $KNbO_3$ to $NaNbO_3$ greatly altered its physical characteristics. The optical properties of the tetragonal phase in $(Na_{0.9}K_{0.1})NbO_3$ are much more similar to those in $KNbO_3$ than to those in $NaNbO_3$. In mixed crystals such as this we observed both domains of parallel extinction and plates oriented in the c direction.

The two tetragonal phases observed optically in pure $NaNbO_3$ were also observed for mixed crystals containing less than 10 percent $KNbO_3$. The temperatures of these optical transitions decreased rapidly with increasing concentration of $KNbO_3$. As in the case of pure $NaNbO_3$, only parallel extinction was observed in the tetragonal phases above 360°C. No examples of complete extinction (i.e., c-axis plates) were found in the twenty or more crystals examined in this range of compositions.

Single crystals large enough for dielectric tests were obtained from the mixed crystal growth of $(Na_{0.9}K_{0.1})NbO_3$. The dielectric constant, measured at a field of 10 v/cm and a frequency of 10 kc/sec, showed two anomalies, corresponding to those obtained in optical observations on the crystal. Hysteresis loops were observed in both the tetragonal and orthorhombic phases, for an ac field of 10 kv/cm.

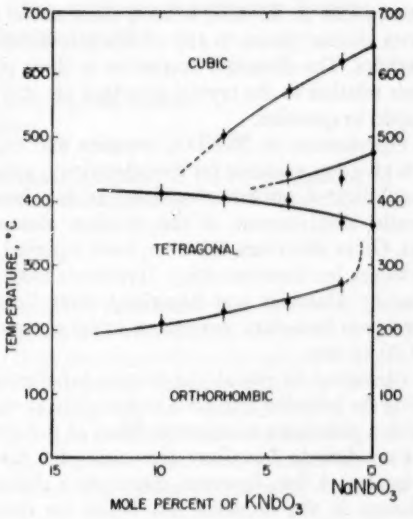

FIG. 7. Phase diagram of $NaNbO_3$-$KNbO_3$ system determined from mixed crystals, showing behavior near pure $NaNbO_3$. The vertical lines show the range of fluctuation of the transition temperatures of the same melt.

TABLE III. Transition energy of $KNbO_3$, $NaNbO_3$, and $(K_{0.1}, Na_{0.9})NbO_3$.

Composition	Lower phase change	Upper phase change
$KNbO_3$	85 cal/mole	190 cal/mole
$(Na_{0.9}, K_{0.1})NbO_3$	20 cal/mole	60 cal/mole
$NaNbO_3$	...	50 cal/mole

VI. DISCUSSION

The optical observations just described point to the existence of three phase transitions in $NaNbO_3$ at 360°, 480°, and 640°C, although the latter two could not be verified by either dielectric or x-ray measurement since the structural perturbation is undoubtedly very small. These two phases are certainly different from the

[20] S. Nagasaki and Y. Takagi, J. Appl. Phys. Japan **17**, 104 (1948).
[21] C. Sykes, Proc. Roy. Soc. (London) **A143**, 422 (1935).

tetragonal phase in $KNbO_3$; in fact, there seems to be no known similar phases in any of the perovskite-type ferroelectrics. The dielectric properties of these phases and their relation to the crystal structure are still very much open to question.

Our experiments on $NaNbO_3$ ceramics and crystals failed to give any evidence for ferroelectricity, although the possibility of antiferroelectricity arising from an antiparallel displacement of the niobium atoms still remains. Other observers, however, have reported positive evidence for ferroelectricity. Hysteresis loops were obtained by Matthias and Remeika,[4] while Vousden[8] observed twin boundary movement under a strong dc field of 20 kv/cm.

We attempted to repeat the latter's experiment by observing the behavior of $NaNbO_3$ crystals in an electric field with a polarizing microscope. Most of the crystals showed no domain boundary movement for fields of 15–20 kv/cm. A few, however, displayed a slight pattern change in the domains just before an electrical breakdown occurred. No positive conclusion could be drawn from the experiments.

It is obvious that the conflicting results could be clarified by assuming Vousden's space group assignment to be in error and by assuming $NaNbO_3$ to have an extremely high coercive field, preventing the observation of hysteresis loops in our dielectric tests. At the same time, however, there is another possible explanation for the disagreement.

The phase diagram shown in Fig. 4 indicates that the ferroelectric tetragonal phase observed in $KNbO_3$ extends to compositions consisting almost entirely of $NaNbO_3$. The ferroelectric orthorhombic phase also extends to within several percent of pure $NaNbO_3$. It is also possible that the addition of other impurities to these mixed crystals would move the ferroelectric phase even closer to pure $NaNbO_3$. Thus a strong electric field might induce the ferroelectric phase in $NaNbO_3$ crystals. This induced ferroelectric phase would be characterized by all the usual phenomena accompanying ferroelectricity, including hysteresis loops and domain boundary movement. In such a case this hypothesis almost exactly fits that proposed by Vousden,[10] who assumed the existence of a ferroelectric state which, under normal conditions, is slightly less stable than a closely related nonferroelectric state. According to Vousden, the ferroelectric structure becomes stable under an applied external field, giving rise to the observed ferroelectric phenomena. This situation is surprisingly similar to the "forced transition by electric field" observed in $PbZrO_3$ [22] and in $Pb(Zr, Ti)O_3$ [23] and $(Ba, Pb)ZrO_3$ [24] solid solutions, for which ample dielectric and structural evidence has been given.

In conjunction with this assumption of a metastable ferroelectric state, it is interesting to note that Roy *et al.*[14] obtained a $NaNbO_3$ compound which showed no extra lines in the powder photograph, by quenching the compound near its melting point. The powder photographs are exactly the same as those usually obtained with $NaNbO_3$, except that the extra lines are missing. After annealing the quenched $NaNbO_3$ overnight at 350°C, the extra lines reappear. This quenched phase could be identical with the induced ferroelectric phase described above; but until the dielectric properties of the quenched phase have been examined, any conclusion would be premature.

It is also interesting to note that the domain movement observed by Vousden can be explained without resorting to an "induced ferroelectricity" hypothesis. If the dielectric constants of a nonpolar crystal differ greatly for different crystallographic directions, a strong electric field can create large energy differences in domains of different orientation. This energy difference may be sufficiently large to cause a domain boundary movement, in such a way that each domain is aligned with the direction of the larger dielectric constant parallel to the external field. The energy difference ΔW may be calculated from $\Delta\epsilon \cdot E^2/8\pi$, where $\Delta\epsilon$ is the difference of the dielectric constant. To obtain an approximate order of magnitude for ΔW, we take $\Delta\epsilon = 1000$, and $E = 20$ kv/cm, which yields $\Delta W = 4\times10^{-3}$ cal/cm^3. Such an energy difference is equivalent to the energy, $P_s \cdot E$, of a crystal having a spontaneous polarization P_s of 1×10^{-6} coulomb/cm^2 at a field of 20 kv/cm. This condition could give rise to the domain boundary movement observed in $NaNbO_3$. The difference of the dielectric constants for different axes of $NaNbO_3$ could be of the same order as those used in the calculation; and since the orthorhombic distortion is extremely small, it is conceivable that the domains are reoriented in a large field. Such a reorientation due to the induced polarization could also lead to an anomalous P *vs* E relationship observed on the oscilloscope.

We are grateful to Dr. R. Roy and Dr. F. Jona for helpful discussions, and to Mr. J. McLaughlin for assistance in specimen preparation and dielectric measurements.

[22] Shirane, Sawaguchi, and Takagi, Phys. Rev. 84, 476 (1951).
[23] E. Sawaguchi, J. Phys. Soc. Japan 8, 615 (1953).
[24] G. Shirane, Phys. Rev. 86, 219 (1952).

Relation between the Width of an X-Ray Line and the Resolving Power of the Double-Crystal Spectrometer

GÖSTA BROGREN
Department of Physics, University of Uppsala, Uppsala, Sweden
(Received June 30, 1954)

The widths of some $K\alpha_1$ lines were measured in a double-crystal spectrometer in the (1,+1) position. It was found that the difference between the experimental width of the line and the width of the rocking curve had a constant value when perfect crystal gratings were used.

THE relation between the width of an x-ray emission line and the resolving power of the double-crystal spectrometer has been investigated in the wavelength range 2285 x-units (the Cr $K\alpha_1$ line) to 708 x-units (the Mo $K\alpha_1$ line). The crystal gratings used were different atomic planes in quartz and calcite. It has been shown previously that the reflection properties of these crystals are in good agreement with the predictions from the dynamical theory for x-ray diffraction, so that these crystals can be considered to have a nearly perfect structure. In this investigation the shape of the rocking curve was calculated for the crystal gratings under consideration and compared with the experimental curves. Only such crystal specimens where the two curves showed a satisfactory agreement were used, so that all these quartz and calcite crystals proved to be perfect. Owing to the dynamical theory the diffraction pattern of position (1,+1) is identical with that of position (1,−1) (the latter being the rocking curve) when the absorption is negligible. When the absorption increases, the pattern in position (1,+1) becomes asymmetric, but in the wavelength range used its width at half-maximum intensity is everywhere nearly the same as that of the rocking curve. The difference in shape between the curves is also slight. Hence, the width of the rocking curve can be used as a measure of the resolving power of the double-crystal spectrometer, for which reason it has been determined for every emission line examined. It was also possible to use crystal gratings with small spacings and high resolving power, since the measurements were carried out on strong spectral lines, mostly $K\alpha_1$ lines.

The results appear in Fig. 1. The width W_R of the rocking curve, the experimental line width W_{exp}, and the true width W_T of the line were found to satisfy the relation

$$W_{exp}=W_T+W_R.$$

If we assume that both the emission line and the rocking curve have the classical line shape, this relation can be derived theoretically.

It should be mentioned that line-width determinations carried out with slightly imperfect crystals gave rise to large deviations from the results in Fig. 1, when the crystal gratings had low resolving power. (Such crystal gratings are for instance calcite 211, quartz $10\bar{1}1$, and quartz $10\bar{1}0$.) When the resolving power was high, small imperfections were unimportant. This can be seen from the measurements with topaz 400 which

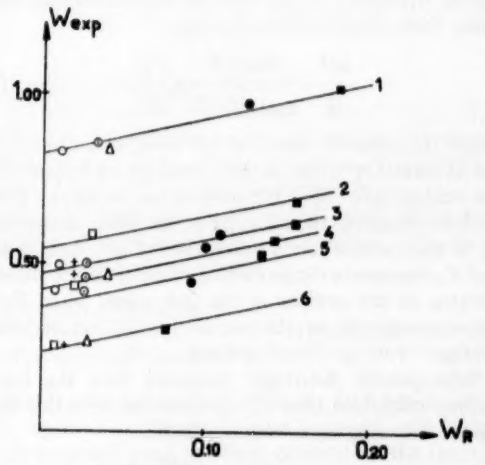

FIG. 1. The full widths W_{exp} of some $K\alpha_1$ lines as functions of the full widths W_R of the rocking curves. The lines are: Fe (1), Co (2), Ni (3), Cu (4), Zn (5), and Mo (6). The following crystal gratings were used: ■ calcite 211, □ calcite 422, ● quartz $10\bar{1}0$, ⊙ quartz $20\bar{2}0$, ○ quartz $30\bar{3}0$, △ quartz $11\bar{2}0$, + topaz 400. The experimental values obtained with Cr $K\alpha_1$ are not shown in the figure, because they fall along curve (1).

are also given in the diagram. This crystal has a mosaic structure, but on account of the high dispersion the mosaic broadening has hardly any influence on the line width.

The above results indicate that the values of x-ray line widths and x-ray energy levels accepted at present are, as a rule, too great.

An extensive report will be published later in *Arkiv för Fysik*.

Interaction of Conduction Electrons and Nuclear Magnetic Moments in Metallic Lithium*

W. KOHN
Department of Physics, Carnegie Institute of Technology, Pittsburgh, Pennsylvania
(Received July 20, 1954)

The probability density at the nucleus of a metallic lithium conduction electron on the Fermi surface is calculated in the spherical approximation, giving the value $P_F=0.11\pm0.01$ atomic unit. This is in good agreement with measurements of the nuclear magnetic resonance shift discovered by Knight and with recent determinations by Schumacher, Carver, and Slichter of the paramagnetic susceptibility.

I. INTRODUCTION

A NUMBER of years ago Knight[1] discovered a significant difference between the frequencies at which nuclear resonance occurs when a given element is in the form of a metal, on the one hand, and when it is part of a nonmetallic compound, on the other. This shift was attributed by Townes *et al.*[2] to the additional magnetic field at the nucleus, ΔH, resulting from a partial alignment of the spins of the conduction electrons. They derived the expression

$$\frac{\Delta H}{H}=\frac{hc\Delta\nu IM}{\mu_I\mu_0(2I+1)}\chi_p\frac{P_F}{P_A}, \tag{1}$$

where the symbols have the following meaning: $\Delta\nu$ is the hyperfine splitting of the atomic ground state; I is the nuclear spin; M is the mass of one atom; μ_I is the nuclear magnetic moment; μ_0 is the Bohr magneton; χ_p is the paramagnetic susceptibility per unit mass; and P_A represents the probability density of the valence electron at the nucleus in the free atom, while P_F is the same quantity for the metallic conduction electrons, averaged over the Fermi surface.

Subsequently Korringa[3] proposed that the longitudinal relaxation time T_1 is connected with this shift by the following approximate relation:

$$T_1=\frac{\mu_0^2}{\pi\hbar(kT)\gamma_I^2}\left(\frac{\Delta H}{H}\right)^{-2}, \tag{2}$$

where $\gamma_I=\mu_I/\hbar I$.

Since all other quantities are known from independent measurements, knowledge of the Knight shift or of T_1 gives one information about the quantity $\chi_p(P_F/P_A)$. In the case of metallic Li, direct measurement of $\Delta H/H$ by Gutowsky and McGarvey[4] leads to the result

$$\chi_p(P_F/P_A)=1.73\pm0.02\times10^{-6}\text{ cgs units}, \tag{3}$$

and preliminary measurements of T_1 by Norberg[5] are in good agreement with this value.

Recent measurements of χ_p by Schumacher *et al.*† give the value,

$$\chi_p=(3.74\pm0.6)\times10^{-6}\text{ cgs mass units}, \tag{4}$$

which is in good agreement with unpublished calculations by Pines.‡ Thus these data indicate that

$$(P_F/P_A)_{\text{expt}}=0.46\pm0.07. \tag{5}$$

It is of interest to examine whether the band picture of the metallic electrons in Li can account for this value. Kohn and Bloembergen,[6] using a variational method with certain s, p, and d functions, suggested by perturbation theory, obtained a value of 1.0, in rather bad agreement with (5). In the present paper, we wish to report a more accurate calculation giving a value,

$$(P_F/P_A)_{\text{theor}}=0.49\pm0.05. \tag{6}$$

This value was obtained with the effective potential constructed by Seitz[7] and by replacing the atomic polyhedron by an equivalent sphere. All checks indicate that the remaining calculational errors within the framework of this model are less than 10 percent.

Before going on to the details of the calculation, we should like to mention the reason for the discrepancy between the present result (6) and the earlier value of Kohn and Bloembergen. It turns out that although the probability of finding the electron in an angular momentum state with $l>2$ is less than 1 percent, the boundary conditions cannot even remotely be satisfied with s, p, and d functions only. The higher angular momentum states, in spite of their small amplitude, play an essential role at the surface of the cell boundary. The present calculation includes states up to $l=6$.

II. DETAILS OF THE CALCULATION

The Quantity P_A

Since we require the ratio P_F/P_A we began by calculating

$$P_A=|\psi_A(0)|^2, \tag{7}$$

* This work was supported in part by the U. S. Office of Naval Research.

[1] W. D. Knight, Phys. Rev. **76**, 1259 (1949).
[2] Townes, Herring, and Knight, Phys. Rev. **77**, 852 (1950).
[3] J. Korringa, Physica **16**, 601 (1950).
[4] H. S. Gutowsky and B. R. McGarvey, J. Chem. Phys. **20**, 1472 (1952).
[5] R. E. Norberg (private communication).
† Schumacher, Carver, and Slichter, Phys. Rev. **95**, 1089 (1954).
‡ D. Pines, Phys. Rev. **95**, 1090 (1954).
[6] W. Kohn and N. Bloembergen, Phys. Rev. **80**, 913 (1951); **82**, 283 (1951).
[7] F. Seitz, Phys. Rev. **47**, 400 (1935); for a correction see W. Kohn and N. Rostoker, Phys. Rev. **94**, 1111 (1954).

where ψ_A is the normalized $2S$ wave function of atomic Li. Using the potential of Seitz,[7] we found

$$(P_A)_{\text{theor}}=0.223a_0^{-3}, \tag{8}$$

where a_0 is the Bohr radius, while the measured hyperfine splitting of the $2s$ state[8] leads to

$$(P_A)_{\text{expt}}=0.231a_0^{-3}. \tag{9}$$

The agreement, to within 4 percent, must be considered excellent and gives one additional confidence in the Seitz potential. Any inaccuracy of this potential, should have a quite negligible effect on the ratio P_F/P_A.

The Metallic Wave Function in the Spherical Approximation

We next calculated the quantity P_F. With an equivalent spherical cell boundary this is the value of $|\psi_F(0)|^2$, where ψ_F is the normalized wave function for any wave vector on the Fermi surface. If we denote the radius of the equivalent sphere by r_s, we must solve the boundary value problem:

$$(-\nabla^2+V(r)-E)\psi(\mathbf{r})=0, \quad r<r_s; \tag{10}$$

$$\psi(\mathbf{r})=e^{2ikr_s\cos\theta}\psi(-\mathbf{r}), \quad r=r_s; \tag{11}$$

$$\partial\psi(\mathbf{r})/\partial r=-e^{2ikr_s\cos\theta}\partial\psi(-\mathbf{r})/\partial r, \quad r=r_s; \tag{12}$$

where k is the magnitude of the wave vector, assumed in the z direction ($kr_s=1.9192$), and θ is the angle between $\mathbf{k}$ and $\mathbf{r}$, if possible $\psi(\mathbf{r})$ can be expanded in terms of the s, p, etc., solutions of (10),

$$\psi(\mathbf{r})=c_0R_0(r)P_0(\cos\theta)+ic_1R_1(r)P_1(\cos\theta)+c_2R_2(r)P_2(\cos\theta)+\cdots, \tag{13}$$

where the R_l are normalized such that $R_l(r_s)=1$ and the c_l, by a simple symmetry argument, are real.

According to the variational theory described in a previous paper,[9] the c_l are determined by the condition that the surface integral,

$$K\equiv\int_S\frac{\partial\psi(\mathbf{r})}{\partial r}\psi^*(-\mathbf{r})e^{-2ikr_s\cos\theta}\sin\theta d\theta, \tag{14}$$

be stationary. When (13) is substituted in (14) one finds that K is a quadratic form in the c_l. The stationary condition leads to a set of linear equations for the c_l, which are compatible provided that

$$\Delta\equiv\begin{vmatrix} 2L_0I_{00} & (L_0+L_1)iI_{01} & (L_0+L_2)I_{02} & \cdots \\ (L_0+L_1)iI_{01} & -2L_1I_{11} & (L_1+L_2)iI_{12} & \cdots \\ (L_0+L_2)I_{02} & (L_1+L_2)iI_{12} & 2L_2I_{22} & \cdots \\ \cdot & \cdot & \cdot & \\ \cdot & \cdot & \cdot & \\ \cdot & \cdot & \cdot & \end{vmatrix}=0, \tag{15}$$

where

$$L_l=\left[\frac{dR_l}{dr}\Big/R_l\right]_{r=r_s},$$

$$I_{ij}=\int_0^\pi e^{-2ikr_s\cos\theta}P_i(\cos\theta)P_j(\cos\theta)\sin\theta d\theta. \tag{16}$$

In practice, the determinant is truncated after a finite number, say $\bar{l}$, of rows and columns and evaluated for a series of energies E which enter only through the L_l. (The latter were found by numerical integration and, for high l, by cruder perturbation methods.) In this way the E for which Δ vanishes is found and the c_l are then evaluated by solving the set of equations which lead to (15). Finally, P_F is given by

$$P_F=c_0^2R_0^2(0)\Big/\sum_{l=0}^{\bar{l}}c_l^2N_l, \tag{17}$$

$$N_l=\frac{4\pi}{2l+1}\int_0^{r_s}R_l^2(r)r^2dr. \tag{18}$$

The results are given in Table I.

It will be noted that if one stops at $l=2$, P_F is much too small.[10] At $l=3$ no solution at all is found. However, at $l=6$, P_F appears to have settled down to within less than 10 percent of its true value.

We have made two checks on this result. If the wave function satisfied the boundary condition (11) exactly we should have, at all angles,

$$\frac{c_1P_1(\cos\theta)+c_3P_3(\cos\theta)+\cdots}{c_0P_0(\cos\theta)+c_2P_2(\cos\theta)+\cdots}\Big/\tan(kr_s\cos\theta)=1. \tag{19}$$

Following is a table of this ratio for $\bar{l}=5$ and 6 (Table II). Again an accuracy of about 5 percent is indicated.

As a second check we have substituted the function (13), with 7 undetermined coefficients into the boundary conditions (11) and (12) at the arbitrarily selected angles, $\theta=30°$, $60°$, $75°$, $90°$, and determined E from the condition that the equations be compatible. The c_l and P_F were then evaluated, the result for the latter being $0.116a_0^{-3}$, agreeing within 6 percent with the best variational result. We tend to favor the latter

TABLE I. Successive variational approximations.

$\bar{l}$	E(ry)	$P_F\times a_0^3$
2	−0.4272	0.046
3	(−0.4065)*	
4	−0.4347	0.075
5	−0.4308	0.114
6	−0.4313	0.110

* Δ has no zero but a minimum at this energy.

[7] M. Fox and I. I. Rabi, Phys. Rev. **48**, 746 (1935).
[8] W. Kohn, Phys. Rev. **87**, 472 (1952).
[10] The value 0.22 of Kohn and Bloembergen was obtained with s, p, and d functions which did not satisfy (10) but were suggested by a perturbation expansion for small k.

TABLE II. Accuracy of variational functions.

θ	0°	30°	60°	75°
$l=5$	1.06	1.04	0.99	0.82
$l=6$	1.04	0.92	0.98	1.05

slightly, since it does not depend on arbitrarily chosen angles.

Combining the last entry of Table I and Eq. (9), and taking into account the error indicated by our checks, we arrive at the result quoted in (6).

III. ADDITIONAL REMARKS

Effect of Actual Cell Boundary

One of the remaining uncertainties of the calculation is the effect of replacing the true cell boundary by an equivalent sphere. Since the required quantity is $|\psi_F(0)|^2$ averaged over the Fermi surface one would expect the equivalent sphere model to give a good approximation, provided that the true $|\psi_F(0)|^2$ does not vary too much over the true Fermi surface. We have the following two indications that the variation is in fact moderate. Kohn and Rostoker[7] have calculated the energy band of metallic Li, using the actual atomic polyhedron. They find that the energies on the Fermi surface, relative to the energy of the $k=0$ state, differ by only 3 percent in the (1,0,0) and (1,1,1) direction. As a second check we have extracted the variational wave functions consisting of s, p, and d states from the calculation of Kohn and Rostoker and have computed $|\psi(0)|^2$ both in the (1,0,0) and (1,1,1) direction. Their ratio is 1.14, indicating a rather moderate variation over the Fermi surface. This result must, however, be viewed with some caution as we have seen that the true wave function cannot be adequately expressed in terms of s, p, and d functions only.[11]

Nature of the Wave Function on the Fermi Surface

Returning to our "spherical" calculation, let us write the wave function in the form,

$$\psi=\sum_{l=0}^{\infty} a_l\varphi_l, \tag{20}$$

where φ_l is a wave function corresponding to angular momentum l, normalized over the equivalent sphere; and let ψ itself be normalized to unity so that

$$\sum_{l=0}^{\infty} |a_l|^2=1. \tag{21}$$

[11] The absolute values of $|\psi_F(0)|^2$ obtained with these functions is very large giving $P_F/P_A\sim 1.3$.

Our variational calculation gives the following results, which agree with those obtained by fitting the boundary conditions at the selected angles within a few percent:

$$|a_0|^2=0.20;\quad |a_1|^2=0.73;\quad |a_2|^2=0.06;\quad |a_l|^2=0.00,\quad l>2. \tag{22}$$

The preponderance of the p function is noteworthy. This is in line with a recent calculation by Schiff[12] who has calculated the wave function at some points on the Brillouin zone boundary and finds that it has p character. Since $|\psi(0)|^2$ therefore vanishes at the zone boundary, Jones and Schiff[13] have anticipated a rather small value of P_F (the Fermi surface is quite close to the zone boundary), a fact which the present calculation bears out.

Perturbation Theory

As first suggested by Bardeen,[14] it is possible to expand the wave function corresponding to the spherical problem (10)–(12) in a power series in k. We do not know any good *a priori* reason why such an expansion should converge well on the Fermi surface. However, this is in fact the case for the energy $E=E_0+E_2k^2+E_4k^4+\cdots$.[14] Keeping two terms gives, in atomic units, $E=-0.423$, three terms give $E=-0.427$, which should be compared with our best variational result of Table I, $E=-0.431$. One can similarly expand $|\psi(0)|^2$ in powers of k (see reference 2). In this way, one finds, in atomic units,

$$|\psi(0)|^2=0.4247-0.9006k^2, \tag{23}$$

if higher terms are neglected. This expansion is certainly good for small k. Further it predicts that $|\psi(0)|^2$ vanishes at $k=0.6868$. The calculation of Schiff[12] shows that $|\psi(0)|^2$ vanishes at the zone boundary which in our spherical model corresponds to $k=0.7533$. Thus the expansion (23) gives good results for $k\approx 0$ and slightly low results for k near the zone boundary. On the Fermi surface where $k=0.5979$ we find

$$|\psi_F(0)|_{\text{pert}}{}^2=0.103,\quad (P_F)_{\text{pert}}/P_A=0.46, \tag{24}$$

which is in remarkably good agreement with the variational result (6) but, as expected, slightly too low.

IV. ACKNOWLEDGMENTS

It is a pleasure to thank Professor H. Jones for many interesting discussions on this subject, and Professors Slichter and Norberg for the communication of their preliminary experimental results. I should like also to thank Mrs. A. Watson for the expert execution of the numerical calculations.

[12] B. Schiff, Proc. Phys. Soc. (London) **A67**, 2 (1954).

[13] H. Jones and B. Schiff, Proc. Phys. Soc. (London) **A67**, 217 (1954).

[14] J. Bardeen, J. Chem. Phys. **6**, 367 (1938); R. Silverman and W. Kohn, Phys. Rev. **80**, 912 (1950); **82**, 283 (1951).

Some Electrical Properties of Natural Crystals of Iron Pyrite

JOHN C. MARINACE
General Engineering Laboratory, General Electric Company, Schenectady, New York
(Received June 21, 1954)

Room-temperature Hall mobilities of natural single crystals of iron pyrite with carrier concentrations of approximately 10^{18}/cm³ were found to be approximately 100 cm²/volt-sec for electrons and 1 for holes. Resistivity as a function of temperature was measured on six samples in the range from −196°C to 403°C; from this measurement the width of the forbidden band was estimated to be 1.2 ev.

ALTHOUGH iron pyrite received some use as a crystal detector in the past, along with the more widely known galena, there is comparatively little information available regarding its electrical properties. The *International Critical Tables* quote some conductivity data[1] by Koenigsberger, Beckman, and Heaps and a Hall coefficient obtained by Smith.[2] The conductivity data were not measured over a temperature range sufficiently wide to permit an estimate of the width of the forbidden band, and the Hall coefficient data were not accompanied by conductivity data which would permit an estimate of carrier mobility.

Because synthesis of iron pyrite crystals suitable for electrical measurements proved to be difficult, natural crystals were selected for measurement. Specimens were sawed from several different single crystals in the approximate dimensions 1×0.5×0.1 cm. These wafers were lapped with carborundum powder and etched with a mixture of 60 parts HNO_3 and 40 parts HF. With a thermoelectric probe, four *p*-type and two *n*-type wafers were selected for measurement, *n*- and *p*-type wafers being eliminated. Although these wafers were cut from single crystals, etching revealed many inhomogeneities, which possibly were due to strains.

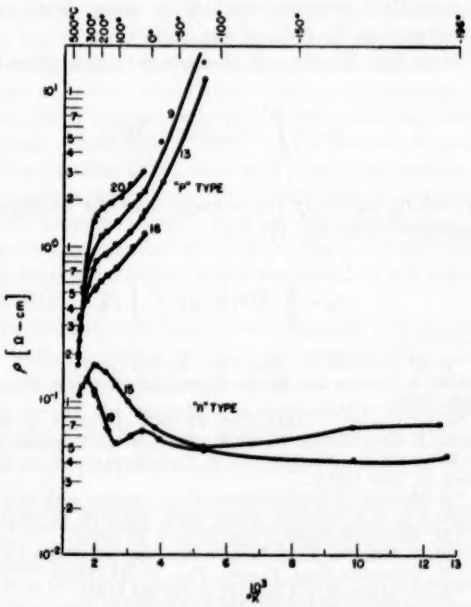

FIG. 1. Resistivity as a function of reciprocal temperature for mineral iron pyrite.

Hall coefficients were measured at room temperature by means of a 10.5-kilogauss magnetic field from a permanent magnet and currents of 10 to 25 ma dc. Results are shown in Table I.

After the Hall-coefficient measurements were made, resistivities as a function of temperature were measured on all six samples in a single run. No protective atmosphere was used. From Fig. 1 the width of the forbidden band can be estimated to be about 1.2 ev.

TABLE I. Room-temperature electrical properties.

Sample No.	Thermoelectric type	R cm³/coul	N 10^{18}/cm³	ρ Ω−cm	Hall μ* cm²/volt-sec
9	*p*	2.8	2.6	2.2	1.3
13	*p*	2.3	3.2	1.6	1.4
15	*n*	−7.6	0.97	0.078	98
16	*p*	1.9	4.1	1.2	1.6
19	*n*	−6.5	1.1	0.063	103
20	*p*	6.3	1.2	3.1	2.0

* Another *n*-type sample not included in this group exhibited an electronic Hall mobility of 168 cm²/volt-sec.

Also evident from Fig. 1 is the striking difference in conductivities between the *n*-type and *p*-type samples at low temperatures. From the slopes of the plots, the acceptor activation energy can be estimated roughly at 0.1 ev, while the donor activation energy is very much less. Because of this wide difference, two of the *p*-type samples and the two *n*-type samples were spectrographically analyzed. However, no distinction between the two types could be made in this way. As a point of interest, these samples had an extremely high purity, considering that they were natural crystals; all four showed silicon as the major impurity in a concentration roughly estimated at 0.03 percent.

I wish to thank W. C. Dunlap of the Research Laboratory for helpful discussion and Mrs. A. P. O'Hara of the Material and Process Laboratory for the spectrographic analyses.

[1] *International Critical Tables* (McGraw-Hill Book Company, Inc., New York, 1933), Vol. 6, pp. 154, 155, 422.
[2] Reference 1, p. 416.

Moment Singularity Analysis of Vibration Spectra*†

MELVIN LAX AND JOEL L. LEBOWITZ
Department of Physics, Syracuse University, Syracuse, New York
(Received July 7, 1954)

The frequency distribution of a crystal is approximated by combining Van Hove's determination of its analytical nature and Montroll's method of moments. The function $G(\omega^2)$ is represented by an expression with the correct behavior at the singularities and at the maximum and minimum frequencies. The behavior between singular points is adjusted smoothly by leaving n undetermined parameters. These parameters are then fixed by using the correct first n moments. As a test, this procedure was applied to the two-dimensional square lattice with nearest and next nearest neighbor interactions, solved exactly for a particular case by Montroll. The approximated distribution function had the right form at the end points, contained terms of the appropriate logarithmic form, and a jump function (with known coefficients). It also included Legendre polynomials with unknown coefficients, which were determined by moments. The difference between the exact and approximate distribution functions was a few percent using only the zeroth moment (normalization). Using higher moments produced a gradual increase in accuracy.

I. INTRODUCTION

THE normal modes of a lattice are eigenvectors of a matrix $M_{ij}^{\alpha,\beta}$ denoted simply by $\mathbf{M}$, where i, j are indices of the cell and α, β are indices of particles in a cell. Using the translational symmetry of the lattice, the problem is customarily reduced to the diagonalization of a matrix $M^{\alpha,\beta}(\mathbf{k})$, denoted briefly by $\mathbf{M}(\mathbf{k})$, where $\mathbf{k}$ is the propagation constant of the wave, and the index α (or β) takes on lZ different values, where l is the dimension of the space and Z the number of atoms per cell. The elements of $\mathbf{M}(\mathbf{k})$ are periodic functions of $\mathbf{k}$, with the periodicity of the reciprocal lattice.

The normalized density of eigenvalues ω^2 associated with the matrix $\mathbf{M}$ can be defined by

$$G(\omega^2)=\langle\delta(\omega^2-\mathbf{M})\rangle, \tag{1}$$

where the average of a matrix $\langle\ \rangle$ is the trace of that matrix divided by its dimensionality. Using the uniform spacing of the propagation constant over one Brillouin zone, Eq. (1) can be reduced to

$$G(\omega^2)=\int\langle\delta[\omega^2-\mathbf{M}(\mathbf{k})]\rangle d\mathbf{k}\Big/\int d\mathbf{k}, \tag{2}$$

where

$$\langle\delta[\omega^2-\mathbf{M}(\mathbf{k})]\rangle=(lZ)^{-1}\,\mathrm{trace}\{\delta[\omega^2-\mathbf{M}(\mathbf{k})]\}$$

$$=(lZ)^{-1}\sum_{n=1}^{lZ}\delta[\omega^2-\omega_n^2(\mathbf{k})].$$

The relation between the frequency distribution $g(\omega)$ and the distribution function of the frequency squared $G(\omega^2)$ is

$$g(\omega)=2\omega G(\omega^2). \tag{3}$$

Since the integral in Eq. (2) cannot be evaluated explicitly except for a few special cases,[1–3] many approximate methods[4] have been used to study $g(\omega)$. Blackman[5] approximates $g(\omega)$ by calculating the frequencies at a large number of points in the Brillouin zone and finding their distribution. This requires a great deal of labor, which has to be repeated for every set of force constants. Houston[6] finds the distribution along special lines in reciprocal space and interpolates for the rest of the Brillouin zone. This method introduces some spurious singularities in $g(\omega)$.[7] Montroll uses the moments of $g(\omega)$ to determine the coefficients of the initial terms in a power series expansion of $g(\omega)$. We shall discuss Montroll's[8,9] moment method in some detail as it forms part of the basis of our work.[10]

From Eq. (1), the nth moment of $G(x)$ is given by

$$m_n=\int_0^1 x^n G(x)dx=\langle\mathbf{M}^n\rangle, \tag{4}$$

or, taking explicitly the average over the propagation constant[11] as in Eq. (2), by

$$m_n=\int\langle\mathbf{M}^n(\mathbf{k})\rangle d\mathbf{k}\Big/\int d\mathbf{k}. \tag{5}$$

* A summary of the essential results of this paper was presented to the Washington meeting of the American Physical Society, April, 1954.

† Supported in part by the Office of Naval Research.

[1] E. W. Montroll, J. Chem. Phys. **15**, 575 (1947).
[2] W. A. Bowers and H. B. Rosenstock, J. Chem. Phys. **18**, 1056 (1950).
[3] G. F. Newell, J. Chem. Phys. **21**, 1877 (1953); H. B. Rosenstock, J. Chem. Phys. **21**, 2064 (1953); H. B. Rosenstock and G. F. Newell **21**, 1607 (1953); H. B. Rosenstock and H. M. Rosenstock **21**, 1608 (1953).
[4] A discussion of some of the methods together with references is given by A. C. Menzies, Repts. Progr. Phys. **16**, 83 (1953).
[5] M. Blackman, Repts. Progr. Phys. **8**, 11 (1941).
[6] W. V. Houston, Revs. Modern Phys. **20**, 161 (1948).
[7] T. Nakamura, Prog. Theoret. Phys. **5**, 213 (1950).
[8] E. W. Montroll, J. Chem. Phys. **10**, 218 (1942).
[9] E. W. Montroll, J. Chem. Phys. **11**, 481 (1943).
[10] For convenience we use units in which the maximum frequency of vibrations ω_L is unity so that $x=\omega^2=(\omega/\omega_L)^2$ covers the range $0\leq x\leq 1$.
[11] T. H. Walnut, J. Chem. Phys. **22**, 692 (1954), calculates the moments directly from $\mathbf{M}$.

Montroll was the first to recognize that the moments m_n are easily computed from traces of powers of $\mathbf{M}(\mathbf{k})$ via Eq. (5). He showed that the first N moments can be used to construct the best approximate distribution function in the sense of least squares, for approximating functions expressed in a power series or a polynomial series containing N terms.[12] For these two choices of expansion, the least squares criterion is equivalent to the requirement that the first N moments of the approximating and exact distribution agree.[13] The rate of convergence of such an expansion is determined by the smoothness of the exact function. Hence, if $G(x)$ is smooth, the use of even a few moments could be expected to give a good approximation.

However, it was found by Montroll,[1] when he did an exact calculation for a two-dimensional square lattice with nearest and next nearest neighbor interactions, that the frequency distribution function was not smooth but contained two logarithmic singularities. Smollett[14] extended Montroll's result to the case of a two-dimensional ionic lattice, taking into account the long-range Coulomb forces between ions. Similar results were obtained by Bowers and Rosenstock[2] for the frequency distribution of vibrations perpendicular to the plane of the lattice. Van Hove[15] subsequently showed that these singularities, far from being accidental, are a necessary consequence of the periodic structure of the lattice. They arise from those vibrations in the neighborhood of critical points $\mathbf{k}_c$ for which $|\text{grad}x_n(\mathbf{k}_c)|=0$. The singularities in $G(x)$ occur at $x_c=x_n(\mathbf{k}_c)$, where $x_n(\mathbf{k})=\omega_n^2(\mathbf{k})$. In two dimensions $G(x)$ will have at least one logarithmic singularity. In three dimensions there will be at least three critical points x_c, where while $G(x)$ remains continuous, its derivative $G'(x_c)$ has an inverse square root singularity.

These considerations show that a smooth approximating function $G_a(x)$, such as a linear combination of polynomials which has the correct first N moments, would converge slowly to $G(x)$ with increasing N. Hence a large number of moments, and a corresponding large amount of labor, would be needed to get a good fit to $G(x)$.

We decided, therefore, to take explicitly into account the analytic nature of $G(x)$ in constructing $G_a(x)$. $G_a(x)$ is represented by an expression with the correct behavior at the singularities and at the end points. The behavior between singular points is adjusted smoothly by leaving n undetermined parameters to be fitted by the moments.[16] In this way the moments are used for approximating a smooth function so that good agreement to $G(x)$ might be expected, even when, only a small number of moments are used. Essentially the same procedure was suggested independently by Rosenstock,[17] who applied it to the body-centered and face-centered cubic lattices. See Sec. III for further discussion of Rosenstock's results.

II. TWO-DIMENSIONAL SQUARE LATTICE

As a test, this procedure, which we call the moment-singularity method was applied to a two-dimensional monatomic square lattice with neighbor and next neighbor interactions. The distribution function obtained by this procedure will be compared (a) with the exact distribution calculated by Montroll,[1] (b) with the distribution obtained by the unmodified method of moments.

For this lattice, $\mathbf{M}(\mathbf{k})$ is a two-by-two matrix:[18]

$$\mathbf{M}(\mathbf{k})=\frac{1}{2}\begin{pmatrix}1+(t-1)c_1-tc_1c_2 & ts_1s_2\\ ts_1s_2 & 1+(t-1)c_2-tc_1c_2\end{pmatrix}, \quad (6)$$

where $c_i=\cos k_i$, $s_i=\sin k_i$, $i=1,2$, $t=(1+\alpha/2\gamma)^{-1}$, and α and γ are neighbor and next neighbor forces, respectively. The two roots of the secular equation are

$$x_\pm=\tfrac{1}{4}[2t(1-c_1c_2)+(1-t)(2-c_1-c_2)] \pm\tfrac{1}{4}[4t^2s_1^2s_2^2+(1-t)^2(c_1-c_2)^2]^{\frac{1}{2}}. \quad (7)$$

The nth moment of $G(x)$ can be found from Eq. (5) by integrating the trace $M^n(k)$ over the Brillouin zone, $-\pi<k_1, k_2\leq\pi$, and dividing the result by $2(2\pi)^2$. Thus, the first moment m_1, is

$$m_1=\int_{-\pi}^{\pi}dk_1\int_{-\pi}^{\pi}dk_2(16\pi^2)^{-1} \times[2-(1-t)(c_1+c_2)-2tc_1c_2]=\tfrac{1}{2}. \quad (8)$$

Montroll has calculated the first six even moments μ_{2n} of $g(\omega)$, in a slightly different way. These are related to the m_n by

$$\mu_{2n}=\int_0^1\omega^{2n}g(\omega)d\omega=\int_0^1x^nG(x)dx=m_n, \quad (9)$$

and their values are

$$\begin{aligned}&m_0=1,\quad m_1=1/2,\quad m_2=(3-2t+2t^2)/8;\\ &m_3=(5-6t+6t^2)/16;\\ &m_4=(35-60t+77t^2-34t^3+17t^4)/128;\\ &m_5=(462-980t+960t^2-265t^3+80t^4-5t^5)/1024.\end{aligned} \quad (10)$$

[12] The use of polynomials as expansion functions will always lead to the same result as the use of a power series, for the same number of terms. The use of orthogonal polynomials greatly simplifies the arithmetic.

[13] If an expansion is made in functions other than polynomials, e.g., an N-term Fourier series, the method of equating moments and the least squares method are distinct for finite N. While knowledge of the first N moments determines a Fourier expansion to N terms, if the moment conditions are applied, this knowledge is insufficient to lead to a least squares solution.

[14] M. Smollett, Proc. Phys. Soc. (London) **A65**, 109 (1952).

[15] L. Van Hove, Phys. Rev. **89**, 1189 (1953).

[16] The fitting between singular points may also be done by any other method, e.g., Blackman's which yields sufficiently accurate results away from the singularities.

[17] H. B. Rosenstock, Phys. Rev. **95**, 617 (1954). A paper reporting this work is in preparation.

[18] For comparison with notation in reference 1: $k_i\to\Phi_i$, $x\to f^2$, $G(x)\to(2f)^{-1}\omega_L g(f)$, we measure the frequency in such units that the largest frequency $\omega_L=1$.

TABLE I. Value of the coefficients of $A_k^{(N)}$ of the Legendre polynomials in the expansion of the nonsingular part of distribution function.

N \ k	$A_0^{(N)}$	$A_1^{(N)}$	$A_2^{(N)}$	$A_3^{(N)}$	$A_4^{(N)}$	$A_5^{(N)}$	$A_6^{(N)}$	$A_7^{(N)}$
$G_a^{(1)}$	−0.1306	−0.1599	0.1568					
$G_a^{(2)}$	−0.1306	−0.2620	0.1568	0.1021				
$G_a^{(3)}$	−0.1306	−0.2620	0.1409	0.1021	0.0159			
$G_a^{(4)}$	−0.1306	−0.2620	0.1409	0.1388	0.0159	−0.0368		
$G_a^{(5)}$	−0.1306	−0.2620	0.1409	0.1388	0.0536	−0.0368	−0.0378	∞
$G_a^{(6)}$	−0.1306	−0.2620	0.1409	0.1388	0.0536	−0.0429	−0.0378	0.0061

An explicit form for all higher moments was found by Walnut.[11]

Because of the symmetry of the problem it is sufficient to work in one quadrant of the Brillouin zone, $0 \leq k_1, k_2 \leq \pi$. In this quadrant the critical points of $x_\pm$ are at

$$(k_1,k_2) = (0,0), (0,\pi), (\pi,0), (\pi,\pi), \text{ when } 0<t<1/5. \quad (11)$$

The values of x, in the two branches $x_\pm(\mathbf{k})$, at these critical points are $(0, 1, 1, 1-t)$ and $(0, t, t, 1-t)$, respectively. For t greater than $1/5$ but less than $1/2$,[19] the x_+ branch has one additional critical point at $\{\cos^{-1}[(t-1)/(4t)], \cos^{-1}[(t-1)/(4t)]\}$, and the value of $x_+(\mathbf{k})$ at that point is $(1+3t)^2/(16t)$.

From the behavior of $x_\pm(\mathbf{k})$ in the neighborhood of the critical points in reciprocal space it is possible to deduce the form of $G(x)$ near the critical values of x,[20] including the value of $G(0)$ and $G(1)$. If the singular part of $G(x)$ is called $F(x)$, then it can be shown that

$$F(x) = B_1 \ln|x-t| + B_2 \ln|x-(1-t)| + B_3 H[x-(1-t)], \quad 0<t<\tfrac{1}{5}, \quad (12a)$$

$$F(x) = C_1 \ln|x-t| + C_2 \ln|x-(1+3t)^2/16t| + C_3 H[x-(1-t)], \quad \tfrac{1}{5}<t<\tfrac{1}{2},$$

where H is the Heaviside unit function, $H(y)=0$, for $y<0$, $H(y)=1$, for $y>0$, and

$$B_1 = -[t(1-2t)]^{-\frac{1}{2}}/\pi^2;$$

$$B_2 = -(1-3t)[t(1-t)(1-2t)(1-5t)]^{-\frac{1}{2}}/\pi^2;$$

$$B_3 = -(2/t\pi^2)\int_0^{\pi/2} d\theta[(1-3t)/t + (1+k^2\sin^2\theta)^{\frac{1}{2}}]^{-1}, \quad k^2 = (3t^2-2t+1)/t^2; \quad (12b)$$

where

$$C_1 = -[t(1-2t)]^{-\frac{1}{2}}/\pi^2;$$

$$C_2 = (16t/\pi^2)(1-t)^{-1}[3(5t-1)(3t+1)]^{-\frac{1}{2}};$$

$$C_3 = [(1-3t)/\pi][t(1-t)(1-2t)(5t-1)]^{-\frac{1}{2}}.$$

The value of $G(x)$ at 0 and 1 is

$$G(0) = (1+t)[t(1+2t-3t^2)]^{-\frac{1}{2}}/\pi; \quad G(1) = t^{-\frac{1}{2}}/\pi. \quad (12c)$$

In order to apply the moment-singularity method we subtracted $F(x)$ from $G(x)$ and approximated the remainder by a linear combination of n Legendre polynomials. The first $n-2$ coefficients of the expansion are determined by the requirement that first $n-2$ moments of the approximate function agree with the exact ones. The remaining two coefficients are then determined by fixing the end points. Hence, when N moments are known, the approximate distribution function $G_a^{(N)}(x)$ is

$$G_a^{(N)}(x) = F(x) + \sum_{k=0}^{N+1} A_k^{(N)} P_k(2x-1), \quad 0 \leq x \leq 1, \quad (13a)$$

where

$$A_k^{(N)} = (2k+1)\int_0^1 P_k(2x-1)[G(x)-F(x)]dx \quad (13b)$$

for $k \leq N-1$, and

$$A_N^{(N)} + A_{N+1}^{(N)} = G(1) - F(1) - \sum_{i=0}^{N-1} A_i^{(N)},$$

$$(-1)^N A_N^{(N)} + (-1)^{N+1} A_{N+1}^{(N)} = G(0) - F(0) - \sum_{i=0}^{N-1} (-1)^i A_i^{(N)}. \quad (13c)$$

Note that $A_k^{(N)}$ is independent of N, the order of the approximation for $k \leq (N-1)$.

When the unmodified method of moments is used to approximate $G(x)$, the approximating function, when N moments are known, $G_m^{(N)}(x)$ is

$$G_m^{(N)}(x) = \sum_{k=0}^{N-1} B_k^{(N)} P_k(2x-1); \quad (14)$$

the $B_k^{(N)}$ are again given by Eq. (13b) with $F(x)$ set equal to zero.

A numerical evaluation of the $A_k^{(N)}$ and the $B_k^{(N)}$ was made for $t=1/3$. This is the value of t for which Montroll[1,18] evaluated $G(x)$ in a closed form, so that

TABLE II. Convergence of the moment-singularity approximating $G_a^{(N)}(x)$ to the exact distribution of $G(x)$ with increasing N. (N is the number of moments used.)

x	$F(x)$	$G_a^{(1)}(x)$	$G_a^{(2)}(x)$	$G_a^{(3)}(x)$	$G_a^{(4)}(x)$	$G_a^{(5)}(x)$	$G_a^{(6)}(x)$	$G(x)$
0	0.450	0.637	0.637	0.637	0.637	0.637	0.637	0.637
0.05	0.528	0.653	0.697	0.689	0.670	0.687	0.689	0.683
0.1	0.620	0.689	0.763	0.752	0.734	0.739	0.739	0.740
0.3	1.36	1.25	1.34	1.34	1.36	1.35	1.35	1.34
1/3	∞	∞	∞	∞	∞	∞	∞	∞
0.4	1.25	1.08	1.12	1.14	1.16	1.17	1.18	1.17
0.5	1.11	0.897	0.897	0.911	0.911	0.937	0.937	0.951
0.6	1.17	0.939	0.890	0.901	0.879	0.891	0.887	0.908
0.7	1.52	1.28	1.20	1.20	1.17	1.16	1.16	1.14
0.75	∞	∞	∞	∞	∞	∞	∞	∞
0.9	0.942	0.755	0.682	0.671	0.688	0.694	0.695	0.733
0.95	0.799	0.637	0.599	0.585	0.604	0.621	0.619	0.631
1	0.6851	0.551	0.551	0.551	0.551	0.551	0.551	0.551

[19] We shall assume, as did Montroll in reference 1, that $t \leq \frac{1}{2}$.

[20] For a discussion see Sec. III of this paper, also Van Hove, reference 15, Secs. II and III. For comparison see Montroll, reference 1.

comparisons can be made. This will indicate how useful the moment-singularity method is.

For $t=1/3$, Eqs. (12) and (13) yield

$$G_a^{(N)}(x)=-(3/\pi^2)\ln|x-\tfrac{1}{3}|-(4/\pi^2)\ln|x-\tfrac{3}{4}|+\sum_{k=0}^{N+1}A_k^{(N)}P_k(2x-1), \quad (15)$$

$$G(0)=2/\pi; \quad G(1)=\sqrt{3}/\pi.$$

The values of the $A_k^{(N)}$ in different orders of approximation $N\leq 6$ are summarized in Table I. The values of the $B_k^{(N)}$, which are all independent of N, are

$$B_0=1, \quad B_1=0, \quad B_2=-0.4167, \quad B_3=0, \quad B_4=-0.2269, \quad B_5=-0.2290. \quad (16)$$

Comparisons between $G(x)$, $G_a^{(N)}(x)$, and $G_m^{(N)}(x)$ are presented in Tables II, III, and IV.

III. CONCLUSION

As can be seen from Table IV, use of the nonsingular method of moments results in a great increase in the accuracy of the approximation over the usual method of moments for the same number of moments. The additional work required to find $F(x)$ was small, for $t=1/3$. For this particular value of t, $x_\pm(\mathbf{k})$ can be expanded in a Taylor series near the critical points, and the behavior of $G(x)$ near the critical points can be read off directly from Van Hove. For other values of t, the critical points (0,0), (π,π) are of the type which Van Hove calls generalized critical points. The behavior of $x_\pm(k)$ near these points is

$$x(\mathbf{k})=x_c+|\xi|^2\psi(\xi/|\xi|)+O(|\xi^3|), \quad \xi=\mathbf{k}-\mathbf{k}_c.$$

To find the form of $G(x)$ near these points, the integral in Eq. (2) has to be evaluated, terms of $O(|\xi^3|)$ being neglected. Transforming to polar coordinates in reciprocal space, the integration over the radial variable can be done immediately by means of the delta function. This leaves an integration over the angle variable, whose evaluation may be quite difficult if it cannot be found in the tables. The integral representing B_3 in Eq. (12b) is one such case.

However, even when the exact form of the singular part of $G(x)$, such as the coefficients multiplying the logarithmic terms in two dimensions, or the square root terms in three dimensions, are not known, convergence would be improved greatly if the approximating function contained terms of the correct singular form. The coefficients of these terms could then be determined by the moments. Thus, for the case considered in this paper, it would have been preferable if the approximating function $G_a(x)$ consisted of polynomials multiplying the logarithmic terms whose value at the critical points is the correct one. This would have taken account of terms in the distribution function of the form $(x-x_c)\ln|x-x_c|$. A smaller number of moments might then have been used to obtain the same accuracy. This was not done because of the extra work involved in solving simultaneous equations for the coefficients of the multiplying polynomials since no orthogonal set would be available. In general, the amount of work required to find more moments has to be balanced against the work involved in solving simultaneous equations.

TABLE III. Convergence of the unmodified moment approximation $G_m^{(N)}(x)$, to the exact distribution of $G(x)$ with increasing N. (N is the number of moments used.)

x	$G_m^{(1)}(x)$	$G_m^{(2)}(x)$ $=G_m^{(3)}(x)$	$G_m^{(4)}(x)$ $=G_m^{(5)}(x)$	$G_m^{(6)}(x)$	$G(x)$
0	1	0.583	0.332	0.103	0.637
0.05	1	0.702	0.655	0.646	0.683
0.1	1	0.808	0.861	0.770	0.740
0.3	1	1.11	1.13	1.20	1.34
1/3	1	1.14	1.14	1.21	∞
0.4	1	1.18	1.13	1.20	1.17
0.5	1	1.21	1.12	1.12	0.951
0.6	1	1.18	1.13	1.06	0.908
0.7	1	1.11	1.13	1.07	1.14
0.75	1	1.05	1.12	1.09	∞
0.9	1	0.808	0.861	0.953	0.733
0.95	1	0.702	0.655	0.664	0.631
1	1	0.583	0.332	0.561	0.551

There is a theorem of Feynman[21] which is useful in finding *some* critical points without diagonalizing $\mathbf{M}(\mathbf{k})$. This theorem states that, if $\mathbf{A}(\alpha)\Psi(\alpha)=\lambda(\alpha)\Psi(\alpha)$ and $\mathbf{A}(\alpha)$ is Hermitian, then

$$\frac{\partial\lambda(\alpha)}{\partial\alpha}=\left(\Psi(\alpha),\frac{\partial\mathbf{A}(\alpha)}{\partial\alpha}\Psi(\alpha)\right).$$

Thus $|\text{grad}\omega^2(k)|=0$ whenever $|\text{grad}\mathbf{M}(\mathbf{k})|=0$. This can happen only at those $\mathbf{k}$ where all the branches have critical points simultaneously.

A great difficulty, in many cases, in finding the analytic form of the distribution, is the location of *all* the critical points. Van Hove's arguments predict only

TABLE IV. Comparison of the unmodified approximation $G_m^{(6)}(x)$, the moment singularity approximation $G_a^{(6)}(x)$, and the exact distribution $G(x)$ when six moments are used.

x	$G_m^{(6)}(x)$	$G_a^{(6)}(x)$	$G(x)$
0	0.103	0.637	0.637
0.05	0.646	0.689	0.683
0.1	0.770	0.739	0.740
0.3	1.20	1.35	1.34
1/3	1.21	∞	∞
0.4	1.20	1.18	1.17
0.5	1.12	0.937	0.951
0.6	1.06	0.887	0.908
0.7	1.07	1.16	1.14
0.75	1.09	∞	∞
0.9	0.953	0.695	0.733
0.95	0.664	0.619	0.631
1	0.561	0.551	0.551

[21] R. P. Feynman, Phys. Rev. **56**, 340 (1939).

the minimum number of critical points but give no upperbound. It is generally easy to find those which are at symmetry points of the Brillouin zone. In most cases investigated thus far,[1-3] these are the only critical points. This might be due to the assumption made in these cases that the forces are of short range. The number of critical points might be expected to increase with the range of the interaction, and their location is then more likely to be at nonsymmetry points of the zone. Rosenstock[17] has devised a method for examining the presence of critical points inside the zone from the behavior of $\omega^2(\mathbf{k})$ on the boundary.

For three dimensions, with short-range forces, when the critical points are at the symmetry points the matrix $\mathbf{M}(\mathbf{k})$, is easy to diagonalize at these points to find the critical frequencies. To find the exact form of the distribution near the critical points x_c, degenerate perturbation theory has to be used to find the eigenvalues in the vicinity of $\mathbf{k}_c$. However, since in three dimensions $G(x)$ does not become infinite at x_c, it might be sufficient to use the right form of $G(x)$ near x_c; the coefficients of the singular part would then be determined by the moment as mentioned above. This would agree with the results of Rosenstock.[17]

PHYSICAL REVIEW VOLUME 96, NUMBER 3 NOVEMBER 1, 1954

Electrical Properties and the Solid-Vapor Equilibrium of Lead Sulfide

ROBERT F. BREBRICK AND WAYNE W. SCANLON
U. S. Naval Ordnance Laboratory, White Oak, Maryland
(Received June 21, 1954)

Natural PbS crystals were exposed to various pressures of sulfur-vapor near 500°C and then quenched. Calculations based on the penetration of p-n junctions gave an interdiffusion constant of 2×10^{-6} cm²/sec at 550°C. The temperature dependence of the Hall coefficient and resistivity for several treated crystals was determined. A forbidden energy gap of 0.37 ± 0.01 ev and an electron to hole mobility ratio of 1.4 was obtained.

I. INTRODUCTION

AT low temperatures the electrical properties of ionic or partially ionic binary compound semiconductors may be attributed to the presence of donor and acceptor levels produced either by foreign atoms or by deviations from stoichiometric proportions. In the absence of appreciable concentrations of foreign atoms the electrical properties are dependent to a large extent upon deviations from stoichiometry. Current statistical models predict that it is possible for all crystalline ionic compounds to show these deviations from stoichiometry.[1] The crystal can exist as a single phase over a range of composition through the inclusion of interstitial atoms and/or vacant lattice sites. While this range of composition is generally too small to be detected chemically it is revealed through variations in electrical properties which are composition sensitive.

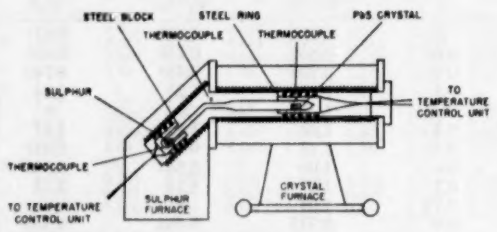

FIG. 1. Apparatus used for treating crystals.

The ability of the crystal to exist as one phase over a range of composition implies some thermodynamic consequences which are important in the preparation of these materials with desired electrical properties. In the case of lead sulfide the equilibrium system, crystal-vapor, has two phases and two components, lead and sulfur. According to the Gibbs phase rule this system possesses two degrees of freedom. Hence when the temperature and vapor pressure of either component are fixed, all of the intensive properties of the system, such as the composition of the crystal and vapor phases, are fixed also. The vapor phase will in general contain two components in a different proportion than the crystal.[2] Therefore, under equilibrium conditions, the crystal can be held at a fixed composition over a range of temperature only by appropriately adjusting the vapor pressure of one of the components or the total pressure. On the other hand, if one of these pressures is held constant and the temperature varied or *vice versa*, then the composition of the crystal will change in general.

In principle, therefore, the composition of a crystalline binary compound can be varied by heat treatments in a controlled atmosphere comprised of its components. In practice, it is necessary to work at those tempera-

[1] R. H. Fowler and E. A. Guggenheim, *Statistical Thermodynamics* (Cambridge University Press, Cambridge, 1949), Chap. XII.

[2] C. Wagner, *Thermodynamics of Alloys* (Addison-Wesley Press, Inc., Cambridge, 1952), p. 67.

tures at which the crystal-vapor equilibrium is established in a reasonable length of time. The determination of this temperature range for lead sulfide and the corresponding vapor pressures of sulfur in equilibrium with the near stoichiometric solid, along with a study of some of the associated electrical properties, are the subject matter of this paper.

II. DIFFUSION RATE IN PbS CRYSTALS

An indication of the time required for the crystal-vapor system to establish equilibrium can be obtained from the times required for an originally *n*-type (excess lead) crystal to become *p*-type (excess sulfur) when exposed to sufficiently high temperatures and sulfur pressures. The necessary composition change will occur first at the crystal surface, and will be subsequently propagated into the crystal interior by a diffusion process. If the crystal is quenched in the early stages of this composition change, it will contain a *p-n* junction which divides its *n*-type interior from its *p*-type exterior. The *p-n* junction can be located electrically by cleaving the crystal and determining the sign of rectification or thermal emf at different points on these cleavage faces. Under certain assumptions the penetration-time data can be used to calculate a diffusion constant and to estimate the time required for the crystal to come to equilibrium with its vapor phase.

The experimental setup is shown in Fig. 1. Two natural PbS crystals with known Hall coefficients and a quantity of sulfur are placed at the opposite ends of a sealed, evacuated quartz tube. The temperatures at the ends of the tube are controlled independently. The crystal temperature is fixed to within $\pm 2°C$, the sulfur temperature to within $\pm 0.5°C$. If the sulfur temperature is lower than that along any other part of the tube, the pressure of sulfur vapor in the tube is the vapor pressure of sulfur at this temperature. The crystals can be quenched at the end of a run by moving away the crystal furnace. In quenching, the crystals cooled to 300°C in about 1 minute and to 200°C in another minute.

In Fig. 2, mid-sections of two crystals run simultaneously are shown to indicate the penetration of a *p-n* junction after sixty minutes. The crystal temperature was 550°C; the sulfur temperature was 123°C. The position of the *p-n* junction was located by a rectification test. An electrolytically sharpened tungsten probe was mounted in a fixed position in the field of view of a comparator microscope, while the PbS crystal was mounted on the micrometer stage. The rectification curve corresponding to a given point on the crystal surface was observed on an oscilloscope screen. Because of the sharp change in the rectification characteristics in crossing the *p-n* junction, its position could be located to a few ten-thousandths of an inch.

If the composition at the crystal-vapor interface is assumed to be constant and the diffusion constant D to

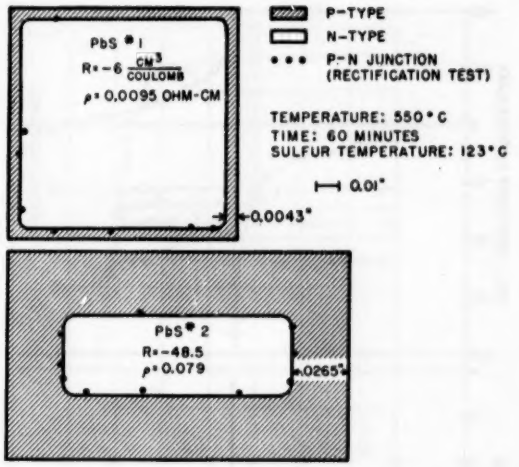

FIG. 2. Cross sections showing the penetration of the *p-n* junction in two crystals of different initial compositions.

be independent of composition, then the appropriate boundary value problem for a crystal of thickness h is

$$\begin{aligned} &\partial C/\partial t = D\partial^2 C/\partial x^2, \\ &C(0,t) = C(h,t) = C_s, \\ &C(x,0) = C_i \quad (0<x<h). \end{aligned} \tag{1}$$

The simplified analysis used here can be carried through with the concentration referring either to that of the lead or sulfide ions. In the following the concentration will be that of the sulfide ions. Then C_s is the constant concentration of sulfide ion at the crystal surface, while C_i is the initial concentration in the crystal. The solution of the boundary value problem is[3]

$$\begin{aligned} \frac{C(x,t)-C_i}{C_s-C_i} &= 1-\frac{4}{\pi}\sum_{\nu=0}^{\infty}\frac{\sin\left[\dfrac{(2\nu+1)x}{h}\right]}{2\nu+1} \\ &\quad\times\exp\left[\frac{(2\nu+1)^2\pi^2 Dt}{h^2}\right] \\ &= S(x,Dt). \end{aligned} \tag{2}$$

Since the initial compositions of the crystals used are such that they are in the exhaustion region at room temperature, the assumption is made that the initial concentration of sulfide ions C_j at a *p-n* junction, and the concentration n of conduction electrons are related by the equation

$$a(C_j-C_i)=n. \tag{3}$$

The constant a is the number of conduction electrons per donor center. By combining Eqs. (2) and (3) the following condition is obtained at the *p-n* junction:

$$n=[a(C_s-C_j)+n]S(x_j,Dt), \tag{4}$$

[3] W. Jost, *Diffusion in Solids, Liquids, Gases* (Academic Press, Inc., New York, 1952), p. 37.

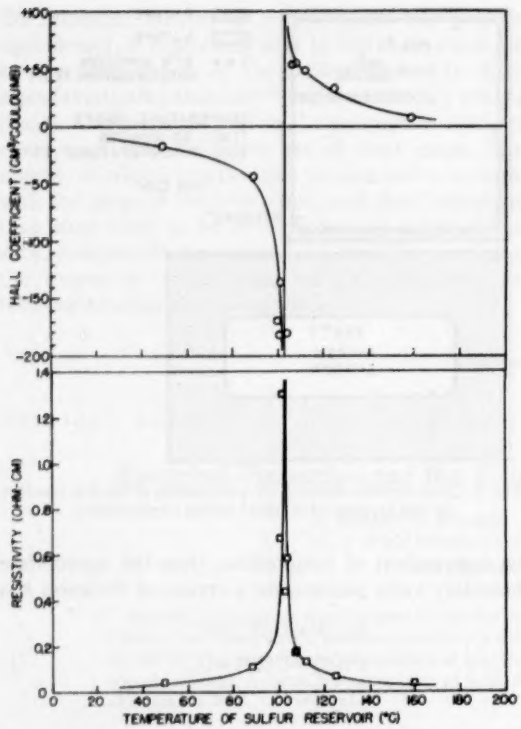

FIG. 3. Room-temperature values of Hall coefficient and resistivity of PbS crystals as a function of sulfur reservoir temperature.

where x_j is the distance of the p-n junction from the crystal surface. This equation contains two unknowns, $a(C_s-C_j)$ and D, which may be evaluated from measurements on two crystals of initially different compositions treated under identical conditions. From the values obtained on the two crystals given in Fig. 2, the diffusion constant obtained is 2×10^{-6} cm²/sec at 550°C. The value of $a(C_s-C_j)$ for the conditions of Fig. 2 is 6×10^{16}.

In subsequent experiments PbS crystals were treated at the somewhat lower temperature of 500°C. It is of interest to estimate the value of the diffusion constant and the time required for a crystal to come essentially to equilibrium with its vapor at this temperature. The results obtained using the value of the diffusion constant at 550°C and the usual equation for the temperature dependence of the diffusion constant,

$$D=D_0\exp[-E/RT], \tag{5}$$

are given in Table I. The lowest value assumed for D_0 is of the order of magnitude expected from elementary derivations.[4] The middle value is of the order of magnitude of the values recently observed in metal alloys. The times given are those required for the concentration change to be 99.8 percent complete in the middle of a 2-mm thick crystal. They are overestimated by the use of the one-dimensional solution of the diffusion equation. In the equilibrium experiments described subsequently diffusion is allowed to proceed for twenty hours.

TABLE I. Estimated rate of approach to equilibrium at 500°C for a 2-mm thick crystal.

D_0	E(kcal)	D(500°)	t(hr)	$\frac{C-C_i}{C_s-C_i}$
2×10^{-4}	7.58	1.5×10^{-6}	5	0.998
2	23	0.81×10^{-6}	9.3	0.998
200	30.3	0.61×10^{-6}	12.3	0.998

The effect of oxidation on the diffusion rate in PbS was also studied. Natural crystals 1.5 to 2.0 mm thick with room-temperature Hall coefficients of $R=-48.5$ cm³/coulomb were used. When such crystals were exposed to sulfur vapor at 500°C for twenty hours with a sulfur reservoir temperature of 124°C, the room temperature values of the Hall coefficient changed to $R=+30$ cm³/coulomb. If, however, the crystal was heated in air for fifteen minutes at 500°C and then exposed to sulfur vapor under the same conditions as above, it was unchanged beneath a surface layer about 0.15 mm thick. The heating in air itself resulted in a surface layer about 0.10 mm thick, beneath which the crystal was unchanged. The surfaces of the oxidized crystals were bluish in color but were less so after exposure to sulfur vapor.

III. EQUILIBRIUM EXPERIMENTS

Small natural crystals of PbS, 2 mm or less thick, were exposed at 500°C to various fixed pressures of sulfur vapor for 20 hours and then quenched to room temperature. The apparatus used is shown in Fig. 1. The sulfur temperatures used ranged from 50°C to 160°C corresponding to a range of sulfur pressures from 3×10^{-5} mm Hg to 3×10^{-1} mm Hg. A thin surface layer, probably formed in the quenching process, could be removed by grinding approximately one mil from each crystal face. The Hall coefficients and resistivities of these crystals were then measured by the standard dc method. The results of such measurements are summarized in Fig. 3 where the room temperature values of the Hall coefficient and resistivity are plotted as a function of the sulfur reservoir temperature. The treatment was reversible in so far that crystals could be changed from n to p and back to n type. As a rule, crystals were used only once. The reproducibility of the treatment was checked by running two or more crystals simultaneously. The electrical properties agreed to within 10 percent in such cases.

The Hall coefficient and resistivity for several crystals treated by this method are shown as a function of temperature from −190°C to 250°C in Fig. 4 (n type) and Fig. 5 (p type). The corresponding curves for two un-

[4] See reference 3, p. 137.

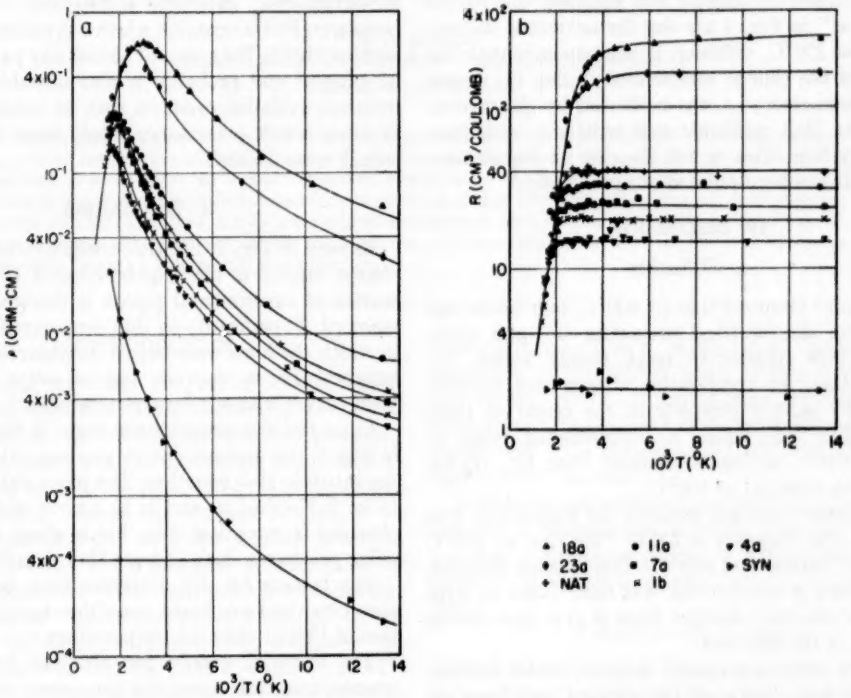

FIG. 4. (a) Resistivity and (b) Hall coefficient for *n*-type PbS crystals as a function of temperature.

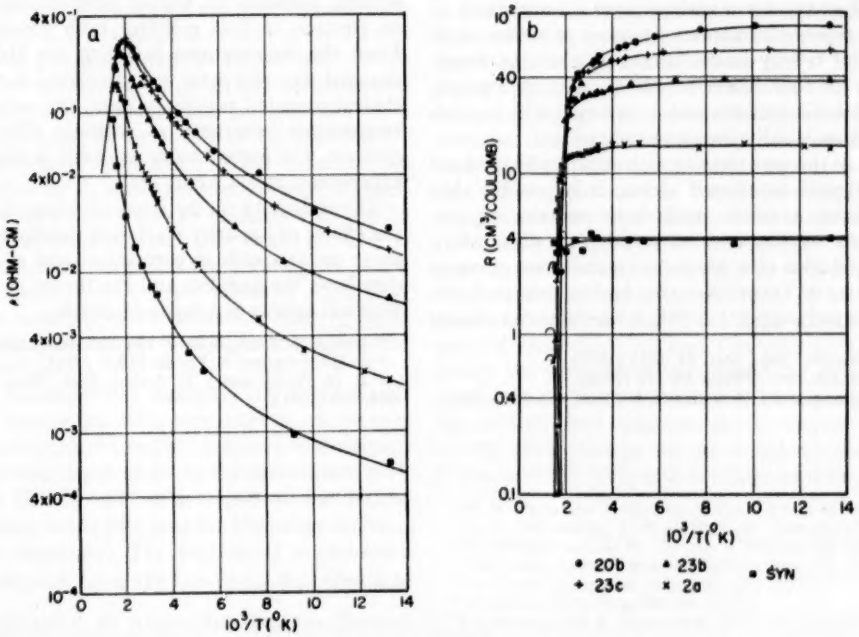

FIG. 5. (a) Resistivity and (b) Hall coefficient for *p*-type PbS crystals as a function of temperature.

treated synthetic crystals are also included. The curves labeled "nat" in Fig. 4 are for the untreated natural PbS. Below 250°C, diffusion is slow enough that the crystals did not change composition during the course of the measurements as was evidenced by the reversibility of the Hall coefficient and resistivity with temperature cycling. This is not the case at higher temperatures as has been pointed out previously.[5]

IV. DISCUSSION

a. Diffusion

Eisenmann[6] observed that at 600°C, four hours was sufficient for the electrical properties of 1-mm thick, synthetic PbS crystals to reach steady values. By assuming that the composition change was between 70 and 99.9 percent complete at the center of these crystals after four hours, a corresponding range of 10^{-7} to 5×10^{-7} cm²/sec is obtained from Eq. (2) for the diffusion constant at 600°C.

The diffusion constant reported for radioactive lead in pressed PbS powders is 2×10^{-11} cm²/sec at 550°C and 5×10^{-11} cm²/sec at 600°C.[7] The average diffusion constant for a p-type powder was three times as large as that for one that changed from p to n type during the course of the diffusion.

Synthetic crystals prepared thus far in this Laboratory, both from fusion of the element and from remelted natural PbS crystals, have a diffusion constant considerably smaller than that found for the natural crystals used here. The synthetic crystals remained unchanged except for a surface layer 0.1 mm thick or less when exposed to various pressures of sulfur vapor at 500°C for twenty hours. However, when run simultaneously for four hours at 850°C, natural crystals, p-type synthetic crystals, and n-type synthetic crystals all reached essentially the same composition.

In view of the experiments with superficially oxidized natural crystals mentioned above, it is possible that the synthetic crystals used here contain oxygen, probably as oxygen ions on sulfide ion sites, which slows the diffusion rate. Since the crystals were grown in sealed quartz or Vycor tubes that had to be heated over 1120°C, the melting point of PbS, it was difficult to insure an oxygen-free, water-free atmosphere. At these temperatures, PbS is unstable relative to oxidation products such as $PbSO_4$, PbO, etc., at almost any partial pressure of oxygen[8] and probably is also unstable relative to incipient oxidation products such as mixed PbS—PbO crystals, which presumably would form if the oxygen supply were limited.

b. Equilibrium

As seen in Fig. 3, the Hall coefficient and resistivity change rapidly in the neighborhood of 104°C, and the scatter of experimental points is therefore more pronounced. Experiments on thin evaporated films of PbS in which the films were heated successively to different temperatures in vacuum and in sulfur atmospheres yield curves with similar characteristics.[9]

From the high-temperature slope of the Hall curves in Fig. 4, the intrinsic energy gap was calculated using the intrinsic Hall equation. The mean value was found to be 0.37 ± 0.01 ev and is in accord with the values obtained from optical data, but is about one-third the value previously derived from Hall data.[10]

The reasons for this difference have been discussed elsewhere[5] and are based upon the change of composition of PbS at elevated temperatures.

The impurity energy gap obtained from the low-temperature Hall curves for the present materials were 0.03 ev for the n-type crystals and 0.001 ev for the p-type crystal.

The Hall coefficients of the p-type crystals, Fig. 5, became negative at higher temperatures, indicating an electron to hole mobility ratio greater than one. From the temperatures at which the Hall coefficient changed sign this ratio was calculated to be 1.4. From the extrapolated resistivity data, the estimated room-temperature resistivity of intrinsic PbS is about 3 ohm-cm. The highest value achieved in the equilibrium experiments was 1.3 ohm-cm.

The resistivity in the impurity range does not show the effects of impurity scattering usually found in nonpolar crystals such as germanium and silicon. Further details on the mobility and the theory of scattering in PbS will appear in a separate article.

[5] W. W. Scanlon, Phys. Rev. **92**, 1573 (1953).
[6] L. Eisenmann, Ann. Physik **38**, 121 (1940).
[7] J. S. Anderson and J. R. Richards, J. Chem. Soc. **1946**, 537.
[8] Bureau of Mines, Bulletin 406, 1937 (unpublished).
[9] H. Hintenberger, Z. Physik **119**, 1 (1942).
[10] E. H. Putley and J. B. Arthur, Proc. Phys. Soc. (London) **B64**, 616 (1951).

Thermal Ionization of Impurities in Polar Crystals. I. Formal Theory

H. D. VASILEFF
Physics Laboratories, Sylvania Electric Products, Bayside, New York
(Received June 28, 1954)

The method of O'Rourke is used to obtain an expression for the thermal ionization rate of an impurity in a polar crystal. The interaction energy of the trapped electron with the optical vibrational modes is assumed to be linear in the normal vibrational coordinates of the lattice. The eigenvalue equations and perturbation of the Born-Oppenheimer adiabatic potential method are employed, leading to a result identical to that of Huang and Rhys. Multiphonon transitions occur only when the configurational constant $S \neq 0$. An approximation of simple form, for the transition rate, can be made only for low temperatures, where the frequency factor s is independent of temperature.

I. INTRODUCTION

IN luminescent materials, the rate of thermal ionization of an impurity center containing a trapped electron is one of the fundamental reaction processes. Afterglow phenomena can in some cases be ascribed to the ejection of an electron from a trap into the empty conduction band, whence the electron returns to an empty luminescent center with the emission of a light quantum. The decay of the afterglow is determined by the rate of ionization P of the traps and a monomolecular decay of emitted light intensity is described by an equation of the form $I=I_0 \exp(-Pt)$. Generally the rate P is assumed to have the form $P=s \exp(-E/kT)$, where s is the frequency factor, of the same order as the vibrational frequency of the lattice, and E is the activation energy corresponding to the depth of the trap below the bottom of the conduction band. It is recognized that calculations of E are quite insensitive to choice of values of s, so that from crystal to crystal one finds values of s ranging from 10^7 to 10^{16} sec^{-1}. Since there appears to be no way of predicting s from known characteristics of the crystal and impurity center, a better understanding of the nature of s is required.

In the analysis of thermostimulated emission, the same expression for P, with s constant, is used. Randall and Wilkins[1] have shown how to calculate trap depths from the temperatures at which glow peaks occur. It is difficult to conclude whether a single glow peak is due to one trap species with discrete values of s and E or whether it is caused by a distribution of traps in depth or s value. Hoogenstraaten[2] is of the opinion that the latter is more likely.

Recently Ellickson[3] has discussed the effect of the variation of energy gap with temperature, on the rate of thermal ionization of traps in phosphors. His assumption that the trap depth varies to the same extent with temperature ($E=E_0-\beta T$) is not justified, but he has called attention to the fact that the frequency factor is temperature dependent. The analysis of a first-order glow curve depends upon the functional dependence of s on the temperature T. Williams and Eyring,[4] in their discussion of metastable levels, obtain from absolute rate theory, $s=AT$. It can be shown by modifying the analysis of Grossweiner,[5] that the William's form of s alters very little the estimated trap depths, provided they are not too shallow.

Several theoretical investigations[6-10] have shown that the rate of thermal ionization of impurities in crystals involves a frequency factor which depends on temperature as well as upon trap depth, so that P has the form

$$P=s(E,T) \exp(-E/kT). \quad (1)$$

Except for the work of Huang and Rhys, these calculations do not apply to traps in polar crystals. However, it will be shown that in this case Eq. (1) gives the general form of P and that $s(E,T)$ decreases with decrease in temperature.

In addition to determining the correct form of $s(E,T)$ it is of interest to examine the problem of multiphonon transitions, which according to Kubo[9] have a high probability of occurring. He ascribes this to the difference of the lattice vibrational frequencies in different electronic states. In the present calculation it will be seen that a multiphonon transition is due fundamentally to a different mechanism, namely, the displacement of the lattice normal coordinates after excitation.

Within the approximation employed the final expression for P reduces identically to that of Huang and Rhys[10] who have omitted all details of its derivation. However, in their theory of light absorption by F centers, they have utilized two constants, S and c, which we shall henceforth term the configurational constant and displacement constant respectively. Lax[11] has utilized these constants in his complete treatment of light absorption by the use of ordered operators and O'Rourke[12] has dealt with the same problem by the use

[1] J. T. Randall and M. H. Wilkins, Proc. Roy. Soc. (London) **A184**, 366 (1945).
[2] W. Hoogenstraaten, J. Electrochem. Soc. **100**, 356 (1953).
[3] R. T. Ellickson, J. Opt. Soc. Am. **43**, 196 (1953).
[4] F. Williams and H. Eyring, J. Chem. Phys. **15**, 289, (1947).
[5] L. I. Grossweiner, J. Appl. Phys. **24**, 1306 (1953).
[6] F. Möglich and R. W. Rompe, Z. Physik **115**, 707 (1940).
[7] Goodman, Lawson, and Schiff, Phys. Rev. **71**, 191 (1947).
[8] D. Curie, J. phys. et radium **12**, 920 (1951).
[9] R. Kubo, Phys. Rev. **86**, 929 (1952).
[10] K. Huang and A. Rhys, Proc. Roy. Soc. (London) **A204**, 406 (1950).
[11] M. Lax, J. Chem. Phys. **20**, 1752 (1952).
[12] R. C. O'Rourke, Phys. Rev. **91**, 265 (1953).

of the density matrix for a harmonic oscillator. It is the latter method, whose effectiveness and simplicity is to be emphasized, that is to be applied to the Huang-Rhys model. In addition, use is made of the "Condon" approximation which becomes exact when the second derivative of the electronic wave function with respect to any normal coordinate vanishes.

II. BASIC EQUATIONS

Following Kubo, we treat the crystal plus impurity center, as a polyatomic molecule, whose Hamiltonian H is given by

$$H=H_R+H_r+V(\mathbf{r},\mathbf{R}), \tag{2}$$

where H_R is the vibratory energy of the crystal nuclei, H_r the energy of the trapped electron, and $V(\mathbf{r},\mathbf{R})$ the interaction of the electron with the nuclei. On the basis of the Born-Oppenheimer[13] adiabatic potential method, we seek solutions of the eigenvalue equations

$$[H_r+V(\mathbf{r},\mathbf{R})]\phi_l(\mathbf{r},\mathbf{R})=E_l(\mathbf{R})\phi_l(\mathbf{r},\mathbf{R}), \tag{3}$$

$$[H_R+E_l(\mathbf{R})]\zeta_{l,n}(\mathbf{R})=E_{l,n}\zeta_{l,n}(\mathbf{R}), \tag{4}$$

where $E_l(\mathbf{R})$ is the adiabatic potential of the lth electronic state and n signifies a vibration state of the nuclei. The wave function of the system in the lth electronic state is thus

$$\Psi_{l,n}(\mathbf{r},\mathbf{R})=\phi_l(\mathbf{r},\mathbf{R})\zeta_{l,n}(\mathbf{R}). \tag{5}$$

The perturbation on the system for a process such as thermal ionization, is determined from the approximate nature of the wave function (5) and is given by

$$H'\Psi_{l,n}=H_R\phi_l\zeta_{l,n}-\phi_l H_r\zeta_{l,n}. \tag{6}$$

Treating the lattice as a continuum and considering the vibratory motion of the nuclei as lattice waves, the Hamiltonian H_R becomes

$$H_R=\tfrac{1}{2}\sum_j^N(\dot{q}_j^2+\omega^2 q_j^2), \tag{7}$$

where q_j is the normal lattice coordinate, ω the angular frequency of vibration, and N the total number of unit cells in the crystal. Since it is generally assumed that the electron interaction with the optical modes is predominant, ω is approximately constant for all modes of vibration in the optical branch. By substituting the corresponding operator in (6), there results

$$H'\Psi_{l,n}=-\hbar^2\sum_j^N\left(\frac{\partial\phi_l(\mathbf{r},\mathbf{R})}{\partial q_j}\cdot\frac{\partial\zeta_{l,n}}{\partial q_j}\right)-\frac{\hbar^2}{2}\sum_j^N\frac{\partial^2\phi_l(\mathbf{r},\mathbf{R})}{\partial q_j^2}\cdot\zeta_{l,n}(\mathbf{R}). \tag{8}$$

[13] M. Born and F. Oppenheimer, Ann. Physik 84, 457 (1927).

From time-dependent perturbation theory, the transition probability from the state (l,n') to a final state (k,n'') in the conduction band is

$$\omega(l,n'\to k,n'')=(2\pi/\hbar)\int_{-\infty}^{+\infty}\rho(E_k)|\langle k,n''|H'|l,n'\rangle|^2\times\delta(E_{k,n''}-E_{l,n'})dE_k, \tag{9}$$

where $\rho(E_k)$ is the state density of the electronic state in the conduction band, and the matrix element is defined as

$$\langle k,n''|H'|l,n'\rangle=\int\Psi_{k,n''}^*H'\Psi_{l,n'}d\mathbf{r}d\mathbf{R}. \tag{10}$$

Thus the total transition probability P is found by averaging (9) over all the initial lattice states n' and summing over all the final n'':

$$P=(2\pi/\hbar)\int_{-\infty}^{+\infty}\rho(E_k)\sum_{n'',n'}p_{n'}|\langle k,n''|H'|l,n'\rangle|^2\times\delta(E_{k,n''}-E_{l,n'})dE_k, \tag{11}$$

where the weighting factor $p_{n'}$ is given by

$$p_{n'}=[\textstyle\sum_{n'}\exp(-E_{l,n'}/kT)]^{-1}\exp(-E_{l,n'}/kT), \tag{12}$$

and the quantities $E_{l,n'}$ and $E_{k,n'}$ are the energies of the system in the initial and final states, respectively.

The thermal ionization rate is found by evaluating expression (11). To this end we shall follow the notation and procedure of O'Rourke. The initial and final state wave functions of the system are

$$\Psi_{l,n'}=\phi_l(\mathbf{r},\mathbf{R})\cdot\zeta_{l,n'}(\mathbf{R}),$$
$$\Psi_{k,n''}=\Omega^{-\frac{1}{2}}\exp(i\mathbf{k}\cdot\mathbf{r})\cdot\zeta_{k,n''}(\mathbf{R}), \tag{13}$$

with the vibrational wave function expressed as a product of N harmonic oscillator wave functions,

$$\zeta_{l,n'}(\mathbf{R})=\prod_j^N X_{n_j'}(q_j')=\prod_j^N|l,n_j'\rangle,$$
$$\zeta_{k,n''}(\mathbf{R})=\prod_j^N X_{n_j''}(q_j'')=\prod_j^N|k,n_j''\rangle. \tag{14}$$

The primes on the coordinates indicate that the normal coordinates for each electronic state are modified by the coupling constants A_j^l and A_j^k for the initial and final states as follows:

$$q_j'=q_j-N^{-\frac{1}{2}}\omega'^2A_j^l=q_j-c_j',$$
$$q_j''=q_j-N^{-\frac{1}{2}}\omega''^2A_j^k=q_j-c_j''. \tag{15}$$

It is assumed that the electronic wave function in the free state is a plane wave independent of the lattice coordinates, and is normalized by the introduction of

the crystal volume Ω. For the present the analytical form of the electronic function for the ground state remains unspecified.

The form of the wave function for a simple harmonic oscillator is given by

$$X_{n_j}(q_j)=\left(\frac{\omega}{\pi\hbar}\right)^{\frac{1}{4}}(2^{n_j}n_j!)^{-\frac{1}{2}}H_{n_j}\left[q_j\left(\frac{\omega}{\hbar}\right)^{\frac{1}{2}}\right]\times\exp\left\{-\frac{1}{2}\left[q_j\left(\frac{\omega}{\hbar}\right)^{\frac{1}{2}}\right]^2\right\}, \quad (16)$$

where the variable q_j and the angular frequency ω correspond to the appropriate electronic state. The connection between the initial state frequency ω' and the final state frequency ω'' is expressed by the phenomenological constant ρ such that $(\omega''-\omega')=\rho\omega'$.

In addition, the system energy is required for each of the two electronic states under consideration; these become

$$E_{k,n''}=\frac{\hbar^2k^2}{2m^*}-\frac{1}{2N}\sum_j^N\frac{(A_j^k)^2}{\omega''^2}+\sum_j^N(n_j''+\tfrac{1}{2})\hbar\omega'',$$
$$E_{l,n'}=-E_l-\frac{1}{2N}\sum_j^N\frac{(A_j^l)^2}{\omega'^2}+\sum_j^N(n_j'+\tfrac{1}{2})\hbar\omega', \quad (17)$$

where $(\hbar^2k^2/2m^*)$ and $-E_l$ are the electron energies in the conduction band (with m^* the effective electron mass) and in the trapped state, respectively, in the absence of electron interaction with the lattice vibrational modes.

Evaluation of Transition Probability

It is convenient to express Eq. (11) in a different manner, by the introduction of the integral representation for the Dirac delta function

$$\delta(\phi)=(1/2\pi\hbar)\int_{-\infty}^{+\infty}dt\exp(it\phi/\hbar),$$

so that P becomes

$$P=(1/\hbar^2)\int_{-\infty}^{+\infty}\rho(E_k)P'dE_k, \quad (18)$$

with

$$P'=\int_{-\infty}^{+\infty}dt\exp(it\omega_{k,l})G_{k,l}(t), \quad (19)$$

$$G_{k,l}(t)=\sum_{n'',n'}p_{n'}|\langle k,n''|H'|l,n'\rangle|^2\times\exp[it\sum_j^N(n_j''+\tfrac{1}{2})\omega''-(n_j'+\tfrac{1}{2})\omega'], \quad (20)$$

$$\hbar\omega_{k,l}=(\hbar^2k^2/2m^*)+E_l^*,$$

$$E_l^*=E_l-\frac{1}{2N}\sum_j^N[(A_j^k)^2/\omega''^2-(A_j^l)^2/\omega'^2].$$

Since the weight factor (12) may be written[14] as the product of the Boltzmann factors for each oscillator we have

$$p_{n'}=\prod_j^N 2\sinh(\beta'/2)\exp\{-(n_j'+\tfrac{1}{2})\beta'\},$$

with $\beta'=(\hbar\omega'/kT)$, then the function $G_{k,l}(t)$ becomes

$$G_{k,l}(t)=\sum_{n'',n'}2\sinh(\beta'/2)\exp[-(n_j'+\tfrac{1}{2})\lambda_j']\times\exp[-(n_j''+\tfrac{1}{2})\mu_j'']|\langle k,n''|H'|l,n'\rangle|^2, \quad (21)$$

with $\lambda_j'=i\omega' t+\beta'$ and $\mu_j''=-i\omega'' t$. From Eq. (8) we obtain for the matrix element of the perturbation due to the ith vibrational mode:

$$\langle k,n''|H_i'|l,n'\rangle=\int_{\mathbf{R}}\zeta_{k,n''}^*(\mathbf{R}'')\left[-\hbar^2\int_{\mathbf{r}}\phi_k^*(\mathbf{r},\mathbf{R}'')\cdot\frac{\partial\phi_l(\mathbf{r},\mathbf{R}')}{\partial q_i}d\mathbf{r}\right]\frac{\partial\zeta_{l,n'}}{\partial q_i}(\mathbf{R}')d\mathbf{R}+\int_{\mathbf{R}}\zeta_{k,n''}^*(\mathbf{R}'')\left[-\frac{\hbar^2}{2}\int_{\mathbf{r}}\phi_k^*(\mathbf{r},\mathbf{R}'')\cdot\frac{\partial^2\phi_l(\mathbf{r},\mathbf{R}')}{\partial q_i^2}d\mathbf{r}\right]\cdot\zeta_{l,n'}(\mathbf{R}')d\mathbf{R}. \quad (22)$$

Within our approximation $\phi_k^*(\mathbf{r},\mathbf{R}'')$ is independent of the lattice coordinates, and we can apply the "Condon" approximation if the first derivative of the ground-state electronic wave function varies slowly with lattice coordinates $\mathbf{R}$. Under this condition the second term on the right-hand side may be ignored since $\partial^2\phi_l(\mathbf{r},\mathbf{R}')/\partial q_i^2$ is approximately zero, and Eq. (22) becomes

$$\langle k,n''|H_i'|l,n'\rangle=M_i(k,l)\int\zeta_{k,n''}[\mathbf{R}'')\cdot\frac{\partial\zeta_{l,n'}(\mathbf{R}')}{\partial q_i}d\mathbf{R},$$

where

$$M_i(k,l)=-\hbar^2\int_{\mathbf{r}}\phi_k^*(\mathbf{r},\mathbf{R}'')\frac{\partial\phi_i(\mathbf{r},\mathbf{R}')}{\partial q_i}d\mathbf{r}.$$

Substituting the vibrational wave functions (14), squaring the modulus and the summing over all vibrational modes, we obtain

$$|\langle k,n''|H'|l,n'\rangle|^2=\sum_i^N|M_i(k,l)|^2\left|\int_{-\infty}^{+\infty}X_{n_i''}(q_i'')\frac{\partial}{\partial q_i}X_{n_i'}(q_i')dq_i\right|^2\times\prod_{j\neq i}^N\left|\int_{-\infty}^{+\infty}X_{n_j''}(q_j'')X_{n_j'}(q_j')dq_j\right|^2=\sum_i^N|M_i(k,l)|^2\left|\left\langle n_i''\left|\frac{\partial}{\partial q_i}\right|n_i'\right\rangle\right|^2\prod_{j\neq i}^N|\langle n_j''|n_j'\rangle|^2, \quad (23)$$

[14] J. Mayer and M. Goeppert-Mayer, *Statistical Mechanics* (John Wiley and Sons, Inc., New York, 1940).

the quantity required in expression (21), which may be simplified to

$$G_{k,l}(t)=\sum_{i}^{N}|M_i(k,l)|^2 H_i\prod_{j\neq i}^{N}G_j, \tag{24}$$

where

$$H_i=\sum_{n_i'',n_i'}\left|\left\langle n_i''\left|\frac{\partial}{\partial q_i}\right|n_i'\right\rangle\right|^2 2\sinh(\beta'/2)$$
$$\times\exp\{-(n_i'+\tfrac{1}{2})\lambda_i'\}\exp\{-(n_i''+\tfrac{1}{2})\mu_i''\},$$
$$G_j=\sum_{n_j'',n_j'}|\langle n_j''|n_j'\rangle|^2\,2\sinh(\beta'/2)$$
$$\times\exp\{-(n_j'+\tfrac{1}{2})\lambda_j'\}\exp\{-(n_j''+\tfrac{1}{2})\mu_j''\}.$$

The procedure followed by both Kubo and O'Rourke in evaluating the matrix elements in H_i and G_j, was to make use of the Slater sum,

$$\rho(x,x'|\xi)=\sum_{n=0}^{\infty}\frac{e^{-(n+\frac{1}{2})\xi}}{\pi^{\frac{1}{2}}\cdot 2^n\cdot n!}H_n(x)H_n(x')\exp\{-\tfrac{1}{2}(x^2+x'^2)\}$$
$$=(2\pi\sinh\xi)^{-\frac{1}{2}}\exp\{-\tfrac{1}{4}[(x+x')^2\tanh(\tfrac{1}{2}\xi)+(x-x')^2\coth(\tfrac{1}{2}\xi)]\},$$

where $H_n(x)$ are the Hermite polynomials. By the use of the vibrational wave function (16), it is easily seen that

$$G_j=2\sinh(\beta'/2)\sum_{n_j'',n_j'}\frac{\alpha''\exp[-(n_j''+\frac{1}{2})\mu_j'']}{(\pi^{\frac{1}{2}}2^{n_j''}n_j''!)}\cdot\frac{\alpha'\exp[-(n_j'+\frac{1}{2})\lambda_j']}{(\pi^{\frac{1}{2}}2^{n_j'}n_j'!)}\int_{-\infty}^{\infty}\int dq_j d\bar{q}_j$$
$$\times H_{n_j''}(\alpha''q_j'')H_{n_j''}(\alpha''q_j'')\exp\{-\tfrac{1}{2}\alpha''^2(q_j''^2+\bar{q}_j''^2)\}H_{n_j'}(\alpha'q_j')H_{n_j'}(\alpha'\bar{q}_j')\exp\{-\tfrac{1}{2}\alpha'^2(q_j'^2+\bar{q}_j'^2)\}$$
$$=2\alpha'\alpha''\sinh(\beta'/2)\int_{-\infty}^{\infty}\int dq_j d\bar{q}_j\rho(\alpha''q_j'',\alpha''\bar{q}_j''|\mu_j'')\rho(\alpha'q_j',\alpha'\bar{q}_j'|\lambda_j')$$
$$=\frac{2\alpha'\alpha''}{2\pi}\sinh(\beta'/2)[\sinh\lambda_j'\sinh\mu_j'']^{-\frac{1}{2}}\int_{-\infty}^{\infty}\int dq_j d\bar{q}_j\exp\{-\tfrac{1}{4}[(q_j''+\bar{q}_j'')^2\alpha''^2\tanh(\tfrac{1}{2}\mu_j'')$$
$$+(q_j''-\bar{q}_j'')^2\alpha''^2\coth(\tfrac{1}{2}\mu_j'')]\}\exp\{-\tfrac{1}{4}[(q_j'+\bar{q}_j')\alpha'^2\tanh(\tfrac{1}{2}\lambda_j')+(q_j'-\bar{q}_j')\alpha'^2\coth(\tfrac{1}{2}\lambda_j')]\},$$

where $\alpha''^2=\omega''/\hbar$ and $\alpha'^2=\omega'/\hbar$. The integral[15] occurring in the above expression has already been evaluated by O'Rourke so that it reduces to

$$G_j=\frac{2\alpha'\alpha''}{2\pi}\sinh(\beta'/2)[\sinh\lambda_j'\sinh\mu_j'']^{-\frac{1}{2}}2\pi(\Lambda_j^2\Omega_j^2)^{-\frac{1}{2}}\exp[-\alpha'^2\alpha''^2(c_j'-c_j'')^2/\Omega_j^2]\cdots, \tag{25}$$

where

$$\Omega_j^2=\alpha''^2\coth(\tfrac{1}{2}\mu_j'')+\alpha'^2\coth(\tfrac{1}{2}\lambda_j'),\quad \bar{\Omega}_j^2=\alpha'^2\coth(\tfrac{1}{2}\mu_j'')+\alpha''^2\coth(\tfrac{1}{2}\lambda_j'),$$
$$\Lambda_j^2=\alpha''^2\tanh(\tfrac{1}{2}\mu_j'')+\alpha'^2\tanh(\tfrac{1}{2}\lambda_j'),\quad \bar{\Lambda}_j'=\alpha'^2\tanh(\tfrac{1}{2}\mu_j'')+\alpha''^2\tanh(\tfrac{1}{2}\lambda_j').$$

The last-defined quantity $\bar{\Lambda}_j^2$ occurs in the evaluation of H_i which may be carried out in the same manner.

$$H_i=2\sinh(\beta'/2)\sum_{n_i'',n_i'}\frac{\alpha''\exp[-(n_i''+\frac{1}{2})\mu_i'']}{(\pi^{\frac{1}{2}}2^{n_i''}n_i''!)}\cdot\frac{\alpha'\exp[-(n_i'+\frac{1}{2})\lambda_i']}{(\pi^{\frac{1}{2}}2^{n_i'}n_i'!)}\int_{-\infty}^{\infty}\int dq_i d\bar{q}_i$$
$$\times H_{n_i''}(\alpha''q_i'')H_{n_i''}(\alpha''\bar{q}_i'')\exp\{-\tfrac{1}{2}\alpha''^2(q_i''^2+\bar{q}_i''^2)\}\frac{\partial}{\partial q_i}\frac{\partial}{\partial\bar{q}_i}H_{n_i'}(\alpha'q_i')H_{n_i'}(\alpha'\bar{q}_i')\exp\{-\tfrac{1}{2}\alpha'^2(q_i'^2+\bar{q}_i'^2)\}$$
$$=2\alpha'\alpha''\sinh(\beta'/2)\int_{-\infty}^{\infty}\int dq_i d\bar{q}_i\varphi(\alpha''q_i'',\alpha''\bar{q}_i''|\mu_i'')\frac{\partial}{\partial q_i}\frac{\partial}{\partial\bar{q}_i}\rho(\alpha'q_i',\alpha'\bar{q}_i'|\lambda_i')$$
$$=\frac{2\alpha'\alpha''}{2\pi}\sinh(\beta'/2)[\sinh\lambda_i'\sinh\mu_i'']^{-\frac{1}{2}}\int_{-\infty}^{\infty}\int dq_i d\bar{q}_i\exp\{-\tfrac{1}{4}[(q_i''+\bar{q}_i'')^2\alpha''^2\tanh(\tfrac{1}{2}\mu_i'')$$
$$+\alpha''^2(q_i''-\bar{q}_i'')^2\coth(\tfrac{1}{2}\mu_i'')]\}\frac{\partial}{\partial q_i}\frac{\partial}{\partial\bar{q}_i}\exp\{-\tfrac{1}{4}[(q_i'+\bar{q}_i')^2\alpha'^2\tanh(\tfrac{1}{2}\lambda_i')+\alpha'^2(q_i'-\bar{q}_i')^2\coth(\tfrac{1}{2}\lambda_i')]\}.$$

[15] O'Rourke's evaluation of G_j is slightly in error. In his expression the exponent of the exponential contains Ω_j^2 rather than $\bar{\Omega}_j^2$. This does not affect his final result, however.

After evaluating the integral, we obtain

$$H_i=(\alpha'\alpha'')^3[\sinh\lambda_i'\sinh\mu_i''\Lambda_i^2\Omega_i^2]^{-1}\times[(1-\rho)^{-\frac{1}{2}}\sinh\lambda_i'+(1-\rho)^{\frac{1}{2}}\sinh\mu_i'']G_i+[(\alpha'\alpha'')^4/\Lambda_i^2\Omega_i^2](\bar{\Lambda}_i/\bar{\Omega}_i)^2(c_i'-c_i'')^2G_i, \quad (26)$$

where the G_i are the functions defined in Eq. (25). Thus for Eq. (24) we obtain for the product:

$$H_i\prod_{j\neq i}^{N}G_j=\left[(\alpha'\alpha'')^3\{\sinh\lambda_i'\sinh\mu_i''\Lambda_i^2\Omega_i^2\}^{-1}\times\{(1-\rho)^{-\frac{1}{2}}\sinh\lambda_i'+(1-\rho)^{\frac{1}{2}}\sinh\mu_i''\}+\frac{(\alpha'\alpha'')^4}{\Lambda_i^2\Omega_i^2}\left(\frac{\Lambda_i}{\Omega_i}\right)^2(c_i'-c_i'')^2\right]\prod_{j}^{N}G_j=K_i\prod_{j}^{N}G_j. \quad (27)$$

When the displacement constants c_i' and c_i'' are put equal to zero, H_i reduces to the form obtained by Kubo. In the evaluation of K_i, we shall neglect ρ which enters as $O(N^{-1})$. The second term in K_i may be neglected in comparison with the first since the c's are $O(N^{-\frac{1}{2}})$ and the first term is proportional to the angular frequency. Thus using the relation

$$[\sinh\lambda_i'\sinh\mu_i''\Lambda_i^2\Omega_i^2]=4\alpha'^2\alpha''^2\sinh^2[\tfrac{1}{2}(\lambda_i'+\mu_i'')],$$

we obtain

$$K_i=\tfrac{1}{4}\alpha'\alpha''\left\{\frac{(1-\rho)^{-\frac{1}{2}}\sinh\lambda_i'+(1-\rho)^{\frac{1}{2}}\sinh\mu_i''}{\sinh^2[\frac{1}{2}(\lambda_i'+\mu_i'')]}\right\}\simeq\frac{\omega'}{4\hbar}[\coth(\beta'/2)+1]e^{i\omega' t}+\frac{\omega'}{4\hbar}[\coth(\beta'/2)-1]e^{-i\omega' t}. \quad (28)$$

O'Rourke has approximated the second factor in (27) by neglecting terms $O(N^{-2})$ under summation, so that

$$\prod_{j}^{N}G_j=\exp\{-S\coth(\beta'/2)\}\times\exp\{-i\omega' tB\coth(\beta'/2)+S\,\mathrm{csch}(\beta'/2)\cos(\omega' t-\phi)\}, \quad (29)$$

where

$$S=\sum_{i=1}^{N}\tfrac{1}{2}\alpha'^2(c_i''-c_i')^2, \quad B=\tfrac{1}{2}N\rho,$$
$$\sin\phi=i\sinh(\beta'/2), \quad \cos\phi=\cosh(\beta'/2).$$

Thus from Eqs. (19), (24), (27), and (28) we obtain, after dropping primes on the frequency factors,

$$P'=\frac{\omega}{4\hbar}\sum|M_i(k,l)|^2\exp\left\{-S\coth\frac{\beta}{2}\right\}\times[\{\coth(\beta/2)+1\}I_-+\{\coth(\beta/2)-1\}I_+], \quad (30)$$

with the integrals I_- and I_+ given by

$$I_\pm=\int_{-\infty}^{+\infty}dt\exp\left\{-i\omega t\left(B\coth(\beta/2)\pm1-\frac{\omega_{k,l}}{\omega}\right)+S\,\mathrm{csch}(\beta/2)\cos(\omega t-\phi)\right\}$$
$$=\frac{2\pi}{\omega}\exp\{i(y\mp1)\phi\}\sum_{p=-\infty}^{+\infty}\delta(y-p)\frac{1}{2\pi}\int_0^{2\pi}dx\times\exp\{i(y\mp1)x+S\,\mathrm{csch}(\beta/2)\cos x\},$$

where the dimensionless quantity

$$y=(\omega_{k,l}'/\omega)-B\coth(\tfrac{1}{2}\beta),$$

may have any integral value p, with the result that the integrals may be expressed in terms of the modified Bessel functions.

$$I_\nu(z)=(2\pi)^{-1}\int_0^{2\pi}dx\exp\{iyx+z\cos x\}.$$

Using the defining relationships for ϕ given in (29) we find

$$\exp[i(y\pm1)\phi]=\exp[-\tfrac{1}{2}(y\pm1)\beta],$$

so that

$$[\coth(\beta/2)\pm1]\exp[i(y\pm1)\phi]=2(e^\beta-1)^{-1}\exp[-\tfrac{1}{2}(y-1)\beta].$$

Consequently expression P' may be simplified to

$$P'=\frac{\pi}{\hbar}\sum_i|M_i(k,l)|^2\exp\{-S\coth(\beta/2)\}\frac{e^{-\frac{1}{2}(y-1)\beta}}{(e^\beta-1)}\times\sum_{-\infty}^{\infty}\delta(y-p)\left[I_{\nu+1}\left(S\,\mathrm{csch}\frac{\beta}{2}\right)+I_{\nu-1}\left(S\,\mathrm{csch}\frac{\beta}{2}\right)\right].$$

Inserting the quantity P' in Eq. (18), we finally obtain the total rate of thermal ionization P:

$$P=\frac{\pi}{\hbar^3}(e^\beta-1)^{-1}\exp\{-S\coth(\beta/2)\}\times\sum_i\int_{-\infty}^{+\infty}|M_i(k,l)|^2\rho(E_k)dE_k e^{-\frac{1}{2}(y-1)\beta}\times\sum_{-\infty}^{+\infty}\delta(y-p)\left[I_{\nu+1}\left(S\,\mathrm{csch}\frac{\beta}{2}\right)+I_{\nu-1}\left(S\,\mathrm{csch}\frac{\beta}{2}\right)\right]. \quad (31)$$

Integration over the electronic states E_k, in the conduction band, may be replaced by integration over the variable y, by employing the defining relationship for y,

$$y=(\omega_{k,l}/\omega)-B\coth(\tfrac{1}{2}\beta).$$

Thus,

$$\hbar\omega_{k,l}=(\hbar^2k^2/2m^*)+E_i^*=y\hbar\omega+B\hbar\omega\coth(\beta/2), \quad (32)$$

and hence

$$dE_k=\hbar\omega dy,$$

$$\rho(E_k)=(4\Omega m^*/h^2)k=(4\Omega m^*/h^2)(2m^*\omega/\hbar)^{\frac{1}{2}}(y-y_0)^{\frac{1}{2}},$$

where

$$y_0=(E_l^*/\hbar\omega)-B\coth(\beta/2).$$

Since we are interested only in those values of y which correspond to transitions to the conduction band, then y must have a minimum positive integral value larger than or equal to y_0, which may or may not be integral. Since thermal ionization implies a transition to any one of the states in the conduction band, the rate of thermal ionization must be the sum of all such transition probabilities as is given by expression (31). If we now make the Huang-Rhys assumption (contrary to Kubo) that the electronic matrix element $M_i(k,l)$ is an insensitive function of k (or y, which increases by unit steps), then it may be removed from under the sign of integration. Thus we put $k=0$ in $M_i(k,l)$. This procedure is valid if the wavelength $(1/k)$ is large compared with the electron orbit of the ground state. With this approximation, the rate of thermal ionization may be written,

$$P=A(e^\beta-1)^{-1}e^{\frac{1}{2}\beta}\cdot\exp[-S\coth(\beta/2)]$$

$$\times\sum_{p>y_0}^{\infty}(p-y_0)^{\frac{1}{2}}e^{-\frac{1}{2}p\beta}[I_{p+1}+I_{p-1}], \quad (33)$$

where

$$A=\frac{\pi\omega}{\hbar^2}\frac{4\Omega m^*}{h^2}\left(\frac{2m^*\omega}{\hbar}\right)^{\frac{1}{2}}\sum_i|M_i(0,l)|^2.$$

The expression for P is identical with the result, expressed in different notation, of Huang and Rhys who employed a different method of derivation. A further approximation may be made by replacing the summation by an integration over the order p of the Bessel functions, the lower limit of integration being y_0. As yet, however, the integral has not been evaluated. A different approach may be followed by putting in the summation $p=p_0+m$ where p_0 and m are integral. The minimum value of p is then p_0, so that $(p_0-y_0)=\delta$ where $0<\delta\leqslant 1$. Equation (33) becomes

$$P=A(e^\beta-1)^{-1}e^{\frac{1}{2}\beta}\cdot\exp[-S\coth(\beta/2)]e^{-\frac{1}{2}p_0\beta}$$

$$\sum_{m=0}(m+\delta)^{\frac{1}{2}}e^{-\frac{1}{2}m\beta}[I_{p_0+m+2}+I_{p_0+m}]. \quad (34)$$

In evaluating the terms in the summation it is convenient to use the series expansion for the modified Bessel function.

$$I_p(x)=\frac{(x/2)^p}{\Gamma(p+1)}\left[1+\frac{(x/2)^2}{1!(p+1)}+\frac{(x/2)^4}{2!(p+1)(p+2)}\right.$$

$$\left.+\frac{(x/2)^6}{3!(p+1)(p+2)(p+3)}+\cdots\right],$$

where Γ is the gamma function.

III. DISCUSSION

Since the argument of the Bessel functions occurring in the final expression (33) for P is proportional to the configurational constant S, the functions will have nonzero values for all finite integral values of p, greater than y_0, provided S is not zero. Thus, multiphonon transitions occur when the displacement constants c_i'' and c_i', for the final and initial states differ for each vibrational mode. A nonzero value of S corresponds physically to a displacement of the adiabatic potential minimum in configuration space, or to a change in the electron-lattice interaction with excitation. On the other hand, if S is zero, only a single-phonon transition is possible in spite of the fact that the lattice vibrational frequency changes on excitation. This is easily seen as follows. When $S=0$, the Bessel functions, and consequently the ionization rate P, reduce to zero except when p is unity, in which case only a single-phonon transition is possible, since from Eq. (32) we have for $y=1$,

$$E_l^*=\hbar\omega+B\hbar\omega\coth(\beta/2)-(\hbar^2k'^2/2m^*), \quad (35)$$

where k' corresponds to the electronic state in the conduction band, to which the transition has occurred. For such a transition there is a range of permissible values for E_l^*, its maximum value corresponding to a minimum possible value for k'. Thus its maximum value is approximately

$$(E_l^*)_{\max}\simeq\hbar\omega+B\hbar\omega\coth(\beta/2). \quad (36)$$

It may be remarked at this point that the approximation made in the formal theory of neglecting the second term in Eq. (26) has no effect on the preceding argument, since when $S=7$, the definition of S given by Eq. (29) implies that $c_i''=c_i'$, so that the second term in Eq. (26) becomes identically zero. Returning now to Eq. (35) it would appear that when $B\coth(\beta/2)>1$, single phonon transitions would take place from electronic levels (E_l^*) having depths greater than $2\hbar\omega$. However, this argument is not as yet conclusive since the magnitude of the phenomenological constant B is not known. We would expect intuitively that as E_l^* increases, so does B, with the result that for very shallow trap depths, B is also very small. Some idea, as to the magnitude of B may be obtained by comparing the theories of O'Rourke, and Huang and Rhys. The frequency of light absorbed corresponding to a transition from an initial state a to a final state b is given by

$$h\nu=\hbar\omega_{b,a}+p\hbar\omega-B\hbar\omega\coth(\beta/2), \quad \text{(O'Rourke)}$$

$$h\nu=\hbar\omega_{b,a}+p\hbar\omega+B'(\bar{n}+\tfrac{1}{2}), \quad \text{(Huang and Rhus)}$$

where $\bar{n}=(e^\beta-1)^{-1}$.

Thus the relation between O'Rourke's constant B and the Huang-Rhys constant B' is expressed by

$$B=(-B'/2\hbar\omega).$$

On comparing their theoretical result, with Pohl's data on light absorption by F centers in KBr crystals, Huang and Rhys deduce that $B'=-0.1$ ev, so that we would conclude that O'Rourke's dimensionless quantity B would be about unity for this particular case. Thus for the case of ionization of shallow traps we would expect B to be much less than unity, with the result that only at very high temperatures will the condition $B\coth(\beta/2)>1$, be obtained. We may conclude that the condition $S\neq 0$ is the more fundamental reason for multiphonon transitions, being contrary to the conclusion of Kubo that a change in lattice vibrational frequencies ($B\neq 0$) leads to an appreciable probability for a multiphonon transition.

In view of the series expansion for $I_\nu(S\,\mathrm{csch}\beta/2)$, it is possible to simplify the expressions (33) or (34) subject to the condition

$$[\tfrac{1}{2}S\,\mathrm{csch}(\beta/2)]^2\ll p_0,$$

since in this case we need retain only the leading term of the series expansion, and Bessel functions of higher order in the summation may be neglected. Expression (34) for P, then yields

$$P=\frac{AS^{p_0-1}\delta^{\frac{1}{2}}}{2^{p_0-1}\Gamma(p_0)}(e^{\beta}-1)^{-1}e^{\frac{1}{2}\beta}\cdot\exp[-S\coth(\beta/2)]\cdot e^{-\frac{1}{2}p_0\beta}[\sinh(\beta/2)]^{-p_0}. \quad (37)$$

The temperature range for which Eq. (37) is valid is determined by the values of S and p_0, and hence by the nature of the impurity center. Calculations, which will be presented at a later time, indicate that, for interstitials in the cubic form of zinc sulfide, $S=1.2$, $A=2.66\times 10^{15}$ and $p_0=12$ at 300°K (for $B\simeq 0$). These values were obtained on the basis of the Simpson[16] model for interstitials. The value for S is reasonable since it is less than the value $S=16$ obtained by Huang and Rhys for excitation of F centers in NaCl. Here S must be smaller since the electronic wave function is more diffuse and the effective ionic charge is less. Since the condition for the validity of Eq. (37) may be expressed as

$$S^2<4p_0\sinh^2(\beta/2)<4[(E_t^*/\hbar\omega)-B\coth(\beta/2)]\sinh^2(\beta/2). \quad (38)$$

Equation (37) is valid up to 300°K where $(\beta/2)\simeq 1.03$ corresponding to $\omega=6.28\times 10^{13}$ sec^{-1} and where a maximum error of 10 percent occurs. Since Eq. (37) can be expressed in the form of a frequency factor $s(E^*,T)$ times a Boltzmann factor $\exp(-p_0\beta)$, typical values of $s(E^*,T)$ are $s(E^*, 300°\mathrm{K})=2.5\times 10^8$ sec^{-1}, $s(E^*, 75°\mathrm{K})=10^8$ sec^{-1} which are of the correct order of magnitude for values obtained from glow curve and phosphorescent decay measurements on zinc sulfide. However, it is seen that the frequency factor decreases with decrease in temperature, at high temperatures and remains constant at low temperature.

If β is large Eqs. (34) or (37) may be further simplified to

$$P=s(E^*)\exp(-p_0\beta), \quad (39)$$

where

$$s(E^*)=Ae^{-S}S^{p_0-1}\delta^{\frac{1}{2}}/\Gamma(p_0).$$

For interstitials in zinc sulfide, Eq. (39) holds quite well up to 300°K where it is less than the correct value by approximately a factor of 10. Low-temperature measurements on phosphorescent decay times should lead to an estimate of the important factor S. We have been unable to simplify Eq. (33) or Eq. (34) for high temperatures.

IV. CONCLUSIONS

The method of O'Rourke leads in a straightforward manner to the expression obtained by Huang and Rhys, for the thermal rate of ionization of impurities in polar crystals. The use of the integral representation for the Dirac delta function is equivalent to the use of Kubo's generating function. The results indicate that the frequency factor depends both on temperature and trap depth.

The writer would like to express his thanks to Dr. J. Fajans for having initially suggested the investigation of the problem.

[16] J. H. Simpson, Proc. Roy. Soc. (London) **A197**, 269 (1949).

Diffusion of Cadmium, Indium, and Tin in Single Crystals of Silver*†

C. T. Tomizuka and L. Slifkin‡
Department of Physics, University of Illinois, Urbana, Illinois
(Received July 26, 1954)

The diffusion coefficient of cadmium, indium, and tin tracers in single crystals of pure silver has been measured as a function of temperature over the range 592–937°C. The activation energies and frequency factors were determined, yielding $D=0.44\exp(-41\,700/RT)$ for the cadmium tracer, $D=0.41\exp(-40\,630/RT)$ for indium, and $D=0.25\exp(-39\,300/RT)$ cm²/sec for tin. These values are in marked disagreement with the older data. The results of the present work are discussed in terms of Lazarus' theory and Zener's theory. Both theories give fair agreement with the experimental data.

INTRODUCTION

It has long been noted that the activation energy for chemical diffusion, i.e., the diffusion of impurities, is often exceedingly smaller than that for self-diffusion in the matrix metal.[1] A similar difference is seen in the values of the frequency factor. Theoretical efforts have been made in the past either to explain this effect[1,2] or to suggest the re-examination of the experimental results.[3–5] The latter approach finds more justification in view of the questionable accuracy of much of the old data.[6] In the first place, in most of the old experiments there was a concentration gradient which was not negligible and hence could have caused large unidirectional currents of imperfections as are seen in Kirkendall effect. Secondly, most of the experiments were carried out on polycrystalline specimens. As was shown by Fisher,[7] Hoffman and Turnbull,[8] Slifkin, Lazarus, and Tomizuka,[9] and Wajda,[10] diffusion along grain boundaries can mask the volume diffusion, especially at low temperatures. Moreover, the availability in recent years of radioactive isotopes of high specific activity has made it possible to obtain considerably greater accuracy in diffusion measurements than previously.

It thus seems evident that the redetermination of the activation energies and the frequency factors for chemical diffusion is necessary. The work reported here satisfies the following conditions: (1) Experiments were carried out on a pure metal and with an extremely dilute solute concentration, by the use of high specific activity radioisotopes. (2) Carefully grown single crystals were employed. (3) A monovalent face-centered cubic metal was chosen for the matrix crystal for ease of theoretical treatment. (4) The elements to be diffused into the metal were chosen in a systematic manner, as those neighboring the matrix metal in the periodic table. (5) Isotopes of long half-life were used to minimize errors. Silver is seen to be quite convenient as a solvent metal. In addition to the availability of high-purity silver, self-diffusion in pure silver has been studied by three independent groups of investigators[8,9,11] with satisfactory agreement in their results. Moreover, the neighboring elements, cadmium, indium, tin, etc., have isotopes of long half-life.

It is hoped that the present determination of the activation energy and the frequency factor as a function of the atomic number of the diffusing elements will be significant in re-appraising the existing theories and will contribute to an adequate understanding of the mechanisms involved in diffusion in metals. The results of the first stage of this general program of investigation have been reported previously.[12]

EXPERIMENTAL

Specimens were prepared from Handy and Harmon silver of 99.99 percent purity. Single crystals were grown in high-purity graphite crucibles in a vacuum furnace with a temperature gradient.[13] Crystals thus grown were etched, cast in plaster, cut into the form of short cylinders, polished mechanically and electrolytically, and annealed to remove any residual strains. They were then etched again to ascertain their monocrystallinity. Acceptable specimens were electroplated on their ends with high specific activity processed radio-isotopes obtained from Oak Ridge National Laboratory. The following plating baths were found to be practical: cadmium-115 (available as a nitrate in acid solution):

* Supported in part by the U. S. Atomic Energy Commission.
† Based on a thesis submitted by C. T. Tomizuka to the University of Illinois in partial fulfillment of requirements for the degree of Doctor of Philosophy in Physics.
‡ Present address: Department of Physics, University of Minnesota, Minneapolis, Minnesota.
[1] R. P. Johnson, Phys. Rev. **56**, 814 (1939); F. Seitz in *Phase Transformations in Solids*, edited by R. Smoluchowski *et al.* (John Wiley and Sons, Inc., New York, 1951).
[2] G. J. Dienes, Phys. Rev. **89**, 185 (1953).
[3] C. Zener, J. Appl. Phys. **22**, 372 (1951); C. Zener, in *Imperfections in Nearly Perfect Crystals*, edited by W. Shockley *et al.* (John Wiley and Sons, Inc., New York, 1952).
[4] A. S. Nowick, J. Appl. Phys. **22**, 1182 (1951).
[5] A. D. LeClaire, Acta Metallurgica **1**, 438 (1953).
[6] W. Seith and E. Peretti, Z. Elektrochem. **42**, 570 (1936). Tabulations of data are seen in W. Jost, *Diffusion in Solids, Liquids, Gases* (Academic Press, Inc., New York, 1952).
[7] J. C. Fisher, J. Appl. Phys. **22**, 74 (1951).
[8] R. E. Hoffman and D. Turnbull, J. Appl. Phys. **22**, 634 (1951).
[9] Slifkin, Lazarus, and Tomizuka, J. Appl. Phys. **23**, 1032 (1952).
[10] E. S. Wajda, Acta Metallurgica **2**, 184 (1954).
[11] W. A. Johnson, Trans. Am. Inst. Mining Met. Engrs. **143**, 107 (1941).
[12] Sonder, Slifkin, and Tomizuka, Phys. Rev. **93**, 970 (1954); Slifkin, Lazarus, and Tomizuka, J. Appl. Phys. **23**, 1405 (1952).
[13] D. Lazarus and D. R. Chipman, Rev. Sci. Instr. **22**, 211 (1951).

$Cd(NO_3)_2$ radioactive, 0.005N; KOH, to make the bath slightly basic (pH 9–10); KCN, 1.5N; with a cadmium anode. Indium-114 (available as an irradiated unit or as a chloride in acid solution): $In_2(SO_4)_3$ radioactive, 0.01N; Na_2SO_4, 0.1N; with an indium and platinum anode. Tin-113 (available as a chloride in acid solution): $SnCl_2$ radioactive, 0.004N; $NaHC_4H_4O_6$, 12N; NaOH, 0.004N; with a zinc anode. A cyanide bath similar to the cadmium plating bath was initially employed for the plating of indium but was discontinued after three specimens were plated due to the instability of the solution. The current density ranged between 8 and 40 ma/dm^2 and the estimated thickness of the plated layer ranged from 10 A to 100 A.

Electroplated specimens were sealed off in evacuated Vycor tubes and placed in controlled furnaces. Furnaces operating at temperatures below 700°C were controlled by an ac resistance bridge with a platinum winding as one arm. To stabilize the operation of the controllers, a motor-driven switch was inserted to cut off the plate voltage of the thyratron momentarily every one-half minute to quench the arc. The furnaces operating at temperatures above 700°C were controlled by Tag Celectrays. In either case the temperature at the specimen was held constant within ±0.5°C over the entire period of diffusion anneal which ranged from several hours to three months, depending on the temperature.

Sectioning was performed on a precision lathe with a specially designed chuck which permitted a wide adjustment of the specimen orientation relative to the lathe axis. In order to eliminate effects of surface diffusion, a thickness of approximately $6(Dt)^{\frac{1}{2}}$ was removed from the side before sectioning, where D is the estimated diffusion coefficient and t the time of anneal. In sectioning, the thickness of each cut varied from one-half mil to a few mils depending on the depth of penetration of the diffused isotope. The zero setting of the dial indicator used in the measurement of depth was determined by electrically insulating the cutting tool and determining the point of electrical contact between the tool and the surface of the specimen.

Each cut from a specimen was assayed by an immersion-type beta counter (N. Wood Counterlab type B, wall thickness 30 mg/cm^2). The counting vessel consisted of a graduated cylinder, a Teflon adaptor at the bottom of the cylinder which served to expel radioactive acid solution from the dead portion of the counter and to hold the bottom tip of the counter tightly, and a Lucite ring at the open end of the cylinder for the centering of the counter. There were markers on the cylinder, the Teflon adapter and the counter, and adjustments were made before each counting so that the markers all coincided. These precautions were employed to insure reproducibility of the counting geometry. In order to eliminate possible differences in the absorption caused by the variation in the density of the solution from one cut to the other, 10-mil silver wire of commercial purity was added to normalize the density. The assaying of the specimens with Sn^{113} isotope was started at least two days after the specimen was taken out of the furnace so that no part of the diffusion of its radioactive daughter In^{113} (1.7 hours half-life) was measured.

To determine the distance accurately, weights of all cuts except the first one at the original surface were added and the mass equivalent of distance was calculated by assuming that the over-all dial-gauge reading of the distance between the front face of the second cut and the end of the last cut was correct. This factor was used to recalculate the center of each cut, including the first. The dial-gauge reading of the depth of the first cut is less reliable because the surface of the specimen is not ideally flat and the point of electrical contact does not always coincide with the zero-point of mechanical cutting.

The above procedure was repeated throughout the entire series of experiments except for one case, diffusion of In at 613°C, where the sectioning was performed[14] on a specially designed precision grinding machine.[15]

RESULTS

A total of 18 diffusion runs were performed, six on each diffusing element, covering the temperature range 592–937°C. Results plotted in Figs. 1–3 show that the specific activity of cuts falls off exponentially as the square of the penetration depth. This fact, as well as the observations of the results of etching the remainders of

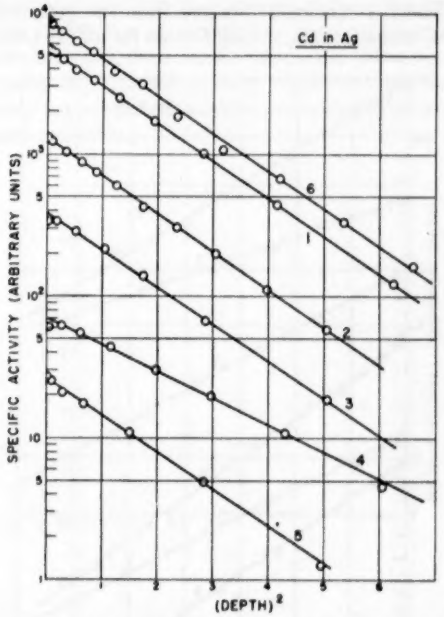

FIG. 1. Penetration curves for diffusion of Cd in Ag. See Table I for the scaling factors for the distance.

[14] Cooperation of Dr. H. Letaw, Jr., is gratefully acknowledged.
[15] Letaw, Slifkin, and Portnoy, Phys. Rev. 93, 892 (1954); also Rev. Sci. Instr. (to be published).

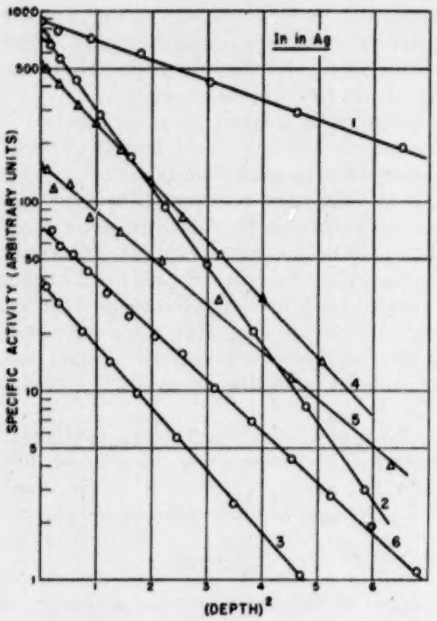

FIG. 2. Penetration curves for diffusion of In in Ag. See Table II for the scaling factors.

the specimens, indicates that there was no observable grain-boundary diffusion taking place due to an accidental recrystallization during the diffusion anneal.

Diffusion coefficients obtained from the penetration curves, temperatures, scaling factors for all the plots in

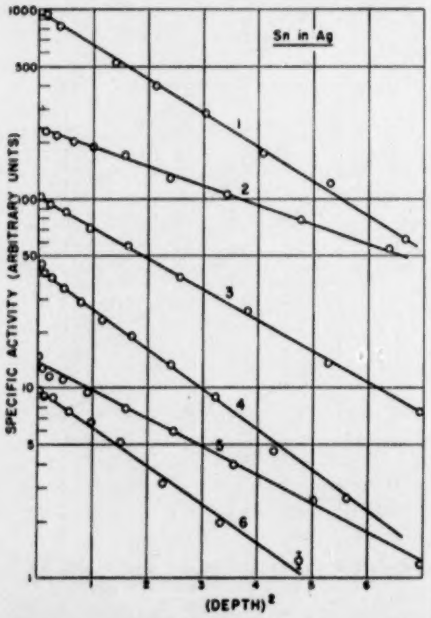

FIG. 3. Penetration curves for diffusion of Sn in Ag. See Table III for the scaling factors.

TABLE I. Diffusion of cadmium in silver.

Curve	Unit of (depth)² (cm²)	Temperature (deg C)	Time (sec)	D (cm²/sec)
1	2.00×10^{-3}	936.8	6.39×10^{4}	1.28×10^{-8}
2	1.29×10^{-3}	862.5	1.25×10^{5}	4.18×10^{-9}
3	6.45×10^{-4}	758.8	3.97×10^{5}	6.74×10^{-10}
4	3.87×10^{-4}	724.0	6.59×10^{5}	3.25×10^{-10}
5	1.29×10^{-4}	651.7	9.47×10^{5}	6.06×10^{-11}
6	2.15×10^{-4}	592.3	7.06×10^{6}	1.25×10^{-11}

Figs. 1–3, and the time of diffusion anneal are given in Tables I–III. Figure 4 represents the data plotted as log$D$ *versus* $1/T$, where T is the absolute temperature. The best least-squares straight lines are given by the equations

$$D_{Cd}=0.44\exp(-41\,700/RT),$$

$$D_{In}=0.41\exp(-40\,630/RT),$$

$$D_{Sn}=0.25\exp(-39\,300/RT),$$

where the subscripts on D indicate the solute and R is the gas constant. Also shown in Fig. 4 are the results of self-diffusion[9] and diffusion of antimony in silver[12] which are given by the equations

$$D_{self}=0.724\exp(-45\,500/RT),$$

and

$$D_{Sb}=0.169\exp(-38\,320/RT).$$

These data and the results of the present measurements are tabulated in Table IV where all D_0's are normalized for the mass number 110 by multiplying by the factor (mass of isotope/110)$^{\frac{1}{2}}$, thus eliminating the difference in jump frequencies due to different isotope masses.

The activation energy H is plotted as a function of the atomic number (i.e., excess valence Z) in Fig. 5. If the value for self-diffusion is excluded, the activation energies are described by the expression: H (in kcal/mole) $=42.8-1.13\,Z$.

Each diffusion coefficient is accurate to about ±2 percent. This precision, the number of measurements and the temperature range determine the activation energy H and the frequency factor D_0, approximately within ±0.5 percent and ±10 percent, respectively.

DISCUSSION OF THE RESULTS

The present results differ radically from the earlier measurements made on the same system by Seith and Peretti.[6] These workers reported the activation energy

TABLE II. Diffusion of indium in silver.

Curve	Unit of (depth)² (cm²)	Temperature (deg C)	Time (sec)	D (cm²/sec)
1	6.45×10^{-4}	936.0	4.17×10^{4}	1.73×10^{-8}
2	1.94×10^{-3}	860.8	8.64×10^{4}	5.89×10^{-9}
3	6.45×10^{-4}	760.0	2.36×10^{5}	8.95×10^{-10}
4	6.45×10^{-4}	715.8	6.05×10^{5}	3.85×10^{-10}
5	3.23×10^{-4}	661.3	1.36×10^{6}	1.30×10^{-10}
6	2.67×10^{-3}	612.7	3.14×10^{5}	3.44×10^{-11}

TABLE III. Diffusion of tin in silver.

Curve	Unit of (depth)^2 (cm^2)	Temperature (deg C)	Time (sec)	D (cm^2/sec)
1	1.29×10^{-3}	937.0	3.96×10^{4}	1.97×10^{-8}
2	6.45×10^{-4}	860.8	9.36×10^{4}	6.20×10^{-9}
3	5.00×10^{-4}	776.0	2.21×10^{5}	1.50×10^{-9}
4	6.45×10^{-4}	722.0	5.83×10^{5}	5.51×10^{-10}
5	2.58×10^{-4}	666.3	1.21×10^{6}	1.51×10^{-10}
6	2.58×10^{-4}	592.3	4.75×10^{6}	2.97×10^{-11}

to be 22.35, 24.4, and 21.4 kcal/mole and D_0 to be 4.9×10^{-5}, 7.3×10^{-5}, and 7.8×10^{-5} cm^2/sec for the diffusion in silver of cadmium, indium, and tin, respectively. In the present work the extreme difference in activation energy and the frequency factor between self-diffusion and chemical diffusion is considerably reduced. The discrepancy between the present results and the older ones cannot be solely due to the existence of grain-boundary diffusion in the old measurements, since the recent determination of the diffusion of antimony in polycrystals of silver[12] agrees with measurements on single crystals except for temperatures below 600°C, where the effect of grain boundaries becomes significant. The existence of still some other short-circuiting paths, as suggested by Zener[3] and Nowick,[4] to explain the low values of the activation energy in the old data seems unwarranted, since in the high-temperature region of the range of measurement the old values of the diffusion coefficient are substantially less than the corresponding values given by the present work. It is possible that the discrepancy was caused by the presence of an appreciable concentration gradient, since the old measurements involved the use of a diffusion couple which consisted of a 2 percent alloy and a pure silver crystal. It is not obvious, however, that the discrepancy is explainable by the flow of unidirectional vacancy currents alone. The possible variation of the diffusion coefficient along the diffusing path, the Kirkendall shift, and the lack of more accurate means of measurement all combined together could very likely have been the reason for the disagreement. Examination of the old data reveals that some of the plots of log$D$ *versus* $1/T$ were not linear but possessed a knee which would subject the accuracy of the measurement itself to some question.

In the light of the present results, it seems imperative that most of the existing data on chemical diffusion which show substantial differences in their values of H and D_0 as compared with the values for self-diffusion be re-examined as a basis for theoretical considerations on chemical diffusion at extremely dilute concentrations. Before accepted, these measurements should be repeated by using high-specific activity radio-isotopes at extremely low solute concentrations and negligible concentration gradients.

TABLE IV. Diffusion in silver.

Isotope	Experimental activation energy (cal/mole)	Frequency factor (normalized) (cm^2/sec)	D_0, Zener (cm^2/sec)	H, Nowick (cal/mole)	Screening constant q(1/A)	D_0, calculated from q, (cm^2/sec)
$_{47}Ag^{110}$	45 500	0.724	0.724	44 900	1.725[a]	...
$_{48}Cd^{115}$	41 700	0.454	0.462	41 720	1.55	0.39
$_{49}In^{114}$	40 630	0.416	0.416	40 770	1.67	0.28
$_{50}Sn^{113}$	39 300	0.255	0.364	40 370	1.70	0.22
$_{51}Sb^{124}$	38 320	0.179	0.331	40 160	1.74	0.16

[a] N. F. Mott, Proc. Cambridge Phil. Soc. 32, 281 (1936).

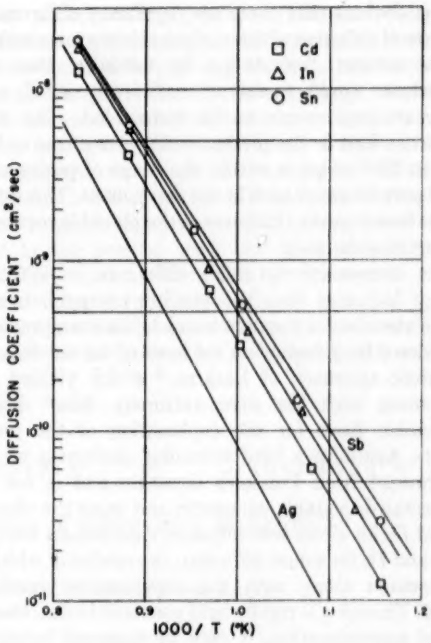

FIG. 4. Diffusion data plotted as log$D$ *versus* $1/T$.

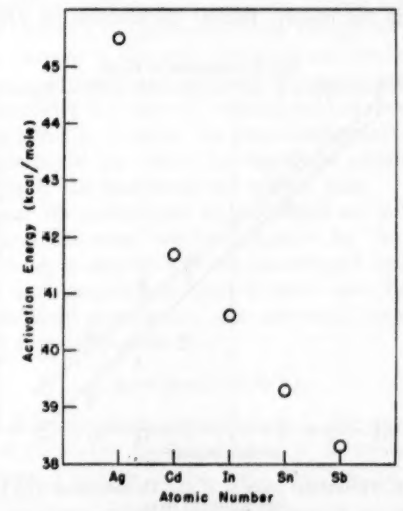

FIG. 5. Activation energy for diffusion in silver plotted as a function of atomic number.

It is obvious that there are significant differences in the rate of diffusion of the various solute atoms and that of the solvent. Speculation by LeClaire[6] that these differences would vanish at sufficiently small solute concentrations seems to be unfounded. The solute concentrations in the present work were of the order of 10^{-4} to 10^{-5} which is within the range of purity of the 99.99 percent silver used in the experiment. This estimation is based on the thickness of the plated layer and the penetration distance.

The comparatively small difference in activation energy indicates that the binding energy between a solute atom and a vacancy is much less than previously considered by Johnson[1] on the basis of the old data. The atomistic approach of Lazarus,[16] which yielded good agreement with the silver-antimony data[12] offers a reasonable basis for the explanation of the present results. Assuming a fixed screening constant q, which is determined from Poisson's equation and is not considered an adjustable parameter and using the observed H and D_0 for silver self-diffusion, calculations are made of H and D_0 for solute diffusion, the results of which are represented along with the experimental results in Fig. 6. Though q is rigidly held constant in the Thomas-Fermi approximation, it may be expected to vary in actual cases as is discussed below. The results of the present work may thus be used as a means of estimating corrections to the screening constant, since all other quantities are known. Lazarus' relation gives $\Delta H/Z$ as a function of q, where $\Delta H = H(\text{solvent}) - H(\text{solute})$ and Z is the excess valence. The experimental values of $\Delta H/Z$ thereby determine q for each solute. These values and the values of D_0 calculated by using these experimentally determined screening constants are listed in Table IV. The value of q varies by 10 percent for Z ranging from 1 to 4, which is consistent with the approximation employed in the theory. Recent calculations by Friedel[17] show that the Thomas-Fermi model is not correct for small odd values of Z. It was shown that in addition to the first valence electrons which are lost to the conduction band, possibly a fraction of a second valence electron of some di- or tetravalent impurities may not be retained in bound states when the matrix is a noble metal. In terms of this view, the present results indicate that such an effect, as in the case of divalent cadmium, results in a smaller value of q. If the case of cadmium be excepted, then the value of q is constant to within ± 2 percent, which gives justification to the model employed in the screening theory. As a further check on the theory of the diffusion in silver, tracers of the elements preceding silver in the periodic table should be studied. A measurement of the diffusion of ruthenium in silver is now under way in this laboratory by using Ru^{103} isotope and the preliminary results indicate the activation energy to be considerably larger than that for self-diffusion in silver. This agrees qualitatively with the screening theory.

According to Zener,[3] D_0 can be estimated from the values of H by the relation

$$D_0 = a^2 \nu \exp(\lambda \beta H / R T_m),$$

where a is the lattice constant, ν the vibrational frequency, λ a numerical constant often taken to be 0.55 for f.c.c. metals, T_m the melting point, and β a constant related to the shear modulus μ by the relation $\beta = d(\mu/\mu_0)/d(T/T_m)$. In very dilute solution all of these quantities except ν and H are those of the solvent metal. An estimation of D_0 was made by approximating ν by the Debye frequency of silver and by using the experimentally determined values of H. The term β was taken to be 0.45, and λ to be 0.54 to normalize the results to the measured values for self-diffusion. The results are given in Table IV along with the estimation of H, which

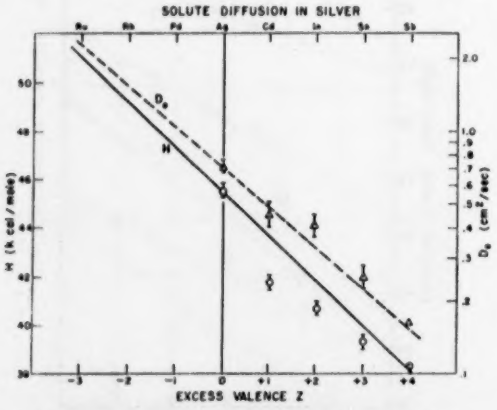

FIG. 6. Theoretical plots of H and D_0 compared with the experimental data.

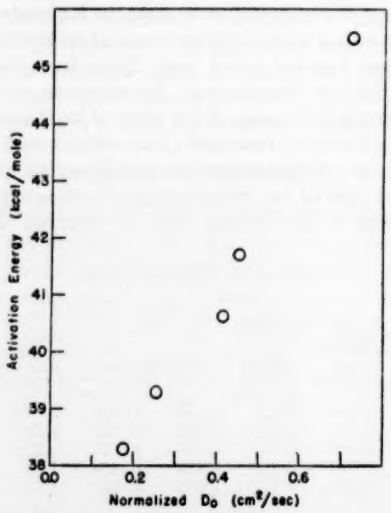

FIG. 7. Plot of H against D_0.

[16] D. Lazarus, Phys. Rev. 93, 973 (1954).
[17] J. Friedel, Phil. Mag. 43, 153 (1952).

is obtained by using only the diffusion coefficients at the highest temperature for all the isotopes and employing Zener's theory as was suggested by the work of Nowick.[4] The values of H and D_0 thus calculated yield excellent agreement with the experimental results for cadmium and indium but significant deviations are seen for tin and antimony. Moreover, they do not reproduce the experimental correlation between H and D_0 which is shown in Fig. 7. Perhaps this discrepancy results from our use of a constant value of ν. It should be noted that Zener's theory shows better agreement with experiment for smaller values of Z where the activation energies predicted by the screening theory deviate appreciably and the situation is reversed for cases of larger Z. It may be that an appreciable portion of the free energy is expended in the changing of configurations other than the straining of the lattice (e.g., the redistribution of the electronic charge) when a relatively large number of extra electrons are attached to the impurity atoms, and that the assumption of Zener's theory is thus violated.

The negative values for the entropy of activation, which were implied by the old data and have been subject to much theoretical speculation, are not observed in the present work and their notion, in all probability, must be discarded for the case of dilute chemical diffusion in f.c.c. metals.

The authors wish to express their gratitude to Dr. F. Seitz and Dr. D. Lazarus for many helpful discussions.

PHYSICAL REVIEW VOLUME 96, NUMBER 3 NOVEMBER 1, 1954

Shapes of Absorption and Emission Lines of Impurities in Solids*

D. L. DEXTER
Institute of Optics, University of Rochester, Rochester, New York, and Solid State Division, Naval Research Laboratory, Washington, D. C.

(Received June 28, 1954)

Existing treatments of band shapes in solids, for the simplest impurity centers, predict Gaussian shape functions. These treatments assume for simplicity that the electronic matrix element is independent of the nuclear wave functions, and that the energy width of the band is negligible compared with the energy of the mid-point of the band. We estimate here the expected magnitude of the effect of correcting these assumptions in typical cases, and find that the emission or absorption band may deviate from a Gaussian by twenty percent or more on the wings.

ABSORPTION and emission spectra are not generally of a simple shape for several possible reasons. In the simplest case, where only a single initial electronic state and a single final electronic state can contribute to the line, where the environment of all the centers is identical, where the transition is far from resonance with the host lattice, and where the configurational coordinate curve for the final electronic state is sufficiently displaced from that for the initial state, an approximate calculation leads to a Gaussian shape function for the absorption or emission spectrum.[1–4] This result depends on the Born-Oppenheimer approximation and on the assumption that the electronic transition probability is independent of the nuclear wave functions, i.e., the wave functions for the lattice vibrations. This assumption is generally made in three parts: (1) the wave function of only one electron is changed during the transition, (2) the electronic matrix element for this one electron is independent of the nuclear wave functions, and (3) the width of the band is negligible as compared with the energy of its mid-point. On configurational coordinate diagrams these assumptions are equivalent to assuming that the electronic transition probability is independent of the configurational coordinate, so that line shapes are determined solely by the geometry of the energy curves.

The purpose of this note is to point out the influence of these approximations upon the calculated line shape. For simplicity and ease of presentation the description will be given in terms of the usual configurational coordinate model (in which the important coordinate is presumably the position of the nearest ions).

In case the ground and excited states are influenced by about the same relative amount[5] by the lattice oscillations, as may be true in a system such as KCl:Tl where both ground and excited state wave functions are relatively compressed, the electronic momentum matrix element is given by

$$\langle \mathbf{p} \rangle = \langle \mathbf{p} \rangle_0 (1 - \Delta R/R), \tag{1}$$

where R is any characteristic length in the wave functions of the center. As the neighbors of the center move and cause a change in the wave function, i.e., in R,

* Research supported in part by U. S. Air Force through the Office of Scientific Research of the Air Research and Development Command.

[1] M. Lax, J. Chem. Phys. **20**, 1752 (1952).
[2] F. E. Williams and M. H. Hebb, Phys. Rev. **84**, 1181 (1951).
[3] R. C. O'Rourke, Phys. Rev. **91**, 265 (1953).
[4] C. C. Klick, Phys. Rev. **85**, 154 (1952).

[5] By the phrase "the same relative amount" we mean the equality of the logarithmic differentials of the damping lengths of the two wave functions.

they also change the energy of the transition between these electronic states by an amount proportional to R^{-2}. Thus the square of the matrix element, which determines transition probabilities, is

$$\langle \mathbf{p} \rangle^2 = \langle \mathbf{p} \rangle_0^2 (1 + \Delta E/E). \tag{2}$$

In the event that the excited state wave function is so diffuse that it is relatively uninfluenced by the vibrations of the nearest neighbors, as is probably the case with the F center, for example, most of the variation in the matrix element will occur because of variations in the ground-state wave function. For the sake of definiteness, let us consider transitions between a $1s$ and a $2p$ state, for which the momentum matrix element is proportional to

$$(a\alpha)^{\frac{1}{2}}/(a+\alpha)^4,$$

where α and a are the damping lengths in the exponentials of the $1s$ and $2p$ wave functions, respectively. Expanding, we find

$$\langle \mathbf{p} \rangle = \langle \mathbf{p} \rangle_0 \left\{ 1 + \Delta\alpha \left(\frac{3}{2\alpha} - \frac{4}{a+\alpha} \right) \right\}. \tag{3}$$

As the neighbors move and cause a change in the $1s$ wave function, its energy likewise changes, and the change in the energy of the transition is $\Delta E = -(2/\alpha)\Delta\alpha |E_{1s}|$, and thus the square of the matrix element is given by

$$\langle \mathbf{p} \rangle^2 = \langle \mathbf{p} \rangle_0^2 \left\{ 1 - \frac{\Delta E}{E} \left[\frac{E}{|E_{1s}|} \left(\frac{3}{2} - \frac{4}{1+a/\alpha} \right) \right] \right\}. \tag{4}$$

The quantity in square brackets is of the order of plus or minus one-tenth; in the case of an isolated atom, the ratio a/α is 2, $|E/E_{1s}|$ is $\frac{3}{4}$, and the coefficient of $\Delta E/E$ is $-\frac{1}{2}$. In actual cases the ratios a/α and $|E/E_{1s}|$ will not be exactly 2 and $\frac{3}{4}$; for the F center in NaCl perhaps better values are 1.5 and 0.8,[6] so that the coefficient of $\Delta E/E$ is $+0.08$.

An absorption band arises from a summation of the contributions from one electronic transition and all possible nuclear transitions. Since the integrated absorption cross section for each individual absorption line is proportional to $\langle \mathbf{p} \rangle^2/E$, the absorption band will not in general be a Gaussian $G(E)$, but rather a function of the form

$$\sigma(E) = E^n G(E), \tag{5}$$

where n may take different values in the various cases mentioned above. For a system such as that discussed in leading to Eq. (2), n will have the value zero because of the cancellation of the effects arising from the magnitude of the matrix element and the energy. In the case of Eq. (4), however, n has the value

$$-1 - \frac{E}{|E_{1s}|} \left(\frac{3}{2} - \frac{4}{1+a/\alpha} \right),$$

or about -1.1 and -0.9 for the two models mentioned after Eq. (4). Thus it appears that at least a small amount of long-wavelength tail on the absorption band may usually be expected.

In emission, on the other hand, the exponent n must be increased by two in each case, because of the $\langle p \rangle^2 E$ dependence of the spontaneous emission probability. (In referring to the emission band shape we shall mean the *number* of photons, rather than the energy, emitted as a function of energy.) Thus for the case treated first, an E^2 factor modifies the Gaussian, and for the other two cases, an approximately linear factor. (It is interesting to note that an approximate mirror-image relation exists between emission and absorption in the latter two cases.)

In typical impurity centers the half-width of a band may be one-tenth of the energy of its mid-point, so that the emission or absorption band may deviate from a Gaussian by twenty percent or more on the wings. This circumstance makes the common practice of analyzing these spectra into sums of Gaussians of questionable significance.

The writer is indebted to Dr. C. C. Klick for interesting discussions on this material.

[6] D. L. Dexter, Phys. Rev. **83**, 435 (1951).

Production and Bleaching of Color Centers in X-Rayed Alkali Halide Crystals*

I. L. MADOR,† R. F. WALLIS, M. C. WILLIAMS, AND R. C. HERMAN
Applied Physics Laboratory, The Johns Hopkins University, Silver Spring, Maryland

(Received July 23, 1954)

The x-ray production and optical and thermal bleaching of color centers in NaCl and LiF have been studied quantitatively in regions of substantially uniform concentration, by making optical absorption measurements in a direction perpendicular to the axis along which the crystals were x-rayed. At room temperature F center growth rate for short x-ray exposures is found to be proportional to the rate of absorption of x-rays. For long exposures the rate of growth of the F band increases greatly near the x-rayed surface. Large M band growth accompanies this increased F band growth. The rate of bleaching of F centers by F light in NaCl has been studied at room temperature for low concentrations where the light absorption is nearly uniform along the light path. Differential equations describing the rates of excitation of F center electrons to the conduction band and the trapping of conduction electrons by negative ion vacancies and holes have been integrated under special conditions. The results are found to be consistent with the experimental data. The rate of thermal bleaching of F centers in NaCl has been studied at temperatures up to 150°C. It has not been found possible to analyze the data in terms of a mechanism involving trapping of conduction electrons by negative ion vacancies and holes. The results of several qualitative experiments to investigate the possible formation of vacancies during x-raying are presented.

I. INTRODUCTION

THE nature and interrelation of the various color centers in alkali halide crystals are fairly well established. However, a detailed understanding of the processes of the formation and decay of color centers appears to be lacking. In part, this is a result of insufficient knowledge of such parameters as describe the initial state of the crystal in terms of single and paired vacancies, impurity content, and mechanical strain. In part, the apparent complexity of the processes requires models that cannot be adequately tested by experimental data presently available. The data obtained on x-rayed crystals has been qualitative rather than quantitative, as a consequence of the fact that most of the optical absorption measurements have been made along a path of nonuniform coloration.

This inhomogeneity arises from the attenuation of the x-ray beam with increasing depth in the crystal. The greatest coloration is at the front face of the crystal, and the concentration gradient depends on the energy distribution in the x-ray beam and the stopping power of the crystal. Measurement of color center concentration by optical absorption has generally been made along the same axis as that of the x-ray beam, thereby giving an integrated value of the absorption through the crystal depth. However, quantitative absorption measurements can be obtained by choosing the direction of the optical absorption light path to be perpendicular to the axis of the x-ray beam. If the light beam is sufficiently narrow, the segment of the crystal observed will be essentially homogeneous in color center concentration. This technique has been used to investigate the growth of color centers by x-ray irradiation and their thermal and optical decay. It appears possible to reduce the apparent complexity of these processes by making a quantitative study of segments having a uniform color center concentration.

II. EXPERIMENTAL

The alkali halide crystals were obtained in various lots from the Harshaw Chemical Company. They were cleaved to 1.5 cm×1.5 cm and to various thicknesses. So-called "thick" and "thin" crystals were ~0.8 cm and less than 0.1 cm, respectively, in the dimension through which the optical absorption was measured. A Picker-Waite diffraction unit with a Machlett tube was employed for the x-ray coloration. The accelerating voltages were in the 30 to 50 kv range, and voltage fluctuations were reduced by a Sola transformer. The x-ray tube had a molybdenum target and beryllium windows 0.5 mm thick, located 2.5 cm from the focal spot. The crystals were mounted ~4 cm from one Be window. The optical absorption measurements were made on a Beckman Model DU spectrophotometer.

The "thick" crystals were x-rayed and the optical density measured in the same brass holder shown schematically in Fig. 1(a). This simplified the problem of handling the crystal during x-raying and transferring to the spectrophotometer in the dark, a precaution taken to avoid optical bleaching. The "thin" crystals were placed between two thicker crystals of the same alkali halide, and the sandwich was clamped between two brass plates. The purpose of the thicker crystals was to eliminate shadows caused by the brass plates during x-raying. For the optical absorption measurements the "thin" crystals were transferred to the holder employed for the "thick" crystals. The holder and crystal sample were mounted in the Beckman spectrophotometer as shown in Fig. 1(b). The crystal was moved perpendicular to the light path by a micrometer screw and absorption readings were taken about every half millimeter. Reproducibility of positioning was

* This work was supported by the Bureau of Ordnance, Department of the Navy.

† Present address: Research Laboratories, National Distillers Products Corporation, Cincinnati, Ohio.

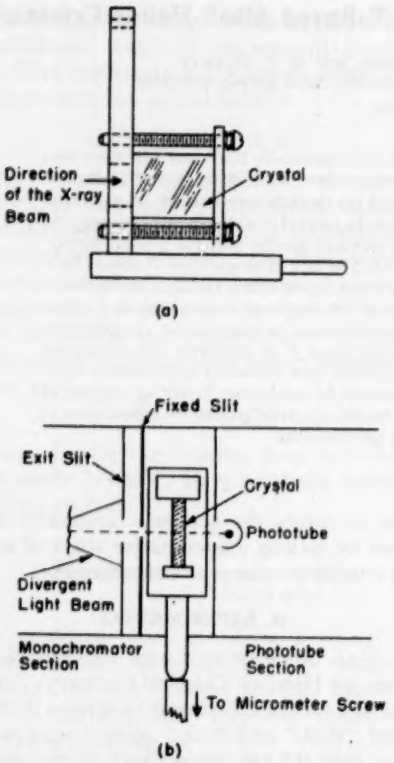

FIG. 1. (a) Crystal holder for x-raying and measuring the optical absorption of alkali halide crystals. (b) Crystal holder mounted in the Beckman spectrophotometer.

assured to $\sim\pm 0.001$ cm by observing the micrometer reading, for which transmission was 50 percent, as the leading edge of the front post passed the optical beam. Since the beam from the exit slit of the Beckman spectrophotometer is divergent, an additional 0.035-cm wide fixed slit was mounted between the variable slit and the crystal. For a Beckman slit of ~ 0.01 cm the width of the beam passing through the crystal was ~ 0.04 cm. All absorption values reported here are $\log_{10}$ of the ratio of the transmission before coloration to that after. Crystals used more than once were bleached of all coloration by heating in an oven at 350°C for two hours.

Optical bleaching of NaCl was accomplished in the spectrophotometer at 464 mμ, the frequency of the F band maximum, with the variable slit set at 1 mm, giving a spectral band width of ~ 35 mμ. After x-raying, and after each bleaching period, about five minutes was allowed for the decay of F' centers before the optical absorption was measured. The total bleaching light flux incident on the crystal was measured with an RCA 929 photocell and found to be ~ 37 μw/cm² or 10^{14} quanta/(cm² sec) on the basis of the calibration data of the manufacturer. Various bleaching light intensities were obtained by placing neutral filters in front of the crystal. The measuring light had a spectral band width of ~ 5 mμ and a flux of ~ 0.6 μw/cm². The bleaching power of the measuring light was negligible, and therefore was neglected in all of the present experiments.

For the study of thermal decay a forced air oven was built around the crystal holder, between the monochromator and detector sections of the spectrophotometer. Oven temperatures were maintained to ± 1°C by a Celectray potentiometer type controller with a thermocouple sensing element. A dummy crystal with another thermocouple imbedded in it was clipped to the back plate of the crystal holder to monitor the temperature.

The optical absorption experiments reported here concerning α and β bands in KI crystals were made at 5° and 78°K in a low-temperature cryostat previously described.[1] The optical absorption measurements in this case were made along the same axis as that of the x-ray coloring beam, and the results are therefore only qualitative.

III. GROWTH OF F CENTERS IN NaCl AND LiF

A. Short X-Ray Exposures

The mechanism for the formation of F centers in alkali halides by x-ray irradiation is not clearly understood.[2] In the absence of a clearly defined model upon which to base calculations it seemed worth while to investigate the applicability of simple relationships between the rate of formation of F centers and the rate of x-ray absorption. For short times for which saturation effects can be neglected, the simplest assumption is that the local rate of production of F centers is proportional to the local rate of absorption of x-rays, as given by the equation

$$(dn_F/dt)_x = -adJ(x)/dx, \tag{1}$$

where $J(x)$ is the intensity of the x-ray beam at depth x in the crystal, a is a constant, and n_F is the concentration of F centers at x. To test Eq. (1) the following calculations were made to determine as a function of depth in the crystal the relative energy absorption per cm³ per sec, which is equal to $-dJ(x)/dx$.

The intensity $J(x,\lambda)$ of a monochromatic x-ray beam of wavelength λ at any depth of penetration x in a crystal is

$$J(x,\lambda) = J_0(\lambda)e^{-\mu x}, \tag{2}$$

where $J_0(\lambda)$ is the energy flux per unit area incident on the crystal face and μ the linear x-ray absorption coefficient of the absorbing crystal.

The unfiltered spectral output of an x-ray tube is not monochromatic but consists of a continuum with characteristic lines superimposed upon it. In this calculation the contribution of the characteristic Mo x-ray lines is neglected. The wavelength distribution of the

[1] W. H. Duerig and I. L. Mador, Rev. Sci. Instr. 23, 421 (1952).
[2] F. Seitz, Revs. Modern Phys. 26, 7 (1954).

continuous x-rays as given theoretically by Kramers[3] and determined empirically by Kuhlenkampf[4] is of the form

$$J_0(\lambda)=D_0Z\lambda^{-2}(\lambda_0^{-1}-\lambda^{-1}), \tag{3}$$

where $J_0(\lambda)$ is the intensity at wavelength λ, D_0 is a constant related to the efficiency of x-ray production, Z is the atomic number of the x-ray target material, and λ_0 is the short-wavelength cutoff.

The linear x-ray absorption coefficient varies with wavelength as[5]

$$\mu=A\lambda^3+B, \tag{4}$$

where A and B are constants depending on the absorbing material.

The total intensity $J(x)$ at any depth in a crystal irradiated with such a heterogeneous x-ray beam may be derived by combination of Eqs. (2–4) and integration over all λ from the short wavelength cutoff, yielding

$$J(x)=D_0Ze^{-Bx}[(J_1/\lambda_0)-J_2], \tag{5}$$

where

$$J_1=\int_{\lambda_0}^{\infty}\lambda^{-2}\exp(-A\lambda^3x)d\lambda \tag{5a}$$

and

$$J_2=\int_{\lambda_0}^{\infty}\lambda^{-3}\exp(-A\lambda^3x)d\lambda. \tag{5b}$$

The relative energy loss per unit volume, or relative absorption rate of the x-ray energy at any depth in the crystal, is the negative of the derivative of $J(x)$ with respect to the distance x in the crystal, and is given by

$$-dJ(x)/dx=-D_0Z\{e^{-Bx}[\lambda_0^{-1}(dJ_1/dx)-(dJ_2/dx)] -Be^{-Bx}[(J_1/\lambda_0)-J_2]\}. \tag{6}$$

The quantities J_1, J_2, and their derivatives may be evaluated in terms of complete and incomplete gamma functions, Γ_∞ and Γ_{u_0}, respectively, with the change of variable $u_0=A\lambda_0^3x$ as follows:

$$J_1=(Ax)^{\frac{1}{3}}\{e^{-u_0}[u_0^{-\frac{1}{3}}+\tfrac{2}{3}u_0^{\frac{1}{3}}] -\tfrac{2}{3}[\Gamma_\infty(5/3)-\Gamma_{u_0}(5/3)]\}, \tag{6a}$$

$$J_2=\tfrac{1}{2}(Ax)^{\frac{1}{3}}\{e^{-u_0}[u_0^{-\frac{1}{3}}+3u_0^{\frac{1}{3}}] -3[\Gamma_\infty(4/3)-\Gamma_{u_0}(4/3)]\}, \tag{6b}$$

$$dJ_1/dx=\tfrac{1}{2}A^{\frac{1}{3}}x^{-\frac{1}{3}}\{e^{-u_0}u_0^{\frac{1}{3}}[\Gamma_\infty(5/3)-\Gamma_{u_0}(5/3)]\}, \tag{6c}$$

and

$$dJ_2/dx=A^{\frac{1}{3}}x^{-\frac{1}{3}}\{e^{-u_0}u_0^{\frac{1}{3}}[\Gamma_\infty(4/3)-\Gamma_{u_0}(4/3)]\}. \tag{6d}$$

By using Eqs. (6)–(6d), numerical values of $-dJ(x)/dx$ were calculated for various values of depth x (in cm) for NaCl and LiF. The constants D_0 and Z were arbitrarily taken as unity since the primary interest was in determining the relative energy loss at different depths in a crystal. Values of μ for each alkali halide crystal were computed for various wavelengths from values of the mass absorption coefficient, μ/ρ, for each element, and the density, ρ, of the crystal. From these values of μ, A and B were computed by a least squares fit to be for NaCl, 49.64×10^{24} cm^{-4} and 0.376 cm^{-1}, respectively, and for LiF, 8.953×10^{24} cm^{-4} and 0.435 cm^{-1}. Values of λ_0 in cm were obtained from the equation $\lambda_0=hc/eV$, where V is the x-ray tube peak accelerating voltage.

Computations of $-dJ(x)/dx$ involving the gamma function expressions were quite laborious. A simpler procedure was therefore developed which yielded essentially the same results. The Kramer's energy distribution was divided into half a dozen wavelength segments. The derivative of Eq. (2),

$$dJ(x,\lambda)/dx=-\mu J_0(\lambda)e^{-\mu x}, \tag{7}$$

was computed by using average values of μ and $J_0(\lambda)$ for each segment. These contributions were then summed to give $dJ(x)/dx$. In this case wavelengths greater than $\sim$2 A were neglected. For this reason the segment approximation is not very accurate for $x<0.1$ cm where the long-wavelength x-rays are strongly absorbed.

The x-ray energy absorbed after a given time of irradiation is proportional to the rate of energy absorption, $-dJ(x)/dx$. The results of the calculations of x-ray energy absorption as a function of depth x, based on the segment method of calculating $-dJ(x)/dx$,

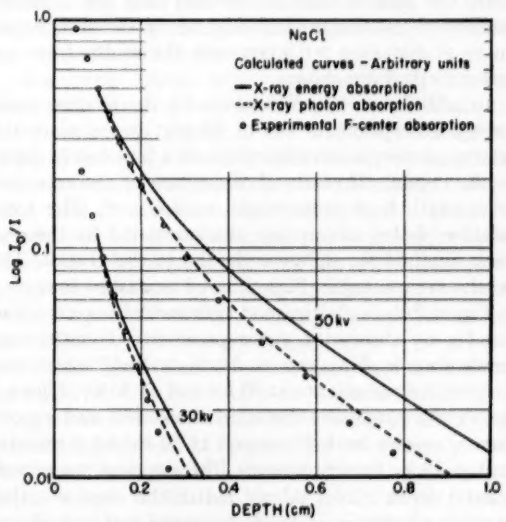

FIG. 2. Comparison of theoretical x-ray absorption and experimental F center concentration as functions of depth in NaCl. The solid line shows the x-ray energy absorbed, the dashed line shows the number of x-ray photons absorbed, and the circles are the observed F center concentrations for short x-ray exposure time (1 minute).

[3] H. A. Kramers, Phil. Mag. **46**, 836 (1923).
[4] H. Kuhlenkampf, Ann. phys. **69**, 548 (1922).
[5] W. T. Sproull, *X-Rays in Practice* (McGraw-Hill Book Company, Inc., New York, 1946), p. 75.

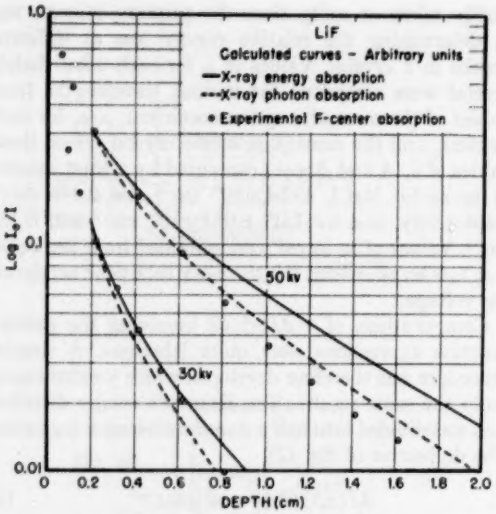

FIG. 3. Comparison of theoretical x-ray absorption and experimental F center concentration as functions of depth for LiF. X-ray exposure times of 2 min (50 kv) and 2.8 min (30 kv).

are shown as solid lines on the semilogarithmic plot in Fig. 2 for NaCl and in Fig. 3 for LiF for 50 and 30 kv x-rays. The intensity incident on the face of the x-rayed crystal, J_0, was assumed to be unknown here. The calculated penetration curves were, therefore, fitted at a depth of 0.1 cm for NaCl and 0.2 cm for LiF to the experimental data for the F center absorption which was measured as a function of depth in the crystal. The experimental points are denoted by circles. Since both the gamma-function method and the segment method of calculation yield very nearly the same depth curve at distances >0.1 cm, only the results from the latter method are shown.

In addition to the calculation for the relative x-ray energy absorption, it was of interest to calculate the relative x-ray photon absorption as a function of depth in the crystal. The rate of absorption of photons with wavelength λ is proportional to $\lambda\mu J_0 e^{-\mu x}$. The total relative photon absorption was calculated by the segment method for different depths in the crystal. The results are plotted in Figs. 2 and 3 as dashed lines.

Figure 2 shows fairly good agreement between calculated x-ray absorption and experimental F center concentrations as functions of depth in NaCl which was x-rayed for one minute at 50 kv and at 30 kv. Figure 3 shows the agreement between calculated and experimental results for LiF x-rayed at 50 kv for 2 minutes and at 30 kv for 2.8 minutes. The slopes of the experimental depth curves do not match the slope of either the calculated energy absorption curve or the calculated photon absorption curve to the exclusion of the other one. We can say that the experimental F center concentrations are approximately proportional to the x-ray absorption as a function of depth through the crystal, but the problem of whether F center formation is more closely related to x-ray energy absorption or photon absorption is unresolved. The reasons for this ambiguity lie partly in experimental error in the determination of the small F center concentrations produced from very short x-ray exposures, and partly in the appearance of saturation effects for exposures long enough to give well-reproducible depth curves. The problem is aggravated by the large range of x-ray energies in the heterogeneous beam available. It is hoped that an experiment can be carried out using monochromatic x-rays with a sufficiently high intensity to allow short times of exposure.

An estimate of the x-ray intensity J_0 at the front face of a crystal is 1.3×10^{16} ev/(cm^2 sec), based on tube operation at 50 kv and 15 ma, and tube efficiency of $\sim1.5\times10^{-9}$. The energy absorbed in the 0.86-cm^3 NaCl crystal in one minute was estimated to be $\sim5\times10^{17}$ ev. The total number of F centers produced in this crystal can be estimated by summing the local concentrations over the depth of the crystal. The local concentration can be found by using Smakula's equation[6]

$$n_F(\text{cm}^{-3}) = 1.28\times10^{17}\frac{n}{(n^2+2)^2}\frac{\alpha W}{f}, \qquad (8)$$

where n is the index of refraction of an uncolored crystal, f is the oscillator strength of the color center,

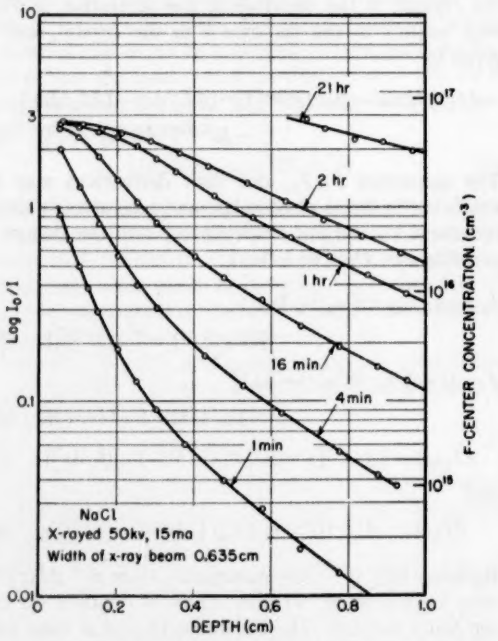

FIG. 4. F center concentration as a function of depth in NaCl for various times of x-ray irradiation.

[6] A. Smakula, Z. Physik **59**, 603 (1930). See also reference 2, footnote 1.

W is the band width in ev at half-maximum, and α is the absorption coefficient at the band maximum given by $\alpha = d_0^{-1} \ln(I_0/I)$, with d_0 taken as the crystal thickness. For NaCl at room temperature $n = 1.54$, $f \sim 0.7$, and $W \sim 0.51$ ev. The total number of F centers produced after a one minute x-ray exposure was $\sim 3 \times 10^{15}$, so that the average energy for the formation of one F center in NaCl is $\sim 10^2$ ev. This can be compared with the values of 18 and 120 ev reported by Schneider[7] and Harten,[8] respectively, for KCl x-rayed at room temperature.

B. Growth for Long X-Ray Exposures

F center concentrations as a function of depth in the crystal are shown in Fig. 4 for NaCl x-rayed for various times at 50 kv. The concentrations range from less than 10^{15} to $\sim 10^{17}$ cm^{-3}. For a particular crystal, absolute values of $\log(I_0/I)$ for a given depth and length of x-ray exposure could be reproduced to $\sim \pm 10$ percent, under the experimental conditions employed. Variations between crystals were somewhat larger than this. The slope of the depth curve at a given depth for a given length of exposure for all crystals of the same alkali halide could be reproduced to ± 1 percent. Variations in the x-ray tube current as well as differences in the treatment of the crystals were responsible for the large scatter in absolute determinations of the concentrations. Changes in the x-ray voltage and slight instability in the Beckman spectrophotometer blank determinations affected the depth curve slope reproducibility.

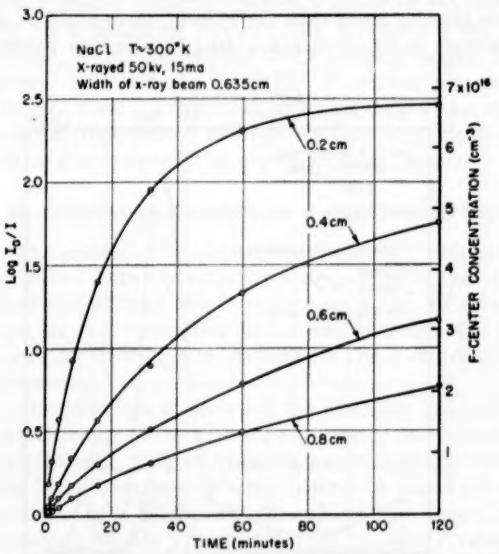

FIG. 5. F center concentration as a function of x-ray exposure time for several depths in NaCl.

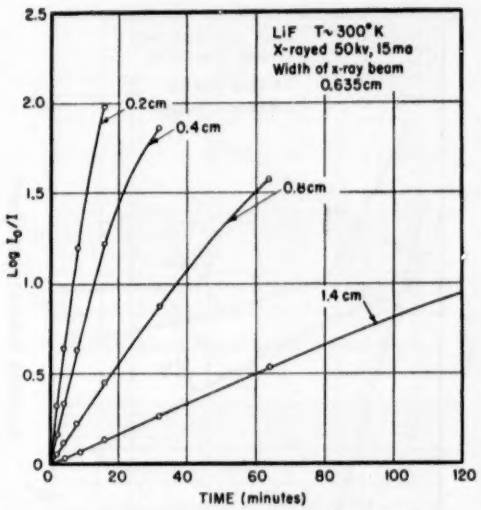

FIG. 6. F center concentration as a function of x-ray exposure time for several depths in LiF.

Figure 5 is a cross plot of data for Fig. 4 and shows F center growth up to two hours of x-ray exposure for several depths in the same NaCl crystal. The growth rate varies markedly through the crystal for the early exposures, and a trend toward saturation soon appears near the x-rayed face. Platt and Markham,[9] Schneider,[7] and Harten[8] have reported qualitatively similar growth curves, although their absorption measurements were taken in the same direction as that of the x-ray beam, and did not show the quantitative differences apparent at various depths in the crystal.

The trend toward saturation appears in the concentration range of ~ 4–6×10^{16} cm^{-3} as shown in the curves taken at depths of 0.2 and 0.4 cm from the x-rayed face of the NaCl. At greater depths the growth rates are not constant, but they vary much more slowly with time than those at the smaller depths. The x-ray intensity incident on the crystal was varied by changing the x-ray tube filament current. The depth curve for a given current and length of exposure was the same within 2 percent as that for one-half the current and twice the length of exposure.

F center growth curves at various depths are shown in Fig. 6 for LiF. In contrast to the behavior of NaCl, the growth rates for LiF are very nearly constant close to the x-rayed face. At optical densities about the same as those for which NaCl showed a trend to saturation, luminescence in the LiF during and following x-ray irradiation had become sufficiently intense to decrease the accuracy of the optical absorption measurements.

Figure 7 shows color center concentration with depth after a thin NaCl crystal had been x-rayed for 2 hours

[7] See E. E. Schneider in J. W. Mitchell, *Fundamental Mechanisms of Photographic Sensitivity* (Academic Press, New York, 1951), p. 13.

[8] H. U. Harten, Z. Physik **126**, 619 (1949).

[9] R. T. Platt, Jr., and J. J. Markham, Phys. Rev. **92**, 40 (1953).

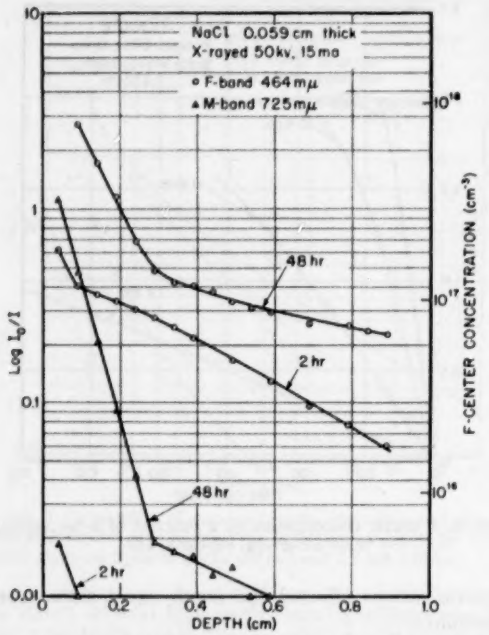

FIG. 7. Color center concentrations as a function of depth in NaCl for 2- and 48-hr x-ray exposure for F band (○) and M band (△).

and 48 hours. For the shorter time the F center curve shows appreciable coloration extending through the crystal. Within 0.1 cm of the x-rayed face there is unexpected increase in F center concentration, greater than the apparent saturation value of $\sim 10^{17}$ cm^{-3}. For the same length of exposure and for depths up to 0.1 cm a small but significant amount of M band is observed.

After 48 hours the F center concentration through the back portion of the crystal is $\sim 10^{17}$ cm^{-3}. Near the front, however, a large increase of F band growth results in concentrations of $\sim 10^{18}$ cm^{-3}. The M band for this exposure is very large in the front and decreases rapidly within the front 0.3-cm region where the F center concentration is $> 10^{17}$ cm^{-3}.

Measurements on other thin NaCl crystals have confirmed the fact that under continued irradiation, and for F center concentrations of $\sim 10^{17}$ cm^{-3}, the growth rate of the F band breaks from the trend toward saturation and rises rapidly. Under these conditions the growth rate of the M band, and also possibly the R and V bands, increase rapidly. The break visible in the depth curves moves into the crystal from the x-rayed face, up to an apparent limiting value which is reached after about 24 hours' exposure to this type of radiation. For NaCl this limiting depth appears to be ~ 0.3 cm for the x-ray intensity employed.

Estermann, Leivo, and Stern[10] reported measurable decreases in crystal density for KCl after x-ray irradiation for several hours with an intensity having the same order of magnitude as was used in the present experiments. This fact leads us to suggest that the large increase in F center growth near the x-rayed surface and the accompanying increase in M center growth are associated with the production of vacancies by the x-rays.

The NaCl crystals x-rayed for long times appear "black" in the portion near the x-rayed face, and yellow in the remaining portion. In Fig. 8 are given three absorption spectra for 35-hour x-rayed NaCl; one was taken in the black portion, one at the diffuse boundary between the black and yellow portions, and one in the yellow portion, at 0.09, 0.29, and 0.49 cm, respectively, from the x-rayed face. Only at the 0.09-cm depth are there indications of appreciable band structure other than the F band. At this depth there is a well defined M band, and indications of two V bands, as well as a long tail on either side of the F band which could include K and R bands.

The half-width of the F band in the yellow portion of this crystal x-rayed for 35 hours is ~ 0.49–0.50 ev, which is about what is observed after short x-ray exposures at any depth. Near the front of the crystal the half-width has grown to ~ 0.61 ev. This variation in half-width is larger than that reported by Mador, Markham, and Platt[11] who included in their study of KBr half-widths at 78°K F bands made by additive coloration as well as x-ray coloration. There may be two reasons for this large half width near the x-rayed face: (1) if the K, V, and R bands in the F band tails are growing faster than the F band, there could be an increase in apparent half-width; (2) the high concen-

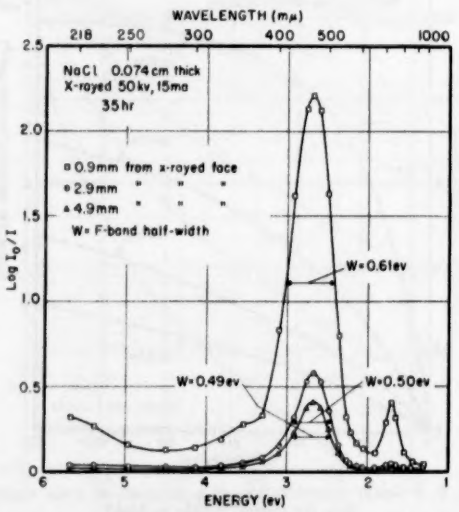

FIG. 8. Absorption spectra of NaCl x-rayed for 35 hr. ▫ in the black portion; ○ at the boundary between the yellow and black portions; △ in the yellow portion.

[10] Estermann, Leivo, and Stern, Phys. Rev. 75, 627 (1949).

[11] Mador, Markham, and Platt, Phys. Rev. 91, 1277 (1953).

tration of imperfections at this depth in the crystal might cause interactions which could increase the true half-width.

Figure 9 shows a large amount of F and M bands extending through the whole depth of an LiF crystal x-rayed for 24 hours. No break similar to that found at 0.3 cm for NaCl is observed for this crystal, but preliminary experiments on a larger LiF sample indicate that a break may occur for this length of exposure at a depth of ~1.8 cm. Another experiment indicates that a similar break occurs in KCl at ~0.15 cm.

An attempt was made to test the hypothesis that vacancy diffusion from a surface is rate determining in F center formation. A NaCl crystal was partially cleaved in the direction perpendicular to that of the x-ray beam, and the whole crystal was x-rayed for 16 minutes. The F center concentration decreased somewhat more rapidly with depth beyond the cleavage plane than in an uncleaved crystal, but it showed no discontinuity at the cleavage plane to indicate anomalous F center growth at the boundary. Absorption measurements were made every 0.25 mm through the cleavage region with a light beam width of ~0.04 cm. For this period of exposure no effect on the rate of growth of F centers caused by proximity to a crystal surface was observed.

On the basis of this study, F center growth at room temperature appears to be divided into three parts. First, there is an early fast growth which is proportional to the relative x-ray absorption through the whole crystal. Secondly, there is a slower growth tending to a saturation concentration through the whole crystal, which for various NaCl samples ranges between $\sim 6\times10^{16}$ and $\sim 2\times10^{17}$ F centers per cm^3. Thirdly, there is an increased growth in the very heavily x-rayed front portion of these relatively large crystals, which is accompanied by growth of other centers.

IV. OPTICAL BLEACHING OF F CENTERS IN NaCl

The analysis of the optical bleaching of F centers is simplified if the crystal is uniformly colored so that the local and average concentrations are equal. In actual practice the nonuniform absorption of x-rays and of bleaching light lead to gradients in the F center concentration.

The technique of orienting the bleaching light path perpendicular to the axis of x-ray permits one to study substantially uniform initial concentrations provided the light beam is sufficiently narrow. A condition of uniform light absorption throughout the region of bleaching may be approximated by choosing F center concentrations and crystal thicknesses so that only a small fraction of the incident light is absorbed.

Observations[12] of photocurrents in x-rayed crystals during irradiation with F light at room temperature

[12] J. J. Oberly and E. Burstein, Phys. Rev. 79, 217 (1950).

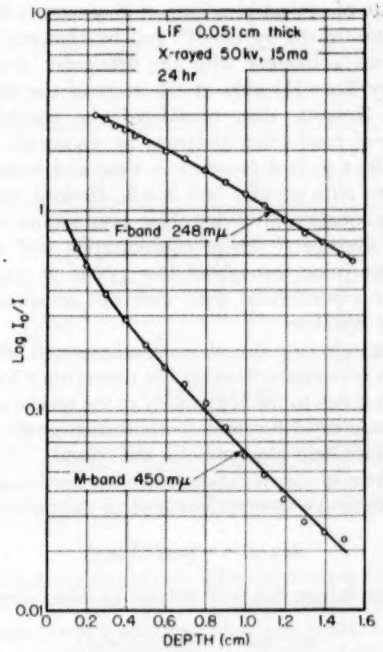

FIG. 9. Color center concentrations as a function of depth in LiF after 24-hr x-ray exposure.

indicate that electrons are transferred to the conduction band in optical bleaching. The conduction electrons may then be captured either by positive holes or by negative ion vacancies. The nonlinear kinetic equations for these processes may be written as

$$dn_F/dt = -\sigma_F I n_F + k_1 n_c n_v, \tag{9}$$

$$dn_c/dt = \sigma_F I n_F - k_1 n_c n_v - k_2 n_c n_h, \tag{9a}$$

$$dn_v/dt = \sigma_F I n_F - k_1 n_c n_v, \tag{9b}$$

$$dn_h/dt = -k_2 n_c n_h, \tag{9c}$$

where I is the local intensity of the bleaching F light, n_F, n_c, n_h, and n_v are the local concentrations of F centers, conduction electrons, holes, and negative-ion vacancies, respectively, σ_F is the cross section for the optical decomposition of F centers, and k_1 and k_2 are rate constants. Conservation of charge and of negative-ion vacancies lead to the equations

$$n_h = n_c + n_F, \tag{10}$$

and

$$n_v^0 + n_F^0 = n_v + n_F = N, \tag{10a}$$

where n_v^0 and n_F^0 are the respective initial concentrations.

A simple limiting case arises if the capture cross section of a vacancy for a conduction electron is negligible, i.e., $k_1 = 0$. Then

$$dn_F/dt = -\sigma_F I n_F. \tag{11}$$

The rate of optical bleaching of F centers in KCl has been investigated by Grant[13] and by Hesketh.[14] Their results are consistent with the first-order decay law given by Eq. (11) only at the start of the bleaching period. Hesketh then considered the possibility of capture of conduction electrons by vacancies. He assumed that n_e is a constant in time and is negligible compared with n_F and that $k_1=k_2$. Hesketh expressed the rate equation involving these assumptions in terms of the average F center concentration and average light absorption throughout the crystal. It was found that the experimental data were not consistent with this rate equation.

Before rejecting the above mechanism it is worthwhile to investigate whether the discrepancy found by Hesketh is due to the nonvalidity of the special assumptions made or to F center concentration gradients and nonuniform light absorption in the crystal.

In terms of our notation involving local concentrations, Hesketh's assumptions lead to the rate equation

$$dn_F/dt=-(\sigma_F I/N)n_F^2, \tag{12}$$

which, on integration with respect to time, gives

$$n_F^0/n_F=1+(n_F^0/N)\sigma_F It. \tag{13}$$

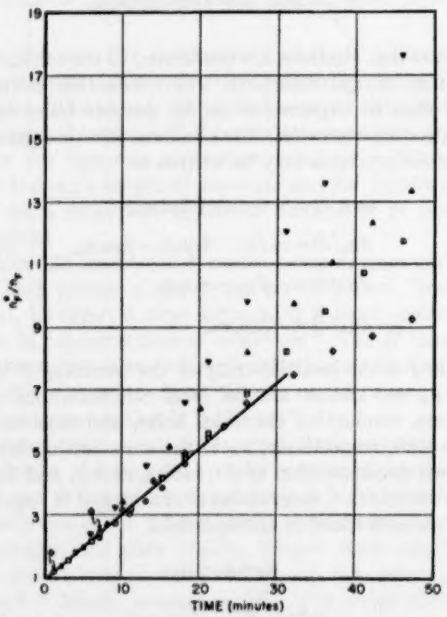

FIG. 10. Reciprocal of the fraction of F centers optically bleached vs time in a "thin" NaCl crystal. Initial F center concentrations (cm^{-3}): ○—3.2×10^{16}; ◇—4.3×10^{16}; □—6.7×10^{16}; △—8.7×10^{16}; ▽—1.4×10^{17}.

[13] D. F. Grant, thesis, University of Durham, Durham, England, 1950 (unpublished). We are indebted to Dr. E. E. Schneider for copies of this thesis and that referred to in reference 14.

[14] R. V. Hesketh, thesis, University of Durham, Durham, England, 1953 (unpublished).

The system of Eqs. (9)–(10a) may be integrated exactly[15] for the case $k_1=k_2$ without placing restrictions on n_e. One obtains

$$\frac{N}{n_F}=\frac{(N/n_F^0)+\alpha[\tau-\beta^{-1}(1-\epsilon^{-\beta\tau})]}{1-\alpha(1-\epsilon^{-\beta\tau})}, \tag{14}$$

where

$$\tau=k_2Nt, \tag{14a}$$

$$\gamma=\sigma_F I/(k_2N), \tag{14b}$$

$$\beta=1+\gamma, \tag{14c}$$

$$\alpha=\gamma/\beta. \tag{14d}$$

The quantity k_2N may be expected[15] to be $\sim10^8$ sec^{-1}. For times long compared with 10^{-8} sec, neglect of the exponential terms is justified and leads to the approximation

$$\frac{n_F^0}{n_F}=1+\gamma-\left(\frac{n_F^0}{N}\right)\left(\frac{\gamma}{1+\gamma}\right)+\left(\frac{n_F^0}{N}\right)\sigma_F It. \tag{15}$$

For ordinary light intensities γ may be expected[15] to be a small number $\sim10^{-8}$ and may be neglected compared with unity. Equation (15) then becomes identical with Eq. (13) derived for a stationary state in the conduction electrons. The special assumptions concerning n_e made by Hesketh appear to be quite well justified for the interpretation of the optical bleaching data. According to Eqs. (13) and (15), a plot of n_F^0/n_F vs t is linear.

Experimental data for the optical bleaching of a "thin" crystal are plotted in Fig. 10. The optical density $\log(I_0/I)$ at the F band maximum is taken to be proportional to the average F center concentration along the light path. For uniform concentrations,

$$\left(\log\frac{I_0}{I}\right)_{t=0}\Big/\left(\log\frac{I_0}{I}\right)_{t=t}=\frac{n_F^0}{n_F}. \tag{16}$$

The curves for the three lowest initial F center concentrations are quite linear over the major portion of the bleaching period. The curves for the two highest concentrations are not linear. After several minutes of bleaching, the slopes are appreciably larger than those for the low concentrations. Although it is not evident in Fig. 10, the experimental data indicate that the initial slopes are somewhat smaller than the low concentration slopes.

In Fig. 11 are plotted optical bleaching data for a "thick" crystal in which the x-rayed region was 6.3 mm thick. The two lower concentrations yield plots of n_F^0/n_F vs t which are fairly linear. The highest concentration shows a smaller slope than the low concentrations in the region $n_F^0/n_F<3$ while at larger values of n_F^0/n_F the slope increases.

[15] Herman, Meyer, and Hopfield, J. Opt. Soc. Am. **38**, 999 (1948).

Since the optical density is proportional to the product of F center concentration and thickness of the x-rayed region, the linear relation between n_F^0/n_F and t has been observed over a tenfold range of n_F^0 values for the two thicknesses employed. The explanation for the results at the high concentrations is not completely clear. At high concentrations the light absorption is not uniform and concentration gradients develop during bleaching. To take into account this effect as well the recapture of electrons by vacancies would require the solution of a nonlinear partial differential equation and has not been attempted as yet.

Some qualitative observations may, however, be made. For uniform initial F center concentrations Eq. (12) may be integrated over the thickness of the crystal. The initial rate of change of the average F center concentration is then found to be proportional to the average light intensity along the light path. The

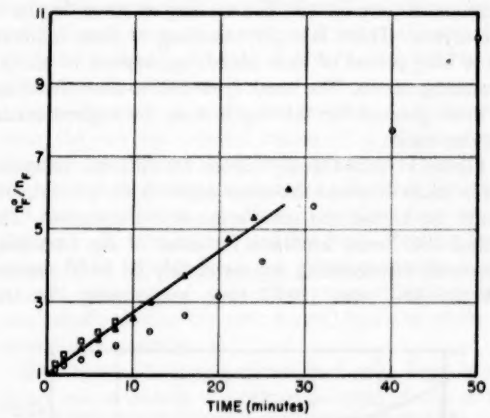

FIG. 11. Reciprocal of the fraction of F centers optically bleached *vs* time in a "thick" NaCl crystal. Initial F center concentrations (cm^{-3}): □—6.7×10^{15}; △—1.7×10^{16}; ○—4.6×10^{16}.

average intensity is smaller for high concentrations than for low concentrations. The initial slopes in the plot of n_F^0/n_F *vs* t may then be expected to be smaller in the former case than in the latter.

The effect of concentration gradients on the rate may be investigated for the case of a constant gradient and uniform light intensity. If the gradient is g, integration of Eq. (12) over the thickness d_0 of the crystal yields

$$dN_F/dt=-(\sigma_F I/N)[(N_F^2/d_0)+(g^2d_0^3/12)], \quad (17)$$

where

$$N_F=\int_0^{d_0} n_F dy. \quad (17a)$$

For $g=0$,

$$dN_F/dt=-(\sigma_F I/N)(N_F^2/d_0). \quad (17b)$$

A constant concentration gradient, therefore, leads to an increased rate over that for a zero gradient and the

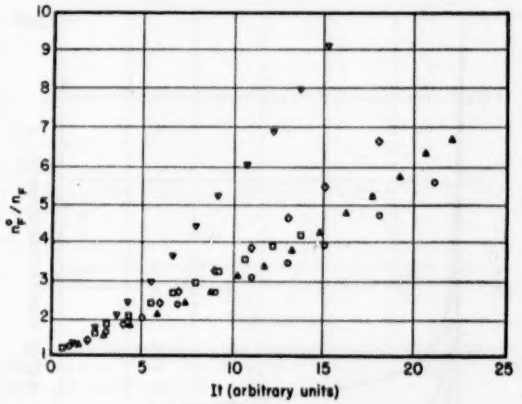

FIG. 12. Reciprocal of the fraction of F centers optically bleached with light of intensity $I=fI_i$ in a "thin" NaCl crystal as a function of It. Initial F center concentrations (cm^{-3}) and relative intensity, f: □—3.2×10^{16}, 0.305; △—3.1×10^{16}, 0.734; ○—3.2×10^{16}, 1.00; ▽—1.39×10^{17}, 0.305; ◇—1.44×10^{17}, 1.00. $I_i=37$ μwatt/cm².

same average concentration. This effect offers a possible explanation for the relatively large slopes found at high concentrations and long bleaching times.

Another variable which affects the slope of the n_F^0/n_F *vs* t plot is the ratio n_v^0/n_F^0. The near coincidence of the plots at low concentrations indicates that in these cases this ratio is nearly constant. The changes in slope found in passing to higher concentrations may involve a variation in n_v^0/n_F^0.

The above discussion indicates that the discrepancy found by Hesketh is not due to the special assumptions concerning n_e and the rate constants, but may be attributed to F center concentration gradients and nonuniform light absorption in the crystal.

Equation (13) predicts that n_F^0/n_F is a function of the product It. In Fig. 12 are plotted experimental data for optical bleaching of a thin crystal for various intensities of the incident light. For the low initial concentrations the curves nearly coincide. This result is consistent with a dependence of n_F^0/n_F on It, and with a nearly constant value of the ratio n_F^0/N for the three examples at low concentrations.

The two curves for high concentrations, on the other hand, show a considerable deviation from one another. This indicates that n_F^0/n_F is a function not only of It but also of some variable such as n_v^0/n_F^0 or of I alone which differs in the two cases.

The initial rate of destruction of F centers specified by Eq. (13) is given by

$$\left(\frac{dn_F}{dt}\right)_{t=0}=-\frac{n_F^0}{N}\sigma_F I n_F^0. \quad (18)$$

If σ_F is the cross section for the absorption of photons, then $\sigma_F=q_1\sigma_F$ where q_1 is the primary quantum efficiency for the destruction of F centers. The local rate of

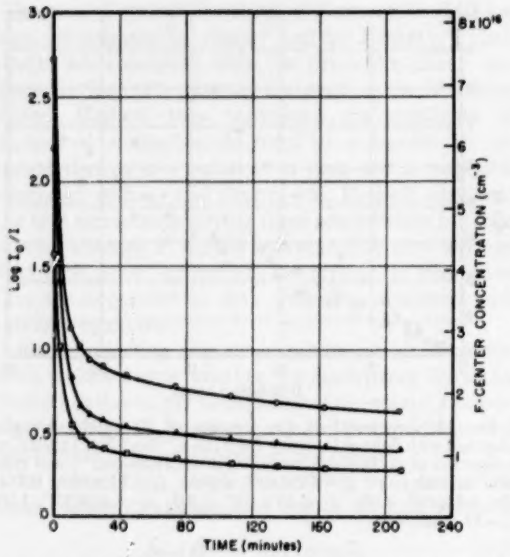

FIG. 13. Thermal bleaching of F centers in a "thick" NaCl crystal at 150°C *vs* time. Initial F center concentrations (cm^{-3}): □—4.3×10^{16}; △—6.0×10^{16}; ○—7.4×10^{16}.

absorption of photons is initially equal to $\sigma_F I n_F^0$. The net quantum efficiency q is defined as the net rate of destruction of F centers divided by the rate of absorption of photons. At $t=0$,

$$q=(n_F^0/N)q_1=[n_F^0/(n_v^0+n_F^0)]q_1. \qquad (19)$$

Initial rates of destruction of F centers in the optical bleaching of NaCl were determined from the experimental data by using Smakula's formula given in Eq. (8). The bleaching light intensity was measured as described in Sec. II. The net quantum efficiency q was then calculated to be ~0.3. Within the limit of experimental error the value of q was found to be the same for the various values of n_F^0 considered. The present result is nearly equal to the value 0.23 found by Camagni and Chiarotti[16] for the initial net quantum yield for the optical bleaching of F centers in x-rayed KCl containing strontium impurity.

A value of q less than unity follows from Eq. (19) if q_1 is less than unity, or if $n_v^0\neq0$, or both. If n_v^0 is proportional to n_F^0, then Eq. (19) indicates a lack of dependence of q on n_F^0. The assumptions that q_1 is unity at room temperature and that $n_v^0>0$ are consistent with the present data, and with the quantum yields obtained by Pick[17] for the transformation of F centers to F' centers in additively colored KCl and NaCl.

V. THERMAL BLEACHING OF F CENTERS IN NaCl

Thermal decay of F centers in "thick" NaCl crystals was studied at various depths through the crystals in the temperature range 29° to 150°C. Prior to a thermal bleaching experiment the F center concentration of a freshly x-rayed NaCl crystal was determined at room temperature. The crystal and holder were then removed from the spectrophotometer while the oven was heated to the desired temperature. Zero time for the run was taken when the crystal was replaced in the hot oven, although it took 5 to 10 minutes for the sample to reach thermal equilibrium. Because the F band λ_{max} shifted towards longer wavelengths as the crystal temperature increased, measurements for the three highest temperature runs were taken at 470 mμ instead of 464 mμ. The room temperature determinations of the initial concentrations were corrected to account for the decrease of the absorption at the band maximum with increasing temperature at constant concentration. This was observed in a separate run, and found to be 0.06 percent per degree.

Figure 13 shows the F center concentration as a function of time for 150°C bleaching at three depths in the crystal. There is rapid bleaching at first, followed by a long period of slow bleaching, typical of all the bleaching curves. The break from fast to slow bleaching is more gradual for the depth with the highest initial concentration.

Figure 14 shows decay curves for different temperatures taken at about the same depth in the crystal, and hence for almost the same original concentration. The initial fast decay accounts for most of the bleaching observed, representing approximately 60 to 80 percent for the 140° and 150°C runs, respectively. In this

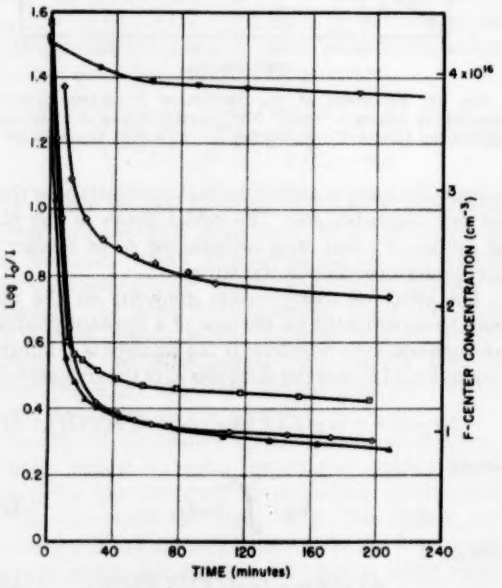

FIG. 14. Thermal bleaching of F centers in a "thick" NaCl crystal *vs* time at various temperatures. Initial F center concentrations ~4.5×10^{16} cm^{-3}. ▽—29°C; ◇—98°C; □—120°C; ○—140°C; △—150°C.

[16] P. Camagni and G. Chiarotti, Nuovo cimento **XI**, 1 (1954).
[17] H. Pick, Ann. Physik **31**, 365 (1938).

temperature range the bleaching rates in the slow portion are the same within experimental error. All the curves decrease continuously with no leveling off, even in the very slow decay just above room temperature. Bleaching was 99 percent complete at 150°C after 92 hours; it was only 86 percent complete at 120° after 120 hours.

Figure 15 is a plot of the reciprocal of the fraction of F centers bleached *vs* time. The initial slopes of the 120°–150° runs are comparable with those observed for the 10^{14} quanta/(cm² sec) F light optical bleaching, but the subsequent lower slopes, representing the break from fast to slow thermal decay, are a departure from the behavior of the optical decay slopes. The room temperature thermal decay shows the same qualitative behavior as that of the higher temperatures.

In a separate experiment a crystal was bleached at 140°C for two hours and then bleached optically at room temperature. The optical decay proceeded at nearly the same rate for the remaining concentration as in a freshly x-rayed crystal, and was not changed by the prior removal of those F centers involved in the initial fast thermal decay.

Luminescence at room temperature was observed from the heavily x-rayed region of a NaCl crystal. Thermoluminescence had been reported in KCl by Grant[13] and Hesketh[14] to accompany thermal bleaching, and was attributed to direct recombination of the F center electron and a positive hole. Heating an x-rayed NaCl crystal on a hot plate produced a substantial amount of blue-white thermoluminescence, particularly during the first several minutes while the crystal was warming up.

The thermal bleaching curves such as in Figs. 14 and 15 are not amenable to analysis in terms of one or two independent monomolecular processes,[13,14] nor can they be explained by the model developed for the optical bleaching involving electron excitation to the conduction band and retrapping.

Thermal bleaching has been considered[14] to involve a tunneling process with a very small activation energy in which the F center electron recombines with a positive hole without entering the conduction band. No activation energy could be determined from the present experiments, though this may be due only to the small temperature range covered. The break from fast to slow bleaching would probably have to be explained in terms of a spatial arrangement of nearby and faraway holes if tunneling were the only process involved.

It is possible that tunneling at the onset of thermal decay might cause sufficient luminescence to produce some optical bleaching, the cessation of which, shortly after the sample attains thermal equilibrium, might contribute to the relatively sharp break back to a purely thermal decay process.

The present experiments on the thermal bleaching of F centers in NaCl have shown a fast decay followed by a slow decay, which, in the absence of knowledge concerning conductivity and luminescence effects are very difficult to analyze to yield an understanding of the mechanisms involved.

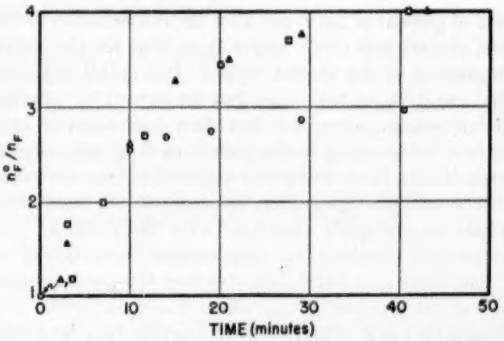

FIG. 15. Reciprocal of the fraction of F centers thermally bleached in a "thick" NaCl crystal *vs* time with initial concentrations $\sim 6.5\times10^{16}$ cm^{-3}. ○—120°C; □—140°C; △—150°C.

VI. VACANCIES

To obtain evidence concerning the role of negative ion vacancies in the growth and decay of F centers, several qualitative experiments were carried out by investigating the relationship of the α and β bands to the F band in KI. The α band is ascribed[18] to the excitation of an ion adjacent to a negative ion vacancy, and the β band to that of an ion adjacent to an F center. Both bands lie in the ultraviolet and are obscured by the tail of the first fundamental except at low temperatures. Even at low temperatures the quantitative determination of their intensities is difficult.

The intensity of the β band is roughly proportional to that of the F band, both during growth by x-raying and bleaching by F light, at 78° and 5°K.[18] The α band can be developed to some extent by x-raying. However, it is also observed in some KI crystals additively colored[19] with excess K and in some KI crystals prior to x-raying. Partial emptying of F centers during the quenching of the additively colored crystals could account for the former case, and divalent negative-ion impurities could account for the latter case. It is also possible that the appearance of the α band at these low temperatures indicates that some single negative-ion vacancies have been frozen in from a higher temperature equilibrium vacancy concentration. For an x-rayed crystal, the largest amounts of α band are observed after F band optical bleaching.

To study the possible formation of negative-ion vacancies during x-ray irradiation a KI crystal was x-rayed and optically bleached at 78°K. This crystal was then cooled to 5°K and x-rayed again. A second KI crystal was x-rayed at 5°K for the first time. The

[18] Delbecq, Pringsheim, and Yuster, J. Chem. Phys. **19**, 574 (1951); **20**, 746 (1952).

[19] R. T. Platt, Jr. and J. J. Markham (private communication).

rate of growth of the F band for the reirradiation of the first crystal was much larger than that for the initial irradiation of the second crystal. This result indicates that negative ion vacancies may be formed by x-raying at low temperatures, and that their concentration may be rate determining in the growth of F centers. On the basis of this, then, one would expect that the concentration of unfilled negative ion vacancies during irradiation would be negligible compared with the F center concentration. However, the simultaneous formation of an F band and an α band indicates that the concentration of unfilled negative ion vacancies is not negligible. The destruction of F centers during x-raying may be a possible explanation for the presence of these unfilled vacancies.

During the α- and β-band studies of KI several other observations were made. As with KBr,[20] a large fraction of the F centers bleach when irradiated with F light at 78° and 5°K, and after bleaching there is partial dark recovery. A low, wide band at 275 mμ[18] grows at low temperatures independent of any x-raying or bleaching, and seems to be caused not by an impurity in the crystal, but possibly by a surface deposit condensed on the crystal.

It appeared likely that vacancies could be involved in the addition and removal of water from natural rock salt crystals as reported by Barnes.[21] We found that water was readily removed from such crystals by heating, as measured by the intensity of absorption at $\sim 3\ \mu$, but all of our attempts to introduce H_2O into natural or synthetic crystals were unsuccessful. The addition was tried by immersion in liquid H_2O under various conditions of pH, temperature, and mechanical deformation, and by heating in steam in a high-pressure bomb.

[20] Markham, Platt, and Mador, Phys. Rev. **92**, 597 (1953).
[21] R. B. Barnes, Phys. Rev. **43**, 82 (1933); **44**, 898 (1933).

VII. CONCLUSION

It has been possible to minimize the difficulties due to nonuniform color center concentrations inherent in x-ray colored crystals by making optical absorption measurements perpendicular to the direction of x-ray penetration.

It appears that there is approximate proportionality between the number of F centers produced and the amount of x-ray radiation absorbed for short times of exposure. The production of large concentrations of both F and M centers after prolonged irradiation as well as the low-temperature rate of growth of F centers in a crystal previously x-rayed and optically bleached indicate that vacancies are created by the x-rays.

Experimental rates of optical bleaching of F centers at low concentrations may be explained on the basis of a set of nonlinear differential equations describing the transfer of F center electrons to the conduction band and trapping of the conduction electrons by holes and vacancies. Observations on thermal bleaching, however, may not be so interpreted at present.

We believe that additional understanding of the mechanisms involved in the formation and bleaching of color centers could be achieved by electrical conductivity measurements in conjunction with determinations of growth and bleaching rates.

VIII. ACKNOWLEDGMENTS

We wish to express our appreciation to Mr. Joel Selbin for his assistance in calculating x-ray penetration curves and Mr. F. Harler, of the Naval Research Laboratory for assistance in cryogenics. We also wish to thank Miss Doris Rubenfeld for her untiring cooperation in the preparation of the illustrations as well as Miss Shirley Thomas and Miss Agnes Fogelgren for typing the manuscript.

Microwave Spectra of the Alkali Halides*

A. HONIG,† M. MANDEL, M. L. STITCH,‡ AND C. H. TOWNES
Columbia University, New York, New York

(Received June 2, 1954)

Data from the microwave spectra of all alkali halides excepting LiF, NaF, KF, RbF, and LiCl are given and analyzed in terms of molecular and nuclear constants. These yield internuclear distances and ionic radii for the gaseous alkali halides, molecular dipole moments, potential constants including four constants for some molecules, amount of covalent character from quadrupole coupling constants and from rotational effects, and mass ratios for isotopes of Li, K, Rb, Cl, and Br.

INTRODUCTION

RECENT advances in microwave spectroscopy at high temperatures[1,2] have made it possible to obtain the pure rotation spectra of most of the alkali halide molecules. With the exception of LiF, NaF, KF, RbF, and LiCl, which involved certain experimental difficulties, experimental results on all the (stable) alkali halides are given here and discussed in terms of various molecular and nuclear properties.

Past experimental work on the alkali halides in the gaseous state include electron diffraction experiments[3] and molecular beam studies.[4–7] The electron diffraction results yielded internuclear distances with a stated 1 percent error, but these have consistently been found to be about 3 percent too large. Until quite recently, molecular beam experiments on alkali halide molecules utilized radio-frequency resonances. The magnetic resonance experiments[5,6] gave information concerning the nuclear magnetic and electric quadrupole moments, and their interaction with the rotating molecule, and the more recent electric resonance[7] experiments yielded, in addition to the molecular hyperfine structure, information concerning the electric dipole moment and moment of inertia of the molecule. However, these last two quantities are not determined with high accuracy by the electric resonance technique. The very recent molecular beam experiments employing microwave frequencies to study pure rotational transitions[8–10] are most similar in scope to the work described in this paper, although the techniques are greatly different. This type of molecular beam measurement of rotational states has been carried out with KCl,[8] KBr,[9] and RbCl,[10] where it yielded a considerable amount of precise information, some of which is included in this treatment.

The present experiments on the alkali halides in the microwave region provide extremely accurate moments of inertia, internuclear distances, and vibration-rotation interaction constants. Accurate mass ratios for the Cl, Br, Li, K, and Rb isotopes have been obtained. In the lighter molecules, the electric quadrupole hyperfine interactions and the electric dipole moments have been measured. The first part of this paper will deal with the experimental results obtained, and later parts discuss the theoretical significance of some of the results.

APPARATUS AND METHOD

The apparatus for this experiment has been thoroughly described in a previous article.[11] It consists essentially of a gold-plated nickel absorption cell enclosed in a vacuum chamber. This wave guide can be heated to temperatures up to 930°C at present. A thin gold-plated nickel strip, hereafter referred to as a Stark plate, runs the length of the guide parallel to the broad face of the wave guide. An alkali halide salt is placed inside the absorption cell which is then heated until sufficient vapor pressure of the salt is present to produce detectable absorptions of microwave power at the resonant frequencies. Application of an oscillating electric field between the Stark plate and the guide frequency modulates the microwave absorption due to molecular resonances, and greatly increases the sensitivity of the instrument. Application of a steady electric field between the Stark plate and the guide provides a means of measuring the electric dipole moment of the molecule. The details of observing the spectra and measuring the frequency are the same as those employed in conventional microwave spectroscopy at room temperature, and have been thoroughly described in other articles.[12]

Unfortunately temperatures in excess of the 930°C presently attainable are necessary for sufficient vapor pressure of LiF and NaF, so the microwave spectra of these molecules could not be obtained. For LiCl, KF, and RbF, various types of experimental difficulties, some of which are related to the high chemical activity

* Research supported jointly by the Signal Corps, U. S. Office of Naval Research and Air Force.
† Now at the University of California, Berkeley, California.
‡ Now at Varian Associates, Palo Alto, California.
[1] Stitch, Honig, and Townes, Phys. Rev. **86**, 813 (1952).
[2] Honig, Stitch, and Mandel, Phys. Rev. **92**, 901 (1953).
[3] Maxwell, Hendricks, and Mosley, Phys. Rev. **52**, 968 (1937).
[4] Rodebush, Murray, and Bixler, J. Chem. Phys. **4**, 372 (1936).
[5] J. B. M. Kellogg and S. Millman, Revs. Modern Phys. **18**, 323 (1946).
[6] D. R. Hamilton, Am. J. Phys. **9**, 319 (1941).
[7] H. K. Hughes, Phys. Rev. **70**, 570 (1946).
[8] Lee, Fabricand, Carlson, and Rabi, Phys. Rev. **91**, 1395 (1953).
[9] Fabricand, Carlson, Lee, and Rabi, Phys. Rev. **91**, 1403 (1953).
[10] R. Braunstein and J. W. Trischka, Quarterly Report, Columbia Radiation Laboratory, August 31, 1953 (unpublished).
[11] Stitch, Honig, and Townes, Rev. Sci. Instr. **25**, 759 (1954).
[12] S. Geschwind, Annals N. Y. Acad. Sci. **55**, 751 (1952).

of these molecules, prevented observation of their spectra. It is hoped that subsequent work will succeed in detection of their spectra.

THEORY

A. Energy of a Rotating Vibrator

The molecular energy levels of a diatomic molecule are based upon the model of a rotating vibrator. If one assumes a Morse potential function of the form[13]

$$V(r-r_e)=D_e(1-e^{-\beta(r-r_e)})^2,$$

the solution of Schrödinger's equation gives the usual energy level expansion:

$$\begin{aligned}W=&\omega_e(v+\tfrac{1}{2})-\omega_e x_e(v+\tfrac{1}{2})^2+\omega_e y_e(v+\tfrac{1}{2})^3+\cdots\\&+B_eJ(J+1)-\alpha_eJ(J+1)(v+\tfrac{1}{2})\\&+\gamma_eJ(J+1)(v+\tfrac{1}{2})^2+\cdots+D_eJ^2(J+1)^2\\&-\beta_eJ^2(J+1)^2(v+\tfrac{1}{2})+\cdots,\end{aligned}$$

where the terms are the familiar band spectra terms[13] and are related to the constants in $V(r-r_e)$. (The third term on the right-hand side is zero for a Morse potential, but is used in the analysis of band spectra.) Since the Morse potential has three independent parameters, only three of the coefficients of the quantum numbers in the energy expansion are independent. Indeed, the agreement of the interrelations between the molecular constants with the experimental values of the constants is a measure of the validity of the Morse potential. For the alkali halides, the high accuracy of the measurements obtained warrants the use of the Dunham potential,[14] which is a power series expansion about the equilibrium internuclear distance r_e of the form

$$V=\sum_{i=2}^{\infty}a_i\left(\frac{r-r_e}{r_e}\right)^i.$$

The Schrödinger equation has been solved for this potential by Dunham and the molecular energy levels are given as

$$F_{v,J}=\sum_{l,j}Y_{lj}(v+\tfrac{1}{2})^lJ^j(J+1)^j.$$

The correspondence between the Y_{lm}'s and the ordinary band spectra constants can be obtained by comparing coefficients of identical powers of the quantum numbers in the energy expansions.

For a $J\rightarrow J+1$ pure rotational transition, the frequency of the transition is given by

$$\begin{aligned}\nu=&2Y_{01}(J+1)+2Y_{11}(J+1)(v+\tfrac{1}{2})\\&+2Y_{21}(J+1)(v+\tfrac{1}{2})^2+4Y_{02}(J+1)^3,\end{aligned}\quad(1)$$

to an approximation required by our experimental accuracy. The Y_{lj}'s with which we are concerned in this present work are:

$$\begin{aligned}&Y_{11}\sim-\alpha_e,\quad Y_{02}\sim D_e,\quad Y_{10}\sim\omega_e,\quad Y_{20}\sim-\omega_ex_e,\\&Y_{21}\sim-\gamma_e,\quad Y_{30}\sim\omega_ey_e,\end{aligned}\quad(2)$$

and Y_{01}, which is related to the rotational constant B_e by

$$Y_{01}=B_e[1+(\beta_{01}B_e^2/\omega_e^2)],$$

where

$$\beta_{01}=(Y_{10}^2Y_{21}/4Y_{01}^3)+(16a_1Y_{20}/3Y_{01})-8a_1-6a_1^2+4a_1^3,$$

and

$$a_1=(Y_{11}Y_{10}/6Y_{01}^2)-1.$$

From a knowledge of Y_{01}, Y_{10}, Y_{20}, Y_{11}, and Y_{21}, the first four coefficients of the power series expansion of the potential can be determined. Expressions relating the Y_{lm}'s to the potential coefficients can be found in Dunham's original paper.

B. Mass Ratios of Isotopes

Under the assumption that the potential function is the same for different isotopic substitutions in a given molecule, very accurate mass ratios can be computed from the experimental data. Denoting the two isotopic species of molecules by M_1X and M_2X, the ratio of the reduced masses is given by

$$\frac{\mu_1}{\mu_2}=\frac{(B_e)_2}{(B_e)_1}=\frac{(Y_{01})_2}{(Y_{01})_1}\left[1+\beta_{01}\frac{B_e^2}{\omega_e^2}\left(\frac{\mu_1}{\mu_2}-1\right)\right]^{-1},\quad(3)$$

and the mass ratio M_1/M_2 is given by

$$M_1/M_2=\frac{(\mu_1/\mu_2)(X/M_2)}{X/M_2-\mu_1/\mu_2+1},$$

with a fractional error of

$$\pm\left[\delta\left\{\frac{X/M_2+1}{(\mu_1/\mu_2)(X/M_2+1-\mu_1/\mu_2)}\right\}\pm\frac{\Delta(1-\mu_1/\mu_2)}{(X/M_2)(X/M_2+1-\mu_1/\mu_2)}\right],$$

where Δ is the fractional error in the mass X and δ is the fractional error in μ_1/μ_2.

C. Hyperfine Structure

Most of the alkali and halogen nuclei have nonzero electric quadrupole moments. The interaction between the nuclear quadrupole moment and the gradient of the electric field at the nucleus is sufficient to account, within the experimental error, for all molecular hyperfine structure observed in the present experiments. The

[13] G. H. Herzberg, *Molecular Spectra and Molecular Structure. I. Spectra of Diatomic Molecules* (D. van Nostrand Company, Inc., New York, 1952), second edition, p. 101.
[14] J. L. Dunham, Phys. Rev. 41, 721 (1932).

Hamiltonian for this interaction is

$$H=\frac{-eqQ}{2I(2I-1)(2J-1)(2J+3)J}[3(\mathbf{I}\cdot\mathbf{J})^2+\tfrac{3}{2}\mathbf{I}\cdot\mathbf{J}-I^2J^2],$$

where Q, the quadrupole moment for the particular nucleus concerned, is given by

$$Q=(1/e)\int\rho(3z_n^2-r^2)dxdydz,$$

and q_m is defined as $(d^2V/dz^2)_M$ at the same nucleus. The z direction lies along the internuclear axis, and V is the electrostatic potential due to all charges outside a small sphere surrounding the nucleus. In cases where both nuclei have sizeable interactions, the Hamiltonian consists of the sum of two expressions of the above form, one for each nucleus.

First-order perturbation theory yields energy levels given by

$$W=W_0+(-eq_mQ)f(I,J,F),$$

$$f(I,J,F)=\frac{\frac{3}{4}C(C+1)-I(I+1)J(J+1)}{2I(2I-1)(2J-1)(2J+3)},$$

$$C=F(F+1)-I(I+1)-J(J+1),$$

in the case of only one nucleus having an appreciable interaction. W_0 represents the unperturbed molecular energy level, and $f(I,J,F)$ is Casimir's function, which has been tabulated in several places.[15] In the few cases where the accuracy of the measurements requires consideration of both nuclear interactions, the energy levels are readily derivable by a technique described by Bardeen and Townes.[16]

In only one case, of all the molecules studied, does second-order perturbation theory seem to be needed. This is in NaI, where the ratio of eqQ_I/B_e is about 1/20. Even here, the magnitude of the contribution of second-order theory just borders on the magnitude of the experimental error. Bardeen and Townes[17] give the matrix elements necessary for computing the appropriate energy levels.

In the heavier molecules, where higher J states were considered due to the low-frequency limit imposed by a given wave-guide size, no hyperfine structure was observed even though eqQ may have been of appreciable magnitude. A glance at relative intensity tables[18] shows that for $J=5$ or higher, $I\leq 5/2$, over 90 percent of the entire line intensity is distributed among $F\rightarrow F+1$ transitions. Also, $f(I,J+1,F+1)-f(I,J,F)$, which is proportional to the frequency shift, becomes smaller with increasing J. Thus, for $J\geq 5$, $I\leq 5/2$, and an eqQ of the order of 100 Mc/sec (this is a large estimate for most of the alkali halides), the total spread of the observable hyperfine components would be of the order of 1 Mc/sec. Several lines within 1 Mc/sec would not be resolved under the conditions of these experiments.

[15] See, for example, P. Kisliuk and C. H. Townes, J. Research Natl. Bur. Standards **44**, 611 (1950).
[16] J. Bardeen and C. H. Townes, Phys. Rev. **73**, 97 (1948).
[17] J. Bardeen and C. H. Townes, Phys. Rev. **73**, 627 (1948).
[18] See H. E. White, *Introduction to Atomic Spectra* (McGraw-Hill Book Company, Inc., New York, 1934), p. 206.

D. Dipole Moments

The energy levels for a diatomic molecule in an electric field have been discussed by Fano.[19] There are three cases into which the calculations naturally fall. Case A: Weak-field case, where $\mu E\ll eqQ$; case B: intermediate-field case where μE is of the same order of magnitude as eqQ, and case C: strong-field case where $\mu E\gg eqQ$. In all of these cases, the quadrupole interaction and electric field energy are small compared to $B_eJ(J+1)$, the rotational energy. All of the molecules for which the dipole moments have been measured in the work described in this paper fall into case A or case C. Case C, the strong-field case, is the simpler one to discuss. Here, J is a good quantum number, and the electric field splits the energy level into $J+1$ levels corresponding to M_J values of 0, ± 1, $\cdots\pm J$. The expression for the energy levels so perturbed is the familiar quadratic Stark effect for molecules:

$$W=W_0+\frac{\mu^2E^2[J(J+1)-3M^2]}{2BJ(J+1)(2J-1)(2J+3)}.$$

These levels may now be perturbed by the electric quadrupole interaction between J and I. In view of the criterion of "strong-field" case, i.e., $eqQ\ll\mu E$ and the fact that the electric field splitting is rarely more than about 10 Mc/sec for the electric fields used in this experiment, the electric quadrupole interaction has not been resolved in these cases.

In the weak field case, I and J combine to form a good quantum number F. The electric field then perturbs the degenerate M_F states. The energy levels in this case are given by

$$W=W_0-\frac{\mu^2E^2}{B}\times\frac{[3M_F^2-F(F+1)][3D(D-1)-4F(F+1)J(J+1)]}{2J(J+1)(2J-1)(2J+3)2F(2F+1)(2F-1)(2F+3)},$$

where

$$D=F(F+1)+J(J+1)-I(I+1).$$

The differences in energy levels divided by h yields the relation between the observed frequency shifts in an electric field and the permanent dipole moment μ of the molecule.

RESULTS

Tables listing measured lines of the molecules whose spectra have been observed are given in Appendix I.

[19] U. Fano, J. Research Natl. Bur. Standards **40**, 215 (1948).

In this section, a discussion of the observed transitions and the information derived from them is given. The actual values of the molecular and nuclear constants appear in the following section, along with other pertinent available data on the alkali halides.

LiBr

The $J=0\rightarrow 1$ transition was observed for Li^7Br^{79}, Li^7Br^{81}, and Li^6Br^{81} at a temperature of about 680°C. Values of Y_{01}, Y_{11}, and Y_{21} have been obtained. The dipole moment of Li^7Br^{79} has been determined for the $v=0$ state. The electric quadrupole coupling constant $(eqQ)_{Br}$ was measured for the $v=0$ states of both Br isotopes and for the $v=1$ state of $LiBr^{81}$.

The calculated reduced mass ratio $\mu(Li^6Br^{81})/\mu(Li^7Br^{81})$ was used to make a rough determination of the percent ionic character of the bond, in a manner identical to that described below for LiI. Since ω_e is not known for LiBr and since it is a quantity necessary for the calculation of Y_{02} and β_{01} which are essential for an accurate mass ratio, it had to be extrapolated from other existing data. The calculation yields a result of 93±35 percent ionic character for the bond.

LiI

The $J=0\rightarrow 1$ transition was measured for both Li^6I and Li^7I at a temperature of about 600°C. Y_{01}, Y_{11}, and Y_{21} for Li^7I, and Y_{01} and Y_{11} for Li^6I have been determined. The dipole moment was measured in the $v=0$ state. The electric quadrupole coupling constant $(eqQ)_I$ has been obtained in the first three vibrational states of Li^7I and in the first two vibrational states of Li^6I.

This molecule is an interesting case for comparison of mass ratio determinations from microwave spectra and from other sources, since this ratio is rather accurately determinable in both cases. Furthermore, since Li is so light, various small effects such as those associated with the position of its valence electron and with L uncoupling of the electrons should be larger than usual and possibly observable.

The mass ratio of the atomic Li isotopes (measured by C. W. Li *et al.*)[20] from nuclear reaction data is 0.8573425±0.0000030. If the Li is in an ionic state in LiI, this gives for the ratio of reduced masses

$$(\mu^6/\mu^7)_{\text{ion}}=0.8637874\pm 0.0000030.$$

If the Li carries all its valence electrons as it rotates in the LiI molecule (i.e., it is neutral), the ratio of reduced masses is

$$(\mu^6/\mu^7)_{\text{atom}}=0.8637985\pm 0.0000030.$$

It may be seen from Table VII and the discussion below that Li in LiI is approximately 90 percent ionic, so that the ratio of reduced masses to be expected lies between the two values above and is

$$(\mu^6/\mu^7)_{\text{LiI}}=0.8637885\pm 0.0000030.$$

The actual ratio obtained from the microwave measurements is

$$(\mu^6/\mu^7)_{\text{measured}}=0.8637888\pm 0.0000020,$$

which is in remarkable agreement with the value obtained from nuclear reactions. The experimental uncertainty corresponds to an error in the mass energy of one of the Li isotopes of only about 12 kev.

The above results may be used in reverse to give a measurement of the amount of ionic character of LiI from its mechanical properties. The result is 87±35 percent. Improved measurements of the masses from nuclear reactions should allow improvement of the accuracy of this result.

The above result may be slightly in error because of some L uncoupling in LiI. However, the effect of L uncoupling would be to decrease the apparent amount of ionic character. Since the ionic character is so near 100 percent, it is evident that L uncoupling is not of great importance in this molecule. Hence it probably gives no appreciable errors in mass ratio measurements in the other alkali halides, since their large moments of inertia would make L uncoupling relatively less important.

NaCl

The $J=1\rightarrow 2$ transitions of both $NaCl^{35}$ and $NaCl^{37}$ were observed at a temperature of about 800°C. Values of Y_{01} and Y_{11} for both isotopes were obtained. The ω_e was measured by comparing the relative intensities of the $v=0$ line of $NaCl^{37}$ and the $v=3$ line of $NaCl^{35}$. The lines lie very close together in frequency and hence the standing wave ratio in the wave guide is fairly constant, giving reliability to the relative intensity measurements. The dipole moment μ was assumed to be the same in the two vibration states, which is probably a fair approximation within the accuracy of the intensity measurements.

NaBr

The $J=1\rightarrow 2$, and the $J=2\rightarrow 3$ transitions have been observed for $NaBr^{79}$ and $NaBr^{81}$ at a temperature of about 780°C. In addition to the Y_{01}, Y_{11}, and Y_{21}, quantities, the Y_{02}, or D_e was obtained from the two J transitions. The quadrupole coupling constant $(eqQ)_{Br^{79}}$ was measured in the $v=0$ state. The $(eqQ)_{Na}$, although a factor of about 10 smaller than $(eqQ)_{Br^{79}}$, was taken into account in interpretation of the observed hyperfine pattern. Accurate measurement of $(eqQ)_{Br}$ for excited vibrational states or for Br^{81} were not made because of difficulty with the overlap of lines of the two Br isotopic species.

NaI

The $J=2\rightarrow 3$ transition was observed at a temperature of approximately 650°C. The Y_{01}, Y_{11}, and Y_{21}

[20] Li, Whaling, Fowler, and Lauritsen, Phys. Rev. **83**, 512 (1951).

were obtained. The $F \rightarrow F+1$ and $F \rightarrow F$ hyperfine components of the transition were completely resolved. The quadrupole coupling constants of I for four different vibrational states were obtained. Effects of second order perturbation theory on the hyperfine levels were of the same order of magnitude as the experimental error, and hence the quadrupole coupling constants were determined by a least square fit to first-order theory.

KCl

The $J=0 \rightarrow 1$ transition of KCl was observed, but no very precise measurements were made because extensive data was already available from molecular beam experiments.[8]

KBr

The $J=0 \rightarrow 1$ transition of KBr had already been accurately measured by the method of molecular beams,[9] and hence no further measurements were made of the spectrum of this molecule.

KI

Lines from the $J=4 \rightarrow 5$, $5 \rightarrow 6$, and $6 \rightarrow 7$ transitions of $K^{39}I$, and a single line from the $J=5 \rightarrow 6$ transition of $K^{41}I$ have been observed at a temperature of about 690°C. The mass ratio of the potassium isotopes was calculated. Hyperfine structure was evident in the $J=4 \rightarrow 5$ transition, but only a rough measurement of $(eqQ)_I$ could be made due to the incomplete resolution.

RbCl

The $J=0 \rightarrow 1$ transition of RbCl had already been accurately measured by the method of molecular beams,[10] and hence no further measurements were made of the spectrum of this molecule.

RbBr

The $J=8 \rightarrow 9$ transition was observed at a temperature of about 730°C for $Rb^{85}Br^{79}$, $Rb^{85}Br^{81}$, and $Rb^{87}Br^{79}$. Y_{01}, Y_{11}, and Y_{21} were determined for $Rb^{85}Br^{79}$, and Y_{01} and Y_{11} for $Rb^{85}Br^{81}$, and $Rb^{87}Br^{79}$. A line was also measured for the $J=7 \rightarrow 8$ transition yielding a value of Y_{02}. The relative intensities of the three neighboring lines $v=0$ of $Rb^{87}Br^{79}$, $v=0$ of $Rb^{85}Br^{81}$, and $v=3$ of $Rb^{85}Br^{79}$ were compared and used in conjunction with the known value of ω_e to indicate how the dipole moment varies with vibration state. The mass ratios of the isotopes of both Br and Rb were calculated from the frequencies for isotopic species.

RbI

The $J=10 \rightarrow 11$, $11 \rightarrow 12$, and $12 \rightarrow 13$ transitions were observed at a temperature of about 660°C. For $Rb^{85}I$, the values of Y_{01}, Y_{11}, Y_{21} and Y_{02} were obtained; for $Rb^{87}I$, the values of Y_{01} and Y_{11}. Relative intensity measurements of the $v=0$ $Rb^{87}I$ and the $v=4$ $Rb^{85}I$ pair of lines, and of the corresponding $v=1$, $v=5$ pair of lines indicate how the dipole moment varies with vibration state. The mass ratio of the Rb isotopes was determined.

CsF

The $J=1 \rightarrow 2$ transition was observed[2] at a temperature of about 700°C and the constants Y_{01}, Y_{11}, and Y_{21} evaluated. The dipole moment was measured in the $v=0$ state.

CsCl

The $J=5 \rightarrow 6$ transition was observed[2] at a temperature of about 720°C. For $CsCl^{35}$, the Y_{01}, Y_{11}, and Y_{21} were determined. For $CsCl^{37}$, Y_{01} and Y_{11} were obtained. Measurement of the two isotopic species allowed a determination of the mass ratio of the two Cl isotopes.

CsBr

The $J=9 \rightarrow 10$, $10 \rightarrow 11$, and $11 \rightarrow 12$ transitions were observed[2] at a temperature of about 690°C. For both $CsBr^{79}$ and $CsBr^{81}$, Y_{01}, Y_{11}, and Y_{21} were determined. Y_{02} was determined for $CsBr^{79}$, using some of the information from the $CsBr^{81}$ spectra and allowing for the dependence of Y_{02} on $1/\mu^2$. ω_e was obtained very roughly from relative intensity measurements assuming no variation of dipole moment with vibration state.

CsI

The $J=15 \rightarrow 16$, $16 \rightarrow 17$, and $17 \rightarrow 18$ transitions were observed at a temperature of about 640°C. Values of Y_{01}, Y_{11}, Y_{21}, and Y_{02} were obtained.

MOLECULAR AND NUCLEAR CONSTANTS OF THE ALKALI HALIDES

In Tables I and II, most of the available molecular data on the alkali halides is included.[1–13, 21–30] Quantities in parentheses ( ) were derived from simple theoretical relations using directly measured quantities. Those in brackets [ ] were obtained by extrapolation of other information in the tables. For some quantities, such as dipole moments, there have been several determinations made by different experimenters. The most accurate value is listed in the tables, and other values are given in the notes accompanying the tables.

---

[21] H. Levi, dissertation, Berlin, 1934 (unpublished).
[22] P. A. Tate, Massachusetts Institute of Technology Quarterly Progress Report, July 15, 1953 (unpublished).
[23] R. F. Barrow and A. D. Caunt, Proc. Roy. Soc. (London) **A219**, 120 (1953).
[24] J. W. Trischka, Phys. Rev. **76**, 1365 (1949).
[25] R. G. Luce and J. W. Trischka, Phys. Rev. **83**, 851 (1951).
[26] J. W. Trischka, Phys. Rev. **74**, 718 (1948).
[27] J. C. Schwartz and J. W. Trischka, Phys. Rev. **88**, 1085 (1952).
[28] Logan, Cote, and Kusch, Phys. Rev. **86**, 280 (1952).
[29] L. Grabner and V. Hughes, Phys. Rev. **79**, 819 (1950).
[30] V. Hughes and L. Grabner, Phys. Rev. **79**, 314 (1950).

TABLE I. Molecular constants. Quantities in parentheses ( ) were derived from simple theoretical relations using directly measured quantities. Those in brackets [ ] were obtained by extrapolation of other information in the tables.

	Y_{01} Mc/sec	B_e Mc/sec	$(-Y_{11})$ α_e Mc/sec	Y_{21} γ_e kc/sec	Y_{02} D_e kc/sec	(Y_{10}) ω_e cm^{-1}	(Y_{20}) $\omega_e x_e$ cm^{-1}	(Y_{30}) $\omega_e y_e$ cm^{-1}	I_e	r_e(A)	r_e el. diff.	μ_e debye
Li^6F												
Li^7Cl^{35}												
Li^7Cl^{37}												
Li^6Br^{81}	19 161.511 ±0.07	19 162.316 ±0.07	(208.75)	(868)	[109]							
Li^7Br^{79}	16 650.570 ±0.05	16 651.186 ±0.05	169.09 ±0.08	(656±40)	[82]	[480]	[1.7]		30.36012	2.1704 ±0.0001		6.19 ±0.15
Li^7Br^{81}	16 650.002 ±0.05	16 617.617 ±0.05	168.58 ±0.08	653±40	[82]							
Li^6I	15 381.448 ±0.08	15 381.986 ±0.08	152.59 ±0.10	(610±20)	(69.0)							
Li^7I	13 286.386 ±0.08	13 286.785 ±0.08	122.62 ±0.10	455 ±50	(51.5)	450[a]	1.5[a]	0.0017[a]	38.04799	2.3919 ±0.0001		6.25 ±0.20
NaF												
$NaCl^{35}$	6536.86 ±0.10	6537.07 ±0.10	48.28	[145]	(8.60)	380[a]	1.0[a]		77.3331	2.3606 ±0.0001	2.48	8.5 ±0.4[b]
$NaCl^{37}$					(8.24)							
$NaBr^{79}$	4534.51 ±0.10	4534.52 ±0.10	28.25 ±0.10	85 ±30	7±3	315[a]	1.15[e,f]	0.0008[a]	111.486	2.5020 ±0.0001	2.61	
$NaBr^{81}$	4509.34 ±0.10	4509.35 ±0.10	28.06 ±0.10	[84]	(4.13)							
NaI	3531.759 ±0.035	3531.778 ±0.040	19.439 ±0.030	46.9 ±6.0	(2.39)	286[a]	0.75[a]	0.001[a]	143.138	2.7115 ±0.0001	2.87	
$K^{39}F$						405[c]	1.45[c,d]					8.62[c]
$K^{39}Cl^{35}$ [f]	3856.370 ±0.007	3856.399 ±0.007	23.680 ±0.001	50 ±1		305[c,d]	0.9[c,d]		131.08913	2.6666 ±0.0001	2.76	10.48[g]
$K^{39}Cl^{37}$ [f]	3746.583 ±0.007	3746.611 ±0.007	22.676 ±0.002	47 ±1								
$K^{41}Cl^{35}$ [f]	3767.394 ±0.007	3767.421 ±0.007	22.865 ±0.001	48 ±1								
$K^{39}Br^{79}$ [h]	2434.947 ±0.007	2434.953 ±0.007	12.136 ±0.001	23 ±1		230[c,d]	0.7[c,d]		203.4372	2.8207 ±0.0001	2.91	10.41[g]
$K^{39}Br^{81}$ [h]	2415.075 ±0.007	2415.081 ±0.007	11.987 ±0.001	22 ±1								
$K^{39}I$	1825.006 ±0.030	1825.012 ±0.030	8.0337 ±0.0018	12.21 ±0.25	1.03 ±0.3	200[c,d,i]	0.5		277.00945	3.0478	3.19	11.05[c]
$K^{41}I$	1756.903 ±0.030											
$Rb^{85}F$						390[c,j]	1.3[c]					
$Rb^{87}F$												
$Rb^{85}Cl^{35}$ [k]		2627.400 ±0.003	13.6008 ±0.0035	21 ±3		270[c]	0.7[c]		192.4077	2.7868 ±0.0001	2.86	
$Rb^{85}Cl^{37}$ [k]												
$Rb^{87}Cl^{35}$ [k]												
$Rb^{85}Br^{79}$	1424.8342 ±0.02	1424.840 ±0.02	5.5782 ±0.0056	7.9 ±1.1	0.45 ±0.20	181[i]	0.35[c]		354.8006	2.9448 ±0.0001	3.02	
$Rb^{85}Br^{81}$	1406.5944 ±0.02		5.461 ±0.011									
$Rb^{87}Br^{79}$	1409.0573 ±0.02		5.4744 ±0.0085									
$Rb^{85}I$	984.3137 ±0.012	984.3166 ±0.012	3.2806 ±0.0012	2.98 ±0.20	−0.234 ±0.035	147[i]	0.25[c]		513.5883	3.1769 ±0.0001	3.22	
$Rb^{87}I$	970.7601 ±0.012		3.2135 ±0.0030									
CsF	5527.27 ±0.04	5527.34 ±0.04	33.13 ±0.05	9 ±12		385[c,l]	1.23[c]		91.4603	2.3453 ±0.0001		7.874[m,n]
$CsCl^{35}$	2161.195 ±0.015	2161.208 ±0.015	10.085 ±0.004	7.1 ±0.7		240[c]	0.6[c]		233.9118	2.9062	3.02	10.40[o]
$CsCl^{37}$	2068.761 ±0.015		9.46 ±0.03									
$CsBr^{79}$	1081.3392 ±0.02	1081.3429 ±0.02	3.7175 ±0.0029	3.1 ±0.4	−0.27 ±0.08	171[c,l]	0.3[c]		467.5039	3.0720 ±0.0001	3.10	
$CsBr^{81}$	1064.5853 ±0.02		3.6313 ±0.0024	3.1 ±0.5								
CsI	708.3568 ±0.02	708.3579 ±0.02	2.0441 ±0.0020	1.45 ±0.40	−0.152 ±0.025	120[c,l]	0.2[c]		713.6686	3.3150 ±0.0001	3.36	12.1[c]

[a] See reference 21.
[b] See reference 22.
[c] See reference 23.
[d] Levi (see reference 21) gives the following values for the potassium halides:

	ω_e (cm^{-1})	$\omega_e x_e$	$\omega_e y_e$
KCl	280	0.9	0.0011
KBr	231	0.7	0.0011
KI	212	0.7	0.001.

[e] See reference 4.
[f] See reference 8.
[g] Reference 4 gives values 9.53 and 10.85 debye for the respective dipole moments of KCl and KBr.
[h] See reference 9.
[i] For the molecules NaBr, KI, RbBr, RbI, CsBr, and CsI, values of ω_e were obtained from the experimental value of Y_{02}, or D_e. These values in cm^{-1} are:

NaBr	235±60,	KI	165±35,
RbBr	169±40,	RbI	134±15,
CsBr	143±25,	CsI	103±18.

[j] Hughes and Grabner (see reference 28) obtain $\omega_e = 340 \pm 68$ cm^{-1}.
[k] See reference 10.
[l] Trischka (see reference 26) reports $\omega_e = 270 \pm 30$ cm^{-1} from relative intensi measurements.
[m] See reference 24.
[n] The present work yielded a value of 7.85±0.25 for the dipole moment of CsF.
[o] See reference 25.

TABLE II. Electric quadrupole coupling constants and dipole moments.

Molecule	Nucleus and ref.	eqQ/h (Mc/sec) $v=0$	$v=1$	$v=2$	$v=3$	Av. over vib. state	μ_{el}(debye) $v=0$	$v=1$	$v=2$
Li^6F	[a]						$\left(\frac{450.2}{I_{v=0}}\right)^{\frac{1}{2}}$	$\left(\frac{469.6}{I_{v=1}}\right)^{\frac{1}{2}}$	
Li^7F	Li^b					+0.408			
Li^7Cl	Li^b					+0.192			
Li^7Br^{79}	Li^b					+0.184			
Li^7Br^{79}	Br	+37.20 ±0.45					6.19 ±0.15		
Li^7Br^{81}	Br	+30.71 ±0.40	+33.19 ±0.20						
Li^7I	Li^b					+0.172			
Li^7I	I	−198.15 ±0.30	−206.5 ±0.30	−212.6 ±1.5			6.64 ±0.20		
Li^6I	I	−199.43 ±0.30	−206.8 ±2.0						
NaF	Na^b					−8.12			
NaCl	Na^b					−5.40	8.5		
NaBr	Na^b					−4.68			
$NaBr^{79}$	Br	+58±2							
NaI	Na^b					−3.88			
NaI	I	−259.87 ±0.60	−264.52 ±0.65	−267.59 ±0.40	−271.03 ±0.20				
$K^{39}F$	K^c	−7.938	−7.828	−7.744	−7.658		7.33	Increase of about 0.8% per vibration	
$K^{39}Cl^{35}$	K^d	−5.656	−5.622	−5.571	−5.511		10.48		10.69
$K^{39}Cl^{35}$	Cl^d	<0.040	+0.075	+0.237	+0.393				
$K^{39}Br^{79}$	K^e	−5.003	−4.984	−4.915			10.41		9.93
$K^{39}Br^{79}$	Br^e	+10.244	+11.244	+12.204					
$K^{39}I$	I^f	−60±10					11.05		
$Rb^{85}F$	Rb^g	−70.31	−69.54	−68.71	−67.99				
$Rb^{85}Cl^{35}$	Rb^h	−52.675	−52.306	−51.903					
$Rb^{85}Cl^{35}$	Cl^h	+0.774	+0.612	+0.470					
CsF	Cs^i	+1.240					7.874	7.945	
CsCl	Cs^j	<4					10.40		
CsCl	Cl^j	<3							
CsI	[f]						12.1		

[a] See reference 27.
[b] See reference 28.
[c] See reference 29.
[d] See reference 8.
[e] See reference 9.
[f] See reference 4.
[g] See reference 30.
[h] See reference 10.
[i] See reference 24.
[j] See reference 25.

GENERAL CONSIDERATIONS CONCERNING TREATMENT OF DATA AND THE NUMERICAL RESULTS

The quantities $[Y_{01}+2Y_{02}(J+1)^2]$, Y_{11}, and Y_{21} for the molecules investigated in this paper were obtained from least square fits to Eq. (1), for lines of a given J transition. Since in most of the molecules, more than three vibrational states were measured, these three molecular parameters could be determined somewhat more accurately than indicated by the errors involved in individual measurements. The Y_{02} and Y_{01} values were also obtained from least square fits to Eq. (1) for lines from different J transitions but the same vibration state.

In general, the accuracy with which Y_{02} is determined is quite poor, and in many cases it gives rise to the principle error in Y_{01}. In calculating the mass ratio of two isotopic species, A and B, the ratio $Y_{01}{}^A/Y_{01}{}^B$ enters, and this ratio is quite insensitive to the error in Y_{02}. Hence, in Table III, more significant figures in the values of Y_{01} may be listed than might at first glance appear warranted, in view of the quoted errors. Use of the theoretical dependence of Y_{11} and Y_{21} on $1/\mu^1$ and $1/\mu^2$, respectively, also helps to decrease errors in the ratio $Y_{01}{}^A/Y_{01}{}^B$ and hence in the mass ratio. Here μ is the reduced mass.

From the values of Y_{02}, the vibration frequencies ω_e can be calculated via the relation $\omega_e=[4B_e{}^3/D_e]^{\frac{1}{2}}$. Thus, values of ω_e have been determined having approximately one-half the percentage error of D_e. In all but one of the cases where this determination was made, the ω_e agrees within the experimental error with the vibration frequencies recently determined by Barrow and Caunt.[23] Nevertheless, our vibration frequencies are consistently lower than those obtained by Barrow and Caunt. Since their method is much more prone to large *systematic* errors than that used here, the results obtained by the above method are of value.

TABLE III. Mass ratios of isotopes obtained from the microwave spectra of alkali halides. An asterisk indicates data from measurements by molecular beam techniques.

	Ratio	Molecule
Cl^{35}/Cl^{37}	0.9459781±0.0000030	CsCl
Cl^{35}/Cl^{37}	0.9459803±0.0000015	$K^{39}Cl$ [a]*
Br^{79}/Br^{81}	0.9753068±0.0000045	CsBr
Br^{79}/Br^{81}	0.9752999±0.0000065	$Rb^{85}Br$
Br^{79}/Br^{81}	0.9753088±0.0000020	$K^{39}Br$ [b]*
Li^6/Li^7	0.8573423±0.0000020	LiI
K^{39}/K^{41}	0.9512250±0.0000070	KI
K^{39}/K^{41}	0.9512189±0.0000015	KCl^{35} [a]*
Rb^{85}/Rb^{87}	0.9770177±0.0000045	RbI
Rb^{85}/Rb^{87}	0.9770146±0.0000055	$RbBr^{79}$

[a] See reference 3.
[b] See reference 4.

In the cases of RbBr and RbI, relative intensities of rotational transitions for various vibrational states were used to determine roughly the change of dipole moment μ with vibration. The relative intensity for vibration states of excitation v_1 and v_2 is given by $[(\mu_{v1})^2/(\mu_{v2})^2]\exp[-h\omega_e(v_1-v_2)/kT]$, so that the dipole moment ratio can be determined if ω_e and T are known. For both RbBr and RbI the data indicate a decrease of μ with increasing vibration state.

A. The Potential Coefficients

The vibration frequency ω_e and the first anharmonic term in the vibration spectra, $\omega_e x_e$, are known for most of the alkali halides to within an accuracy of about 10 percent. These constants, in conjunction with the Y_{01}, Y_{11}, and Y_{21} values afford sufficient information for the computation of the first four potential coefficients in the Dunham expansion. The potential energy has been expressed by Dunham in the form

$$V=hca_0\xi^2(1+a_1\xi+a_2\xi^2+a_3\xi^3+\cdots),$$

where $\xi=(r-r_e)/r_e$, $a_0=\omega_e^2/4B_e$, and both B_e and ω_e are expressed in cm^{-1}.

The dependence of all the a_i's on the value of ω_e limits the accuracy with which the potential coefficients are known. In addition, the errors increase as one goes to successively higher terms. Table IV gives the coefficients a_0, a_1, a_2, and a_3. The quantities $\mathfrak{a}_1$, $\mathfrak{a}_2$, and $\mathfrak{a}_3$ appearing beside the corresponding a's are explained in the following section. Rough estimates of the reliability of the a's would be as follows:

	Error due to uncertainty in ω_e	Error due to uncertainty in $\omega_e x_e$
a_0	±20%	
a_1	± 7%	
a_2	±20%	± 8%
a_3	±50%	±25%

The values of ω_e and $\omega_e x_e$ used were those given by Barrow and Caunt for the K, Rb, and Cs halides, and those given by Levi for the Na halides and for LiI. The ω_e and $\omega_e x_e$ for LiBr were estimated to be 480 cm^{-1}, and 1.7 cm^{-1}, respectively. Even in cases such as CsF and CsBr where Barrow and Caunt's values appear to be too high, they were none the less used for the sake of uniformity.

The potential constants can be related to the physical properties of the molecules. Rittner[31] has recently used an expression for the energy of a completely ionic diatomic molecule of the form,

$$W(r)=\varphi+Ae^{-r/\rho}-c'/r^6+\tfrac{1}{2}h\nu_0+(h\nu_0/e^{h\nu_0/kT}-1)-\tfrac{1}{2}kT,$$

where

$$\varphi=-\frac{e^2}{r}-\frac{e^2(\alpha_1+\alpha_2)}{2r^4}-\frac{2e^2\alpha_1\alpha_2}{r^7},$$

and A is a repulsion constant. Here φ is the electrostatic contribution to the potential energy, α_1 and α_2 are the polarizabilities[32] of the alkali and halogen ions, respectively, ρ is a repulsion constant, and c' is a measure of Van der Waal's attractive force between ions. If $W(r)$ is expanded about r_e, the resulting expression is

$$W(r-r_e)=C+hc\mathfrak{a}_0\left(\frac{r-r_e}{r_e}\right)^2+hc\mathfrak{a}_1\mathfrak{a}_0\left(\frac{r-r_e}{r_e}\right)^3+hc\mathfrak{a}_2\mathfrak{a}_0\left(\frac{r-r_e}{r_e}\right)^4+hc\mathfrak{a}_3\mathfrak{a}_0\left(\frac{r-r_e}{r_e}\right)^5,$$

where C is a constant term of no importance to the potential coefficients, and

$$\mathfrak{a}_0=-\frac{1}{hc}\left\{\frac{e^2}{r_e}+\frac{5e^2(\alpha_1+\alpha_2)}{r_e^4}+\frac{21c'}{r_e^6}+\frac{56e^2\alpha_1\alpha_2}{r_e^7}-\frac{r_e^2A}{2\rho^2}e^{-r_e/\rho}\right\},$$

$$\mathfrak{a}_1=\frac{1}{hc\mathfrak{a}_0}\left\{\frac{e^2}{r_e}+\frac{10e^2(\alpha_1+\alpha_2)}{r_e^4}+\frac{56c'}{r_e^6}+\frac{168e^2\alpha_1\alpha_2}{r_e^7}-\frac{r_e^3A}{6\rho^3}e^{-r_e/\rho}\right\},$$

$$\mathfrak{a}_2=-\frac{1}{hc\mathfrak{a}_0}\left\{\frac{e^2}{r_e}+\frac{17.5e^2(\alpha_1+\alpha_2)}{r_e^4}+\frac{126c'}{r_e^6}+\frac{420e^2\alpha_1\alpha_2}{r_e^7}-\frac{r_e^4A}{24\rho^4}e^{-r_e/\rho}\right\},$$

$$\mathfrak{a}_3=\frac{1}{hc\mathfrak{a}_0}\left\{\frac{e^2}{r_e}+\frac{28e^2(\alpha_1+\alpha_2)}{r_e^4}+\frac{252c'}{r_e^6}+\frac{924e^2\alpha_1\alpha_2}{r_e^7}-\frac{r_e^5A}{120\rho^5}e^{-r_e/\rho}\right\}.$$

The agreement of the quantities $\mathfrak{a}_1$, $\mathfrak{a}_2$, and $\mathfrak{a}_3$ with the experimentally determined coefficients a_1, a_2, and a_3 is a measure of the applicability of Rittner's expression for the energy. For the purpose of calculating $\mathfrak{a}_1$, $\mathfrak{a}_2$, and $\mathfrak{a}_3$, the experimental values of α_1 and α_2 can be used. London[33] has shown how the Van der Waal's constant c' can be estimated with the aid of the

[31] E. S. Rittner, J. Chem. Phys. **19**, 1030 (1951).
[32] Values used are those of L. Pauling, Proc. Roy. Soc. (London) **A114**, 181 (1927). See also reference 31.
[33] F. London, Z. Physik **63**, 245 (1930).

optically determined energy levels of the alkali ions and the electron affinities of the halogen ions.

From the experimental values of ω_e and r_e, both A and ρ can be determined from the equations,

$$(dW/dr)_{r_e}=0,$$

$$(d^2W/dr^2)_{r_e}=\text{force constant}.$$

This determination of course makes $\mathfrak{a}_0$ identical to a_0. The values computed for $\mathfrak{a}_1$, $\mathfrak{a}_2$ and $\mathfrak{a}_3$ are listed in parenthesis in Table IV for comparison with the experimental values.

The agreement must be considered quite satisfactory with the exception of LiBr and LiI.

B. Electron Diffraction Values of Internuclear Distances

On comparing the r_e values obtained by microwave spectroscopy with those obtained from electron diffraction measurements (corrected for the average over vibration states[31]), it is seen that the electron diffraction measurements are consistently larger, in most cases by amounts exceeding the experimental error. The magnitude of the discrepancy appears to vary systematically, being of the order of four percent for the lighter molecules, and decreasing progressively for the heavier molecules. (See Table I.) A possible reason for this discrepancy is a small percentage of dimerization of the vapors. This would not affect any of the spectroscopic results, but would make the electron diffraction values larger, since in a dimer, one would expect the average internuclear distance to be larger than that for a monomer.

TABLE IV. Potential coefficients a_0, a_1, a_2, and a_3 are determined from the experimental data. $\mathfrak{a}_1$, $\mathfrak{a}_2$, and $\mathfrak{a}_3$ are obtained from Rittner's theoretical expressions.

	a_0	a_1	($\mathfrak{a}_1$)	a_2	($\mathfrak{a}_2$)	a_3	($\mathfrak{a}_3$)
LiF							
LiCl							
LiBr	1.02	−2.45	(−1.71)	5.5	(+1.18)	−14	(+ 1.54)
LiI	1.14	−2.56	(−1.75)	6.0	(1.68)	−15	(+ 0.28)
NaF							
NaCl	1.66	−3.14	(−3.01)	9.2	(5.71)	−31	(− 8.0)
NaBr	1.64	−3.16	(−3.09)	7.4	(6.0)	−16	(− 8.2)
NaI	1.74	−3.23	(−3.32)	8.8	(7.0)	−26	(−11.0)
KF	1.41						
KCl	1.81	−3.43	(−3.46)	10.0	(7.7)	−32	(−12.8)
KBr	1.63	−3.35	(−3.35)	9.1	(7.4)	−26	(−11.5)
KI	1.64	−3.41	(−3.50)	9.1	(7.9)	−25	(−13.4)
RbF	1.78						
RbCl	2.08	−3.66	(−3.92)	11.8	(10.0)	−42	(−19.1)
RbBr	1.73	−3.49	(−3.53)	10.3	(8.1)	−33	(−13.7)
RbI	1.64	−3.49	(−3.55)	10.2	(8.0)	−32	(−13.6)
CsF	2.01	−3.21	(−3.35)	8.4	(7.0)	−26	(−10.8)
CsCl	2.00	−3.59	(−3.83)	10.6	(9.5)	−35	(−17.6)
CsBr	2.03	−3.72	(−4.03)	11.7	(10.5)	−41	(−20.8)
CsI	1.53	−3.45	(−3.53)	9.2	(7.9)	−26	(−13.2)

TABLE V. Internuclear distances and additivity of ionic radii. All distances are in angstrom units.

	F Internuclear distance	XCl-XF difference	Cl Internuclear distance	XBr-XCl difference	Br Internuclear distance	XI-XBr difference	I Internuclear distance
Li					2.1704	0.2215	2.3919
NaH-LiH difference					0.3316		0.3196
Na			2.3606	0.1414	2.5020	0.2095	2.7115
KH-NaH difference			0.3060		0.3187		0.3363
K			2.6666	0.1541	2.8207	0.2271	3.0478
RbH-KH difference			0.1202		0.1241		0.1291
Rb			2.7868	0.1580	2.9448	0.2321	3.1769
CsH-RbH difference			0.1194		0.1272		0.1381
Cs	2.3453	0.5609	2.9062	0.1658	3.0720	0.2430	3.3150

C. Ionic Radii

It has been found that the sum of assigned ionic radii in alkali halide crystals can satisfactorily account for the observed internuclear distances in the crystals[34] if certain factors concerning the crystal environment are taken into account. This might suggest a similar degree of constancy of ionic bonding radii in the vapors. In a former paper,[2] this has been investigated for the molecules KCl, KBr, CsCl, and CsBr. Table V gives a more complete picture of how constant the ionic radii are. Variations in the differences $r_e(XH_1)$ minus $r_e(XH_2)$ for various alkalis (X's) or $r_e(X_1H)$ minus $r_e(X_2H)$ for various halogens indicate deviation from the so-called "additivity rule."

Schomaker and Stevenson[35] have modified the additivity criterion by allowing the bond distance to be sensitive to the relative amounts of ionic and covalent character present. Their modification of the internuclear distance depends linearly upon the electronegativity difference, and hence does not affect the departure from additivity present in Table V. A quadratic dependence on the electronegativity difference would affect the additivity departure. However, the alkali bromide-iodide sequence is inconsistent with any simple scheme for modifying the internuclear distances that involves only the relative electronegativities. This might be expected, since the polarization of the atomic electrons plays an important role in determining the structure of alkali halide molecules in the vapor state, and the polarizabilities vary greatly from one alkali or halogen to the next.

Undoubtedly similar deviations from the additivity rule as large as 0.01A or 0.02A exist for other types of bonds. However, the alkali halides afford a particularly clear case for examination of these deviations, since

[34] L. Pauling, *The Nature of the Chemical Bond* (Cornell University Press, Ithaca, 1944), second edition, p. 343.

[35] V. Schomaker and D. P. Stevenson, J. Am. Chem. Soc. 63 37 (1941).

TABLE VIa. Ionic radii in angstrom units.

Ion	Diatomic molecule set No. 1	Diatomic molecule with allowance made for polarization and bond type set No. 2	Solid crystal
Li^+	0.478	0.498	0.607
Na^+	0.825	0.786	0.958
K^+	1.131	1.091	1.331
Rb^+	1.251	1.217	1.484
Cs^+	1.371	1.358	1.656
F^-	0.974	1.100	1.341
Cl^-	1.535	1.485	1.806
Br^-	1.689	1.600	1.951
I^-	1.917	1.778	2.168

they are a large group of molecules with essentially the same simple type of bond.

It is of course the great accuracy of microwave determinations of internuclear distances which allows the relatively small deviations from additivity of ionic radii to be examined in detail. If precision of only about 1 percent is required for internuclear distances, a set of ionic radii can be constructed which satisfactorily gives internuclear distances for the alkali halides. If a standard radius is chosen by Pauling's method[36] for KCl, for example, the ionic radii listed in set No. 1 of Table VIa are obtained. The internuclear distances given by the radii are compared with measured values in Table VIb.

If internuclear distances are determined simply by an attractive Coulomb potential A/r and a repulsive potential B/r^n, it can be shown that the internuclear distance should be $r=(nB/A)^{1/(n-1)}$. In most crystalline alkali halides $A=e^2$ times the Madelung constant 1.748, and the repulsion is due to six nearest neighbors. In an isolated molecule, $A=e^2$, and the repulsion is due to only one nearest neighbor. To a rough approximation, r is, in fact, given by $(nB/A)^{1/(n-1)}$, where n and B are obtained from available information on solids. However, good agreement cannot be expected, since the values of r in isolated molecules are considerably different from those in solids, and the appropriate values of n may be different. In an isolated molecule, there is an additional attractive potential due to the polarizability of each ion. Allowing for this attractive interaction, the internuclear distance should be approximately $r=[nB/A]^{1/(n-1)}-[4(\alpha_1+\alpha_2)/(n-1)r^3]$, where α_1 and α_2 are the polarizabilities of the two ions involved. Allowing for the term $-4(\alpha_1+\alpha_2)/(n-1)r^2$ lessens the agreement between experimental measurements and predictions of internuclear distance from this simple extrapolation of information about the solid alkali halides.

TABLE VIb. Internuclear distances for the gaseous alkali halides.

Molecule	Observed internuclear distance in angstrom units	Sum of ionic radii from set No. 1 of Table VIa	Calculated internuclear distance from ionic radii of set No. 2, Table VIa
LiF		1.452	1.527
LiCl		2.013	2.022
LiBr	2.1704	2.167	2.166
LiI	2.3919	2.395	2.392
NaF		1.799	1.840
NaCl	2.3606	2.361 (standard)	2.356
NaBr	2.5020	2.514	2.500
NaI	2.7115	2.742	2.727
KF	2.55*	2.105	2.129
KCl	2.6666	2.666 (standard)	2.666 (standard)
KBr	2.8207	2.821 (standard)	2.815
KI	3.0478	3.048 (standard)	3.051
RbF		2.225	2.246
RbCl	2.7868	2.787 (standard)	2.793
RbBr	2.9448	2.941	2.944
RbI	3.1769	3.168	3.182
CsF	2.3453	2.345 (standard)	2.346
CsCl	2.9062	2.906 (standard)	2.911
CsBr	3.0720	3.060	3.065
CsI	3.3150	3.288	3.307

* Measured roughly by resonance between Stark components with molecular beam techniques. (See reference 29.)

[36] L. Pauling, reference 34, p. 344.

A useful empirical expression for internuclear distances of these molecules can be constructed which fits the experimental data to an accuracy of about 0.005 A. Such an expression is

$$r=r_1+r_2-0.410[(\alpha_1+\alpha_2)/r^3]+0.175[(X_F-X_{Cs})-(X_2-X_1)],$$

where X_1 and X_2 are the electro negatives of atoms 1 and 2, respectively. The values of r_1 and r_2 in this expression are taken equal to those for the crystal ionic radii obtained by Pauling[34] multiplied by the factor 0.820. From the discussion above, the ratio of distances in the vapor and crystalline phases may be expected to be

$$\frac{r\ (\text{vapor})}{r\ (\text{crystal})}=\left[\frac{nB}{(6nB/1.748)}\right]^{1/(n-1)}=(0.29)^{1/(n-1)}.$$

This ratio equals 0.820 when n is between 7 and 8, which is a reasonable average value for n in the solid alkali halides. As is expected, the polarization term shortens the internuclear distance. The term involving the electronegativities is somewhat similar to that introduced by Schomaker and Stevenson. It has little theoretical justification, especially since the alkali halides are almost entirely ionic. However, its introduction does allow an improved fit to experimentally determined internuclear distances.

Table VIa lists the set of radii (No. 2) which are 0.820 times Pauling's radii[37] for solid alkali halides, and Table VIb allows comparison between calculated and measured internuclear distances. These radii are not of great interest in themselves, but they should allow fairly accurate estimation of internuclear distances of the alkali halides which have not yet been measured.

D. Electric Quadrupole Coupling Constants

In "ionic" substances such as the alkali halides the quadrupole coupling constant is the resultant of several

[37] L. Pauling, reference 34, p. 64.

small terms of different signs, and hence it is particularly difficult to predict theoretically.

Quadrupole coupling constants of the halogens are most easily treated, since for a covalently bonded halogen, the single p electron missing from the valence shell of the halogen produces a large coupling constant,[38] and in some of the alkali halides the covalent character is large enough (although quite small) to make this source of coupling dominant. An isolated negative halogen ion has zero quadrupole coupling. For covalent bonds, coupling constants near -110.4 Mc/sec, 769.8 Mc/sec, and -2292.4 Mc/sec are to be expected for Cl^{35}, Br^{79}, and I^{127}, respectively (F has zero quadrupole moment). Coupling constants for these atoms in the alkali halides are very much less than the above numbers, but are always of the same sign. In some cases (such as NaI) the coupling constants are large enough to indicate fairly clearly that the relatively small covalent character produces the dominant contribution to the coupling constant. In others (such as KCl), the coupling constants are so small that other effects are surely of importance. These include contributions due to the electric field of the neighboring alkali, and that due to distortions of the valence shell of electrons by polarization.

The quadrupole coupling constants of the halogens probably give the clearest available evidence on the amount of covalent character in the structure of the alkali halides. If the measured coupling constants are devided by the coupling constant given above for purely covalent bonds, one obtains the results listed in Table VII. The covalent character of the alkali halide bonds is given approximately by these numbers.[38] It may be noted that in accordance with expectations the covalent character obtained from Table VII decreases with increasing electronegativity of the halogens I, Br, and Cl. However, LiI appears to be slightly less covalent than NaI from this table in spite of the fact that the electronegativity difference between Li and I is less than that between Na and I. This may be due to effects of polarization or other contributions to the coupling constant in the two molecules, or it may simply be due to the fact that covalent character depends on other variables in addition to the electronegativity difference. The small size of Li, for example, can be expected to lower the energy of the ionic state of LiI by comparison with that of NaI.

The results listed in Table VII give further evidence that the alkali halides are almost purely ionic. They also show, however, that some of the alkali halides involving the least electronegativity differences have a small amount of covalent character.

Quadrupole coupling constants for the alkalis are more difficult to understand than those for the halogens because both the ionic and the atomic states of the alkali elements have spherical distributions of electrons and hence zero quadrupole coupling constants. The coupling constants observed in the molecule are evidently due to distortions or excitations of the electron shells about the alkali atoms, and to charges on the adjacent halogens.

[38] C. H. Townes and B. P. Dailey, J. Chem. Phys. **17**, 782 (1949).

TABLE VII. Ratio of quadruple coupling constant for the halogens to that due to a single p electron.

Molecule	Ratio
KCl	0.0004
KBr	0.013
KI	0.026
NaBr	0.075
NaI	0.113
LiBr	0.048
LiI	0.086

E. Electric Dipole Moments

Table VIII lists the values of the dipole moments calculated from Rittner's[31] expression,

$$\mu = er_e - \frac{[r_e^4 e(\alpha_1+\alpha_2)+4er_e\alpha_1\alpha_2]}{r_e^6-4\alpha_1\alpha_2},$$

where α_1 and α_2 are the ionic polarizabilities. The experimental dipole moments obtained by molecular beams or microwave spectroscopy are also listed, for comparison. The calculated values are consistently lower, even for the LiBr and LiI, which have considerable covalent character. The polarizabilities may possibly be in error, but it seems more likely that the disagreement is primarily because the classical model used is not adequate for computing reliable induced dipole moments.

TABLE VIII. Comparison of dipole moments calculated from polarized ion model with experimental values.

	μ calculated	μ experimental
LiF		
LiCl		
LiBr	5.139	6.25 ±0.15
LiI	5.375	6.64 ±0.20
NaF		
NaCl	7.770	8.5 ±0.4
NaBr	7.959	
NaI	7.993	
KF		
KCl	9.180	10.48 ±0.03
KBr	9.576	10.41 ±0.02
KI	9.922	(11.05)
RbF		
RbCl	9.450	
RbBr	9.925	
RbI	9.762	
CsF	7.278	7.874±0.012
CsCl	9.363	10.40 ±0.10
CsBr	9.974	
CsI	10.612	(12.1)

ACKNOWLEDGMENTS

The authors wish to express their thanks to Mr. C. Dechert, foreman of the Columbia Radiation Laboratory shop, to Mr. A. Marshall, and to other members of the shop. Their ingenuity and cooperativeness contributed greatly to the success of these experiments. We should also like to thank Mr. G. Dousmanis, who aided in the calculations.

APPENDIX I. MEASURED FREQUENCIES IN MC/SEC FOR MICROWAVE TRANSITIONS OF THE ALKALI HALIDES

LiBr: $J=0 \rightarrow 1$.

Transition	$v=0$ state	$v=1$	$v=2$
	Li^7Br^{79}		
$F=3/2 \rightarrow 5/2$	33 130.30±0.10		32 461.52±0.10
$F=3/2 \rightarrow 3/2$	33 139.50±0.10		
$F=3/2 \rightarrow 1/2$	33 122.44±0.30		
	Li^7Br^{81}		
$F=3/2 \rightarrow 5/2$	33 063.96±0.10	32 729.14±0.10	32 397.13±0.10
$F=3/2 \rightarrow 3/2$	33 071.53±0.10	32 737.53±0.10	
$F=3/2 \rightarrow 1/2$	33 057.54±0.25	32 722.60±0.10	
	Li^6Br^{81}		
$F=3/2 \rightarrow 5/2$	38 112.72±0.10		

LiI: $J=0 \rightarrow 1$.

Transition	$v=0$	$v=1$	$v=2$
	Li^7I		
$F=5/2 \rightarrow 7/2$	26 460.14±0.10	26 217.11±0.10	25 975.62±0.20
$F=5/2 \rightarrow 5/2$	26 418.44±0.10	26 173.72±0.10	25 931.21±0.20
$F=5/2 \rightarrow 3/2$	26 477.88±0.10	26 235.65±0.10	25 995.48±0.40
	Li^6I		
$F=5/2 \rightarrow 7/2$	30 620.17±0.10	30 317.79±0.20	
$F=5/2 \rightarrow 5/2$	30 578.28±0.10		
$F=5/2 \rightarrow 3/2$	30 638.10±0.15	30 336.40±0.40	

NaCl: $J=1 \rightarrow 2$.

$v=0$	$v=1$	$v=2$	$v=3$
	$NaCl^{35}$		
26 051.1±0.75	25 857.6±0.75	25 666.5±0.75	25 473.9±0.75
	$NaCl^{37}$		
25 493.9±0.75	25 307.5±0.75	25 120.3±0.75	

NaBr

Rotational transition	Hyperfine transition	$v=0$	$v=1$	$v=2$	$v=3$	$v=4$
			$NaBr^{79}$			
$J=1 \rightarrow 2$	$F=5/2 \rightarrow 7/2$ $3/2 \rightarrow 5/2$	18 080.13±0.10	17 968.42±0.20	17 856.57±0.10		
	$F=1/2 \rightarrow 3/2$ $5/2 \rightarrow 5/2$	18 095.95±0.15[a]	17 082.5±0.8[a]			
	$F=3/2 \rightarrow 3/2$	18 070.07±0.10				
$J=2 \rightarrow 3$	$F=7/2 \rightarrow 9/2$ $5/2 \rightarrow 7/2$	...	26 952.98±0.10[a]	26 785.63±0.10[a]	26 621.8±0.8[a]	26 455.8±0.8[a]
	$F=3/2 \rightarrow 5/2$ $1/2 \rightarrow 3/2$	...	26 956.30±0.30[a]	26 789.51±0.30[a]	...	...
			$NaBr^{81}$			
$J=1 \rightarrow 2$	$F=5/2 \rightarrow 7/2$ $3/2 \rightarrow 5/2$	17 980.48±0.20[a]	17 868.49±0.10			
	$F=3/2 \rightarrow 3/2$	17 971.0±0.5[a]				
$J=2 \rightarrow 3$	$F=7/2 \rightarrow 9/2$ $5/2 \rightarrow 7/2$	...	26 803.55±0.10[a]	26 639.9±0.8[a]	26 475.0±0.8[a]	
	$F=3/2 \rightarrow 5/2$ $1/2 \rightarrow 3/2$	...	26 806.32±0.40[a]	26 643.2±0.8[a]	...	

[a] Due to overlap of neighboring lines, the above figures do not necessarily represent true line positions, but rather maxima corresponding to the designated transition. The true line positions can be calculated from these.

NaI: $J=2\rightarrow 3$.

Transition	$v=0$	$v=1$	$v=2$	$v=3$	$v=4$
$F=9/2\rightarrow 11/2$	21 135.35±0.20	...	20 903.62±0.20	20 788.73±0.20	20 674.43±0.2
$F=7/2\rightarrow 9/2$	21 137.49±0.20	21 021.50±0.20	20 906.05±0.20	20 791.24±0.20	20 676.96±0.2
$F=5/2\rightarrow 7/2$	21 124.58±0.20	21 008.40±0.20	20 892.92±0.20	20 777.70±0.20	20 663.68±0.2
$F=3/2\rightarrow 5/2$	21 111.67±0.20	...	20 879.61±0.20	20 764.43±0.40	...
$F=1/2\rightarrow 3/2$	21 108.64±0.20	...	...	...	...
$F=9/2\rightarrow 9/2$	...	20 970.52±0.20	20 854.59±0.20	20 738.98±0.20	...
$F=7/2\rightarrow 7/2$		same frequencies as $7/2\rightarrow 9/2$ transitions			
$F=5/2\rightarrow 5/2$	21 148.85±0.20	...	20 917.89±0.20	20 803.00±0.20	...
$F=3/2\rightarrow 3/2$	21 141.93±0.20	...	...	...	...
$F=1/2\rightarrow 1/2$	...	...	...	...	...

KI

v	$J=4\rightarrow 5$	$J=5\rightarrow 6$	$J=6\rightarrow 7$
		$K^{39}I$	
0	18 209.77±0.10[a]	21 851.32±0.10	25 492.81±0.15
1	18 129.61±0.20	21 755.19±0.10	25 380.71±0.15
2	...	21 659.38±0.10	25 268.95±0.15
3	...	21 563.91±0.10	25 157.04±0.30
5	...	21 373.63±0.10	...
6	...	21 279.07±0.10	...
7	...	21 184.73±0.10	...
		$K^{41}I$	
0		21 036.78±0.10	

[a] The shape of this line was used to obtain $(eqQ)_I$. The frequency given is the peak of the line. A secondary maximum occurred at a frequency 18 208.97 ±0.10 Mc/sec.

RbBr

Rotational transition	Vibration state	$Rb^{85}Br^{79}$	$Rb^{87}Br^{79}$	$Rb^{85}Br^{81}$
$J=8\rightarrow 9$	0	25 596.03±0.10	25 312.99±0.10	25 268.84±0.10
	1	25 495.98±0.10	25 214.65±0.10	25 170.56±0.10
	2	25 396.14±0.10	25 116.57±0.10	25 072.63±0.10
	3	25 296.52±0.10		
	4	25 197.32±0.10		
$J=7\rightarrow 8$	0	22 752.29±0.10		

RbI

Rotational transition	Vibration state	$Rb^{85}I$	$Rb^{87}I$
$J=12\rightarrow 13$	0	25 547.52±0.10	25 196.01±0.10
	1	25 462.28±0.10	25 112.84±0.10
	2	25 377.33±0.10	25 029.38±0.10
	3	25 292.65±0.10	
	4	25 207.88±0.20	
	5	25 123.45±0.10	
	6	25 038.99±0.10	
$J=11\rightarrow 12$	1	23 503.98±0.10	
	2	23 425.51±0.10	
$J=10\rightarrow 11$	0	21 617.58±0.10	

CsF: $J=1\rightarrow 2$.

Vibration state	Frequency
0	22 038.51±0.20
1	21 898.21±0.40
2	21 757.58±0.60
3	21 617.09±0.60
4	21 477.5±1.0

CsCl: $J=5\rightarrow 6$.

Vibration state	$CsCl^{35}$	$CsCl^{37}$
0	25 873.11±0.10	24 767.86±0.10
1	25 752.16±0.20	24 654.86±0.30
2	25 631.58±0.20	24 541.40±0.50
3	25 511.25±0.20	
4	25 390.36±0.40	
5	25 270.0 ±0.6	
6	25 150.1 ±0.6	
7	25 031.0 ±0.6	
8	24 911.2 ±0.6	

CsBr

Isotopic species	Vibration state	$J=9\rightarrow 10$	$J=10\rightarrow 11$	$J=11\rightarrow 12$
$CsBr^{79}$	0	21 588.57±0.10	23 747.17±0.10	...
	1	21 514.48±0.20	23 665.60±0.20	25 816.53±0.20
	2	21 440.65±0.20	23 583.87±0.20	25 648.95±0.20
	3	21 366.36±0.20	23 502.95±0.20	25 550.22±0.20
	4	21 292.40±0.20	...	...
	5	21 218.66±0.20	23 340.26±0.20	
	6	...	23 259.19±0.20	
	7		23 178.25±0.20	
	8		23 097.97±0.20	
$CsBr^{81}$	0	21 254.44±0.10	23 379.53±0.10	25 504.69±0.10
	1	...	23 299.79±0.20	...
	2		23 220.22±0.20	
	3		23 140.61±0.20	
	4		23 061.38±0.20	

CsI

Vibration state	$J=15\rightarrow 16$	$J=16\rightarrow 17$	$J=17\rightarrow 18$
0	22 632.26±0.10	24 046.40±0.10	25 460.53±0.10
1	22 567.02±0.10	23 976.96±0.10	25 387.04±0.10
2	...	23 907.70±0.10	25 313.66±0.10
3		23 838.47±0.10	...

APPENDIX II. DATA FOR DETERMINATION OF DIPOLE MOMENTS.

LiBr

Data on $J=0\rightarrow 1$, $F=3/2\rightarrow 5/2$, $v=0$, Li^7Br^{79} line.

Voltage (volts)	Frequency (Mc/sec)
+ 4.0	33 130.30±0.10
+27.0	33 132.02±0.10
+50.2	33 136.96±0.10

LiI

Data on $J=0\rightarrow 1$, $F=5/2\rightarrow 7/2$, $v=0$, Li^7I line.

Voltage (volts)	Frequency (Mc/sec)
0	26 460.14±0.10
23.3	26 462.23±0.10
47.0	26 468.60±0.20
70.3	26 478.56±0.20

CsF

Data on $J=1\rightarrow 2$, $v=0$, line.

Voltage (volts)	Frequency (Mc/sec)	
	$M=0$ component	$M=1$ component
0	22 038.51±0.20	22 038.51±0.20
25[a]	22 034.05±0.30	22 039.89±0.30
50[a]	22 026.63±0.40	22 047.31±0.40
75[a]	22 013.68±0.50	22 056.21±0.50

[a] These are not the true voltages, but the dipole moment was determined by direct comparison with the OCS molecule. The actual voltage is within 10 percent of the stated values.

Calibration of electric field strength in guide *vs* voltage on Stark plate, using CH_3Cl^{37} ($J=0\rightarrow 1$, $F=3/2\rightarrow 5/2$, $K=0$ line).

Voltage (volts)	Frequency (Mc/sec)
−4.0	26 179.22±0.05
19.3	26 179.35±0.05
43.0	26 179.78±0.05
66.3	26 180.53±0.10
89.5	26 181.58±0.10
136.6	26 184.79±0.10

Ionization Produced by 5-Mev Alpha Particles in Argon Mixtures

C. E. MELTON, G. S. HURST, AND T. E. BORTNER
Health Physics Division, Oak Ridge National Laboratory, Oak Ridge, Tennessee

(Received May 17, 1954)

It is shown that when small amounts of impurities are added to argon extra ionization is produced by alpha particles moving through the gas. These effects are studied as a function of the ionization potential of the added impurity and it is found that the ionization increases even when the ionization potential is much higher than the well-known metastable state of argon.

INTRODUCTION

IT is known that small traces of impurities in some of the noble gases greatly increase the amount of ionization produced by alpha particles losing their energy in the gas.[1,2] Most of the investigations have been concerned with helium, and the decrease in the value of W (alpha-particle energy divided by number of ion pairs produced) was attributed to a discharge of the metastable state of the noble gas by an impurity which had an ionization potential less than or equal to the metastable level. In this reaction the impurity was ionized and the resultant ion pairs collected, thus lowering the W value. For example, if argon, whose ionization potential is 15.7 volts, is added to helium, the reaction

$$He^*+A \rightarrow He+A^++e^-$$

can take place since the excitation energy of the metastable state of helium (He^*) is greater than the ionization potential of argon. In fact, Biondi[3] has measured the cross section of this reaction and reports 1.0×10^{-16} cm^2. Sharpe[4] found an increase in ionization when carbon dioxide was added to argon. This increase could not be explained by the type of reaction described above since the ionization potential of carbon dioxide is greater than the metastable state in argon.

In the present work a systematic study of argon was made by adding to it other gases in measured percentages and observing their effect on the W value. The gases for the argon mixtures were selected to meet the requirement of a continuous range of ionization potentials from 8.5 ev to 15.7 ev, in order to study the effect both above and below the well-known metastable state in argon at 11.5 ev.

A somewhat similar investigation was carried out concurrently in Europe by Bertolini, Bettoni, and Bisi.[5] The results for the five gases they studied compare favorably with the results of this investigation; however, the complete results from this investigation do not support their conclusion, namely, that the lower the ionization potential of the foreign gas the higher the maximum ionization. The five gases for which they reported results will support this conclusion, but this is not true for other gases, as is shown by Fig. 7.

EXPERIMENTAL RESULTS

A description of the apparatus has previously been reported.[6] An uncollimated Pu^{239} alpha source was placed in the center of a large parallel-plate ionization chamber, and the ionization produced was measured by means of an accurately calibrated capacitor, a stable high-voltage supply, a vibrating-reed electrometer, and a potentiometer. Great care was exercised to assure purity of the gases investigated. They were obtained in the extra pure form and further purified by fractional distillation. In some cases the ionization was measured during a continuous gas flow through the chamber.

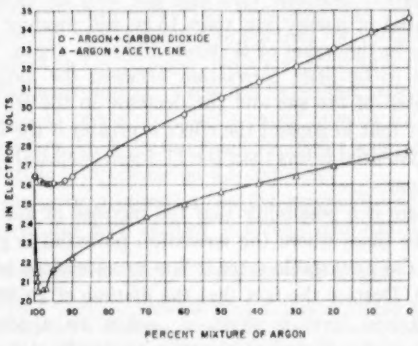

FIG. 1. W values for Pu alpha particles in mixtures of argon+carbon dioxide and argon+acetylene.

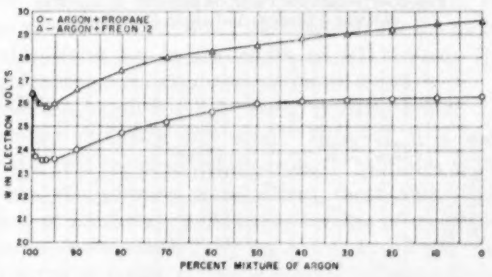

FIG. 2. W values for Pu alpha particles in mixtures of argon+propane and argon+Freon-12.

[1] Jesse, Forstat, and Sadauskis, Phys. Rev. **88**, 417 (1952).
[2] T. E. Bortner and G. S. Hurst, Phys. Rev. **90**, 160 (1953).
[3] M. A. Biondi, Phys. Rev. **88**, 660 (1952).
[4] J. Sharpe, Proc. Phys. Soc. (London) **A65**, 859 (1952).
[5] Bertolini, Bettoni, and Bisi, Phys. Rev. **92**, 1586 (1953).
[6] T. E. Bortner and G. S. Hurst, Phys. Rev. **93**, 1236 (1953).

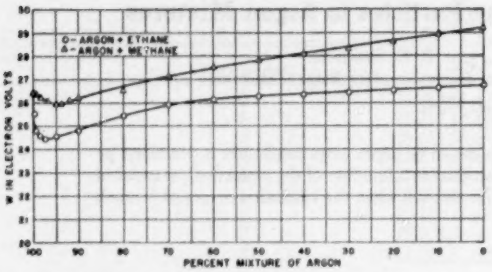

FIG. 3. W values for Pu alpha particles in mixtures of argon+ethane and argon+methane. ■

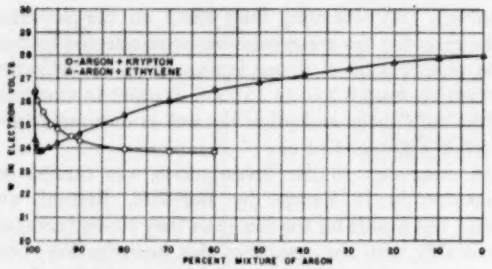

FIG. 4. W values for Pu alpha particles in mixtures of argon+krypton and argon+ethylene.

In Figs. 1–6 results are given for argon and various gas mixtures. The value of W in electron volts per ion pair is plotted on the ordinate, and the percent mixture of each gas on the abscissa. The percent of argon is given at each point; the remaining percentage consists of the gas indicated. It is interesting to note that large increases in ionization occur at very small percentages of impurities in argon. Acetylene gives a greater effect than any other gas investigated although it has an ionization potential much higher than some of the other gases. The results shown in these figures are believed to be correct to within one-half of one percent.

Figure 7 is a plot of the minimum W values observed, as a function of the ionization potentials of the gas component which is added to argon. The numbers in parentheses are the percents of the impurities required to give the minimum values for W. In the case of krypton the plotted "minimum" W value, 24.2, is simply the W value at the mixture giving the maximum deviation of the experimental curve from a straight line drawn through the W values of pure argon and pure krypton.

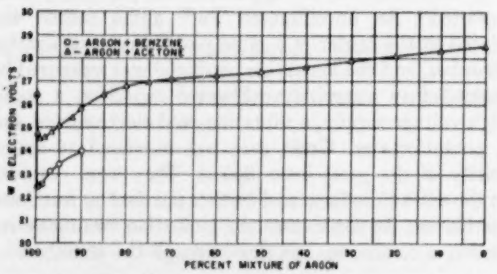

FIG. 5. W values for Pu alpha particles in mixtures of argon+benzene and argon+acetone.

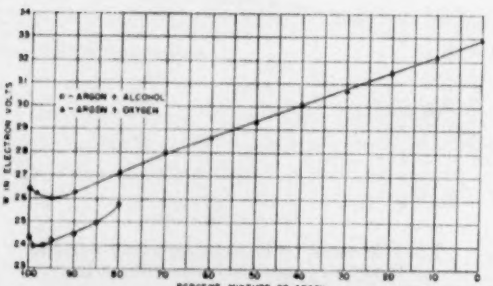

FIG. 6. W values for Pu alpha particles in mixtures of argon+alcohol and argon+oxygen.

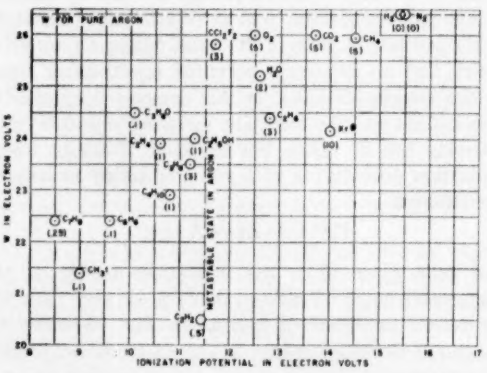

FIG. 7. Summary of effects of impurities on minimum W values for alpha particles in argon. The numbers in parentheses are the percents of the impurities required to give the minimum values of W.

CONCLUSIONS

Figure 7 indicates that any gas with an ionization potential of energy less than 15 ev will produce a decrease in the value of W when added to argon. There seems to be little correlation between the ionization potential of the gas and the decrease in the W value, except that in general the effect is greater if the ionization potential is less than the 11.5-volt metastable level in argon.

There is a possibility that the increase in ionization for the cases where the ionization potential is greater than the metastable state is due to an excited level in argon. Despite the fact that the lifetime of an atom in an excited level is short, it makes an appreciable number of collisions with other molecules before returning to the ground level. Consider a mixture of argon (95 percent) and methane (5 percent) at atmospheric pressure and room temperature. Then if the average velocity of the argon atoms is assumed to be unaffected by the methane, the number of collisions

of the argon atoms with methane molecules would be approximately 10^8 per second per excited argon atom. The assumption that the cross section measured by Biondi for the destruction of metastable helium by argon applies to the argon-methane reaction leads to approximately 5×10^6 destructions (hence ionizations) per second per excited argon. Therefore an excited state lifetime of only a few microseconds would be long enough to explain the observed increases in ionization. The generally larger increases in ionization in impurities whose ionization potential is less than the 11.5-volt metastable state can be attributed to the utilization of the energy in the metastable state as well as that of the excited state in producing ionization.

PHYSICAL REVIEW VOLUME 96, NUMBER 3 NOVEMBER 1, 1954

Hyperfine Structure of Nitrogen*

MARK A. HEALD† AND ROBERT BERINGER
Sloane Physics Laboratory, Yale University, New Haven, Connecticut
(Received July 23, 1954)

The magnetic resonance spectrum of the ^4S ground state of atomic nitrogen-14 has been observed using the microwave absorption method. The magnetic-dipole hyperfine interaction constant is

$A=10.45\pm0.02$ Mc/sec.

No evidence was obtained for electric quadrupole interaction.

INTRODUCTION

THE observation of magnetic resonance transitions between hyperfine sublevels in atoms is useful for measuring hyperfine interaction energies and, in many cases, for obtaining the nuclear moments as such. This is an important technique for evaluating nuclear quadrupole moments. The interaction of nuclear moments with a single valence electron outside closed shells can be calculated quite reliably.[1] A generally successful procedure for obtaining nuclear moments from a knowledge of the hfs interaction constants has been developed for this case and can be immediately extended to the case of a closed shell less one electron.[2] The situation with several valence electrons is considerably more complicated.[3] Goudsmit has evaluated theoretically the magnetic interaction for special configurations on *LS* coupling[4]; Breit and Wills have treated intermediate coupling.[5] Trees has developed generalized formulas, in terms of Racah's tensor algebra for complex spectra, for both the magnetic-dipole and electric-quadrupole interactions on *LS* coupling.[6]

In the present investigation the magnetic resonance technique has been applied to atomic nitrogen. It was initially hoped that fine-structure and hyperfine-structure interaction constants could be measured for both the ground and metastable states of the nitrogen atom, and that perhaps some estimate of the quadrupole moment of N^{14} could be obtained. However, useful analysis of observed spectra is severely limited by the presence of considerable configuration interaction in nitrogen. Experimental difficulties have prevented observation of magnetic resonance spectra from the metastable states. Observations in connection with the atomic-nitrogen source are, however, of some interest in the long-standing problem of "active" nitrogen.

The ground electronic configuration of the nitrogen atom is $2p^3$, which forms the Russell-Saunders terms ^4S, ^2D, and ^2P. The $^4S_{\frac{3}{2}}$ state is the normal ground state; the doublet states are metastable. It is well-known that the N^{14} nucleus possesses both magnetic-dipole and electric-quadrupole moments. According to the nonrelativistic *LS* coupling formulas of Goudsmit and Trees, the magnetic hfs interaction constant for the ground state vanishes; the constants for the metastable states are in the region of 100 Mc/sec. The quadrupole interaction vanishes for all states.

Since nitrogen is a light atom, deviations from *LS* coupling should be very small.[7] However, it is well-known that the observed electrostatic splittings of the ground-configuration terms depart significantly from those of *LS* theory, presumably because of configuration interaction with $2p^23p$ states.[8] Although the fine-structure intervals of the metastable doublet states would vanish according to *LS* coupling theory, small

* Assisted by the Office of Naval Research and the du Pont Company.

† du Pont Company Fellow in Physics. Now at Project Matterhorn, Princeton University, Princeton, New Jersey. This work is part of a dissertation presented to Yale University for the Ph.D. degree.

[1] H. B. G. Casimir, *Interaction Between Atomic Nuclei and Electrons* (Teyler's Tweede Genootschap, Haarlem, 1936).
[2] Davis, Feld, Zabel, and Zacharias, Phys. Rev. **76**, 1076 (1949).
[3] H. Lew, Phys. Rev. **91**, 619 (1953).
[4] S. Goudsmit, Phys. Rev. **37**, 663 (1931).
[5] G. Breit and L. A. Wills, Phys. Rev. **44**, 470 (1933).
[6] R. E. Trees, Phys. Rev. **92**, 308 (1953).
[7] D. R. Inglis, Phys. Rev. **38**, 862 (1931).
[8] E. U. Condon and G. H. Shortley, *Theory of Atomic Spectra* (Cambridge University Press, London, 1935), p. 198.

negative splittings are observed in optical spectra which indicate the effects of spin-other-orbit and configuration interactions.[9]

Some years ago Jackson and Broadway performed a Stern-Gerlach experiment in an attempt to measure the magnetic moment of the product of a nitrogen discharge.[10] The trace on their chemical target indicated the presence of a component with $M_J g_J = \pm\frac{1}{3}$, which corresponds to the $^2P_{\frac{1}{2}}$ metastable state. However, they were unable to account satisfactorily for the absence of any indication of other states, all of which have larger Mg values (e.g., $^2P_{\frac{1}{2}}: Mg = \pm\frac{2}{3}, \pm 2$; $^4S_{\frac{3}{2}}: Mg = \pm 1, \pm 3$). It would also seem that, for any magnetic field reasonable in a Stern-Gerlach type of experiment, a virtually complete Paschen-Back effect would occur for the nearly-degenerate $^2P_{\frac{1}{2}}$ and $^2P_{\frac{3}{2}}$ states (whereupon $Mg = 0, \pm 1, \pm 2$) which would invalidate the evidence for the presence of the $^2P_{\frac{1}{2}}$ state. In view of these inconsistencies, it appears that little confidence can be placed in their conclusions.

With the exception of the atomic nitrogen source, the experimental technique used in the present investigation was identical to that used in our precision measurement of the electron g factor in atomic hydrogen.[11] Atomic nitrogen vapor was pumped in a fused-silica tube through a 9185-Mc/sec resonant cavity located in a modulated, proton-controlled magnetic field. Absorption of microwave energy by the atomic vapor was detected when the magnetic field was adjusted such that a magnetic resonance transition coincided with the cavity frequency.

ATOMIC NITROGEN SOURCE

The production of atomic nitrogen is intimately connected with the phenomenon of "active nitrogen." Nitrogen excited in discharge tubes of certain types manifests greatly enhanced chemical activity and a yellow glow which persists after the excitation is removed, under some conditions remaining visible for an hour or more. The afterglow consists of certain well-known band systems of the neutral nitrogen molecule. The mechanism of this afterglow has been the subject of extensive investigation for many years. It is well established that the essential component of active nitrogen is atomic nitrogen, and that the necessity of three-body collisions (or chemical reactions) to bring about recombination of the atoms is responsible for the main features of long life and high energy content.

In order to explain the selective enhancement of the particular band systems present in the afterglow, it is necessary to assume that the metastable ^2D and ^2P atomic states as well as the metastable $A^3\Sigma_u^+$ molecular state are essential to the process. The theory of Cario and Kaplan[12] therefore postulated that a considerable fraction of the atoms in active nitrogen are in the metastable states. An extensive series of experiments by Okubo and Hamada, however, indicated that the actual concentration of metastable components is very small.[13] Cario was able to preserve the energetic function of the metastable atoms by assuming them to be short-lived intermediate products in a chain of interactions producing the afterglow.[14] Frost and Oldenberg searched unsuccessfully for infrared absorption bands due to the metastable molecular state and concluded that the metastable components, both molecules and atoms, have lifetimes of only a millisecond or less.[15] There are nonradiative processes of atomic recombination in addition to the process producing the visible afterglow.[16] Indeed, Rayleigh has estimated that only about 0.1 percent of the atoms and molecules present contribute to the afterglow under the brightest conditions.[17] Oldenberg has recently discussed some aspects of the active nitrogen problem.[18]

Active, or atomic, nitrogen is not formed in a high-voltage dc discharge of the type which is so successful for hydrogen.[11,19] A pulsed rf (electrodeless) discharge[20] or a condensed discharge[21] is required. The latter is a relaxation-oscillator arrangement in which the discharge tube, sometimes with a series air spark-gap, forms the intermittent element. In either type the dynamic nature of the process allows high fields to exist throughout the discharge tube rather than to be concentrated in the small region of the cathode fall of a dc glow discharge.

In the present investigation a condensed discharge was used to obtain nitrogen atoms in the ground ^4S state. A high-voltage power supply charged a 5-μf capacitor through a 20 000-ohm resistor. A long U-shaped tube with aluminum electrodes (identical to that used in our atomic hydrogen work)[11] was connected in parallel with the capacitor; discharge occurred about eight times per second. The 5-kv unloaded output of the power supply was reduced to a time-average of about 3.2 kv at 100 ma with relaxation-oscillator load. The walls of the discharge-tube exit tubulation were coated with metaphosphoric acid. Rayleigh observed that this treatment significantly prolonged the life of the afterglow.[20]

Tank nitrogen was introduced into the discharge tube near the electrodes by means of a reducing valve

[9] Aller, Ufford, and Van Vleck, Astrophys. J. **109**, 42 (1949).
[10] L. C. Jackson and L. F. Broadway, Proc. Roy. Soc. (London) **A127**, 678 (1930).
[11] R. Beringer and M. A. Heald, Phys. Rev. **95**, 1474 (1954).
[12] G. Cario and J. Kaplan, Z. Physik **58**, 769 (1929).
[13] J. Okubo and H. Hamada, Phys. Rev. **42**, 795 (1932).
[14] G. Cario, Z. Physik **89**, 523 (1934).
[15] A. A. Frost and O. Oldenberg, Phys. Rev. **48**, 66 (1935).
[16] D. E. Debeau, Phys. Rev. **61**, 668 (1942).
[17] Lord Rayleigh, Proc. Roy. Soc. (London) **A176**, 1 (1940).
[18] O. Oldenberg, Phys. Rev. **90**, 727 (1953).
[19] R. W. Wood, Phil. Mag. **44**, 538 (1922).
[20] Lord Rayleigh, Proc. Roy. Soc. (London) **A151**, 567 (1935).
[21] J. H. Greenblatt and C. A. Winkler, Can. J. Research **B27**, 721 (1949).

and capillaries. The pressure of the vapor in the microwave cacity was of the order of 0.1 mm; the discharge-tube pressure was somewhat higher.

With the arrangement just described, it was found that the condensed discharge, after running a few minutes, would cease operating unless water vapor was introduced by bubbling the input nitrogen through a water bottle. Apparently the peak fields available were insufficient to initiate discharge in dry nitrogen. Subsequently the discharge tube was shortened from 1.4 m to 0.9 m total length to increase the peak field. The condensed discharge then operated dependably with dry nitrogen, although the intensities of the visible afterglow and the magnetic resonance spectrum from the ^4S state were greatly diminished. The original intensities were immediately restored and sustained upon introduction of water vapor. There is considerable evidence that impurities do have an important effect on the characteristics of active nitrogen.[22] The present observation that afterglow and ground-state-atom concentration are dependent on the presence of a significant amount of water does not, however, seem to follow from previous results.[20] The Wood's-tube condensed discharge, with water vapor present, proved to be a dependable and copious source of ground-state nitrogen atoms. The afterglow was easily visible in the pumping line as far as the diffusion pump, about six feet from the discharge tube.

An extensive search was made for magnetic resonance spectra from the metastable ^2D and ^2P states, using a number of different types of discharge. No trace of these spectra was found. It was felt that the most promising source used in this search consisted of the production of active (i.e., ground-state-atomic) nitrogen with the condensed discharge and then subjecting the vapor stream to a weak electrodeless discharge of some sort immediately preceding the microwave cavity. The usefulness of a second discharge was suggested by the experiments of Bay and Steiner, who obtained the optical spectrum of atomic nitrogen from a second discharge tube in this manner; the intensity of the atomic lines correlated with that of the afterglow in the vapor stream emerging from their first discharge tube.[23] The proximity of the second discharge to the cavity was an effort to utilize short-lived (millisecond) metastable discharge products, such as the doublet states. It would appear that the input nitrogen should be free from impurities, including water vapor, to prolong the metastable lifetime.[15,22] However, its necessity in producing afterglow left unclear the desirability of either presence or absence of the water vapor. The greatly reduced ground-state spectrum from the "dry" condensed discharge could be interpreted as indicating that most of the atoms were in the metastable states. If so, assuming a total atomic concentration comparable to that from the "wet" discharge, then the metastable spectra should have been easily observable. It seems more reasonable that the dry discharge did not produce atoms of any sort so effectively.

The second discharge was a high-voltage ac transformer with interrupted primary.[22] The cavity entrance sleeve and a turn of heavy wire served as the external electrodes. A standard induction coil and a constant amplitude (CW) rf oscillator were also tried.

No attempt has been made to employ a carrier gas, such as helium.[24] The possibility of using a Philips-type discharge tube located in the magnetic field and immediately preceding the microwave cavity has been considered as a method of reducing to a minimum the transit time between discharge region and cavity. While this proposal has not been tried experimentally, it seems doubtful that it would prove to be a satisfactory source of metastable nitrogen atoms. For our present spectrometer we estimate very roughly that a concentration of the order of a percent is necessary in a given state.

GROUND-STATE SPECTRUM

A three-line spectrum arising from the $^4S_{\frac{3}{2}}$ ground state of the N^{14} atom was observed. The lines were of equal intensity and width and were equally spaced. This spectrum, corresponding to the strong-field (Back-Goudsmit) case, indicates a small magnetic hyperfine interaction but gives no evidence for electric quadrupole interaction.

For an atom with $J=\frac{3}{2}$ and $I=1$ there are twelve magnetic sublevels. The first-order strong-field energies are given by[2,3]

$$W(M_I M_J)=AM_IM_J+M_Jg_J\mu_0H+M_Ig_I\mu_0H.$$

The observed magnetic resonance spectrum consisted of the nine transitions of the type $\Delta M_J=\pm 1$, $\Delta M_I=0$. In the pure strong-field case these occur as three triply-degenerate lines, the separation of which is a measure of the magnetic hfs interaction constant A. At somewhat lower fields the off-diagonal hyperfine interactions must be included and these degeneracies would be removed. Quadrupole hfs would also remove the degeneracies. The sign of A cannot be obtained from the magnetic resonance spectrum.

Two major precision runs were made which agreed to 1.2 ppm. A constant microwave transition frequency $\nu\sim 9185$ Mc/sec was maintained throughout a run. The magnetic field at which the central line occurred was measured as a proton resonance frequency $\nu_p\sim$

[22] J. Kaplan, Phys. Rev. 54, 176 (1938).
[23] Z. Bay and W. Steiner, Z. physik. Chem. B3, 149 (1929).
[24] T. R. Merton and J. G. Pilley, Proc. Roy. Soc. (London) A107, 411 (1925); O. S. Duffendack and R. A. Wolfe, Phys. Rev. 34, 409 (1929).

13.96 Mc/sec. Each of the side lines was separated from the central line by a proton frequency $\delta\nu_p \sim 16$ kc/sec. The "peak-to-peak" line width[25] of each line was about 0.09 gauss (equivalent to 250 kc/sec in transition frequency at constant field). The 30-cycle/sec field-modulation peak-to-peak amplitude was also 0.09 gauss. The calculated asymmetry of the side lines about the central line due to off-diagonal hfs contributions is 20 cps in proton frequency, which was not quite observable. The calculated splitting of the three nearly degenerate components of each of the side lines due to this same effect is 40 cps, or ten percent of the observed line width.

We obtained the following results:

$$-\frac{g_J}{g_p}=\frac{\nu}{\nu_p}\left[1-\left(\frac{\delta\nu_p}{\nu_p}\right)^2+\cdots\right]=658.1631\pm0.0010,$$

$$|A|=\delta\nu_p(\nu/\nu_p)=10.45\pm0.02 \text{ Mc/sec},$$

$$|B|<0.03 \text{ Mc/sec}.$$

[25] The spectrometer detector displays essentially the derivative of the absorption line-shape; see Fig. 6 of reference 11.

A small correction term arising from the off-diagonal hfs interaction has been included in evaluating the g-factor ratio. For LS coupling neglecting relativistic effects, $g_J(^4S_{\frac{3}{2}}\text{N})$ is identical with the electron spin g factor. We have not evaluated relativistic corrections. Since no evidence for quadrupole hfs was detected, an upper limit for the quadrupole interaction constant $B(=eQq)$ has been estimated on the basis of line width.

DISCUSSION

The formulas of Trees for nonrelativistic LS coupling indicate that both the magnetic and quadrupole hfs interactions vanish in the ^4S state. The observed small but nonvanishing magnetic interaction is probably due to configuration interaction with $2p^23p$ or possibly $2s2p^23s$. The estimated interaction due to slight breakdown of LS coupling would contribute only a small portion of the observed splitting. Configuration interaction problems of this type have been considered by Koster and by Sachs.[26]

The authors are grateful to Dr. R. E. Trees for helpful correspondence.

[26] G. F. Koster, Phys. Rev. **86**, 148 (1952); M. Sachs, Phys. Rev. **90**, 1058 (1953).

Microwave Absorption Spectra of MnO_3F and ReO_3Cl*†

ALI JAVAN, *Department of Physics, Columbia University, New York, New York*

AND

A. ENGELBRECHT, *Research Institute of Temple University, Temple University, Philadelphia, Pennsylvania*

(Received June 8, 1954)

The microwave spectra of MnO_3F and ReO_3Cl near 1-cm wavelength have been studied. From the spectra of the first molecule and its isotopic species $Mn(O^{16})_2O^{18}F$, the structural parameters were determined as:

$$Mn-O=1.586\text{ A},\quad Mn-F=1.724\text{ A},\quad \angle(O,Mn,F)=108°27'.$$

The nuclear quadrupole coupling constant of Mn^{55} was measured as $eqQ=16.8$ Mc/sec. Because of the spin and statistics of O^{16} nuclei not all of the rotational states are allowed. It was found that, whereas in the ground vibrational states only states with K a multiple of three are permissible, in the excited vibrational states of the perpendicular normal modes the states with $K-l$ a multiple of three can occur. For $K=l=\pm1$ appreciable l-type doubling was observed. The amounts of l doubling and their corresponding values of α_z were determined for MnO_3F. The molecular dipole moment of this molecule was found to be $\mu=1.5$ Debye units. The hyperfine structure of ReO_3Cl gives for the ratio of quadrupole moments of the two abundant isotopes of Re a value of $Q_{Re^{187}}/Q_{Re^{185}}=1.067\pm0.045$ and for the quadrupole coupling constant of Re^{187}, $eqQ=253$ Mc/sec. This coupling constant and the known optical value of the quadrupole moment of Re^{187} give some information about the electronic structure of the molecular bonds, from which an approximate value of the nuclear quadrupole moment of Mn^{55} was obtained as $Q=0.55\times10^{-24}$ cm^2.

MOLECULES containing the elements Mn and Re are not easily obtainable in the gaseous state for microwave or electron diffraction study. Partly for this reason experimental data on the covalent radii of these elements has previously been limited to certain anomalously large radii measured for Mn in crystalline MnS_2 and similar compounds. Isolation[1] in 1950 of the molecule MnO_3F allowed the microwave measurement of its rotational spectrum reported below. This plus the microwave spectrum[2] of ReO_3Cl give the first accurate determinations of the geometry of bonds of Mn and Re.

The single stable isotope Mn^{55} has a spin of 5/2 and hence a quadrupole moment which produces a hyperfine structure in the rotational spectrum giving some information about the value of the quadrupole moment. The two isotopes Re^{187} and Re^{185} which occur in nature in relative abundance, 61.8 percent and 38.2 percent, respectively, also have spin 5/2 and give quadrupole hyperfine structure from which a fairly accurate measure of the ratio of their two quadrupole moments is obtained.

The spectrometer used for the measurements was a Stark modulation type of more or less conventional design except for the absorption cell and gas handling system. Both molecules MnO_3F and ReO_3Cl are highly reactive and rather unstable. Their handling required special care which will be described in a subsequent paper.[3]

ROTATIONAL SPECTRUM

The observed spectrum of MnO_3F and ReO_3Cl show clearly that the molecules are symmetric tops. The three oxygen atoms are located at the corners of an equilateral triangle forming the base of a pyramid with the metal at its apex. The halogen is on the symmetry axis.

The allowed rotational transitions of such a molecule involve a change of total angular momentum $\Delta J=\pm1$ with no change of K, the projection of J on the symmetry axis. In the absence of hyperfine structure, the frequency of a transition of this kind is independent of quantum number K except for a small factor due to centrifugal stretching of the molecule, and given by $\nu=2B(J+1)$, where $B=h/(8\pi^2I_B)$. I_B is the moment of inertia of the molecule about a direction perpendicular to the symmetry axis.

When J is greater than zero, lines due to molecules having several different values of K are superimposed. The quadrupole interaction mentioned above causes a splitting of the rotational lines which depends on the absolute value of K.[4] Hence the hyperfine structure may be complicated due to the superposition of patterns belonging to different K states. However, in the cases of $Mn(O^{16})_3F$ and $Re(O^{16})_3Cl$ not all values of K are permissible because of the statistics and spin of O^{16}. O^{16} nuclei have zero spin and follows Bose-Einstein statistics so that only those states occur which remain symmetric under any permutation of the three oxygen nuclei.

These molecules belong to point group C_{3v}. Since permutations of the three oxygen nuclei is isomorphous with operations of the point group C_{3v}, totally symmetric wave functions belong to irreducible represen-

* Work supported by the U. S. Atomic Energy Commission.

† Submitted by Ali Javan in partial fulfillment of the requirement for the degree of Doctor of Philosophy in the Faculty of Pure Science at Columbia University.

[1] A. Engelbrecht and A. V. Grosse, J. Am. Chem. Soc. **76**, 2042 (1954).

[2] Amble, Miller, Schawlow, and Townes, J. Chem. Phys. **20**, 192 (1952).

[3] J. Lotspeich and A. Javan (to be published).

[4] J. Bardeen and C. H. Townes, Phys. Rev. **73**, 97 (1948).

tation of class A. It can be shown[5] that, when K is a multiple of three, the rotational wave function can be reduced to belong to classes A or B of the point group C_{3v}. Rotational wave functions with K other than a multiple of three are doubly degenerate and belong to the irreducible representation of class E. In the ground vibrational state, the total vibrational wave function belongs to class A or B according to whether the molecule is in the symmetric or antisymmetric inversion state. Hence only states with K a multiple of three can form total symmetric wave functions and, therefore, are allowed.

In contrast to the ground state, values of K not a multiple of three can occur in some excited vibrational states. Molecules such as MnO_3F have six different normal frequencies of oscillation. Three of these correspond to three pairs of doubly degenerate modes and when excited can give rise to internal angular momentum. These modes are known as perpendicular modes and the other three are nondegenerate and known as parallel modes. The internal angular momentum for the vth excited state of a degenerate mode can take values corresponding to the quantum number l, where l is a positive or negative integer running by steps of two from $+v$ to $-v$.

Vibrational wave functions of a pair of degenerate normal modes transform in a way which is fairly similar to that of the rotational wave function under permutations of the three oxygen nuclei. When $|l|$ is a multiple of three, this wave function can hence be put in a form to belong to classes A or B, but for $|l|$ other than a multiple of three it belongs to class E.[5] In the latter case, this wave function when combined with rotational wave function of E symmetry can furnish wave functions of classes A and B because the result would have symmetry of $E\times E=A+B+E$. Thus values of K not a multiple of three become permissible when a doubly degenerate mode of class E is excited. An explicit form of the transformations of the total rotation-vibrational wave functions shows that the criterion for the permissible states is that $|K-l|$ be a multiple of three.

In the presence of internal angular momentum, the rotational energy levels undergo a first-order Coriolis splitting,[6] (K-type doubling), which in the absence of centrifugal stretching is independent of J. The contribution to the energy levels due to this term is $2C_v\zeta Kl$, where $C_v=h/8\pi^2I_{zz}c$, ζ is the Coriolis coupling constant. The two members of this doublet correspond to positive or negative signs of the product Kl. The frequency of the rotational transition is unaffected by the presence of this splitting due to the lack of dependence on J. However, the levels corresponding to $|K-l|$ a multiple of three which are the only permissible values as discussed above, undergo further an l-doubling splitting. When $K=l=\pm1$, the amount of splitting[5,6] is given by $q_lJ(J+1)$, and rotational transitions are manifested as doublets with separations $\Delta\nu=2q_l(J+1)$ in a transition $J+1\leftarrow J$. For higher values of K and l, the l doubling is very small, and the splitting of the corresponding rotational lines are undetectable.

TABLE I. Hyperfine structure of MnO_3F for the ground vibrational state and first excited state $v_6=1$. The experimental errors where not indicated are less than 50 kc/sec.

Transition	Measured frequency Mc/sec	Calculated frequency Mc/sec
$v=0$, $K=0$		
$9/2\leftarrow9/2$	24 777.526	24 777.517
$5/2\leftarrow3/2$	24 775.949	24 775.949
$7/2\leftarrow5/2$	24 775.125	24 775.117
$11/2\leftarrow9/2$	24 774.445	24 774.437
$9/2\leftarrow7/2$	24 774.250	24 774.277
$7/2\leftarrow7/2$		
$5/2\leftarrow3/2$	24 773.85±0.15	24 773.984
$5/2\leftarrow5/2$	24 773.505	24 773.549
$1/2\leftarrow3/2$	24 772.39±0.1	24 772.477
$3/2\leftarrow5/2$	24 771.56±0.1	24 771.589
$v_6=1$, $K=2$		
$3/2\leftarrow1/2$, $1/2\leftarrow1/2$	24 755.95±0.15	24 736.06
$11/2\leftarrow5/2$, $9/2\leftarrow9/2$, $9/2\leftarrow3/2$, $7/2\leftarrow3/2$, $7/2\leftarrow1/2$	24 738.20	24 738.22
$7/2\leftarrow7/2$, $5/2\leftarrow5/2$, $3/2\leftarrow5/2$	24 740.60	24 740.62
$9/2\leftarrow7/2$, $7/2\leftarrow7/2$, $5/2\leftarrow7/2$	24 741.49	24 741.46
$v_6=1$, l_2, $K=1$		
$3/2\leftarrow3/2$, $1/2\leftarrow1/2$	24 768.00	24 768.03
$11/2\leftarrow9/2$	24 768.38	24 768.40
$9/2\leftarrow7/2$, $7/2\leftarrow7/2$, $3/2\leftarrow1/2$	24 769.14	24 769.10
$7/2\leftarrow5/2$, $5/2\leftarrow3/2$	24 769.55	24 769.52
$9/2\leftarrow9/2$	24 770.68	24 770.71

SPECTRUM OF MnO_3F

The rotational transition $J=3\leftarrow2$ of this molecule is particularly suitable for study of hyperfine structure. According to the above discussions, in the ground vibrational state only $K=0$ can occur. The first excited states of degenerate modes provide transitions with $K=\pm1$ and $K=\pm2$ displaced from the position of the ground state transition according to their corresponding values of α_v. Because of l-type doubling the $K=\pm1$ transitions are manifested as doublets. The two components of each doublet are symmetrically located on either side of $K=\pm2$ transition for the same excited vibrational state. The values of α_v and the amounts of l-type doublings are large enough to prevent any

[5] G. Hertzberg, *Infrared and Raman Spectra of Polyatomic Molecules* (D. Van Nostrand Company, Inc., New York, 1945).

[6] M. Johnston and D. M. Dennison, Phys. Rev. 48, 868 (1935). See also reference 12.

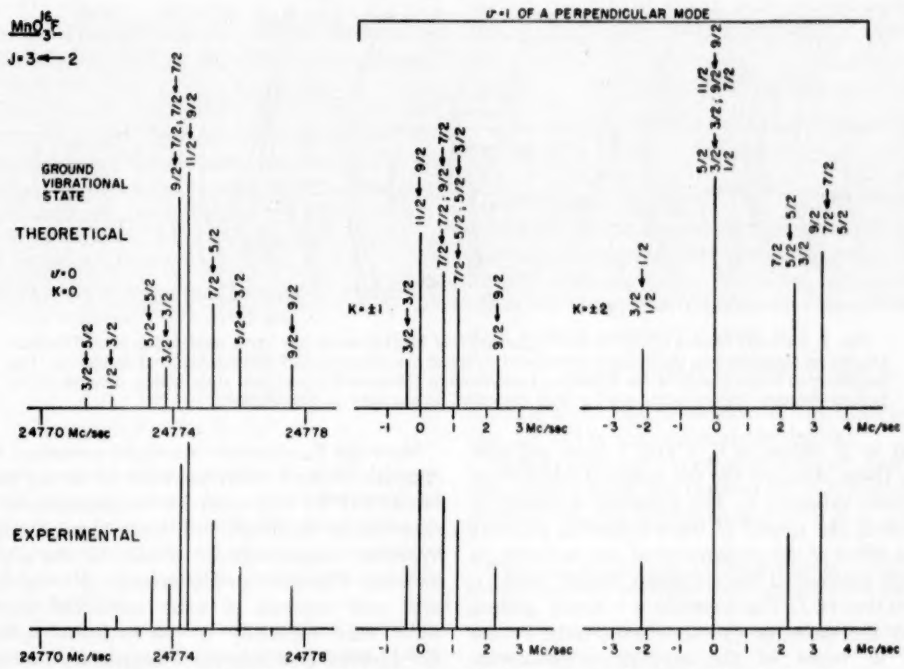

FIG. 1. The quadrupole hyperfine structure of MnO_3F in the rotational transition $J=3 \leftarrow 2$.

superposition of hyperfine structures arising from different values of K.

The hyperfine structure verifies a spin 5/2 for Mn^{55} and gives $eqQ=16.8$ Mc/sec and $B_0=4129.106\pm0.004$ Mc/sec. In Table I the measured lines for the ground vibrational state and the first excited state of one of the degenerate modes are listed. In Fig. 1 observed hyperfine structures are compared with the theoretical patterns. The hyperfine patterns of the first excited vibrational states of the three perpendicular normal modes are identical. This indicates that there is no detectable change of the coupling constant eqQ in these excited states. Table II contains the list of values of α_v and l-type doubling constants q_l for the three degenerate normal modes and α_v of one of the nondegenerate modes. Also a rough estimate of the normal frequencies of oscillation is given on the basis of the observed relative intensities.

The second excited states of the perpendicular modes and the excited state $v_6=1$, $v_5=1$ were also observed. Since in these cases, the total angular momentum due to vibration corresponds to $l=\pm2$ or $l=0$, the allowed values of K are $K=\pm2$, $K=\pm1$, and $K=0$.

A recorder tracing of over-all spectra of the excited vibrational states of the perpendicular modes discussed above appears in Fig. 2. This tracing was taken under a low Stark modulation field, hence only lines corresponding to $K=\pm1$ and $K=\pm2$ which can show a first-order Stark splitting are detected. Since the tracing was taken under relatively low resolution conditions, only the hyperfine splittings of the $K=\pm2$ lines could be seen, these being larger than the splittings of the $K=\pm1$ transitions.

SPECTRA OF $Mn(O^{16})_3O^{18}F$ AND STRUCTURAL PARAMETERS

The size and geometry of MnO_3F depends on three independent parameters. They can be taken as the distances Mn−O, Mn−F and the angle $\angle$(O,Mn,F). The moment of inertial I_B, obtained from the B value of $Mn(O^{16})_3F$ is not alone sufficient to yield values for these parameters. In order to obtain enough experimental data for determining completely the structure of the molecule, the rotational spectrum of the isotopic species $Mn(O^{16})_2O^{18}F$ was examined. Due to the presence of O^{18}, the C_{3v} symmetry of this molecule is destroyed, and hence all of the asymmetric rotor energy levels are permissible.

The rotational transition $J=3 \leftarrow 2$ was observed and the stronger hyperfine components of the transitions which in the limiting case of a symmetric prolate rotor

TABLE II. Vibrational and l-type doubling constants and approximate normal vibration frequencies of MnO_3F.

Normal mode	α_v(Mc/sec)	q_l(Mc/sec)	ω(cm^{-1})
6	5.87	9.81	350
5	−12.80	16.20	470
4	14.38	5.90	600
3	7.77		400

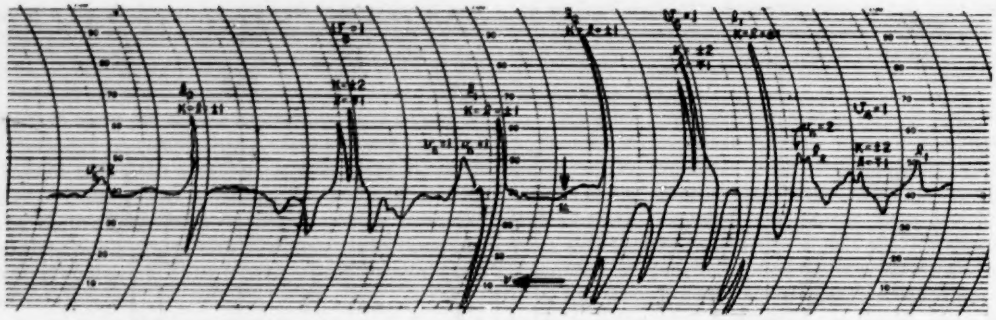

FIG. 2. Recorder tracing of the $J=3 \leftarrow 2$ transition of MnO_3F under low Stark modulation field. The lines are due to transitions in the excited vibrational states of the perpendicular normal modes of oscillation. The frequency ν_0 is the center of the hyperfine transitions in the ground vibrational state which, because of the high modulation field requirements for their detection, do not show on this tracing.

correspond to K values of 0, 1 and 2 show patterns similar to those obtained for the molecule $Mn(O^{16})_3F$ with the same values of K. The difference is mainly in a reduction of the spread of these hyperfine patterns due to the effect of the asymmetry of the molecule on the average gradient of the molecular electric field q_J, in the direction of J. The molecule is a nearly prolate rotor, and the quantity q_J can conveniently be expanded[7,8] in terms of the asymmetry parameter $b_p=(C-B)/(2A-C-B)$, where A, B, and C are the three rotational constants in decreasing order of magnitude. For $K=1$ and $K=2$ this expansion to the second power of b is given by

$$K=1,$$

$$q_J=\frac{q_m}{(J+1)(2J+3)}\left\{3-J(J+1)\mp\frac{J(J+1)}{2}\eta+(\tfrac{3}{2}b^2-b\eta)\frac{f(J,2)}{4}\pm\frac{3}{128}\eta b^2 f(J,2)J(J+1)\right\};$$

$$K=2,$$

$$q_J=\frac{q_m}{(J+1)(2J+3)}\left\{12-J(J+1)+(\tfrac{3}{2}b^2-b\eta)\times\left[\frac{f(J,3)}{6}-\frac{f(J,1)}{2}\right]\mp(\tfrac{3}{2}b^2-b\eta)\frac{f(J,1)}{2}\right\},$$

where, in the case of a nearly prolate rotor, the upper and lower signs correspond to the upper and lower asymmetric rotor energy levels, respectively, and

$$f(J,n)=\tfrac{1}{4}[J^2-n^2][(J+1)^2-n^2],\quad q_m=\partial^2V/\partial Z_m^2,$$

$$\eta=\left(\frac{\partial^2V}{\partial X_m^2}-\frac{\partial^2V}{\partial Y_m^2}\right)\Big/q_m.$$

Z_m is the principal axis of the least moment of inertia and Y_m is that of the largest.

[7] G. Knight and B. T. Feld, Report No. 123, Massachusetts Institute of Technology Research Laboratory of Electronics, 1949), (unpublished).

[8] J. Kratchman, J. Chem. Phys. (to be published).

Since the Z_m direction is rotated somewhat from the direction of the F−Mn bond due to the asymmetry of $Mn(O^{16})_2O^{18}F$, this quantity is consequently smaller than that of the $Mn(O^{16})_3F$, hence the splittings of the hyperfine components are smaller for the asymmetric molecule. The effect of the terms in $(\frac{3}{2}b^2-b\eta)$ is a slight shift and removal of some accidental degeneracies which exist especially in the hyperfine splittings of $K=2$ levels. This removal of degeneracy produces only a small splitting and shows only as a broadening of the absorption lines.

Table III contains a list of the measured lines, from which the three rotational constants can be obtained as

$$A=4488.81\pm0.3 \text{ Mc/sec},$$
$$B=4098.088\pm0.01 \text{ Mc/sec},$$
$$C=3963.552\pm0.01 \text{ Mc/sec}.$$

On the basis of these constants, values of eqQ and η can be calculated from the coupling constant eqQ of $Mn(O^{16})_3F$ by expressing the electric field gradient tensor in the coordinate system coinciding with the principal axes of the asymmetric molecule. The values obtained are $eq_mQ=16.4$ Mc/sec, $\eta=0.044$. These values fit the observed hyperfine patterns, indicating that there is no detectable change of the electronic structure resulting from a substitution of O^{18} in the molecule.

The centrifugal stretching of the molecule is small and less than experimental error. In terms of the limiting case of a symmetric prolate rotor an upper limit to the centrifugal distortion coefficient D_{JK} can be given as 10 kc/sec from the relative position of different rotational transitions in the spectrum.

The three rotational constants are inversely proportional to the principal moments of inertia of the molecule from which three structural parameters can be evaluated. The main source of uncertainty on this determination is due to the zero-point vibrations.[9] These cause slight change in the $\angle(O^{18}-Mn-F)$ angle

[9] Townes, Holden, and Merritt, Phys. Rev. 74, 1113 (1948).

and Mn−O^{18} distance compared to ∠(O^{16}−Mn−F) and Mn−O^{16}. The available data on the two isotopic species can not be used for separately evaluating all parameters involving O^{18} and O^{16}. However, if it is assumed that isotopic substitution affects only the bond angle, a fit of the spectrum can be obtained with the ∠(O^{18},Mn,F) angle 2′ smaller than that for O^{16}. On the other hand, if Mn−O bond is assumed to be shortened by one part in one thousand due to the substitution of O^{18} for O^{16}, then the O−Mn−F angle must change by 10′ for the isotopic substitution.

The best values of structural parameters and errors expected from zero-point vibrations are

$$\text{Mn}-\text{O}=1.586\pm0.005\text{ A},$$
$$\text{Mn}-\text{F}=1.724\pm0.005\text{ A},$$
$$\angle(\text{O,Mn,F})=108°27'\pm7'.$$

These parameters are rather sensitive to slight changes in the angle and the distance due to the substitution of O^{18}. However, the projection of the Mn−O distance on a plane perpendicular to Mn−F axis is quite insensitive to these changes and can be determined more accurately as 1.5020 A±0.0001 A.

We can obtain a value for the covalent radius of doubly bonded Mn by subtracting the covalent radius of doubly bonded oxygen from our measured bond lengths Mn−O. The ionic character of this bond is not expected to have a large effect on the bond length; thus one obtains the double bond radius for Mn as 1.04 A.

Since the amount of ionic character of Mn−F bond is not known, the single-bond radius of Mn can not be determined precisely. However, ignoring ionicity of this bond, a radius of 1.08 A is obtained for the single-bond radius of Mn. The presence of ionic character in the bond shortens the bond length; hence, this value should be considered as a lower limit.

The anomalously large bond radius of about 1.50 A[10] reported for the octahedral radius of bivalent Mn in MnS_2, $MnSe_2$, and $MnTe_2$ is in striking contrast with our observed bond radii.

It should be noted that the angle ∠(O,Mn,O) is very close to a tetrahedral angle obtained ordinarily for structurally similar molecules formed by tetravalent atoms.

The degeneracy of a pair of degenerate normal modes of oscillation in the molecule $Mn(O^{16})_3F$ is removed when one of the oxygens is replaced by O^{18}. However, it is expected that the separation of vibrational levels corresponding to such a pair in the molecule $Mn(O^{16})_2O^{18}F$ is small and of the same order as the rotational frequencies, so that appreciable perturbation will occur. Hence modified Coriolus interactions and l-doubling effects[11] may be observable. Unfortunately, the absorption lines due to the molecule $Mn(O^{16})_2O^{18}F$ in the excited vibrational states were so weak that these effects could not be clearly observed.

DIPOLE MOMENT

The molecular electric dipole moment μ of MnO_3F is measured by a study of the Stark effect in the transition $J=3\leftarrow2$. Because of the large Stark splitting of the lines corresponding to $K=\pm1$ and $K=\pm2$, it was preferred to make the measurements on the transitions in an excited perpendicular vibrational mode. The l-type doublet with $v_6=1$ was chosen for this purpose. The change in energy due to Stark effect for each rotational level of such a doublet is given by[12]

$$\Delta E=[(\Delta W/2)^2+\mu^2E^2\phi^2]^{\frac{1}{2}}-\Delta W/2,$$

where ϕ is the matrix element of the direction cosine, and ΔW is the separation of the doublet.

In the absence of hyperfine interaction, there are two well-defined Stark components for each member of the observed doublet corresponding to $M_J=1$ and $M_J=2$

TABLE III. Measured lines of $Mn(O^{16})_2O^{18}F$. ν_0 is the frequency of the rotational transition after correction for the hyperfine splitting.

Transition $J'_{K_{-1}'K_1'}\rightarrow J_{K_{-1}K_1}$	$F'\leftarrow F$	Measured frequency (Mc/sec)	ν_0(Mc/sec)
	11/2 ← 9/2	23 966.310±0.040	
$3_{12}\leftarrow2_{12}$	9/2 ← 7/2		23 966.710
	7/2 ← 7/2	23 967.106±0.040	
	7/2 ← 5/2		
	5/2 ← 3/2		
$3_{03}\leftarrow2_{02}$			24 076.35±0.3
	3/2 ← 1/2	24 181.70±0.150	
	1/2 ← 1/2		
$3_{22}\leftarrow2_{21}$	5/2 ←		
	3/2 ← 3/2		
	1/2 ←		
	11/2 ←	24 183.70±0.05	24 184.90
	9/2 ← 9/2		
	7/2 ←		
	9/2 ←		
	7/2 ← 7/2	24 186.85±0.1	
	5/2 ←		
$3_{21}\leftarrow2_{20}$	5/2 ←		
	3/2 ← 3/2		
	1/2 ←		
	11/2 ←	24 292.35±0.08	
	9/2 ← 9/2		24 293.45
	7/2 ←		
	9/2 ←		
	7/2 ← 7/2	24 295.45±0.1	
	5/2 ←		
$3_{12}\leftarrow2_{11}$	11/2 ← 9/2	24 365.64±0.030	
	9/2 ← 7/2	24 366.331±0.060	24 366.05
	7/2 ← 7/2		
	7/2 ← 5/2	24 366.80±0.050	
	5/2 ← 3/2		
	9/2 ← 9/2	24 367.89±0.030	

[10] L. Pauling, *Nature of the Chemical Bond* (Cornell University Press, Ithaca, 1948).

[11] H. H. Nielsen, Revs. Modern Phys. **23**, 90 (1951).

[12] R. G. Shulman and C. H. Townes, Phys. Rev. **77**, 500 (1950).

which under a reasonable amount of electric field can be separated appreciably from their allied zero-field lines. For fields of this order of magnitude, the nuclear quadrupole interaction can be considered approximately as a small perturbation and causes a hyperfine pattern for each of the Stark components. The main sources of error in this measurement were due to an incomplete resolution of the hyperfine structure of these components which, owing to the inhomogeneity of the electric field, are ordinarily broader than the zero-field lines, However, the line shapes could clearly be recognized as those caused by the expected structures and their centers measured. The magnitude of the electric field was chosen such that the Stark components were completely removed from the total range of the hyperfine structure of the zero-field transitions.

The measurements of the electric field were made by a study of the Stark effect in the molecule OCS which has a known dipole moment. It was found that, in spite of the high instability of MnO_3F, it can coexist together with the molecule OCS for a reasonable length of time. Both samples were admitted simultaneously into the wave guide and their Stark splittings studied under the same field.

Table IV contains a list of the measured splittings. The values given for each setting of the electric field is an average for the Stark splittings of the two members of the doublet. From this table we obtain $\mu=1.5\pm0.2$ for the dipole moment of MnO_3F.

All of the measurements on MnO_3F were made at a temperature of about $-60°$ centigrade.

CHEMICAL PREPARATION OF $Mn(O^{16})_2O^{18}F$

The details of the preparation of MnO_3F appears elsewhere.[1] The O^{18} was introduced in the following way. One gram of $KMn(O^{16})_4$ was refluxed for 42 hours with 4 cc of H_2O^{18}(5 percent O^{18}). Then the water was distilled off, and the enriched $KMnO_4$ was used for the preparation of $Mn(O^{16})_2O^{18}F$. For this purpose it was reacted with about 1 cc of SO_3HF, and the effluent MnO_3 collected in Kel-F traps, Purification was carried out by repeated distillation with an excess of enriched $KMnO_4$ to remove the last traces of SO_3HF and HF.

SPECTRUM OF ReO_3Cl

The rotational transitions $J=5\leftarrow4$ and $6\leftarrow5$ of this molecule are studied for hyperfine structure. There are two nuclei in this molecule with sizable contributions to the quadrupole interaction energy, namely Re and Cl. Due to these interactions, spins of both Re and Cl nuclei are coupled to the rotational angular momentum J. Our observation shows that the energy of interaction of the Re nucleus is considerably larger than that of the Cl nucleus. Hence to a good approximation the energy levels can be designated with quantum numbers corresponding to F_1 and F, where F_1 is the resultant angular momentum obtained by addition of the spin of the Re nucleus to the rotational angular momentum J and F is that obtained by further addition of the spin of the Cl nucleus. The selection rules for allowed transitions are $\Delta F_1=0$ or ±1 and $\Delta F=0$ or ±1.

TABLE IV. Stark splitting of the l doublet, $v_t=1$.

E(volts/cm)	(Mc/sec), $M_J=1$	(Mc/sec), $M_J=2$
57.5		3.2
80	1.5	5.55
86	1.9	

The hyperfine pattern is complicated by the presence of a large number of hyperfine components. Furthermore, there is an overlap of hyperfine structures due to either of the two Re isotopes in both of our observed rotational transitions. For example, the isotopic shift of the lines corresponding to $J=6\leftarrow5$ is 7.4 Mc/sec while the spread due to hyperfine structure is about 15 Mc/sec. The presence of two Cl isotopes does not cause any complication since isotopic shift due to Cl is large, and the hyperfine patterns are well separated.

In order to differentiate decisively between components belonging to either of the two isotopic species in Re, spectroscopy was done on a small quantity of ReO_3Cl prepared with Re metal enriched almost to 100 percent in Re^{187}. The observed spectrum of this sample for the transition $J=6\leftarrow5$ provided a clear identification of those components of the spectrum which were due to the Re^{187} isotope. Most of the final measurements were performed on normal isotopic material.

From analysis of observed lines a spin 5/2 for both Re isotopes is verified and the following constants are obtained:

$$eqQ_{Re^{187}}=253\pm6 \text{ Mc/sec},$$

$$eqQ_{Re^{185}}=270\pm6 \text{ Mc/sec},$$

$$eqQ_{Cl^{35}}=-34 \text{ Mc/sec},$$

$$B_0 \text{ for } Re^{185}O_3{}^{16}Cl^{35}=2094.20 \text{ Mc/sec},$$

$$B_0 \text{ for } Re^{187}O_3{}^{16}Cl^{35}=2093.58 \text{ Mc/sec}.$$

In Fig. 3 the observed structure for $K=\pm3$ and $K=0$ are compared separately with the theoretical patterns. The $K=0$ lines show Stark effect only to the second order. Their presence could conveniently be suppressed for the measurements on the $K=\pm3$ transitions, by using relatively low Stark modulation field. However, under such a field, often there was unfavorable interference from the Stark components of different absorption lines in the pattern. It was necessary to adjust separately the amplitude of the Stark modulation field for each specific line. This difficulty prevented acceptably accurate measurements of some of the components. For example, the $K=\pm3$ transitions at about 25 123 Mc/sec (refer to Fig. 3) were so badly masked by the Stark components of the various nearby lines that in order to free these transitions from such interferences a larger modulation field seemed to be required. However, under higher fields, the transition $K=0$, $17/2\leftarrow$

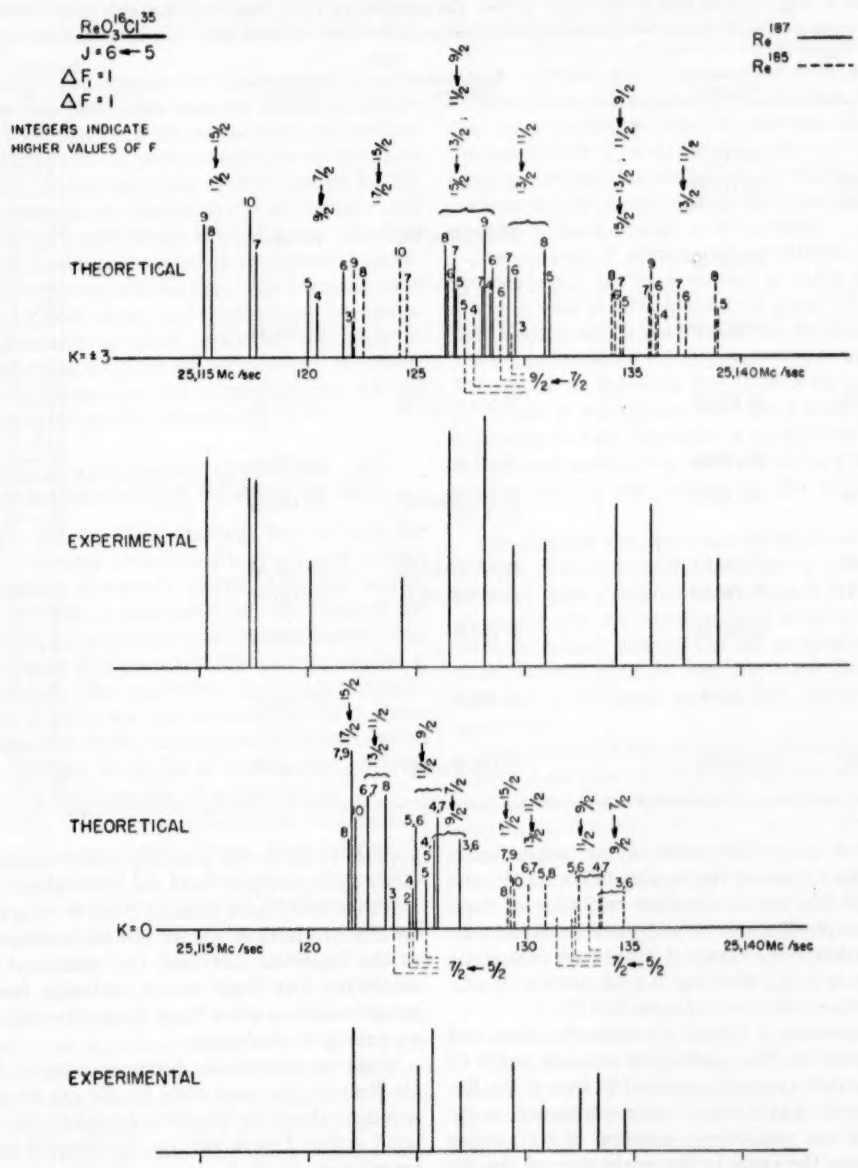

FIG. 3. The quadrupole hyperfine structure of ReO_3Cl in the $J=6 \leftarrow 5$ transition arising from quadrupole couplings of Re and Cl nuclei. The spectrum is a superposition of the transitions originating from the two isotopic species in Re.

15/2 began to show appreciable microwave absorption, and thus no accurate measurements of these lines were possible.

For the measurements on the $K=0$ lines, advantage was taken of the extreme Stark sensitivity of $K=\pm 3$ transitions. By subjecting the molecules to a dc electric field, it was possible to split these lines into Stark components considerably removed from their zero-field positions and make measurements on the $K=0$ transitions which undergo virtually no splitting.

As can be seen from Fig. 3, there are frequently several lines superimposed within a range of about 500 kc/sec. In such cases, although a complete resolution was not achieved, the line shapes were observed to be in agreement with those predicted from the theoretical hyperfine pattern.

TABLE V. The measured lines of ReO_3Cl, in Mc/sec. The experimental error where not indicated is about 0.1 Mc/sec.

Re^{187} Experimental frequency	Re^{187} Theoretical frequency	Re^{185} Experimental frequency	Re^{185} Theoretical frequency	Transition $F' \leftarrow F$	$J=6 \leftarrow 5$ $F_1' \leftarrow F_1$
				$K=\pm 3$	
25 115.33	25 115.37			$\begin{cases}9 \leftarrow 8\\8 \leftarrow 7\end{cases}$	$17/2 \leftarrow 15/2$
25 117.36±0.06	25 117.37			$10 \leftarrow 9$	$17/2 \leftarrow 15/2$
25 117.66±0.04	25 117.59			$7 \leftarrow 6$	$17/2 \leftarrow 15/2$
		25 124.35±0.06	25 124.37	$\begin{cases}10 \leftarrow 9\\7 \leftarrow 6\end{cases}$	$17/2 \leftarrow 15.2$
25 120.10	25 120.10			$\begin{cases}5 \leftarrow 4\\4 \leftarrow 3\end{cases}$	$9/2 \leftarrow 7/2$
25 126.52	25 126.54	25 134.24	25 134.23	$\begin{cases}8 \leftarrow 7\\7 \leftarrow 6\end{cases}$	$15/2 \leftarrow 13/2$
				$\begin{cases}6 \leftarrow 5\\5 \leftarrow 4\end{cases}$	$11/2 \leftarrow 9/2$
25 128.15±0.05	25 128.24	25 135.82±0.06	25 135.93	$\begin{cases}9 \leftarrow 8\\6 \leftarrow 5\end{cases}$	$15/2 \leftarrow 13/2$
				$\begin{cases}7 \leftarrow 6\\6 \leftarrow 5\end{cases}$	$11/2 \leftarrow 9/2$
25 129.47	25 129.40	25 137.40	25 137.29	$\begin{cases}7 \leftarrow 6\\6 \leftarrow 5\end{cases}$	$13/2 \leftarrow 11/2$
25 130.93±0.06	25 131.06	25 138.80±0.07	25 138.95	$\begin{cases}8 \leftarrow 7\\5 \leftarrow 4\end{cases}$	$13/2 \leftarrow 11/2$
				$K=0$	
25 122.08±0.05	25 122.03	25 129.42±0.08	25 129.36		$17/2 \leftarrow 15/2$
25 123.45±0.20	25 123.54	25 130.80±0.2	25 130.97	$\begin{cases}5 \leftarrow 9\\8 \leftarrow 6\end{cases}$	$13/2 \leftarrow 11/2$
25 125.00	25 124.90	25 132.56	25 132.47	$\begin{cases}5 \leftarrow 4\\6 \leftarrow 5\end{cases}$	$11/2 \leftarrow 9/2$
				$5 \leftarrow 4$	$7/2 \leftarrow 5/2$
25 125.75	25 124.90	25 133.38	25 133.45	$\begin{cases}4 \leftarrow 3\\5 \leftarrow 2\end{cases}$	$9/2 \leftarrow 7/2$
				$\begin{cases}4 \leftarrow 3\\7 \leftarrow 6\end{cases}$	$11/2 \leftarrow 9/2$
25 127.03±0.06	25 126.96	25 134.59±0.07	25 134.59	$\begin{cases}3 \leftarrow 2\\6 \leftarrow 5\end{cases}$	$9/2 \leftarrow 7/2$

The excited vibrational states of the perpendicular normal modes appear at frequencies below 25 110 and above 25 140 Mc/sec. A complete resolution of these lines was not possible due to additional complications of the *l*-type doublings. However, there were indications that the amount of *l* doubling is considerably smaller than that observed in the molecule MnO_3F.

Table V contains a list of the measured lines and their theoretical fit. The quadrupole coupling of the Cl nucleus is treated as small compared to that of the Re.

It is expected that a higher-order calculation in the treatment of the quadrupole coupling of Cl nucleus would improve the error in the evaluation of the Re coupling constant from our measured data. This requires a complete solution of the secular determinants obtained in the Hamiltonian of the quadrupole interaction for the case of two nuclei.[4] However, the effect of the Cl quadrupole coupling can be eliminated in a calculation of the difference of the quadrupole coupling constants of the two Re isotopes. One obtains for this difference a value of 17±1.5 Mc/sec, with the coupling constant for Re^{185} larger than that for Re^{187}.

Although complete measurements were not carried out on the $J=5 \leftarrow 4$ transition, the relative position of components of hyperfine pattern of this transition appears to agree well with the above constants and its study gave a helpful check on their values.

Amble *et al.*[2] have measured the B values of ReO_3Cl for different isotopic species without a complete solution of the hyperfine structure. Our measured values are consistant with their results, although their approximate evaluation of the Re quadrupole coupling constant appears to be incorrect.

From the interatomic distances given by Amble *et al.* for ReO_3Cl, the bond radii for Re can be obtained as was done above for Mn. One obtains for the Re double-bond radius 1.21 A and for the single-bond radius a lower limit of 1.25 A.

The angle $\angle$(O,Re,O) is very close to the angle $\angle$(O,Mn,O) observed in MnO_3F indicating structural similarity of these two molecules.

The ratio of the nuclear quadrupole moments of Re^{185} and Re^{187} can be gotten by dividing the values of their quadrupole coupling constants giving

$$Q_{Re^{187}}/Q_{Re^{185}}=1.067\pm0.045.$$

While the quadrupole moment of Re^{187} is known satisfactorily from optical data,[13] there is apparently an uncertainty in the value of quadrupole moment of the

[13] H. Schuler and H. Korsching, Z. Physik 105, 168 (1937).

Re^{185}.[14] The above value of the ratio of these two moments fixes a value of 2.8×10^{-24} cm^2 for Re^{185} from that of the Re^{187}.

Kopfermann[15] has suggested an approximate proportionality of the deviation, $\delta\mu$, of magnetic dipole moments from the Schmidt limits and the electric quadrupole moments in pairs of isotopes of the same spin differing by two neutrons. In the case of Re the magnetic moments are known for both isotopes and their ratio of $\delta\mu$ is 1.05 which is close to our observed ratio of their quadrupole moments and hence in agreement with Kopfermann's relation. The existence of a correlation between these two moments can be understood qualitatively in most cases on the basis of approach to strong coupling approximation.[16] However, such close agreement in this proportionality for the case of Re may be purely coincidental.

MOLECULAR ELECTRONIC STRUCTURE AND NUCLEAR QUADRUPOLE MOMENT OF Mn^{55}

Ordinarily the coupling constant eqQ is used for estimating Q through an evaluation of q from a reasonable assignment of valence electrons to the atomic orbitals.[17] However, in these molecules the state of the bonding electrons is complex and not well known. The valence electrons of heptavalent Mn and Re contain s, p, and d orbitals. The possibility of obtaining an electronic wave function for the molecular bonds in terms of these orbitals is rather unfeasible since little is known about the manner in which d orbitals are involved, particularly in the formation of double bonds.

Fortunately, the nuclear quadrupole moments of both Re isotopes are known. Hence, knowledge of the coupling constants eqQ for Re isotopes in the molecule ReO_3Cl can be used for experimentally determining q at the nucleus of Re in this molecule, which in turn gives some information about the bonding electrons. The value of q obtained in this way is $q=1.4\times10^{15}$ esu.

The gradient of electric field at the nucleus of Re can be calculated for a pure p electron by studying fine structure of the optical spectra of ReI.[18] Under an assumption of an approximate LS coupling, the splitting of Z^6p° multiplet together with Z^5p° can be solved for the spin-orbit coupling constant,[19] which subsequently furnishes the quantity $\langle 1/r^3\rangle$ for the $6p$ electron of Re necessary for an evaluation of its q. In this way one obtains $\langle 1/r^3\rangle=21.6\times10^{24}$ cm^{-3}, giving $q(p_\sigma)=8.13\times10^{15}$ esu for a p_σ orbital (σ standing for $m=0$). In this calculation it is necessary to know the effective value of Z near the nucleus. The value used for $Z_{\text{effective}}$ is 69 as suggested by Barnes and Smith.[20]

The value of q for a pure d electron can also be obtained approximately from optical data, which show that q due to a d electron is about 25 times smaller than that for a p electron (see also reference 17). Although the presence of d electrons may effect q through their bearings on the population of p orbitals, the direct contribution of d electrons to the observed q is, from the above, small enough to be ignored.

The amount of unbalanced p electrons u_p,[17] defined by $q=u_pq(p_\sigma)$, can be evaluated by using above values of $q(p_\sigma)$. One obtains a value of about 20 percent for this quantity which is a measure of the deviation of the p electrons from an equal population of all p orbitals. The sign of u_p indicates that there is an excess of perpendicular p orbitals, p_π, over the p orbitals along the symmetry axis p_σ. The value of u_p obtained for ReO_3Cl can be used to deduce an estimate of the gradient of the electric field at the nucleus of Mn in the molecule MnO_3F.

The chemical and structural similarity of ReO_3Cl and MnO_3F discussed earlier, indicate a close similarity between their chemical bonds. Hence it is reasonable to assume that the atomic orbitals involved in the bond formations have more or less the same relative populations in both cases so that the same amount of unbalanced p electrons u_p may be assumed for both molecules.

The gradient of electric field at the nucleus of Mn for a pure p electron can be evaluated, as was done in the case of Re, from optical fine structure of MnI. One obtains $\langle 1/r^3\rangle=0.9\times10^{24}$ cm^{-3} for the $4p$ electrons of Mn leading to $q(p_\sigma)=2.4\times10^{15}$ esu. The value of this quantity for a d electron is estimated as about 25 times smaller than that for a p electron indicating that the arguments used in this connection in the case of Re holds also for Mn. This value of $q(p_\sigma)$ together with an assumption of 20 percent unbalanced p electron gives $q=0.45\times10^{15}$ esu as an estimate of the gradient of the molecular electric field at the nucleus of Mn.

Using the above value of q and the observed coupling constant $eqQ=16.8$ Mc/sec, one obtains a value of $Q=0.55\times10^{-24}$ cm^2 for the nuclear quadrupole moment of Mn^{55}. The probable error in this result is difficult to assess because it depends primarily on the differences between Mn and Re bonding orbitals. However, there seems to be little reason to doubt the correctness of the sign of Q, and probably the value is correct to within a factor of two. This value was reported in a short abstract several months ago.[21] Since then Murakawa and Kamei[22] have measured this quantity from optical hyperfine structure of MnI. Their value is 0.4 ± 0.2, which agrees with our result and indicates the validity of the approximate calculation used here.

[14] J. E. Mack, Revs. Modern Phys. **22**, 64 (1950).
[15] H. Kopfermann, Naturwiss. **38**, 29 (1951).
[16] A. Bohr and B. R. Mottelson, Kgl. Danske Videnskab. Selskab. Mat.-fys. Medd. **27**, No. 16 (1953).
[17] C. H. Townes and B. P. Dailey, J. Chem. Phys. **17**, 782 (1949).
[18] W. F. Meggers, Bur. Standards J. Research **6**, 1027 (1931).
[19] H. E. White, *Introduction to Atomic Spectra* (McGraw-Hill Book Company, Inc., New York, 1934).
[20] R. G. Barnes and W. V. Smith, Phys. Rev. **93**, 95 (1954).
[21] Javan, Silvey, Townes, and Grosse, Phys. Rev. **91**, 222 (1953).
[22] K. Murakawa and T. Kamei, Phys. Rev. **92**, 325 (1953).

The nucleus of Mn^{55} is one of the exceptions to Meyer's rules for nuclear spin.[23] This nucleus is thought to have 5 protons in $f_{7/2}$ orbits outside of a closed shell which are coupled to a total spin 5/2. The observed sign and the exceptionally large quadrupole moment of this nucleus is consistent with the expected value of such a state. In fact, for all possible spins consistent with Pauli's exclusion principle which one can expect from a $(f_{7/2})^5$ configuration, the state of total spin 5/2 gives the largest positive quadrupole moment. It is remarkable that all nuclei which are exceptions to the normal shell structure rules for spin have a ground state with an exceptionally large positive quadrupole moment,[24] as is found here for Mn^{55}.

The authors wish to thank Dr. G. Silvey for preparing samples of ReO_3Cl, Dr. A. V. Grosse for his interest in the preparation of the Mn compounds, and Mr. J. Lotspeich for his construction of the wave guide and the gas-handling system used in this experiment. Thanks are also due various personnel of the Columbia Radiation Laboratory.

We should like to take this opportunity to express our appreciation to Professor C. H. Townes for his guidance throughout the course of this research.

[23] M. G. Meyer, Phys. Rev. 78, 16 (1950).

[24] S. A. Moszkowski and C. H. Townes, Phys. Rev. 93, 306 (1954).

PHYSICAL REVIEW VOLUME 96, NUMBER 3 NOVEMBER 1, 1954

Electric Excitation of Au^{197}†

C. F. Cook,* C. M. Class, and J. T. Eisinger‡
The Rice Institute, Houston, Texas

(Received July 30, 1954)

The gamma radiation emitted from Au^{197} following the electric excitation of the nucleus by protons of from 2 to 5 Mev has been studied. The angular distributions and absolute yields of the two intense gamma rays of the spectrum at 279 and 555 kev have been measured. The angular distributions of these two gamma rays were found to agree well with those calculated for $5/2 \rightarrow 3/2$ ($M1+E2$) and $7/2 \rightarrow 3/2$ ($E2$) transitions, respectively, the excitation being $E2$ in both cases. The yield from the 279-kev state was observed to increase with beam energy in the manner predicted by theory for electric quadrupole excitation. On the basis of the Bohr-Mottelson unified model of the nucleus the results indicate a larger than expected cross section for the formation of the 555-kev state. Values for the quadrupole moment and magnetic moment of the ground state of gold calculated from the cross section for the formation of the 279-kev state agree with spectroscopic values.

INTRODUCTION

THE low-lying states of Au^{197} have been accessible heretofore through the beta decay of Hg^{197} and Pt^{197}, and through the decay from the metastable state excited by the inelastic scattering of neutrons.[1,2] On the basis of the Hg^{197}-Au^{197} decay, Mihelich and de-Shalit have proposed a level scheme for gold having excited states at 77, 268, 279, and 409 kev, as shown in Fig. 1, which is compatible with the observed gamma ray and internal conversion electron spectra. The results from inelastic neutron scattering indicate that the 409-kev state is metastable. Spin assignments of $1/2^+$ or $3/2^+$ have been made to both the 77- and 268-kev levels. Both values are consistent with the available data, although the $1/2^+$ assignment is preferred for the 77-kev state. Some evidence also supports the prediction of the shell model that the 279-kev and 409-kev levels are $d_{5/2}$ and $h_{11/2}$ states, respectively.

Recent work has shown that the low-energy states of gold can also be reached by electric (or Coulomb) excitation of the nucleus. Using a beam of 3-Mev alpha particles Heydenburg and Temmer[3] have observed gamma rays emitted subsequent to excitation having energies of 77, 191, and 279 kev, which can be identified as due to transitions between the known levels listed. The 191- and 279-kev gamma rays have also been found with proton bombardment,[4,5] and in addition, a gamma ray of 555 kev has been reported which is now assigned to a new level of that energy.[6]

Further study of the gamma radiation due to the Coulomb excitation of gold has been undertaken in the

† Supported in part by the U. S. Atomic Energy Commission. A preliminary account of some of this work was given at the Austin, Texas and Washington, D. C. meetings of the American Physical Society.

* Now at the University of Florida, Gainesville, Florida.
‡ Now at the Bell Telephone Laboratories, Murray Hill, New Jersey.

[1] J. W. Mihelich and A. de-Shalit, Phys. Rev. 91, 78 (1953).

[2] A. A. Ebel and Clark Goodman, Phys. Rev. 93, 197 (1954); Martin, Diven, and Taschak, Phys. Rev. 93, 199 (1954).

[3] N. P. Heydenburg and G. M. Temmer, Phys. Rev. 93, 906 (1954).

[4] W. I. Goldburg and R. M. Williamson, Phys. Rev. 94, 747 (1954).

[5] Class, Cook, and Eisinger, Phys. Rev. 94, 809 (1954).

[6] Goldburg, Cox and Williamson, Phys. Rev. 95, 628 (1954).

work reported here. As has been pointed out,[7,8] this method of excitation is particularly suitable for studying the collective properties of the nucleus, which are described by the unified model of Bohr and Mottelson.[8,9] According to the model, nuclei in the region of mass values removed from closed shell configurations are subject to large deformations which result in a spectrum of low-lying "rotational" states. Because of these deformations large quadrupole matrix elements are associated with the rotational states which cause them to be especially susceptible to electric excitation by the $E2$ component of the radiation field of the incident particle. States due to single particle excitations may, of course, appear in addition to those associated with the collective motion.

The rotational states for an even-odd nucleus have spins which follow the sequence $I=I_0, I_0+1, \cdots$, and are at energies

$$E_I=(\hbar^2/2\vartheta)[I(I+1)-I_0(I_0+1)],$$

where ϑ is the effective moment of inertia (proportional to the square of the nuclear deformation). A similar formula applies for even-even nuclei. Departures from this purely rotational spectrum may occur as a result of centrifugal distortion and perturbations due to neighboring vibrational states. These effects are expected to be small for nuclei far removed from closed-shell configurations, and this is amply confirmed by experiment.[9-11]

In the case of gold, which is close to the magic nuclide Pb, the pure rotational model predicts 12:5 for the ratio of the energies of the second to first rotational states, while the 555- and 279-kev levels which are presumably rotational in character, are in the ratio of 2:1. This departure can be understood in a semi-quantitative way as due to the effects mentioned above. However, other features associated with rotational levels, such as an appropriate sequence of spin values and suitable $E2$ transition probabilities should be retained by these states. Experiments pertaining to these points are reported on in this paper. By measuring the angular distribution of the gamma radiation from these levels with respect to the beam, information relating to their spins was obtained. The observed functional dependence of the yield of these radiations on the energy of the bombarding particle allowed a check on certain of the assumptions in the theory of the excitation process to be made; and finally, the measurement of the absolute yield permitted a comparison of the experimental values of the reduced transition probabilities with those predicted by the unified model.

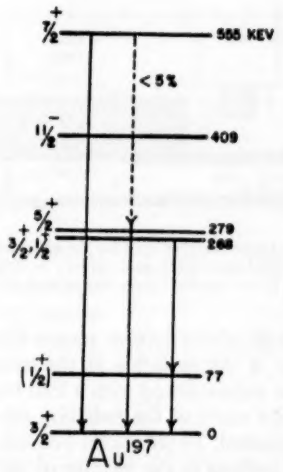

FIG. 1. Energy level diagram of Au^{197}. The arrows indicate transitions observed in Coulomb excitation. Spin assignments are taken from reference 1 and the present work.

APPARATUS AND PROCEDURE

Targets of gold, 99.95 percent pure,[12] were bombarded with protons accelerated by the Rice Institute 6.0-Mev Van de Graaff generator. After deflection through a 90° analyzing magnet, the resolution of the beam was ±10 kev, and the absolute energy was known to ±10 kev. The proton current incident on the target was measured with a current integrator of the type described by Watt.[13]

For the yield measurements, a thin gold target was used in order to reduce the inaccuracies of the stopping power calculation. The target was a gold foil 0.00011 inch thick (about 300 kev for 2-Mev protons) mounted at 45° to the beam. For the angular distribution measurements, it was possible to use a thick target (0.005 inch) since the distributions are not very sensitive to the beam energy.

Background radiation presented a serious problem throughout the experiment but was especially important with the thin target used for the yield measurements. In this case, unless the beam was absorbed on emerging from the target in such a way as to produce relatively little background radiation, the gamma rays under examination were obscured. To reduce this background the target chamber was constructed as shown in Fig. 2, so that the beam was absorbed in lead. Lead was chosen because no level is excited by protons in the energy range up to 5 Mev. By stopping the beam two feet beyond the target-counter position, it was possible to

[7] T. Huus and Č. Zupančič, Kgl. Danske Videnskab. Selskab, Mat.-fys. Medd. 28, No. 1 (1953).
[8] A. Bohr and B. Mottelson, Kgl. Danske Videnskab. Selskab, Mat.-fys. Medd. 27, No. 16 (1953); hereafter referred to as B-M.
[9] A. Bohr, *Rotational States of Atomic Nuclei* (Ejnar Munksgaards Forlag, Copenhagen, Denmark, 1954).
[10] G. M. Temmer and N. P. Heydenburg, Phys. Rev. 94, 1399 (1954).
[11] F. Asaro and I. Perlman, Phys. Rev. 91, 763 (1953).
[12] Based on a spectroscopic analysis. The targets were prepared from gold foil obtained from Baker & Company, 113 Astor Street, Newark 5, New Jersey.
[13] B. E. Watt, Rev. Sci. Instr. 17, 334 (1946).

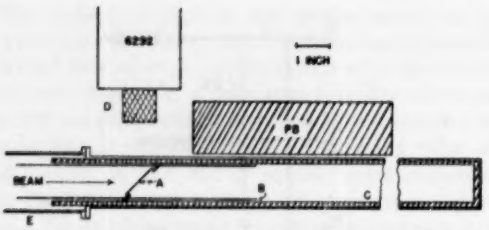

FIG. 2. The target chamber used for the absolute yield measurements. A: a 0.0001-inch thick gold target; B: 0.004-inch tin foil; C: lead lining; D: a 1-inch×1-inch NaI crystal; E: beam tube.

take advantage of the inverse square effect to reduce the intensity of the radiation at the counter. Further shielding was accomplished with a lead block placed so as to intercept much of the radiation produced as the beam was absorbed. To reduce the bremsstrahlung[14] due to scattered protons in the vicinity of the counter, the inner surfaces of the chamber were lined with 0.004-inch thick tin foil. The target chamber was located 20 feet from the analyzing magnet and at this distance the accelerator background was negligible. These measures reduced the background at $E_p<4.0$ Mev to about 15 percent of the total intensity of the photopeaks of the 279- and 555-kev lines. With increasing beam energy, the background rose to about 40 percent at $E_p=5.2$ Mev and at higher energies it prevented significant data being obtained.

The target chamber for the angular distribution measurements was a cylinder of copper 2 inches in diameter and 6 inches deep, which was mounted with its axis transverse to the beam tube. The target and a quartz plate used to position the beam were mounted on a rod free to rotate and slide along the axis of the chamber, and a divided head was provided so that the target could be accurately positioned from outside the chamber at any desired angle to the beam. The gamma-ray counter was mounted on an aluminum platform which rotated about an axis carefully aligned to coincide with the axis of the chamber. Background in these measurements was chiefly due to bremsstrahlung resulting from the scattering of the beam in the thick gold target. However, the improvement in yield due to the greater target thickness caused the problem to assume less importance.

The gamma rays were detected with a conventional NaI(Tl) scintillation spectrometer which had a resolution of 10 percent for 660-kev radiation. Standard electronic circuits were used for amplification, pulse-height analysis, and recording. The spectrometer was calibrated with gamma rays from Hg^{203}, I^{131}, Sn^{113}, and Cs^{137} sources.

The principal problem encountered in analyzing the data was in estimating the amount of background to be subtracted from the photopeak of the gamma rays being measured. This subtraction was guided by data on the shape of pure gamma-ray lines. The spectra of Hg^{203} and Cs^{137} radiations were taken with the sources mounted in the target positions of both chambers and by making use of the peak to valley ratio, resolution, and the location of the upper edge of the photopeak of the pure lines the magnitude of the background was estimated. Subtraction of the background resulted in line shapes for the gold gamma rays which agreed well with the pure lines from radioactive sources. Such measurements also showed that scattering material external to the target chamber had a negligible effect on the line shape. In the case of the angular distribution measurements, sources mounted in the target position made it possible to check the symmetry of the target and counter assemblies.

To make absolute yield measurements, it was necessary to determine the efficiency of the counter assembly. This was done by placing a standardized I^{131} source[15] in the target position under conditions identical to those under which the yield data were taken. Appropriate corrections were made to take into account the difference in the energies of the gamma rays from I^{131} and gold.

RESULTS AND DISCUSSION

1. Spectrum

Figure 3 shows the spectrum of radiation obtained from a thick target of gold when bombarded with 3.0-Mev protons with a 1-mm thick gold absorber used to attenuate the target x-rays. Gamma rays having energies of 191, 279, and 555 kev can be identified. A known gamma ray of 77 kev was obscured in these measurements due to the x-rays from Au^{197}, while

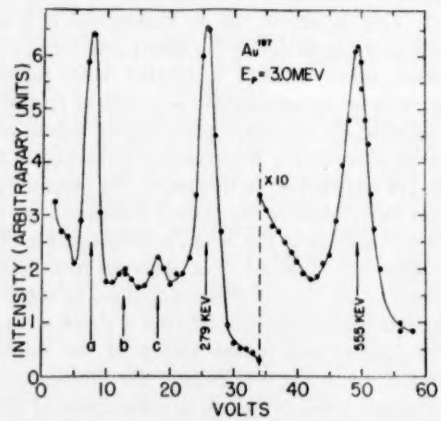

FIG. 3. The pulse-height distribution of gamma radiation from a thick gold target bombarded with 3.0-Mev protons obtained with a NaI crystal using a 1-mm gold absorber. Peaks *a*, *b*, and *c* correspond to the gold *K* x-ray, the Compton edge of the 279-kev gamma ray, and a 191-kev gamma ray.

[14] Č. Zupančič and T. Huus, Phys. Rev. **94**, 205 (1954).

[15] The source was calibrated by the National Bureau of Standards and was made available to us by Miss F. Garrett of the Radio-isotope unit of the V. A. Hospital, Houston, Texas.

possible gamma rays of 276 or 287 kev corresponding to transitions between the 555- and 279- or 268-kev levels could not have been observed with the available resolution. However, a search for gamma-gamma coincidences in this region showed that less than 5 percent of the 279-kev radiation resulted from a cascade from the 555-kev level. (This result was also obtained by Williamson.[6]) No evidence was found for a 478-kev gamma ray corresponding to a transition between the 555- and 77-kev levels. Since the 555-kev level is almost certainly a spin 7/2 state, as will be shown below, the absence of this gamma ray would seem to favor the choice of a spin assignment of 1/2 for the 77-kev level out of the two possibilities of 1/2, 3/2 allowed on the basis of the beta decay measurements.[1] The transitions observed with Coulomb excitation are indicated in Fig. 1. Other transitions in either excitation or decay are presumably negligible because of the large spin changes involved.

2. Angular Distributions

It has been shown by Alder and Winther[16] that information on the spins of electrically excited states can be obtained by measuring the angular distribution of the subsequent gamma radiation with respect to the beam. Figure 4 shows the experimental angular distributions obtained for the 279- and 555-kev radiations at beam energies of 3.0 and 4.4 Mev, respectively. The counter subtended a solid angle of 0.13 steradian and a 1-mm thick gold absorber was again used to reduce the x-ray intensity. The data were corrected for absorption in the target (5 mils gold), background and the finite angle subtended by the counters. Errors shown in Fig. 4 are statistical, but systematic errors due to uncertainties in background subtraction could change the asymmetries by about 3 percent.

The angular distribution data were analyzed under the assumption that the excitation of the state in question occurs by an electric quadrupole transition, which is in keeping with the Bohr-Mottelson theory, as discussed above. Transitions from the excited state may, of course, go by either $E2$ or $M1$ radiation or by a mixture of these. For Au^{197}, which has a ground state spin of 3/2, the only states accessible under this assumption which would result in anisotropic distributions are those having spins 5/2 and 7/2. The angular distribution corresponding to the $7/2\rightarrow 3/2$, $E2$ transition has been calculated at the appropriate beam energy using the following expression given by Alder and Winther[16]:

$$W(\theta)=1+a_2(\xi)B_2P_2(\cos\theta)+a_4(\xi)B_4P_4(\cos\theta), \quad (1)$$

where the $a_k(\xi)$ are energy dependent factors which enter because of the electric character of the excitation process, the B_k are the gamma-gamma correlation

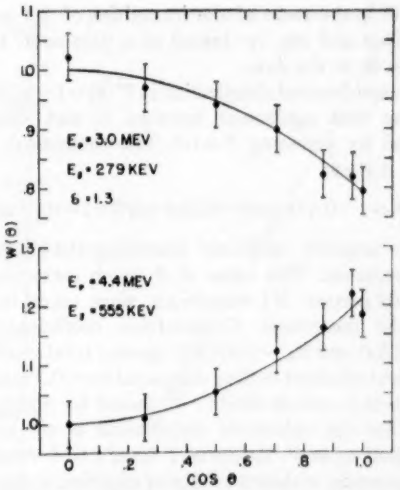

FIG. 4. The angular distributions of the 279-kev and 555-kev gamma rays from gold measured between 0 and 90 degrees to the beam. The curves were obtained from least square fits to the data.

coefficients tabulated by Biedenharn and Rose,[17] and the P_k are the Legendre polynomials.[18] Expression (1) when evaluated for $E_\gamma=555$ kev and cast in a form easily compared with experiment gives

$$W(\theta)=1+0.248\cos^2\theta-0.014\cos^4\theta\approx 1+0.23\cos^2\theta.$$

This distribution is to be compared with $W(\theta)=1+0.21\cos^2\theta$ obtained by a least squares fit to the data for the 555-kev radiation shown in Fig. 4. The agreement between the calculated and observed distributions appears adequate to assign a spin 7/2 to the level.

The observed negative anisotropy of the 279-kev gamma-ray angular distribution obviously excludes the possibility of a $7/2\rightarrow 3/2$, $E2$ transition. Indeed, a $5/2\rightarrow 3/2$, $E2$ transition is also excluded since this leads to a small positive coefficient for the $\cos^2\theta$ term, and although a $5/2\rightarrow 3/2$, $M1$ transition gives a negative coefficient, the anisotropy amounts to only 7 percent. However, by considering a mixture of $M1$ and $E2$ radiations, it is possible to obtain an anisotropy compatible with the experimental results for a $5/2\rightarrow 3/2$ transition. The angular distribution for this case is given by

$$W(\theta)=1+\frac{(0.0365-0.362\delta-0.0715\delta^2)}{1+\delta^2}a_2(\xi)P_2(\cos\theta)+\frac{0.49}{1+\delta^2}a_4(\xi)P_4(\cos\theta), \quad (2)$$

[16] K. Alder and A. Winther, Phys. Rev. **91**, 1578 (1953).

[17] L. C. Biedenharn and M. E. Rose, Revs. Modern Phys. **25** 729 (1953).

[18] The error in the coefficients made in neglecting the effect of the thick target is small because of the form of the yield curve and the slow variation of $a_k(\xi)$ with energy.

where δ^2 is the ratio of the intensities of $M1$ and $E2$ transitions and can be treated as a parameter to give the best fit to the data.

The experimental distribution is $W(\theta)=1-0.21\cos^2\theta$, and the best agreement between it and theory is achieved by assuming $\delta^2=1.7$. The theoretical distribution is then

$$W(\theta)=1-0.174\cos^2\theta-0.014\cos^4\theta\approx 1-0.19\cos^2\theta,$$

and the negative coefficient describing the asymmetry is a maximum. This value of δ^2 which corresponds to about 63 percent $M1$ transitions, when taken together with the theoretical K-conversion coefficients[19] $\alpha_K{}^2=0.08(E2)$ and $\beta_K{}^1=0.50(M1)$ gives a total conversion coefficient of about 0.35 as compared to $\sim$0.3 measured by Mihelich and de-Shalit.[1] It should be noted, however, that the calculated distribution is not strongly dependent upon δ^2. Values of δ^2 from 1 to 3 would lead to anisotropies within the range of experimental error.

3. Yield Measurements

The cross sections measured for the emission of gamma rays from the 279- and 555-kev levels are shown in Figs. 5 and 6, and for comparison the theoretical yield-curve for excitation by $E2$ transitions is also shown, normalized to the experimental data at about 4 Mev. The data were corrected for the finite thickness of the target and the angular distribution of the radiation. The errors indicated are due to some arbitrariness in the subtraction of background. Systematic errors in the absolute calibration of the counter contribute an uncertainty of about 20 percent to the scale of the cross sections.

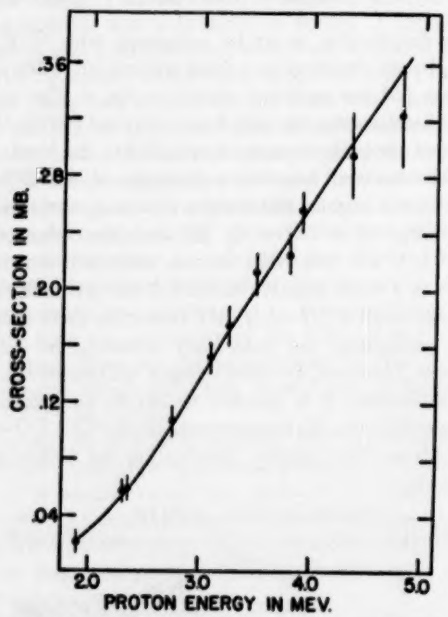

FIG. 5. The cross section in millibarns from the 279-kev gamma radiation as a function of the energy of the incident protons. The theoretical curve which is shown is normalized to the data at 4.0 Mev.

The theoretical yields have been calculated from the cross-section formula of Alder and Winther,[16]

$$\sigma=\frac{2\pi^2}{25}\frac{1}{Z_2{}^2e^2}\left(\frac{Mv}{\hbar}\right)^2 B(E2)g_2(\xi), \qquad (3)$$

where Z_2e is the charge of the target nucleus, v is the relative velocity, M is the reduced mass, and $B(E2)$ is the reduced electric quadrupole transition probability. The definition of the parameter ξ of reference 16 has been replaced here by the more rigorous definition,

$$\xi=\frac{Z_1Z_2e^2}{\hbar}\left(\frac{1}{v_f}-\frac{1}{v_i}\right),$$

in order to improve the agreement with the experimental data in the low-energy region. Z_1 is the charge of the incident particle and $v_{i,f}$ are the relative velocities before and after the excitation. For excitation energies which are small compared to the bombarding energy this definition approaches that given by Alder and Winther. The factor $g_2(\xi)$ involves integrals over the orbit of the impinging particle which are evaluated numerically under the assumption that the path of the particle is a classical trajectory. This implies that the energy lost in the excitation process must be small in comparison to the kinetic energy of the interacting particle.

The agreement observed between the theoretical yield and the experimental measurements for the 279-kev transition supports the assumption of $E2$ excitation and also indicates sufficient accuracy in the evaluation of the trajectory factor. For the 555-kev transition, detectable yields occur when the excitation energy is as much as 20 percent of the energy of the impinging proton, so that a deviation from the theoretical yield might be expected at low bombarding energies. This is, indeed, observed as seen in Fig. 6 for the range of $E_p<3.5$ Mev. That this discrepancy could be due to multipole excitation other than $E2$ is not believed likely in view of the results on the angular distribution of this radiation.

To get the total cross section for the excitation of the 279-kev state, the probability of decay by internal conversion must be taken into account. From the experimentally determined K-conversion coefficient of $\sim$0.3 and a K/L ratio of 6,[1] a total cross section of 0.35 mb for the excitation of this level at $E_p=4.0$ Mev was obtained. The total cross section for the excitation of the 555-kev state is 0.26 mb at the same proton energy, the correction for internal conversion and decay by cascades being assumed negligible.

[19] Rose, Goertzel, Spinrad, Harr, and Strong, Phys. Rev. 83, 79 (1951).

4. Discussion

From the experimental total cross sections for the excitation of the 279- and 555-kev states and the theoretical cross section formula (3), the reduced transition probabilities $B(E2)$ were calculated. If the states are assumed to have rotational character, the $B(E2)$ are given by the unified model as

$$B(E2)=\frac{15}{16\pi}e^2Q_0^2\frac{I_0}{(I_0+1)(I_0+2)}, \quad I_0\rightarrow I_0+1, \quad (4)$$

and

$$B(E2)=\frac{15}{8\pi}e^2Q_0^2\frac{1}{(2I_0+3)(I_0+2)}, \quad I_0\rightarrow I_0+2, \quad (5)$$

where Q_0 and I_0 are the intrinsic nuclear quadrupole moment and spin of the ground state. By using spins of 5/2 and 7/2 for the 279- and 555-kev states, respectively, and the ground state spin of 3/2, Q_0 has been calculated from the above formulas. From the data for the 279-kev transition, $Q_0=1.9\times10^{-24}$ cm² has been obtained while that from the 555-kev transition yields $Q_0=3.0\times10^{-24}$ cm². This Q_0 is related to the spectroscopically measured quadrupole moment Q by

$$Q=[I_0/(I_0+1)][(2I_0-1)/(2I_0+3)]Q_0,$$

so that the two cross section measurements yield values for Q of 0.4×10^{-24} and 0.6×10^{-24} cm², respectively. Recent measurements[20] of the hyperfine structure of Au give $Q=(0.56\pm0.1)\times10^{-24}$ cm².

Quadrupole moments of other nuclei derived in a similar manner from the collective model matrix elements have been found to be systematically smaller than those obtained from spectroscopic measurements (see B-M, VIId, iii). In view of this, the larger value of Q deduced from the 555-kev transition data suggests that the cross section for the excitation of this state is greater than would be expected from the theory. That a difficulty exists here is also indicated by the ratio of the reduced transition probabilities for the 279- and 555-kev states which is independent of Q_0. From formulas (4) and (5), $B(279):B(555)$ is expected to be 9:5 while the experimental ratio is of the order of 1:2. A similar comparison for the first two levels of Ta^{181}

[20] W. von Siemens, Ann. Physik 13, 158 (1953).

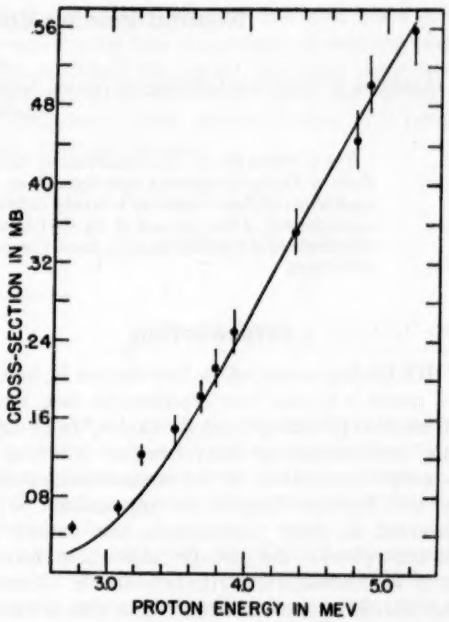

FIG. 6. The cross section in millibarns for the 555-kev gamma radiation as a function of the energy of the incident protons. The theoretical curve which is shown is normalized to the data at 4.2 Mev.

gave excellent agreement between experiment and theory.[9]

By making use of the Q_0 and $M1$ to $E2$ ratio determined for the 279-kev transition, the ground-state magnetic moment of gold was calculated (see B-M, IVb and VII 18, 20) to be ~0.13 nm as compared to 0.13±0.01 nm as measured by the atomic beam method.[21] These data also enable the intensity of the cascade transition from the 555-kev level through the 279-kev level to be calculated and compared with the intensity of the cross-over transition (see B-M, VII 18, 19, 20). Seven percent of the decays were computed to occur by the cascade route whereas the coincidence measurements gave an upper limit of about 5 percent.

We wish to acknowledge several helpful comments by Dr. T. Huus of the Institute for Theoretical Physics, Copenhagen, Denmark.

[21] G. Wessel and H. Lew, Phys. Rev. 92, 641 (1953).

Neutron Binding Energies from (d,p) Q Values*†

N. S. WALL‡
Department of Physics and Laboratory for Nuclear Science, Massachusetts Institute of Technology, Cambridge, Massachusetts
(Received July 9, 1954)

The Q values for the (d,p) reactions on some 27 targets whose neutron numbers are around the closed shells of 50 and 82 neutrons were determined. The general interpretation of these results and the specific application of these results to a variety of problems is discussed. In general, the results show a break of approximately 2 Mev at each of the shell edges. The technique used was that of a NaI scintillation spectrometer and is described in some detail. Comparison is also made with previous measurements by different techniques.

I. INTRODUCTION

THE binding energy of the last neutron B_n in many nuclei is known from experimental data such as (d,p) reaction Q values,[1] (γ,n) thresholds,[2] (n,γ) experiments,[3] and radioactive decay energies.[4] Much of this information is contained in the excellent summaries of Way[5] and Feather.[6] Despite the large amount of data represented in these compilations, one notices that there are regions of the periodic table where there is a paucity of information, particularly in the vicinity of nuclei with 82 or more neutrons. With this in mind, it was decided to study a number of (d,p) reactions in order to obtain additional values of B_n. From a study of (d,p) reactions one can also find the mass differences between various nuclei, the location of excited states, and other information. Following a brief discussion of the experimental technique, the results and their interpretations will be presented.

II. APPARATUS AND EXPERIMENTAL PROCEDURE

A. Emergent Beam and Electronic Equipment

The experiments reported here were performed using the M.I.T. cyclotron as a source of 15.1-Mev deuterons. The beam focusing arrangement, as well as many features of the scattering chamber, have been described in detail elsewhere.[7] The major experimental difference between the present experiments and those of Harvey,[1] using the same general apparatus, was in the energy measurement technique. Whereas his techniques involved the use of range-energy measurements, the present experiments used a NaI scintillation spectrometer in combination with an absorber of sufficient thickness to stop elastically scattered deuterons.

The scintillation spectrometer was essentially that described by Stoddart and Gove,[8] except that an RCA 6199 rather than an RCA 5819 photomultiplier was used. The high-voltage supply for the photomultiplier was the same as the one described by Higinbotham[9] and was stable enough to cause no fluctuations greater than 10 kev equivalent of the 10–15 Mev proton energy loss in the NaI crystal. The output of the photomultiplier drove a cathode follower adjacent to it. The cathode follower signal was then brought out of the scattering chamber through a vacuum seal and into a highly stabilized inverter and another cathode follower preamplifier. This preamplifier fed the 50-foot cable carrying the signal from the scattering chamber room, through the concrete shielding, to the electronic equipment area outside. The signal was then amplified by a linear amplifier designed by Hugh F. Stoddart of the M.I.T. cyclotron group. The basis for this amplifier was the non-overloading amplifier described by Chase and Higinbotham.[10]

Pulse-height measurements were made with a single-channel analyzer of the type described by Johnstone.[11] External biasing was used so that the bias could be "stepped" automatically. The same stepping arrangement which changed the bias caused the differential pulse-height scaling circuit output to go into an appropriate register. The stepping relays performing these actions were actuated by the beam monitor reaching a predetermined number of counts.[12] The monitor consisted of another scintillation counter which could could either see the same area of the target as the spectrometer, or could be placed in such a position so as to see the elastically scattered deuterons from a thin gold foil near the beam catcher. In either case, the entire beam target area was seen by the spectrometer and the monitor. The output of the monitor counter was scanned with an integral discriminator and then

* This work is based in part on material submitted in partial fulfillment for the Ph.D. degree at Massachusetts Institute of Technology.

† This work was supported in part by a joint program of the U. S. Office of Naval research and the U. S. Atomic Energy Commission.

‡ Now at the Department of Physics, University of Rochester, Rochester, New York.

[1] J. A. Harvey, Phys. Rev. **81**, 353 (1951).
[2] Sher, Halpern, and Mann, Phys. Rev. **84**, 387 (1951).
[3] Kinsey, Bartholomew, and Walker, Phys. Rev. **78**, 77, 481 (1950); Canadian J. Phys. **31**, 1025 (1953).
[4] A. H. Wapstra, thesis, University of Amsterdam, 1953 (unpublished).
[5] K. Way (private communication).
[6] N. Feather, Phil. Mag. Supplement **2**, 141 (1953).
[7] Boyer, Gane, Harvey, Deutsch, and Livingston, Rev. Sci. Instr. **22**, 310 (1951).
[8] H. F. Stoddart and H. E. Gove, Phys. Rev. **87**, 262 (1952).
[9] W. A. Higinbotham, Rev. Sci. Instr. **22**, 429 (1951).
[10] R. Chase and W. A. Higinbotham, Rev. Sci. Instr. **23**, 34 (1952).
[11] C. W. Johnstone, Nucleonics **11**, 36 (1953).
[12] M.I.T. Laboratory for Nuclear Science Progress Report, November 30, 1952 (unpublished).

set below the pulse height corresponding to elastic deuterons. The discriminator could be varied over a large range without significant changes in the counting rate; that is to say, the monitor was insensitive to small changes in energy or amplification.

The various scaling circuits used are those described in reference 7.

B. Targets

For most of the nuclei studied in these experiments, thin (10–20 mg/cm²) metallic or elemental foils could not be obtained easily. In addition, since it was desired to study a large number of separated isotopes,[13] it was necessary to have the targets in a readily recoverable form. Therefore, a compound of the element to be studied containing only carbon, hydrogen, or oxygen was ground to a fine powder and mixed with a solution of polystyrene dissolved in benzene. This slurry was then spread onto a glass plate and allowed to dry at room temperature. The resulting foil could then be peeled off the glass with a razor blade.[14]

The reason for using only compounds of carbon, hydrogen, or oxygen lies in the fact that these elements are practically monoisotopic and the abundant isotopes have ground-state Q values lower than most of the nuclei studied. In addition, these nuclei are lighter than any of those studied so that the proton groups corresponding to levels of the same Q value, of the elements studied, had higher energy in the laboratory frame of reference.

C. Q-Value Determinations

The ratio of the pulse heights corresponding to the maxima of the spectra of the clearly resolved ground and first excited states of C^{13} was measured in order to determine the beam energy as well as the relationship between energy and pulse height rapidly and precisely.[15] By assuming a set of beam energies and calculating this ratio by means of the Q equation for each assumed energy, one could find the ratio corresponding to the actual beam energy. Then, knowing the beam energy as well as the target thickness, angle of counter, and absorber thickness, one can calculate the energy lost in the crystal by the ground-state proton group. The absorber thickness as well as the other factors just mentioned are also considered in ratio calculation.

The actual analysis of the pulse-height data is carried out in the following manner. From the pulse-height measurement we can find the proton energy loss in the NaI crystal. With the range-energy curves of Smith[16] as modified by Harvey[1] it is possible to calculate the proton energy when the particles leave the target. Then, using the relative stopping powers as measured by Harvey[1] and knowing the deuteron beam energy, one can calculate both the proton and deuteron energies at the center of the target. Knowing these particle energies at the centers of both targets, one can calculate the unknown Q value relative to that of a reference target, from the equation

$$Q_x - Q_r = (E_{p_x} - E_{p_r}) - (E_{d_x} - E_{d_r}) + \frac{(E_{p_x} + 2E_{d_x})}{A_x} - \frac{(E_{p_r} + 2E_{d_r})}{A_r} - 2\left[\frac{(2E_{p_x}E_{d_x})^{\frac{1}{2}}\cos\theta_x}{A_x} - \frac{(2E_{p_r}E_{d_r})^{\frac{1}{2}}\cos\theta_r}{A_r}\right],$$

where E_p and E_d refer to proton and deuteron energies, the subscripts x and r refer to the unknown and known Q-value groups, respectively, A is the mass of the residual nucleus, and θ is the angle of the detector with the incident beam.

In order to minimize the effect of any systematic errors, the present measurements were made by comparing the proton groups from the nucleus under consideration to a proton group corresponding to a reaction of well-known Q value.[1] Frequently this was the C^{13} end group from the $C^{12}(d,p)C^{13}$ reaction in either the target polystyrene or, usually, the same polyethylene target used to measure the beam energy. A consideration of possible causes of systematic errors leads one to believe they introduce no significant error in the final result, at least to the accuracy of these experiments.[17]

On the other hand, when one considers other sources of error,—that is, errors which affect the unknown Q-value proton group differently from the reference group, one finds as the largest single factor the inability to locate accurately the maximum of the spectrum. This difficulty in locating spectral maxima is due directly to the over-all poor energy resolution of the technique used. When one considers effects such as photomultiplier statistics and energy straggling in the absorber, one sees that the energy spread of a clearly resolved proton group is about 500–600 kev (full width at half-maximum) for the targets used. Consequently, errors as large as 200–300 kev can be introduced in the location of the energy of the proton group under consideration. Figure 1 illustrates the over-all resolution of this setup for the ground-state proton group from C^{13}.

The other main source of error in these measurements is the error in target thickness. The thickness is measured by comparing the energy of the proton groups from the C^{13} ground state reaction in the target to those coming from the reference target. Since we are measuring a small difference between two large quantities, the technique is somewhat insensitive. However, it is

[13] These isotopes were supplied by the Staple Isotopes Division, Oak Ridge National Laboratory.

[14] N. S. Wall and J. W. Irvine, Jr., Rev. Sci. Instr. (to be published).

[15] F. Ajzenberg and T. Lauritsen, Revs. Modern Phys. **24**, 321 (1952).

[16] J. H. Smith, Phys. Rev. **71**, 39 (1947).

[17] N. S. Wall, Ph.D. thesis, Massachusetts Institute of Technology, October, 1953 (unpublished).

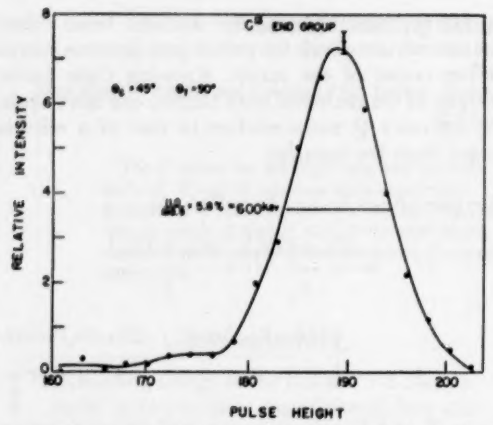

FIG. 1. Spectrum of $C^{12}(d,p)C^{13}$ ground-state to ground-state reaction. The abscissa is given in terms of absolute pulse height as determined by a precision pulser.

believed no errors of greater than 50 kev are introduced in this manner. The best criterion of the errors in these experiments is, however, a comparison between the present results and other measurements; for example, Sr^{89}, Sn^{121}, and Bi^{210}.

III. RESULTS

The experimental results of the ground state Q-value determinations are given in Table I. The location of any excited states that could be resolved are listed in the third column of this table. In most cases, these excitation energies were determined using the equation given above with the ground-state Q value as the reference. For the energy of particles, and the heavy nuclei examined here, the excitation energy is practically equal to the difference of the outgoing proton energies corresponding to the ground-state and excited-state proton groups.

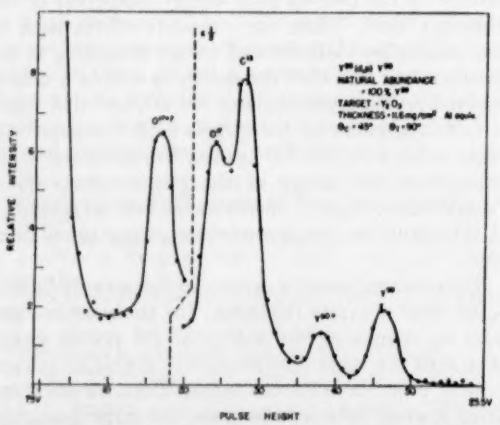

FIG. 2. The $Y^{89}(d,p)Y^{90}$ spectrum. The abscissa in this figure as well as Figs. 3 and 4 is given in arbitrary pulse heights. The absolute pulse heights can be found from the notations at either border indicating the pulse height in volts.

Figures 2–4 show the proton spectra from several typical targets. Figure 2 shows the clearly resolved end group and first excited states from a thin, uniform Y_2O_3 in polystyrene target. Figure 3 shows the analysis necessary to interpret the spectrum and derive the ground-state Q value for the $Ce^{140}(d,p)Ce^{141}$ reaction. Since the Q value as determined here is only about 450 kev higher than the C^{13} Q value, and C^{12} is probably present to a much higher concentration in the target, the Ce^{141} end proton group is on the high-energy side of the C^{13} end group and not clearly resolved from it. The graphical analysis was based on an analysis of the different causes of spread such as energy straggling, and the energy dependence.[17] Figure 4 shows the spectrum from the reaction $Mo^{92}(d,p)Mo^{93}$. This target was a suspension of MoO_3, enriched to about 87 percent Mo^{92}, in polystyrene. The spectrum again illustrates

TABLE I. Experimental results.

Residual nucleus	Q value of ground state reaction Mev	Excitation energies Mev
Ca^{43}	2.80±0.30	
Sr^{85}	5.25±0.30	
Sr^{87}	6.26±0.20	
Sr^{89}	4.29±0.15	
	3.20±0.20	1.09
Rb^{84}	6.2 ±0.3(?)	
		1.5(?)
Rb^{88}	3.75±0.20	
Y^{90}	4.41±0.05	
		1.17±0.06
Zr^{92}	4.46±0.05	
Mo^{95}	5.63±0.05	
		0.91±0.10
		1.41±0.10
		2.23±0.10
		2.73±0.10
Zr^{96}	4.19±0.05	
		0.9 ±0.2
Mo^{97}	4.51±0.30	
Mo^{98}	6.06±0.10	
		2.5 ±0.3
Cd^{113}	4.10±0.09	
		0.55±0.08
Cd^{116}	$3.52^{+0.15}_{-0.06}$	
Sn^{121}	3.92±0.07	
Sn^{126}	3.52±0.07	
		1.16±0.08
		2.77±0.10
		3.41±0.10
		4.09±0.10
Te^{125}	4.25±0.07	
Te^{126}(?)	5.0 ±0.2	
I^{128}	4.35±0.05	
Cs^{134}	4.50±0.10	
La^{140}	2.87±0.10	
Ce^{141}	3.17±0.10	
Ce^{142}	2.86±0.07	
		0.90±0.15
Pr^{142}	3.42±0.30	
		0.62±0.10
Nd^{143}	3.79±0.08	
		0.70±0.10
Sm^{155}	3.36±0.30	
Bi^{210}	1.94±0.03	

the difficulties in resolving single levels, although in this particular reaction the end group is clearly resolved.

For some of the targets studied the end proton group was resolved even more poorly than the Ce^{141}. This was attributed to poor targets (i.e., too thick or not sufficiently uniform), or low-lying levels. In other cases, however, the end groups were resolved more clearly than the Y^{90} ground-state group.

Table II lists the binding energy of the last neutron in each of the nuclei studied, as well as comparisons of these measurements with measurements made by means of other techniques and reactions. In particular, the

TABLE II. Neutron binding energies in Mev and comparison with Metropolis-Reitwiesner predictions.

Nucleus	B_n (obs)	B_n (calc)	B_n (obs) $-B_n$ (calc)	Other measurements	Ref.
$_{20}Ca^{49}$	5.0	4.1	+0.8		
$_{38}Sr^{85}$	7.48	7.92	−0.4		
$_{38}Sr^{87}$	8.49	7.18	+1.3	(n,γ) 8.42 (d,p) 8.52±0.20	a b
$_{38}Sr^{89}$	6.52	6.53	0	(d,p) 6.55±0.10 (d,p) 6.55±0.20	c b
$_{37}Rb^{85}$	8.4	6.8	+1.6		
$_{37}Rb^{88}$	5.98	6.12	−0.1		
$_{39}Y^{90}$	6.64	7.06	−0.4		
$_{40}Zr^{93}$	6.69	6.88	−0.2	(d,p) 6.56±0.10	b
$_{42}Mo$	7.86	8.47	−0.6	(d,p) 8.31±0.2	b
$_{40}Zr^{95}$	6.42	6.28	+0.1		
$_{42}Mo^{97}$	6.7	7.2	−0.5	(γ,n) 7.1 ±0.3	d
$_{42}Mo^{98}$	8.29	9.04	−0.8		
$_{48}Cd^{113}$	6.33	6.83	−0.5	(γ,n) 6.44±0.15	e
$_{48}Cd^{115}$	5.75	6.36	−0.6		
$_{50}Sn^{121}$	6.15	6.17	0	(d,p) 6.2 ±0.3	b
$_{50}Sn^{125}$	5.75	5.33	+0.4		
$_{52}Te^{125}$	6.48	6.47	0	(γ,n) 6.50±0.2	e
$_{52}Te^{128}$?	7.2	8.1	−0.9		
$_{53}I^{128}$	6.58	6.33	+0.3		
$_{55}Cs^{134}$	6.73	6.16	+0.6		
$_{57}La^{140}$	5.10	6.00	−0.9		
$_{58}Ce^{141}$	5.40	6.30	−0.9		
$_{58}Ce^{143}$	5.09	5.93	−0.9		
$_{59}Pr^{142}$	5.65	6.60	−1.0		
$_{60}Nd^{143}$	5.02	5.89	−0.9		
$_{62}Sm^{155}$	5.58	5.69	−0.1		
$_{83}Bi^{210}$	4.17	5.82	−1.7	(n,γ) 4.17±0.015 (d,p) 4.14±0.03	a b

[a] See reference 3.
[b] See reference 1.
[c] See F. B. Shull and C. E. McFarland, Phys. Rev. **89**, 489 (1953).
[d] See reference 33.
[e] See reference 2.

measurements on Te^{125}, Cd^{113}, and Mo^{97} should be noticed. The measurements given in the last column of Table II are all of such a nature that they would set an upper limit on the neutron binding energy (6).[18,19] On the other hand, since the ground-state proton group may not have been observed, the (d,p) reaction only leads to a lower limit on the neutron binding energy. (From conservation of energy the binding energy of the last neutron equals the Q value of the ground-state to

[18] The measurement on Mo^{97} was made by using the Cu^{63} threshold as 10.9 Mev. The recent re-evaluation of this to 10.6 Mev (see reference 19) would make the (γ,n) and (d,p) agreement very close.
[19] Birnbaum, Harth, Seren, and Tobin, Phys. Rev. **91**, 474(A) (1953).

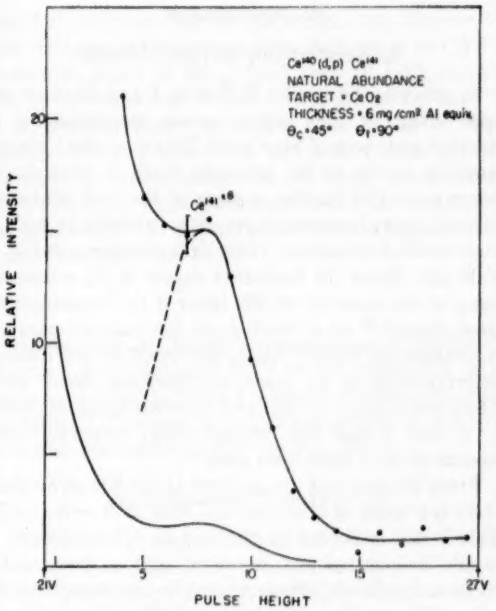

FIG. 3. The $Ce^{140}(d,p)Ce^{141}$ spectrum. See Fig. 3 for explanation of abscissa.

ground-state (d,p) reaction plus the binding energy of the deuteron, 2.23 Mev.) It is therefore worth noting the agreement between these two methods as it lends confidence to the general approach of deriving binding energies from either (d,p) or (γ,n) reactions. Table II also lists the binding energy expected on the basis of the semiempirical mass formula.[20,21]

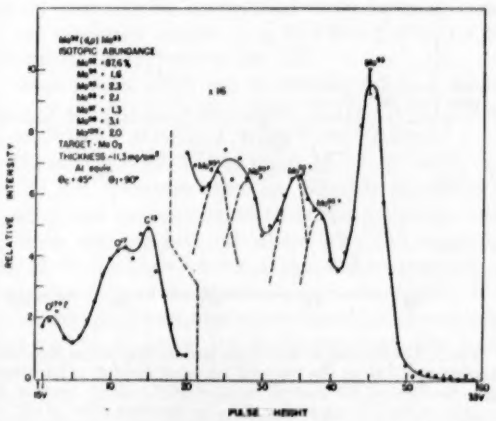

FIG. 4. The $Mo^{98}(d,p)Mo^{99}$ spectrum. See Fig. 2 for explanation of abscissa.

[20] R. Metropolis and G. Reitwiesner, Atomic Energy Commission Report NP-1980, 1950 (unpublished).
[21] E. Fermi, *Nuclear Physics* (University of Chicago Press, Chicago, 1950).

IV. DISCUSSION

A. Relationship to Shell Model

In general, the results in Tables I and II show the same effect at shell edges as the measurements of Harvey[1] and those of Sher *et al.*[2] That is, at the "magic" numbers of 50 or 82 neutrons there is pronounced decrease in the binding energy of the last neutron.[22] There is now, however, more data available at each of these shells than before. These data are shown in Fig. 5. This plot shows the measured values of B_n minus the value of B_n expected on the basis of the semiempirical mass formula[20] as a function of the neutron number. No values are plotted which are based on the indirect determination of B_n from, for example, decay data. The main content of this plot is based upon references 1, 2, and 3 and the present work; however, other sources of data have been used.[23]

From this plot one can see that at the 50 and 82 shells there is a break of about 2.0–2.3 Mev in $B_n - B_n$ (calc). This break is similar to the one at 126 neutrons.[1] It should be pointed out, however, that at none of the shells is this break *directly* related to the strength of the spin-orbit coupling since the level filled just after the magic number is not a member of the same doublet filled at or just before it. In order to evaluate any spin-orbit parameter one would therefore have to know the order of the levels before a spin-orbit perturbation is introduced. This in turn is related to a particular nuclear model.

In Fig. 5 there are three points just prior to $N=50$ representing B_n for Sr^{85}, Kr^{85},[24] and Sr^{86}.[2] These values

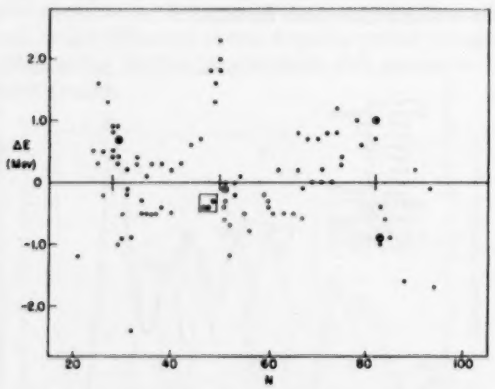

FIG. 5. The binding energy of the last neutron minus the binding energy expected on the basis of the semiempirical mass formula as a function of the neutron number of the target nucleus. The double circles indicate two nuclei with the same value of ΔE, and the heavy circle indicates three nuclei with the same value of ΔE. The three nuclei enclosed in the box are doubtful measurements and are discussed in Sec. IV-A of the text.

are in pronounced disagreement with other nuclei in this general vicinity.

Sr^{85}.—The Sr^{85} measurement reported here may be low due to the fact that the targets used in these experiments had only about 45 percent Sr^{84} and about 15 percent Sr^{86}. B_n for Sr^{85} should be somewhat higher than B_n for Sr^{87}, since Sr^{85} has a smaller neutron excess. If for some reason the intensity of the Sr^{85} ground-state proton group was less than the intensity of the Sr^{87} group, then it may have escaped observation.

Sr^{86}.—The B_n for Sr^{86} again should be somewhat higher than that of Sr^{88}. Since Sr^{86} is present in only low abundance in natural Sr, the neutrons corresponding to the (γ,n) reaction on Sr^{86} may have been missed in the measurements of Sher *et al.*[2]

Kr^{85}.—With respect to Kr^{85}, Wheeler *et al.* mention that the actual binding energy may be some 0.9 Mev higher, but feel that it is unlikely. However, even with a B_n 0.9 Mev higher $B_n - B_n$ (calc) would still be low as compared to other nuclei in this region.

Relative to the shell model, it should be pointed out that $B_n(Ca^{49})$ does not show the effect of either neutron number 28 or proton number 20. This is similar to the cases of V^{52} and Fe^{55},[1] but a behavior unlike that of the Ti isotopes as analyzed by Pieper.[23] However, when Pieper's data is compared to the mass formula, no "magic effect" is observed. (See Fig. 5.)

It should also be noted that of the nuclei referred to in Fig. 5 in the region around $N=35$, those lying above the $B_n - B_n$ (calc) $=0$ line are mostly even-A nuclei, whereas those below the line are odd-A nuclei. This may be entirely a result of the fact that the mass formula[21] pairing term $\delta/A^{\frac{1}{2}}$ is poorly estimated in this mass region.

B. Double β Decay

As has been pointed out in an earlier paper[25] the neutron binding energies for Te^{125} and Sn^{125} along with the decay energies of Sn^{125} and Sb^{125} allow one to conclude that there is 2.4 ± 0.3 Mev available for the double β decay of Sn^{124}. In a similar fashion one can show that there is at least 4.3 ± 0.3 Mev available for the decay of Ca^{48} to Ti^{48}. In this case, however, the decay energies are not known to sufficient accuracy[26] for the result to be meaningful even though it agrees with the mass spectroscopic data, 4.34 ± 0.11 Mev.[27]

C. Mo^{98}

On the basis of the compound nucleus theory of nuclear reactions, the neutron capture cross section of a particularly stable nucleus, such as the magic number nuclei, should be low as compared to a normal

[22] M. G. Mayer, Phys. Rev. **78**, 16 (1950); Haxel, Jensen, and Suess, Z. Physik **128**, 295 (1950).
[23] G. Pieper, Phys. Rev. **88**, 1299 (1952).
[24] Wheeler, Schwartz, and Watson, Phys. Rev. **92**, 121 (1953).
[25] N. S. Wall, Phys. Rev. **92**, 1526 (1953).
[26] Hollander, Pearlman, and Seaborg, Revs. Modern Phys. **25**, 469 (1953).
[27] Collins, Nier, and Johnson, Phys. Rev. **86**, 407 (1952); **84**, 717 (1951).

nucleus.[28,29] Mo^{98}, as well as other nuclei with from 56–60 neutrons, shows an anomalously low capture cross section.[30] Mo^{98}, therefore, should show a particularly high binding energy for the last neutron, since Mo^{97} seems to be a normal nucleus compared to others in that region. (See Table II.) However, the binding energy of the last neutron is 8.29 Mev or compared to the mass formula the difference $B_n - B_n$ (calc) is equal to -0.8 Mev. The average difference in this region of the periodic table is only about -0.4 Mev.

It may be that the last neutron in Mo^{99} is only very loosely bound relative to Mo^{98}. Then the neutron added to Mo^{98} would enter the compound nucleus in a region of low level density. However, at other magic numbers there is a relative increase of $B_n - B_n$ (calc) just before the shell edge, whereas here none is observed. Consequently, the nuclei that show an anomalously low cross section, in this region of the periodic table, might do so for another reason, or the compound nucleus theory may be inadequate here.[31]

D. Bi^{210}

The Q value of the highest-energy proton group from the reaction $Bi^{209}(d,p)Bi^{210}$ has been measured and found to be 1.94 ± 0.03 Mev, in excellent agreement with Harvey[1] and Kinsey.[3] It is felt that this proton group does not truly represent the ground state of Bi^{210}, but several excited states of about 400–500-kev excitation too closely spaced to be resolved in the present experiments. The following paper on the angular distributions of the protons from the $Q=1.94$-Mev level will discuss this point in greater detail.

E. Sn^{125}, Mo^{93}, Y^{90}, Ce^{143}, Pr^{142}, Nd^{143}

These nuclei show excited states which, at least within the resolution of the present experiments, are clearly resolved and have a several hundred kilovolt spacing, for the first excited state, and in some cases higher levels.

Y^{90}, Pr^{142}, and Nd^{143} have one neutron over a closed shell, Ce^{143} has three, but Sn^{125} is not too close to either the 50 or 82 shells. On the other hand, Sn^{125} is proton magic and therefore, if the neutrons and protons are coupled as in the collective model,[31] one might expect such a level structure.

F. Cd^{113}

The ground state of Cd^{113} is believed to be unstable relative to In^{113}.[26] Because there is a large spin difference between the ground states of these nuclei, as well as a low but unknown energy difference, the lifetime for this decay should be quite long. An isomer in Cd^{113} is known to decay to the ground state of In^{113}, but the energy of excitation of this isomer is not known.[26] If it is assumed that the excited state found in these experiments is the same as the isomer then one can calculate the decay energy for the ground-state transition. From the data given in Table I and the Cd^{113m} decay energy,[27] the ground-state decay energy of Cd^{113} should be 0.04 ± 0.08 Mev.

G. Mo^{92}

On the basis of Harvey's measurement of $B_n(Mo^{93})$, Feather[6] has estimated Mo^{92} to be 0.08 ± 0.35 Mev capture-unstable to Nb^{92}. Using the value for B_n given in Table II, however, a similar calculation shows Nb^{92} is unstable to decay to Mo^{92} by 0.53 Mev.

H. Calculated Values of B_n

Though no measurements of the sort given below were used in Fig. 5, from appropriate total decay energies and known B_n values, B_n for other nuclei can be found. For example:

$$Ce^{140}+n=Ce^{141}+B_n(Ce^{141}),$$
$$Ce^{141}\xrightarrow{\beta} Pr^{141}+E_{\beta 1},$$
$$Pr^{141}=Pr^{140}+n-B_n(Pr^{141}),$$
$$Pr^{140}\xrightarrow{\beta} Ce^{140}+E_{\beta 2}.$$

Adding these four equations and using the value 5.40 Mev given in Table II for $B_n(Ce^{141})$ as well as 0.58 Mev for $E_{\beta 1}$ and 3.25 Mev for $E_{\beta 2}$,[26] one finds $B_n(Pr^{141})=9.2\pm0.3$ Mev. This agrees quite nicely with the value 9.4 ± 0.3 Mev as given by Hanson.[32] This latter value should probably be lowered 0.3 Mev, however, since it was measured relative to a 10.9-Mev $Cu^{63}(\gamma,n)Cu^{62}$ threshold. See footnote in Sec. III.

Other values which can be determined in a similar manner are $B_n(Kr^{88})\leq 6.8$ Mev; $B_n(In^{113})=9.13$ Mev; $B_n(La^{141})=6.7$ Mev; and $B_n(Ba^{140})=6.32$ Mev.

The author would like to thank Mr. E. F. White and the M.I.T. cyclotron crew for valuable assistance in building and maintaining much of the equipment used in these experiments. He would also like to thank Mr. H. F. Stoddart for the design and construction of the major part of the electronic instrumentation. It is a pleasure to acknowledge many valuable conversations with Dr. H. E. Gove, Dr. Katherine Way, Dr. J. W. Irvine, Jr., and Dr. J. A. Harvey. A particular debt of gratitude is due Professor Martin Deutsch for the guidance, advice, and training the author received from him.

[28] J. Blatt and V. Weisskopf, *Theoretical Nuclear Physics* (J. Wiley & Sons, Inc., New York, 1952).
[29] H. Hurwitz and H. Bethe, Phys. Rev. **81**, 898 (1951).
[30] D. Hughes, Phys. Rev. **91**, 1423 (1953).
[31] K. Ford, Phys. Rev. **90**, 29 (1953).
[32] J. M. Cassidy, Phys. Rev. **83**, 483 (1951).
[33] Hanson, Duffield, Knight, Diven, and Palevsky, Phys. Rev. **76**, 578 (1949).

Proton Angular Distributions from Deuteron Bombardment of Bi^{209}, Pb^{207}, and Y^{89}†*

N. S. WALL‡
Department of Physics and Laboratory for Nuclear Science, Massachusetts Institute of Technology, Cambridge, Massachusetts
(Received July 9, 1954)

The proton angular distributions in the (d,p) reactions on Bi^{209}, Pb^{207}, and Y^{89} have been measured and an attempt made to interpret the results on the basis of the Butler stripping theory. The neutron added to Y^{89} is consistent with an $l_n=2$ prediction. The last neutron in Pb^{208} shows a similarity to an $l_n=1$, non-Coulomb theory angular distribution, but the Bi^{210} case is not readily capable of being interpreted with this theory. The results of these experiments are analyzed on the basis of the shell model and the systematics of the binding energy of the last neutron.

I. INTRODUCTION

THE interpretation of the binding energy of the last neutron[1,2] in terms of the shell model depends on the angular momentum of the state in which the neutron is captured. According to the theory of deuteron stripping[3-6] the angular distribution of the outgoing protons from a (d,p) reaction yields, directly, the orbital angular momentum value l_n of the captured neutron. Though this technique does not measure the total angular momentum of the resultant nucleus, it does limit it to certain values, derived from the conservation of angular momentum.[3] The present paper reports an attempt to ascertain whether the measured Q-values of (d,p) reactions can be used to determine the spin-orbit coupling in the $5g$ and $7i$ shells from the binding energies of the 50th and 51st or the 126th and 127th neutron respectively.

Pb^{208}, Bi^{210}

In the case of the Bi^{210} neutron binding energy it is believed that the protons observed do not correspond to Bi^{210} in the ground state, and therefore the binding energy as derived from the $Bi^{209}(d,p)Bi^{210}$ Q-value is too low. The main reason for this belief is the failure of a cycle involving, in addition to the Q-values of the $Bi^{209}(d,p)Bi^{210}$ and $Pb^{208}(d,p)Pb^{209}$ reaction, well established masses, decay energies, and Q-values to close.[1,2,7,8] If one assigns the entire discrepancy to the Bi^{210} Q-value, the Bi^{210} ground state should actually be about 500 kev lower than experiments to date indicate.[1,2,8] By accepting some very general results from deuteron stripping theory this discrepancy can be readily understood on the basis of the model of Bi^{210} as given by Pryce.[9]

The differential cross section $d\sigma/d\omega$ for a (d,p) stripping reaction can be written

$$\frac{d\sigma}{d\omega}\propto\frac{(2I+1)}{(2J+1)}|\langle M\rangle|^2, \tag{1}$$

where $|\langle M\rangle|^2$ is equivalent to a matrix element between the initial and final states and J and I are the total angular momenta corresponding to these states, respectively.[3-6] This matrix element contains one term expressing the probability of finding a proton of an appropriate momentum in the deuteron and another representing the capture of the stripped neutron by the nucleus. It should be remarked that the value of the matrix element here is assumed to be independent of I. If, however, this is not the case but $|\langle M\rangle|^2$ is not too dependent on I, the conclusions below are still valid.

The model of Pryce[9] gives a ground state of Bi^{210} of minimum spin, that is the j of the neutron is antiparallel to that of the proton. On the basis of the shell model the last neutron in Bi^{210} is expected to be in a $g_{9/2}$ configuration with the proton in the $h_{9/2}$ configuration of Bi^{209}.[10] Following Pryce these two nucleons would couple to give an $I=0$ ground state for Bi^{210}, with a series of nine excited states with $I=1, 2\cdots9$. These latter states are closely spaced in energy and are separated by several hundred kev from the $I=0$ ground state.

The spin of Ra E, Bi^{210} has recently been found to have the value $I=1$ by K. F. Smith, as quoted in a paper to be published on Ra E by E. A. Plassman and L. M. Langer. If the last neutron configuration is $h_{11/2}$ then the conclusions above are essentially the same, the statistical weight factor being 2.5 percent. If, however, the neutron configuration is $g_{9/2}$ so that a $g_{9/2}$ neutron and an $h_{9/2}$ proton couple to give a ground state of $I=1$, then this whole picture is probably incorrect.

The (d,p) experiments performed to date have not been of sufficiently high resolution to be able to dis-

† This work is based in part on material submitted in partial fulfillment for the Ph.D. at Massachusetts Institute of Technology.

* This work supported in part by a joint program of the U. S. Office of Naval Research and the U. S. Atomic Energy Commission.

‡ Now at the University of Rochester, Rochester 3, New York.

[1] N. S. Wall, preceding paper [Phys. Rev. **96**, 664 (1954)].
[2] J. A. Harvey, Phys. Rev. **81**, 353 (1951).
[3] S. T. Butler, Proc. Roy. Soc. (London) **A208**, 559 (1951).
[4] P. B. Daitch and J. B. French, Phys. Rev. **87**, 900 (1952).
[5] F. L. Friedman and W. Tobocman, Phys. Rev. **92**, 93 (1953).
[6] A. B. Bhatia *et al.*, Phil. Mag. **43**, 485 (1952).
[7] J. R. Huizenga *et al.*, Phys. Rev. **79**, 908 (1950).
[8] B. B. Kinsey *et al.*, Phys. Rev. **78**, 77 (1950).
[9] M. H. L. Pryce, Proc. Phys. Soc. (London) **A65**, 773 (1952).
[10] P. F. A. Klinkenberg, Revs. Modern Phys. **24**, 63 (1952).

tinguish the various components of the excited multiplet of Bi^{210}. The ground state however would have been resolved providing it had a moderate, (2 percent–3 percent), intensity relative to the unresolved multiplet. On the basis of the stripping theory, as given above, the general result that the differential cross section depends upon the statistical weight of the initial and final levels leads to the conclusion that the intensity of the ground state should be 1 percent, that of the excited multiplet for the $h_{9/2}$, $g_{9/2}$ configuration. (The excited multiplet corresponds to the $Q=1.94$-Mev proton group.) The fact that we are dealing with nuclei for which the deuteron energy used is comparable to the Coulomb barrier probably does not introduce too large an error, providing the reaction still goes by stripping. The Coulomb field will, however, introduce a small effect since the barrier penetration factor is energy dependent, and this comes into $|\langle M\rangle|^2$.

To determine the validity of the deuteron stripping under a condition of deuteron energy comparable to barrier height the $Pb^{207}(d,p)Pb^{208}$ ground-state reaction was investigated. In this case since the spins of both the initial and final nuclei are known l_n is uniquely determined. If the non-Coulomb theory is valid in this case the proton angular distribution should be predictable. Any quantitative difference between the observed and the predicted distributions can be attributed in a large part to the Coulomb effect.

Y^{90}

In the case of the $Y^{89}(d,p)Y^{90}$ ground-state (g.s.) reaction information is desired on the angular momentum of just the captured 51st neutron to see if it is a member of the same spin-orbit doublet as the 50th neutron. The 50th neutron is believed to be in a $5g_{9/2}$ level.[10] If the 51st neutron is a $5g_{7/2}$ configuration the difference in the binding energies of these two neutrons should be directly related to the spin-orbit coupling parameter.[11] It should be noted, however, that the difference in binding energies should be corrected, because the two nuclei involved have a different neutron excess.[1,2] This fact is taken into account by determining the difference Δ between the observed binding energy and the binding energy expected on the basis of the semiempirical mass formula.[12,13] The difference between $\Delta(Y^{90})$ and $\Delta(Y^{89})$ is then the magnitude of the spin-orbit coupling.

Actually the stripping analysis only gives the orbital angular momentum value of the captured particle. To the extent to which we are interpreting the shell model, however, it is valid to use the shell model prediction to determine the alignment of the spin of the captured particle relative to its orbital angular momentum.

II. EXPERIMENTAL PROCEDURES

The technique used in these experiments was very similar to that of Black.[14] 15.1-Mev deuterons from the M.I.T. Cyclotron were brought into the scattering chamber in a well collimated beam. The counter could be placed at any angle from about 5°–150° to the beam. The detector was a NaI scintillation spectrometer with an absorber, in front of it, either of polystyrene or Al thick enough to stop elastic deuterons. The angular position of the counter was determined by means of a helical potentiometer coupled to the movable arm on which the counter was mounted. This arrangement gave a resistance linearly proportional to the angular displacement of the arm. The zero angle was found by comparing angles on either side of zero degrees at which the intensity of elastically scattered deuterons was equal. In this manner angles could be measured with relative ease to an accuracy of about $\frac{1}{2}$°.

The electronic equipment used is described in the preceding paper[1] and elsewhere.[15]

III. RESULTS

The angular distributions from the $Pb^{207}(d,p)Pb^{208}$ (g.s.), $Bi^{209}(d,p)Bi^{210}$ ($Q=1.94$ Mev group), and $Y^{89}(d,p)Y^{90}$ (g.s.) are shown in Figs. 1, 2, and 3. The

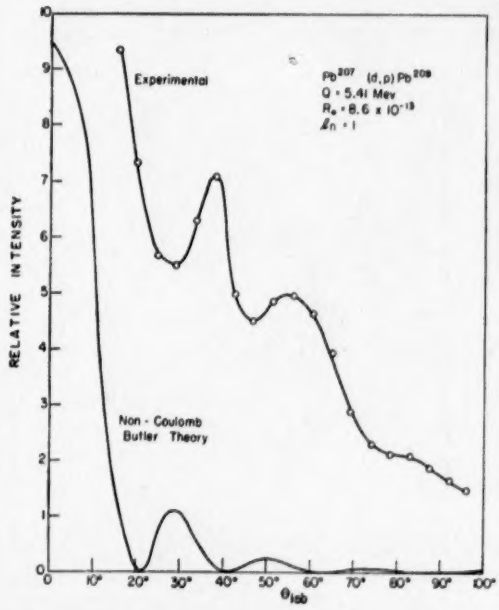

FIG. 1. The angular distribution of the protons from the ground state to ground state $Pb^{207}(d,p)Pb^{208}$ reaction.

[11] D. R. Inglis, Revs. Modern Phys. 25, 390 (1953).
[12] E. Fermi, *Nuclear Physics* (University of Chicago Press, Chicago, 1950).
[13] N. Metropolis and G. Reitwiesner, Atomic Energy Commission Report NP-1980, 1950 (unpublished).
[14] C. F. Black, Ph.D. Thesis, Massachusetts Institute of Technology, January, 1953 (unpublished).
[15] K. Boyer *et al.*, Rev. Sci. Instr. 22, 310 (1951).

angles are given in the laboratory system since, for the heavy nuclei studied, the laboratory and center-of-mass angles are the same within the accuracy of measurement. The probable error of the relative intensity is believed to be less than 10 percent at each point. The forward angles on the Pb^{208} curve were measured with both an Al and a polystyrene absorber since the proton resulting from (d,p) reactions in the Al, produced by deuterons scattered by the target foil, had an energy comparable to that of the Pb^{208} protons. The protons from the $C^{12}(d,p)C^{13}$ reaction in the polystyrene absorber had much lower energy[1] and therefore did not interfere. Also plotted in these figures are the angular distributions expected on the basis of the Butler expression for the angular distribution.[3] It should also be pointed out that though no absolute measurements of the Bi or Pb cross sections were made one can use Harvey's results on these two nuclei to obtain absolute values. His data gives the cross sections at 50° as 1.4 and 0.25×10^{-27} cm²/steradian for Bi and Pb, respectively.[2] The Bi^{210} angular distribution is in agreement with that of Gove.[16]

IV. OBSERVATIONS AND CONCLUSIONS

Y^{90}

The Y^{90} g.s. angular distribution is consistent with the 51st neutron being in a $d_{5/2}$ state. From a study of radioactive decay schemes, and nuclear moments one can see that the first few neutrons over the $N=50$ shell occupy a $d_{5/2}$ state.[17] Much of this information is contained in references 10 and 18. Since the 51st neutron is therefore not in the $g_{7/2}$ member of the $5g$ doublet, the binding energy difference cannot be attributed solely to spin-orbit coupling. Any evaluation of the spin-orbit coupling parameter must therefore depend upon the position of the levels before the spin-orbit perturbation is introduced.

The angular distribution of the proton group corresponding to the first excited state of Y^{90} was also measured. As one can see in Fig. 2 of reference 1, the observed width of this proton group is slightly larger than that of the ground state indicating a possible additional unresolved level. Furthermore at small angles the C^{13} proton groups interfere with the Y^{90*} proton groups to a certain degree making the determination of the intensity of the Y^{90*} somewhat inaccurate. The angular distribution which is observed, however, qualitatively resembles that of an $l_n=0$ Butler distribution. It should be mentioned that Holt and Marsham[19] obtain fair agreement with experiment for the angular distribution of the protons corresponding to the first excited state of Sr^{89}, in the reaction $Sr^{88}(d,p)Sr^{89}$, by assuming a mixture of $l_n=0$ and $l_n=3$. On the basis of the shell model it would be expected that these two nuclei have the same neutron configurations.

Pb^{208} and Bi^{210}

The Pb^{208} g.s. angular distribution has relative maxima and minima which correspond, at least in the location of these maxima and minima, to those of an $l_n=1$ distribution neglecting Coulomb forces. It is believed that the effect of the Coulomb field will be to

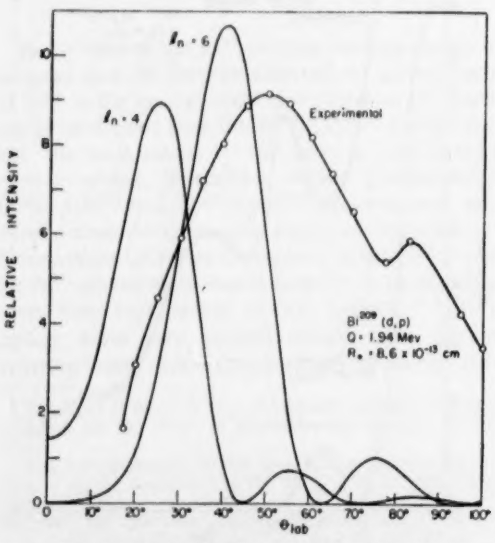

FIG. 2. The angular distribution of the $Q=1.94$ Mev proton group from the reaction $Bi^{209}(d,p)Bi^{210}$.

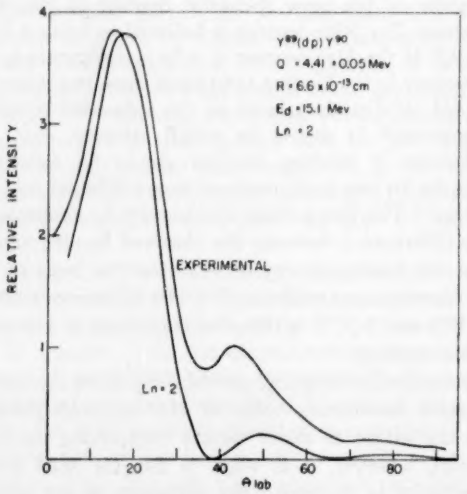

FIG. 3. The angular distribution of the ground state to ground state $Y^{89}(d,p)Y^{90}$ reaction.

[16] H. E. Gove, Phys. Rev. 81, 364 (1951).

[17] The $d_{5/2}$ assignment for odd-odd nuclei follows if one assumes the shell model predictions for the proton and the (2,−) ground state configuration.

[18] J. M. Hollander *et al.*, Revs. Modern Phys. 25, 469 (1953).

[19] J. R. Holt and T. N. Marsham, Proc. Phys. Soc. (London) A66, 565 (1953).

"fill in" the minima.[20] If this is the case, there seems to be a reasonable agreement between theory and experiment.

On the other hand, in the case of Bi^{210} there does not seem to be much similarity between the experimental angular distribution and the distribution expected for either $l_n=4$ or $l_n=6$, the values expected on the basis of the shell model. The fact that the distribution differs from the Pb^{208} g.s. distribution in having a minimum at small angles would lead one to conclude that $l_n \geq 2$. Consistent with the interpretation of a high l_n value for the last neutron in the Bi^{210} is the observation that no proton group occurs with an intensity of 1/30 the intensity of the $Q=1.94$ Mev state at an angle of 45°.[1] The nonsimilarity between the predicted and observed distributions may be because approximations of the stripping theory with respect to the Coulomb interaction are worse for larger angular momentum transfers or that for large l_n the reaction may not be Butler stripping. One unfortunately is therefore unable to assign an l_n value to the last neutron in Bi^{210}.

Odd-Even Effect

An explanation, as offered above for the low-intensity Bi^{210} g.s., would be consistent with Harvey's[2] observation of low (d,p) cross sections for odd $N-$even Z target nuclei relative to isotopes of the same element and even N, if the matrix elements for nearby isotopes were similar. For example, Harvey gives, at an angle of 20°,

$$\frac{d\sigma}{d\omega}(Zr^{92}) \Big/ \frac{d\sigma}{d\omega}(Zr^{91}) = \frac{1}{40}.$$

If in both cases the last neutron is in a $d_{3/2}$ state, the relative differential cross section would be

$$\left[\frac{2I(Zr^{92})+1}{2J(Zr^{91})+1}\right]\left[\frac{2J(Zr^{90})+1}{2I(Zr^{91})+1}\right] = \frac{1}{[2J_i+1]^2} = \frac{1}{36},$$

where J_i is the total angular momentum of the resultant nucleus for the reaction involving the lighter target nucleus.

In the case of the Ti isotopes, however, where the last neutron is probably in a $f_{7/2}$ state, the expected ratio is $1/[2J_i+1]^2=1/64$, whereas the observed ratio is only about 0.10.

However, many of the nuclei given by Harvey have relative differential cross sections in agreement with the supposition that the matrix elements for nearby nuclei are similar to within a factor of 2 or 3. It may be that for those nuclei where there is serious disagreement, the l_n in each case is different. Factors other than the statistical weight would then be expected to cause such a difference.

[20] W. Tobocman (private communication).

PHYSICAL REVIEW VOLUME 96, NUMBER 3 NOVEMBER 1, 1954

Determination of the Ranges and Straggling of Low-Energy Alpha Particles in a Cloud Chamber

S. Barile, R. Webeler, and G. Allen
Lewis Flight Propulsion Laboratory, National Advisory Committee for Aeronautics, Cleveland, Ohio

(Received June 14, 1954)

Ranges of 105 alpha particles with energies of 0.48, 0.545, and 0.615 Mev as fixed by a velocity selector have been measured by the use of a low-pressure cloud chamber. From the results of these measurements the average ranges R_{Av} and the straggling coefficients in air at 15° and 760 mm were calculated for these three energies. The values of R_{Av} were found to be respectively 0.299, 0.327 and 0.354 cm; and the values of the standard deviation were respectively 0.011, 0.0135, and 0.010 cm. After a correction to take into account the difference in definition, the R_{Av}'s are two to three percent higher than those following from a range-energy curve given by Bethe.

INTRODUCTION

THE theoretical expression obtained by Bethe for the energy loss of charged particles in a gas gives, if the effects of the binding of the K-shell electrons of the atoms of the gas are taken into account, quite accurate results for alpha particles down to about 5 Mev.[1] For energies below this, its usefulness is limited because of (1) the difficulty of calculating the L-shell binding correction if the atoms of the gas are of low atomic number, (2) the breakdown of the Born approximation upon which Bethe's derivation is based, and finally, (3) the occurrence below about 1 Mev of an additional complication in the stopping process itself, namely, charge exchange, for which as yet no satisfactory theoretical treatment exists.[2] Hence, the range-

[1] M. S. Livingston and H. A. Bethe, Revs. Modern Phys. 9, 261 (1937).

[2] Further details and references are to be found in the review article by H. A. Bethe and J. Ashkin in *Experimental Nuclear Physics* (John Wiley and Sons, Inc., New York, 1953), Vol. I, Part II.

energy relation for alpha particles below 5 Mev must be based largely on experimental measurements.

Experimental range values are obtained, in general, either from direct measurements of track lengths observed in a cloud chamber or from various types of measurements with ionization chambers.[2] The range-energy relation in the low-energy region that has been generally adopted is based on the experiments of Holloway and Livingston[3] in which the specific ionization along the path of polonium alphas in air was measured. In order to obtain from their results a range-energy relation, it is necessary to know w, the average energy lost per ion pair formed in air as a function of the energy of the alpha particle. Recently, w was measured by Jesse *et al.*[4,5] for energies between 0.3 and 5.3 Mev. Jesse and Sadauskis[5] and Bethe[6] have used these results to construct the corresponding range-energy relation. This relation will be referred to as the "Bethe 1950" relation in order to distinguish it from an earlier one (1937).[1]

This relation is in good agreement with some well established range-energy points above 1.5 Mev obtained from cloud-chamber studies of alpha particles produced by nuclear reactions whose energy values have been quite precisely determined. Recently, Cook *et al.*[7] made some range determinations by measuring the Bragg ionization curves of artificially accelerated alphas of energies between 0.01 and 0.25 Mev. Their results are in good agreement with Bethe's 1950 relation, which in this range was obtained by an extrapolation of Jesse and Sadauskis' results to low energies. There is, however, a discrepancy between Bethe's 1950 relation and the results of some "absolute" range measurements carried out by Jesse and Sadauskis in the course of the above-mentioned investigation. Thus, for a range of 0.790 cm in air the direct measurements gave an energy value 0.04 Mev lower than the 1.611 Mev read from the curve.

The most widely quoted cloud-chamber investigation of low-energy alpha particles (0.01 to 0.3 Mev) is that of Blackett and Lees.[8] They investigated 38 tracks of low-energy alpha particles in a low-pressure cloud chamber, the particles originating in collisions between polonium alphas and helium atoms in the chamber. In order to obtain from the configuration of the tracks the energy of the slow alphas, these investigators had to estimate the energy of the other (faster) alphas emerging from the collision by measuring their track lengths and employing Briggs'[9] range-energy relation. Later experiments showed Briggs' energy values to be 9 percent too low at 5.30 Mev, and consequently Bethe increased all of Briggs' and Blackett and Lees' energy values by this proportion in constructing his 1937 range-energy curve.[1] Nevertheless, the resulting curve still gives energies considerably below those obtained from the Bethe 1950 relation for a given range.

Furthermore, there is a much more recent cloud-chamber investigation by Mills[10] covering the energy range between 0.01 and 0.35 Mev. He employed a chamber which was filled with a mixture of forty percent water vapor and sixty percent helium and operated at a pressure of 45 mm of mercury before expansion. The slow alphas were obtained from elastic collisions of collimated monoenergetic neutrons with the helium in the chamber. In order to make his air equivalent range agree with that following from Bethe's 1950 range-energy curve[6] at about 0.3 Mev, Mills assumed that a large increase in the amount of water vapor took place throughout the chamber as a result of the expansion. Since the diffusion of water vapor under the conditions existing in the chamber is too slow to account for an appreciable increase in the vapor by the evaporation of water from the walls, he postulated the presence of small invisible droplets suspended throughout the body of the chamber. Mills' and Bethe's curves disagree, however, at other energies.

The lack of agreement between ionization and direct cloud-chamber measurements in the extreme low-energy region indicates a need for further measurements below 1 Mev. Since the results of the previous cloud-chamber investigations appear questionable, it would seem that any new experimental determinations would be most valuable if they were to be based on the cloud-chamber method. Furthermore, the error in the ionization measurements may be greatest below 1 Mev because complications arise in determining the end point of the range and because processes other than ionization (and excitation) begin to contribute appreciably to the energy loss.

The determination of ranges in the cloud chamber has the further advantage that one obtains quite directly the amount of range straggling. This latter quantity is of especial interest at low energies because the relative straggling should tend to increase as a larger proportion of the energy loss is due to nuclear collisions. At a somewhat higher energy (1.2 Mev) than those considered here, Bøggild[11] found a relative range straggling for alphas amounting to about 2 percent, although that due to electronic processes alone can be expected to be only about 1 percent.[12] Some doubt is cast on Bøggild's results, however, because of the fact that his experiments were done in such a way that the quantity measured was the combined straggling of

[3] M. G. Holloway and M. S. Livingston, Phys. Rev. **54**, 18 (1938).
[4] Jesse, Forstat, and Sadauskis, Phys. Rev. **77**, 782 (1950).
[5] W. P. Jesse and J. Sadauskis, Phys. Rev. **78**, 1 (1950).
[6] H. A. Bethe, Revs. Modern Phys. **22**, 213 (1950).
[7] Cook, Jones, and Jorgensen, Phys. Rev. **91**, 1417 (1953).
[8] P. M. S. Blackett and D. S. Lees, Proc. Roy. Soc. (London) **A134**, 658 (1932).
[9] G. H. Briggs, Proc. Roy. Soc. (London) **A114**, 341 (1927).
[10] R. G. Mills, Rev. Sci. Instr. **24**, 1041 (1953). See also: R. G. Mills, University of California Radiation Laboratory Report UCRL 1815, 1952 (unpublished).
[11] J. K. Bøggild, Nature **161**, 810 (1948).
[12] N. Bohr, Kgl. Danske Videnskab. Selskab, Mat.-fys. Medd. **18**, 8, 128 (1948).

alpha particles and lithium ions which had to be divided somewhat arbitrarily into the contributions of the two particles.

We have decided therefore to make a study of the range and straggling of alpha particles for energies below one Mev by the use of a low-pressure cloud chamber. Since at least a part of the difficulties encountered in the previous cloud-chamber studies arises from the fact that the initial energy of the low-energy alpha particles was always determined in a somewhat indirect fashion, we arranged the experiment so that the energy of the particles was known when they entered the chamber. For this purpose we made use of a natural alpha emitter (polonium) as a source of low-energy particles. The alphas were first slowed down and then entered an energy selector of sufficiently good resolution which permitted the particles having the desired energy to enter the chamber.

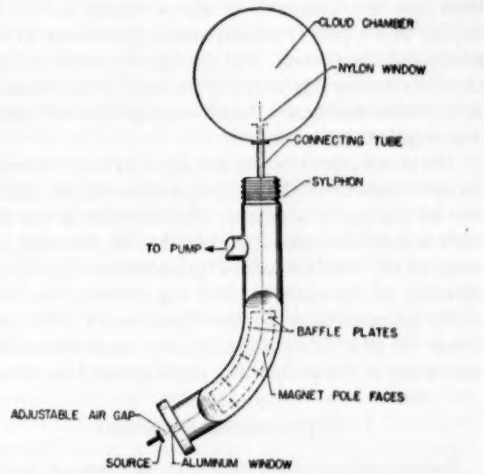

FIG. 1. Schematic diagram of the experimental arrangement.

EXPERIMENTAL METHOD

Description of Apparatus

The experimental arrangement is shown in the diagram in Fig. 1. The alpha particles emitted by the polonium source were slowed down in passing through the (adjustable) air gap and the aluminum window before entering the magnetic analyzer. The particles of the desired energy were selected by the analyzer and were admitted to the cloud chamber through a thin nylon window.

The details were as follows. The source,[13] which had an average strength of 5 to 10 millicuries, was plated on a metal disk mounted on a micromanipulator which, in turn, was rigidly attached to the analyzer. The analyzer was constructed as shown in the figure. The six baffle plates, which were staggered in order to facilitate pumping, defined an annular channel of a mean curvature of 16.5 cm, a width of 0.6 cm, and a length of 14 cm. For a given magnetic field, the disposition of these plates essentially determined the mean energy of the particles traversing the spectrograph while the aperture and the resolving power depended also on the location and size of the exit window. In order to facilitate the process of aligning the instrument, the exit tube, to which the window is attached, was joined to the rest of the spectrograph by a sylphon.

A geometrical analysis of the allowed trajectories was carried out which showed that for the energies of interest to us (0.40 to 0.65 Mev) the resolving power of the velocity selector amounted to about 1.5 percent in momentum for incident particles with a uniform distribution in magnitude and direction of momentum. The pressure in the analyzer was kept below 6×10^{-6} cm, so that there was presumably no appreciable contribution from scattering in the gas. Since the particles after passing through the aluminum window had a larger spread in momentum, the energy dispersion of those entering the cloud chamber was essentially determined by the velocity selector. The magnetic field which was varied in strength between 8200 and 7300 gauss, was produced by an electromagnet with pole pieces of the shape indicated in the figure and a pole gap of 1.4 cm. In order to prevent the magnet from overheating, it was excited for only about ten percent of the cycle of the cloud chamber. For reasons stated above, it is desirable that most of the range of the particles leaving the velocity selector be in the cloud chamber. Therefore, the window between the chamber and the analyzer should be just thick enough to withstand the pressure difference between the chamber and the analyzer (between 13 and 20 cm of Hg). It was found that a nylon film about 0.04 mg/cm^2 thick, backed up by a perforated plate was satisfactory for this purpose. The film consisted of 8 layers prepared in the usual fashion.[14]

The cloud chamber was of the horizontal type and cylindrical in shape, with a height of 3.2 cm unexpanded, and a diameter of 25 cm. The chamber was filled with a mixture of hydrogen gas and water and ethyl alcohol vapor. At the operating temperature of 20.5°C the pressure before expansion amounted to 12.25 cm for the hydrogen, 1.50 cm for the water, and 2.24 cm for the alcohol, the last two pressures being the equilibrium values above a 50-50 volume mixture of the corresponding liquids. The expansion ratio employed was 1.25, and the cycling time was one minute, the sequence of operations being governed by an electronic controller.

We had investigated previously[15] the question of whether it is necessary to limit the natural sensitive time of the chamber for an experiment of this sort. We found that, under the conditions specified above, this

[13] This source was obtained from the Canadian Radium-Uranium Corporation.

[14] Brown, Febber, Richards, and Saxon, Rev. Sci. Instr. **19**, 818 (1948).

[15] S. Barile and R. Webeler, Rev. Sci. Instr. **25**, 389 (1954).

time (for the formation of sharp tracks) is 0.014 sec during which period the expansion goes from 90 to 99 percent of completion. The change of conditions in the chamber during this period is too small to introduce any appreciable errors, and therefore no special arrangement was required.

The cloud chamber was arranged so that two stereoscopic views could be obtained on a single negative, one by the use of a mirror. The direction of the direct view was at an angle of 3°, and that of the other, at an angle of 15° with the axis of the chamber. The direction of entry of the particles into the chamber was essentially perpendicular to the direction of both views. From the two views of a track any large deflections or curvature in the path of the particle could be detected.

Experimental Procedure

Before taking cloud-chamber pictures of particles with a given energy entering the chamber, the position of the source and the position of the exit window were adjusted as follows. The nylon window was replaced by a glass plate coated with silver-activated zinc sulfide which served as a scintillation counter in conjunction with a photomultiplier tube mounted inside the cloud chamber. The air gap between the source and the entrance window was adjusted with the aid of the micromanipulator, and the position of the exit window was varied by moving the cloud chamber with respect to the spectrograph, so as to give a maximum counting rate with the desired magnetic field.

The same arrangement was also used to determine the air equivalent of the nylon exit window at 0.615 Mev (which was one of the energies investigated). The source position and the alignment of the selector were adjusted as described, and a nylon film of the correct thickness was interposed between the entrance window and the baffle plate system of the analyzer by means of a vacuum-tight seal. The air gap was then varied by moving the source with the micromanipulator and the new source position corresponding to a maximum counting rate located. The change in the air gap thus produced was found to be 0.046 cm which was taken as the air equivalent of the film. This value agrees within 5 percent with the calculated air equivalent given in a later section.

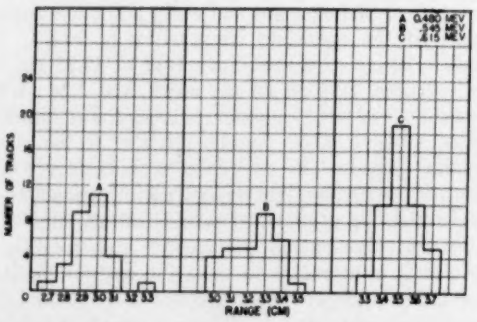

FIG. 2. Distribution of track lengths of alpha particles in a cloud chamber filled with hydrogen, water vapor, and ethyl alcohol vapor at respective pressures of 12.25 cm, 1.50 cm, and 2.24 cm.

Cloud-chamber photographs were obtained in this fashion with three settings of the analyzer corresponding to alpha particle energies E_0 of 0.615, 0.545, and 0.48 Mev and were analyzed as follows. The stereoscopic pictures were projected to full size by using the camera with which they were taken as a projector and adjusting its position so that the image of a ruler photographed alongside the chamber appeared in its natural size. Measurements of the total track length on the projection of the direct view were made by the use of dividers set at 3 mm. Since near the window the alpha particles did not have any visible droplet trail, the length of the missing portion of the track was simply taken as being equal to the length of a straight line from the window to the beginning of the visible portion of the track, drawn so as to be tangent at this point. Tracks having kinks were excluded from consideration because it was difficult to obtain their lengths with any accuracy. Since such tracks were in any case few in number, neglecting them cannot have affected the results appreciably. However, tracks which showed sudden changes in droplet density as a consequence of charge exchange were used if otherwise normal.

The range usually quoted is simply the projection x of the total path on a line parallel to the direction of the particle at the beginning of the path. Therefore, in order to compare our results with this conventional range, we measured this quantity for each track. From x and r', the average length of the track in two dimensions, the (most probable) true length r in three dimensions can be estimated. A simple consideration shows that on the average $r=2r'-x$, if $(r'-x)$ is small enough as was the case here. The resulting distributions for r' which are based on 105 tracks, are shown in Fig. 2 for the three energies mentioned.

DISCUSSION OF RESULTS

(a) General

The results of an investigation of the present sort are usually presented in terms of the parameters of the distribution of ranges of individual particles in air. The range itself is ordinarily represented by the arithmetic mean range in air, R_{Av}; the median range, R_m; or the extrapolated range R_e. To define the extrapolated range, it is necessary to consider the number-distance curve, which represents the number of particles with a range equal to or larger than a given distance as a function of this distance. If now a line is drawn tangent to this curve at the point of steepest slope, the abscissa of the point at which it intersects the range axis is equal to R_e. The straggling is usually specified in terms of the range straggling coefficient which is equal to $1/\sqrt{2}$ times the

TABLE I. Average range R_{Av}, median range R_m, extrapolated range R_e, and straggling coefficient σ (standard deviation of R_{Av}) for low-energy alpha particles in air at a temperature of 15°C and 760-mm pressure as a function of the initial energy E_0.

E_0 (Mev)	No. of tracks	R_{Av} (cm)	R_m (cm)	R_e (cm)	σ (cm)	σ/R_{Av}
0.480	29	0.299	0.304	0.317	0.011	0.037
0.545	30	0.327	0.334	0.350	0.0135	0.042
0.615	46	0.354	0.358	0.370	0.010	0.029

reciprocal of the standard deviation σ of the distribution, or in terms of the so-called "straggling" which we take as $s=R_e-R_m$.

(b) Ranges in Air

In order to obtain the parameters for air from the experimental results, it is necessary to know the composition of the gas in the chamber at the time the measured tracks are produced and the stopping powers of its constituents and of those of the nylon window relative to air. While the range of pressures of the hydrogen in the chamber during the sensitive time can be inferred from the position of the piston (the expansion being 90 to 99 percent completed), the variation of the vapor pressure of the alcohol-water mixture during the motion of the piston cannot. It seems plausible, however, that up to the end of the sensitive time, the number of atoms which constitute the vapor will remain essentially the same as that which would prevail if no evaporation took place—at least in the parts of the chamber away from the walls.

The following equations hold for R_{Av}, the equivalent average range in air at atmospheric pressure and 15°C of a particle having an energy E_0; for t, the thickness of the nylon window traversed by a particle of incident energy E_0 and emergent energy E_f; and for r_{Av}, the average length of a track in the cloud chamber:

$$R_{Av}=\int_{E_0}^{0}\frac{dE}{(dE/dx)_a},\quad t=\int_{E_0}^{E_f}\frac{dE}{(dE/dx)_n},\quad r_{Av}=\int_{E_f}^{0}\frac{dE}{(dE/dx)_c},\tag{1}$$

where the denominators in the integrands of Eqs. (1) are the stopping powers of air, nylon, and the cloud-chamber mixture, respectively. The stopping power of any mixture or compound may be expressed in terms of that of air by

$$dE/dx=(dE/dx)_a\sum_i p_i(N_i/N_a)\equiv(dE/dx)_aP,\tag{2}$$

where p_i and N_i are, respectively, the relative atomic stopping power and number of atoms per unit volume for the ith element present, and N_a is the number of atoms per unit volume for air. The expressions $\sum_i p_i(N_i/N_a)$ for nylon and for the cloud-chamber gas will be referred to as P_n and P_c, respectively.

In order, then, to determine the equivalent ranges in air from our results, one needs the values of p for the elements H, C, O, and N. For the first two elements Livingston and Bethe[1] give curves for p against E for E greater than 2 Mev and also list separately values of p for several energies. In the case of hydrogen the value read from the curve differs slightly from that given in the text. In order to estimate p in the energy range of interest to us, the curve for hydrogen was altered so as to go through the tabulated point and both curves were then extrapolated to zero energy taking into account the tendency of the curvature to increase slightly with decreasing energy. The values of atomic stopping power for oxygen were obtained by extrapolating to zero energy some recent measurements of the molecular stopping power of water[16] and subtracting the contribution of the hydrogen. The values for oxygen so obtained were, in turn, used to compute the atomic stopping power for nitrogen from the known composition of air.

Over the small energy interval between E_0 and E_f the change in the quantity P_n is insignificant and may be neglected without further consideration. The change in P_c amounts to two percent in the energy interval from 0.1 to 0.6 Mev. Thus if the value of P_c is taken as constant in this range and equal to that at $E_0/2$, only a small error is introduced. With the above approximations, the first of Eqs. (1) becomes

$$R_{Av}=P_nt+P_cr_{Av}.\tag{3}$$

The values computed for P_n are practically the same for alpha particles of the three energies studied and result in a value of 0.044 cm for P_nt. This value is five percent lower than that following from the direct experimental investigation described above. Because the contribution of the corresponding term in Eq. (3) to R_{Av} is small relative to that of the other term, the corresponding error in R_{Av} is negligible. The value obtained for P_c was 0.103 under our conditions of operation. The average and median ranges R_{Av} and R_m are given in columns 3 and 4 of Table I.

In order to make a comparison with the ranges following from Bethe's 1950 curve, it is necessary to express our results in terms of projected ranges. For this purpose, we give in Table II, together with Bethe's mean values $\bar{X}$, the quantities X_{Av} and X_m, which represent, respectively, the average and median of the

TABLE II. Projected average and median ranges X_{Av} and X_m of low-energy alpha particles in air at a temperature of 15°C and 760-mm pressure as a function of the initial energy E_0; X_{Av} and X_m, present investigation; $\bar{X}$, Bethe's 1950 curve.

E_0	X_{Av} (cm)	X_m (cm)	$\bar{X}$ (cm)	$(X_{Av}-\bar{X})/X_{Av}$	$(X_m-\bar{X})/X_m$
0.480	0.293	0.298	0.285	0.027	0.044
0.545	0.321	0.328	0.312	0.028	0.049
0.615	0.348	0.352	0.340	0.023	0.034

[16] H. G. de Carvalho and H. Yagoda, Phys. Rev. 88, 273 (1952).

sum of the air equivalents of the projected track lengths in the gas of the chamber and the nylon window. While, by making a comparison in this way, one can assure that the ranges are defined in the same way as far as geometrical considerations are concerned, it should be pointed out that the definition of the mean range (Bethe) is based on the "specific ionization curve of a single alpha particle" while our definitions $X_{\bar{N}}$ and X_m are based on the number range distribution.

It can be seen that our $X_{\bar{N}}$'s are about two to three percent higher than the ranges $\bar{X}$ following from Bethe,s curve, and that our values of X_m are still higher.

There were three chief potential sources of systematic errors in our range determinations. In the first place' the (extrapolated) stopping powers relative to air which were used to convert the measured ranges to ranges in air may have been inaccurate. Secondly, there may be some doubt as to the locations of the end points of the tracks. Thirdly, the total amount of water and alcohol vapor present in the chamber may have changed during the expansion due to evaporation of some of the excess liquid either from the walls of the chamber or from small invisible droplets dispersed through the gas (Mills' process).

No estimate can be made of the errors resulting from any inaccuracies in the values of the relative stopping powers used. Any errors of the last two types mentioned, however, would necessarily tend to make the ranges which were obtained for air at atmospheric pressure smaller than the true ranges. Thus, the difference between our results and Bethe's 1950 curve, which is in the opposite direction, cannot be explained on this basis.

(c) Straggling

Columns 6 and 7 of Table I contain the standard deviation σ and the coefficient of variation $\sigma/R_{\bar{N}}$, respectively. In order to determine the straggling one has to estimate the effect of the energy spread of the alpha particles leaving the velocity selector. As mentioned before, geometrical considerations show that the maximum spread is 1.5 percent in the momentum and is, therefore, 3 percent in the energy (independent of the setting of the analyzer). It follows from our results that the slope of the range energy curve is about 0.4 cm/Mev for the energies in question and, hence, the resulting spread in the measured ranges due to this cause alone amounts to about two percent of the range. For any distribution the standard deviation is by definition less than half the spread; and in the present case, on physical grounds, the standard deviation in the ranges associated with the finite resolution of the spectrograph is very much less than half the corresponding spread in the ranges. Even if the standard deviation from this cause was as large a fraction as 0.01 of the range it would make a contribution of only about ten percent to the measured values of σ and $\sigma/R_{\bar{N}}$. Therefore the straggling due to the finite resolution of the analyzer can be neglected and the coefficients σ listed in the table may be taken as a measure of the true straggling. In view of the number of tracks measured, one may consider the individual σ's given in the table to be correct to about fifteen or twenty percent.

According to Bohr,[12] the value of σ/R which one would expect on the basis of electronic collisions would amount to somewhat less than 0.01, independent of energy and stopping material. It follows therefore that the straggling at these energies is mostly due to charge exchange and nuclear collisions, processes which become relatively more important near the end of the track. Thus the true value of σ should be nearly independent of the energy for short range alpha particles.

Therefore it is possible to compute this quantity more accurately from a properly weighted rms average of the σ's for the three energies. The resulting value of $\sigma=0.012$ cm agrees well with the value of 0.014 cm obtained by Bøggild[11] for alpha particles of a range of 0.7 cm in air (about twice our ranges), which verifies the assertion that most of the straggling occurs at the end of the path.

We can also compute the extrapolated range R_e and the straggling s from the number range curves following from Fig. 2; however, it is rather difficult to locate the points of inflection in the individual curves. Consequently, we assumed that s is the same for all three energies just as σ proved to be and constructed from them a single number range curve constructed by superposing the three curves so that the points corresponding to their averages all coincided. The value of s thus obtained is 0.016 cm; the extrapolated ranges given in column 5 of Table I were computed from the relation $R_e=R_m+s$ using this value of s.

ACKNOWLEDGMENTS

The authors are indebted to Dr. Gerhart Groetzinger, Dr. Philip Schwed, and Dr. Howard C. Volkin for many stimulating discussions.

Variations in the Isotopic Abundances of Neon and Argon Extracted from Radioactive Minerals*

GEORGE W. WETHERILL† ‡
Department of Physics, University of Chicago, Chicago, Illinois and Argonne National Laboratory, Lemont, Illinois
(Received May 21, 1954)

Large excesses of Ne^{21}, Ne^{22}, and A^{38} have been found in uranium and thorium minerals. These abnormal abundances are ascribed to (α,n) and (α,p) reactions in the minerals. It is shown that it is possible that a part of the atmospheric Ne^{21} originated in this way.

I. INTRODUCTION

THE most careful determination of the isotopic abundances of neon and argon was made by Nier.[1] However, his investigation, as well as the earlier ones, was restricted to the analysis of atmospheric neon and argon. In the course of some experiments on spontaneous fission of uranium and thorium,[2] the neon and the argon from the radioactive minerals pitchblende, euxenite, and monazite were analyzed in a mass spectrometer in order to see if any variations in their isotopic abundances could be found. Gross variations were found which are presumably a consequence of nuclear reactions induced by the natural radioactivity of these minerals. During the course of this work similar variations in the abundance of argon were reported by Fleming and Thode.[3]

II. EXPERIMENTAL METHODS

The gases occluded within the minerals were released by fusing the mineral with NaOH in vacuum and chemically reactive gases removed by use of the apparatus shown in Fig. 1 as described in a previous paper.[2] After most of the chemically reactive gases were cleaned up, the helium and the small quantities of neon present were separated from the rest of the inert gases by absorbing the heavier gases on activated charcoal held at -195°C and pumping the helium and neon into the gas separator (Fig. 2) with the Toepler pump. After some further purification the xenon, krypton, and argon were again absorbed on charcoal and sealed off. The gas separator was used to separate neon from helium. It is essentially the same as the gas separator constructed and used by Arrol, Chackett, and Epstein.[4] Their separator was patterned after one designed by Glückauf[5] which is used in Paneth's laboratory at Durham. A similar apparatus was used by Aston[6] in an attempt to separate the isotopes of neon. The operation of the apparatus has been described by Glückauf.[5] The separation is effected by the fractional adsorption of neon and helium on activated charcoal. The apparatus consists of a series of four 100-cc Toepler pumps with a dead space between each of them consisting of a U-tube containing 2.5 g of activated charcoal. Fractionation is achieved because this dead space has a larger effective volume for neon than it has for helium causing the efficiency of the pump to be greater for helium.

By use of this apparatus the heavy fraction was depleted in helium by a factor of several thousand with a loss of neon of about 15 percent. The neon is then treated in the final purifier, adsorbed on the neon sample charcoal C_4, and sealed off.

The gas samples were analyzed in the mass spectrometer described previously.[2]

The sample tubes containing the gases adsorbed on charcoal were sealed onto the sample system of the mass spectrometer and the gas introduced by the use of conventional glass breakoffs. The argon sample tubes containing about 0.5 g of charcoal were held at -100°C with ethyl alcohol cooled with liquid nitrogen. At this temperature most of the argon was desorbed. The neon sample tubes contained about 10 g of charcoal. The neon was first observed with the charcoals at liquid nitrogen temperature and then another set of data was taken at -100°C, at which temperature all the neon was desorbed.

The gas flowed into the mass spectrometer through an orifice of about 0.001-in. diameter. Since molecular flow was maintained at all times, the measured isotope ratios represented the isotopic composition of the gas in the reservoir behind the orifice. In some cases it was necessary to correct for the change in isotopic composition of the gas in this reservoir with time, since the lighter isotopes flow through the leak more rapidly than the heavier ones, causing the gas remaining in the reservoir behind the leak to become enriched in the heavier isotopes. The mass spectrometer used was equipped with an electron multiplier, and, since the sensitivity of the electron multiplier varied slightly with mass, it was necessary to apply a correction of about two per-

* This work was supported in part by a grant from the National Science Foundation.
† This work was done while the author held a U. S. Atomic Energy Commission predoctoral fellowship at the University of Chicago.
‡ Present address: Department of Terrestrial Magnetism, Carnegie Institution of Washington, Washington, D. C.
[1] A. O. Nier, Phys. Rev. **79**, 450 (1950).
[2] George W. Wetherill, Phys. Rev. **92**, 907 (1953).
[3] W. H. Fleming and H. G. Thode, Phys. Rev. **90**, 857 (1953).
[4] Arrol, Chackett, and Epstein, National Research Council of Canada, declassified document CRC-297.
[5] E. Glückauf, Proc. Roy. Soc. (London) **A185**, 98 (1946).
[6] F. W. Aston, *Mass Spectra and Isotopes* (Longmans, Green and Company, New York, 1941), p. 33.

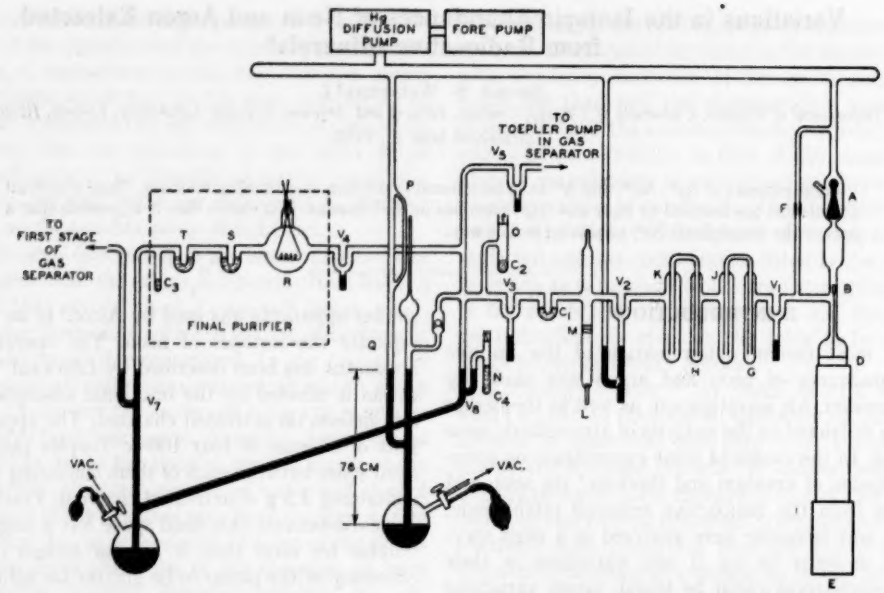

FIG. 1. Apparatus for the extraction of inert gases from minerals. A. Magnetic valve; B. Stirring rod; C_1. Tube containing .5 g of activated charcoal; C_2. Tube containing .5 g of activated charcoal; C_3. Tube containing .5 g of activated charcoal; C_4. Tube containing 10 g of activated charcoal; D. Nickel furnace; E. Electric heater winding; F. Constriction for sealing off; G. Magnesium perchlorate trap; H. Potassium hydroxide trap; L. Calcium vapor furnace; M. Quartz-pyrex graded seal; N. Neon sample tube; O. Argon, krypton, xenon sample tube; P. McCleod gauge; Q. McCleod exhaust; R. Tungsten bulb; S. Copper oxide trap; T. Magnesium perchlorate trap.

cent per mass unit. The discrimination was determined by measuring samples of normal gas and comparing the results with the accepted values of the isotope ratios as given by Bainbridge and Nier.[7]

III. EXPERIMENTAL RESULTS AND DISCUSSION

1. Variations in the Isotopic Abundances of Neon

Mass spectrometric determinations were made of neon extracted from pitchblende, euxenite, and monazite. The isotope ratios as well as estimates of the absolute quantity of the gas contained in the mineral are given in Table I. It is believed that the gas observed here is neon rather than some impurity for the following reasons:

TABLE I. Isotope ratios and absolute quantities of neon from radioactive minerals.

Sample	Size of sample	Age $\times 10^{-8}$ yr	Percent uranium	Percent thorium	Isotope ratios 21/20[a]	Isotope ratios 22/20[a]	Excess Ne^{21} cc STP/g[b]
Atmospheric[c]					0.00283	0.0970	
Belgian Congo Pitchblende	20.0 g	650[d] 215[e]	44.	0	0.00519 ±0.00017	0.103 ±0.005	1.36×10^{-7}
Brazilian Monazite	13.8 g	460[f]	0.2	6	0.402 ±0.024	0.0954 ±0.011	8.7×10^{-9}
Madagascar Euxenite	109.6 g	60[e] ~600[f]	6.0	3.5	1.05 ±0.09	4.72 ±0.32	8.0×10^{-9}

[a] The errors shown represent the mean deviations of the peak heights.
[b] Mass spectrometer calibrated with krypton tracer.
[c] See reference 7.
[d] Alfred O. Nier, Phys. Rev. 55, 153 (1939).
[e] Helium age, as calculated from the quantity of helium obtained from the mineral and the uranium content.
[f] Uranium-lead ages. These ages were measured in this laboratory.

(1) The electron-accelerating potential in the ion source was adjusted to a value so low that doubly charged interfering ions such as A^{40++} and CO_2^{++} could not be present.

(2) It was possible to resolve completely the interfering H_2O^{18} peak from the neon peak at mass 20.

(3) At no time, even when the background of the mass spectrometer was so high that the instrument could not be used to analyze the krypton and xenon samples, was a background peak of any kind observed at mass 21.

(4) Separate aliquots of the neon were taken from activated charcoal at temperatures of $-195°C$ and $-100°C$; the ratios were the same in both cases.

(5) During the course of the measurements the pressure in the ion source dropped by a factor of at least four. The isotope ratios did not change.

(6) The pressure in the source decayed with time as the gas in the reservoir was depleted in every case with the decay constant characteristic of neon.

It should be noted that the Ne^{21} is always anomalously high; in the extreme case of the euxenite the

[7] K. T. Bainbridge and A. O. Nier, Preliminary Report No. 9, Nuclear Science Series, National Research Council (unpublished).

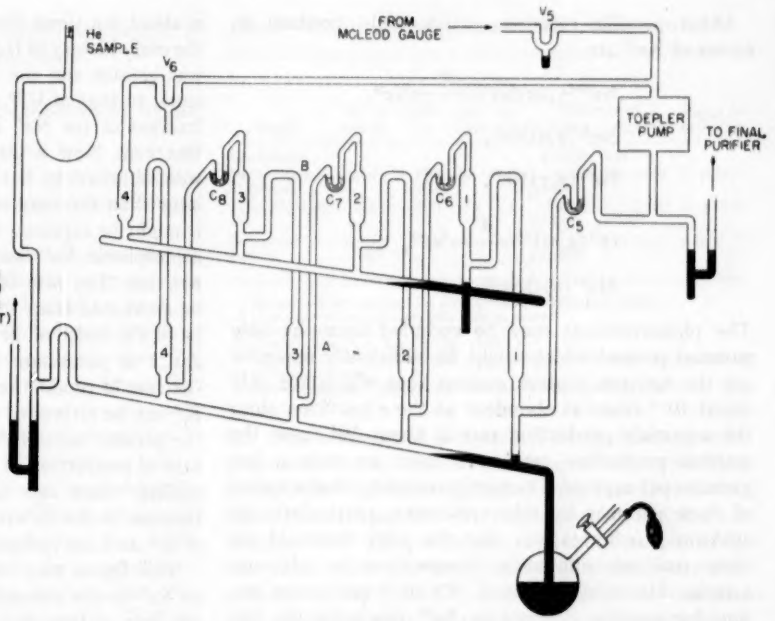

FIG. 2. Gas separator for separating neon from helium.

Ne^{21}/Ne^{20} ratio is 370 times normal. Any impurity at mass 20 or 22 would cause an effect in the opposite direction. The Ne^{22}/Ne^{20} ratios are approximately normal in the pitchblende and the monazite, but in the euxenite the Ne^{22} abundance is about 50 times the normal abundance. It is possible that the errors in the Ne^{22}/Ne^{20} ratios for the pitchblende and the monazite mask small variations which would be revealed by a more careful investigation. The relatively small change in the Ne^{21}/Ne^{20} ratio in the pitchblende was caused by the presence of a large quantity of normal neon in the sample, as it may be seen that the absolute excess of Ne^{21} is greater in the pitchblende than it is in either of the other two samples. This normal neon probably had its origin in "memory" in the mass spectrometer. Shortly before the pitchblende sample was analyzed a large sample of normal neon was run; apparently a sufficient quantity remained in the instrument to interfere with the pitchblende analysis.

The values for the excess Ne^{21} can be relied on as a measure of the quantity of the gas in the sample to within a factor of two. The relative values are reliable within twenty percent.

The variations in isotopic abundance found here are much greater than those which could be produced by any natural chemical isotopic fractionation or by fractional diffusion of isotopes. These variations must be attributed to a natural nuclear process. It appears that the most likely process for producing this excess Ne^{21} is the nuclear reaction $O^{18}(\alpha,n)Ne^{21}$. All three minerals contain oxygen as a major constituent and the (α,n) reaction on oxygen is well-known.[8] The yield of this reaction on O^{16} is zero, since for this isotope the Q for the reaction is -12.2 Mev. The yield from O^{17} may be expected to be less than that from O^{18}, since this isotope is less abundant and the Q values are similar ($+0.6$ and -0.7, respectively); it is difficult in this experiment to see the effect of the reaction with O^{17} because of the relatively large amount of normal Ne^{20} present.

A calculation of the quantity of Ne^{21} which would be produced in the pitchblende by this reaction by the polonium α-particles, if we use the yield for oxygen given by Roberts, indicates that about 9×10^{-8} cc/g would be produced if the target could be considered to be pure oxygen, all the reaction to be with the isotope O^{18}, and the age of the mineral taken to be the helium age. The helium age is used rather than the lead age because it probably includes a better measure of the ability of the mineral to retain inert gases. The fact that the mineral was not pure oxygen will reduce the amount of Ne^{21} which might be expected by a factor of about three, while the fact that there are seven other α particles emitted from uranium will increase this estimate by a factor of about eight. The differing energies of the natural α particles will not affect the order of magnitude of this estimate. Thus the expected amount is in approximate agreement with the actual quantity 1.4×10^{-7} cc/g which was found.

[8] J. H. Roberts, U. S. Atomic Energy Commission Report MDDC-731, 1947 (unpublished). A summary of the studies which have been made of (α,n) reactions was made by H. L. Anderson, Preliminary Report No. 3, Nuclear Science Series, National Research Council (unpublished).

Other possible reactions which might produce an excess of Ne^{21} are

$$Na^{23}(\gamma,2n)Na^{21} \xrightarrow{\beta^+} Ne^{21},$$

$$Ne^{22}(\gamma,n)Ne^{21},$$

$$Ne^{20}(n,\gamma)Ne^{21},$$

$$O^{18}(\alpha,p)F^{21} \xrightarrow{\beta^-} Ne^{21},$$

$$Mg^{24}(n,\alpha)Ne^{21}.$$

The photoreactions may be excluded since the only gammas present which might be sufficiently energetic are the neutron capture gamma rays which are only about 10^{-6} times as abundant as the α particles, since the α-particle production rate is about 10^7 times the neutron production rate[2] and there are only a few gammas per capture. The high probability of absorption of these gammas by other processes, particularly by electron pair formation, plus the high threshold for these reactions eliminates competition by photoreactions. The relatively small (4×10^{-25} cm^2) cross section for neutron capture in Ne^{20} precludes the formation of approximately equal amounts of Ne^{21} by neutron capture in this isotope. The high threshold (4.66 Mev) for the (α,p) reaction plus the fact that the emitted proton will have to traverse the Coulomb barrier of the nucleus makes this reaction seem less likely than the (α,n) reaction. The (n,α) reaction on magnesium to produce Ne^{21} has a threshold of about 2 Mev. Also, because of the Coulomb barrier of about 6 Mev, the emission of low-energy α-particles is improbable. Therefore even higher neutron energies are required. If all the neutrons formed in the mineral reacted in this way with magnesium, about ten times as much Ne^{21} would be produced by this process as by the $O^{18}(\alpha,n)$ mechanism. However, because of the fact that magnesium is usually present in these minerals only to a few tenths of a percent and because of the small number of neutrons with sufficient energy, it should be expected that this magnesium reaction is much less likely.

It is interesting to calculate the amount of Ne^{21} which may be formed by this (α,n) reaction in ordinary rocks. The monazite contained about six percent thorium, while the average uranium and thorium concentrations of igneous rocks are about four and twelve parts per million respectively.[9]

Thus the α activity of these average rocks is about 1/2500 of that in the monazite. If it is assumed that the abundance of normal neon in these rocks is the same as in monazite, then in these rocks the ratio of excess Ne^{21} to normal Ne^{20} will be 1.6×10^{-4}. Thus the Ne^{21} produced by nuclear reactions contributes about 6 percent of the Ne^{21} in ordinary rocks if their ages are the same as that of the monazite. However, the age of the earth is about ten times the age of the monazite, and during the early history of the earth, the abundance of uranium was greater and the α activity due to U^{235} was about equal to that of U^{238}. Thus it may be seen that a large fraction of the Ne^{21} in rocks was probably formed in this way. Now if the neon in the earth's atmosphere were obtained by out-gassing of the crust at some time later than the very early stages of the earth's history, it might be expected that an appreciable fraction of the atmospheric Ne^{21} was formed by this natural nuclear reaction. The rate of production of Ne^{21} in rocks can be estimated from the data presented in this paper to be of the order of 10^{-20} cc STP/g yr. Taking the abundance of potassium in igneous rocks as 2.6 percent[10] the rate of production of A^{40} from the disintegration of K^{40} can be estimated to be 9×10^{-14} cc STP/g yr. Thus the present ratio of the rate of production of A^{40} to the rate of production of Ne^{21} is about 10^7. Four thousand million years ago this ratio was about twice this, because of the difference between the decay constants of K^{40} and the isotopes of uranium.

This figure may be compared with the ratio of A^{40} to Ne^{21} in the atmosphere, 2.0×10^5, as calculated from the data of Paneth.[11] Therefore, if the atmosphere was formed by out-gassing of the crust and if argon and neon were out-gassed to the same extent, this calculation indicates that between 1 and 2 percent of the Ne^{21} in the atmosphere today originated from this nuclear reaction. In this calculation it is assumed that the ratio of potassium to uranium plus thorium throughout the region of the crust which is out-gassed is the same as the average calculated for igneous rocks relatively near the surface. If deep rocks contribute significantly this assumption may not be valid. Furthermore, it is possible that the uranium and thorium minerals in these rocks, e.g., zircon, may lose gas more readily owing to damage of the crystal structure by alpha-particles. If for these reasons the contribution of excess Ne^{21} to the atmosphere is greater it may be noted that this effect will affect estimates of the cosmic abundances of neon based on interpolating the odd isotope abundance curve at mass 21 and then multiplying by the observed atmospheric isotopic abundances.[12]

The excess Ne^{22} found in the euxenite can probably be attributed to the similar reaction $F^{19}(\alpha,n)Na^{22}$. The high yield for this reaction reported by Roberts[8] indicates that the extra Ne^{22} could be produced by only a few tenths percent of fluorine provided it were located within a few microns of the alpha source. However, it is not known whether fluorine can be expected to be this favorably located. For this reason it would be very difficult to calculate whether or not it is reasonable to expect this much Ne^{22} to be produced by this process. The evidence is not sufficiently strong to exclude the

[9] K. Rankama and T. G. Sahama, *Geochemistry* (University of Chicago Press, Chicago, 1950), pp. 570, 632.

[10] See reference 9, p. 423.

[11] F. A. Paneth, Quart. J. Roy. Meteorol. Soc. **65**, 303 (1939).

[12] Harrison Brown, Revs. Modern Phys. **21**, 625 (1949).

reactions $F^{19}(\alpha,p)Ne^{22}$ and $Mg^{25}(n,\alpha)Ne^{22}$ although it is believed that these reactions are less likely.

2. Variations in the Isotopic Abundances of Argon

Mass spectrometric determinations were made of argon extracted from pitchblende, Ceylon monazite, and euxenite. The results of these measurements are shown in Table II.

The constancy of the ratios when aliquots of the gas are taken from charcoal at different temperatures and when the pressure in the source changes because of the depletion of the reservoir together with the fact that the known impurity peaks did not change when the pressure of the gas in the reservoir was increased by decreasing its volume indicates that the ratios observed were not seriously affected by background impurities.

In every case the abundance of A^{36} is below normal; this is probably caused by the decay of small amounts of potassium present in the mineral. The anomalously low A^{36}/A^{38} ratio found in pitchblende, and to a much smaller extent in the other minerals, is in agreement with the measurements of Fleming and Thode.[3] The situation here is quite similar to the excess Ne^{22} in euxenite. The reactions which should be considered are

$$Cl^{35}(\alpha,n)K^{38}\xrightarrow{\beta^+}A^{38}, \quad Q=-5.46 \text{ Mev};$$

$$Cl^{35}(\alpha,p)A^{38}, \quad Q=0.42 \text{ Mev};$$

$$K^{41}(n,\alpha)A^{38}, \quad Q=-1.0 \text{ Mev}.$$

The Q values were calculated from reaction energies given by Roberts,[8] and atomic masses were given by Collins, Nier, and Johnson.[13]

Again the first two reactions require the presence of significant quantities of chlorine within range of the α-particles. The yield of the (α,n) reaction is low, primarily because of the high threshold for the reaction; most of the alphas will have energies below the threshold. For those with energies just above the threshold the cross section will be small. The (n,α) reaction on potassium seems unlikely because of the nine-Mev barrier that the α-particle must penetrate in order to leave the nucleus. However, this reaction has the advantage that the potassium need not be intimately associated with the uranium or thorium. From the amount of radiogenic A^{40} present, the potassium concentration is in the range of a few-tenths percent or less. This fact also makes this reaction unlikely. Thus, though the evidence is not definite, the (α,p) reaction on chlorine seems the most likely possibility.

[13] Collins, Nier, and Johnson, Phys. Rev. **84**, 717 (1951).

TABLE II. Data on argon extracted from radioactive minerals.

Sample	Wt. of sample	Age $\times 10^{-6}$ yr	Percent uranium	Percent thorium	Isotope ratios 36/40[a]	36/38[a]	Excess A^{36} cc STP/g[b]
Atmospheric[c]					0.00338	5.35	
Belgian Congo Pitchblende	20.0 g	650[d] 215[e]	44	0	0.00233 ±0.0005	1.61±0.04	2×10^{-3}
Ceylon Monazite	53.2 g	535[f]	0.3	7.8	0.00266 ±0.0005	4.71±0.20	6×10^{-10}
Madagascar Euxenite	109.6 g ~600[f]	60[e]	6	3.5	0.00321 ±0.0005	4.72±0.15	9.5×10^{-11}

[a] The errors shown represent the mean deviations of the peak heights.
[b] Mass spectrometer calibrated with krypton tracer.
[c] See reference 7.
[d] Alfred O. Nier, Phys. Rev. **55**, 153 (1939).
[e] Helium age as calculated from the quantity of helium obtained from the mineral and the uranium content.
[f] Uranium-lead ages. These ages were measured in this laboratory.

IV. ACKNOWLEDGMENTS

The writer wishes to express appreciation to C. Patterson for instruction in the chemical techniques used in the lead analyses and for the use of some purified reagents, to G. Tilton for several uranium analyses, to D. F. Peppard and J. P. Marble who supplied mineral samples, to O. Joensuu for emission spectrometric lead analyses, and to R. J. Hayden who was responsible for the construction of the mass spectrometer used in this investigation and who prepared the krypton tracers which were used.

Especial thanks must be given to M. G. Inghram whose counsel and encouragement guided this work from its inception to its completion.

Disintegration of Li^6 and Li^7 by 0.24-Mev Tritons

K. W. Allen,* E. Almqvist, J. T. Dewan,† and T. P. Pepper,‡
Chalk River Laboratory, Atomic Energy of Canada Limited, Chalk River, Ontario, Canada
(Received July 28, 1954)

The energy distributions of charged particles emitted in the bombardment of Li^6 and Li^7 by 0.24-Mev tritons have been obtained by magnetic analysis and by measuring pulse heights in a proportional counter. Q values for the reactions $Li^6(t,d)Li^7$, $Li^6(t,p)Li^8$, and $Li^7(t,\alpha)He^6$ were found to be 0.986±0.007 Mev, 0.790 ±0.011 Mev and 9.79±0.03 Mev, respectively. The latter, when combined with other accurately measured Q values, leads to a He^6-Li^6 mass difference of 3.55±0.03 Mev, which is in agreement with the most recent β-ray measurements. Evidence is also presented for an excited state of He^6 at 1.71±0.01 Mev above the ground state.

I. INTRODUCTION

THE reactions produced by the bombardment of light elements with tritium and He^3 in general have large Q values and sometimes lead to the formation of residual nuclei which cannot easily be produced in other ways. A systematic study of these reactions has been made possible by the technique[1] developed in this laboratory for handling and recovering small quantities of tritium and He^3 gases used in the ion source of a specially designed low-voltage accelerator.[2] The present paper deals with the energy distributions of the protons, deuterons and α-particles emitted when the lithium isotopes are bombarded with 0.24-Mev tritons. With a Li^6 target, the reactions $Li^6(t,d)Li^7$, $Li^6(t,p)Li^8$ and $Li^6(t,\alpha)He^5$ have been observed as well as a continuum of α-particles from the three-body disintegration $Li^6(t,n)2\alpha$ proceeding directly or via virtual α-emitting states of Be^8. With Li^7 as a target, two groups of α-particles from the reaction $Li^7(t,\alpha)He^6$ were observed leading to the ground state of He^6 and to a previously unreported excited state at 1.71 Mev. These groups were superimposed on an α-particle continuum from the various multibody disintegrations that are possible. Brief accounts of these experiments have already been published.[3]

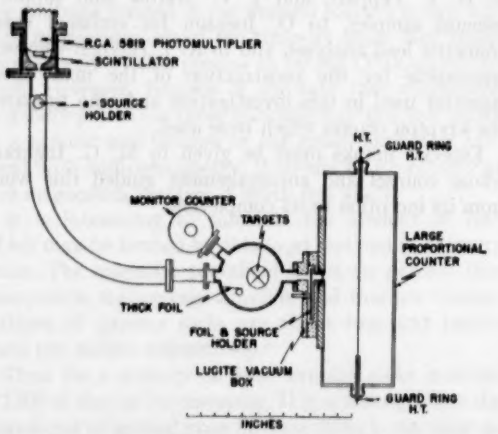

FIG. 1. Diagram showing arrangement of target chamber, magnetic analyzer and proportional counters.

II. EXPERIMENTAL TECHNIQUE

A. Accelerator and Gas Recovery

The low-voltage accelerator and gas recovery system have been described in detail elsewhere.[1,2] Hydrogen containing 15 percent tritium was fed into the rf ion source through a palladium leak at the rate of about 10 cc per hour. More than 96 percent of the gas leaving the ion source was recovered by a differential pumping system employing mercury diffusion pumps. The exhaust gas from the last pump, which was modified to operate against a backing pressure of 15 mm of mercury, was absorbed at room temperature in pyrophoric uranium contained in a stainless steel reservoir. By heating the reservoir to about 450°C, the hydrogen-tritium mixture was re-evolved in a pure state and used again in the ion source. A magnetic valve controlled from a vacuum gauge was provided to prevent air entering the pyrophoric uranium in the event of a leak developing in some part of the apparatus.

B. Target Assembly

The particle detectors used in this work consisted of a large proportional counter which recorded energy distributions of disintegration particles directly, and a ZnS(Ag) screen and photomultiplier which detected particles after their passage through a 90° analyzing magnet. In each case the sizes of the amplified pulses were displayed on a thirty-channel pulse-height analyzer.[4] The arrangement of the apparatus is shown diagrammatically in Fig. 1.

The vertical beam from the accelerator was deflected in a 90° magnet whose field was chosen to select the

* Now at the University of Liverpool, Liverpool, England.
† Now with Schlumberger Well Surveying Corporation, Houston, Texas.
‡ Now with Isotope Products Ltd., Oakville, Ontario, Canada.
[1] K. W. Allen and E. Almqvist, Rev. Sci. Instr. **24**, 70 (1953).
[2] Allen, Almqvist, Dewan, and Pepper, Can. J. Phys. **29**, 557 (1951).
[3] Pepper, Allen, Almqvist, and Dewan, Phys. Rev. **85**, 155 (1952); Dewan, Pepper, Allen, and Almqvist, Phys. Rev. **86**, 416 (1952).
[4] Moody, Howell, Battell, and Taplin, Rev. Sci. Instr. **22**, 551 (1951).

mass-3 component (T^+ and H_3^+ ions). This component of the beam, after collimation by $\frac{3}{16}$-in. diameter apertures 4 in. apart, was allowed to bombard one of four targets mounted on a water-cooled insulated assembly. The target assembly could be moved on vacuum seals so that any one of the four targets could be brought into the bombarding position facing either a magnetic analyzer or a large proportional counter. In the working position a target was inclined at 45° to both the ion beam and the particle detector. The collimation and entrance apertures were such that disintegration particles emitted at 90±2° to the beam were recorded. However, because of the low bombarding energy employed, this angular spread did not cause appreciable broadening of the particle energy distribution.

An additional small proportional counter was provided on one side of the target chamber to monitor the yield when the magnetic analyzer was in use.

C. The Magnetic Analyzer

Disintegration particles from the target were deflected through 90° in a homogeneous magnetic field on a radius of curvature of 20 cm. The field was variable up to a maximum of 15 000 gauss and the current through the coils was electronically stabilized. Relative values of the magnetic field were measured by the voltage developed across a coil rotating in the fringing field and driven by a synchronous motor. Absolute calibration was made by means of known particle groups. As normally set up, the resolution of the magnetic analyzer was about 2 percent in momentum (total width at half-height). The particles were detected by their scintillations in a ZnS(Ag) screen viewed by a 5819 photomultiplier. The ZnS screen was made by dusting the powder on to a piece of cellulose tape and shaking off the excess. The screen was mounted on the end of a short Lucite light pipe shaped at the other end to fit the surface of the photomultiplier. The photomultiplier was provided with mu metal and iron shields to reduce the effect of the stray field of the analyzing magnet on its operation. The pulses from the photomultiplier, after suitable amplification, were dispalyed on a thirty-channel pulse-height analyzer.[4]

D. The Proportional Counter

The large proportional counter used for measuring the energies of disintegration particles was constructed from an aluminum cylinder 5 in. in diameter and 15 in. long. It was provided with a mica window $\frac{1}{4}$ in. in diameter and 1 mg cm^{-2} thick. The mica window was plugged into the counter wall on an O-ring vacuum seal, so that windows could be changed easily in case of failure. The inner conductor was a tungsten wire 0.010 in. in diameter, supported at either end by copper to glass seals incorporating a guard ring construction.

TABLE I. α-particle energy calibration points obtained from radioactive sources and nuclear reactions.

Source	α-particle energy (Mev)	Reference
$D(l,\alpha)n$	3.43	a
U^{233}	4.823	b
Pu^{239}	5.150	c
Am^{241}	5.476	d
Cm^{242}	6.100	d
$Li^7(p,\alpha)He^4$	8.76	a

[a] Energies are those at 90° to 0.24-Mev beam. Q values were calculated from the masses (see reference 5).
[b] See reference 6.
[c] See reference 7.
[d] See reference 8.

The counter was filled to a pressure of 70 cm of mercury with a gas mixture consisting of welding argon with 1 percent carbon dioxide added. Particles entering through the mica window crossed the counter in a direction perpendicular to the wire in its central region. The counter was normally used with a gas amplification of five, obtained with the wire about 2400 volts positive with respect to the outer cylinder. The best resolution was obtained immediately after filling, when the total width at half-maximum was 1.5 percent of the mean pulse height for 8.75-Mev α-particles from the $Li^7(p\alpha)He^4$ reaction. The width deteriorated to ~2.5 percent in a few hours, and then stayed constant for long periods. Counter pulses were taken from the central wire through a 50-$\mu\mu$f ceramic condenser to a preamplifier mounted on the end of the counter. Thence, the pulses were led to a linear amplifier and pulse-height analyzer which were located near the control desk of the accelerator. Pulse heights were always referred to the output of a stable pulse generator which was connected to the input of the preamplifier via a 5-$\mu\mu$f condenser.

A wheel carrying aluminum absorbers and α-particle sources for calibration purposes was mounted *in vacuo* between the counter and the target. Table I lists the energy calibration points which were used.[5-8]

III. DISINTEGRATION OF Li^6

The possible exothermic reactions, with Q values calculated from the masses,[5] are:

$$Li^6+T=Li^7+D^2+0.988 \text{ Mev}, \quad (1)$$

$$Li^6+H^1+0.799 \text{ Mev}, \quad (2)$$

$$2He^4+n+16.100 \text{ Mev}, \quad (3)$$

$$He^5+He^4+15.2 \text{ Mev}, \quad (4)$$

$$Be^8+n+16.004 \text{ Mev}. \quad (5)$$

The low-energy deuterons and protons from reactions (1) and (2) were studied with the magnetic analyzer,

[5] Li, Whaling, Fowler, and Lauritsen, Phys. Rev. **83**, 512 (1951).
[6] T. E. Cranshaw and J. A. Harvey, Can. J. Research **A26**, 243 (1948).
[7] F. Asaro and I. Perlman, Phys. Rev. **88**, 828 (1952).
[8] Asaro, Reynolds, and Perlman, Phys. Rev. **87**, 277 (1952).

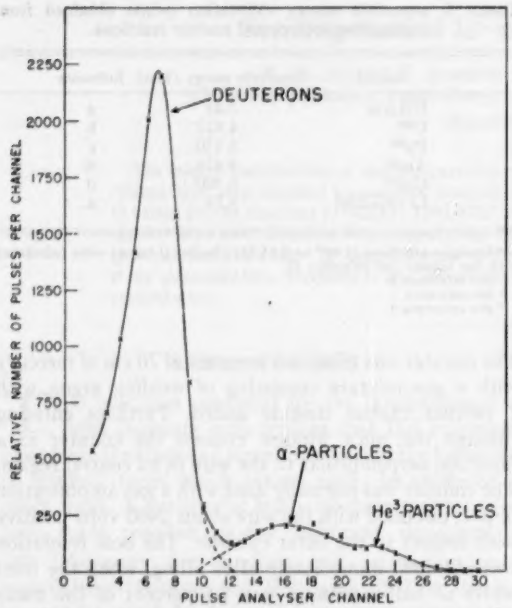

FIG. 2. The pulse-height distribution from a ZnS(Ag) screen produced by different particles with the same $H\rho$. The energies are: deuterons 0.866 Mev, α-particles 1.74 Mev, and He^3 particles 2.32 Mev.

and the α-particles from reaction (3), (4), and (5) with both the analyzer and the proportional counter. Thick targets of lithium fluoride were used in which the isotopic content of the lithium was 99.4 percent Li^6, 0.6 percent Li^7. The triton bombarding energy was 0.24 Mev.

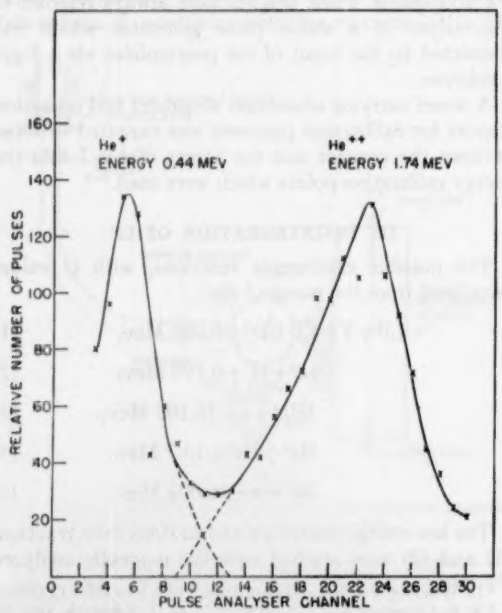

FIG. 3. Pulse-height distribution from ZnS(Ag) screen produced by singly and doubly charged α-particles with the same momentum-to-charge ratio.

A. The Reactions $Li^6(t,d)Li^7$ and $Li^6(t,p)Li^8$

A preliminary investigation with the magnetic analyzer revealed two strong deuteron groups from reaction (1) superimposed on a background of α-particles from reactions (3), (4), and (5). Disintegration particles from the reaction $Li^6(p,\alpha)He^3$, which was produced by 80-kev protons arising from the HHH^+ component of the ion beam, were also observed.

It so happened that, under the conditions of this experiment, the magnetic field required to bend the ground state deuterons on to the detector also selected doubly charged α-particles and He^3 particles from the $Li^6(p\alpha)He^3$ reaction. At the low bombarding energy of 80 kev and at 90° to the beam, these α-particles and He^3 particles had almost identical momenta and were not resolved by the magnet. Figure 2 shows a pulse-height analysis for a magnetic field close to the ground-state deuteron peak from reaction (1). The deuterons are quite well separated from the α-particles and He^3 particles, which are barely resolved. The calculated energy ratios for deuterons, doubly charged α-particles and He^3 particles with the same magnetic rigidity are 1:2:2.67; the estimated pulse-height ratios are 1:2.1:2.9. If only α-particles can reach the ZnS screen, then a pulse-height spectrum similar to that of Fig. 3 is observed. This curve was obtained by bombarding a Li^7 target with tritons, with the analyzing magnet setting the same as for Fig. 2. The two groups are singly and doubly charged α-particles, and the ratio of pulse heights is about 0.25, as it should be if the response of the ZnS screen is proportional to α-particle energy. These measurements suggest that the light output of ZnS(Ag) is proportional to the energy of heavy particles incident upon it, and independent of their nature, as is generally believed. Presumably this will only be true for short-range particles, for loss of light by scattering and absorption will be serious in the thicker layers of ZnS required to stop more energetic particles. Thus a ZnS screen forms a very convenient energy sensitive detector for use with a magnetic analyzer in the low-energy region, where a window is undesirable.

The momentum distributions of the deuterons and protons from the reactions $Li^6(t,d)Li^7$ and $Li^6(t,p)Li^8$ are shown in Fig. 4. The two intense groups are deuterons associated with the formation of Li^7 in the ground state and in the well-known 478-kev excited state. The weak proton group was readily detected when the ZnS screen was covered with aluminum foil just sufficiently thick to stop α-particles with the same momentum as the protons. The dashed curve represents the contribution from the reaction $Li^6(p,\alpha)He^3$, which was separated from the deuterons by analysis of the

pulse-height distribution from the detector as noted above.

B. Q Values and Discussion

It was found that the ground-state deuteron group coincided exactly in momentum with the α-particles and He^3 particles from the reaction $Li^6(p,\alpha)He^3$, within the accuracy of these measurements which was about 0.5 percent in momentum. As the Q value for the $Li^6(p,\alpha)He^3$ reaction has been measured accurately in several laboratories, it provided an excellent calibration for determining the Q value of the $Li^6(t,d)Li^7$ reaction. Taking a value of 4.023 ± 0.002 Mev for the former, which is a weighted mean of the best measurements,[5,9] the latter was found to be 0.986 ± 0.007 Mev. Allowance was made for an oil layer equivalent to 0.005 cm air on the target. The thickness of this oil layer was estimated very roughly by measuring the yield of α-particles from the $D(t,\alpha)n$ reaction when the target was turned to face the proportional counter on the other side of the target assembly. As the H.T. set had never had deuterium in it, it was assumed the source of deuterium was the natural isotopic content of hydrogenous vapors which condensed on the target. It is known that the deuterium contamination can be reduced very considerably by heating the target.[10] This estimate of the thickness of the oil layer was almost certainly too low as some of the oil must have been carbonized by the beam. The Q value is however fairly insensitive to the amount of oil on the target since both calibrating α-particles and deuterons go through it. A correction of +5 kev was made for thick target effect.

TABLE II. Comparison of measured Q values with those calculated from the masses.

Reaction	Calc. Q (Mev)	Meas. Q (Mev)
$Li^6(t,d)Li^7$	0.988	0.986 ± 0.007
$Li^6(t,p)Li^8$	0.799	0.790 ± 0.011

If the energy of the first excited state of Li^7 is assumed to be 0.478 ± 0.007 Mev,[11] the Q of the reaction $Li^6(t,d)Li^7$ becomes 0.508 ± 0.007 Mev. From this value, and the measured separation in momentum of the low energy deuterons and protons from the reaction $Li^6(t,p)Li^8$, the Q value of the latter reaction was found to be 0.790 ± 0.011 Mev. Corrections for an oil layer and thick target effect were included. Comparison of the measured Q values with those calculated from the masses is made in Table II. The difference between the two measured Q values, 0.196 Mev, may also be compared with the directly measured Q value of the reaction $Li^7(d,p)Li^8$; i.e., 0.191 ± 0.001.[12]

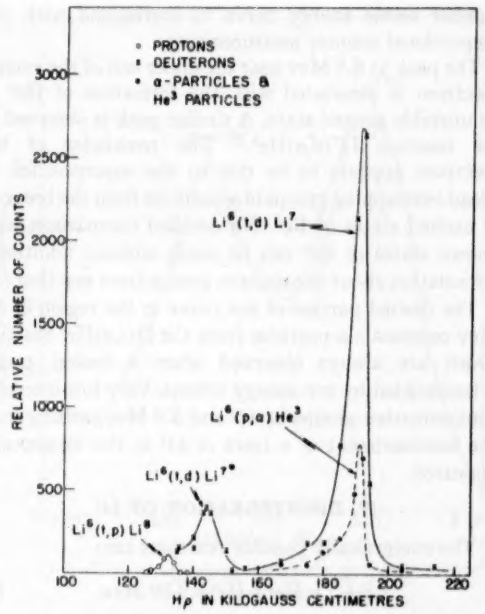

FIG. 4. Protons and deuterons from Li^6+T reactions observed at 90° to a 0.24-Mev triton beam. The dashed curve represents He^3 particles and α-particles produced by 80-kev protons on Li^6.

C. α-Particles from Li^6+T

The energy spectrum of α-particles from reactions (3), (4), and (5) obtained from magnetic deflection and proportional counter measurements is shown in Fig. 5. In the magnetic measurements, the intensity of doubly charged α-particles was obtained by integrating the area under the upper peak in the pulse analyzer curve (compare Fig. 3). The data were then corrected for charge exchange in the target[13] and plotted on a

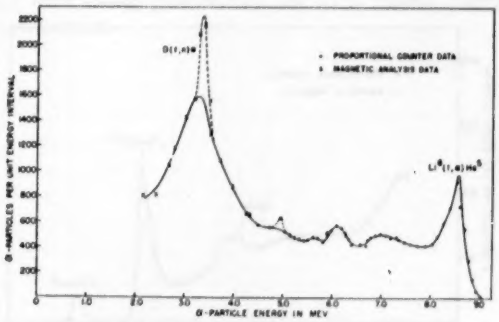

FIG. 5. The 90° α-particle energy distribution from Li^6+T reactions at a triton energy of 0.24 Mev.

[9] Collins, McKenzie, and Ramm, Proc. Roy. Soc. (London) **A216**, 242 (1953).
[10] Allen, Almqvist, Dewan, Pepper, and Sanders, Phys. Rev. **82**, 262 (1951).
[11] Hornyak, Lauritsen, Morrison, and Fowler, Revs. Modern Phys. **22**, 291 (1950).
[12] Williamson, Browne, Craig, and Donahue, Phys. Rev. **84**, 731 (1951).
[13] G. H. Briggs, Proc. Roy. Soc. (London) **A114**, 341 (1927).

number *versus* energy curve to correspond with the proportional counter measurements.

The peak at 8.5 Mev near the upper end of the energy spectrum is associated with the formation of He^5 in its unstable ground state. A similar peak is observed in the reaction $Li^7(d,\alpha)He^5$.[14] The remainder of the spectrum appears to be due to the superposition of broad overlapping groups of α-particles from the breakup of excited states of Be^8. No detailed comparison with known states of Be^8 can be made without additional information about the neutron groups from reaction (5).

The dashed portion of the curve in the region of 3.4 Mev represents α-particles from the $D(t,n)He^4$ reaction which are always observed when a cooled target is bombarded by low-energy tritons. Very low-intensity contamination groups at 4.9 and 5.9 Mev, arising from the bombardment of a trace of Li^7 in the target, also appeared.

IV. DISINTEGRATION OF Li^7

The energetically possible reactions are:

$$Li^7+T=He^6+He^4+9.79 \text{ Mev}, \quad (1)$$

$$=2He^4+2n+8.85 \text{ Mev}, \quad (2)$$

$$=Be^9+n+10.42 \text{ Mev}, \quad (3)$$

Reaction (2) may also represent the final products of two step processes via the unstable nuclei He^5 and Be^8 or through virtual excited states of He^6 and Be^9.

The bombardments were carried out at a triton energy of 0.24 Mev, using thick targets of LiF and Li_2SO_4 in which the isotopic content of the lithium was 99.91 percent Li^7 and 0.09 percent Li^6. The results are shown in Fig. 6, identical energy spectra being observed for each type of target. In addition to the α-particle continuum from reaction (2), there are prominent groups at 5.93 and 4.91 Mev and a double peak at $\sim$3.5 Mev.

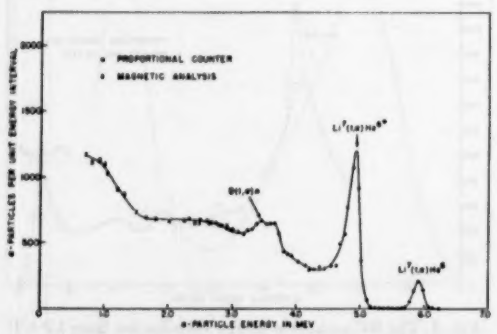

FIG. 6. The 90° α-particle energy distribution from the Li^7+T reactions at a triton energy of 0.24 Mev.

[14] Williams, Shepherd, and Haxby, Phys. Rev. **52**, 390 (1937).

Mass of He^6

The group at 5.93 Mev is associated with the formation of He^6 in its ground state. The energy of this group was determined accurately by allowing the α-particles to enter the counter simultaneously with α-particles from Cm^{242}. In this way any small shifts in counter calibration between runs were eliminated. Such small shifts in pulse height, dependent on over-all counting rate in the counter, are known to occur. An expanded portion of the pulse-height distribution (Fig. 7) shows the two groups clearly resolved. The separation of the peaks was found to be 0.165 ± 0.017 Mev. Asaro, Reynolds, and Perlman[8] have shown that the α-particle spectrum from Cm^{242} is complex, 73 percent of the α-particles being emitted with an energy of 6.110 ± 003 Mev and 27 percent with an energy of 6.064 ± 0.003 Mev; residual groups account for less than 0.1 percent of the total intensity.[15] Therefore, if a weighted mean of 6.100 ± 0.003 is taken for Cm^{242}, the energy of the ground-state α-particle group becomes 5.945 ± 0.017 Mev after corrections totalling $+0.010$ Mev are added for thick target effect and for an oil layer on the target. The Q value of the reaction $Li^7(t\alpha)He^6$ is then calculated to be 9.79 ± 0.03 Mev.

It may be shown that the energy equivalent of the mass difference He^6-Li^6 is $(Q_1+Q_2)-(Q_3+Q_4)$, where Q_1, Q_2, Q_3, and Q_4 are respectively the Q values of the reactions $Li^7(p,\alpha)\alpha$, $T(\beta)He^3$, $Li^6(p,\alpha)He^3$, and $Li^7(t,\alpha)$-He^6. The following values were assumed for the Q values: $Q_1=17.343\pm0.007$ Mev,[5,9] $Q_2=0.0186\pm0.0002$ Mev,[16] $Q_3=4.023\pm0.002$ Mev,[5,9] $Q_4=9.79\pm0.03$ Mev. Thus,

$$He^6-Li^6=3.55\pm0.03 \text{ Mev}.$$

If the mass of Li^6 is assumed to be 6.01703, the mass of He^6 is, therefore, 6.02084 ± 0.00003.

Excited States of He^6

The strong group of α-particles at 4.9 Mev (Fig. 6) is believed to be associated with the first excited state of He^6. The energy of the group was found by direct comparison with α-particles from Pu^{239} ($E=5.150$ Mev) which were allowed to enter the target simultaneously with those from the Li target. The mean energy derived from these runs was 4.91 ± 0.02 Mev. From the directly measured energy difference of 1.03 ± 0.01 Mev between this group and the ground state group, the energy of the first excited state was found to be 1.71 ± 0.01 Mev.

The double peak at $\sim$3.5 Mev is believed to be a superposition of the usual T+D α-particles at 3.43 Mev and the ground-state He^6 particles associated with the 5.945-Mev α-particles. There is no evidence for the existence of other excited states of He^6 from the 90° α-particle spectrum (Fig. 6). However, in the course of

[15] Asaro, Thompson, and Perlman, Phys. Rev. **92**, 694 (1953).
[16] Curran, Angus, and Cockcroft, Phil. Mag. **40**, 53 (1949). G. C. Hanna and B. Pontecorvo, Phys. Rev. **75**, 983 (1949).

some measurements of the angular distribution of the two prominent groups, a third group of α-particles was observed at backward angles. This group is believed to be associated with a second excited state of He^6 at 3.35 Mev. A fuller discussion of this state will appear in a forthcoming publication.

DISCUSSION

Before the present measurements were made, the best value for the He^6-Li^6 mass difference appeared to be that given by the end point of the β-ray spectrum, 3.215 ± 0.015 Mev.[17] However, this value was inconsistent with earlier measurements of the same quantity by absorption techniques,[18,19] and also with the observation that the neutron threshold for the production of He^6 radioactivity in the reaction $Be^9(n,\alpha)He^6$ was greater than 0.6 Mev.[20] This latter observation implies that the He^6-Li^6 mass difference must be greater than 3.44 Mev. There is no evidence for a γ ray associated with the β-particles.[19] This puzzling discrepancy is now clear since the end point of the β spectrum has been remeasured as 3.50 ± 0.05 Mev,[21] which is in agreement, within experimental error, with the value obtained here from reaction Q values.

The first excited state of He^6 is unstable against dissociation into an α-particle and two neutrons by 0.78 Mev, and it may be inferred that the dissociation does take place because no group of He^6 particles corresponding to the 4.9-Mev α-particles was observed. Indeed it would be surprising if the breakup did not take place. Although unstable against three body disintegrations, this excited state cannot break up into He^5 and a neutron and may be quite narrow. The observed width of the 4.9-Mev group was not noticeably greater than the experimental width for a particle of this energy, which suggests that the width of the excited state of He^6 is probably not greater than about 100 kev.

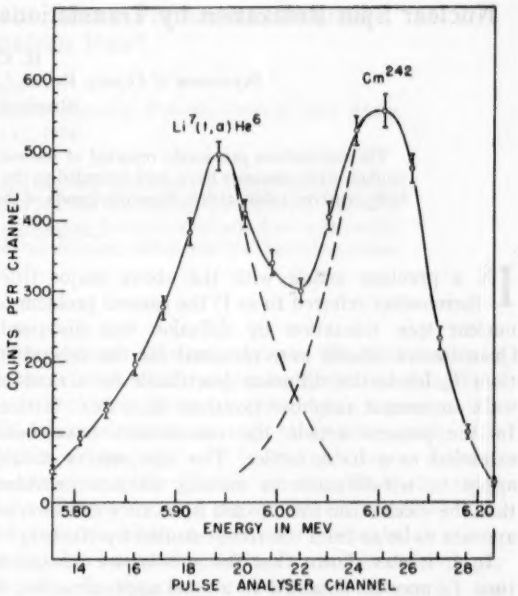

FIG. 7. The pulse-height distribution obtained when α-particles from the $Li^7(t,\alpha)He^6$ reaction and from Cm^{242} are admitted to the counter simultaneously through the same window. Observation at 90° to a 0.24-Mev triton beam.

ACKNOWLEDGMENTS

The cooperation of the Isotopes Branch of this laboratory under the direction of Mr. M. H. Thomas, who extracted the tritium gas, is gratefully acknowledged. We are also indebted to Professor B. W. Sargent and Dr. L. G. Elliott for their interest in this work, and to Mr. G. J. Leighton and Mr. J. Rothfels for much technical assistance. The separated Li^6 and Li^7 were kindly provided by the U. S. Atomic Energy Commission.

[17] V. Perez-Mendez and H. Brown, Phys. Rev. **77**, 404 (1950).
[18] T. Bjerge and K. J. Brostrom, Kgl. Danske Videnskab. Selskab, Mat.-fys. Medd. **16**, No. 8 (1938); H. S. Sommers, Jr., and R. Sherr, Phys. Rev. **69**, 21 (1946).
[19] W. J. Knox, Phys. Rev. **74**, 1192 (1948).
[20] Allen, Burcham, and Wilkinson, Proc. Roy. Soc. (London) **A192**, 114 (1947).
[21] Wu, Rustad, Perez-Mendez, and Lidofsky, Phys. Rev. **87**, 1140 (1952).

Nuclear Spin Relaxation by Translational Diffusion. II. Diffusion in a B.C.C. Lattice

H. C. TORREY
Department of Physics, Rutgers University, New Brunswick, New Jersey
(Received July 30, 1954)

The calculations previously reported of nuclear spin relaxation time when relaxation is influenced by random-walk processes have been extended to the case of random walk to nearest neighbor positions in a body-centered cubic lattice. Some corrigenda of the previous work are noted.

IN a previous article with the above major title[1] (hereinafter referred to as I) the general problem of nuclear spin relaxation by diffusion was discussed. Quantitative results were obtained for the relaxation time T_1 for lattice diffusion describable by a random walk to nearest neighbor positions in a f.c.c. lattice. In the present article the calculations have been extended to a b.c.c. lattice. The new results should apply to self-diffusion in metallic lithium provided that the mechanism in this case is vacancy diffusion as appears to be so from the recent studies by Norberg.[2]

In I, it was shown that the spin-lattice relaxation time T_1 may be obtained to a good approximation, if one assumes relaxation to be due to dipolar coupling rendered time-dependent by lattice diffusion of the above type, from the equation

$$T_1^{-1}=(8\pi/5)\gamma^4\hbar^2I(I+1)(n/k^3l^3\omega)\psi(k,\tfrac{1}{2}\omega\tau),$$

where

$$\psi(k,y)=yG(k,y)+2yG(k,2y)$$

and

$$G(k,y)=\int_0^\infty J_{\frac{1}{2}}^2(kx)\frac{1-\sin x/x}{(1-\sin x/x)^2+y^2}\frac{dx}{x}.$$

In these equations the parameter k depends on the lattice structure and is given by

$$k^3=(4\pi/3)n_0b^{-3}l^{-3}/\textstyle\sum_k r_k^{-6},$$

where n_0 is the number of sites in a unit cell, b is the lattice parameter, and l is the distance between nearest neighbor sites.

For a b.c.c. lattice $n_0=2$, $l=\frac{1}{2}\sqrt{3}b$, and[3] $\sum_k r_k^{-6}=29.045/b^6$. From these data we obtain for a b.c.c. lattice $k=k_b=0.76293$.

With this value of k we have computed the function $\psi(k_b,y)$ by numerical methods. Its values are given in Table I.

TABLE I. Table of the function $\psi(k_b,y)$ and of $\delta\psi=\psi(k_f,y)-\psi(0.74335,y)$; ($k_b=0.76293$, $k_f=0.74280$).

y	$\psi(k_b,y)$	$\delta\psi\times10^5$
0	0	0
0.025	0.04043	−4
0.05	0.07394	−6
0.10	0.12866	−6
0.15	0.17172	−6
0.20	0.20542	−6
0.25	0.23137	−5
0.30	0.25094	−4
0.35	0.26543	−2
0.40	0.27571	−1
0.45	0.28264	0
0.50	0.28693	+1
0.55	0.28907	2
0.5922	0.28955 (max)	
0.60	0.28953	3
0.65	0.28864	4
0.70	0.28681	4
0.80	0.28086	6
0.90	0.27304	6
1.00	0.26417	7
1.20	0.24535	7
1.40	0.22686	8
1.60	0.20967	8
1.80	0.19415	8
2.00	0.18024	7
2.25	0.16497	7
2.5	0.15174	6
3.0	0.13029	6
3.5	0.11380	5
4.0	0.10083	5
5.0	0.08189	4
6.0	0.06883	3
7.0	0.05930	3
10.0	0.04181	2
20.0	0.02102	1
30.0	0.01403	1
40.0	0.01052	1

In I we stated a value of $\sum_k r_k^{-6}$ for a f.c.c. lattice. We had obtained this value by summing directly over a large number of lattice sites and by integration over the remainder. It has since come to our attention that this sum has been computed by more accurate methods[3] and that the correct value is $115.631b^{-6}$. This value is 0.2 percent larger than that used in I and leads to the value $k=k_f=0.74280$ for a f.c.c. lattice. This new value of k results in small changes in the function $\psi(k_f,y)$ reported in I. Although these changes are not significant experimentally, we reproduce them for completeness in the third column of Table I. The numbers in this column should be added to the tabulated values of $\psi(k,y)$ in Table II of article I in order to obtain $\psi(0.74280,y)$. Also the value of y at maximum ψ is changed to 0.6027 for the new value of k. The corresponding value of $\psi_{\max}$ is 0.29063. These corrections were obtained by linear extrapolation from the previous results for $k=0.74335$ and the present results for $k=0.76293$. Incidentally, Eq. (84) of I was incorrectly reproduced and should contain a factor k^{-1} on the right.

The author is indebted to Mr. James Simpson for help in computational work.

[1] H. C. Torrey, Phys. Rev. **92**, 962 (1953).
[2] R. E. Norberg, University of Illinois (private communication).
[3] J. E. Jones and A. E. Ingham, Proc. Roy. Soc. (London) **A107**, 636 (1925).

Direct Quantitative Observation of the Three-Photon Annihilation of a Positron-Negatron Pair*

J. K. Basson
National Physical Laboratory, Council for Scientific and Industrial Research, Pretoria, Union of South Africa
(Received January 11, 1954)

Three-photon annihilation of the positron with a negatron has been determined quantitatively as well as qualitatively by the simultaneous observation of the emitted photons with scintillation counters. The ratio of the reaction cross sections for two- and three-photon annihilation has been determined as $\sigma_{2k}/\sigma_{3k}=402 \pm 50$. This is in agreement with the theory of Ore and Powell but definitely differs from the theoretical values obtained by Lifshitz and by Ivanenko and Sokolov.

INTRODUCTION

THE possibility that an appreciable part of positron-negatron reactions might result in annihilation with the radiation of three photons, was first theoretically postulated by Lifshitz[1] and by Ivanenko and Sokolov[2] and a short while later by Ore and Powell.[3] They all used the time-independent perturbation theory to compute the cross section for three-photon annihilation. The influence of Coulomb binding was neglected and plane wave functions were assumed for the initial and final states of the positron-negatron system. Similar results were obtained but with different numerical values.

When the positron and negatron meet in free space they can be considered to form a bound system similar to that of the hydrogen atom, as suggested by Wheeler.[4] The triplet or singlet state is formed depending on whether the spins of the positron and negatron are parallel or antiparallel. These states are called respectively *ortho-* and *para*-positronium. Transitions between the two are strictly forbidden.[3]

The singlet state is annihilated with the emission of two quanta, while the triplet state has to emit three quanta in order to conserve the total spin. Because of the multipole nature of the last process, *ortho*-positronium has a lifetime (1.4×10^{-7} sec[3]) markedly longer than that of *para*-positronium (1.25×10^{-10} sec[4]), and threefold annihilation has a correspondingly smaller chance of occurring.

The optical spectrum of positronium has not yet been observed,[5] but the formation of the triplet atom in gases has been observed experimentally by Deutsch[6] with Na^{22} as the positron emitter. In a gas at normal temperature and pressure, the positronium atom will undergo thermal collisions at the rate of the order of 10^{12} per second. This may result in the de-excitation of the triplet state to the singlet state, with resulting two- instead of three-photon annihilation, in a gas (such as NO) where electron exchange takes place easily. The number of delayed ($\sim10^{-7}$ sec) coincidences between the emission of the gamma quantum from the decay of the Na^{22} nucleus and the appearance of an annihilation quantum when the positron is brought to rest in the gas, has been measured by Deutsch in different gas mixtures. In the case of nitrogen, for example, the number of delayed coincidences—due to the formation of *ortho*-positronium—is markedly decreased by the addition of a few percent of NO. The electrons from the positronium atom are easily exchanged during a collision with an unpaired electron (from the NO) with opposite spin. Furthermore, by observing the number of delayed coincidences from positron capture in freon (where this exchange is almost nonexistent) as a function of the pressure and extrapolating to zero pressure, Deutsch found for the lifetime of the *ortho*-positronium a value in good agreement with the theoretical value of Ore and Powell.

When the positrons are brought to rest in a solid no positronium is formed. The smallest Bohr radius of the positronium atom is about one angstrom,[7] while the lattice distances in a crystal are of the order of only a few angstroms. Because of the intense perturbing influence of the ionic and electronic fields that it would experience, a positronium atom could not exist in a solid. The positron moves through the substance till it is brought to rest and then it is annihilated by a negatron without any real binding by any one of them. (According to Heitler,[8] the chance that a positron with an energy of 0.55 Mev, from Na^{22}, will be destroyed before being brought to rest, is about 3 percent.) The particles which are annihilated can therefore be regarded as quite free and the ratio of two- to three-photon annihilation therefore equals the ratio of the reaction cross sections, i.e., σ_{2k}/σ_{3k}.

* This work forms part of a thesis submitted in August, 1953, to the University of Pretoria in partial fulfillment of the requirements for the degree of D.Sc.

[1] E. M. Lifshitz, Doklady Akad. Nauk. S.S.S.R. **60**, 207 (1948).

[2] D. Ivanenko and A. Sokolov, Doklady Akad. Nauk. S.S.S.R. **61**, 51 (1948).

[3] A. Ore and J. L. Powell, Phys. Rev. **75**, 1696 (1949).

[4] J. A. Wheeler, Ann. N. Y. Acad. Sci. **48**, 219 (1946).

[5] J. D. Fox and J. Korringa, Ned. Tijdschr. Natuurk. **18**, 304 (1952).

[6] M. Deutsch, Phys. Rev. **82**, 455 (1951); **83**, 866 (1951).

[7] The Bohr radius of the hydrogen atom is $a=\hbar^2/me^2=0.525$A. The effective mass of the electron in the positronium atom is half of that in the hydrogen atom. Its Bohr radius is therefore 1.05A.

[8] W. Heitler, *The Quantum Theory of Radiation* (Oxford University Press, London, 1944), p. 231.

The first direct observation of this three-photon process was made by Rich,[9] who obtained threefold coincidences from three scintillation counters spaced around a Cu^{64} source of positrons. He did not obtain quantitative results accurate enough to discriminate between the various theoretical results. With the aid of NaI(Tl) counters, De Benedetti and Siegel[10] measured the three-photon disintegration rate of Na^{22} positrons, stopped in aluminum. Owing to lack of knowledge of source strength and counter efficiencies, they could only report a correspondence within a factor of two with the theory of Ore and Powell.[10a]

It was therefore considered worthwhile to make an accurate, direct determination of σ_{2k}/σ_{3k}, since it would, apart from its relation to positron-negatron annihilation, yield a method of testing the theoretical foundation of the computations.

CALCULATIONS

The different ways in which a positron-negatron pair can be annihilated are determined by the laws of energy and momentum conservation. In the case of three-photon annihilation these laws reduce to

$$\text{energy conservation: } k_1+k_2+k_3=2m; \quad (1)$$

$$\text{momentum conservation: } \mathbf{k}_1+\mathbf{k}_2+\mathbf{k}_3=0. \quad (2)$$

Figure 1 gives the spectrum of the individual photons according to Ore and Powell. The type of annihilation with the greatest probability is that in which one quantum has an energy m and the other two are emitted in the opposite direction. This form of annihilation is impractical to observe due to the intense background of two-photon annihilation. In this work a symmetrical 120° setup has been chosen as it also simplifies the calculation of the fraction of all threefold annihilations observed with our experimental setup. In this case the three photons have the same energy, i.e., $\frac{2}{3}m=340$ kev.

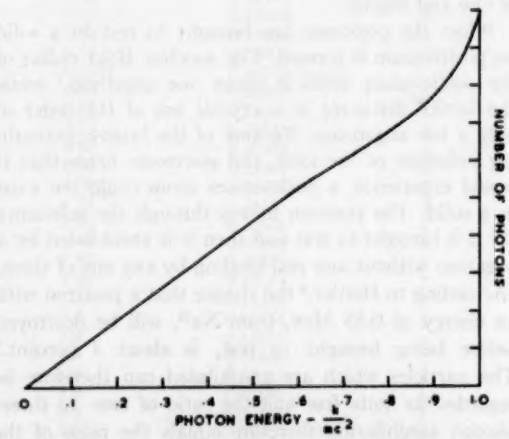

FIG. 1. Energy spectrum of individual photons from the three-photon annihilation of an electron and a positron—Ore and Powell.

Equation (2) of Ore and Powell[3] gives the probability of three-photon annihilation in terms of the matrix H_{FA} (which gives the relation between the initial and final states of the system) and ρ_F (the phase density of the final states per unit energy interval)

$$dP=2\pi|H_{FA}|^2\rho_F. \quad (3)$$

Substituting the values of $|H_{FA}|^2$ and ρ_F from their Eqs. (4) and (5) gives

$$dP=\frac{2e^6\kappa^3}{3\pi^2m^4}[(1-\cos\alpha)^2+(1-\cos\beta)^2+(1-\cos\gamma)^2]\times dk_1dk_2d\Omega_1,$$

where α, β, and γ are the angles between k_2 and k_3, k_3 and k_1, and k_1 and k_2, respectively, and $1/\kappa$ is twice the Bohr radius. The term dP is the probability that the positron and negatron are annihilated to give three photons such that the energy of photon 1 lies between k_1 and k_1+dk_1, with direction in the small solid angle $d\Omega_1$ and the energy of photon 2 between k_2 and k_2+dk_2. These three conditions completely determine the manner of annihilation.

To normalize, we have to divide dP by P the total probability of threefold annihilation which, according to Ore and Powell, is

$$P=\frac{1}{3\tau}=\frac{16e^6\kappa^3}{9\pi m^2}(\pi^2-9).$$

This gives dW, the fraction of all threefold annihilation within the limits dk_1, dk_2, and $d\Omega_1$,

$$dW=dP/P=\frac{3}{8\pi m^2(\pi^2-9)}[(1-\cos\alpha)^2+(1-\cos\beta)^2+(1-\cos\gamma)^2]dk_1dk_2d\Omega_1. \quad (4)$$

Resolving (2) into its X and Y components (with the X axis in the direction of k_1 (see Fig. 2) gives

$$k_1+k_2\cos\gamma+k_3\cos\beta=0,$$
$$k_2\sin\gamma-k_3\sin\beta=0.$$

(All the Z components disappear as the X-Y plane is chosen so that the three photons fall in it.) Furthermore $\alpha+\beta+\gamma=2\pi$. Therefore

$$k_1=\frac{2m\sin\alpha}{\sin\alpha+\sin\beta+\sin\gamma},$$

$$k_2=\frac{2m\sin\beta}{\sin\alpha+\sin\beta+\sin\gamma},$$

$$k_3=\frac{2m\sin\gamma}{\sin\alpha+\sin\beta+\sin\gamma}.$$

[9] J. A. Rich, Phys. Rev. **81**, 140 (1951).
[10] S. De Benedetti and R. Siegel, Phys. Rev. **85**, 371 (1952).
[10a] For references to further work on this subject, see M. Deutsch in *Progress in Nuclear Physics*, edited by O. R. Frisch (Academic Press, New York, 1953), Vol. 3, p. 131.

This gives k_1 and k_2 as functions of α and β. Equation (4) can now be transformed by means of the Jacobian,

$$\frac{\partial(k_1,k_2)}{\partial(\alpha,\beta)}=\frac{4m^2\sin\alpha\sin\beta\sin\gamma}{(\sin\alpha+\sin\beta+\sin\gamma)^3},$$

and becomes

$$dW=\frac{3}{2\pi(\pi^2-9)}[(1-\cos\alpha)^2+(1-\cos\beta)^2+(1-\cos\gamma)^2]\times\frac{\sin\alpha\sin\beta\sin\gamma}{(\sin\alpha+\sin\beta+\sin\gamma)^3}d\alpha d\beta d\Omega. \quad (5)$$

Since $d\alpha$, $d\beta$, and $d\Omega$ are small angles in this experimental setup, the probability can be assumed to be constant over the range $d\alpha$, $d\beta$, and $d\Omega$ and equal to that at $\alpha=120°$ and $\beta=120°$. Substituting in (5) gives

$$dW=\frac{3}{8\pi(\pi^2-9)}d\alpha d\beta d\Omega. \quad (6)$$

Now α and β can vary from 0 to 2π and Ω from 0 to 4π. Therefore the fraction of the total α,β,Ω phase space observed is

$$B=\frac{1}{16\pi^3}d\alpha d\beta d\Omega. \quad (7)$$

This gives the fraction of all random threefold annihilations which can be observed with our setup, assuming the probability to remain constant within its limits. Furthermore, the three photons are emitted in the same plane. This factor B is now calculated by means of elementary coordinate geometry as follows:

A random plane intersecting all three counters is given by

$$lx+my+nz=0, \quad (8)$$

where l, m, and n are the directional cosines of its orthogonal. Also,

$$l^2+m^2+n^2=1. \quad (9)$$

The equations for the circular front surfaces of the counters are:

Counter 1:

$$x=R,\qquad y^2+z^2=r^2, \quad (10)$$

where R equals the distance from source to counter and r the radius of each counter;

Counter 2:

$$x-\sqrt{3}y+2R=0,\qquad x^2+y^2+z^2=R^2+r^2; \quad (11)$$

Counter 3:

$$x+\sqrt{3}y+2R=0,\qquad x^2+y^2+z^2=R^2+r^2. \quad (12)$$

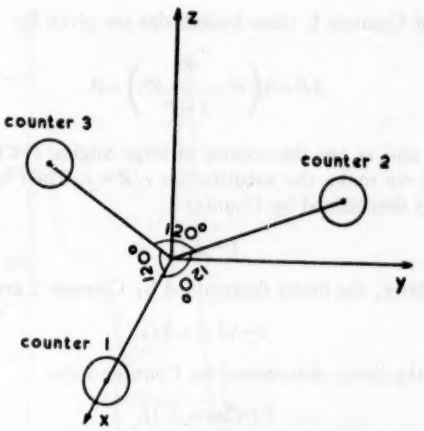

FIG. 2. Positions of front surfaces of scintillation counters with respect to our coordinate system.

The random plane now intersects the three counters in lines AB, CD, and EF. Solving for AB from Eqs. (8), (9), and (10) gives

$$AB=4\left(r^2-\frac{l^2}{1-l^2}R^2\right).$$

Similarly,

$$CD=4\left[r^2-\frac{(l-\sqrt{3}m)^2}{4-(l-\sqrt{3}m)^2}\cdot R^2\right],$$

$$EF=4\left[r^2-\frac{(l+\sqrt{3}m)^2}{4-(l+\sqrt{3}m)^2}\cdot R^2\right].$$

The fraction of all three-photon annihilations, in one specific plane, through the three counters, is

$$6\times\frac{AB}{2\pi R}\times\frac{CD}{2\pi R}\times\frac{EF}{2\pi R},$$

where AB, CD, and EF are functions only of $l(=\cos\phi)$ and $m(=\cos\theta)$. The factor 6 is introduced as there are 6 possible ways of annihilation giving photons in the three directions. The fraction of all planes with directional angles between ϕ and $\phi+d\phi$, and θ and $\theta+d\theta$ is therefore

$$dB=6\times\frac{AB}{2\pi R}\times\frac{CD}{2\pi R}\times\frac{EF}{2\pi R}\times\frac{d\theta}{2\pi}\times\frac{d\phi}{2\pi}.$$

The total fraction observed by our setup is

$$B=\frac{6}{(2\pi)^4}\int\int\frac{AB\cdot CD\cdot EF}{R^3}d\theta d\phi. \quad (13)$$

This integration takes place over the ranges of θ and ϕ where the plane still cuts all three counters. At the limits the plane touches one or more of the counters.

For Counter 1, these boundaries are given by

$$AB=4\left(r^2-\frac{l^2}{1-l^2}R^2\right)=0.$$

As l and m are the cosines of large angles, $l^2\ll 1\gg m^2$. Also, we make the substitution $r/R=f$. Then for the limits determined by Counter 1,

$$l=\pm f.$$

Similarly, the limits determined by Counter 2 are

$$l-\sqrt{3}=\pm 2f;$$

and the limits determined by Counter 3 are

$$l+\sqrt{3}m=\pm 2f.$$

Now $l=\cos\phi$ and therefore $d\phi=-dl/(1-l^2)^{\frac{1}{2}}\approx -dl$; similarly $d\theta\approx -dm$. Substituting further $a=l/f$ and $b=\sqrt{3}m/f$ in (13) gives

$$B=\frac{12f^5}{\sqrt{3}(2\pi)^5}\int\int\{(1-a^2)[4-(a-b)^2]\times[4-(a+b)^2]\}^{\frac{1}{2}}dbda,$$

where the integration takes place within the limits given by

$$a=\pm 1,\quad a-b=\pm 2,\quad a+b=\pm 2.$$

Numerical integration gives

$$B=\frac{12f^5}{\sqrt{3}(2\pi)^5}\times 13.8. \tag{14}$$

Substituting (7) and (14) into (6) gives

$$dW=\frac{3}{8\pi(\pi^2-9)}\times 16\pi^3 B$$

$$=0.665f^5.$$

Now the fraction of space subtended by each counter is $\Delta\Omega/4\pi=\pi r^2/4\pi R^2=\frac{1}{4}f^2$. Therefore,

$$dW=21.3(\Delta\Omega/4\pi)^{5/2}.$$

The probable error of this calculation is less than 2 percent.

EXPERIMENTAL PROCEDURE

Three NaI(Tl) scintillation counters were placed around the Na^{22} source (as NaCl) in a container of aluminum which was thick enough to stop all the positrons. The 2.5-cm×4-cm diameter crystals were mounted directly on the 5819 photomultipliers with silicone grease and MgO as reflector. Jordan-Bell amplifiers were used with shorted delay-line shaping of the input pulses and connected to conventional differential discriminators. The output pulses from the discriminators were fed into a threefold coincidence circuit. It was found that the resolving time could be decreased to 4.5×10^{-7} sec before losing any genuine coincidences.

The number of genuine coincidences, observed with this setup, is given by

$$K_3=\frac{\sigma_{3k}}{\sigma_{2k}+\sigma_{3k}}Ne_1e_2e_3dW, \tag{15}$$

where N=disintegration rate of Na^{22} source, e_1=efficiency of Counter 1, e_2=efficiency of Counter 2, and e_3=efficiency of Counter 3. Substituting the value that we obtained for dW gives

$$\frac{\sigma_{2k}}{\sigma_{3k}}=\frac{N\times e_1e_2e_3}{K_3}\times 21.3\left(\frac{\Delta\Omega}{4\pi}\right)^{5/2}-1.$$

Each parameter on the right-hand side of this equation was determined separately.

Determination of N

The disintegration rate of the Na^{22} was determined with a 4π counter as 0.436 ± 0.013 rutherford.

Determination of $\Delta\Omega/4\pi$

The solid angles subtended at the source by the different counters were first made equal. Two counters were placed on opposite sides of the source. Counter 1 was fixed at about 9 cm distance while the position of counter 2 could be read on a scale. The windows of both discriminators were adjusted on the 510-kev annihilation peak, and twofold coincidences were observed for various distances from Counter 2 to source. When the solid angle of Counter 2 is bigger than that of Counter 1, the coincidence counting rate is determined by Counter 1 and is constant. As soon as Counter 2 is moved farther away from the source, the coincidence counting rate is determined by the solid angle of Counter 2 and the counting rate drops. Counter 2 could therefore be adjusted to a position with solid angle equal to that of Counter 1. Now the individual counting rates are given by

$$N_1'=2Ne_1'\Delta\Omega/4\pi,$$
$$N_2'=2Ne_2'\Delta\Omega/4\pi,$$

where e_1' is the efficiency of Counter 1 for 510-kev photons and e_2' is the efficiency of Counter 2 for 510-kev photons. The coincidence rate is

$$K_{12}=2Ne_1'e_2'\Delta\Omega/4\pi,$$

as every photon into Counter 1 is accompanied by one in the direction of Counter 2. This gives

$$\Delta\Omega/4\pi=N_1'N_2'/2NK_{12}.$$

Now Counter 2 is moved to the 120° position such that its counting rate, and therefore its solid angle,

remains the same. The accidental twofold coincidence rate is determined in this position. The expression $\Delta\Omega/4\pi$ was found to be 1.41×10^{-2}.

The same procedure was repeated with Counters 1 and 3, giving $\Delta\Omega/4\pi=1.38\times10^{-2}$. The average value was taken as $(1.40\pm0.04)\times10^{-2}$.

Determination of e_1, e_2, and e_3

The efficiencies of the three counters for 340-kev radiation were determined with an I^{131} source emitting 364-kev photons instead of the Na^{22}. The I^{131} source had been calibrated with the 4π counter. It emits the following gamma rays with intensities as indicated:[11] 80 kev—2.17 percent; 163 kev—<0.5 percent; 284 kev—5.3 percent; 364 kev—80.0 percent; 637 kev—9.3 percent; 722 kev—2.8 percent.

With the window of the differential discriminators adjusted to the region from 200–450 kev, the 80-kev and 163-kev photons could be neglected. The scintillation spectra of the 722-kev and 637-kev photons were extrapolated from the high-energy region to 200 kev in analogy with the spectrum of the 662-kev photons from Cs^{137} and with due regard to their relative intensities. Only the photopeak of the 284-kev photons falls inside the discriminator window and this peak was drawn from the knowledge of its intensity and the resolution of the scintillation counter (see Fig. 3). The area of these three curves falling inside the region 200–450 kev was subtracted from the total gamma spectrum, giving the fraction due to the 364-kev photons as 0.88. Now the efficiency of the nth counter is given by

$$e_n=\frac{0.88N_n}{0.80D\times\Delta\Omega/4\pi},$$

where N_n is the counting rate of scintillation counter n and D is the disintegration rate of the I^{131} source.

The efficiencies of the three counters were found to be $e_1=0.357$, $e_2=0.305$, and $e_3=0.369$ (6 percent probable error). It was then assumed that the efficiencies for 340-kev photons would be near enough to these values—after adjusting the bias of the discriminator 24 kev lower.

Determination of K_3

Threefold coincidences were determined with the discriminator bias adjusted to the 340-kev photopeak—the window width remaining the same. The random coincidence rate was determined with one of the counters lifted out of the plane but with exactly the same individual counting rate. We obtained a total counting rate (coplanar) of

$$K_3+T_3=2.93\pm0.12 \text{ per minute},$$

[11] R. E. Bell and R. L. Graham, Phys. Rev. **86**, 212 (1952).

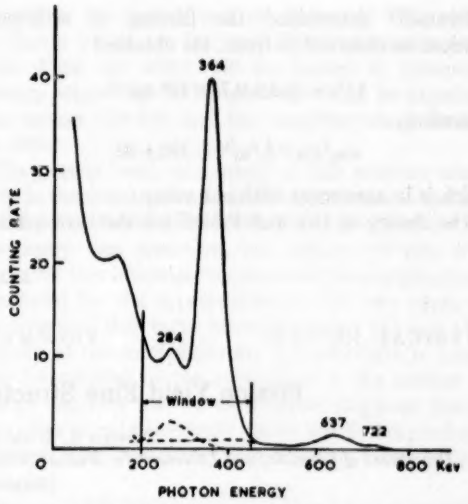

FIG. 3. Pulse distribution of photons from I^{131} showing the window of the differential discriminator as well as the extrapolated 284-, 637-, and 722-kev spectra.

and a random counting rate (out of plane) of

$$T_3=1.65\pm0.09 \text{ per minute}.$$

Therefore, the true threefold coincidence rate is

$$K_3=1.28 \text{ per minute}.$$

Substituting these values in (15) gave

$$\sigma_{2k}/\sigma_{3k}=402\pm50.$$

DISCUSSION

The difference in threefold coincidence counting rate with one counter in or out of the plane cannot be ascribed to anything else than the emission of three simultaneous quanta by the source. The annihilation of the positron by a negatron, with emission of three quanta instead of the usual two, has therefore been quantitatively confirmed by direct observation of the three quanta.

The following values for the ratio σ_{2k}/σ_{3k} between the cross sections for two- and three-photon annihilation have been obtained previously:

Theoretically

Ore and Powell[3]	370
Lifshitz[1]	235
Ivanenko and Sokolov[2]	1670

Experimentally

Rich[9] and De Benedetti and Siegel[10] observed the three-photon annihilation directly, but could only state that the order of magnitude of the effect corresponded with the value of Ore and Powell.

Deutsch[6] determined the lifetime of *ortho*-positronium as observed in freon. He obtained

$$1/^3\tau = (6.8 \pm 0.7) \times 10^6 \text{ sec}^{-1}.$$

Therefore,

$$\sigma_{2k}/\sigma_{2k} = \tfrac{1}{2}\,{}^3\tau/{}^1\tau = 398 \pm 40,$$

which is in agreement with our value.

The theory of Ore and Powell for the three-photon annihilation of a positron-negatron pair has therefore been directly confirmed. The numerical results of Lifshitz and Ivanenko and Sokolov are definitely in disagreement with our experimental results.

The author would like to express his indebtedness to the South African Council for Scientific and Industrial Research for permission to publish this paper, and to Dr. S. J. du Toit, head of the Nuclear Physics Division, for suggesting this problem.

PHYSICAL REVIEW VOLUME 96, NUMBER 3 NOVEMBER 1, 1954

Fission Yield Fine Structure in the Mass Region 99–106*

DONALD R. WILES† AND CHARLES D. CORYELL
Department of Chemistry and Laboratory for Nuclear Science, Massachusetts Institute of Technology, Cambridge, Massachusetts

(Received July 20, 1954)

Fission yield measurements were carried out in the mass region 99 to 106 to investigate previously postulated fine structure related to nuclear closed shells. Radiochemical data were obtained in this mass region in the fission reactions $U^{235}(n,f)$, $U^{238}(\gamma,f)$, $U^{235}(d,f)$, and $U^{238}(d,f)$ for the yields of Mo^{99}, Mo^{101}, Mo^{105}, Ru^{103}, Ru^{105}, and Ru^{106}. Fine structure spikes were found in all reactions. It was found that the mass position of the spikes can be explained by the assumption that primary fission fragments with 82 neutrons or 50 protons and their complements have an enhanced yield as a result of selectivity in the fission process itself. Agreement was also found with two previously known reactions: $U^{233}(n,f)$ and Cm^{242} spontaneous fission. Fine structure is also predicted for several other fission reactions.

I. INTRODUCTION

SINCE the discovery of fission in 1939, a great deal of work has been done by nuclear chemists to investigate the problem of the distribution of mass between the fission fragments. It was found quite early that fission is asymmetric, and that the distribution of mass could be described,[1] at least approximately, by a smooth curve with two broad maxima. This fact has been verified many times, for many fission reactions, and although the shape and mass position of the yield-mass curve may change somewhat, all cases of low- and medium-energy fission seem to follow the same type of mass distribution.

Several significant departures from the smooth distribution curve have been discovered, however, and in certain mass regions the smooth curve is found to be totally inadequate. The earliest indication of anomalous yields was reported by Thode and Graham,[2] who found that the measured yields of Kr^{84} and Xe^{134} were about 35 percent too high to lie on any continuous smooth curve. Stanley and Katcoff[3] found the cumulative yield of I^{136} in the thermal-neutron fission of U^{235} to be 3.1 percent, while the next member of the same chain, Xe^{136}, whose independent fission yield was estimated[4] to be about 0.4 percent, had been found by Thode and Graham[2] to have a cumulative yield of 6.1 percent. This indicated a much higher independent yield for Xe^{136} than could easily be explained. Still another anomalous fission yield was found by Macnamara, Collins, and Thode,[5] in that the fission yield of Xe^{132} was found to be 6.3 percent instead of the expected 5.0 percent. Recent studies[6,7] have led to somewhat higher absolute values for the xenon fission yields.

These so-called fine-structure phenomena, as known up to that point, were explained satisfactorily by Glendenin.[8] He postulated that in all cases where a primary fission fragment contains one neutron in excess of a closed shell (i.e., contains 51 or 83 neutrons) this extra loosely bound neutron is immediately lost. This neutron loss, considered to be entirely independent of

* This work was supported in part by the U. S. Atomic Energy Commission.

Presented in partial fulfillment for the Ph.D. degree in the Department of Chemistry, Massachusetts Institute of Technology, Cambridge, Massachusetts, November, 1953. The findings of this study were reported briefly at the Hauptversammlung of Die Deutsche Bunsen Gesellschaft, Bayreuth, Germany, May 28–29, 1954; to be published in Z. Electrochemie.

† Present address: Kjemisk Institutt, Blindern-Oslo, Norway.

[1] See, for example, C. D. Coryell and N. Sugarman, editors, *Radiochemical Studies: The Fission Products* (McGraw-Hill Book Company, Inc., New York, 1951), National Nuclear Energy Series, Vol. 9, Div. IV.

[2] H. G. Thode and R. L. Graham, Can. J. Research **A25**, 1 (1947).

[3] C. W. Stanley and S. Katcoff, J. Chem. Phys. **17**, 653 (1949).

[4] Glendenin, Coryell, and Edwards, Paper 52 of reference 1.

[5] Macnamara, Collins, and Thode, Phys. Rev. **78**, 129 (1950).

[6] S. Katcoff and W. Rubinson, Phys. Rev. **91**, 1458 (1953).

[7] A. C. Pappas, Laboratory for Nuclear Science, Technical Report No. 63, Massachusetts Institute of Technology, September, 1953 (unpublished).

[8] L. E. Glendenin, Laboratory for Nuclear Science and Engineering, Technical Report No. 35, Massachusetts Institute of Technology, August, 1949 (unpublished).

the known prompt neutron emission, results in a decrease in yield at the mass of the shell-plus-one fragment, and an equal increase in yield at the mass of the closed-shell fragment. The high fission yields of masses 133 and 134, and the anomalous yields at mass 136 were thus explained semiquantitatively as the influence of the 82-neutron shell on neutron emission. It should be noted that although this postulate has been modified by Wiles,[9] who considered the amount of neutron loss to be a function of the neutron-proton ratio as compared with the same ratio for stable nuclei, and by Pappas,[7] who extended the postulate to the third, fifth, and seventh neutrons in excess of a closed shell, based on studies of shell effects in neutron-binding energies and the emission of neutrons from fission fragments, the underlying principle of neutron loss remains essentially as conceived by Glendenin.[8]

This shifting of mass yield, as explained by Glendenin, requires that a depression in fission yields occur at about masses 135–137, to balance the excess at masses 133 and 134. Wiles,[9] in a mass-spectrometer study of the fission-produced cesium isotopes of masses 133, 135, and 137, found that no such dip occurs. To explain this, it was proposed[9] that in addition to the neutron-loss mechanism of Glendenin, an additional effect occurs, namely, that primary fission fragments with a closed shell of 82 neutrons have a somewhat enhanced yield. This "extra" primary yield or selectivity was postulated to be some function of the expected unperturbed yield of that fragment, as calculated using the postulate of equal charge displacement.[4] Fission-yield calculations based on this proposal, and on a slightly modified form of Glendenin's original hypothesis, were found to fit the experimental data quite well from mass 132 to mass 137. Pappas[7] found good agreement between the predicted and the measured values in the mass region 130 to 150 except at masses 134 and 135, where the observed values were somewhat higher than expected. In order to account for this, he, too, found it necessary to include some enhanced yield for 82-neutron fragments, as well as a lower probability for neutron emission from these fragments.

It is a necessary consequence of this proposed selectivity in the fission process that the fragment which is complementary to the 82-neutron fragment must also have an enhanced yield. It was predicted by Wiles,[10] and at about the same time independently discovered by Glendenin, Steinberg, Inghram and Hess,[11] that a fine-structure spike occurs at mass 100 in the thermal-neutron fission of U^{235}. Primary selectivity expected for 50 neutrons would occur near masses 84–85 and 147–149 in the thermal-neutron fission of U^{235}, where the fission yields are low and changing rapidly with mass. Thus the effect will be harder to interpret. Primary selectivity for 50 protons would be expected near masses 129–131 and the complementary masses 103–105.

The present work is a study of this primary selectivity in the fission process, and of its relation to nuclear closed shells, $N=82$ and $Z=50$. The region of the complementary fine structure, i.e., masses 99–105, was chosen for this investigation to avoid the complications introduced by the superposition of the two types of fine structure that occur between masses 132 and 137. A study of the complementary fine structure is somewhat complicated by the uncertainty in the number of prompt neutrons lost by each fission fragment before it becomes an experimentally observable fission product. However, this was found not to be a very serious obstacle.

Fission yields can be determined by the mass-spectrometric method only for samples which have undergone very large amounts of fission. Radiochemical determinations permit study of a much greater variety of fission processes, but pains must be taken to compare β activities on an absolute basis. Gaps occur in the information where species are too short lived to be determined quantitatively, such as at mass numbers 96, 98, 100, and 104.

II. EXPERIMENTAL

Fission yields have been determined for 14.6-min Mo^{101} and 11.0-min Mo^{102} relative to 67-hr Mo^{99}, and for 67-hr Mo^{99}, 43-day Ru^{103}, 4.5-hr Rh^{105}, and 1.0-yr Ru^{106}, all relative to 12.8-day Ba^{140}. These yields were measured in the thermal-neutron fission of U^{235}, the 13-Mev photofission of U^{238}, and in the 15-Mev deuteron fission of U^{235} and U^{238}.

Irradiation Procedures

The thermal-neutron irradiations were done at the M.I.T. cyclotron, where neutrons are produced by the $Be(d,n)$ reaction. The neutrons were thermalized by the 4-inch thick walls of a paraffin block which held the sample. The samples were irradiated either as solid UO_3 or as a solution of UO_2Cl_2 in 12M HCl.

For the photofission experiments, irradiations were made in the 13.5-Mev electron beam of the M.I.T. linear accelerator. The maximum energy of the electrons was 13.5 Mev, the most probable electron energy was 13.0 Mev. The electrons were stopped in a $\frac{1}{4}$-inch lead plate, placed immediately in front of the sample, which gave rise to a complete spectrum of bremsstrahlung with maximum energy just over 13 Mev. Irradiations were made on UO_3.

Deuteron irradiations were made in the external beam of the M.I.T. cyclotron. The energy of the deuterons striking the target was 15 Mev. Irradiations were made on natural UO_3 (U^{235}), and on nearly pure

[9] D. R. Wiles, M.Sc. thesis in chemistry, McMaster University, Hamilton, Ontario, Canada, October, 1950 (unpublished); Wiles, Smith, Horsley, and Thode, Can. J. Phys. **31**, 419 (1953).

[10] D. R. Wiles, Laboratory for Nuclear Science, Quarterly Report, Massachusetts Institute of Technology, August, 1951 (unpublished).

[11] Glendenin, Steinberg, Inghram, and Hess, Phys. Rev. **84**, 860 (1951).

U^{235}, in the form of U_3O_8, kindly loaned by the U. S. Atomic Energy Commission.

In some cases, the samples to be irradiated were so small (~10 mg) as to involve possible loss of fission fragments by recoil, or loss of fission-produced xenon by gaseous effusion. In such cases, the samples were tightly wrapped in several thicknesses (~12 mg/cm² total) of aluminum foil, and this foil was dissolved and processed with the sample.

Chemical Procedures

Molybdenum was separated from the fission mixture by extraction into diethyl ether from 6*N* HCl, after addition of Te^{IV}, Te^{VI}, and Mo^{VI} carriers. After back extraction into water, impurities such as Ga, Sb, Te, and other elements which are extracted slightly under these conditions were removed by scavenging with $Fe(OH)_3$. Technetium was found to follow the molybdenum almost completely up to this point, and rhenium was here added to act as hold-back carrier. The molybdenum was finally precipitated from the hot, buffered solution by 8-hydroxyquinoline (oxine). When the short-lived molybdenum isotopes were being studied, it was found that the separation could be done in about fifteen minutes. For this fast separation, in which only a small amount (~1 mg total weight) of molybdenum oxinate was separated, drying of the sample was done by washing the sample, on the filter paper, first with boiling water, then with dioxane, and finally with ether. The chemical yield was of no importance in these cases, because Mo^{99} was used as an internal standard for fission. The samples were mounted as the oxinate. Tracer tests showed that separation from technetium in this fast procedure is better than a factor of 200, and that separation from tellurium is a factor of 10^3 or better. Separation from all other fission products is expected to be much better than 10^5.

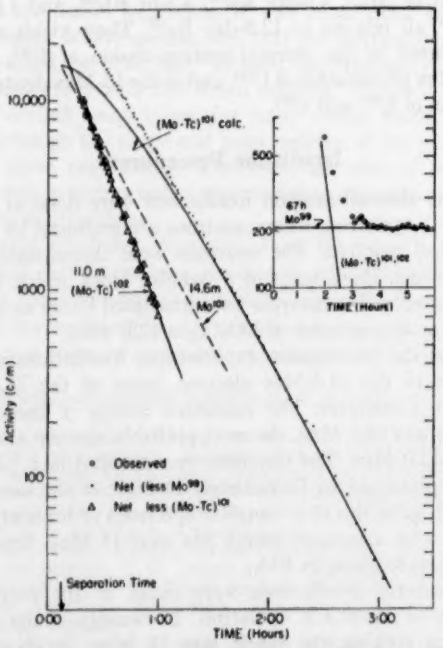

FIG. 1. Analysis of Mo-Tc decay curve.

When 67-hr Mo^{99} was being studied relative to Ba^{140}, the separation was done by the same method, but care was taken to get a stoichiometric compound, without coprecipitated reagent. Drying was done in an oven at 110° for fifteen minutes. The carrier was standardized by the same procedure.

Ruthenium separation was done by distillation of the tetraoxide with carrier from a perchloric acid solution of the fission mixture. Separation from technetium was done by precipitating the hydrous oxide, RuO_2, by reduction of the alkaline solution with alcohol. This precipitate was dissolved in HCl, and ruthenium metal was precipitated by reduction with powdered magnesium. The metal precipitate was filtered and washed with water, alcohol, and ether, and dried at 110° for ten minutes. When essentially weightless sources were needed, an aliquot, containing <20 micrograms of ruthenium, was evaporated to dryness on the source mounting. The chemical yield was determined colorimetrically by the thiourea method, using an identical aliquot.

Barium was separated by precipitation at 0°C as $BaCl_2 \cdot H_2O$ by HCl-ether reagent (1 part diethyl ether, 5 parts concentrated HCl). The precipitate was dissolved in water, and a ferric hydroxide scavenging was performed. The chloride precipitation was repeated twice, and the final precipitate was filtered and dried with alcohol, ether, and suction.

Beta Counting

The standard mounting for samples consisted of a 21-mm diameter filter paper disk (14.6 mg/cm²) onto which the sample was filtered, supported by Scotch Tape (8.5 mg/cm²), in a 1-inch hole in a 2¾-inch by 3¼-inch card. The sample was covered with a film of polystyrene (2.5 mg/cm²). For counting, this sample was supported by an aluminum shelf arrangement, about 2 cm below an end-window G. M. counter (Tracerlab TGC-1). The whole counting assembly was in an aluminum-lined lead shield with 1½-inch walls.

In order to compensate for scattering and absorption of the beta radiation by the counting assembly, by the air gap, and by the sample itself, appropriate corrections were made. The corrections used were nearly identical with those of Pappas,[7] which are derived from the work of Zumwalt,[12] Engelkemeir *et al.*,[13] and

[12] L. R. Zumwalt, Unclassified Report MonC-397 (unpublished); Atomic Energy Commission Report AECU-507 (unpublished).

[13] Engelkemeir, Seiler, Steinberg, and Winsberg, Paper 4 of reference 1.

TABLE I. Decay data used. Values marked with an asterisk (*) are from references 9 and 14; all others are from reference 15.

Species	Half-life	β-energies (Mev)
Mo^{99}	67 hr	1.23, 80%; 0.45, 20%
Mo^{101}	14.6 min*	1.2*, 70%*; 2.2*, 30%*
Tc^{101}	14.3 min*	1.4*
Mo^{102}	11.0 min*	1.2*±0.3
Tc^{102}	<25 sec	~3.5*
Ru^{103}	43 days	0.217
Ru^{105}	4.5 hr	1.15
Rh^{105m}	45 sec	~0.11 (ε^-)
Rh^{105}	36.5 hr	0.57
Ru^{106}	1.0 yr	0.04
Rh^{106}	30 sec	3.3 (weighted average)
Ba^{140}	12.8 days	1.02, 60%; 0.48, 40%
La^{140}	40.0 hr	1.32, 70%; 1.67, 20%; 2.3, 10%

Pappas.[7] Corrections could only be estimated for the equilibrium pair, 11.0-min Mo^{102}→<25-sec Tc^{102}, because of the uncertainty in the β energies. The error is felt to be small, however, because all of these samples were very thin (~1 mg/cm²), so that the self-scattering and self-absorption corrections were small and not strongly dependent on the beta energy. The counting correction factors (by which the observed counting rates were divided) for these thin molybdenum samples were 1.03, 1.06, and 1.04, respectively, for Mo^{99}, Mo^{101}, and Mo^{102}.

All counting rates were corrected for coincidence losses (determined as 1.2 percent per 100 counts/second), for chemical yield, for the size of aliquot used, and for the fraction of saturation activity produced in the irradiation.

In determinations of the fission yields of the short-lived molybdenum isotopes, counting of samples was begun 25-35 minutes after the end of the irradiation, and continued every minute for about two hours. After this time, counting was done every five minutes for 2–3 hours more, and then every fifteen minutes for several hours to establish the slope of the 67-hr Mo^{99}–6.0-hr Tc^{99m} growth-decay curve, and give the initial activity of the Mo^{99}. The long-lived molybdenum could then be subtracted from the gross activity. The tail of the remaining curve was a pure growth-decay curve of the 14.6-min Mo^{101}–14.3-min Tc^{101}.[14] A calculated curve for the total activity of this pair, computed using the calculated counting efficiency of Tc^{101} equal to 0.98 times that of the Mo^{101}, was fitted to the tail of the observed curve after subtraction of Mo^{99}. The upper end of this fitted curve gave the activity of the Mo^{101} at separation time. Subtraction of this computed curve from the observed points (less Mo^{99}) gave the decay curve of Mo^{102}–Tc^{102}. Considerable confidence in the precision of this method is given by the fact that the slope of this last decay curve was in every case found to be within ±0.3 minute of the half-life of 11.0 minutes found[14] for Mo^{102}. These successive subtractions are shown in Fig. 1 for a typical analysis.

[14] D. R. Wiles, Phys. Rev. **93**, 181 (1953); D. R. Wiles and C. D. Coryell (to be published).

Counting of Ru^{103}, which has a 217-kev β, was done from a <20-microgram sample, evaporated on a ~50 microgram/cm² film of Parlodion. A careful β absorption curve taken of this sample was extrapolated to zero absorber according to a 4.5-mg/cm² initial half-thickness, to give the total activity.

The half-lives and β energies used in this work are given in Table I.[9,14,15]

The half-lives of the zirconium and niobium isotopes of masses 101 and 102 are not known, so parent corrections could not be made at these masses. A careful estimate of the half-lives, using shell-specialized parameters[16,17] for the semiempirical mass formula, and the energy—half-life correlations of beta-decay theory, showed that Zr^{102} and Nb^{101} could have half-lives as long as 2 minutes, or as short as about one second. From this calculated maximum half-life, the maximum possible error can be calculated. In all experiments, separation times were such that the precursors would have completely decayed before separation. The possible error, then, would result only from failure to correct for production, by decay of the parent, of the desired species after the end of the irradiation. The error, which is always positive, can be derived directly from the standard decay laws, and amounts to

$$\text{Error} = \frac{T_{\frac{1}{2}}(\text{parent})}{T_{\frac{1}{2}}(\text{daughter}) - T_{\frac{1}{2}}(\text{parent})}.$$

Using a parent half-life of 2 minutes, and assuming no independent formation of the daughter, the maximum error is computed to be 16 percent for Mo^{101} and 22 percent for Mo^{102}. This error is a constant, and is independent of the nature and the time of the irradiation. An appreciable independent yield of the daughter (which is very likely in both these cases) would decrease the error. It must be emphasized that these surprisingly large errors represent maxima only, and it is probable that the real errors are much smaller, perhaps negligible. (For example, the highly likely process of branched β^- decay would greatly decrease the calculated half-life and correspondingly reduce the error.)

TABLE II. Fission yields obtained in this work. Precision is expressed as standard deviation of the mean value. Italicized values were used as reference. Parentheses indicate values of doubtful validity.

Type	Mo^{99}	Mo^{101}	Mo^{102}	Ru^{103}	Ru^{105}	Ru^{106}	Ba^{140}
$U^{235}(n,f)$	5.9 ±0.2	5.4 ±0.2	4.1 ±0.2	1.4	0.83±0.2		*6.2*
$U^{238}(\gamma,f)$	6.8 ±1.0	6.5 ±1.0	5.0 ±0.8	(1.4)	3.15±0.3		*5.77*
$U^{238}(d,f)$	1.27±0.02	1.30±0.04	1.06±0.03	0.22	1.16±0.06	0.31	*1.00*
$U^{235}(d,f)$	1.42±0.09	1.27±0.12	0.86±0.05	0.44	0.90±0.04	0.60	*1.00*

[15] Hollander, Perlman, and Seaborg, Revs. Modern Phys. **25**, 469 (1953).

[16] Coryell, Brightsen, and Pappas, Phys. Rev. **85**, 732 (1952); and Laboratory for Nuclear Science Quarterly Report, Massachusetts Institute of Technology, August, 1952 (unpublished).

[17] C. D. Coryell, Ann. Revs. Nuclear Sci. **2**, 305 (1953).

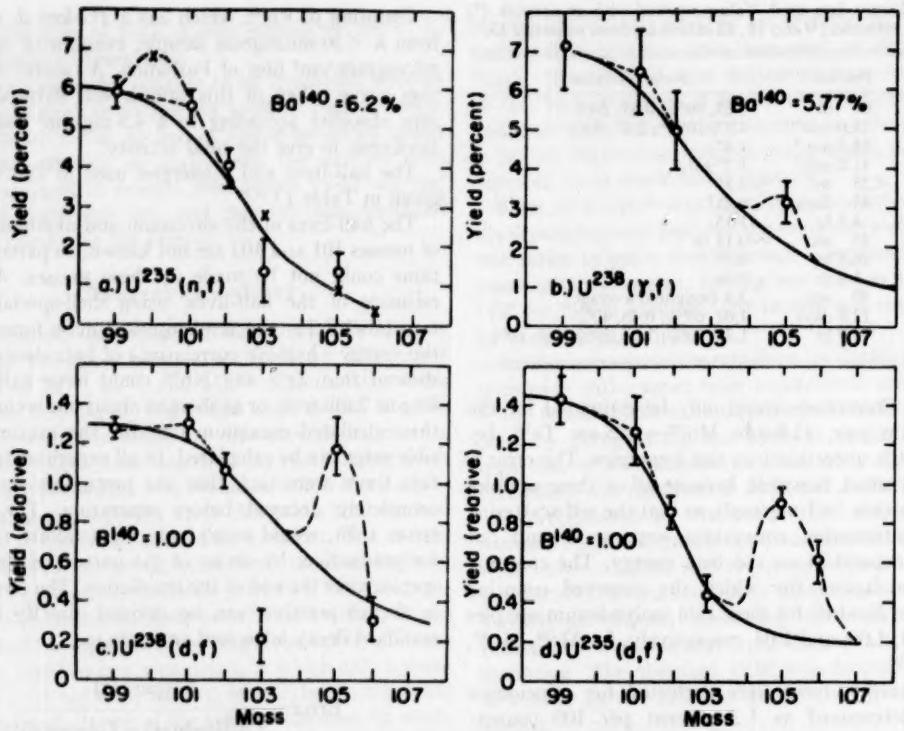

FIG. 2. Fission yields determined in this thesis. (o = this work; × = others.)

The fission yield values obtained in this work are given in Table II and are shown graphically in Fig. 2. The value of 6.2 percent is taken[1,7] for Ba^{140} in $U^{235}(n,f)$ and that of 5.77 percent is taken for Ba^{140} in $U^{238}(\gamma,f)$ according to Richter.[18] The fission yields for $U^{238}(d,f)$ and $U^{235}(d,f)$ are compared to Ba^{140} as unity. The value for Mo^{99} in $U^{235}(n,f)$ is in good agreement with the absolute value, 6.14±0.16 percent, reported by Terrill *et al.*[19] The value for Ru^{103} in $U^{235}(n,f)$ is less reliable than that of Hardwick[20] (2.85 percent), and little weight can be given to the values for Ru^{103} and Ru^{106} in Table II and Fig. 2.

In Fig. 2, the observed yields are shown as open circles, and the values given by Glendenin *et al.*[11] and by Hardwick[20] as crosses. The points for Mo^{99}, Mo^{101}, and Mo^{102} are joined by a dotted line to indicate that the relative values for the fission yields of these isotopes are known with greater precision than the absolute values, because of having been determined relative to Mo^{99}. The solid line is a proposed hypothetical "smooth curve" of fission yields, drawn with some personal prejudice. The dashed line indicates the observed fission yield curve. The difference between the observed fission yields (dashed line) and the smooth curve (solid line) is considered to be the "fine-structure yield." The magnitude of this fine-structure yield is of only qualitative interest, because of the uncertainty in the position of the smooth curve. The mass location of the fine structure, on the other hand, is felt to be quite reliable. There may be some doubt as to whether the fine structure indicated at mass 101 in parts (b), (c), and (d) of Fig. 2 is real, or whether it might be an error resulting from the parent correction discussed earlier. Moreover, the minimum shown in the dashed curve of Fig. 2b [$U^{238}(\gamma,f)$] is perhaps exaggerated. This, however, is not very important to the following discussion of fine structure.

Two other cases of complementary fine structure have been reported—in the thermal-neutron fission reaction $U^{233}(n,f)$, a fine-structure spike occurs[21] at mass 99, and in the spontaneous fission reaction $Cm^{242}(f)$, a fine-structure peak is found[22] at masses 105–106.

[18] H. G. Richter, Ph.D. thesis in Chemistry, Massachusetts Institute of Technology, August, 1952 (unpublished); H. G. Richter and C. D. Coryell, Phys. Rev. **95**, 1550 (1954).
[19] Terrill, Scott, Gilmore, and Minkkina, Phys. Rev. **92**, 1091 (1953).
[20] W. H. Hardwick, Phys. Rev. **92**, 1072 (1953).
[21] Steinberg, Glendenin, Inghram, and Hayden, Phys. Rev. **95**, 867 (1954).
[22] E. P. Steinberg and L. E. Glendenin, Phys. Rev. **95**, 431 (1954).

III. DISCUSSION

In an attempt to interpret the nature of this fine-structure effect, the following assumptions were made:

(1) The fine structure observed in the mass 99–106 region is caused by a primary selectivity in the fission process which favors[9] certain nuclei having a closed shell of 82 neutrons.

(2) It is assumed that those closed-shell nuclei are favored for which a high independent yield is predicted by the postulate of equal charge displacement.[4,7] The observations would thus not show up the yield increases for closed-shell nuclei of low smooth-curve yields.

(3) It is assumed that on an average, the fragment complementary to the closed-shell fragment will lose 2 prompt neutrons.

(4) A similar treatment should be applicable to the 50-proton shell.

Calculation of the expected unperturbed yield, as required by the second assumption, was done according to the method of Pappas,[7] based on the principle of equal charge displacement from stability for the most probable member of fission chains. The effect of shells on the variation of most stable charge, Z_p, with mass number, A, is included in Pappas' work.[7]

TABLE III. Closed-shell nuclei having high independent yields in fission, and their complements.

	$N=82$ Closed shell			$Z=50$ Closed shell		
		Complements			Complements	
Type of fission	Favored nuclei	Before neutron loss	After neutron loss	Favored nuclei	Before neutron loss	After neutron loss
$Th^{232}(\gamma,f)$	Sn^{132}	Zr^{100}	Zr^{98}	Sn^{130}	Zr^{102}	Zr^{100}
	Sb^{133}	Y^{99}	Y^{97}	Sn^{131}	Zr^{101}	Zr^{99}
				Sn^{132}	Zr^{100}	Zr^{98}
$Th^{232}(n,f)$	Sn^{132}	Zr^{101}	Zr^{99}	Sn^{131}	Zr^{102}	Zr^{100}
	Sb^{133}	Y^{100}	Y^{98}	Sb^{132}	Zr^{101}	Zr^{99}
$U^{233}(n,f)$	Sb^{133}	Nb^{101}	Nb^{99}	Sn^{129}	Mo^{105}	Mo^{103}
	Te^{134}	Zr^{100}	Zr^{98}	Sn^{130}	Mo^{104}	Mo^{102}
$U^{235}(n,f)$	Sb^{133}	Nb^{103}	Nb^{101}	Sn^{130}	Mo^{106}	Mo^{104}
	Te^{134}	Zr^{102}	Zr^{100}	Sn^{131}	Mo^{105}	Mo^{103}
$U^{238}(\gamma,f)$ and $U^{238}(f)$	Sn^{132}	Mo^{106}	Mo^{104}	Sn^{131}	Mo^{107}	Mo^{105}
	Sb^{133}	Nb^{105}	Nb^{103}	Sn^{132}	Mo^{106}	Mo^{104}
	Te^{134}	Zr^{104}	Zr^{102}			
$U^{233}(d,f)$	Sb^{133}	Mo^{102}	Mo^{100}	Sn^{128}	Nb^{107}	Nb^{105}
	Te^{134}	Nb^{101}	Nb^{99}	Sn^{129}	Nb^{106}	Nb^{104}
	I^{135}	Zr^{100}	Zr^{98}			
$U^{235}(d,f)$	Sb^{133}	Mo^{104}	Mo^{102}	Sn^{129}	Tc^{108}	Tc^{106}
	Te^{134}	Nb^{103}	Nb^{101}	Sn^{130}	Tc^{107}	Tc^{105}
				Sn^{131}	Tc^{106}	Tc^{104}
$U^{238}(d,f)$	Sn^{132}	Tc^{108}	Tc^{106}	Sn^{131}	Tc^{109}	Tc^{107}
	Sb^{133}	Mo^{107}	Mo^{105}	Sn^{132}	Tc^{108}	Tc^{106}
$Pu^{239}(n,f)$	Sb^{133}	Tc^{107}	Tc^{105}	Sn^{129}	Ru^{111}	Ru^{109}
	Te^{134}	Mo^{106}	Mo^{104}	Sn^{130}	Ru^{110}	Ru^{108}
				Sn^{131}	Ru^{109}	Ru^{107}
$Cm^{242}(f)$	Te^{134}	Ru^{108}	Ru^{106}	Sn^{129}	Pd^{113}	Pd^{111}
	I^{135}	Tc^{107}	Tc^{105}	Sn^{130}	Pd^{112}	Pd^{110}

The distribution of yield along the chain is the same as that first proposed by Glendenin *et al.*[4] This calculation has been performed for all cases for which there are fine-structure data available for comparison. The predictions of favored nuclei under these assumptions are given in Table III.

It is evident that the predicted mass location of the complementary fine structure is dependent on the number, ν, of prompt neutrons emitted by the complementary fragment. The number $\nu=2$ was chosen partly for the sake of convenience, and is quite likely not accurate. There is evidence[7] that the total number of prompt neutrons emitted in near-symmetric fission may be as low as 1.4. The region of present study is further from symmetrical fission, where ν is believed to be considerably larger. The number of neutrons lost by the complementary fragment must probably be between 1.5 and 2.0.

Table IV gives the comparison of the mass numbers observed for fission spikes with those predicted as in Table III. We are grateful to Dr. L. E. Glendenin and Dr. E. P. Steinberg for advance communication of some of their mass-spectrometric yield data[21] for $U^{233}(n,f)$ and radiochemical yield data[22] for $Cm^{242}(f)$. The remaining identifications of fine structure spikes come from Fig. 2. The fission yield of Mo^{100} in thermal-neutron fission of U^{235} is from reference 11.

It is to be noted that the experimental data reported in Table IV encompass spreads of 4 charge units and 5 neutrons in nuclei undergoing fission, and in addition a broad spread of excitation energies from spontaneous fission through fission induced by 15-Mev deuterons. There is a fairly good correlation between observed masses of fine-structure spikes and those predicted from the assumption of a primary selectivity of closed-shell structures when the mass numbers for closed-shell

TABLE IV. Comparison of observed and calculated complementary fine structure.

Type of fission	Mass location of predicted fine structure		Mass of observed fine structure
	$N=82$ shell	$Z=50$ shell	
$Th^{232}(\gamma,f)$	97–98	98–100	...
$Th^{232}(n,f)$	98–99	99–100	...
$U^{233}(n,f)$	98–99	103[a]	...
$U^{235}(n,f)$	100–101	104[a]	100–101
$U^{238}(\gamma,f)$			101[b]
	102–104	105	105
$U^{238}(f)$	102–104	105[a]	...
$U^{233}(d,f)$	98–100	104–105	...
$U^{235}(d,f)$	101–102		101[b]
		104–106	105–106
$U^{238}(d,f)$			101[b]
	105–106	106–107	105
$Pu^{239}(n,f)$	104–105	107–109[a]	...
$Cm^{242}(f)$	105–106	110–111[a]	...

[a] Fine-structure effects are expected to be quite small here because of low yield.
[b] The apparent fine structure at this mass is small.

effects occur in regions of substantial smooth-curve yields. In $U^{235}(n,f)$, the effect at mass 100 (mass spectrometric yield determination) is more prominent than that at mass 101. In the next two entries in Table IV, the mass 101 effect seems to be small, but for these and $U^{238}(d,f)$ mass 100 data are not available. The rapid fall of yields for thermal-neutron fission and spontaneous fission on approaching symmetrical fission[1,22] tends to minimize effects of the 50-proton shell.

Attempts have been made to define an empirical yield enhancement curve for closed-shell species which would be a function of smooth-curve independent yields. Such a treatment serves to support the correlations of Table IV, but is at present on too speculative a basis for detailed confidence. The accumulation of more experimental data on independent fission yields in selected cases should help ground such treatment. Treatment at the level presented in this paper predicts a relatively large separation in the $U^{233}(d,f)$ curve for the spikes complementary to $N=82$ (masses 97–99) and complementary to $Z=50$ (masses 103–105).

The statistical theory of Fong[23] provides one mechanism for selectivity of closed-shell species in the fission process. The enhanced stability of closed-shell configuration in one of the two fragments implies greater internal energy in the fission mode, thus giving higher statistical weights and fission yields for these modes. This enhancement should be slowly diluted out with increasing energy in the fission process.

Sincere thanks are expressed to the operating staffs of the M.I.T. Cyclotron and Linear Accelerator. Of these, Dr. John Winhold and Messrs. Earl White and Frank Fay have been particularly generous with their time. Mrs. Charleen Vanelli and Mrs. Grace Rowe have assisted greatly in the preparation of the manuscript, which was kindly proofread by J. W. Winchester and R. C. Fix.

The authors express their gratitude to the United States Atomic Energy Commission for supplying nearly pure U^{235}, which led directly to the discovery of the 50-proton effect.

[23] P. Fong, Ph.D. Thesis in Physics, University of Chicago, 1953 (unpublished); and P. Fong, Phys. Rev. **89**, 332 (1953).

PHYSICAL REVIEW VOLUME 96, NUMBER 3 NOVEMBER 1, 1954

γ Rays from the $C^{13}(p,\gamma)N^{14}$ and $Na^{23}(p,\gamma)Mg^{24}$ Reactions

B. Hird, C. Whitehead, J. Butler, and C. H. Collie
Clarendon Laboratory, Oxford, England

(Received July 14, 1954)

The γ rays from the 554-kev resonance of $C^{13}(p,\gamma)N^{14}$ and the 310-kev resonance of $Na^{23}(p,\gamma)Mg^{24}$ have been measured with a three-crystal pair spectrometer. Energies and intensities were measured and cascades detected by coincidence measurements. The 5.7-Mev γ-ray from $C^{13}(p,\gamma)N^{14}$ is 0.7 ± 0.6 percent of the intensity of the main 8.05-Mev radiation. The most intense radiation from $Na^{23}(p,\gamma)Mg^{24}$ was the 1.38-Mev line, and no 2.76-Mev radiation was observed.

THE three-crystal pair spectrometer[1,2] is well suited to measure weak γ rays in the presence of more intense radiation of higher energy. We have used it to investigate the γ rays from the 554-kev resonance of the $C^{13}(p,\gamma)N^{14}$ and the 310-kev resonance of $Na^{23}(p,\gamma)Mg^{24}$ reactions.

$C^{13}(p,\gamma)N^{14}$

The pair pulse-height energy distribution curve is shown in Fig. 1. The energy calibration is based upon RdTh (2.62 Mev) and Po–Be (4.45 Mev) and the assumption that the main component has an energy of 8.05 Mev.[3] The intensities of the lines, obtained from the pair cross section values of Mann, Meyerhof, and West,[4] was found to be:

Energy (Mev)	8.05	5.7 ± 0.15	4.05 ± 0.05	2.35 ± 0.02	1.66 ± 0.03
Relative intensity	100	0.7 ± 0.6	12.5 ± 2	15 ± 5	17 ± 4.

The shape of the pair peak was estimated for each energy. The asymmetrical shape of the peaks arises partly because of bremsstrahlung and electron escape and partly because all the triple coincidences do not correspond to pair formation in the central crystal. It is possible to obtain a triple coincidence when the Compton-scattered γ ray is captured in one side crystal and the bremsstrahlung from the Compton electron is captured in the other. The assumptions made in calculating the shape of pair spectrum peaks were checked by comparison with the measured shape of the known γ rays from the $F^{19}(p,\gamma)O^{16}$ and the $B^{11}(p,\gamma)C^{12}$ reac-

[1] B. Hird and C. Whitehead, Proc. Phys. Soc. (London) **67**, 644 (1954).
[2] H. I. West and L. G. Mann, Rev. Sci. Instr. **25**, 129 (1954).
[3] F. Ajzenberg and T. Lauritsen, Revs. Modern Phys. **24**, 321 (1952).
[4] Mann, Meyerhof, and West, Phys. Rev. **92**, 1481 (1953).

tions. The relative intensities of the observed γ rays can easily be obtained by quadrature once the shape of the peaks is known.

Part of the observed 2.35-Mev radiation was due to N^{13}, but this could be accurately estimated since it continued after the beam had been switched off.

The difficulty in interpretation caused by the fact that the 4.05-Mev γ ray has very nearly the same energy as the crossover radiation from the 2.35-Mev and 1.66-Mev cascade can be resolved by coincidence measurements.

The 4.05-Mev, 2.35-Mev, and 1.66-Mev lines were found to be in coincidence. This enables the 4.01-Mev crossover transition of the 2.35, 1.66-Mev γ-ray cascade to be distinguished from the 4.05-Mev radiation. Its intensity was found to be 5±5 percent of the 2.35, 1.66-Mev cascade.

Our results are in agreement with the energy level scheme discussed by Ajzenberg and Lauritsen[3] (Fig. 1, inset).

Our crossover intensity is less than that found by Woodbury, Day, and Tollestrup[5] in an investigation using a single-crystal spectrometer. Our intensity for the 5.7-Mev radiation agrees with that found experimentally in a single crystal measurement by Clegg and Wilkinson,[6] and we can exclude their alternative explanation that it was due to a 5.08-Mev line. We have discussed the point with Dr. Beghian,[7] who is now in agreement with our results.

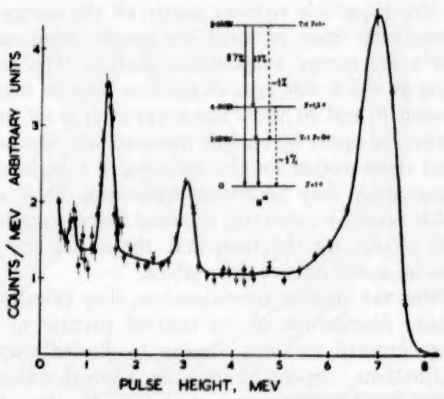

FIG. 1. Pair spectrometer pulse-height distribution of the γ rays from the $C^{13}(p,\gamma)N^{14}$ reaction.

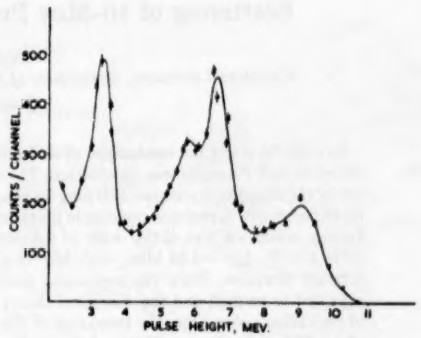

FIG. 2. Pair spectrometer pulse-height distribution of the γ rays from the $Na^{23}(p,\gamma)Mg^{24}$ reaction.

$Na^{23}(p,\gamma)Mg^{24}$

Thick targets of NaCl and Na_2SO_4 were bombarded with about 100 μa of protons.

The observed pulse-height distribution is shown in Fig. 2. The energies and relative intensities obtained were:

Energy (Mev)	10.6±0.2	7.67±0.1	6.7±0.2	4.11±0.05	1.38±0.02
Relative intensity	72±10	75±10	13±3	57±6	105±20.

The 6.7-Mev peak had the correct shape when the background due to the two higher lines was subtracted. The relative intensities were determined by the method already described, except for the 1.38-Mev line, all the measurements on which were made with a single-crystal spectrometer.

These results are in good agreement with the recent measurements of Carlson, Geer, and Nelson,[8] and show that the 1.38-Mev line is not fed from the well-known 4.14-Mev level of Mg^{24}. The peak at 4.11 Mev was found to be significantly broader than would be expected from a single γ ray. This provides further evidence in support of the decay scheme suggested by Carlson, Geer, and Nelson,[8] according to which this line is a superposition of two lines of approximately the same energy.

[5] Woodbury, Day, and Tollestrup, Phys. Rev. **92**, 1199 (1953).
[6] A. B. Clegg and D. H. Wilkinson, Phil. Mag. **44**, 1269 (1953).
[7] Hicks, Husain, Sanders, and Beghian, Phys. Rev. **90**, 163 (1953).
[8] Carlson, Geer, and Nelson, Phys. Rev. **94**, 1311 (1954).

Scattering of 10-Mev Protons on Carbon and Magnesium*

GERHARD E. FISCHER†
Radiation Laboratory, Department of Physics, University of California, Berkeley, California
(Received June 21, 1954)

In order to study the mechanism of excitation of nuclear levels by inelastic scattering, a scattering chamber of 36-inch diameter was constructed. The deflected beam of the Berkeley 60-inch cyclotron was brought out of the shielding by means of strong focusing magnets. Particles from the nuclear reactions were detected by either of two systems, a quadruple proportional-counter telescope, or a coincidence crystal spectrometer. Energy resolution was of the order of 2.5 percent. The angular distribution of protons from the reactions $C^{13}(p,p')C^{13*}$, $Q=-4.43$ Mev, and $Mg^{24}(p,p')Mg^{24*}$, $Q=-1.38$ Mev, were found to be peaked in the forward direction. Since the compound nucleus is excited to about 13 Mev, where the level density is expected to be high and the statistical theory of the nucleus should hold, it is proposed that two processes of excitation occur. One, the formation of the compound nucleus and its subsequent decay—symmetrically about 90°; two, direct collision of the incident proton with a nucleon on the surface shell of the nucleus. The elastic scattering of protons on the above nuclei was also studied and interference maxima were found. Three new levels are believed to have been confirmed in magnesium.

I. INTRODUCTION

THE inelastic scattering of particles on nuclei has been used by a large number of investigators as a way of exciting nuclear energy levels. The actual mechanism of the transfer of energy and angular momentum, however, has not been quite clear. Rhoderick[1] was the first to be concerned with this problem, for he found that the angular distribution of the inelastically scattered protons from the 1.38-Mev level in magnesium-24 was peaked in the forward direction. He was unable to reconcile this result with the idea that the excitation proceeded through compound nuclear formation. Other investigators,[2–6] working with bombarding energies of 7.3, 9.5, and 32 Mev, have also found anisotropies in the angular distribution of inelastically scattered protons. Wolfenstein[7] showed that the angular distribution arising from the decay of the compound nucleus need not be isotropic, but that if the excitation be high enough so that the density of compound nuclear states is high and the states overlap, the distribution should at least be symmetric about 90°. This follows from the assumption that interference terms between outgoing waves of different parity cancel out. Two processes that have nothing to do with the compound nucleus suggest themselves to explain the observed anisotropies. They are: either electric charge excitation,[8] or a direct collision of the incident proton with a nucleon on the surface shell of the nucleus. Electric excitation is tentatively ruled out by the large size of the observed cross section. Recently Gugelot[9] and Eisberg[10] have suggested the direct collision idea in connection with level-density determinations by inelastic scattering.

For the direct collision theory, we will follow an analysis given by Austern, Butler, and McManus[11] for $X(n,p)Y$ reactions which should be equally applicable to (n,n'), (p,n), and (p,p') reactions. These authors suggest that the direct collision process can compete with compound nuclear formation because the struck particle receives nearly all the energy and consequently may get over the barrier more readily than a low-energy evaporation particle. The energy region in which this type of reaction may be found is between 10 and 30 Mev. The lower limit is set by the barrier, the upper by nuclear transparency. The anticipated cross section for the emission of a high-energy proton group may be several millibarns. They arrive at this figure by correcting the total free n-p scattering cross section for the time that the initial and final particles spend outside the nucleus.

Using the impulse approximation, they calculate the angular distribution of the emitted particle to have sharp forward maxima, similar to Butler stripping distributions, depending on the allowed values of orbital-angular-momentum transfer. If the struck particle can be assumed to be in a single-particle state, they show that the angular distribution becomes especially simple. It is the purpose of this paper to show that the observed angular distribution of inelastically scattered protons on magnesium can be in part accounted for in this way.

A by-product of this investigation was the measurement of the elastic scattering of 10-Mev protons on magnesium and carbon. Renewed interest in this type of scattering has been expressed recently by Cohen,[12]

* The work was performed under the auspices of the U. S. Atomic Energy Commission.
† Present address: Department of Physics, Columbia University, New York.
[1] E. H. Rhoderick, Proc. Roy. Soc. (London) **201**, 348 (1950).
[2] H. E. Gove and H. F. Stoddart, Phys. Rev. **86**, 572 (1952).
[3] Burcham, Gibson, and Rotblat, Phys. Rev. **92**, 1266 (1953).
[4] Baker, Dodd, and Simmons, Phys. Rev. **85**, 1051 (1952).
[5] R. Britten, Phys. Rev. **88**, 283 (1952).
[6] R. M. Eisberg and G. Igo, Phys. Rev. **93**, 1039 (1954).
[7] L. Wolfenstein, Phys. Rev. **82**, 690 (1951).
[8] R. Huby and H. C. Newns, Proc. Phys. Soc. (London) **A64**, 619 (1951).
[9] P. C. Gugelot, Phys. Rev. **93**, 425 (1954).
[10] R. Eisberg, Phys. Rev. **94**, 739 (1954).
[11] Austern, Butler, and McManus, Phys. Rev. **92**, 350 (1953).
[12] B. L. Cohen and R. V. Neidigh, Phys. Rev. **93**, 282 (1954).

who finds a remarkable number of diffraction maxima and minima.

II. EXPERIMENTAL METHOD[13]

The arrangement of the experimental apparatus is shown schematically in Fig. 1. The deflected molecular hydrogen beam may be traced from the deflector through a $\frac{1}{4}$-inch collimating slit to the target port and into the iron snouts. Shielded from the fringing magnetic field of the machine by the iron, it passes into a long brass pipe to the 36-inch scattering chamber and subsequently to the Faraday cup for integration.

Focusing is achieved by two magnetic quadrupole lenses.[14] These lenses, whose design and action is illustrated in Fig. 2, increase the beam intensity through an eighth-inch-square collimating hole by a factor of 400 over the intensity obtainable without the lenses. Maximum beam current is 0.8×10^{-6} amp. Accurate positioning screws are provided on the mount to permit movement of the beam to the desired location. A set of three collimators defines the beam axis in the chamber.

The required motions of targets and counters in the scattering chamber are carried out by remote control.

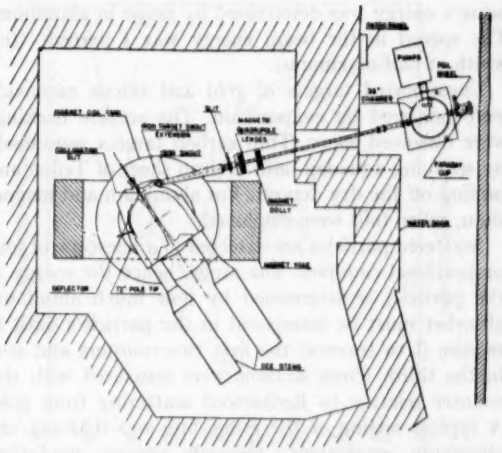

FIG. 1. Schematic diagram of the emergent beam apparatus at the 60-inch Berkeley cyclotron.

An average time of 15 minutes was consumed in reaching an operating pressure of 3×10^{-5} mm Hg. A 100 percent feedback electrometer was used to measure the charge collected by the Faraday cup and the

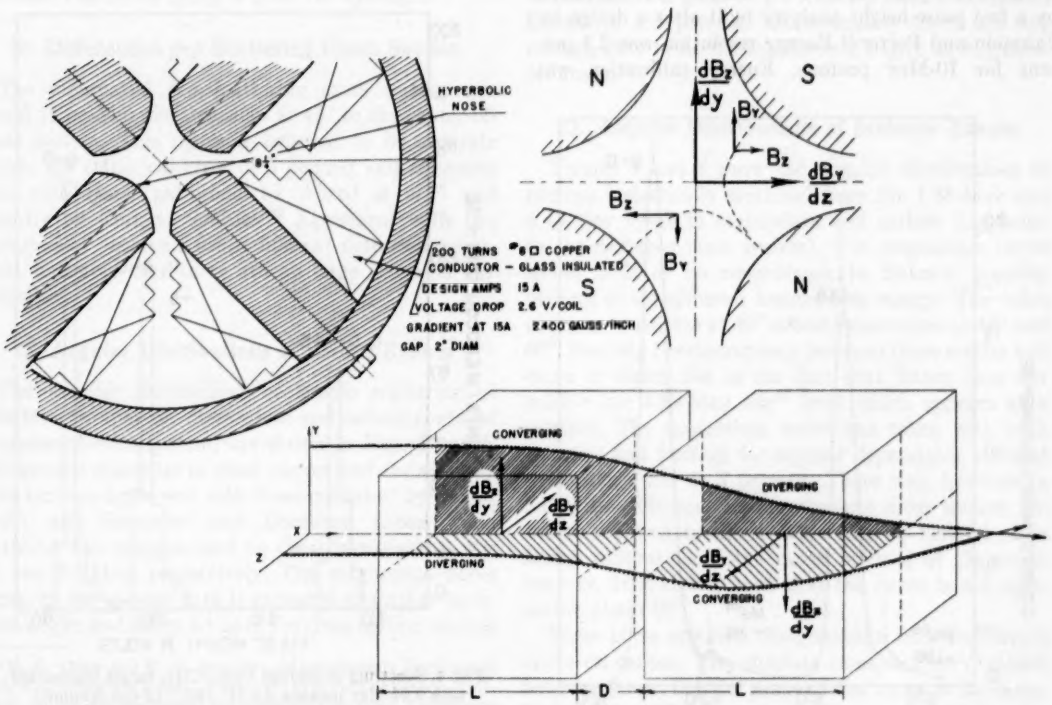

FIG. 2. Design parameters and illustration of the double-focussing properties of a magnetic lens system. $1/F=K^2L^2(\frac{1}{2}L+D)$, $K=(1/BR)(dB_y/dz)$. (Illustration after Courant, Livingston and Snyder.) See reference 14.

[13] A detailed account of the experimental technique employed may be found in University of California Radiation Laboratory Report UCRL-2546 (unpublished).

[14] Courant, Livingston, and Snyder, Phys. Rev. 88, 1190 (1952).

beam's energy was determined by range in aluminum. The spread in the beam energy was 1 percent (full width at half-maximum).

Unsupported targets of gold and silicon monoxide were prepared by evaporation. The acetate backings were dissolved away. Thin carbon targets were made by spraying aquadag onto a clean sheet of Teflon and peeling off the dry deposit. For aluminum and magnesium, rolled foils were employed.

Scattered particles are detected in a telescope of four proportional counters. The range, hence the energy of the particle, is determined by how much aluminum absorber must be interposed in the particle's path to require it to traverse the first two counters and stop in the third. Cross sections were measured with this counter relative to Rutherford scattering from gold. A typical setting of the range bite was 0.57 mg/cm² aluminum equivalent. Over-all energy resolution, largely dependent on the range straggling of the particles in the aluminum absorbers and the spread in the beam itself, was about 2.5 percent (full width at half-maximum).

Another mode of particle detection was the use of a sodium iodide crystal spectrometer in coincidence with a thin proportional counter. The thin counter identified the particle by its dE/dx. Pulse heights were measured by a fast pulse-height analyzer built after a design by Fairstein and Porter.[15] Energy resolution was 2.5 percent for 10-Mev protons. Energy calibration was achieved by identifying the observed inelastic proton groups with known levels in aluminum,[16] silicon,[17] and oxygen. Fifteen groups in all were used. Energies can be estimated to ±0.1 Mev. Angular resolution was one degree.

III. RESULTS AND CONCLUSIONS

A. Particle Groups from Magnesium and Carbon

Figure 3 shows a partial spectrum of protons resulting from the bombardment of naturally occurring magnesium with 10-Mev protons. Easily identified are the elastic and first inelastic levels of magnesium-24. It is evident that in measuring the yield from the 1.38-Mev level, the small satellite arising from Mg^{26}, whose abundance is 11.3 percent, must be subtracted. The other satellite is a contribution from the 0.46-Mev level in Mg^{26}. Other particle groups were observed with both counters corresponding to the 4.13–4.24-Mev doublet in Mg^{24} (not resolved), to the 1.89- and 2.84-Mev levels in Mg^{26}, and to 0.6- and 3.4-Mev levels in Mg^{25}. Three further groups were clearly seen with the crystal counter, corresponding to Q values of 6.3±0.1, 5.9±0.1, and 5.1±0.1 if calculated for Mg^{24}. These have in part been reported also by Hausman *et al.*,[18] Gove and

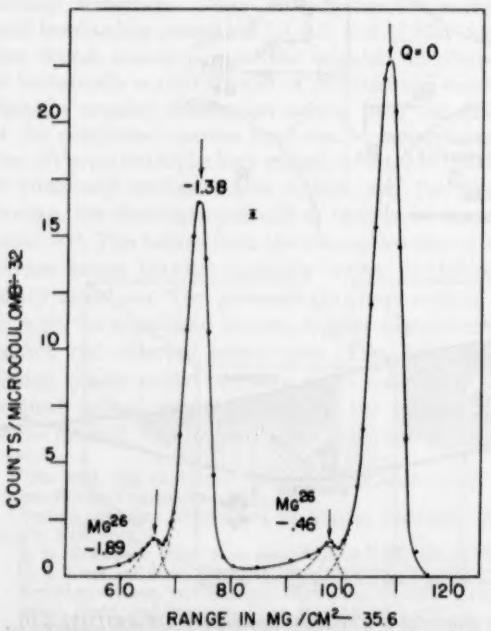

FIG. 3. Partial spectrum of protons from the reaction $Mg(p,p')Mg^*$ at 90° and 10 Mev (Range interval = 0.57 mg/cm².)

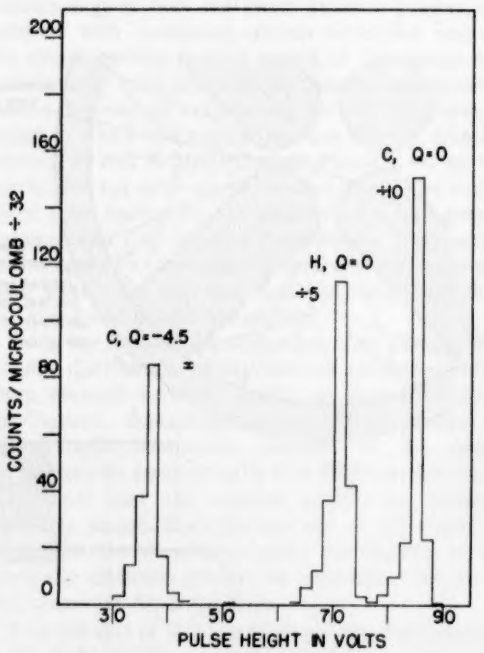

FIG. 4. Spectrum of protons from $(CH)_n$ target bombarded with 9.94-Mev protons, $\theta = 24°$ (lab). (2-volt window).

[15] E. Fairstein and F. M. Porter, Rev. Sci. Instr. **23**, 650 (1952).

[16] Reilley, Allen, Arthur, Bender, Ely, and Hausman, Phys. Rev. **86**, 857 (1952).

[17] D. E. Alburger and E. M. Hafner, Revs. Modern Phys. **22**, 376, 343 (1950).

[18] Hausman, Allen, Arthur, Bender, and McDole, Phys. Rev. **88**, 1296 (1952).

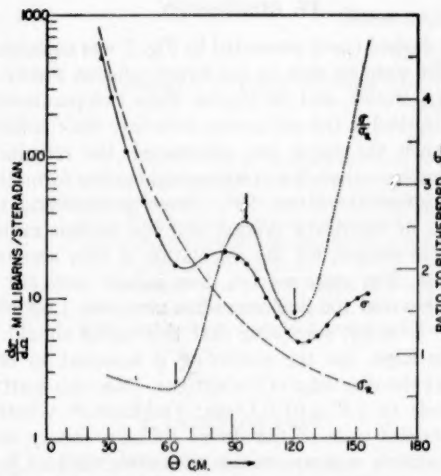

FIG. 5. The angular distribution of elastically scattered protons from Mg at 10 Mev.

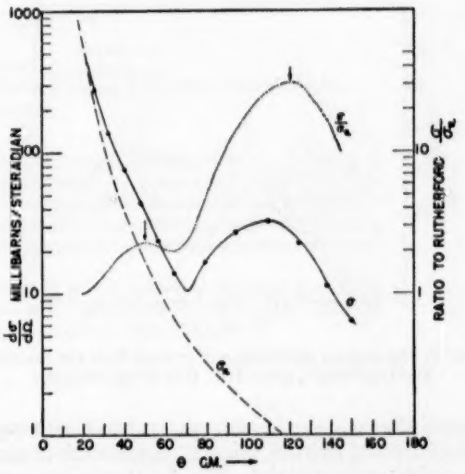

FIG. 6. The angular distribution of elastically scattered protons from carbon at 10 Mev.

Stoddart,[19] and Baker, Dodd, and Simmons.[4] The 6.3-Mev level has previously been assigned to Mg^{24}.[20] Figure 4 shows the spectrum of protons from a polystyrene $(CH)_n$ target bombarded with 9.94-Mev protons. The center group is from the hydrogen.

B. Differential *p-p* Scattering Cross Section

The differential *p-p* scattering cross section was found to be 54.6 mb/steradian at 48° in the center-of-mass system. This figure is believed to be accurate within the statistical error of 3 percent and compares well with those published by Allred *et al.*,[21] and recently by Cork at 9.6 Mev.[22] Agreement with two independent observers using different detection equipment indicates that there are no large errors in our technique.

C. Angular Distributions of Elastic Events

The angular distribution of elastic scattering of 9.94-Mev protons on magnesium and carbon (reduced to center-of-mass system) are shown in Figs. 5 and 6. The general character of these curves and the absolute cross sections agree well with those published by Baker, Dodd, and Simmons[4] and Burcham, Gibson, and Rotblat.[3] The energies used by these investigators was 9.6 and 9.5 Mev, respectively. The magnesium curve shown in the present data is extended to further backward angles and shows a rise in the cross section leading to a second maximum. Since these data were taken at the same time as the hydrogen cross section was measured, it is felt that the absolute cross sections are accurate to within ±3 percent. The angular measurement is good to ½°. Relative cross sections are known to 2.5 percent. Unfortunately there are not enough data to fix the interference angles with greater accuracy.

D. Angular Distributions of Inelastic Events

Figures 7 and 8 show the angular distributions of protons inelastically scattered from the 1.38-Mev and 4.43-Mev levels in magnesium and carbon (corrected to the center-of-mass system). The magnesium curve shows little or no resemblance to Baker's, possibly because of the different bombarding energy. The value of the cross section at 30° is well below those at 45° and 60°. Possibly the discrepancy between these results and those of Baker lies in the fact that Baker does not resolve the 1.89-Mev Mg^{26} level which appears as a satellite. The magnesium curve was taken with both counters and findings for angular dependance checked with each other to 3 percent. There was, however, a 5 percent difference in the absolute cross section between the two methods. This can be blamed on a faulty calibration of the range interval of the range counter. It is clearly seen that the curve is not symmetric about 90°.

There is no essential disagreement with Burcham's curve on carbon. The absolute cross sections obtained here are lower, but the shape of the curve is the same. I disagree with their conclusion that the curve is symmetric about 90° because the points of these data, although not as many in number, have better statistics (1.5 percent). They fall within their quoted statistical error. An examination was made to see whether the

[19] H. E. Gove and H. F. Stoddart, Massachusetts Institute of Technology Progress Report, February, 1952 (unpublished), p. 67.
[20] K. Boyer, Massachusetts Institute of Technology, Laboratory of Nuclear Science and Engineering Progress Report, July, 1950 (unpublished), p. 174.
[21] Allred, Armstrong, Bondelid, and Rosen, Phys. Rev. **88**, 433 (1952).
[22] B. Cork, University of California Radiation Laboratory Report UCRL-2373 (unpublished).

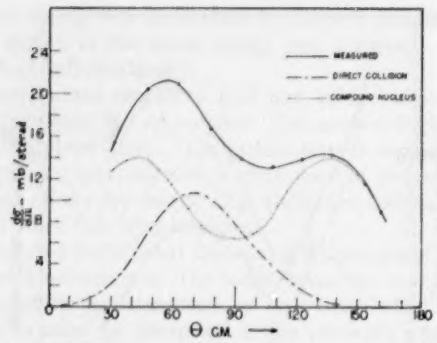

FIG. 7. The angular distribution of protons from the reaction $Mg^{24}(p,p')Mg^{24*}$, $Q=-1.38$. (For detail see text.)

counter efficiency varied with energy, hence with angle, of the incoming particle. Possible asymmetries in target alignment were checked. The conclusion was that errors from these sources were 3 percent at the very most. No data exist for 45°, for at this angle the hydrogen elastic peak overlaps the inelastic peak and a subtraction of the hydrogen cross section cannot be made accurately.

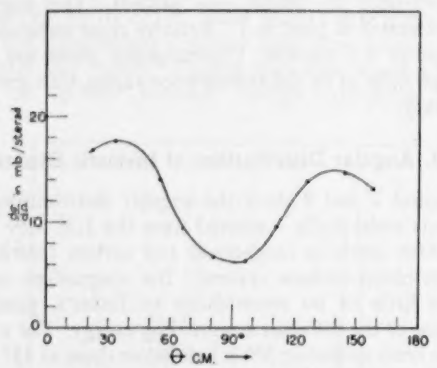

FIG. 8. The angular distribution of protons from the reaction $C^{13}(p,p')C^{13*}$, $Q=-4.4$.

IV. DISCUSSION

The dashed curve presented in Fig. 7 was calculated from the simplest case in the direct collision theory of Austern, Butler, and McManus. Only two parameters were required in the calculation to satisfy the condition that when the curve was subtracted, the remaining contribution—that due to compound nuclear formation—be symmetric about 90°. These parameters, the amount of the direct process and the nuclear radius, are quite unique, for the calculation is very sensitive to them. The cross section does indeed turn out in millibarns and the nuclear radius used was 1.6×10^{-13} $A^{\frac{1}{3}}$ cm. It is not surprising that this radius should be a little large, for the scattering is assumed to take place at the very edge of the nucleus. (Neutron scattering leads to $1.57\times10^{-13}A^{\frac{1}{3}}$ cm: Feshbach.)[23] Whether the simplest case of the direct collision theory may be applied to magnesium (an even-even nucleus), and whether a statistical theory may be applied to the compound nuclear part (only 10 levels enter at this excitation) is not certain, but the results indicate that this is a start on the problem.

As for the elastic data, it is interesting to note that the angles at which diffraction effects are found in carbon and magnesium at 10 Mev are all proportional to those found by Cohen at 20 Mev by the same factor, namely, 1.39. If diffraction effects should indeed be proportional to λ, the wavelength of the incident proton in the center-of-mass system, the factor should be 1.48.

The author wishes to express his sincere gratitude to Professor A. C. Helmholz for his valuable guidance and support in all phases of the work. The ample assistance of Mr. Robert Ellis and Mr. F. Vaughan is gratefully acknowledged. The author is also indebted to Dr. Warren Heckrotte for several discussions on the analysis of the inelastic data and to all the members of the 60-inch cyclotron crew and staff who made this investigation possible.

[23] H. Feshbach and V. F. Weisskopf, Phys. Rev. 76, 1550 (1949).

Resonances in $Li^7(p,n)Be^7$†

ROBERT K. ADAIR
University of Wisconsin, Madison, Wisconsin, and Brookhaven National Laboratory, Upton, New York

(Received July 30, 1954)

An investigation of experimental data concerning the $Li(p,n)$ reaction indicates that the resonance at 2.25-Mev proton energy is due to the influence of a spin 3, isotopic spin 1, even parity level of Be^8, 19.2 Mev above the ground state, and that the background reaction intensity is predominantly the result of a spin-1 state of odd parity, and a spin-2 state of odd parity and isotopic spin 0. Cross sections, angular distributions, and neutron polarizations calculated on this basis are in good agreement with previous experimental measurements of these quantities.

The neutron and proton widths of the isotropic spin-1 state in Be^8 are related to the neutron width of the corresponding isotopic-spin-1 state of Li^8, 2.3 Mev above the ground state, in a manner consistent with the transition probability relationships expected of a nuclear isotopic spin multiplet.

I. INTRODUCTION

MEASUREMENTS of the reaction constants of the $Li^7(p,n)Be^7$ reaction by Taschek and Hemmendinger[1] have been analyzed by Breit and Bloch,[2] who concluded that the experimental results were most likely indicative of an odd parity level in Be^8, 19.2 Mev above the ground state. The observed angular distribution was interpreted as indicating an interference between states of opposite parity and hence the reaction background was believed to be due primarily to P-wave neutrons. Breit and Bloch noted that an alternative view was also admissible; the resonance resulted from the interaction of P-wave neutrons. Since the centrifugal barrier is high for P-wave neutrons and protons, the explanation in terms of a P-wave resonance appeared to require an improbably strong resonance strength, indicating that the explanation in terms of an $L=0$ resonance was more likely.

However, in the five years which have elaspsed since this interpretation was published, a considerable body of experimental information has been accumulated which bears obliquely on this problem. In particular, the occurrence of strong or broad resonances has been shown to be common,[3] and the best value of the effective nuclear radius to use in barrier calculations appears to be rather larger[3] than that used by Breit and Bloch. If a larger radius is used in the calculations, the computed height of the barrier is lower, the resonance strength required for P neutrons is not as large, and the objections to the consideration of a P-wave resonance are weakened. It has recently been emphasized that the charge independence of nuclear forces has important consequences on nuclear reactions.[4,5] Since the Be^8 states of interest in the $Li(p,n)$ reaction have a definite isotopic spin and break up into the states Li^7+n and Be^7+p, which differ only in isotopic spin, transition probability relationships will obtain[5] which should aid considerably in interpreting the data. In view of these considerations it seemed that it would be useful to reinvestigate this problem.

II. ASSIGNMENT OF RESONANCE PARAMETERS

The lowest isotopic spin one level in Be^8, corresponding to the ground state of Li^8, appears to lie about 16.9 Mev above the ground[6] state of Be^8. Resonant scattering of neutrons by Li^7 indicates the presence of a state in Li^8, 2.3 Mev above the ground state,[7] which has a spin of 3 and even parity.[8] Charge independence of nuclear forces then necessitates the presence of an equivalent state in Be^8 which appears to be the 19.2-Mev state identified with the resonance in the $Li(p,n)$ reaction.

Arguments independent of the presence of the Li^8 state support the assignment of spin 3 and even parity to the Be^8 level. The value of the reaction cross section at resonance must be

$$\frac{(2J+1)}{(2I+1)(2S+1)}\pi\lambda^2\frac{4\Gamma_n\Gamma_p}{(\Gamma_n+\Gamma_p)^2}, \tag{1}$$

where J is the spin of the compound state and I and S are the spins of the interacting particles, $\frac{1}{2}$ and $\frac{3}{2}$. The Γ_n and Γ_p are the widths for neutron emission and proton emission respectively, and λ is the wavelength/2π of the incident proton. The resonant part of the $Li(p,n)$ cross section reaches a maximum value[9] of nearly 0.25 barn, at an incident proton energy of 2.25 Mev. The maximum value allowed is $(2J+1)/8\times0.375$ barns, when $\Gamma_n=\Gamma_p$. This immediately excludes states of $J=1$ and allows $J=2$ only in the somewhat improbable event

† Work supported by the U. S. Atomic Energy Commission and the Wisconsin Alumni Research Foundation.

[1] R. Taschek and N. Hemmendinger, Phys. Rev. **74**, 373 (1948).
[2] G. Breit and I. Bloch, Phys. Rev. **74**, 397 (1948).
[3] T. Teichmann and E. P. Wigner, Phys. Rev. **87**, 123 (1952).
[4] L. A. Radicati, Proc. Phys. Soc. (London) **A66**, 139 (1953).
[5] R. K. Adair, Phys. Rev. **87**, 1041 (1952).
[6] M. Gell-Mann and V. Telegdi, Phys. Rev. **91**, 169 (1953).
[7] R. K. Adair, Phys. Rev. **79**, 1018 (1950).
[8] P. Stelson and W. Preston, Phys. Rev. **84**, 162 (1951).
[9] The cross section values of reference 1 refer to energies based on a scale where the $Li(p,n)$ threshold is 1.86 Mev. The energies have been recalculated for the purpose of this report, on the basis of the presently accepted scale where the $Li(p,n)$ threshold is 1.882 Mev.

that Γ_n is nearly equal to Γ_p. The large value of the Li(p,n) cross section near threshold indicates the background part of the reaction cross section must be largely the result of S-wave neutrons. This conclusion is strongly substantiated by the high value found for the inverse Be$^7(n,p)$Li^7 reaction cross section at thermal neutron energies.[10] The variation[1] with energy at resonance of the part of the differential cross section proportional to $\cos\vartheta$ is characteristic of the interference of an S-wave background with P waves at a resonance. Since Li^7 has odd parity the state in Li^8 must then be even. Since there is evidence that α particles are not emitted appreciably from this level,[11] we can, on these grounds, further exclude the possibility that the state has spin 2 and isotopic spin 0, as such a state should have a high probability for disintegration into two alpha particles.

If it is assumed on the basis of these arguments that the Be^8 state has spin 3, even parity, and isotopic spin one, it presumably forms a charge multiplet together with the 2.3-Mev state in Li^8 and a presently undiscovered state of B^8. Since the states of the charge multiplet are in the continuum it is possible to obtain information concerning the equivalence of the wave functions of states comprising the multiplet by examining the widths for particle emission. If nuclear forces are charge-independent, the wave functions of the compound states and the wave functions of the final states will differ, respectively, only in isotopic spin space. We can write the isotopic spin wave functions of the mirror nuclei Li^7 and Be^7 as $\varphi_{\frac{1}{2}}{}^{\frac{1}{2}}$ and $\varphi_{\frac{1}{2}}{}^{-\frac{1}{2}}$, the neutron and the proton $\tau_{\frac{1}{2}}{}^{\frac{1}{2}}$ and $\tau_{\frac{1}{2}}{}^{-\frac{1}{2}}$, respectively, and the Li^8 and Be^8 levels as $T_1{}^1$ and $T_1{}^0$, where the subscript represents the total isotopic spin and the superscript stands for the third component. Only the isotopic spin part of the matrix elements for the breakup of Li^8 and Be^8 will differ. These are easily calculated:

$$\begin{aligned}&(T_1{}^1|\,\varphi_{\frac{1}{2}}{}^{\frac{1}{2}}\tau_{\frac{1}{2}}{}^{\frac{1}{2}})=1,\\&(T_1{}^0|\,\varphi_{\frac{1}{2}}{}^{\frac{1}{2}}\tau_{\frac{1}{2}}{}^{-\frac{1}{2}})=(T_1{}^0|\,\varphi_{\frac{1}{2}}{}^{-\frac{1}{2}}\tau_{\frac{1}{2}}{}^{\frac{1}{2}})=1/\sqrt{2};\\&(T_0{}^0|\,\varphi_{\frac{1}{2}}{}^{-\frac{1}{2}}\tau_{\frac{1}{2}}{}^{\frac{1}{2}})=-(T_0{}^0|\,\varphi_{\frac{1}{2}}{}^{\frac{1}{2}}\tau_{\frac{1}{2}}{}^{-\frac{1}{2}}).\end{aligned}\qquad(2)$$

We write the whole matrix element as γ_s for (Li^8|Li^7+n), γ_p for (Be^8|Li^7+p), and γ_n for (Be^8|Be^7+n). The reaction widths, Γ, will be equal[12] to $2k\gamma^2(F^2+G^2)^{-1}$, where k is the wave number and F and G are the usual regular and irregular free-particle radial wave functions[13] evaluated at an effective nuclear radius a. By following Christy and Latter,[14] a radius a of $1.45(A^{\frac{1}{3}}+1)\times10^{-13}$ cm was used in the calculations. If one allows for the variation of level shift with energy,[15] $|\gamma_s|$ was found to be equal to $(1.6\times10^{-13}$ Mev cm$)^{\frac{1}{2}}$ from the measured width of the Li^8 level. From relations (1), $\gamma_n=\gamma_p=(0.8\times10^{-13}$ Mev cm$)^{\frac{1}{2}}$, where only the relative signs of the γ are important. A resonance energy $E=E_\lambda-\Delta=1.96$ Mev was assigned in the center-of-mass system, and the resonant part of the Li(p,n) cross section was calculated by using the relation

$$\sigma_{np}=\frac{2J+1}{(2S+1)(2I+1)}\,\frac{\pi\lambda^2\Gamma_n\Gamma_p}{(E+\Delta-E_\lambda)^2+\Gamma^2/4}.\qquad(3)$$

The points on Fig. 1 show the measured values of the total Li(p,n) cross section.[1] The difference between the dashed line and the solid line represents the resonance contribution calculated from relation 2. The excellence of the fit to the resonance cross section variation shown by the experimental points is evidence for the charge independence of nuclear forces and that $(F^2+G^2)^{-1}$ evaluated at a radius of $1.45(A^{\frac{1}{3}}+1)\times10^{-13}$ cm is a good measure of barrier penetrability.

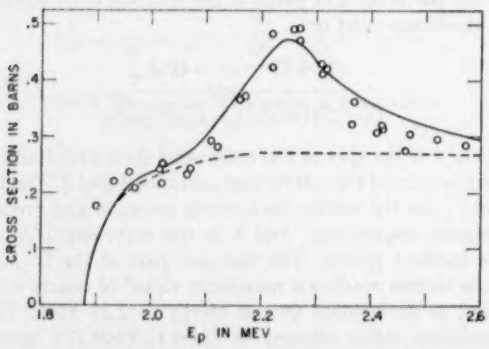

FIG. 1. Total Li(p,n) reaction cross section. The points are taken from the data of reference 1. The solid curve represents the cross section calculated from the considerations of this paper. The area beneath the dashed line is the contribution of the S-wave reaction, the area between the dashed and solid curve is the resonance cross section.

III. S-WAVE INTERACTION

The part of the P-wave neutron amplitude in which the Z component of the total intrinsic spin is conserved will be coherent with, and interfere with, the neutron S-wave amplitude associated with the same spin multiplicity. The magnitude of the interference term will then be proportional to the quintet S-wave neutron amplitude, the coherent part of the P-wave amplitude, and the cosine of the phase angle between them. Since the S wave is isotropic, the interference term will have the angular dependence of the P wave, which, since the Z component of the spin is conserved, will be proportional to $\cos\vartheta$, where ϑ is the angle between the incident proton beam and the reactant neutrons measured in the center-of-mass system. As the phase and magnitude of the P-wave amplitude can be determined from the

[10] Reported by G. C. Hanna at the Birmingham Conference on Nuclear Physics, July, 1953 (unpublished).

[11] Heydenburg, Hudson, Inglis, and Whitehead, Phys. Rev. **73**, 241 (1948).

[12] E. Wigner and L. Eisenbud, Phys. Rev. **72**, 29 (1948).

[13] Bloch, Hull, Broyles, Bouricius, Freeman, and Breit, Revs. Modern Phys. **23**, 147 (1951).

[14] R. F. Christy and R. Latter, Revs. Modern Phys. **20**, 185 (1948).

[15] R. G. Thomas, Phys. Rev. **81**, 148 (1951).

resonance parameters, the experimentally observed values of the part of the differential cross section which is proportional to $\cos\vartheta$ will be a measure of the phase and magnitude of the S-wave neutron amplitude.

From the magnitude of the total background reaction cross section as well as the large values of the part of the angular distribution proportional to $\cos\vartheta$, it appears that the cross section for production of both triplet and quintet states of Be^7 and an S-wave neutron must be large in terms of the maximum allowed by the conservation laws: $(2J+1)\pi\lambda^2/8$. It seems probable, then, that the main contribution to the reaction amplitude for each intrinsic spin state is due either to a broad nearby level of Be^8, or to the tails of a number of far away states, almost all of which have the same isotopic spin. Since, from relation (1), the reaction matrix elements of states with different isotopic spin differ in sign, reaction amplitudes for such states will on the average interfere destructively, reducing the reaction cross section. A reaction amplitude can be represented conveniently in terms of the reduced derivative matrix of Wigner and Eisenbud, and Teichmann and Wigner.[3,12,16] A reaction amplitude then takes the form

$$A=g\lambda_p\exp(i\delta_n+i\delta_p)\times\frac{ik_p^{\frac{1}{2}}(F_p^2+G_p^2)^{-\frac{1}{2}}R_{np}k_n^{\frac{1}{2}}(F_n^2+G_n^2)^{-\frac{1}{2}}}{1-\frac{1}{a}\sum_{j=n,p}R_{jj}\left[\frac{d\ln(F_j^2+G_j^2)^{\frac{1}{2}}}{d\ln k_j a}+ik_j a(F_j^2+G_j^2)^{-1}\right]},\quad(4)$$

where δ_n is equal to the hard sphere scattering phase shift for neutrons; $\exp 2i\delta_n=(G_n-iF_n)/(G_n+iF_n)$ and δ_p is a similar phase shift for protons;

$$\exp 2i\delta_p=\frac{G_p-iF_p}{G_p+iF_p}\frac{l+i\eta\cdots 1+i\eta(i\eta)!}{l-i\eta\cdots 1-i\eta(-i\eta)!},\quad(5)$$

where $\eta=3e^2/\hbar V$. The g is a geometric quantity depending on the orbital angular momentum, intrinsic spins of the reacting particles, total angular momentum of the state, and the channel spin. As written here, g includes the spins and angular dependence characteristic of those states. The values of g for the S-wave and P-wave amplitudes were computed[17] using the Clebsch-Gordon coefficients tabulated by Condon and Shortley.[18] The elements of the R matrix R_{jk} equal $\sum_\lambda \gamma_{j\lambda}\gamma_{k\lambda}/E_\lambda-E$, where $\gamma_{j\lambda}=(\hbar^2/2\mu)^{\frac{1}{2}}\int X_\lambda V_j dS$, where X_λ is a nuclear eigenfunction, V_j is the wave function in the channel j, and the integration over the nuclear surface includes a summation over intrinsic spins and isotopic spins. When one value of the isotopic spin T is dominant, from relation 1: $R_{nn}=R_{pp}=(-)^{T+1}R_{np}$, and the phase of the scattering amplitude will depend upon the value of T. Since the interference intensity is proportional to the cosine of the phase angle between the amplitudes of different states, the sign of the interference term will depend upon the relative isotopic spin of the two states. The dashed line in Fig. 2 shows the value of the coefficient of $\cos\vartheta$ derived by Taschek and Hemmendinger from their experimental results, and the solid line represents a calculated value of $\cos\vartheta$. For this computation the single-level approximation was used for the P-wave resonance; $R_{jk}=\gamma_j\gamma_k/(E_\lambda-E)$ with the parameters introduced in Sec. II. Far from a resonance, R will not vary strongly with energy. For the quintet S-wave amplitude, R was chosen to be 7×10^{-13} cm and the isotopic spin was taken as zero. If the quintet S-wave isotopic spin were one, the sign of the asymmetry coefficient would be reversed and in contradiction with the experimental results. The sign of R used for the S-wave resonance is that which would result from the contribution of far-off high energy levels. Actually the results are not sensitive to the magnitude of R if $R>a$. Also shown in Fig. 1 are the coefficients of $P_2(\cos\vartheta)$ determined from the measured angular distributions and calculated from the P-wave reaction parameters. The agreement is not bad when the large error involved in extracting this quantity from the experimental data is considered.

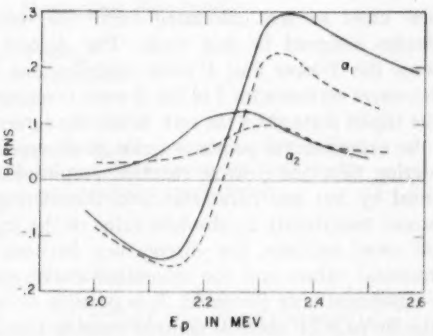

FIG. 2. Energy dependence of the coefficients a_1 and a_2 of the Legendre polynomial fit to the center of mass differential cross sections. As in reference 1 the units of the a's are adjusted so that $4\pi d\sigma/d\omega=a_0P_0(\cos\vartheta)+a_1P_1(\cos\vartheta)+a_2P_2(\cos\vartheta)$. The dashed lines are the experimental results from reference 1; the solid lines represent the values calculated in this report.

We can obtain no information on the triplet S-wave reaction from an examination of the S-P interference term because states of different total spin do not interfere in differential cross section. Since the background reaction cross section is larger than the conservation laws permit for quintet S-wave scattering alone, and the asymmetry in the scattering is satisfactorily accounted for by quintet states, it appears that the triplet S-wave interaction is important. For the sake of definiteness the same parameters were used to calculate the triplet cross section as were used for the quintet state. The solid curve in Fig. 1 represents the total

[16] J. M. Blatt and L. C. Biedenharn, Revs. Modern Phys. 24, 258 (1952), in particular, Eqs. (5, 6).
[17] See, for example, reference 11.
[18] E. U. Condon and G. H. Shortley, *Theory of Atomic Spectra* (Cambridge University Press, Cambridge, 1935).

reaction cross section calculated from the reaction amplitudes assigned in this work. The dashed line separates the S-wave and P-wave contributions. The quintet states accounts for $\frac{5}{8}$ of the S-wave cross section and the triplet state gives the rest. While the agreement with the experimental points is quite good, especially considering that the S-wave reaction amplitudes are described by but one parameter, and considering the 12 percent uncertainty in absolute value of the experimental cross sections, the discrepancy between the experimental values and the theoretical curve appear to be significant near threshold. It is possible to calculate the $Be^7(n,p)Li^7$ thermal neutron cross section from the $Li^7(p,n)Be^7$ cross section using the principle of detailed balance. If the Be^7 thermal neutron cross section is the result of isolated definite resonances in each of the two spin states application of relations 1 and 2 shows that the maximum total cross section allowed is

$$\sigma_{np}=4\pi k_n^{-2}\frac{\Gamma_n\Gamma_p}{(\Gamma_p+\Gamma_n)^2}\approx 4\pi k_n^{-2}\frac{\Gamma_n}{\Gamma_p}$$
$$=4\pi\lambda_n\lambda_p(F_p^2+G_p^2)\approx 1.85\times 10^4 \text{ barns.} \quad (6)$$

While the cross section calculated from the parameters of this paper is almost equal to that maximum, it is considerably lower than the value of about 5×10^4 barns reported by Hanna.[10]

So high a $Be^7(n,p)$ thermal cross section, and equally, so fast a rise of the $Li^7(p,n)$ reaction cross section near threshold cannot then be attributed solely to a resonance if the concept of charge independence of nuclear forces is to be retained. Rather, as can be seen from Eq. (3), the high cross sections must be the result of interference between states of different isotopic spins which have R-matrix elements R_{np} of the same sign. A simple example is the interference of two states of different isotopic spins, one lying above, one below threshold. The $T=1$ state which appears to contribute may be related to the Li^8 state, reported by Levine *et al.*[19]

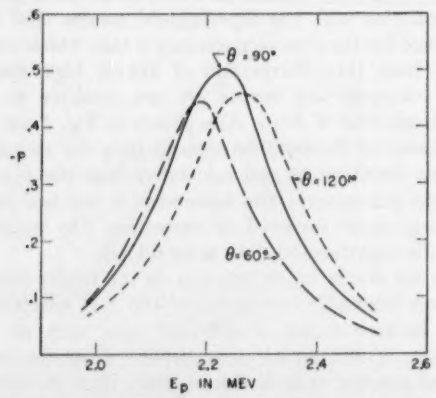

FIG. 3. Values of the polarization P of neutrons produced by the $Li(p,n)$ reaction as calculated from the parameters of this paper.

IV. NEUTRON POLARIZATION

The existence of the isolated spin-3 even-parity state of Be^8 is an effect of the strong spin-orbit coupling found in nuclei. In general a spin-orbit force will result in a polarization of the products of a nuclear reaction. Since effects of the spin-orbit energy are determined kinematically from the parameters of the resonance, without the necessity of obtaining further information concerning the source of this energy, it is possible to calculate the polarization of the neutrons from the $Li(p,n)$ reaction. The polarization of neutrons in the X direction, where Z is the direction of the incident protons, will be equal to $(A^*|\sigma_x|A)/(A^*|A)$, where A represents the total reaction amplitude, including spins, and σ_x is the usual spin operator. The calculation, which was straightforward, was performed by the usual addition and resolution of angular momentum vectors,[16] using for the P-wave and quintet S-wave amplitudes the values discussed previously. Although the σ_x operator will mix states of different total spin, triplet and quintet states do not interfere in this case[18] because the initial Li^7+p triplet and quintet states are incoherent and total spin is conserved in the approximation used; that is, neglect of D and F waves.[20] Therefore, the polarization depends only upon the quintet amplitudes and is likely to be fairly reliable. Figure 3 shows the polarization of neutrons emitted at angles of 60°, 90° and 120° in the center-of-mass system as a function of neutron energy. To be properly compared with experimental data the curves should be shifted to higher energy by about 25 kev, which is the energy discrepancy between the experimental and measured angular distributions at resonance as shown in Fig. 3. A measurement[21] of the polarization at an angle of 66° in the center-of-mass system at a proton energy of 2.23 Mev gave a result of $P=-0.53\pm 0.06$ as compared to a value of about -0.45 taken from the parameters of this paper. Considering the approximations made in the calculations the agreement seems satisfactory.

It might be expected that the protons scattered at these energies will also be partially polarized.

[19] Levine, Bender, McGruer, and Vogelsang, Phys. Rev. **95**, 640 (1954).

[20] I wish to thank Dr. C. N. Yang, who clarified these considerations for me.

[21] Adair, Darden, and Fields, Phys. Rev. **96**, 503 (1954).

Energy Distribution of Nuclear Reaction Products

H. H. BARSCHALL AND J. L. POWELL*
University of Wisconsin, Madison, Wisconsin
(Received June 1, 1954)

In a reaction involving two product particles the distribution in energy of either product particle measured in the laboratory system is the same as the distribution in angle in the zero-momentum system. This relation is valid relativistically and irrespective of the reaction energy. Some applications are discussed.

DIRECT measurements of the angular distribution of the products of nuclear reactions or of scattering processes are frequently more difficult to perform than measurements of the distribution in energy of product or recoiling particles. For this reason it is worth pointing out that the two distributions are related in a very simple manner, if there are only two product particles involved and if a single process occurs.

It is well known that, in single collisions between monoergic neutrons and protons, all neutron or proton energies up to the energy of the primary neutrons are produced with equal probability provided the neutron energy is sufficiently low that the scattering is isotropic in the c.m. system. This relation has been generalized to all nonrelativistic elastic collision processes.[1] It has been shown that the distribution in energy of the recoil particles as measured in the laboratory system is the same as the angular distribution with respect to $\cos\theta$ of the scattered particles in the c.m. system. It is the purpose of this note to point out that the relationship holds also for relativistic energies and for exoergic or endoergic collisions.

Assume that the product particles are numbered 1 and 2. Let $\mathbf{p}$ and E be the momentum and (relativistic) energy and let primed quantities refer to the laboratory system, while unprimed quantities are measured in the system of zero momentum: $\mathbf{p}_1+\mathbf{p}_2=0$. If the zero-momentum system moves with a velocity $\mathbf{v}$ with respect to the laboratory system, the energy of particle 1 in the laboratory system is

$$E_1'=(1-v^2/c^2)^{-\frac{1}{2}}(E_1-|\mathbf{p}_1||\mathbf{v}|\cos\theta),$$

where θ is the angle between $\mathbf{v}$ and $\mathbf{p}_1$, i.e., the scattering angle in the zero-momentum system if scattering is being considered. For a given reaction, the energy E_1' depends only on $\cos\theta$, and the energy distribution function $N(E_1')$ in the laboratory system and the angular distribution function $P(\cos\theta)$ in the zero-momentum system are related by

$$N(E_1')|dE_1'|=P(\cos\theta)|d(\cos\theta)|,$$

and therefore

$$N(E_1')=(1-v^2/c^2)^{\frac{1}{2}}P(\cos\theta)/|\mathbf{p}_1||\mathbf{v}|.$$

This shows that the angular distribution in the zero-momentum system expressed in terms of $\cos\theta$ is the same as the energy distribution in the laboratory system. The energy spectrum is contained in an energy range of width $2|\mathbf{p}_1||\mathbf{v}|(1-v^2/c^2)^{-\frac{1}{2}}$.

This theorem is especially useful for reactions induced by uncharged particles when it is possible to measure the ionization produced by one of the product particles, particularly in the cases of elastic and inelastic scattering of neutrons. Another example is the photodisintegration of the deuteron. By measuring the energy distribution of the photo-protons it is possible to determine directly the angular distribution of the disintegration processes.[2] For reactions induced by neutrons and photons some difficulty may arise in measuring the energy distribution of one of the reaction products separately, if both products are charged particles. If the two product particles have sufficiently different masses, it is, however, still possible to observe the distribution in ionization for each product.

Another problem to which this theorem applies is the disintegration of monoergic mesons in flight. Here $\mathbf{v}$ is the velocity of the meson before disintegration. In the reference system of the meson all directions of emission of the product particles are equally probable. Consequently the energy distribution of the product particles in the laboratory system is a constant between the limits given previously. Such an energy distribution has been observed by Panofsky, Aamodt, and Hadley[3] for the γ rays from the decay of neutral π mesons.

* Now at Lockheed Aircraft Corporation, Van Nuys, California.
[1] H. H. Barschall and M. H. Kanner, Phys. Rev. **58**, 590 (1940).
[2] Bishop, Beghian, and Halban, Phys. Rev. **83**, 1052 (1951).
[3] Panofsky, Aamodt, and Hadley, Phys. Rev. **81**, 565 (1951).

Emission of High-Energy Gamma Line from C^{12}†

DAVID COHEN, BURTON J. MOYER, HARLAN SHAW, AND CHARLES WADDELL
Radiation Laboratory, Department of Physics, University of California, Berkeley, California

(Received June 21, 1954)

A gamma ray of energy 15.2 Mev has been observed with a 180° pair spectrometer in the bombardment of carbon by protons of energy 30–340 Mev. The line is also seen in deuteron bombardment of B^{11}, but not of B^{10}. These facts, along with energetics arguments and clear spectrometer separation from known lines in excited Be^8, strongly indicate an excited C^{12} origin for the line. It is tentatively proposed that the excited C^{12} level here involved is a $T=1$ state for which isotopic spin selection rules forbid a disintegration into three alpha particles.

IN connection with studies of proton bremsstrahlung, in which a 180° pair spectrometer is used to analyze the photon spectrum, a gamma line at 15.2±0.2 Mev has been observed which is believed to arise from the excited C^{12} nucleus. Such a line was suggested in Wilson's[1] experimental bremsstrahlung data on proton bombardment of carbon, but his methods did not permit resolution of the line.

Figure 1 shows this gamma emission revealed by the pair spectrometer as it appears superimposed upon the bremsstrahlung, viewed at 90° from the beam direction, in the bombardment of carbon by 340-Mev protons in the Berkeley cyclotron. The cyclotron target could be pushed in to a radius where the proton energy was 30 Mev; and at this energy the bremsstrahlung is negligible, leaving the line emission as shown in Fig. 2.

The breadth of the line as here shown is essentially entirely instrumental, and a more precise evaluation of its true energy awaits calculation of the instrumental line shape. Calibration of the spectrometer was accomplished by the floating-wire technique, and a calibration test of the spectrometer upon the 17.6-Mev gamma line from Be^{8*} indicates that the energy error is within the limits given above.

The assignment of the line to C^{12*} is based upon the following facts.

(A) It is present with a carbon target for proton energies ranging from 30 to 340 Mev, and is not observed in proton bombardment of Be, B, and O.

(B) It has been observed in deuteron bombardment of B^{11} in which deuterons of 18, 30, and 50 Mev were incident on a thick target. It is not observed in the deuteron bombardment of B^{10}. Recent work[2] at Indiana gives definite indication of high-energy (about 15-Mev) gamma emission from 11-Mev deuteron bombardment of a thick boron target (presumably natural boron which is 81 percent B^{11}).

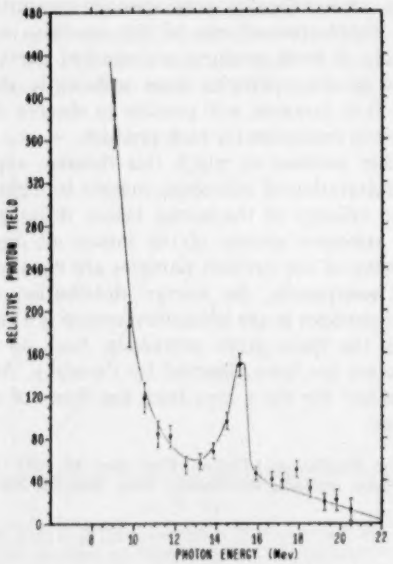

FIG. 1. Photon spectrum from 340-Mev proton bombardment of carbon.

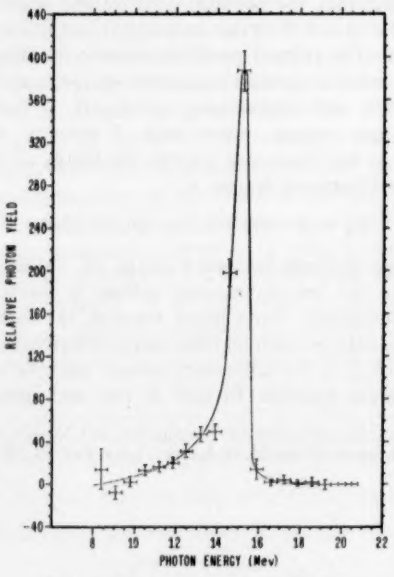

FIG. 2. Photon spectrum from 30-Mev proton bombardment of carbon.

† This work was done under the auspices of the U. S. Atomic Energy Commission.

[1] Richard Wilson, Phys. Rev. 85, 563 (1952).

[2] V. K. Rasmussen (private communication).

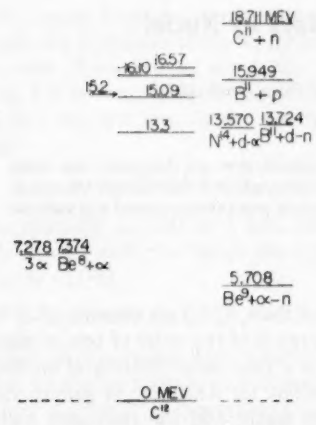

FIG. 3. Energy level diagram.

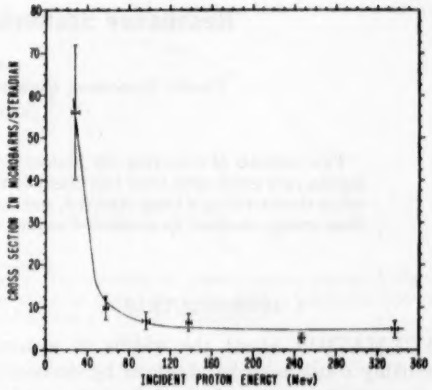

FIG. 4. Differential cross section for production of 15.2-Mev photons at 90° *vs* energy of protons incident upon carbon targets.

(C) A level below 15.95 Mev in C^{12} cannot decay by neutron or proton emission, as is made evident by Fig. 3. Consequently such a level must either disintegrate into three alpha particles or into Be^8 plus an alpha, or decay by gamma emission. If the gamma process is to predominate, a selection rule must operate which suppresses the alpha processes in the decay from this level.

Absolute values of the differential cross section for producing these gamma-ray photons into unit solid angle at 90° were roughly determined by a thermocouple monitoring of target temperature. This is related to beam energy loss in the target, and thus, at a known energy, to beam traversal of the target. The absolute efficiency of the spectrometer is calculated from established pair-production cross sections and geometry. In Fig. 4 is illustrated the dependence of the yield of the level in question upon energy of bombarding protons, with a carbon target.

It seems reasonable to propose tentatively[3] that the alpha disintegration may be considerably forbidden by isotopic spin considerations, which would be the case if this C^{12*} level were a $T=1$ state. This allows dipole gamma emission in the transition to the C^{12} ground state.[4] Upon this basis the B^{12}, C^{12*}, and N^{12} would form the isotopic triplet. The 15.09-Mev C^{12*} level listed by Ajzenberg and Lauritsen[5] may be the one here in question.

Attempts to produce this gamma emission by the alpha bombardment of Be^9, employing 170-Mev alphas upon a Be target of sufficient thickness to stop them, have not given a detectable yield. This apparent failure to produce the required state by $Be^9(\alpha,n)C^{12*}$ may be understood in terms of the $T=1$ proposal advanced above; since a process which amounts essentially to the coalescence of three alpha particles, with the release of the loosely bound neutron, could not develop a $T=1$ state.

Helpful discussions with Professor M. A. Ruderman are acknowledged.

[3] This suggestion has come to us by private communication from the group at the California Institute of Technology.

[4] L. Radicati, Phys. Rev. **87**, 521 (1952).

[5] F. Ajzenberg and T. Lauritsen, Revs. Modern Phys. **24**, 321 (1952).

Resonance Scattering of Gamma Rays by Nuclei

A. M. CORMACK
Physics Department, University of Cape Town, Cape Town, South Africa
(Received June 21, 1954)

Two methods of observing the nuclear resonance scattering of gamma rays are discussed: one using gamma rays which arise from transitions to the ground state of a nucleus which is the same as the one in which the scattering is being observed, and the other using gamma rays of small energy spread and variable mean energy obtained by means of Compton scattering.

1. INTRODUCTION

INFORMATION about the widths of gamma-ray emitting states may be obtained by delayed coincidence methods if the lifetimes of the states are greater than about 10^{-10} second, for in this case the lifetime may be measured directly and hence the width may be deduced. Because of the limitations of present-day coincidence circuits, this method will not work for lifetimes much shorter than 10^{-10} second, and the widths have to be inferred either indirectly, from reactions involving particles, or directly, by measuring the resonance scattering of gamma radiation. Two methods of obtaining gamma rays of approximately the right energy for resonance scattering are: to use gamma rays which arise from a transition to the ground state of a nucleus which is the same as the nucleus in which the resonance scattering is being investigated (method *A*), and to use a source of variable energy gamma rays such as could be obtained by allowing monoenergetic gamma rays to undergo Compton scattering (method *B*). The difficulties inherent in both of these methods and ways of overcoming them are discussed below.

The cross section for resonance scattering may be written.

$$\sigma=\frac{g\lambda^2\Gamma^2}{8\pi[(E_0-E)^2+(\Gamma^2/4)]}, \tag{1}$$

where g is a statistical factor of order unity,[1] and λ, E, E_0, and Γ are, respectively, the wavelength and energy of the incident gamma rays, the resonance energy, and the width of the level. The maximum value of σ is of order 10^{-21} cm^2 for gamma rays of energy 1 Mev. Approximate expressions for Γ have been given by Weisskopf,[2] which show that the conditions for large Γ are large E_0, small multipole order, and large mass number.

2. RESONANCE SCATTERING BY METHOD *A*

Suppose that a nucleus N is stationary when it emits a gamma-ray of energy E_γ in flight. Since the gamma has a momentum (E_γ/c), N must have a recoil energy of $(E_\gamma^2/2Mc^2)$ where M is the mass of N. If the gamma ray is scattered by another nucleus, S, of the same species as N, then S will also recoil with an energy $(E_\gamma^2/2Mc^2)$ so that the appropriate energy E to insert in (1) is less than E_0 by an amount (E_γ^2/Mc^2). Since this last energy is of the order of tens of electron volts, whereas Γ is a very small fraction of an electron volt, the cross section for scattering of gamma rays from N will be very small, and the resonance scattering will be hidden in the background of Compton, Rayleigh, and Thomson nuclear scattering.[3] This fact has been pointed out by several writers[4,5] who have suggested that by making N move towards S at the instant of emission, E_γ will be Doppler-shifted towards E_0, and this will result in a larger value for σ than would be the case if N were stationary. Moon[4] has achieved this relative motion of N and S by rotating the source in the neighborhood of the scatterer, and choosing his geometry so that the bulk of the scattering occurs when the source is moving towards the scatterer. While his results indicate the presence of resonance scattering, his statistics are such that only a rough estimate of Γ may be made.*

Relative motion of N and S will occur if the emission of the gamma by N has been immediately preceded by the emission of either an electron or a gamma ray. The emission of the first particle will set N in motion and the energy of the gamma ray of interest will be Doppler-shifted accordingly. The simplest case will occur when the source nuclei N are in the form of a gas, so that they will move with the recoil velocity resulting from the emission of the first particle as long as they do not undergo collisions.

If the first particle is a gamma ray of energy E_1, it is easily shown that the energy spectrum of gamma rays from the nuclei N in any direction is a constant between $E_\gamma[1-(E_1/Mc^2)]$ and $E_\gamma[1+(E_1/Mc^2)]$ and is zero everywhere else. The effective cross section $\bar{\sigma}$, for gamma rays with this energy distribution is found from (1) to be

$$\bar{\sigma}=(g\lambda^2\Gamma^2Mc^2/8\pi E_\gamma E_1)[\tan^{-1}\{2E_\gamma(E_1-E_\gamma)/\Gamma Mc^2\}+\tan^{-1}\{2E_\gamma(E_1+E_\gamma)/\Gamma Mc^2\}]. \tag{2}$$

Weisskopf's formulas[2] show that the conditions for

[1] E. Guth, Phys. Rev. **59**, 325 (1941).
[2] V. Weisskopf, Phys. Rev. **83**, 1073 (1951).
[3] P. B. Moon, Proc. Phys. Soc. (London) **A63**, 1189 (1950).
[4] P. B. Moon, Proc. Phys. Soc. (London) **A64**, 76 (1951).
[5] S. Devons, *Excited States of Nuclei* (Cambridge University Press, London, 1949).
* *Note added in proof.*—A considerable improvement in the moving source technique has been effected recently by Moon and his collaborators (Proc. Phys. Soc. (London) **A66**, 956 (1953); and **A67**, 601 (1954)).

large $\bar{\sigma}$ are, again, large resonance energy and mass number, and low multipole order. If E_1 and E_γ are of the same order of magnitude, say 1 Mev, the second term in Eq. (2) is very nearly $(\pi/2)$. If $E_1 > E_\gamma$ by as little as 1 kev, the first term is also nearly $(\pi/2)$, and in this case

$$\bar{\sigma} = (g\lambda^2 \Gamma M c^2 / 8 E_\gamma E_1). \tag{3}$$

If $E_1 < E_\gamma$, again by as little as 1 kev, the two terms will nearly cancel and, by using the approximation $\tan^{-1} x = (\pi/2) - (1/x)$,

$$\bar{\sigma} = (g\lambda^2 \Gamma^2 M^2 c^4 / 8\pi E_\gamma^2 [E_\gamma^2 - E_1^2]). \tag{4}$$

The large difference between the expressions Eq. (3) and Eq. (4) may be used as an independent method of inferring the order of emission of gamma rays in cascade. For example, if the 1.33 and 1.17 Mev gammas of Ni^{60} were emitted in that order, Eq. (3) would show $\bar{\sigma}$ to be about 3×10^{-27} cm^2 when $\Gamma = 10^{-4}$ ev. If the order were reversed, Eq. (4) would give $\bar{\sigma} = 4 \times 10^{-31}$ cm^2.

If the first particle emitted is an electron rather than a gamma ray, the spectrum of the gamma rays from the source is more complicated. Kofoed-Hansen[6] has given an expression for the momentum spectrum of nuclei recoiling after beta decay, and from this the energy spectrum of the Doppler-shifted gamma rays may be calculated. The result for a beta spectrum with maximum energy $2mc^2$ is shown in Fig. 1. The intensity is plotted against $\xi = [M(E - E_\gamma)/mE_\gamma]$, where m is the electron mass. The curve is symmetrical about $\xi = 0$ and the ordinates have been chosen to make the area under the whole curve unity. A gamma ray with the same *momentum* as the maximum momentum of the electrons would give rise to a rectangular spectrum within the same limits as the spectrum following beta decay, and would thus give rise to a larger cross section if the Doppler shift was just not large enough to compensate for the loss of energy by recoils. A gamma ray with an *energy* equal to the maximum beta-ray energy would not be similarly effective.

The condition for the validity of the above considerations is that the half-life of the state being investigated should be smaller than the reciprocal of the collison frequency in the gas, i.e., smaller than (mean free path/mean velocity). Since the velocity of sound, V, in a gas is given by[7] $V = v_m(\gamma\pi/8)^{\frac{1}{2}}$, where γ is the ratio of specific heats and is of order unity, and v_m is the mean velocity of the molecules, the condition may be stated that the half-life should be less than (mean free path/velocity of sound in the gas). This condition is satisfied for the states of interest here, with lives less than 10^{-10} sec.

When the atoms of the source are in solid and not gaseous form, the situation is more difficult to analyze in view of the paucity of exact knowledge of the elastic

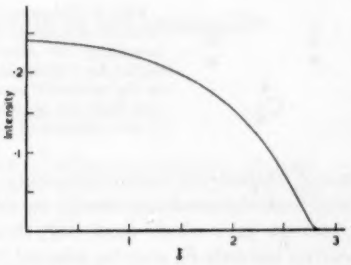

FIG. 1. The intensity of gamma rays of energy E emitted by nuclei recoiling after beta decay with a maximum energy $2mc^2$, plotted against $\xi = [M(E - E_\gamma)/mE_\gamma]$.

forces binding atoms in a crystal lattice. Some progress may be made by considering a linear Blackman model of the crystal lattice, i.e., a set of identical mass points, mass m, with a constant spacing s, joined together with identical springs with force constant k. The equations of motion of the chain may be readily solved with the initial conditions that the displacements of all the particles is zero and that the initial velocities of all but the nth are zero, the nth particle having the initial velocity v_0. This is a model of the system of interest in which an atom is set in motion by the emission of the first particle. The velocity of the $(n \pm r)$th particle is given as a function of time t by

$$v_{n\pm r}(t) = v_0 J_{2r}(2\alpha t), \tag{5}$$

where $\alpha = (k/m)^{\frac{1}{2}}$. The velocity of the nth particle is thus $v_0 J_0(2\alpha t)$, which falls to zero for the first time when $t = (1.2/\alpha)$. $J_p(x)$ reaches its maximum when $x \approx p$, hence the velocity of the $(n \pm r)$th particle will be a maximum when $t = (r/\alpha)$, and, since it is displaced a distance rs from the nth particle, the velocity of propagation of the disturbance will be $V_s = \alpha s$. Thus the velocity of the nth particle will be zero for the first time when $t = (1.2s/V_s)$. Since V_s is obviously the velocity of sound in the solid, the results of this section will still be valid if the half-life of the state under investigation is small compared to (interatomic distance/velocity of sound). In view of the agreement between the form of the conditions of validity for solids and gases, it is apparent that this criterion will also hold for liquids, i.e., half-life short compared to (interatomic distance or mean free path in the liquid/velocity of sound in the liquid). If these conditions are not fulfilled, then the velocity of the atom after the emission of the first particle will diminish because of dissipation of energy in liquids and solids and will be modified and generally diminished by collisions in gases. The Doppler shift and hence $\bar{\sigma}$ will then be smaller than the value given by Eq. (2).

In all of the above considerations it has been assumed that the distribution of recoil velocities after the emission of the first particle is isotropic, so that there will be as many nuclei recoiling away from the scatterer as are moving towards it, and hence as many of the

[6] O. Kofoed-Hansen, Phys. Rev. **74**, 1785 (1948).
[7] A. B. Wood, *Text-book of Sound* (G. Bell & Sons, London, 1944).

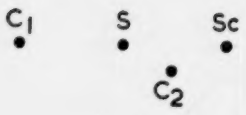

FIG. 2. Schematic arrangement of coincidence method for increasing the effective cross section for resonance scattering in the scatterer Sc of gamma rays from the source S. C_1 and C_2 are counters in coincidence.

gamma rays of interest will have their energy Doppler-shifted away from the resonance energy as towards it. However, gamma rays which have had their energy Doppler-shifted towards E_0 may be selected by means of the coincidence circuit shown in Fig. 2. C_1 and C_2 are detectors, S is the source, and Sc is the scatterer. C_2 is shielded from direct radiation from S. If a coincidence between C_1 and C_2 is registered, one will know that the gamma ray which reached C_2 from S via Sc was emitted by an atom moving towards Sc, since the first particle went in the direction of C_1. This will result in a much larger cross section than would be obtained using unselected gamma rays. Experiments on these lines are in progress in this laboratory. An obvious, but not readily applicable, extension using three scintillation counters is to make one of the phosphors the scatterer and to register coincidences between the other two but not triple coincidences. For large scattering angles this will eliminate the Compton scattering completely and give the advantage of selected gamma rays mentioned above.

3. RESONANCE SCATTERING BY METHOD B

Suppose that it is possible to obtain gamma rays with an energy spectrum which is constant and equal to $(1/E_m)$ in the range $(E_0'\pm\frac{1}{2}E_m)$, and zero everywhere else, where E_0' is the resonance energy corrected for recoil. The effective cross section $\bar{\sigma}$ is found from (1) to be

$$\bar{\sigma}=(g\lambda^2\Gamma/2\pi E_m)\tan^{-1}(E_m/\Gamma), \tag{6}$$

and, if E_m is as small as a few ev, $\tan^{-1}(E_m/\Gamma)\approx(\pi/2)$. Hence (8) may be approximated to by

$$\bar{\sigma}=(g\lambda^2\Gamma/4E_m). \tag{7}$$

$\bar{\sigma}$ will still have this value if the center of the spectrum is displaced by nearly $\pm(E_m/2)$ as long as E_m is large compared to Γ. Hence, as the center of the spectrum is moved from outside this range through it and outside it again, $\bar{\sigma}$ will change from a small to a large value and back again, "small" and "large" depending on the value of E_m. In the case of the 0.487-Mev level in Li^7, which has a width of about 0.01 ev,[8] $\bar{\sigma}=1.8\times10^{-26}$ cm^2, or about 2 percent of the Compton cross section in Li if $E_m\approx9$ kev.

A gamma-ray beam with a spread of a few kev and a mean energy which may be varied continuously may be obtained by the use of the Compton effect in a primary scatterer. If gamma rays with an energy E_p are scattered by an angle θ, the energy of the scattered radiation E is given by the Compton formula

$$E=E_p[1+\{E_p(1-\cos\theta)/mc^2\}]^{-1}; \tag{8}$$

and the spread in energies ΔE due to a spread of scattering angles $\Delta\theta$ is

$$\Delta E=\frac{(E_p^2/mc^2)\sin\theta\Delta\theta}{[1+\{E_p(1-\cos\theta)/mc^2\}]^2}, \tag{9}$$

from which it is seen that, for a given $\Delta\theta$, ΔE is smallest when $\theta\approx0$ or π. For a given E_p, the smallest value of ΔE will occur for $\theta\approx\pi$, but this region suffers from the disadvantages that the differential Compton cross section is smallest here, and, more important, that the maximum energy in this region is $(mc^2/2)$, no matter how high E_p. Thus for most purposes the region of small θ will be important.

If annihilation radiation was used as a source for the investigation of the resonance scattering from the 0.487-Mev Li^7 level, the right energy of gamma rays from the primary scatterer would be obtained for a scattering angle of about 21°. Equation (9) shows that $\Delta\theta$ should be 3.3° in order to obtain $\Delta E=9$ kev, which gives $\bar{\sigma}=1.8\times10^{-26}$ cm^2. If a more favorable source were used, with E_p less than 0.51 Mev, the same ΔE would be obtained with an even larger value of $\Delta\theta$. The geometry of the experiment could be chosen without great difficulty to give such a value of $\Delta\theta$. It would be determined by the finite extension of source, primary scatterer, and lithium scatterer, and would give a cross section somewhat larger than the value mentioned since the energy distribution of the gamma rays would then be peaked about the average value, instead of having the rectangular shape assumed in the derivation of Eq. (7).

The main difficulty is to obtain a large enough intensity of Compton gammas, scattered at just the right angle. This may be done by using a scatterer in the form of part of a surface of revolution, the axis being the line joining source and scatterer, and the profile being a circle. Gamma rays from all parts of the surface will then be scattered through the same angle. Strong sources, careful screening, and possibly the use of coincidence methods to reduce background will be necessary since the counting rates obtainable in double scattering experiments of this kind will not be high.

4. CONCLUSIONS

The methods outlined should prove useful in the study of high-energy, low-multipole order gamma-ray transitions. Because of the short lives of the states involved and the low internal conversion coefficients, etc., these transitions are not readily accessible by the methods which have proved so fruitful in the investigation of lower-energy, higher-multipole order transitions.

[8] J. M. Blatt, and V. Weisskopf, *Theoretical Nuclear Physics* (John Wiley and Sons, Inc., New York, 1952).

Calorimetric Determination of the Half-Life of Polonium-210

J. F. EICHELBERGER, K. C. JORDAN, S. R. ORR, AND J. R. PARKS
Mound Laboratory, Monsanto Chemical Company, Miamisburg, Ohio*
(Received May 14, 1953; revised manuscript received July 14, 1954)

Six determinations have been made of the half-life of polonium with four different steady-state, resistance-bridge calorimeters and five different samples of polonium. These six values of the half-life have been weighted and combined to give a grand-mean value of the half-life of 138.4005±0.0051 days (internal consistency) or ±0.0058 day (external consistency).

INTRODUCTION

MOUND Laboratory has been engaged in the development of calorimeters to be used in the measurement of radioactivity. The quality of the various calorimeter designs was judged by measurements on small localized sources of heat. Polonium-210 was used for the small sources of heat. Polonium is practically an ideal heat source for calorimetric measure because of its simple decay scheme. The polonium isotope decays to stable lead by the emission of essentially monoenergetic alpha particles and of one gamma ray per 10^5 alphas.[1]

During the course of our work, a large number of measurements were made with several samples of different over-all dimensions and with different amounts of polonium. The testing of a calorimeter of new design extended over a period of two to four months, and even in this length of time fairly precise values of the half-life of the samples were calculated from the accumulated data. It was decided to continue to obtain data over a longer period of time so that more precise values of the half-life would be obtained. The precisions of these determinations were used as one of the measures of the success of the calorimeter designs. Since our data and results were of unusually high precision, we believed it desirable to publish the information. The very precise value of the half-life of polonium allowed the use of these samples as reference heat sources in calorimetry research.

Since the identification of polonium by Curie[2] as a naturally occurring radioactive element, there have been many determinations of the half-life of polonium-210. Gmelin's Handbuch[3] lists 28 determinations of the half-life. Beamer and Easton[4] in two determinations obtained a value of the half-life of polonium-210 of 138.3 days±0.1 percent. More recently, Ginnings, Ball, and Vier[5] obtained a value of 138.39±0.14 days.

CALORIMETER DESIGN

The calorimeters used in this work were developed from the steady-state, resistance-bridge type used by Rutherford and Robinson[6] in the measurement of radioactivity by the calorimetric method. The Mound Laboratory development work was directed towards obtaining a knowledge of materials of construction and of dimensional dependence sufficient to permit the design of a calorimeter with arbitrary sensitivity, precision, stability, sample volume, sample-power range, and time to reach equilibrium. In the course of the work, the "heat-distribution error" of a calorimeter was used as a measure of the calorimeter's accuracy. The heat-distribution error of a calorimeter is defined as the maximum-percent difference among the measured values of a small constant-electric-power source placed at various positions in the available sample volume. Polonium properly enclosed can serve as such a source, if its half-life is accurately known.

A description of a resistance-bridge calorimeter and the method of operation is contained in Beamer and Easton's paper.[4] The operating parameters of the calorimeters used in the half-life measurements are summarized in Table I.

DESCRIPTION OF SAMPLES

Five different polonium-210 samples were used during a period of three years. The polonium was prepared by standard methods[4,7] but was sealed in containers fashioned to fit the calorimetric-research needs. The chemical purity of these samples was not accurately known. However, the precision of the half-life measurements indicated that over the period of the measure-

TABLE I. Operating parameters of the calorimeters.

Calorimeter	Electrical sensitivity (μv/mw)	Time to reach 0.01 percent of equilibrium (min)	Sample-container inside dimensions Diameter (in.)	Height (in.)	Heat distribution error (%)	Thermal resistance (°C/w)
A	59.5	360	$2\frac{3}{32}$	$2\frac{11}{16}$	0.15	26
B	54.4	75	$1\frac{3}{16}$	3	0.05	4.3
C	438.	75	$\frac{1}{4}$	$\frac{3}{4}$	not measured	80
D	204.	75	$\frac{1}{4}$	3	0.3	8

* Mound Laboratory is operated by Monsanto Chemical Company for the U. S. Atomic Energy Commission.

[1] Zajac, Broda, and Feather, Proc. Phys. Soc. (London) **60**, 501 (1948).

[2] M. Curie, Compt. rend. **126**, 1101 (1898).

[3] L. Gmelin, *Handbuch der Anorganischen Chemie, System Number 12, Polonium und Isotope* (Verlag Chemie, g. m. b. H., Berlin, 1941).

[4] W. H. Beamer and W. E. Easton, J. Chem. Phys. **17**, 1298–1300 (1949).

[5] Ginnings, Ball, and Vier, J. Research Natl. Bur. Standards **50**, No. 2, 75–79 (1953).

[6] E. Rutherford and H. Robinson, Phil. Mag. **7**, 202 (1904).

[7] Isotopics **2**, No. 4, 1 (1952); **3**, No. 2, 6–14 (1953).

TABLE II. Description of samples.

No.	Mount	Inner container Material	Inner container Height (in.)	Inner container Diameter (in.)	Outer container Material	Outer container Height (in.)	Outer container Diameter (in.)	Atmosphere	Initial watts		Method of deposition
I	platinum	platinum	1¾	½	pyrex	2½	⅝	helium	0.47891	±0.00005	electrodeposition
II	platinum	none	...	...	platinum	7/16	¼	noncontrolled mixture	0.0165429	±0.0000015	electrodeposition
III	platinum	platinum	1¾	½	pyrex	2½	⅝	helium	0.25586	±0.00001	volatilization
IV	platinum	platinum	1¾	½	pyrex	2¼	⅝	helium	0.28334	±0.00002	volatilization
V	inside of hollow sphere	none	...	...	metal sphere	...	1⅞	noncontrolled mixture	1.14697	±0.00004	volatilization

ments only negligible quantities of radioactive impurities could have been present. Gamma counts and neutron counts of the samples did not indicate the presence of any radioactive impurities in measurable amounts.

A brief description of each sample, its preparation, and container is presented in Table II.

APPARATUS FOR MEASUREMENT AND CONTROL

All electrical equipment used in the measurements was of the highest accuracy and precision that was commercially obtainable. Potentials were measured with a Leeds and Northrup Wenner standardizing potentiometer whose accuracy was ±0.01 percent and whose precision was more exact. Currents were calculated from the measurement of the potential drop across Leeds and Northrup National Bureau of Standards type resistors by means of the potentiometer. The National Bureau of Standards type resistors had accuracies of ±0.01 percent and more exact precisions. The potentiometer was standardized by means of a Leeds and Northrup Eppley standard cell whose voltage was accurate to ±0.01 percent and was more precise. Bridge currents and heater currents were obtained from Willard low-discharge batteries.

The calorimeter bath contained a resistance bridge which served as the sensitive thermal element for a Leeds and Northrup type proportional-control system. The temperature of the bath was held constant to within 0.001°C during a measurement. Most of the measurements were made in a room controlled to ±0.2°F. Some of the measurements were made in a room controlled to ±1.0°F. The calorimeters did not show any drift or instability which could be attributed to variations in room temperature.

DISCUSSION OF MEASUREMENTS

The introduction of the sample into the calorimeter caused the internal temperature of the calorimeter to rise until the power loss to the bath was equal to the power supplied by the sample. The change in the potential difference across the bridge in the calorimeter was observed until equilibrium was reached. After the measurement of the equilibrium potential, the sample was removed, and current was then introduced into the calibrating heater in an amount sufficient to cause nearly the same bridge unbalance as was caused by the sample. The heater resistance was concurrently measured, and the power output which was computed for the heater was taken to be the power output of the sample after the heater power was linearly corrected for the difference in bridge unbalance between the sample and heater. After the performance of the calorimeter was well known, an alternative technique was used. A reference heater was compared to the calibrating heater. Power was then supplied by the reference heater in one side of the calorimeter at the same time that the sample was in the other side. Every 10 minutes, the bridge potential was measured, and the bridge current and heater current were readjusted if they had drifted slightly from their preselected values.

Each half-life in Table III was calculated from the respective decay constant which was determined by a least squares fit of the determinations of the power output of the sample and the times at which the equilibria were reached to the equation of logarithmic decay

$$\ln N = \ln N_0 - \lambda t, \tag{1}$$

where t = the time (days), λ = the decay constant (days^{-1}), N_0 = the sample size at time $t=0$ (atoms), and $T_{\frac{1}{2}} = \ln 2/\lambda$ = the half-life (days).

The determination of λ and N_0 was made by the standard least squares procedure which is used to fit a set of data (x_i, y_i) to a straight line,

$$y = a + bx, \tag{2}$$

where the set x_i (the times) are presumed to be accurately known, and the set y_i (the observed power outputs) are presumed to have random errors. Power

TABLE III. Values of the half-life of polonium-210.

Calorimeter	Sample	Time covered by measurements (days)	Number of observations	Half-life (days)	Probable error (days)
A	I	250	19	138.391	0.023
B	III	617[a]	32	138.401	0.012
B	IV	357	32	138.408	0.014
B	V	352	36	138.4059	0.0068
C	II	153	20	138.410	0.024
D	IV	105	24	138.314	0.024

[a] Only two measurements were taken after the 284th day.

output is directly proportional to the number of atoms. The appropriate equations for calculating a and b and their precisions may be derived or found in standard references on statistical treatment of data,[8] and they are tabulated here as Eqs. (3) through (9), inclusive.

The residuals d_i are

$$d_i=y_i-y(x_i)=y_i-a-bx_i. \tag{3}$$

The values of a and b are found from the equations

$$a=[(\sum x_i^2)(\sum y_i)-(\sum x_i)(\sum x_iy_i)]/D, \tag{4}$$

$$b=[n(\sum x_iy_i)-(\sum x_i)(\sum y_i)]/D, \tag{5}$$

$$D=n(\sum x_i^2)-(\sum x_i)^2, \tag{6}$$

(where n is the number of measurements for each half-life determination).

The probable errors of y_i, a, and b have been determined from equations given by Birge.[9] Birge's formulas can be derived by the application to Eqs. (4), (5), and (6) of the usual equations for the determination of the probable error of a function whose variables have known probable errors.[10] The probable error of a single power measurement $p(y_i)$ is found directly from the residuals

$$p(y_i)=0.6745[\sum d_i^2/(n-2)]^{\frac{1}{2}}. \tag{7}$$

The probable errors, $p(a)$ of a and $p(b)$ of b, are:

$$p(a)=p(y_i)[\sum x_i^2/D]^{\frac{1}{2}}, \tag{8}$$

$$p(b)=p(y_i)[n/D]^{\frac{1}{2}}. \tag{9}$$

An examination of Eq. (1) discloses that a constant-percent error in the values of the sample power N cannot influence the value of the decay constant λ. The effect of such an error is to produce a parallel displacement of the line causing an error in the determination of $\ln N_0$ only. This situation is important to the determination of the half-life, because it means that, as long as experimental conditions are duplicated for every power determination, the half-life value is more accurate than the power determinations and should approach the precision of the power determinations.

Six values of the half-life of polonium-210 have been calculated from the data on five samples taken with four calorimeters. The results are given in Table III.

A grand-mean value of the half-life can be computed from the individual values which were determined. In this procedure, each value of the half-life X_i is given a weight inversely proportional to the square of its probable error p_i.

$$\bar{X}=\Sigma\left[\frac{k^2}{p_i^2}\cdot X_i\right]\Big/\Sigma\left[\frac{k^2}{p_i^2}\right]. \tag{10}$$

Birge[9] has given a test for the consistency of the individual means which enter into the calculation of the grand mean. The means are considered consistent if

$$hx=m^{\frac{1}{2}}\left\{0.67\left[\frac{\sum[(X_i-\bar{X})/p_i]^2}{m-1}\right]^{\frac{1}{2}}-1\right\}<1.83, \tag{11}$$

where m is the number of means combined into the grand mean. The data of Table III when substituted into Eq. (11) give a value of 0.15, and therefore the means are consistent. The probable error $p(\bar{X})$ of the grand mean $\bar{X}$ is

$$p(\bar{X})=(\sum 1/p_i^2)^{-\frac{1}{2}}. \tag{12}$$

Since the six half-lives of Table III are compatible, they have been combined by Eq. (10) to give a grand mean of the half-life $\bar{T}_{\frac{1}{2}}$ with a probable error determined from Eq. (12).

$$\bar{T}_{\frac{1}{2}}=138.4005\pm0.0051 \text{ days}.$$

The probable error of the grand mean can also be calculated with the equation for combining means possessing external consistency:

$$p(\bar{X})=0.6745\left\{\frac{\sum[(X_i-\bar{X})/p_i]^2}{(m-1)\sum(1/p_i)^2}\right\}^{\frac{1}{2}}. \tag{13}$$

With $X=138.4005$ and the data of Table III, Eq. (13) gives

$$\bar{T}_{\frac{1}{2}}=138.4005\pm0.0058 \text{ days}.$$

The calorimeters, samples, and conditions of measurement were very similar throughout the measurements, so that there should be a high degree of internal consistency in the data. The application of Eq. (13) to these data appears rather meaningless in terms of evaluating the effects on the half-life of any constant errors of the method. Equation (12) determines precision only since it involves only probable errors and in no way includes deviations from the grand mean. Thus the quoted probable errors are primarily a measure of the precision of the method. Accuracy of the method rests both on the precision of the measurements and on the fact that the slope of a straight line is being determined rather than the absolute location of the line.

ACKNOWLEDGMENT

The authors wish to make the following acknowledgments to Mr. D. G. Anger who participated in part of the work; Mr. W. J. Haubach, Jr., and Mr. J. H. Wright who participated in the construction of the apparatus; Mrs. M. F. Hausenstein, Mrs. Roy Taylor, Miss M. E. Harvil, and Mrs. C. B. Heyd who accumulated the major portion of the data and performed part of the calculations; and Miss M. A. Geiger, Dr. H. H. Fox, and Dr. G. R. Grove who aided in the critical evaluation of the work.

[8] A. D. Worthing and J. Geffner, *Treatment of Experimental Data* (John Wiley and Sons, Inc., New York, 1943), first edition.
[9] R. T. Birge, Phys. Rev. **40**, 207 (1932).
[10] H. Margenau and G. M. Murphy, *The Mathematics of Physics and Chemistry* (D. Van Nostrand Company, Inc., New York, 1943), first edition.

Fission and Total Reaction Cross Sections for 22-Mev Protons on Th^{232}, U^{235}, and U^{238}

G. H. McCormick* and B. L. Cohen
Oak Ridge National Laboratory, Oak Ridge, Tennessee

(Received June 24, 1954)

Absolute excitation functions for (p,f) reactions in Th^{232}, U^{235}, and U^{238} were measured by radiochemical techniques; at 21.5 Mev, the cross sections are 0.83, 1.31, and 1.28 barns, respectively (±15 percent in each case). Cross sections for (p,xn) reactions in U^{238} were found to be quite small. The total reaction cross sections correspond to a nuclear radius of $(1.55\pm0.1)A^{\frac{1}{3}}\times10^{-13}$ cm. Some advantages of determining the nuclear radius by total reaction cross sections are pointed out, and the discrepancy between electromagnetic and nuclear determinations of the nuclear radius is discussed.

MEASUREMENTS of cross sections for neutron-induced fission on various target isotopes and for various incident neutron energies are widely scattered through the literature. Excitation functions (i.e., cross sections as a function of energy) for charged-particle-induced fission have been measured by Jungerman[1] and by Jungerman and Wright[2] using alpha particles and deuterons. Tewes and James[3] have measured the $Th(p,f)$ excitation function, though not on an absolute scale. No absolute cross sections have been reported, however, for proton-induced fission.

Fission cross sections in the medium energy region are especially interesting because, as will be shown, they are essentially a measure of the total reaction cross section, a quantity which, while of great importance in nuclear reaction theory, is generally difficult to measure. This quantity is of more basic importance when determined for protons than for deuterons or alphas, since, in the latter cases, the interpretation is complicated by the structure of the incident particle.

In addition to the fact that excitation functions for (p,f) reactions are of considerable interest, the experimental problems in carrying out the measurements have been greatly simplified by the recent studies of fission mass distributions from proton-induced fission.[3-6] As a result of this work, fission cross sections can be measured by determinations of the radiochemical yield of a single fission product. Measurements of excitation functions for proton-induced fission in Th^{232}, U^{238}, and U^{235} using the internal, circulating 22-Mev proton beam of the ORNL 86-inch cyclotron were therefore undertaken.

The experimental methods used for measurements of excitation functions have been described previously.[7] The energy of the incident protons was lower (21.9 Mev) and somewhat less homogeneous (full width at half-maximum $\simeq$ 0.7 Mev, maximum energy = 22.4 Mev) than in the previous work. Relative excitation functions were determined by bombardment of foil stacks of natural uranium metal, thorium metal, and U^{238}-oxide plated on platinum, with appropriate absorbers interspersed. The stopping powers of uranium and thorium were determined experimentally relative to that of copper (they were about 65 percent of the copper stopping power). The fission product used most consistently was 17-hr Zr^{97} (in equilibrium with 73-min Nb^{97}), although several checks were made with 85-min Ba^{139} and 9.7-hr Sr^{91}.

Absolute cross sections were determined in separate runs employing copper foils. The current was then obtained from the known cross section for the $Cu^{63}(p,n)$ reaction[8] in the region of its broad maximum at about 13 Mev. A large number of determinations (25 for U^{238}, 13 for Th^{232}, and 8 for U^{235}) was carried out. As a check on the method, measurements were made of the cross section for production of Na^{22} by proton bombardment of magnesium and compared with the measurement of that cross section by Batzel and Coleman[9] in the region of its broad minimum near 20 Mev. The magnesium cross section obtained by comparison with copper was larger than the value from reference 9 by 20 percent; in order to take this discrepancy into account, cross sections measured by the copper comparison were reduced by 10 percent.

The maximum error in the ratio of the cross section for production of Zr^{97} to the $Cu^{63}(p,n)$ cross section is estimated to be about 20 percent. The uncertainty in the absolute cross sections on which the measurements are based should not be larger than 20 percent, and errors due to energy uncertainties in the comparison of the cross sections are very small. Errors in the determination of fission yields from the smooth curve (this was necessary in the case of U^{235} and U^{238}) are generally about 5 percent in the regions of Zr, Sr, and Ba; neither studies of fission fine structure[10] nor the direct determi-

* ORINS Fellow from Chemistry Department, Denver University, Denver, Colorado.

[1] J. Jungerman, Phys. Rev. **79**, 632 (1950).
[2] J. Jungerman and S. C. Wright, Phys. Rev. **74**, 150 (1948).
[3] H. A. Tewes and R. A. James, Phys. Rev. **88**, 860 (1952).
[4] Fowler, Jones, and Paehler, Phys. Rev. **86**, 71 (1952).
[5] Jones, Timnick, Handley, and Paehler (private communication).
[6] Timnick, Handley, and Paehler (private communication).
[7] Cohen, Newman, Charpie, and Handley, Phys. Rev. **94**, 620 (1954).
[8] S. N. Ghoshal, Phys. Rev. **80**, 939 (1959).
[9] R. E. Batzel and G. H. Coleman, Phys. Rev. **93**, 280 (1954).
[10] See, for example, A. C. Pappas, Atomic Energy Commission Report AECU 2806 (unpublished). Other references are listed therein.

nations of the yields of these nuclides in thermal fission[11] or proton-induced thorium fission[4] give any indication that their yields are abnormal. Considering the fact that the Ba and Sr checks agree well with the Zr data, it is believed that uncertainties in the fission yields could not contribute errors larger than 8 percent to the absolute fission cross sections. While the sum of these effects gives a rather large maximum possible error (~50 percent), the *probable* error in the absolute cross section for U^{238} is less than 15 percent. The errors in the ratios of the cross sections for U^{235} and Th^{232} to that of U^{238} are considerably smaller.

The absolute cross section for $U^{238}(p,f)$ was determined to be 1.28 barns at 21.5 Mev. The ratios of the cross sections for Th^{232} and U^{235} to that of U^{238} at this energy were found to be 0.65 ± 0.06 and 1.02 ± 0.10, respectively. The thorium value is based largely on the Zr^{97} fission yield from reference 4, which, after remaining at roughly 4.15 percent for proton energies from 9 to 19.5 Mev, suddenly falls to 3.63 ± 0.09 percent at 21.1 Mev. If this jump is assumed not to be real so that the fission yield remains at about 4.15 percent, the ratio of the Th^{232} to U^{238} cross sections becomes 0.57.

The excitation functions for fission in U^{238} and Th^{232} are shown in Figs. 1 and 2, normalized to the above absolute values. In order to determine the total reaction cross sections, it is necessary to obtain some estimate of cross sections for competing reactions. The principal reactions to be considered are (p,xn), i.e., (p,n), $(p,2n)$, $(p,3n)$, etc. Tewes and James[4] have measured the (p,n) and $(p,3n)$ cross sections for Th^{232}; their excitation functions indicate that $(p,3n)$ is predominant at 21 Mev, and they found its cross section to be about 35 percent of the fission cross section. Their measurement is indicated in Fig. 2. Measurements of the (p,n) and $(p,3n)$ cross sections and excitation functions for U^{238} were made by comparing yields of Np^{236} and Np^{238} with those of Zr^{97}. Since the neptunium determinations require carrier-free radiochemistry, the results are somewhat inaccurate. Chemical yields from the organic-solvent extractions were estimated by counting the activity in aliquots from repeated extractions from both the solvent and acid phases. Several other tests were made to ascertain that the neptunium recovery efficiency was high. The final activities were identified as Np^{236} and Np^{238} (in the high-energy and low-energy foils, respectively) by half-life, absorption characteristics, and rough determinations of the gamma-ray spectrum. The $(p,3n)$ excitation function is shown in Fig. 1. Its shape indicates that it is the predominant (p,xn) reaction at 21.5 Mev. Its absolute value at that energy, 32 ± 13 mb, represents an essentially negligible difference between the fission cross section and the total reaction cross section for U^{238}. The (p,n) cross section was found to be 4 ± 2 mb at 14 Mev, and somewhat less at higher energies.

The fact that the fission cross section is considerably smaller in Th^{232} than in U^{238} was also found in the case of alpha- and deuteron-induced fission; it now seems

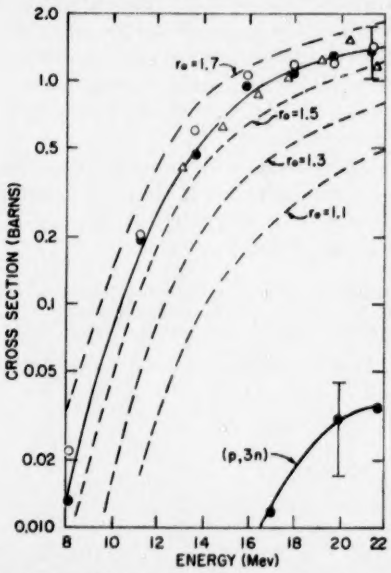

FIG. 1. Fission and $(p,3n)$ excitation functions for protons on U^{238}. The dashed curves are the theoretical total reaction cross sections for various nuclear radii.

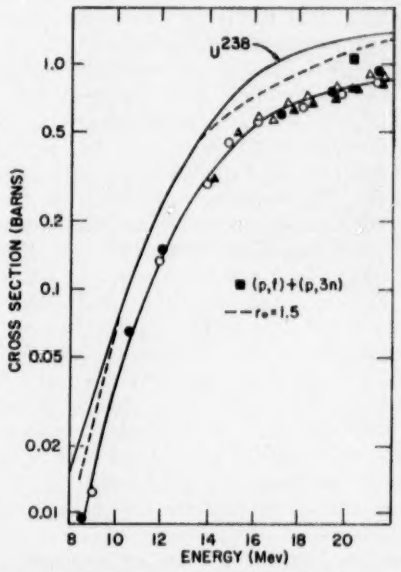

FIG. 2. Fission excitation function for protons on Th^{232}. The point labeled $(p,f)+(p,3n)$ is based on the ratio of $(p,3n)$ to (p,f) cross sections from reference 4. The dashed curve is the theoretical total reaction cross section for $r_0=1.5$, and the line labeled "U^{238}" is from Fig. 1.

[11] C. D. Coryell and N. Sugarman, editors, *Radiochemical Studies: The Fission Products* (McGraw-Hill Book Company, Inc., New York, 1951), Appendix, National Nuclear Energy Series, Plutonium Project Record, Vol. 9, Div. IV.

quite evident that this is due to less effective competition of (p,xn) reactions in the case of U^{238}.

The principal quantity of theoretical interest that can be derived from these measurements is the nuclear radius. The total reaction cross section can be expressed as a product of the geometric cross section [approximately $\pi(R+\lambda)^2$], a Coulomb factor, and a "sticking probability." At energies well above the Coulomb barrier, the Coulomb factor merely takes into account the fact that the path of an incident charged particle approaching a nucleus is hyperbolic rather than rectilinear. The exact quantum mechanical results can be reproduced with reasonable accuracy by a simple classical calculation from Newtonian mechanics.[12] This calculation is quite insensitive to the distribution of charge inside the nucleus. The "sticking probability" has a maximum value of unity and is well known to approach that value closely for the cases under consideration. Furthermore, it will be seen that the interesting feature of these measurements is the large value of the cross section; this feature would be unchanged if the "sticking probability" were less than unity. Measurements of total reaction cross sections at energies well above the Coulomb barrier therefore have a considerable advantage over determinations of the nuclear radius by Coulomb barrier penetration[13] [such as the half-life—energy relationship in alpha decay and low-energy (p,n) excitation functions] or by total neutron cross sections[13] which are difficult to interpret theoretically. The interpretation of the nuclear radius determined from total reaction cross sections is very straightforward, and essentially classical—when an incident particle passes within that distance of the center of the nucleus, a nuclear reaction takes place.

Figure 1 shows the theoretical total reaction cross section for $r_0=1.1$, 1.3, 1.5, and 1.7 (nuclear radius $=r_0A^{\frac{1}{3}}\times10^{-13}$ cm), calculated as described by Shapiro *et al.*[14] Comparison of these curves with the data indicates that $r_0=1.55\pm0.1$. Considering the uncertainties involved, $r_0=1.5$ is within the expected error, but values lower than about 1.3 seem to be completely out of the question. The same conclusion is obtained from the U^{235} and Th^{232} cross sections. It is interesting to note that this value of r_0 is in excellent agreement with the only other existing measurement of a total reaction cross section at energies well above the Coulomb barrier, Kelly's determination of the (p,n), $(p,2n)$, and $(p,3n)$ cross sections for bismuth.[15]

The fact that this value of r_0 is considerably larger than that found from the electron scattering[16] and from μ-mesonic x-ray fine structure[17] measurements (although it is in general agreement with determinations by other nuclear methods)[13] is at first surprising. However, this discrepancy between the determinations of the nuclear radius by electromagnetic and nuclear methods may perhaps be explained as follows: Electromagnetic measurements determine the radius at which the absolute value of the nuclear wave function becomes different from zero; since the nuclear wave function determines the spatial distribution of the nucleons considered as points—there is nothing in the wave function which indicates that a point nucleon is the center of a nuclear force—electromagnetic experiments determine the spatial distribution of these "point" nucleons. Nuclear experiments, however, determine the radius at which the incident particle first experiences a nuclear force. This happens when it comes within the range of the nuclear force of the "point" nucleons in the target nucleus. Thus, radius determinations by nuclear experiments should be larger by the range of nuclear forces than determinations by electromagnetic experiments. For the heaviest nuclei, this represents a difference of about 25 percent, which approximately accounts for the discrepancy.

The authors would like to acknowledge the many helpful suggestions of W. H. Jones (Consultant from Emory University), A. F. Roemer, Jr., and F. Moore in some of the chemical separations.

[12] J. M. Blatt and V. F. Weisskoff, *Theoretical Nuclear Physics* (John Wiley and Sons, Inc., New York, 1952).
[13] Summarized in reference 12, p. 15.
[14] M. M. Shapiro, Phys. Rev. **90**, 171 (1953); Feshbach, Shapiro, and Weisskoff, U. S. Atomic Energy Commission Report NYO 3077 (unpublished).
[15] E. Kelly, University of California Radiation Laboratory Report UCRL 1044 and private communication.
[16] Hofstadter, Fechter, and McIntyre, Phys. Rev. **92**, 978 (1953).
[17] V. L. Fitch and J. Rainwater, Phys. Rev. **92**, 789 (1953).

Energy Levels of Al^{27}†

C. P. Browne, S. F. Zimmerman, and W. W. Buechner
Physics Department and Laboratory for Nuclear Science, Massachusetts Institute of Technology, Cambridge, Massachusetts
(Received July 12, 1954)

Proton groups inelastically scattered from Al^{27} were observed with a high-resolution magnetic analyzer. Bombarding energies between 5.6 and 8.4 Mev were provided by an electrostatic generator. Twenty-two levels have been observed up to 6-Mev excitation. Discrepancies with previous work, both as to number and position of levels, appear. A level at 1.777 Mev in Si^{28} was also measured.

I. INTRODUCTION

A FEW of the energy levels of the Al^{27} nucleus have been seen by several investigators,[1] while Reilly *et al.*[2] have made an extensive survey of the levels up to about 5.7 Mev using inelastically scattered protons. Their cyclotron gave a bombarding energy of 8 Mev, and magnetic analyzers measured input and output energies with good resolution.

In connection with other work on the MIT-ONR electrostatic generator, some of the aluminum levels around 5-Mev excitation were observed. The measured excitations did not agree with the published values. In attempting to account for the discrepancy, these levels were measured again with inelastic proton scattering, and this led to an investigation of the whole aluminum spectrum up to 6-Mev excitation. A preliminary report of the present work has been given.[3]

II. EQUIPMENT AND PROCEDURE

The generator and magnetic analyzer gave proton beams of energies ranging from 5 to 8.4 Mev with a spread in energy of 0.1 percent. An 0.5 mm×5 mm entrance slit defined the beam spot on the targets. An annular magnetic spectrograph was used to measure the energy of particles scattered at 90 degrees to the incident beam. The uniform magnetic field of the spectrograph focused the scattered particles onto a nuclear emulsion after a 180-degree deflection. This instrument has been briefly described in a recent paper.[4]

The annular magnet was calibrated with polonium alpha particles, the $B\rho$ for which was taken to be 3.31588×10^5 gauss-centimeters, and the beam analyzer was then calibrated against this magnet using elastically scattered particles. The input energy was remeasured in this way for each run. The magnetic fields were measured with nuclear resonance fluxmeters. The scattering angle was measured by optical means and checked by observing the energy difference between elastic groups scattered from a heavy and a light nucleus (gold and lithium).

Two types of targets were used. For much of the initial survey, thin aluminum-foil targets, which produced an energy spread in the scattered-particle group several times the analyzer resolution, were used. These gave the maximum peak heights and assured detection of weak groups. A thin layer of aluminum evaporated onto thin Formvar was then bombarded, and each of the groups observed from the targets was carefully studied. The energy width of the groups from these evaporated targets was essentially that caused by the effective analyzer resolution. Levels spaced as closely as 15 kev were easily resolved with these targets.

The region of excitation from the ground state to 4 Mev was surveyed at a bombarding energy of 6.57 Mev; from 3.6 to 4.9 Mev, at an energy of 7.04; and from 4.3 to 5.85 Mev, at an energy of 8.17. The region of excitation from 2.7 to 5.3 Mev was also covered at 7.58 Mev, and that from 5.0 to 6.0, at 8.45 Mev. An energy of 5.64 was used in addition to measure the two levels of lowest excitation. With two exceptions, all levels were seen with at least two bombarding energies.

III. RESULTS

Figure 1 shows a composite plot of the proton groups observed from the thin evaporated targets. The regions in the figure where no data are shown were found in the experiments with the foil targets to be free of groups from aluminum. At each bombarding energy, the intensities of the groups from different targets have been normalized against the elastic group. Because of insufficient collimation of the beam, and possibly other effects, the relative intensities do not reproduce well; therefore, the intensities shown should be regarded as approximate.

From the foil-target data (not shown), it can be stated that no groups, other than those shown in Fig. 1, with intensities greater than 5 percent of the first excited-state group appear up to an excitation of 5.3 Mev. From 5.3- to 6.0-Mev excitation, the intensity limit is based on the data shown in the top curve of Fig. 1. In this region, it is possible that a group of about one-quarter the intensity of the weakest one shown could have been missed. There is some evidence for a

† This work has been supported in part by the joint program of the U. S. Office of Naval Research and the U. S. Atomic Energy Commission.

[1] P. M. Endt and J. C. Kluyver, Revs. Modern Phys. **26**, 95 (1954).

[2] Reilly, Allen, Arthur, Bender, Ely, and Hausman, Phys. Rev. **86**, 857 (1952).

[3] S. F. Zimmerman and C. P. Browne, Phys. Rev. **94**, 749 (1954).

[4] Buechner, Sperduto, Browne, and Bockelman, Phys. Rev. **91**, 1502 (1953).

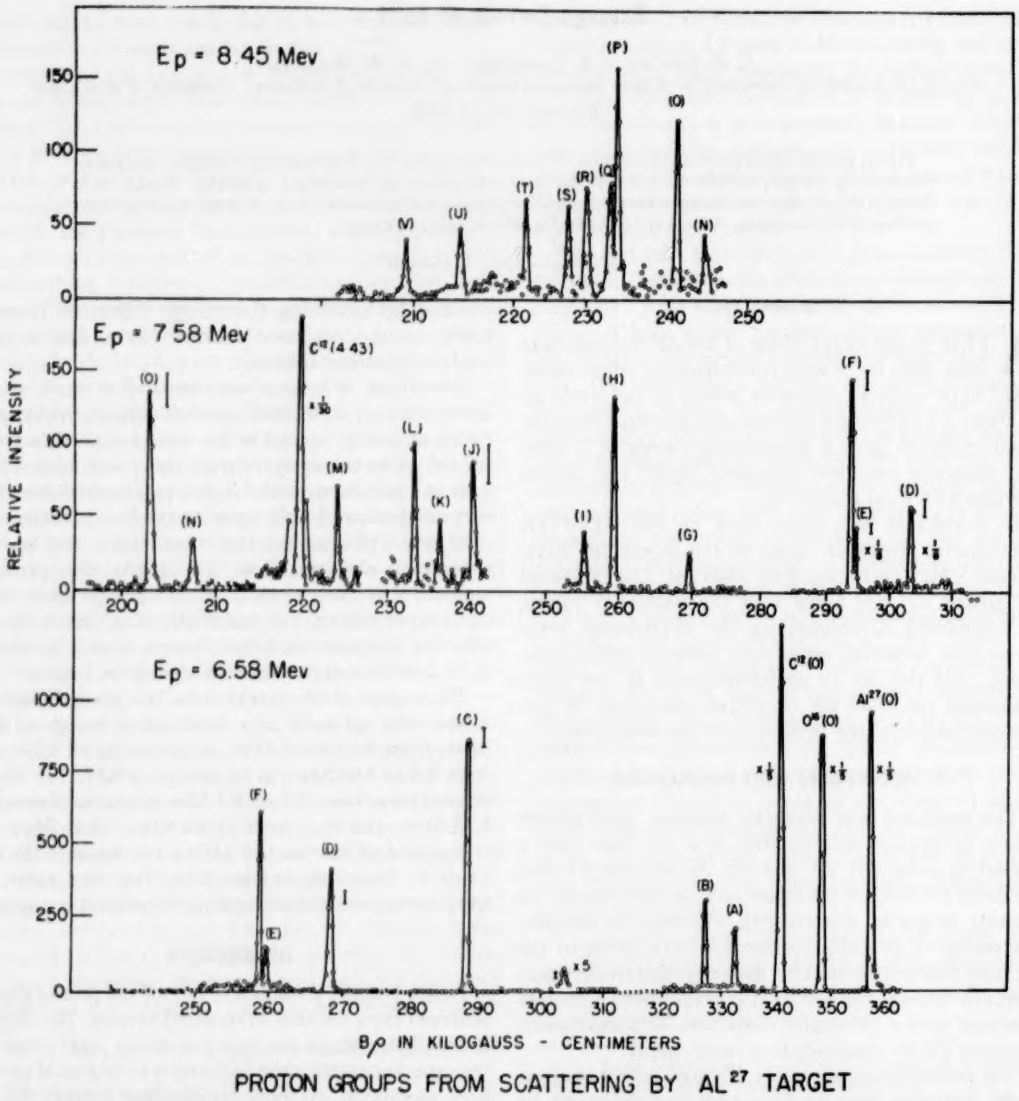
Ep = 8.45 Mev
Ep = 7.58 Mev
Ep = 6.58 Mev
RELATIVE INTENSITY
Bρ IN KILOGAUSS - CENTIMETERS
PROTON GROUPS FROM SCATTERING BY AL27 TARGET

FIG. 1. Composite plot of protons scattered from Al^{27}. Various thin evaporated targets on Formvar backings were used. The peak heights have been normalized to the elastic groups for each target. Regions of excitation in Al^{27} for which no data are shown were observed at other bombarding energies and showed no groups. Groups from excited levels of Al^{27} are labeled alphabetically. Points marked by crosses are from a foil target.

group between groups T and U ($B\rho=218$, Fig. 1). On two exposures at 8.45 Mev, a number of tracks significantly above background appeared. However, on a third exposure at this energy and at a bombarding energy of 8.17, no group appeared in this region of excitation. Another group appeared on one exposure between P and O ($B\rho=237$, Fig. 1), but failed to repeat.

The alphabetically labeled groups in Fig. 1 have been assigned to excited states of Al^{27}. The assignment is based on the constancy of the relative intensity of groups from the foil and evaporated targets and the observation of the change of energy of the scattered group with changing bombarding energy. The region containing the elastically scattered groups was carefully studied to insure that the target did not contain appreciable amounts of contamination other than carbon and oxygen. Since Formvar was used as a target backing, elastic and inelastic groups from carbon and oxygen are to be expected; however, as their energies are well-known, they may be easily identified.

The group labeled V is the only one for which a

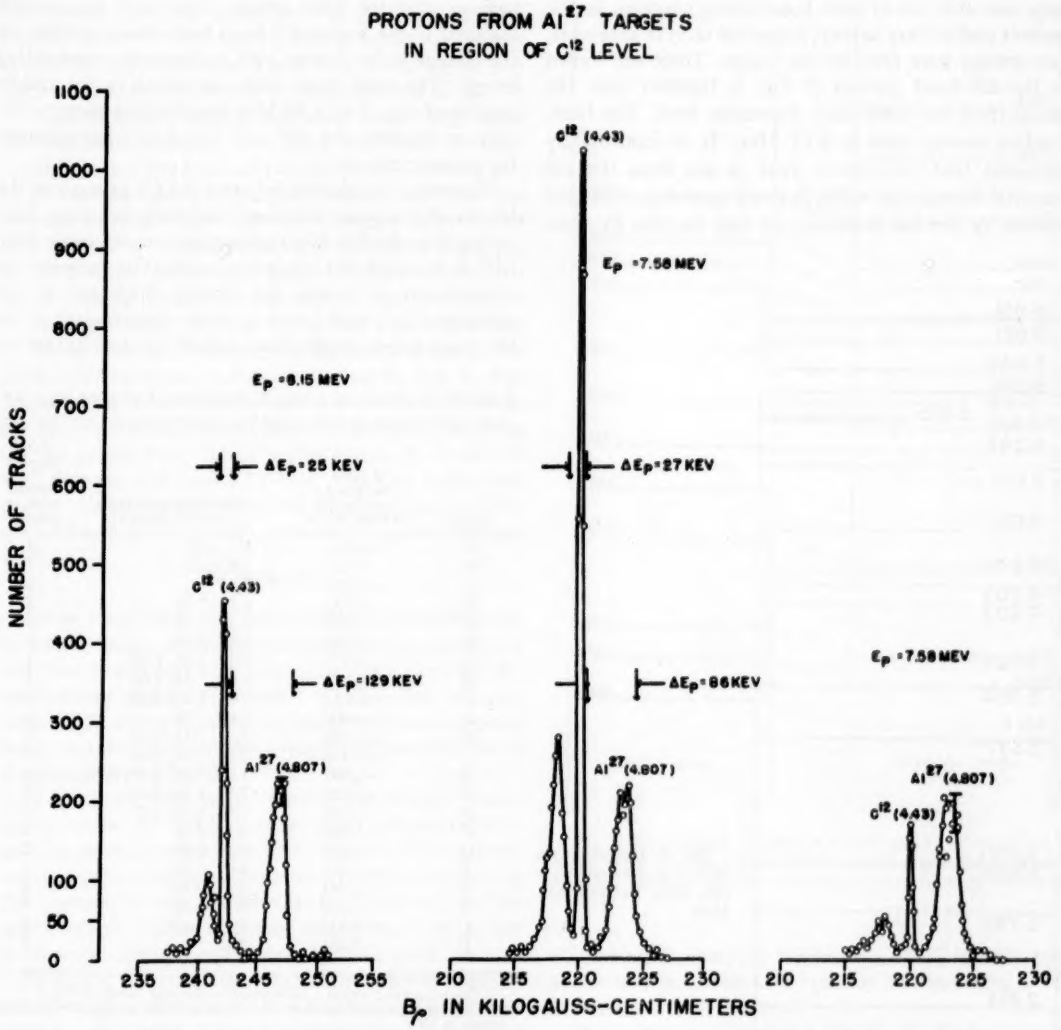

FIG. 2. Evidence for assignment of two proton groups to carbon contamination on front and back surface of aluminum foil target. For explanation, see text.

reservation in assignment must be made. It was observed only once, this being the run shown in the top part of Fig. 1.

In addition to the groups assigned to Al^{27} and to C^{12} and O^{16}, Fig. 1 shows a very weak group at $B\rho=304$ in the lower part of the figure. This latter group has been observed at four bombarding energies between 5.2 and 7 Mev. From its observed change in energy, it may be assigned to a nucleus of mass 28 ± 4. If it is assumed to be from Si^{28}, the excitation is 1.777 Mev. This corresponds to a known level.[5] As a check, a target of evaporated SiO_2 was bombarded immediately after the aluminum. An extremely intense group was found at the same position. Based on the intensity of the group relative to the elastic group from silicon for the SiO_2 target, it was estimated that the amount of silicon contamination on the aluminum target needed to give the observed inelastic peak would give an elastic group that would be lost in the background at the base of the elastic group from Al^{27}. Silicon contamination has been observed before in the annular magnet and might be expected as a contaminant in the foil targets, and it is not surprising to find it here. There is therefore no evidence for an Al^{27} group at 1.8 Mev, as seen by some researchers.[1]

The region containing the group associated with the 4.43-Mev level in C^{12} is of particular interest, as Reilly *et al.* report two levels in Al^{27} that would give groups

[5] R. A. Peck, Phys. Rev. **76**, 1279 (1949); H. T. Motz and D. E. Alburger, Phys. Rev. **86**, 165 (1952).

very near this one at their bombarding energies. In the present preliminary survey, where foil targets were used, two groups were seen in this region. These are shown in the left-hand portion of Fig. 2, together with the group from the 4.807-Mev aluminum level. The bombarding energy here is 8.15 Mev. It is immediately apparent that the central peak is not from the foil material because its width is much narrower than that caused by the foil thickness, as may be seen by comparison with the 4.807 group. This peak was readily assigned to the known C^{12} level from measurements on the change in its energy with a change in bombarding energy. The same three peaks are shown in the middle portion of Fig. 2 for 7.58-Mev bombarding energy. The spacing between the Al^{27} and C^{12} groups has changed the proper amount.

However, the spacing between the C^{12} group and the left-hand group has remained essentially constant, indicating that the left-hand group also cannot come from Al^{27}. It is noted that the energy separation between the two groups is closely the energy thickness of the aluminum foil, and hence it seems apparent that the left-hand group arises from carbon contamination on the back side of the foil. Straggling and nonuniformity of the foil would account for its width. Reilly used a fresh foil in investigating this region and did not report any group from carbon. The right-hand portion of Fig. 2 shows the result of bombarding, at 7.58 Mev, a new foil that had not previously been used. It is seen that the groups assigned to carbon on the two surfaces are greatly reduced in intensity but are still comparable to the intensity of the group from aluminum. The emulsion technique allowed this whole plot to be recorded simultaneously, and undoubtedly this target had considerably less bombardment than Reilly required to plot the region point by point using a counter.

With the thin evaporated aluminum layers on thin Formvar backings, a single intense group is seen from

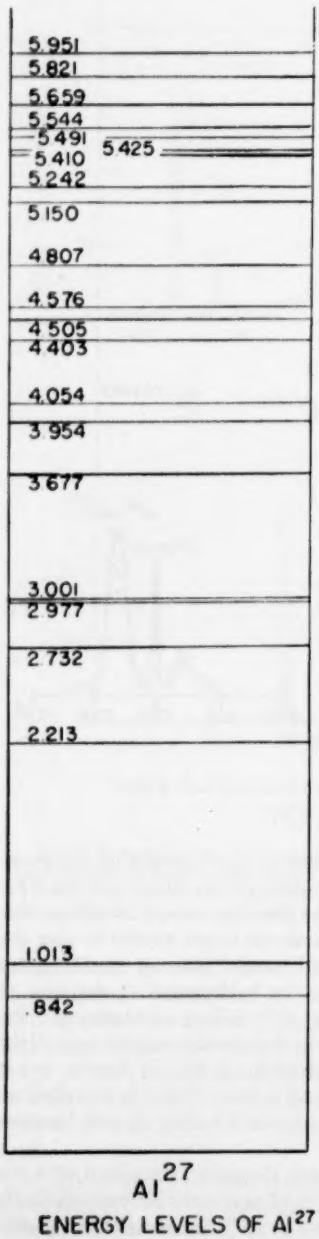

FIG. 3. Energy levels of $^{29}Al^{27}$ as determined in this work. Values are in Mev.

TABLE I. Q values for inelastic scattering of protons from Al^{27}.

Group[a]	Q value weighted average all ±0.006 Mev[b]	Bombarding energies at which observed[c]	Total number of observations used in average[d]
A	−0.842	5.6, 6.57	4
B	−1.013	5.6, 6.57	3
C	−2.213	6.57	2
D	−2.732	6.57, 7.58	3
E	−2.977	6.57, 7.58	2
F	−3.001	6.57, 7.58	2
G	−3.677	6.57, 7.04, 7.58	4
H	−3.954	7.04, 7.58, 8.00	3
I	−4.054	7.04, 7.58, 8.00	3
J	−4.403	7.04, 7.58	2
K	−4.505	7.04, 7.58, 8.16	3
L	−4.576	7.04, 7.58, 8.16	3
M	−4.807	7.04, 7.24, 7.58, 8.16	6
N	−5.150	7.58, 8.16, 8.45	3
O	−5.242	7.58, 8.16, 8.45	3
P	−5.410	8.17, 8.45	2
Q	−5.425	8.17, 8.45	2
R	−5.491	8.17, 8.45	2
S	−5.544	8.17, 8.45	3
T	−5.659	8.17, 8.45	3
U	−5.821	8.17, 8.45	3
V	−5.951	8.45	1

[a] The letters in Column 1 correspond to the peak labels of Fig. 1.
[b] Column 2 gives the Q value which is numerically equal to the excitation energy in Al^{27}.
[c] Column 3 lists the bombarding energies used to measure each group.
[d] Column 4 gives the total number of measurements used in the average for each Q value.

the carbon level, as shown in Fig. 1. The region of excitation in Al^{27} obscured by this group at one energy is clear at other energies. There is no evidence for any aluminum group between the groups labeled *M* and *N*.

The measured *Q* values, which are numerically equal to excitation energies, are listed in Table I. Each number is the weighted average of the values from two to six separate exposures, none of which vary from the average by more than 8 kev. The bombarding energies and number of measurements for each level are given in the last two columns of Table I. The level diagram for Al^{27}, as determined in this work, is shown in Fig. 3.

The discrepancy between the present work and that of Reilly *et al.* is illustrated by the comparison of the level schemes above 4-Mev excitation in Fig. 4. The present values are about 70 kev lower. This difference gradually decreased toward lower excitations, vanishing for the lowest level. As discussed above, no levels are seen between 4.81 and 5.15 Mev. The two levels near 3 Mev with 24-kev spacing and the two near 5.4 Mev with 15-kev spacing were unresolved in the previous work.

IV. ERRORS

Errors involved in the measurements included errors in measurement of group positions on the emulsions, analyzer calibration with polonium alpha particles, determination of scattering angle, measurement of magnetic fields, variation of input energy between measurement of elastic and inelastic groups, and possible effects of target contamination.

It is felt that the major part of the over-all uncertainty stated in Table I arises from errors in determining the radius of the particle trajectory by measurements on the emulsion. This comes from uncertainty in the position of the emulsion both while it is in the spectrograph during exposure and while it is in the microscope during measurement of track positions.

Evidence that the error caused by carbon buildup on the targets is negligible is contained in Fig. 2. The target used to give the groups shown in the center of the figure had been bombarded considerably longer than any target used for final energy measurements. The width of the group from carbon on the surface is still just the analyzer resolution. Thus, the stopping power of the carbon layer cannot be more than a few kilovolts.

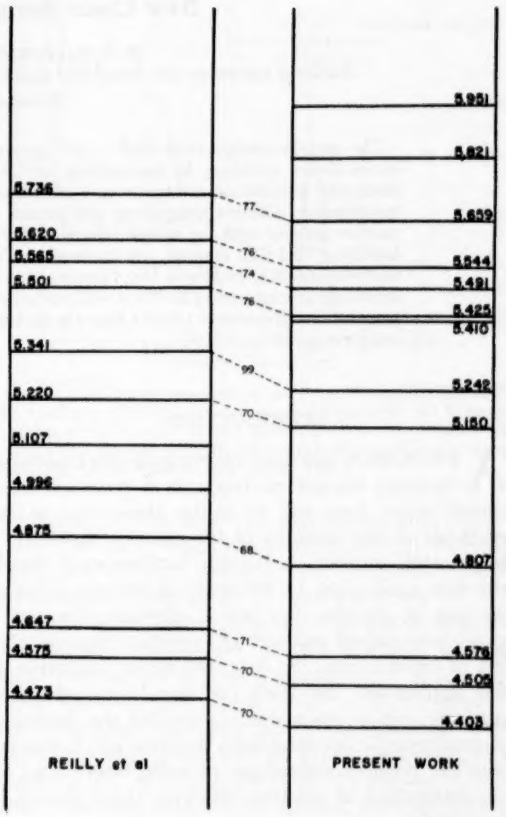

FIG. 4. Comparison of present values and those obtained by Reilly *et al.* for the excited states of Al^{27} above 4.4 Mev. The numbers between the two level diagrams are energy differences in kev.

It is a pleasure to thank Dr. C. K. Bockelman for help in taking some of the data and our plate readers Mr. W. A. Tripp and Miss Janet L. Frothingham for their faithful measurements on the nuclear emulsions.

New Chain Barium-126—Cesium-126

M. I. KALKSTEIN AND J. M. HOLLANDER
Radiation Laboratory and Department of Chemistry, University of California, Berkeley, California
(Received July 9, 1954)

The neutron-deficient chain Ba^{126}—Cs^{126} has been produced from nitrogen-ion bombardments of indium in the 60-inch cyclotron, by the reaction $In^{115}(N, 3n)$. Studies have been made of this new chain with a 50-channel scintillation spectrometer, a scintillation coincidence spectrometer, and a time-of-flight mass spectrograph. Element assignments and genetic relations have been verified chemically, and the mass number assigned with the isotope separator. Ba^{126} decays principally by orbital electron capture with a half-life of 96.5±2.0 minutes, and its daughter Cs^{126} is a positron emitter of 1.6±0.2 minute half-life and electron capture branching of 18±4 percent. The decay of Cs^{126} proceeds by allowed transitions, ~62 percent to the ground state of Xe^{126} and ~38 percent to the first excited state at 385 kev. The positron spectrum has a maximum energy of 3.8±0.4 Mev. On the basis of its decay properties, Cs^{126} appears to have a ground-state configuration of (1+).

INTRODUCTION

A PROGRAM has been underway in this laboratory to study the nuclear reactions of cyclotron-accelerated heavy ions and to utilize these ions in the synthesis of new isotopes of the heaviest elements.[1–4] In principle at least, heavy-ion bombardment should also find application to the study of neutron deficient isotopes of medium and low Z elements, because it provides an almost unique way to prepare these isotopes free of heavier ones. To date, the major limitation on this application has been the low beam intensities available, which has severely restricted the feasibility of spectroscopic investigations. Nonetheless, it was felt that the possible advantages of using heavy ions for the production of neutron deficient nuclei should be examined.

In the work reported here, a new neutron-deficient chain, $_{56}Ba^{126}$—$_{55}Cs^{126}$, has been produced by the irradiation of indium ($Z=49$) targets in the nitrogen ion beam of the Crocker 60-inch cyclotron. The genetic relationship between these nuclides has been verified by means of chemical "milking" experiments, and their radiations have been studied with NaI and anthracene scintillation detectors coupled to a 50 channel differential analyzer. Some coincidence studies have also been made by using the scintillation coincidence spectrometer. Assignment to the mass-126 chain has been accomplished by means of a time-of-flight mass spectrometer. Barium-126 is found to have a half-life of 96.5 minutes, and to decay by orbital electron capture. Its daughter, $_{55}Cs^{126}$, decays with a 1.6-minute half-life, chiefly by the emission of positrons of maximum energy about 3.8 Mev.

A 12-minute barium activity, which may be Ba^{127} or possibly Ba^{124}, has also been observed in some short nitrogen ion bombardments of indium. This will be reported only briefly, since no detailed study of this nuclide has been undertaken.

BOMBARDMENT CONDITIONS

In most of the bombardments, targets of indium oxide (In_2O_3)[5] weighing ~100 mg were mounted in 0.25- or 0.5-mil platinum envelopes for use with the internal heavy ion probe. A few runs were also made using targets of indium metal melted to the copper backing plate of a water-cooled probe. Irradiations were made at a dee radius of 23.5 inches. The energy of the nitrogen ion beam has a continuous distribution with a maximum of ~140 Mev.[3] Because of the thick targets used, it was not possible to monitor the beam during bombardments, but nitrogen ion currents measured separately have averaged around 0.1 microampere. Bombardment times were either short (two to five minutes) or of the order of an hour, depending upon the half-lives of the barium activities being studied.

CHEMICAL PURIFICATIONS

A pure barium fraction was prepared initially from the indium metal or oxide targets by a procedure involving the precipitation of $Ba(NO_3)_2$ with fuming HNO_3 followed by precipitation of $BaCl_2$ with "ether-HCl" reagent.

The rapid "milkings" of cesium from solutions containing the Ba^{126}—Cs^{126} equilibrium mixture made use of sodium cobaltinitrite as a precipitant for cesium. The $Cs_2Co(NO_2)_6$ precipitate was quickly dissolved in fuming HNO_3, and several $Ba(NO_3)_2$ scavenges performed. The entire procedure consumed less than three minutes.

EXPERIMENTAL RESULTS

Half-Lives

The barium chemical fractions from the nitrogen ion bombardments of indium exhibited, after the decay of an

[1] Miller, Hamilton, Putnam, Haymond, and Rossi, Phys. Rev. 80, 486 (1950).
[2] Ghiorso, Thompson, Street, and Seaborg, Phys. Rev. 81, 154 (1951).
[3] Rossi, Jones, Hollander, and Hamilton, Phys. Rev. 93, 256 (1954).
[4] Ghiorso, Rossi, Harvey, and Thompson, Phys. Rev. 93, 257 (1954).

[5] The In_2O_3 powder was prepared from Indium Corporation of America 99.97 percent metal by HNO_3 solution, hydroxide precipitation, and finally ignition to the oxide.

initial ~12-minute component, a single activity which followed a period of 96.5±2.0 minutes through as many as ten half-lives without deviation. When the chemical purification was performed more than an hour after the end of bombardment, only the 97-minute activity appeared in the barium fraction, proving its chemical identity as an isotope of barium.

By making a series of rapid chemical separations of cesium away from a solution containing the 97-minute barium activity, a cesium daughter has been isolated whose half-life was measured from five milkings to be 1.5±0.3 minutes.

Mass Assignment

With the aid of M. C. Michel, the mass assignment of the new Ba−Cs chain has been made on a medium-resolution, high-transmission (~20 percent) isotope separator employing the time-of-flight principle.[6]

The sample, containing ~10^5 dis/min of the 97-minute barium in equilibrium with its cesium daughter, was deposited onto a tungsten filament in the form of ~50 μg $BaSO_4$. Because of the weakness of this source, it did not seem feasible to attempt collection of barium ions, consequently advantage was taken of the much greater ionization efficiency of the short-lived cesium daughter. By "flashing" the ion source at a temperature sufficient to ionize cesium but not vaporize barium it was possible to collect cesium ions alone, accomplishing simultaneously both chemical and mass separation. By so retaining barium on the filament, the experiment could be repeated several times with essentially no loss in yield of cesium at the collector end.

After flashing the source for ~10 seconds, the vacuum system was quickly let down to air, and the collector plate removed for counting. This procedure consumed about two minutes. Activity was found to collect only at the mass-126 position, and this decayed with a half-life of 1.6±0.2 minutes. The new chain is thus identified as Ba^{126}−Cs^{126}, produced by the reaction $In^{115}(N, 3n)Ba^{126}$.

Gamma Spectra

Nitrogen ion bombardments of around an hour's duration yielded less than 10^6 disintegrations per minute of the Ba^{126}−Cs^{126} chain, so it was not possible to utilize high resolution magnetic spectrometers in an examination of the beta and gamma spectra. Consequently, we have made use principally of a NaI(Tl) scintillation detector coupled to a 50-channel differential analyzer designed by Ghiorso and Larsh.[7]

TABLE I. Positron and x-ray abundances.

	Ba^{126}+Cs^{126} equilibrium	− Cs^{126}	= Ba^{126}
X-rays	~1.2	0.18	~1
β^+	~0.8	0.82	~0
Total	2.0	1.0	1.0

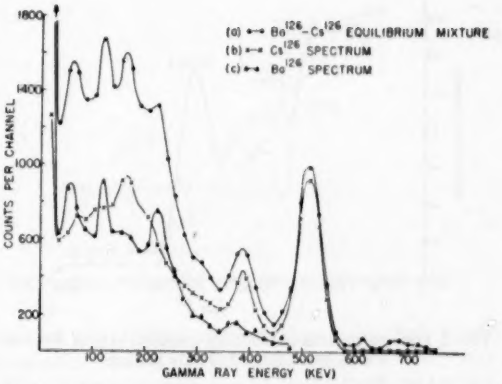

FIG. 1. (a) Gamma spectrum of Ba^{126}−Cs^{126} equilibrium mixture. Ordinate at 30-kev channel equals 6100 counts. (b) Gamma spectrum of Cs^{126}. (c) Gamma spectrum of Ba^{126}, obtained by subtracting *b* from *a*. [The 510-kev peak of Fig. 1(b) has been normalized to the 510-kev peak of Fig. 1(a).]

In these experiments, the gamma-ray spectrum of the barium-cesium equilibrium mixture was first studied, and it was verified that all peaks decayed with a 97-minute half-life. Then a pure sample of the 1.5-minute cesium daughter was prepared by the "milking" procedure described above, and its gamma spectrum was examined. The spectrum due to the 97-minute barium parent was then obtained by making the appropriate subtraction of the cesium spectrum from that of the equilibrium mixture. Figure 1 shows the spectrum between 0 and 750 kev of the equilibrium mixture, the pure Cs^{126}, and the subtracted spectrum obtained for the Ba^{126} parent. It is noted, from the observed relative abundances and from the equilibrium conditions prevailing, that the x-rays (at ~30 kev) belong mainly to the Ba^{126} while the annihilation radiation accompanies the decay of Cs^{126}.

The gamma spectrum of Cs^{126} is quite simple; other than annihilation radiation and ~30-kev x-rays only a gamma ray of 385±5 kev is in evidence. The peak (in Fig. 1(b)) at ~170 kev is due to 180° backscattered annihilation radiation, and that at ~75 kev is the lead fluorescent x-ray generated in the counter shield. From the observed[8] photopeak abundances, it is calculated that Cs^{126} decays principally by positron emission, with an electron capture branching of 18±4 percent. The 385-kev gamma ray appears in 38±7 percent of the disintegrations. No gamma ray of energy greater than 600 kev is observed with an abundance higher than 5 percent of the disintegrations.

The gamma spectrum of Ba^{126}, obtained by sub-

[6] W. E. Glenn, University of California Radiation Laboratory Report UCRL-1628, January, 1952 (unpublished); M. C. Michel and D. H. Templeton, Phys. Rev. **93**, 1422 (1954).

[7] A. Ghiorso and A. E. Larsh (to be published).

[8] The calibration of the scintillation spectrometer is described in the Appendix.

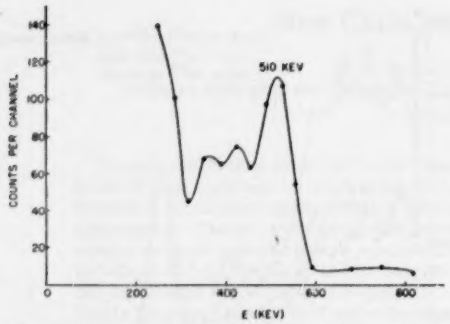

FIG. 2. Gamma-gamma coincidence counting rate of 385-kev γ rays as a function of gate setting.

traction, is more complex. Gamma rays of 225±10 kev and 700±30 kev are definitely observed, with relative intensities 3:1. A weak gamma ray at ~900 kev is probable. The peak at 115 kev appears to be largely backscattered 225-kev radiation, since its relative intensity varies with position of the source in the counter shield. X-rays are the predominant feature of the decay of Ba^{126}, but because of the uncertainties accompanying the subtraction of the gamma spectra and because of the unknown contribution of x-rays from internal conversion of the gamma-rays, a ratio of electron capture to positron emission in Ba^{126} cannot be given with confidence.

The direct decay of the gamma-ray lines from the 1.6-minute Cs^{126} was observed by performing the fast cesium "milking" from the parent, placing the separated cesium fraction into the scintillation spectrometer, and photographing the dials of the spectrometer with a Leica camera at half-minute intervals following each "milking." By subtraction of the dial readings of one negative from those of the next negative, the spectrum during each half-minute period could be examined. In this way, decay curves have been constructed for the integrated photopeaks of the annihilation gamma ray, the 385-kev gamma ray, and for the K x-rays; all exhibit a half-life of 1.6±0.2 minutes, through five half-lives.

Beta Spectrum

The end point of the positron spectrum was measured in a sample of the Ba−Cs equilibrium mixture by means of an anthracene scintillation crystal coupled to the 50-channel analyzer, and also by absorption in beryllium. Both methods gave a value of 3.8±0.4 Mev. As noted above, these positrons are associated with the decay of Cs^{126}.

Coincidence Measurements

Several experiments were done in which the Ba^{126}−Cs^{126} chain was examined with a coincidence scintillation spectrometer designed by J. O. Rasmussen. The apparatus consists of a NaI or anthracene gate detector coupled to a single-channel analyzer, and a NaI coincidence detector coupled to the 50-channel analyzer. In these experiments, the resolving time was $\approx 8\times10^{-8}$ second. The anthracene detector in the gate circuit was employed when positron-gamma coincidences were being examined; for gamma-gamma coincidences NaI crystals were used in both circuits. The two crystals were shielded from each other by a 2-inch lead brick and beryllium absorbers were placed in front of the gamma-ray detector to absorb electrons.

Although the short half-life of the activity under study prevented the accumulation of sufficient events per experiment to give good statistics, several qualitative results were obtained by sweeping the gate channel over the gamma spectrum in increments of ~35 kev and recording the coincident gamma spectrum at 90° on the 50-channel analyzer. Figure 2 is a plot of the coincidence rate at ~385 kev on the 50-channel analyzer as a function of gate setting, showing a maximum rate at a gate setting of ~510 kev. Figure 3 similarly indicates the coincidence rate at ~510 kev, showing a maximum at a gate setting of ~385 kev. These experiments verified that the 385-kev gamma ray follows positron decay in Cs^{126}. They also serve to point out that there is no gamma ray of ~500 kev following positron decay of Cs^{126}, since few 500-500 gamma-gamma coincidences are observed. An upper limit of 4 percent per disintegration can be set for a possible gamma ray at ~500 kev. This fact could not be deduced from the gross gamma spectrum alone, because of interference from the prominent 510-kev annihilation peak. Even those few 510γ-510γ coincidences that are observed at 90° might be explained as being due to annihilation-annihilation coincidences, since an appreciable fraction of positrons annihilate in flight, giving annihilation quanta at angles other than 180° with respect to each other.

In scanning high energies on the gate, a maximum of gamma-gamma coincidences in the region of 225 kev was obtained when the gate was set at ~700 kev, offering some evidence that the 225-kev gamma ray in

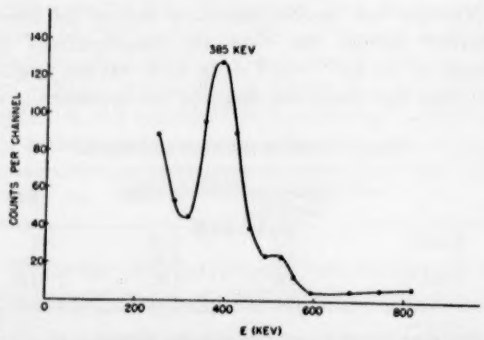

FIG. 3. Gamma-gamma coincidence counting rate of 510-kev γ rays as a function of gate setting.

Ba^{126} may be in coincidence with the 700-kev gamma ray.

Using the anthracene crystal in the gate circuit, positron-gamma coincidences were run at 180°. With a gate setting $\ll 3$ Mev, coincidences were observed at $\sim$390 kev and $\sim$510 kev. At a gate setting of $\sim$3.5 Mev, the $\sim$390-kev peak was not observed, but the positron-annihilation coincidences remained. Since no gamma ray other than that at 385 kev is observed in the decay of Cs^{126}, it is inferred from the above that a ground-state positron transition takes place between Cs^{126} and Xe^{126}.

CONCLUSIONS

From the observed positron and gamma-ray abundances in Cs^{126}, some conclusions can be drawn about its decay scheme. Log*ft* values of 4.7 and 4.8 are calculated[9] for the positron decay to the ground and first excited states of Xe^{126}, respectively. These are both within the range of values expected for "allowed" transitions, and suggest that the configuration of the ground state of Cs^{126} is (1+), since (0+) and (2+) doubtless represent the configurations of the first two states in Xe^{126}. The energy of the first excited state of Xe^{126} found in this work, 385±5 kev, is in agreement with that reported from studies of the beta decay of I^{126} by Perlman and Friedlander[10] (386±2 kev) and by Mitchell *et al.*[11] (395±5 kev).

In a further study of the radiations of I^{126}, Perlman and Welker[12] have reported a second excited state in Xe^{126} at $\sim$870 kev, with a configuration also (2+). It is of interest to note that in the present study this state was not observed from the decay of Cs^{126}. A limit of 4 percent for the population of this state was set by the absence of coincidences between the 510-kev gamma ray and a gamma of 485 kev which would be expected to de-excite an 870-kev state if the spin sequence were (2+)→(2+)→(0+) as reported by Perlman and Welker. If the same selection rules are operative for decay of Cs^{126} to all these states, one would expect an 870 kev (2+) state in Xe^{126} to be populated from Cs^{126} to the extent of perhaps 20 percent, which is substantially above our experimental upper limit. A cross-over gamma ray of 870 kev was also not observed in the gamma spectrum of Cs^{126}, but its expected abundance might be as low as the upper limit of 5 percent set from the gross gamma spectrum.

Because only a rough measurement of the positron energy of Cs^{126} could be obtained in these experiments, the disintegration energy cannot be specified precisely. However, the value of 4.8±0.4 Mev follows the general trend of the energy surface shown by the "beta-systematics" curves of Way and Wood.[13]

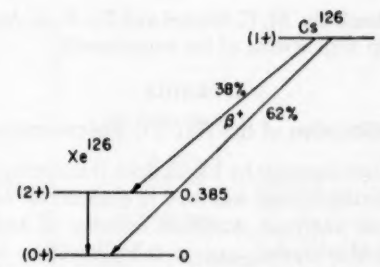

FIG. 4. Decay scheme of Cs^{126}. (β^+ should read β^++EC.)

The electron capture branching of Cs^{126}, 18±4 percent, compares with a figure of $\sim$16 percent predicted from the theoretical curves of Feenberg and Trigg[14] for allowed transitions with $Z=54$ and positron abundances and energies as reported here.

A decay scheme consistent with these data is presented in Fig. 4.

THE 12-MINUTE BARIUM ACTIVITY

In several short nitrogen-ion bombardments of indium, an approximately 12-minute activity appeared in the barium fractions in lower yield than the 97-minute Ba^{126}. This activity may be Ba^{127}, produced by the $In^{115}(N, 2n)$ reaction. Barium-127 has been observed by Lindner and Osborne,[15] who have shown that it decays with a 12-minute half-life into 6.3-hour Cs^{127}. Although no 6-hour "tail" has been seen in the Geiger counter decay curves of our barium fractions, the low $\beta+$/EC branching ratio (<10 percent) of Cs^{127} reported by Mathur and Hyde[16] would indicate that this isotope could have a counting efficiency low enough to have escaped detection in our gross decay curves.

On the other hand, it is possible that the half-life of the unknown isotope Ba^{124} could be of the order of 12 minutes, if it decays by an allowed transition. Such a half-life would require a disintegration energy of $\sim$3 Mev, which is not an unreasonable value.[13] Barium-124 would be produced in these experiments by $In^{113}(N, 3n)$ and $In^{115}(N, 5n)$ reactions.

ACKNOWLEDGMENTS

We would like to thank A. Ghiorso, Professor J. G. Hamilton, W. B. Jones, and G. B. Rossi, and the crew of the 60-inch cyclotron for their constant efforts to develop and improve the heavy ion beams, and for their assistance to us in making these bombardments. It is also a pleasure to acknowledge helpful discussions with Professor J. O. Rasmussen and Dr. E. K. Hyde,

[9] S. A. Moszkowski, Phys. Rev. **82**, 35 (1951).
[10] M. L. Perlman and G. Friedlander, Phys. Rev. **82**, 449 (1951).
[11] Mitchell, Mei, Maienschein, and Peacock, Phys. Rev. **76**, 1450 (1949).
[12] M. L. Perlman and J. Welker, Phys. Rev. **95**, 133 (1954).
[13] K. Way and M. Wood, Phys. Rev. **94**, 119 (1954).
[14] E. Feenberg and G. Trigg, Revs. Modern Phys. **22**, 406 (1950).
[15] M. Lindner and R. Osborne, July, 1952 (private communication).
[16] H. Mathur and E. K. Hyde, Phys. Rev. **95**, 708 (1954).

and to thank Dr. M. C. Michel and Dr. F. A. Asaro for their help with several of the experiments.

APPENDIX

Calibration of the NaI(Tl) Spectrometer

A $1\frac{1}{2}$-inch diameter by 1-inch thick thallium activated sodium iodide crystal was used in conjunction with the 50-channel analyzer. A diffuse reflector of MgO surrounded the crystal, and a thin beryllium window separated it from the sample. The crystal was bonded to a thin quartz disk which in turn was optically coupled to a Dumont 6292 photomultiplier tube by a layer of mineral oil. With this arrangement, a resolution of 8 percent was obtained at 661 kev. An aluminum-lined lead shield housed the detector assembly, and samples were mounted in a standard G-M tube five position shelf holder. In these experiments, most measurements were made at a distance of ~1.5 inches from the crystal, which represented a geometry of 5.1 percent (as determined with the 60-kev gamma ray of a standardized Am^{241} sample).

Energy calibration of the spectrometer was made during each experiment, with the following gamma-ray standards: Am^{241} (60 kev), U^{235} (143, 184 kev), Au^{198} (412 kev), Cs^{137} (32, 661 kev), and Na^{22} (510 kev, 1.28 Mev). In addition, the annihilation radiation of Cs^{128} served as an internal standard, so that any shift in the energy scale could be observed and corrected.

The following counting efficiencies were used to calculate the relative intensities of the various gamma rays:

X-rays (Cs, Xe)	100 percent
225 kev	63
385 kev	28
510 kev	17
700 kev	11

We have determined the counting efficiencies of gamma rays at 412 kev (Au^{198}), 510 kev (Na^{22}), 661 kev (Cs^{137}), 1.28 Mev (Na^{22}), and 1.33 Mev (Co^{60}), using a $4\text{-}\pi$ counter to determine the absolute disintegration rates of the standard samples. The results of these measurements were all within 5 percent of the efficiencies obtained from the data of Bell *et al.*[17,18] for the experimental conditions used here. Because of this agreement, the Oak Ridge curves were used to determine the efficiencies at other gamma-ray energies.

The observed x-ray intensities were corrected for fluorescence yield and absorption by comparison with the x-rays from a Cs^{137} standard examined under identical experimental conditions.

[17] Bell, Heath, and Davis, Oak Ridge National Laboratory Report ORNL-1415, 1952 (unpublished).
[18] Bell, Hughes, Davis, Jordan, and Randall, Oak Ridge National Laboratory Report ORNL-1415, 1952 (unpublished).

PHYSICAL REVIEW VOLUME 96, NUMBER 3 NOVEMBER 1, 1954

Neutral Pion-Deuteron Production in 400-Mev n-p Collisions*

R. A. SCHLUTER
Institute for Nuclear Studies, The University of Chicago, Chicago, Illinois
(Received June 17, 1954)

The reaction $n+p\rightarrow d+\pi^0$ has been studied in a high-pressure hydrogen-filled diffusion cloud chamber. A total of 102 deuterons were identified by a technique of ionization measurement in conjunction with momentum measured in the 10 500-gauss magnetic field. From the laboratory deuteron angle and momentum, the pion angle and the incident neutron energy can be deduced with good resolution, provided the pion is emitted backward in the center-of-mass system. Proton recoils were observed simultaneously, from which the incident neutron flux and energy spectrum were determined. The energy spectrum is centered at 400 Mev with a spread of ±25 Mev. From 52 events occurring in the backward direction the angular distribution of pion emission was found to be consistent with $(0.28_{-0.14}{}^{+0.36}+\cos^3\bar{\psi}_\pi)$, where the limits include 70 percent of the probability and $\bar{\psi}_\pi$ is the pion angle in the center-of-mass system. The observed excitation function and total cross section determined from 60 events is consistent with $(0.47\pm0.08)\eta^3$ millibarn, where η is the center-of-mass pion momentum in rest mass units. These results agree, within the accuracy of the measurements, with the prediction of charge independence that the ratio of this reaction to $p+p\rightarrow d+\pi^+$ should be $\frac{1}{2}$.

Eight cases of internal conversion of the neutral pion were seen, four accompanied by deuterons and four by protons, the later giving evidence on neutral pion creation with unbound final nucleons.

I. INTRODUCTION

THE experiment reported here is a study of the reaction $n+p\rightarrow d+\pi^0$ in a high-pressure diffusion cloud chamber, with 400±25-Mev neutrons produced by the University of Chicago 170-inch synchrocyclotron. The total cross section as well as the angular distribution were measured. Since deuterons rather than neutral pions were detected, there is in this experiment no ambiguity due to the presence of pions produced with unbound final nucleons. The general plan of the experiment is this: deuterons produced in collisions of 400-Mev neutrons with protons in a high-pressure hydrogen

* Research supported by a joint program of the U. S. Office of Naval Research and the U. S. Atomic Energy Commission.

diffusion cloud chamber were identified by a technique of ionization measurement combined with momentum measurement. From deuteron angle and momentum, and knowledge of the incident beam direction, the pion angle in the center-of-mass system and the incident neutron energy in the laboratory system were deduced for each event. Proton recoils in the forward direction were used to determine the incident neutron flux and energy spectrum.

The principal theoretical interest in this reaction arises from the hypothesis of approximate charge independence in the pion-nucleon interaction. The principle of charge independence reduces to three the number of independent matrix elements required to describe single pion production in nucleon-nucleon collisions. This simplification, together with a phenomenological description of the nucleon-nucleon force, provides a framework in which a consistent explanation of the gross features of these processes, such as meson energy spectrum and variation of yield with incident energy, has been attained,[1] and the success of this scheme is support for the charge independence hypothesis.

An acute further test is afforded by the experimental check of relations predicted by charge independence to exist among the various pion creation cross sections. The simplest of these relations,

$$\sigma(n+p\rightarrow d+\pi^0)=\tfrac{1}{2}\sigma(p+p\rightarrow d+\pi^+), \qquad (1)$$

is found for reactions in which the final nucleons are bound deuterons, because the deuteron has isotopic spin 0 whereas an unbound neutron and proton can have isotopic spin 1 or 0. Under charge independence the two reactions of Eq. (1) are merely different orientations in isotopic spin space of a state of total isotopic spin 1, the factor $\frac{1}{2}$ coming from the fact that only half of the $n+p$ states have isotopic spin 1. The similarity of angular distributions predicted by Eq. (1) has been previously confirmed. The angular distribution for $n+p\rightarrow d+\pi^0$ was measured by Hildebrand;[2] that for $p+p\rightarrow d+\pi^+$ was obtained by detailed balance from the reaction $d+\pi^+\rightarrow p+p$, which was measured by Durbin, Loar, and Steinberger.[3]

At the energy of this experiment (pions produced with an energy of about 50 Mev in the center-of-mass system) the important final states and corresponding initial states allowed by conservation of parity, angular momentum, and isotopic spin for the reaction $n+p\rightarrow d+\pi^0$ are given in Table I. The angular distributions are for unmixed transitions. The total angular distribution must be symmetric about 90° in the center-of-mass system, because the initial states are symmetric with respect to isotopic spin and the initial nucleons are therefore indistinguishable. There is evidence from pion scattering experiments[4] that the pion-nucleon interaction is strong in two-particle states of spin $\frac{3}{2}$ and isotopic spin $\frac{3}{2}$. Such states are components only of final state (c), so we expect that this transition will be strong[5] and that there will be (1) a prominent $\cos^2\theta$ term in the angular distribution and (2) a predominantly η^3 dependence of the cross section, where η is the center-of-mass momentum in rest-mass units. This has been experimentally confirmed for the analog reaction $p+p\rightarrow d+\pi^+$.

TABLE I. Final states and corresponding initial states in $n+p\rightarrow d+\pi^0$.

	Initial	Deuteron	Pion	J	Parity	Ang. dist.
(a)	$^3P_1$	$^3S_1$	S	1	−	isotropic
(b)	$^1S_0$	$^3S_1$	P	0	+	isotropic
(c)	$^1D_2$	$^3S_1$	P	2	+	$\frac{1}{4}+\cos^2$

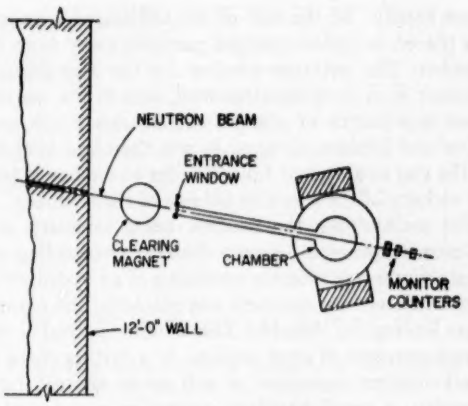

FIG. 1. Experimental arrangement.

II. EXPERIMENTAL ARRANGEMENT

The general experimental arrangement is shown in Fig. 1. The neutrons were produced in a 2-inch thick beryllium target placed in the circulating proton beam at radius 76 inches, corresponding to a nominal proton energy of 450 Mev. Neutrons emitted directly forward pass through 1-inch collimators at either side of the 12-foot steel shield wall. The angular divergence of the neutron beam was about 0.2°. Near the cyclotron side, an 11-inch long paraffin plug was inserted into the beam under conditions such that a single neutron scattering would almost certainly remove the neutron from the beam. The purpose of this filter was to suppress neutrons of energies less than about 100 Mev. Neutrons of such energies are particularly injurious to diffusion cloud-chamber operation because they produce highly ionizing recoil protons copiously, and these deplete the

[1] K. M. Watson and K. A. Brueckner, Phys. Rev. **83**, 1 (1951); M. Gell-Mann and K. M. Watson, Ann. Rev. Nuc. Sci. (to be published); A. H. Rosenfeld, Phys. Rev. **96**, 130, 139 (1954).

[2] R. H. Hildebrand, Phys. Rev. **89**, 1090 (1953), and private communication.

[3] Durbin, Loar, and Steinberger, Phys. Rev. **84**, 581 (1951).

[4] Anderson, Fermi, Martin, and Nagle, Phys. Rev. **91**, 155 (1953).

[5] K. A. Brueckner and K. M. Watson, Phys. Rev. **86**, 923 (1952).

vapor supply. At the exit of the collimator a magnet was placed to deflect charged particles away from the chamber. The entrance window for the high-pressure chamber is $\frac{1}{32}$-inch stainless steel, and in the neutron beam is a source of charged secondaries which steal vapor and confuse pictures. It was therefore mounted on the end of a 5½-foot tube in order to remove it from the vicinity of the sensitive volume of the chamber.

For maintaining the neutron beam intensity at a delicate compromise between chamber overloading and empty pictures, a monitor consisting of an hydrogenous target followed by counters was placed in the neutron beam leaving the chamber. This monitor played no role in measurement of cross section. As a further check on cloud-chamber operation as well as on neutron beam intensity, a small auxiliary camera was mounted to provide test pictures at frequent times during the run without interrupting operation or disturbing the main camera. This camera viewed the heart of the sensitive volume and permitted continual photographic check on cloud-chamber operation.

The chamber itself operated at a pressure (when cold) of 22 atmospheres. It has an inside diameter of 18 inches and maintains a sensitive depth of 2 inches to 3 inches. It is provided with a nonpulsed magnetic field of 10 500 gauss. A proton resonance device was built for measuring the field at several positions in the chamber, and a flux meter using a coil and electronic integrator used to map intermediate regions. The magnetic field varies by one percent across the useful diameter of the chamber, and by about 0.5 percent per cm in the vertical direction in the sensitive volume. Corrections have been made for these variations, although error in radius of curvature measurement usually dominates, as discussed in Sec. III.

The chamber was photographed by a stereoscopic camera whose eyes converge at a total angle of 16°. The camera uses 35-mm Eastman Kodak Linagraph Ortho film, and Leitz Hektor 28-mm lenses which give a minification of 18. Photography is synchronized with the cyclotron oscillator high-voltage power source so that the flash occurs 114 milliseconds after the particles arrive. The clearing field of about 80 volts/cm is removed about four seconds before tracks are formed and reapplied immediately after photography. The interval between exposures was 27 seconds, somewhat longer than in usual diffusion cloud-chamber operation, in order that the chamber could recover fully between pulses. Full recovery and a minimum of localized regions of vapor depletion in the sensitive volume were necessary in order to obtain clear origins of charged recoils. This requirement, plus the fact that the tracks dealt with were relatively heavily ionizing, necessitated the precautions already mentioned, i.e., low-energy neutron filter in the beam, distant chamber entrance window, relatively long interval between pictures, and the auxiliary camera. In addition, great care was taken in shielding of the experimental room and the removal of weakly radioactive objects from the vicinity of the chamber during the runs.

III. SCANNING PROCEDURE

The pictures were analyzed by projection through the identical optical system used in photography in order to eliminate distortion of optical origin. Replicas of the plate glass cloud chamber windows were mounted before the lenses. Film shrinkage is negligible provided the time between photography and projection is not more than a few months.

The projection system was designed to allow accurate and rapid angle and momentum measurement. Over 10 000 pictures were scanned and several thousand tracks measured at an over-all rate of about one picture per minute.

The tracks were projected onto a table which tilts about an axis (the ϕ axis) fixed perpendicular both to the direction of the incident beam and to the projection axis. The ϕ axis can be translated horizontally and vertically in order that the origin of a track may be brought into coincidence at a point on the ϕ axis. See Fig. 2. On the table is a protractor to measure the angle in the plane of the table. The table is adjusted so that $\phi=0$, $\theta=0$ is the direction of the incident beam to within the accuracy of alignment of the cloud chamber, which is to within a few tenths of a degree. This alignment was checked by study of the process $n+p\rightarrow p+p+\pi^-$.[6] All final particles are charged, and the resultant momentum direction, which is that of the incident neutron, can be determined. The full angular spread of the neutron beam is 0.2°.

The film was adjusted in the projector by means of three fiducial markers located at the bottom of the chamber. The images of these markers were adjusted by film motion to obtain stereoscopic coincidence at the proper height of the table.

The momentum of a particle was obtained by measuring the radius of curvature in the plane of the table by means of a set of thin plastic sheets scribed with radii in steps of 2.5 cm. The radii measured in this experiment were in the range 180 to 330 cm and were usually measured to the nearest step of 2.5 cm, thereby

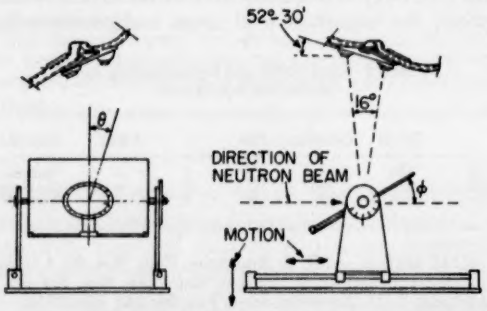

FIG. 2. Essential geometrical features of the scanning projector.

[6] S. C. Wright and R. A. Schluter, Phys. Rev. 95, 639 (1954).

giving an accuracy in momentum of about one percent. This is the greatest contribution to error in momentum measurement. Superposition of these curves on the track images makes discernible any single Coulomb scatterings of a few tenths of a degree or more. Such scatterings might otherwise lead to error in momentum measurement.

The momentum P in Mev/c is given by

$$P=\frac{H_0\rho'}{3333}\cos\phi\left(1-\frac{\theta^2}{4}\right)$$

to second order in θ, where ρ' is the radius measured in the plane of the table, H_0 is the vertical magnetic field in gauss, and the correction term arises from the fact that although the track is a section of a helix, the table is not, in general, exactly in the osculating plane of the helix. For $\theta\approx\frac{1}{10}$ the correction is 0.2 percent.

The magnetic field is nearly constant throughout the usable chamber volume. Correction for its variation in the vertical direction has been made in deuteron measurement.

IV. DETECTION OF DEUTERONS

Deuterons were distinguished from recoil protons by momentum and by a method of ionization measurement. The method and its empirical justification are described, followed by a discussion of factors affecting track image width, and a summary of conditions which it is believed must prevail in order that consistent ionization measurements can be made.

Direct ionization measurement in a high-pressure diffusion cloud chamber must rely on gross features of track appearance, such as width, because counting of individual droplets is not feasible. For example, in hydrogen at 25 atmospheres pressure and 220°K a minimum-ionizing particle produces about 200 ion pairs per cm, a 400-Mev proton twice this.[7] These densities are far too large for usual photographic resolution. Furthermore, densely packed droplets coalesce, so that the number of individual droplets is not simply related to the number of ions. In a diffusion cloud-chamber supersaturation is always present so that ions cannot be dispersed by delaying the onset of drop growth.

In this experiment pictures were scanned in a unit magnification projector as described in Sec. III. The tracks are nearly normal to the projection axis. A simple width-measuring device, two intersecting lines scribed on thin transparent plastic [Fig. 3(a)], was superposed on the track image and adjusted by means of a low-power magnifier so that the skew lines enclose an interval of three times the apparent track width. This criterion avoids obscuring the track edge by the lines, as would occur if the device were adjusted to exactly track width. The widths range from 0.3 to 0.6 mm. Always a particular "eye" of the stereo camera was used and portions of a track near to "holes" of local

[7] R. H. Frost and C. E. Nielsen, Phys. Rev. **91**, 864 (1953).

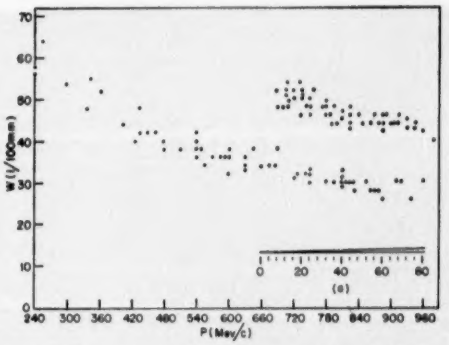

FIG. 3. Apparent track widths W measured at the projector by device sketched at (a), *vs* momentum P.

vapor depletion were avoided. When widths measured in this way are plotted against momentum, the points fall into separate groups as shown in Fig. 3. The identification of events in the deuteron group was checked in every case by comparing the track in question with protons nearby in the same picture. This check is easiest if there are present protons of the same momentum as the deuteron (and 40 percent the ionization) and protons of half the momentum (and the same ionization); however protons between these particular limits of momentum are always present and can also serve as checks. Such protons ionize less than a deuteron although they have less momentum. Figure 4 shows a deuteron (a) of momentum 1010 Mev/c (250 Mev), a proton (b) of the same momentum (437 Mev), and a proton (c) of half the momentum (127 Mev). It is seen that in ionization (a) and (c) are similar and noticeably exceed (b).

The deuteron group includes several tracks accompanied by electron pairs, resulting from internal conversion of a neutral pion gamma ray. These cases are identifiable as deuterons by kinematical arguments alone, without resort to ionization.

The validity of width measurements made in this way was verified separately by measuring track widths on the film with a recording microdensitometer. Every second deuteron was so measured, and also a comparable number of protons of various momenta, making a total of about 100. In Fig. 5 a typical microdensitometer trace is shown, and the width is defined as illustrated there. Widths measured in this way were consistently proportional to widths measured at the projector by the method described above and when plotted against momentum gave two adequately separated groups of points, as shown in Fig. 5. The microdensitometer used here is not a means of scanning, but rather an objective verification of the measuring technique used in scanning.

The relation between track width on the film and particle momentum depends on many factors, some of which are sketched here for the purpose of showing that in this experiment the width was mainly of optical

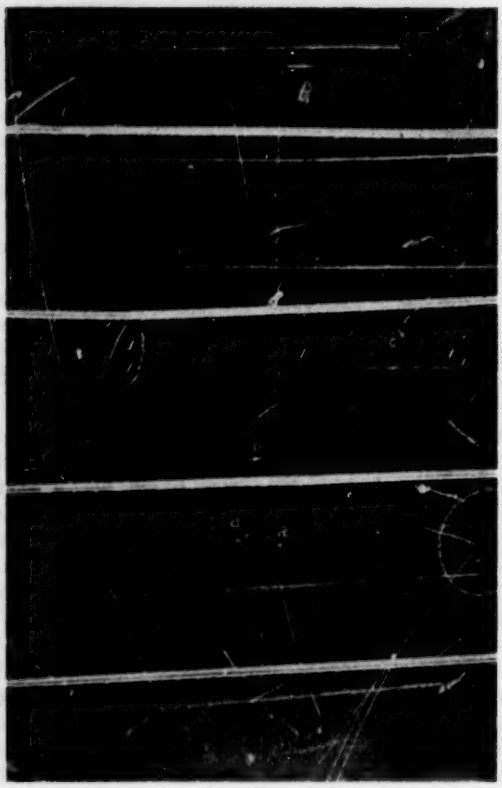

FIG. 4. Cloud-chamber picture showing deuteron (a), proton (b) of same momentum as deuteron, proton (c) of half that momentum, and electron pair (d) from internally converted neutral pion.

origin. At other than extreme relativistic energies the initial column of ions is effectively a line, except for recognizable delta rays. After formation, the ions diffuse at a rate depending on droplet size, which depends in turn on the rate of droplet growth, and therefore on the local density of vapor within the track volume and the rate of inward diffusion of vapor. For the cloud chamber used in this experiment the radius to which droplets have diffused at the time of photography is of the order of a few hundredths of a millimeter, a distance considerably smaller than the measured track half-widths. The increase in width is due to optical aberrations and film turbidity and granularity. This point was checked by photographing under typical conditions a very fine wire; the photographic image width was found to vary with about the 0.4 power of the illumination in the region of widths of interest in this experiment. Since the width is observed to vary with about the 0.2 power of the rate of ionization, the light scattered must vary approximately as the square root of the ionization, showing that droplet size does indeed depend on the density of ionization.

It is clear that obtaining consistent results in measuring ionization demands that tracks be formed in regions of the same supersaturation, that illumination be uniform, that the scattering angle of light into the camera be the same, that the optical settings of the camera be constant, and that the film be developed uniformly. In this experiment the first three conditions were approximated by using a well-collimated neutron beam thereby confining events to a nearly constant height and distance from the light source. Furthermore, the rather long interval of 27 seconds between pictures allowed full recovery of the chamber and lessened fluctuations of vapor density, as did the precautions to lessen unwanted background described in Sec. II.

V. MEASUREMENT OF DEUTERONS

A chamber picture is conveniently divided into 7 sections by the images of the clearing grid wires, which are at right angles to the neutron beam. In order to have sufficient track length for accurate momentum measurement only deuterons originating in sections 2, 3, and 4 (the part of the chamber nearest the entrance window) were recorded. As a check on scanning efficiency, 1400 pictures containing 29 deuterons were carefully scanned a second time, and no additional deuterons were discovered.

Each deuteron was found to satisfy the kinematical relations displayed in Fig. 6, where P_d and ψ_d are the laboratory momentum and angle of the deuteron.[8] For each incident neutron energy T_n the possible deuteron angles and momenta in the laboratory lie on a curve on which the center-of-mass angle $\bar{\psi}_\pi$ of neutral pion emission can be marked off as a parameter. In general a given laboratory system angle and momentum for the deuteron correspond to a particular incident neutron energy and center-of-mass angle of pion emission. How-

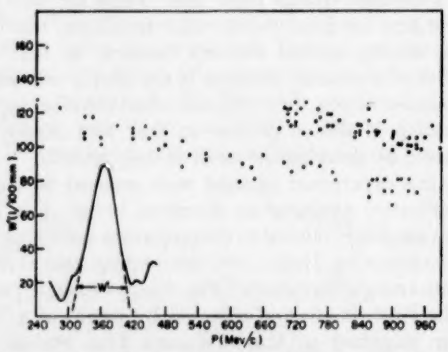

FIG. 5. Track widths W', measured by means of recording microdensitometer, vs momentum. A typical densitometer trace is shown with the width W' defined.

[8] Deuterons could conceivably be produced in radiative capture of neutrons by protons. The cross section for radiative capture at 400 Mev is estimated by detail balance from the inverse reaction, high-energy photodisintegration of the deuteron, to be about 10^{-30} cm^2. The probability that one such event occurred in this experiment is about 1/10.

ever in the region of $\bar{\psi}_\pi = 30°$ to 80° curves for various T_n overlap, and T_n cannot be determined. Also the pion angle is not determined as sharply in this region. For these reasons, the center-of-mass angular distribution of pions and the excitation function for the reaction were found using only pion angles of 90° to 180°, where energy and angular resolution is good.

Each event was plotted on a graph like Fig. 6, and the meson angle and incident neutron energy read off. The intervals of error are shown by the rectangle in Fig. 6.

A total of 102 deuterons have been plotted in the angular distribution, 74 from runs with neutrons produced by a beryllium target and for which the neutron flux and spectrum have been measured as described in Sec. VI, and 28 from a shorter run with similar experimental arrangement, except that a deuterated paraffin target was used for neutron production.

Of the 102, 50 involve meson production forward in the center-of-mass system and 52 backward. This is in satisfactory agreement with a distribution symmetric about 90° in the center-of-mass system.

These events in the backward hemisphere, the hemisphere in which angular and energy resolution is relatively good, are listed in Table II. Groups A and B are deuterons produced by neutrons made in a beryllium and a deuterated paraffin target, respectively.

The angular distribution in intervals of $\mu = \cos\bar{\psi}_\pi$ is given in Table III. A normalized angular distribution of the form $F(A,\mu) = (A+\mu^2)/(A+\frac{1}{3})$ was fitted to these points by the statistically efficient maximum likelihood method.[9] Under the assumption that $F(A,\mu)$ is an adequate theoretical description of the reaction, the likelihood that a given set of experimental points should have occurred is proportional to Q, where

$$Q = \prod_{i=1}^{52} F(A,\mu_i). \tag{2}$$

In Fig. 7 Q is plotted as a function of the parameter A to be determined. The range of A containing 70 percent of the area under $Q(A)$ is given by $A = 0.28_{-0.14}^{+0.26}$. The average energy of the neutrons making the pions in this angular distribution is 392 Mev, corresponding to a center-of-mass momentum and energy of the pion of 130 Mev/c and 53.3 Mev, respectively. Hildebrand[2] studied this reaction in the same beam using counter techniques and found $A = 0.21 \pm 0.06$. These limits are shown in Fig. 7.

TABLE II. Compilation of neutral pion production events used in determining angular distribution. The quantity T_n is the incident neutron energy and $\bar{\psi}_\pi$ the center-of-mass pion angle for each event.

A				B	
T_n	$\bar{\psi}_\pi$	T_n	$\bar{\psi}_\pi$	T_n	$\bar{\psi}_\pi$
440	31	390	2	415	17
435	52	390	19	395	8
435	68	390	33	395	18
425	45	390	48	395	87
425	81	390	78	390	18
425	87	385	20	390	55
420	8	385	27	385	39
420	56	380	17	385	43
415	51	380	50	380	51
415	67	380	90	380	80
405	30	375	41	370	49
405	33	365	50	365	40
405	62	365	60	365	68
405	79	360	26	355	21
400	42	355	80	350	38
400	70	330	61	345	40
395	33	320	70	340	9
		315	41		

TABLE III. Number of events in intervals of μ, the cosine of the center-of-mass pion angle.

μ	1.0–0.8	0.8–0.6	0.6–0.4	0.4–0.2	0.2–0	
No.	18	16	5	7	6	$\Sigma = 52$

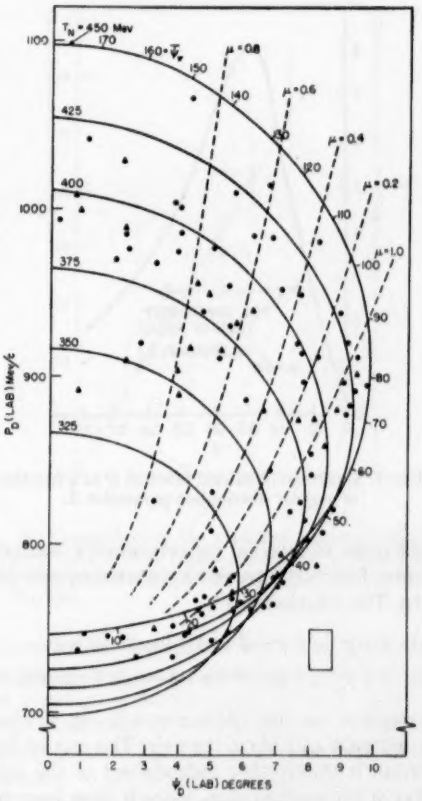

FIG. 6. Kinematics of pion-deuteron formation in $n-p$ collisions. The term T_n is incident neutron energy, ψ_d and P_d are laboratory angle and momentum of the deuteron, respectively, and $\bar{\psi}_\pi$ is the center-of-mass angle of pion emission. The dots represent events in run with beryllium target, the triangles events in run with deuterated paraffin target. The experimental error of these points is given by rectangle.

[9] N. Arley and R. Buch, *Introduction to the Theory of Probability and Statistics* (John Wiley and Sons, Inc., New York, 1950), p. 142.

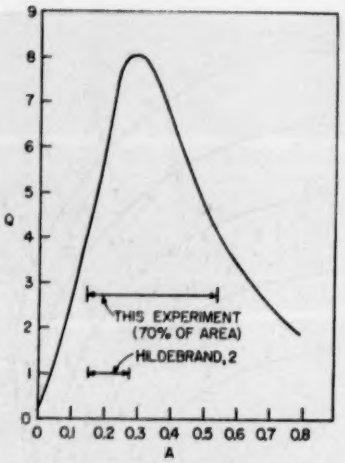

FIG. 7. Maximum likelihood function Q as a function of angular distribution parameter A.

Eight cases of internal conversion of a neutral pion were seen, four accompanied by deuterons and four by protons. The reactions are

(A) $n+p \rightarrow d+\pi^0 \rightarrow d+$pair$+$gamma ray.

(B) $n+p \rightarrow n+p+\pi^0 \rightarrow n+p+$pair$+$gamma ray.

An example of reaction (A) is shown in Fig. 4, where (a) is the deuteron and (d) is the pair. The rate of internal conversion is presumably independent of the mode of creation of the neutral pion, since it lives long enough to escape its birthplace. The calculated[10] internal conversion coefficient is 0.0063 (per gamma ray) which agrees fairly well with the value 0.0080 ± 0.0016 found in observations of neutral pions created in slow π^- capture by protons.[11] From the calculated rate of internal conversion one would expect one or two rather than four conversions in the 102 neutral pions studied in this experiment; in fact the probability that four or more conversions should occur is about 5 percent.

The four cases of reaction (B) give a crude estimate of the rate of neutral pion creation with unbound final nucleons. Using the theoretical internal conversion coefficient, one would expect these four cases to be accompanied by about 300 unconverted pions with unbound final nucleons, compared to 102 pions with bound final nucleons. The unbound reaction appears to be favored by a factor of the order of 3.

It has been pointed out by Serber[12] that deuterons produced in the reaction $p+p \rightarrow d+\pi^+$ should be polarized. Such polarization present in the reaction studied in this experiment might be detected by scattering of the deuterons in the hydrogen of the chamber. No such scatterings were observed. If the cross section is geometrical, the probability of such a scattering in this experiment is $\frac{1}{3}$. The scattering of polarized deuterons by larger nuclei may show asymmetry, in which case the insertion of a plate into the chamber might yield enough scatterings to permit study of the polarization. Such a plate should have low thermal conductivity in order to minimize its effect on chamber operation.

[10] R. H. Dalitz, Proc. Phys. Soc. (London) **A64**, 667 (1951).
[11] Lindenfeld, Sachs, and Steinberger, Phys. Rev. **89**, 531 (1953).
[12] Cited in K. Watson and C. Richman, Phys. Rev. **83**, 1256 (1951).

VI. INCIDENT NEUTRON BEAM MEASUREMENTS

A sufficient number of neutron recoil protons were measured to (1) make statistical errors due to their number small compared with that of the deuterons, (2) obtain the neutron energy spectrum, and (3) to measure the $n-p$ angular distribution for small proton angles. That the latter should be in accord with published data on the $n-p$ angular distribution is a check on scanning methods.

While deuterons were measured, as mentioned, in regions 2, 3, and 4 of the chamber, protons were measured in region 3 only. This procedure gave about 9 protons measured per deuteron. Scanning criteria were: radius of curvature 210 cm or greater (momentum $\geqq 700$ Mev/c, energy ≥ 235 Mev) and the angles of the projector table (Fig. 2) ϕ and θ each less than 30°. Protons from the reaction $n+p \rightarrow n+p+\pi^0$, mentioned in Sec. V, very rarely have 235 Mev or more, so they introduce negligible error in the $n-p$ scattering measurement. The time for measurement of one proton was 4–6 minutes. The relativistic center-of-mass angle of the proton and the laboratory energy of the incident neutron were determined by means of a computational routine requiring about 1½ minutes per event.

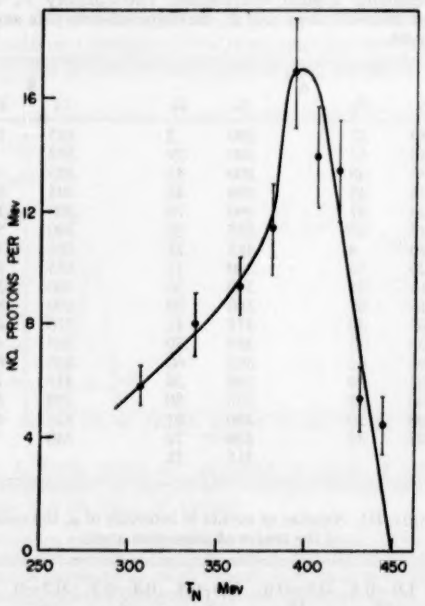

FIG. 8. Energy spectrum of incident neutron beam.

The neutron energy spectrum is shown in Fig. 8 and is derived from protons with center-of-mass angle less than 45°. The small variation of the total scattering cross section with energy has been taken into account. The energy resolution varies with the quality and length of the proton track; in most cases the energy half-width is about four percent. This spectrum is similar to the spectrum determined by Nedzel[13] using counter techniques in the same neutron beam.

In Fig. 9 the relative angular distribution for protons in the center-of-mass system is shown in integrated form. The ordinate gives the relative number of events with scattering angle cosine less than μ. Only protons produced by neutrons of energy greater than 365 Mev are included, in order that the distribution can be compared with the results of Hartzler and Siegel[14] in a neutron beam with a very similar energy spectrum and using a detector with a threshold of about 365 Mev. Their results for the relative angular distribution have been converted to integrated form, normalized to ours by a multiplicative factor, and plotted as a line in Fig. 9. The agreement is satisfactory.

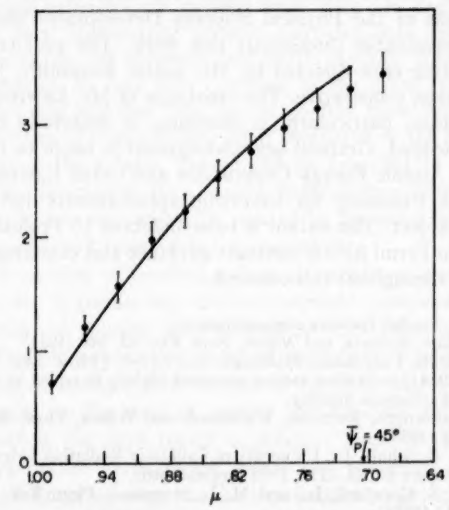

FIG. 9. Comparison of $n-p$ scattering angular distribution obtained in this experiment (points with probable errors) with results of Hartzler and Siegel (reference 14) (line). The ordinate gives the relative number of events above a given value of μ, where μ is the cosine of the proton angle $\bar{\psi}_p$ in the center-of-mass system.

[13] V. A. Nedzel, Phys. Rev. **94**, 174 (1954).
[14] A. J. Hartzler and R. T. Siegel, Phys. Rev. **93**, 928 (1954) and **95**, 185 (1954).

VII. TOTAL DEUTERON CROSS SECTION

It is expected that the cross section for $n+p \rightarrow d+\pi^0$ should have at these energies the approximate form:

$$\sigma = \alpha\eta^3, \tag{3}$$

where η = center-of-mass pion momentum in rest-mass units. The comparison of this equation with the empirical excitation determined from a small number of events is best done in the following way. Let n_{di} and n_{pi} be the numbers of deuterons and protons produced in some given interval of incident neutron energy. If the excitation follows Eq. (3), then the ratio n_{di}/n_{pi} is proportional to η_i^3, where η_i corresponds to the given energy interval and it is assumed that the $n-p$ scattering cross section varies little over the energy range 300–450 Mev. The sum of the ratios up to some value of η will be proportional to η^4. In Fig. 10 this sum is plotted against η^4 and the points are seen to be in reasonable agreement with a straight line, showing that the experimental variation of yield with energy is consistent with Eq. (3).

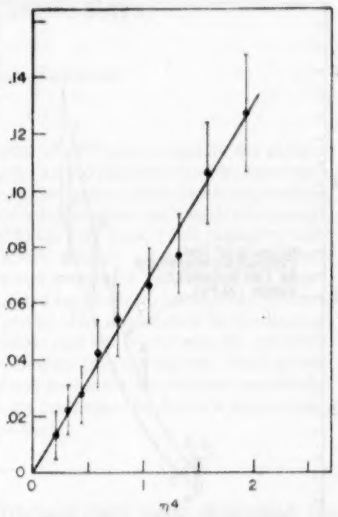

FIG. 10. Comparison of the empirical excitation function in $n+p \rightarrow d+\pi^0$ with η^3. The results are plotted in integrated form and therefore are plotted against η^4. The ordinate represents $\Sigma_{\eta_i \leq \eta}(n_{di}/n_{pi})$.

We now determine the constant α. The number of n_{di} of deuterons produced by neutrons in the energy interval i is

$$n_{di} = \alpha\eta_i^3 L_i/C, \tag{4}$$

where L_i is the number of neutrons in energy interval i passing through the chamber and $1/C$ is the number of scattering centers per cm^2. The number n_{pi} of protons produced with center-of-mass angle less than 45° by neutrons in the same energy interval i is

$$n_{pi} = (S\delta/K)(L_i/C), \tag{5}$$

where S is the total $n-p$ scattering cross section and δ is given by

$$\delta = \int_0^{45°} \frac{d\sigma_{np}}{d\Omega} d\Omega \Big/ \int_0^{\pi} \frac{d\sigma_{np}}{d\Omega} d\Omega. \tag{6}$$

The factor $K = 2.84$ accounts for the fact that a larger section of each picture was scanned for deuterons than

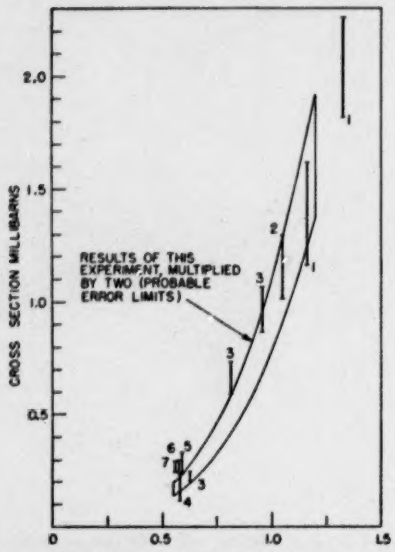

FIG. 11. Comparison of two times the total cross section for $n+p\rightarrow d+\pi^0$ with the total cross section for $p+p\rightarrow d+\pi^+$, as a test of charge independence. Points are: 1, Stadler (reference 15); 2, Fields *et al.* (reference 17); 3, Durbin *et al.* (reference 3); 4, Cartwright *et al.* (reference 18); 5, Clark *et al.* (reference 16); 6. Crawford and Stevenson (reference 20); 7, Schulz (reference 19) normalized by Rosenfeld (reference 1) to Crawford and Stevenson (reference 20).

for protons. The total number of deuterons N_d is given by

$$N_d=\frac{\alpha}{S\delta}K\sum_i \eta_i^3 n_{pi}, \tag{7}$$

where it is assumed that δ and S are not strongly varying with energy. This experiment, then, determines directly $\alpha/S\delta$ to be 0.058 ± 0.0088.

From the result of Hartzler and Siegel[14] the factor δ is found to be 0.240 ± 0.010. The error given is determined by first maximizing and then by minimizing δ within the probable errors of Hartzler and Siegel's points.

The total $n-p$ scattering cross section S has been measured by Nedzel[13] in the same neutron beam used in this experiment and is 33.7 ± 1.3 mb. Combining S and δ with our result, we find

$$\sigma(n+p\rightarrow d+\pi^0)=(0.47\pm0.08)\eta^3 \text{ millibarns}. \tag{8}$$

At 392 Mev, the mean incident energy of events in this experiment, the cross section is 0.41 ± 0.07 mb. The comparison of Eq. (8) with data on the reaction $p+p\rightarrow d+\pi^+$ is made in Fig. 11, in which *twice* Eq. (8) is plotted in order that Eq. (1) may be checked directly. The charged pion production results plotted in Fig. 11 come from the inverse reaction measured by Stadler,[15] by Durbin *et al.*,[3] and by Clark *et al.*,[16] and from the direct pion production reaction measured by Field *et al.*,[17] Cartwright *et al.*,[18] by Schulz,[19] and by Crawford *et al.*[20] The agreement, within the errors of the experiments, is a confirmation of Eq. (1) predicted by charge independence.

VIII. CONCLUSION

With regard to experimental methods, the operation of a high-pressure hydrogen diffusion cloud chamber under conditions such that the angle, momentum and ionization of positive recoils could be measured has been described. The conditions permitting consistent ionization measurement have been discussed.

With regard to the reaction $n+p\rightarrow d+\pi^0$ studied here, it was found that the total cross section agrees within the accuracy of the experiment with the prediction of charge independence in the pion-nucleon interaction. The angular distribution found agrees with the previous measurement[2] made by an entirely different method. Cases of internal conversion of the neutral pion give evidence that neutral pion production with unbound final nucleons occurs at a rate comparable to that for production with bound final nucleons.

The author is grateful for the pleasure of association with Dr. S. C. Wright during the development and use of the cloud-chamber system. The skill of Mr. R. Barrons of the Physical Sciences Development Shop was invaluable throughout this work. The cyclotron operating crew directed by Mr. Lester Kornblith, Jr., was most cooperative. The assistance of Mr. Lawrence Rosenson, particularly in scanning, is gratefully acknowledged. Grateful acknowledgment is made to the U. S. Atomic Energy Commission and to the Eastman Kodak Company for fellowship appointments during this project. The author is most indebted to Professor Enrico Fermi for his constant guidance and encouragement throughout this research.

[15] H. Stadler (private communication).
[16] Clark, Roberts, and Wilson, Phys. Rev. **83**, 649 (1951).
[17] Fields, Fox, Kane, Stallwood, and Sutton [Phys. Rev. **95**, 638 (1954)] total cross section amended slightly in report to the 1954 Washington meeting.
[18] Cartwright, Richman, Whitehead, and Wilcox, Phys. Rev. **91**, 677 (1953).
[19] A. G. Schulz, Jr., University of California Radiation Laboratory Report UCRL-1756, 1952 (unpublished).
[20] F. S. Crawford, Jr., and M. L. Stevenson, Phys. Rev. **91**, 468 (A) (1953).

Anisotropy of High-Energy Cosmic Rays

LEVERETT DAVIS, JR.
California Institute of Technology, Pasadena, California
(Received July 16, 1954)

Review of the evidence indicates that a magnetic field of the order of 10^{-5} gauss probably lies along a spiral arm of the galaxy. If so, any anisotropy observed in high-energy cosmic radiation must be associated with this field. Anisotropy might be due to: (a) acceleration by Fermi's mechanism, either by his longitudinal collisions or by betatron effects; (b) diffusion along field lines toward a region where the cosmic rays escape from the galaxy; (c) inhomogeneities in cosmic-ray density normal to the field lines. From symmetry considerations theoretical expressions are developed for the cosmic-ray flux as a function of direction and for the resulting sidereal time dependence of extensive showers as a function of latitude and the orientation of the detecting apparatus. If atmospheric effects can be corrected for, the main harmonics predicted are the first and second, the second being mainly due to anisotropy produced by acceleration. In the absence of detailed calculations based on a specific theory of the origin of cosmic rays and on the way the extensive showers are detected, the amplitude of the harmonics must be determined from experiment. Preliminary reports of measurements by Cranshaw and Galbraith and by Farley and Storey seem to indicate tentatively that the magnetic field is as described above and that cosmic rays are accelerated by Fermi's mechanism; the measurements of Daudin and Daudin require some other explanation.

I. INTRODUCTION

IT is the purpose of this paper to consider theoretically the anisotropy of the cosmic-ray flux and the sidereal time dependence to be expected for extensive air showers if a galactic magnetic field of about 10^{-5} gauss lies along a spiral arm of the galaxy. Some variation with sidereal time would be expected in the output of any cosmic-ray measuring apparatus that rotates with the earth if the cosmic-ray flux here depends on its direction with respect to the galaxy. It is simplest to try to study this anisotropy by investigating extensive air showers since they are produced by very high-energy primary particles that are not affected by the magnetic field of the earth or, it will be assumed, by any field confined to the solar system. Since the assumed field cannot confine these primary particles to a region very small compared to the thickness of the galaxy, they might be expected to show more anisotropy than would lower-energy particles, which, however, could be treated in the same way if the effects of local fields are allowed for.

A number of possible causes of anisotropy are well known. If cosmic rays travel in straight lines, a distribution of sources concentrated in the plane of the Milky Way or at the center of the galaxy would lead to an anisotropic flux. Motion of the solar system with respect to the sources[1] would also produce such an effect if the rays travel in straight lines. If cosmic rays diffuse through the galaxy by scattering from small knots of magnetic field embedded in gas clouds and separated by field-free regions, anisotropy would be produced by boundary effects.[2,3] However recent information on the galactic magnetic field suggests that it extends throughout a spiral arm with quite a regular structure that must determine the character of the anisotropy.[4] If this is the case, observations on the sidereal time dependence of extensive showers should provide evidence bearing on the local direction of the galactic magnetic field and on the way in which cosmic rays receive their energy but should provide very little evidence concerning the location of the original sources of cosmic rays.

Since this entire treatment assumes the presence of a galactic magnetic field, the evidence for it should be reviewed. No method has yet been suggested by which the material in the galaxy can supply as much power to cosmic rays as to starlight, which gets its energy from nuclear sources. Since the observed flux of cosmic rays is about equal to that of starlight, cosmic rays cannot travel in straight lines. They must be held in the galaxy for times of the general order of a million years. Magnetic fields seem to be required in any mechanism that can do this. Once magnetic fields are accepted, the argument that Dungey and Hoyle[5] used to try to prove that there is no galactic magnetic field can be used to show that the field must be at least $B=6\times10^{-6}$ gauss. For unless it is this large, its energy density, $B^2/8\pi$, will be less than that of the cosmic rays, which would then push the magnetic field aside and expand until their energy density was smaller than that of the field.[5a] The observed polarization

[1] A. H. Compton and I. A. Getting, Phys. Rev. **47**, 817 (1935).
[2] G. Cocconi, Phys. Rev. **83**, 1193 (1951).
[3] Morrison, Olbert, and Rossi, Phys. Rev. **94**, 440 (1954).
[4] L. Davis, Bull. Am. Phys. Soc. **29**, No. 6, 18(A) (1954).
[5] J. W. Dungey and F. Hoyle, Nature **162**, 888 (1948).
[5a] *Note added in proof.*—Dr. Arnulf Schlüter has pointed out in a private communication that this overlooks the influence of forces, such as those of gravity, that could prevent the expansion of a weaker field through their action on the interstellar gas in which the field is embedded. However, it seems significant that the forces due to gravitation, cosmic rays, random motions of the gas clouds, and magnetic fields all appear to be of the same general order of magnitude. Even though no theory yet explains this in detail, the point tends to make more plausible the assumption of a magnetic field strength of the order of 10^{-5} gauss.

of starlight suggests[6,7] that the galactic magnetic field is roughly uniform and in the plane of the galaxy, perhaps running along a spiral arm. There appears to be a root-mean-square deviation of the order of 5° to 10° in the planes of polarization of neighboring stars.[8] Hence there should be corresponding deviations in the direction of the field that must be due to magneto-hydrodynamic waves, and this implies[6,9] that the field is of the order of 10^{-5} gauss. Chandrasekhar and Fermi[9] show that such a field is required to explain the stability of the spiral arms of the galaxy; the lateral pressure due to the magnetic field can support the gravitational forces attracting the interstellar gas and dust towards the axis of the spiral arm whereas kinetic pressures are much too low. Fermi's most successful modification[10] of his theory of the origin of cosmic rays uses a magnetic field directed along the spiral arms; magneto-hydrodynamic waves in this field supplying the energy to the cosmic rays. If such fields were formed[11] by turbulence and a contraction of the galaxy from spherical to disk form in its early history, the conductivity is great enough so that they would be expected to persist for many billion years. Biermann and Schlüter[12] and Biermann[13] conclude from a study of the turbulent motion of ionized gases in a galaxy of the present shape that in a few billion years fields of this strength would be formed even if one started with no magnetic field.

These arguments make plausible the assumption of a magnetic field of about 10^{-5} gauss running along the spiral arms and suggests the investigation of its consequences, including its effect on the isotropy of cosmic rays. The main consequence for cosmic rays is that each particle is constrained to spiral around a particular line of force, following it wherever it may go with, perhaps, occasional reversals of the direction of motion along the line of force and with some very slow transverse diffusion due to inhomogeneities in the field. Even a proton whose energy is 10^{16} ev will move in a helix whose maximum radius (when the helix angle is 90°) in a field of 10^{-5} gauss is 3.5 light years, a small distance on a galactic scale.

For convenience in analysis it will be assumed throughout this paper that the magnetic field within a few light years of the solar system is uniform but is part of a larger field having a somewhat complicated structure. On a galactic scale, the magnetic lines of force will be assumed in general to lie in a parallel bundle that starts from one end of a spiral arm at the rim of the galaxy, follows the arm around several turns, connects to another arm near the galactic center, spirals out to the rim along this arm, and then spreads out to give a very weak dipole field in intergalactic space. Observationally, the distribution of stars and gas along a spiral arm is far from uniform. Thus, by the argument of Chandrasekhar and Fermi,[9] at any point where the mass density and hence the gravitational forces drop off a bit, the lateral pressure of the magnetic field, and, one might also add, of the cosmic radiation, will expand the field laterally. The remaining dust and gas will tend to slide down the lines of force away from this bulge. This further reduces the gravitational forces there and allows the field to bulge out still more. Hence it must always be borne in mind that at a number of places along the spiral arm there may be leaks where some of the lines of force escape into intergalactic space. Assume that the sun is not in such a region. Even in the most nearly uniform regions the magnetic field strength should decrease as one moves out from the axis of the spiral arm. Only then is there a gradient in the pressure of the magnetic field to support the gravitational forces. Superposed on this static field are magneto-hydrodynamic oscillations covering an extensive spectrum of wavelengths. For waves in which regions having dimensions of a few light years move in phase, the root-mean-square deviation of the lines of force appears to be[8] of the order of 0.1 radian. Although ordinary turbulence is suppressed by the strong magnetic field and the conductivity of the gas, waves should be generated by the hydrodynamic forces that ordinarily would generate turbulence from the nonrigid rotation of the galaxy. These waves may be thought of as transient inhomogeneities of all sizes superposed on the nearly uniform static field. The magnetic fields of the earth and sun will be disregarded because of the very high energies of the primary cosmic-ray particles considered.

II. CAUSES OF ANISOTROPY

The isotropy in the cosmic-ray flux depends both on the structure of the galactic magnetic field and on the origin assumed for the cosmic rays. A widely accepted theory of their origin holds that by some electromagnetic process involving varying magnetic fields large amounts of energy are given to ions, probably in the neighborhood of stars, but possibly in particularly turbulent and strongly magnetized gas clouds. There are then two possibilities. The first is that this initial process supplies substantially all the energy that the particles ever get and that their subsequent history is a slow diffusion out of the galaxy. The large number of heavy primaries shows that collisions with gas atoms are unimportant. The second possibility is that the initial process gives only an energy of the general order of a Bev per nucleon, and that further energy is supplied over periods of millions

[6] L. Davis, Phys. Rev. **81**, 890 (1951).
[7] L. Davis, *Vistas of Astronomy*, edited by A. Beer (Pergamon Press, London, to be published).
[8] G. Stranahan, Astrophys. J. **119**, 465 (1954).
[9] S. Chandrasekhar and E. Fermi, Astrophys. J. **118**, 113 (1953).
[10] E. Fermi, Astrophys. J. **119**, 1 (1954).
[11] This possibility was suggested in conversation by F. Hoyle.
[12] L. Biermann and A. Schlüter, Phys. Rev. **82**, 863 (1951).
[13] L. Biermann, in *Kosmische Strahlung*, edited by W. Heisenberg (Springer-Verlag, Berlin, 1953), second edition, pp. 47–65.

of years by interactions with the galactic magnetic field as suggested by Fermi.[10] He considered interactions in which the particle is reflected from a moving inhomogeneity in the magnetic field in a way that adds momentum along the magnetic field only. This should tend to make an anisotropic distribution of cosmic ray flux with greater intensity along the field lines than at right angles to them. Alternatively acceleration could be due to "betatron collisions",[14] i.e., to passage through regions where the magnetic field varies with time. The principal advantages of the betatron mechanism are that it seems easier to add energy at a high rate and that there is not the difficulty found in Fermi's mechanism where, when a particle gains some energy, it is difficult to gain more because it escapes from his "trap." Although the betatron mechanism initially adds momentum normal to the field, this is converted into momentum added parallel to the field when the particles spiral along the lines of force from the region where the field is increasing with time to a region where the field has its average value.[14a]

Further anisotropy will be introduced by the acceleration process if the probability of escape from the system depends on the steepness of the spirals in a different way than does the probability of acceleration. Now the steeper the helices, the more rapidly particles diffuse away along the lines of force, while the flatter the helices, the more easily a particle is accelerated both by Fermi's collision process and by the betatron process. Hence if these processes are important in supplying energy to cosmic rays, there is a tendency for the flux of particles in a given energy range to be greater normal to the field than parallel to it. Whether acceleration produces an anisotropy of this character or one of the opposite character as described in the previous paragraph depends on which tendency dominates. With either accelerating mechanism, inhomogeneities in the magnetic field whose scale is less than the radius of the helix tend to make the flux more nearly isotropic by scattering particles from one helix into another of different helix angle or pitch.

There are additional sources of anisotropy that apply both to such accelerating mechanisms and to the case in which the initial process supplies all the energy. If the particles diffuse along the lines of force out of the galaxy either at the end of a spiral arm or at a region of low mass density where there is a bulge in the field, there will be a net flux along the field lines towards the nearest point of escape. Scattering by inhomogeneities and the collisions described by Fermi will contribute to the flux in the opposite direction. Apparatus should detect a minimum flux when directed along the lines of force in a direction leading to the nearest escape point; it should detect an intermediate flux for directions at right angles to the lines of force; and should detect the maximum flux when directed along the lines of force away from the nearest escape point.

A further source of anisotropy is the fact that the cosmic-ray energy density should decrease, together with the magnetic field strength as described above, as one moves out from the axis of a spiral arm of the galaxy. This could be due to a decrease in the rate of acceleration of cosmic rays by Fermi's mechanism as the field strength decreases. It could be contributed to by diffusion normal to the lines of force caused by inhomogeneities in the field. Since particles would escape into nearly field free intergalactic space at the surface of the spiral arm, the density would decrease from the center out. The very high-energy particles with large radii of curvature should be more inhomogeneous than lower-energy particles. In the absence of all other reasons for a decrease in cosmic-ray density, the decrease in magnetic field strength will require it, since as soon as the source of cosmic rays builds up their energy density in a region to the point where the force they exert on the field is greater than that of gravity on the interstellar gas, the magnetic field will be pushed outward. This decreases the density of particles and decreases the energy of each one by the betatron effect. If for any of these reasons there is a variation in cosmic-ray density as one moves in a plane normal to the lines of force, there will be a corresponding anisotropy observed in the cosmic-ray flux. The flux observed along the lines of force and in the directions in which the density changes most rapidly will have an intermediate value. The maximum and minimum fluxes, as shown in Fig. 1, will be measured along the line orthogonal to both these directions.

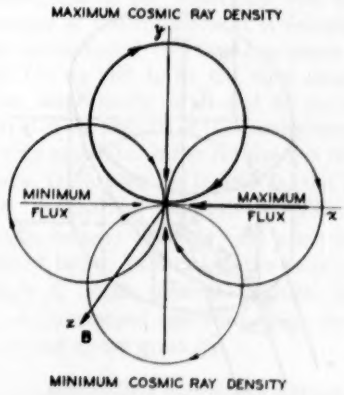

FIG. 1. Anisotropy in flux due to inhomogeneity in density. The circles are projections on the xy plane of helices; their widths indicate the number of particles involved. The straight arrows indicate the flux in the different directions.

[14] L. Davis, Phys. Rev. **93**, 947 (1954).

[14a] The author is indebted to Dr. Schlüter for pointing out that, as a consequence of the theorem that the magnetic moment of a charged particle in a magnetic field is an adiabatic invariant for changes in the field both with time and with position, the betatron mechanism has the same effect on the isotropy as Fermi's collision mechanism.

III. DESCRIPTION OF THE ANISOTROPY

The anisotropy produced in these various ways will now be described analytically. Introduce Cartesian coordinates with origin at the point of interest, for us the solar system. Take Oz along **B**, the direction of the locally uniform magnetic field, and Oy in the direction in which the cosmic ray density increases most rapidly. Each particle describes a helix about a line parallel to Oz. Six quantities are required to completely specify the motion of a particle. Let them be $R, \beta, \psi, x_A, y_A, t_A$; where, as shown in Fig. 2, x_A, y_A are the coordinates of the point A at which the axis of the helix intersects the xy plane, β is the constant angle, called the helix angle, between **B** and the tangent to the trajectory, $R\sin\beta$ is the radius of the cylinder on which the helix is wound, $\psi-\frac{1}{2}\pi$ is the azimuthal angle of the line from A to the point P at which the trajectory intersects the xy plane, and t_A is the time at which the particle in question crosses the plane. Thus R, which is the radius of the circle in which the particle moves when $\beta=90°$, fixes the kinetic energy E of a particle of given charge and rest mass. If one measures the flux of cosmic radiation as a function of direction, β and ψ are the polar and azimuthal angles, respectively, of the axis of the narrow cone within which the apparatus receives the particles. They locate $-\mathbf{v}$, where $\mathbf{v}$ is the velocity of the particle.

A complete description of the cosmic-ray flux is given by defining

$$N(R,\beta,\psi,x_A,y_A,t_A)\sin\beta\cos\beta dR d\beta d\psi dx_A dy_A dt_A \quad (1)$$

to be the number of particles with parameters in the indicated range, dt_A being taken large enough so that N can be regarded as a continuous function. The trigonometric factors are chosen to make N a constant in the homogeneous isotropic case. In the steady state

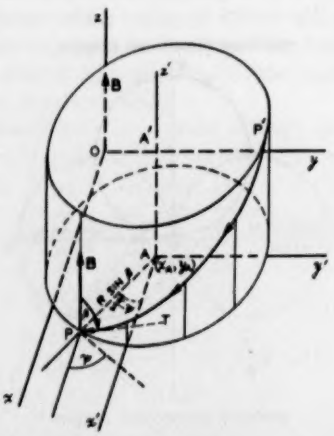

FIG. 2. Parameters used to describe a helical trajectory, $P'P$, shown wound on a cylinder with axis $A'A$ and radius $R\sin\beta$. PT is tangent to the trajectory and is located by the angles β and ψ.

N is not a function of t_A. The axes were oriented so that N is not a function of x_A. Strictly this might be impossible for more than one energy; assume it is possible for all energies of interest. Assume that N is independent of ψ; this is equivalent to the assumption that there would be no periodic variation if O were displaced along **B**. Finally, require that P fall on O so that

$$y_A = R\sin\beta\cos\psi. \quad (2)$$

Thus $N(R,\beta,y_A)$ can be expanded in the series

$$\begin{aligned} N(R,\beta,y_A) &= \Sigma b_{kn}(R) y_A{}^k P_n(\cos\beta) \\ &= \Sigma b_{kn}(R) R^k (\sin\beta\cos\psi)^k P_n(\cos\beta), \end{aligned} \quad (3)$$

where P_n is the usual Legendre polynomial.

The analysis is started with a definition of N since it is what will be determined by any theory of the accelerating process and of the interactions with the inhomogeneities in the galactic magnetic field. However, the quantity of experimental interest is the value at the position O and the time t of $F(E,\beta,\psi,t)dE$, the number of particles in the energy range dE received per unit time, solid angle, and area normal to the beam in a narrow cone whose axis is directed along β,ψ. The connection between F and a completely general N may be found to be

$$\begin{aligned} &F(E,\beta,\psi,t) \\ &\quad = (dR/dE)N(R,\beta,\psi,-R\sin\beta\sin\psi, R\sin\beta\cos\psi, t), \end{aligned} \quad (4)$$

either by evaluation of the Jacobian of the coordinate transformation or by consideration of the geometrical factors involved. The factor dR/dE in (4) allows for the change from R to E. The factor $\sin\beta d\beta d\psi$ in (1) measures the solid angle, and the factor $\cos\beta$ in (1) allows for the fact that for F area is taken normal to the beam while for N it is taken in the xy plane. For an N which, as discussed above, depends only on its first, second, and fifth arguments and which can be expanded in the series (3), F is easily expressed in a similar series. If only low-order terms need be considered at present, the series can be written

$$\begin{aligned} F(E,\beta,\psi) = \bar{F}(E)[&1+\Delta_D\cos\beta \\ &-(4/3)\Delta_A P_2(\cos\beta)+\Delta_I\sin\beta\cos\psi], \end{aligned} \quad (5)$$

where

$$\begin{aligned} &\bar{F}(E) = (dR/dE)b_{00}, \quad \Delta_D = b_{01}/b_{00}, \\ &\Delta_A = -3b_{02}/4b_{00}, \quad \Delta_I = Rb_{10}/b_{00}. \end{aligned} \quad (6)$$

Throughout the rest of this paper all terms arising from those given in (5) will be retained but all higher-order terms omitted in (5) will be ignored. No attempt will be made here to deduce theoretical values of the Δ's; they will be regarded as parameters to be determined by experiment.

The new coefficients, which are evidently functions of E, are defined as in (6) in order to have simple physical meanings. The identification of the terms in the series with the different sources of anisotropy is

easily made from the symmetry properties of each. $\bar{F}$ is essentially the mean cosmic ray flux averaged over all directions. [To make this hold precisely when more terms in the series are used, one must replace $(y_A/R)^k$ in (3) by $T_k(\sin\beta\cos\psi)$, where T_k is the Tschebyscheff polynomial of the first kind.[15]] The term in Δ_A gives the main contribution to the anisotropy resulting from an acceleration uniformly distributed throughout the spiral arms of the galaxy. The sign is so chosen that Δ_A is positive if the likelihood of greater acceleration from the flatter helices is more important than the increase in steepness produced by acceleration. In the reverse case, Δ_A is negative. The term in Δ_D gives the main contribution to the anisotropy resulting from any net diffusion along a line of force. The coefficient Δ_D will be positive when the Oz axis from which β is measured is directed toward the region where most of the cosmic rays originate and away from the nearest region where they escape from the galaxy. The term Δ_I gives the main contribution of any inhomogeneity in the cosmic ray density; its coefficient is positive for particles having a positive charge if Oz is directed along $\mathbf{B}$ and Oy along the direction in which the density increases most rapidly. In each case the numerical factor is so chosen that 2Δ is the maximum possible variation with direction in $F/\bar{F}$ due to the term in question.

If observation yields values of these coefficients, it will be important to know to what extent each coefficient arises solely from the indicated mechanism. Terms having the symmetry of those in Δ_D and Δ_I can arise from the acceleration mechanism only if there is some inhomogeneity, such as a limited region of vigorous acceleration, and in this case interpretation of Δ_D and Δ_I as due to diffusion and inhomogeneity is still justified. Diffusion will tend to produce mostly odd harmonics; hence it would not be expected to contribute much to the coefficient of $P_2(\cos\beta)$. If the density of cosmic rays varies reasonably smoothly over distances of the order of the radius of a spiral arm, one might expect that in (3) quadratic terms in y_A would be less important than linear terms until R approached the radius of the spiral arm. Thus neither diffusion nor inhomogeneity should produce terms having the symmetry of P_2, and if such terms are found, they must be due to acceleration. Diffusion contributes terms in $P_n(\cos\beta)$, i.e., in powers of the cosine of the angle between the axis of the detecting apparatus and $\mathbf{B}$. Inhomogeneity contributes terms in $(\sin\beta\cos\psi)^k$; i.e., in powers of the cosine of the angle between the axis of the detecting apparatus and $\mathbf{e}_T$, a transverse unit vector along Ox that may be defined independently of coordinate systems as being in the direction of (grad N)$\times\mathbf{B}$ for positive particles. Thus it seems impossible to distinguish observationally between anisotropy due to diffusion along the lines of force and that due to inhomogeneity at right angles to the lines unless one has some other means of determining the direction of $\mathbf{B}$ or of $\mathbf{e}_T$. Of course, from one point of view there is very little difference between the two sources of anisotropy since a difference in cosmic-ray energy density will be associated with each of them.

[15] W. Magnus and F. Oberhettinger, *Special Functions of Mathematical Physics* (Chelsea, New York, 1949), p. 78.

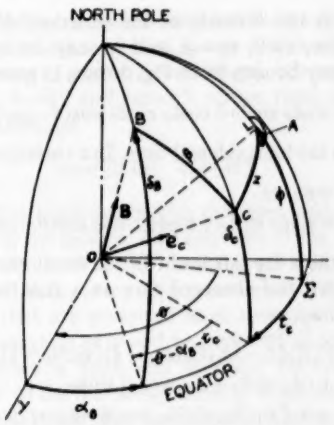

FIG. 3. The celestial sphere seen from the outside. O is the center of the earth, OL is in the direction of the radius vector to the laboratory, OB is the direction of $\mathbf{B}$, OC is the direction of the axis of the apparatus, and γ is the vernal equinox. As the earth rotates, γ and B remain fixed, C, L, and Σ move together to the right.

IV. SIDEREAL TIME DEPENDENCE

This anisotropy in cosmic ray flux means that any apparatus that rotates with the earth will have an output that varies with sidereal time provided adequate corrections for atmospheric effects can be made and provided sufficient data are available to make the statistical fluctuations small enough. To connect the above description of the anisotropy with expressions for the output of the apparatus it is necessary to use the usual astronomical coordinate systems as shown in Fig. 3. Let α_B and δ_B be the right ascension and declination, respectively, of $\mathbf{B}$ and let α_T and δ_T be those of $\mathbf{e}_T$. Let $\mathbf{e}_C$, the axis of the narrow cone in which the detecting apparatus measures the flux of incoming cosmic rays, be located by t_C and δ_C, the local hour angle and declination, respectively. The averaging procedures to be used when the cone is not narrow will be considered below. In terms of the more convenient zenith angle z, (angle from the vertical to $\mathbf{e}_C$) and azimuth, A, (measured eastward from the northern horizon), t_C and δ_C are given by

$$\begin{aligned}\sin\delta_C &= \sin\varphi\cos z + \cos\varphi\sin z\cos A,\\ \cos\delta_C\cos t_C &= \cos\varphi\cos z - \sin\varphi\sin z\cos A,\\ \cos\delta_C\sin t_C &= -\sin z\sin A,\end{aligned} \tag{7}$$

where φ is the latitude of the observer. For vertical observation, $z=0$, $\delta_C=\varphi$, and t_C may be taken to be zero. It may be seen from Fig. 3 that, in general,

$$\cos\beta=\sin\delta_B\sin\delta_C+\cos\delta_B\cos\delta_C\cos(\theta-\alpha_B-t_C), \quad (8)$$

where θ is the local sidereal time. In a corresponding way

$$\sin\beta\cos\psi=\mathbf{e}_C\cdot\mathbf{e}_T$$
$$=\sin\delta_T\sin\delta_C+\cos\delta_T\cos\delta_C\cos(\theta-\alpha_T-t_C). \quad (9)$$

When these are put into (5), the result can be simplified to give the observed flux as a function of local sidereal time.

$$\begin{aligned}F(E,\theta)=\bar{F}(E)\{&1-3\Delta_A(\sin^2\delta_B-\tfrac{1}{3})(\sin^2\delta_C-\tfrac{1}{3})\\&+(\Delta_I\sin\delta_T+\Delta_D\sin\delta_B)\sin\delta_C\\&-\Delta_A[\sin2\delta_B\sin2\delta_C\cos(\theta-\alpha_B-t_C)\\&+\cos^2\delta_B\cos^2\delta_C\cos2(\theta-\alpha_B-t_C)]\\&+\Delta_D\cos\delta_B\cos\delta_C\cos(\theta-\alpha_B-t_C)\\&+\Delta_I\cos\delta_T\cos\delta_C\cos(\theta-\alpha_T-t_C)\}. \quad (10)\end{aligned}$$

In general, what is observed is the cosmic-ray flux in a wide cone and a wide energy range. Accordingly the flux at the top of the atmosphere given by (10) must be multiplied by $S(E,z,A)$, which can be regarded as the effective area of response to primaries of energy E coming from a direction defined by z, A, and the result integrated over A, z, and E. Since this effective area depends in a complicated way on the geometry of the experimental apparatus, its depth in the atmosphere, and the structure of the shower produced by the primary particle, only a partial treatment will be attempted. Assume that the apparatus detects coincidences in an array of some kind of counters in a horizontal plane. Suppose it to have a horizontal axis of symmetry whose azimuth measured eastward from north is A_S. Then since rotation of the apparatus through 180° about a vertical axis should not change the counting rate, the effective area is of the form

$$S(E,z,A)=\sum S_n(E,z)\cos2n(A-A_S). \quad (11)$$

The predicted mean rate of response when statistical fluctuations are averaged out is therefore

$$\Phi(\theta)=\int\int\int S(E,z,A)F(E,\theta)\sin z\,dA\,dz\,dE. \quad (12)$$

Substitute (11), (10), and (7) in (12), introduce the abbreviation

$$M_n(E,z)=2\pi S_n(E,z)\bar{F}(E)\sin z, \quad (13)$$

and evaluate the integrals over A to get

$$\begin{aligned}\Phi(\theta)=&\int\int M_0[1+(\Delta_D\sin\delta_B+\Delta_I\sin\delta_T)\sin\varphi\cos z-3\Delta_A(\sin^2\delta_B-\tfrac{1}{3})(1-\tfrac{3}{2}\sin^2z)(\sin^2\varphi-\tfrac{1}{3})]dz\,dE\\&-\left[\int\int M_0\Delta_A(1-\tfrac{3}{2}\sin^2z)dz\,dE\right][\sin2\delta_B\sin2\varphi\cos(\theta-\alpha_B)+\cos^2\delta_B\cos^2\varphi\cos2(\theta-\alpha_B)]\\&+\left[\int\int M_0\Delta_D\cos z\,dz\,dE\right]\cos\delta_B\cos\varphi\cos(\theta-\alpha_B)+\left[\int\int M_0\Delta_I\cos z\,dz\,dE\right]\cos\delta_T\cos\varphi\cos(\theta-\alpha_T)\\&+\frac{1}{4}\left[\int\int M_1\Delta_A\sin^2z\,dz\,dE\right][-(3\sin^2\delta_B-1)\cos^2\varphi\cos2A_S+\sin2\delta_B\sin2\varphi\cos2A_S\cos(\theta-\alpha_B)\\&-\cos^2\delta_B(1+\sin^2\varphi)\cos2A_S\cos2(\theta-\alpha_B)+2\sin2\delta_B\cos\varphi\sin2A_S\sin(\theta-\alpha_B)\\&-2\cos^2\delta_B\sin\varphi\sin2A_S\sin2(\theta-\alpha_B)]. \quad (14)\end{aligned}$$

It is of interest to note that only the first two terms of (11) affect the result, and that the only second harmonics are those due to Δ_A. Even when the counters lie on a single straight line, no second harmonics are introduced by Δ_D or Δ_I.

The above treatment omits one factor that could be important. $S(E,z,A)$ depends on solar time because of variations in the state of the atmosphere. It is well known that if the corrections for this are not adequate, S will also have first and second harmonics on sidereal time, even when averaged over a year. This is because of seasonal effects. Hence observation of first and second harmonics on sidereal time of the cosmic-ray flux implies anisotropy only if the corrections for atmospheric effects are known to be adequate or if a differential method of observing is used that cancels out atmospheric effects.

V. INTERPRETATION OF OBSERVATIONS

There are several types of observations that can be made to test this theory and perhaps to obtain information on the galactic magnetic field and the origin of cosmic rays. One procedure is to determine the first and second harmonics on sidereal time of the flux of nearly vertical extensive showers, correcting for

atmospheric effects, which have periods of a solar day and a year. If this is done with identical apparatus at different latitudes so that the dependence on φ can be used to partially disentangle the terms in (14), it is possible in principle to determine the values of α_B, δ_B, an integral involving Δ_A, and two integrals involving the remaining quantities. Variation of the range of z, the zenith angle, over which the apparatus responded might be helpful. From shower theory one could get $S(E,z,A)$ and by examination of the integrals, one might get some estimate of the Δ's.

A second procedure, that would largely eliminate the need for corrections for atmospheric effects, would be to make simultaneous continuous measurements of the flux in two or three narrow cones for which z was the same but for which δ_C, as given by (7), had quite different values. A particularly simple case would be that in which $\varphi=z=45°$, $\delta_C=0$, 45°, and 90°. In principle, measurement of the constant term and the first and second harmonics on sidereal time of the flux differences for three values of δ_C would determine Δ_A, α_B, δ_B, and three combinations of the other terms from which it is not quite possible to determine Δ_D, Δ_I, α_T, and δ_T. Observations in more directions or at more latitudes do not provide new algebraic equations; they just improve the statistical accuracy of the information obtained from three directions. When it is stated here that Δ_A is determined, it is meant of course that an integral over E of Δ_A times $S(E,z,A)$ as given by shower theory is determined. The above-mentioned constant terms alone, that is, the differences in the average values of the fluxes for three directions, would give the values of $\Delta_A(\sin^2\delta_B-\frac{1}{3})$ and $(\Delta_D \sin\delta_B+\Delta_D \sin\delta_I)$, information that would be very significant if it were not that $\sin^2\delta_B$ is expected to be about $\frac{1}{3}$.

A third procedure that would give data at a more rapid rate than the second and that might be less difficult to carry out would be to detect extensive showers for all azimuths and over as wide a range of z as possible, preferably at mountain top elevations where oblique showers are more common, and to record the direction of each shower either with cloud chambers, by accurate timing measurements, or perhaps by other means.

Sufficient experimental data do not seem to be available for any of these methods to be used at present. The procedure that will now be followed is to take the few astronomical hints available and estimate the directions of $\mathbf{B}$ and $\mathbf{e}_T$. By using this as a working hypothesis, to be modified or discarded if the results are unsatisfactory, Eqs. (10) and (14) will be tested for consistency with the available observational results.

As discussed in Sec. I, the galactic magnetic field is likely to run along the spiral arms of the galaxy with local deviations of perhaps 5° or 10°. Astronomical evidence[16] indicates that the sun is within a spiral arm, but not on its axis, and that in our neighborhood this spiral arm runs in a direction whose galactic coordinates are $l=40°$, $b=0°$ and hence[17] whose right ascension and declination are

$$\alpha_B=20 \text{ hr}, \quad \delta_B=35°. \tag{15}$$

Following the spiral arm in this direction leads towards the center of the galaxy. This estimate of the direction of $\mathbf{B}$ is corrobroated by the observation[18] that near this direction not many stars show interstellar polarization, and those that are polarized have essentially random planes of vibration as would be expected[7] if one looked along the lines of force and observed the component of $\mathbf{B}$ normal to the line of sight due to small waves in $\mathbf{B}$. Although the spiral arm has considerable structure if one looks at stars and dust, it may not have as much structure if one looks at $\mathbf{B}$ and cosmic rays. Assuming this, one can make a very tentative statement as to the direction of $\mathbf{e}_T$. Assume that the spiral arm is roughly elliptical in cross section, with major axis extending 3000 light years in the galactic plane and minor axis 1000 light years normal to this plane. The sun is, say, 50 light years north (on the side of the north galactic pole) of the plane and 1000 light years from the axis of the spiral arm. One might therefore expect that $\mathbf{e}_T$ would be tangent at the sun to an ellipse whose plane is normal to the axis of the spiral arm and which is similar to the cross section of the arm. Thus it should be within about 10° of the direction $b=90°$, which is the same as

$$\alpha_T=12.3 \text{ hr}, \quad \delta_T=28°. \tag{16}$$

Since nothing is known as to the sense of $\mathbf{B}$, $\mathbf{e}_T$ is just as likely to have the opposite direction, which is

$$\alpha_T=0.3 \text{ hr}, \quad \delta_T=-28°. \tag{17}$$

Without a knowledge of the $\Delta(E)$'s and of $S(R,z,A)$ it is impossible to evaluate the integrals in (14). However, a reasonable estimate for comparison with experiment can be obtained by assuming that S is zero except for z near zero and that $S\Delta$ is zero except in a narrow band of energy. Then the relative amplitudes and the phases of the various harmonics can be predicted with the results shown in the bottom half of Table I, where it must be remembered that the Δ's may depend on E. These results can be compared with the experimental results—shown in the top half of the table—obtained by Cranshaw and Galbraith[19]

[16] The structure described here is an idealized model mainly based on information supplied by Professors Guido Münch and J. L. Greenstein. Any errors made in the interpretation of the information they supplied seems likely to be less important than the other uncertainties involved.

[17] Landolt-Bornstein, *Zahlenwerte und Funktionen* (Springer, Berlin, 1952), sixth edition, Vol. 3.

[18] W. Hiltner, Astrophys. J. 114, 241 (1951), Fig. 7b.

[19] T. E. Cranshaw and W. Galbraith (to be published).

TABLE I. Comparison of experimental and theoretical variations in the rate of extensive air showers, expressed as Fourier series with fundamental period one sidereal day. The theoretical values are based on (15) and (16).

Location Latitude, φ Harmonic	Harwell[d] 52° 1st	 2nd	Pic du Midi[e] 43° 1st	 2nd	Aukland[f] −37° 1st	 2nd
Experimental results						
Energy of primary (ev)	5×10^{14}		6×10^{14}		10^{14}	
Amplitude (%)	4.9±1.5[a]	3.5±1.5	1.5±0.75	Present	1.43±0.38[b]	0.41±0.25[b]
Time of maximum (hr)[c]	10.5±1.3	4.5±1.0	21.0		17.6 ±1.0	2.0 ±2.3
Theoretical results						
Effects of acceleration						
Amplitude (%)	$0.91\Delta_A$	$0.25\Delta_A$	$0.94\Delta_A$	$0.36\Delta_A$	$0.90\Delta_A$	$0.43\Delta_A$
Time of maximum (hr)	8	2	8	2	20	2
Effects of diffusion						
Amplitude (%)	$0.51\Delta_D$	Absent	$0.60\Delta_D$	Absent	$0.65\Delta_D$	Absent
Time of maximum (hr)	20		20		20	
Effects of inhomogeneity						
Amplitude (%)	$0.54\Delta_I$	Absent	$0.65\Delta_I$	Absent	$0.70\Delta_I$	Absent
Time of maximum (hr)	12		12		12	

[a] All errors given are standard deviations.
[b] The second harmonic does not appear to have been corrected for a seasonal effect that changed the first harmonic from an amplitude of (1.10±0.26) percent with maximum at (19.8±0.9) hr to the values given. The method of correction used seems to be an analytically convenient development of the procedure of J. L. Thompson, Phys. Rev. **55**, 11 (1939). Its basic assumption is that there is no annual variation in the phase of the diurnal component on solar time of the atmospheric effect. This assumption is known to be false for barometric pressure and hence presumably is false for other atmospheric effects. However, if no other correction for such effects is made, this correction appears to be desirable since the seasonal variation in their phase is probably less important than the variation in amplitude. The residual error seems likely to be of the same order of magnitude as the correction.
[c] All times are local sidereal time.
[d] See reference 19.
[e] See reference 20.
[f] See reference 21.

at Harwell, by Daudin and Daudin[20] at Pic du Midi, and by Farley and Storey[21] at Auckland. The energies listed are the approximate energies of the primaries that produce most of the showers recorded. Similar results, but with lower statistical significance, are obtained at neighboring energies by Cranshaw and Galbraith and by Daudin and Daudin. It is at once apparent that the standard deviations in the experimental results are small enough so that they must be taken seriously, but are not quite small enough, particularly if one considers the uncertainties introduced by the atmospheric diurnal effects, to make a conclusive test of the theory. The results of Cranshaw and Galbraith and those of Farley and Storey could be explained as due exclusively to acceleration with $\Delta_A>0$ which implies that the preferential acceleration from the flatter helices dominates. They could also be explained as a mixture of roughly equal parts of acceleration and diffusion since this would augment the first harmonic relative to the second in the Southern Hemisphere and decrease it in the Northern. Unless the Δ's vary strongly with energy, there seems to be no way to explain simultaneously the three sets of experimental results, mainly because the phases obtained at Harwell seem inconsistent with those from Pic du Midi. The results of Daudin and Daudin taken together with those of Farley and Storey would imply that the dominant effect is that of diffusion if it were not that then the second harmonics are hard to explain. Of course they could be due to atmospheric effects or to large even spherical harmonics produced by diffusion. It will be noted that if the direction of $\mathbf{e}_T$ is given by (16), the resulting phases in the last row of the table agree rather poorly with the observations. If the direction is given by (17), the amplitudes are unchanged but the times of maximum are advanced 12 hr, which does not improve the agreement. If the increased pitch on acceleration dominates the production of anisotropy, i.e., if $\Delta_A<0$, and if α_B were 8 hr rather than the value given in (15), the only change in the table would be that the second harmonics would have their maxima at 8 hr and 20 hr local sideral time. Since the observations seem to indicate that it is the minima rather than the maxima of the two harmonics that coincide, and since this is an astronomically implausible direction for $\mathbf{B}$, it appears unlikely that $\Lambda_A<0$.

It appears, therefore, that until the statistical effects in the observational data are further reduced, until corrections for atmospheric effects are known with considerable assurance, and until the allowances to be made for the variation in the energy selected at the different laboratories are settled, it will be difficult to decide with confidence whether or not the theory described above fits the observations and to determine which factors dominate in the production of anisotropy. If it were not for the results of Daudin and Daudin, one would say that at present the observations tend to support the above theory and to favor the assumption that the dominant term is a positive Δ_A, or perhaps

[20] A. Daudin and J. Daudin, Proceedings of the Bagneres-de Bigorre Conference, July, 1953 (unpublished).
[21] F. J. M. Farley and J. R. Storey, Nature **173**, 445 (1954); also (private communication).

an equal mixture of Δ_A and Δ_D. If this is the case, it can be regarded as evidence favoring a relatively uniform galactic magnetic field directed along a spiral arm of the galaxy. The field strength could not be an order of magnitude less than 10^{-5} gauss or there would be more anisotropy in the highest energy particles observed by Cranshaw and Galbraith. It is also implied then that cosmic rays are accelerated by the Fermi mechanism rather than exclusively by processes taking place at the original ion sources.

The author is very grateful to Professor J. L. Greenstein and Professor Guido Münch for most helpful discussions and to Dr. W. Galbraith and Dr. F. J. M. Farley for information sent in advance of publication and for their comments on a preliminary version of this theory.

PHYSICAL REVIEW VOLUME 96, NUMBER 3 NOVEMBER 1, 1954

Age-Dependent Branching Stochastic Processes in Cascade Theory*

A. T. Bharucha-Reid
Department of Mathematical Statistics, Columbia University, New York, New York
(Received June 1, 1954)

A brief introduction to the recent Bellman-Harris theory of branching stochastic processes is given in the nomenclature of cascade theory; and a simple model in cascade theory formulated as an age-dependent branching process is given.

INTRODUCTION

THE theory of branching stochastic processes has been used on many occasions in the development of mathematical models of cascade phenomena (e.g., cosmic-ray showers, neutron multiplication, etc.).[1–6] Recently Bellman and Harris[7] have developed a theory of age-dependent branching processes which appears to have important applications in the physical and biological sciences. The purpose of this communication is twofold: first, to give a brief introduction to the Bellman-Harris theory in the nomenclature of cascade theory; and second, to present a simple model for the electron population of a cosmic-ray shower. The model considered is a modification of the Furry process.

In the Bellman-Harris theory the distance or thickness, say τ, travelled by a particle (electron, neutron, etc.) from its formation until it is transformed is a random variable with general distribution $G(\tau)$, $0<\tau<\infty$; i.e., $G(\tau)$ is the integral distribution for all paths of length less than or equal to τ. At the end of its path of travel the particle is transformed into n particles with probabilities q_n, $n=0, 1, \cdots$, each particle having the same distribution $G(\tau)$ for the distance it will travel before being transformed. For example, q_0 is the probability of absorption, q_1 is the probability that one new particle will be formed, the original one being absorbed, q_2 is the probability that two new particles will be formed (the original one being absorbed), etc. The random variable τ measures the distance to the next point of regeneration. We remark that the age-dependence is only for the total cross section, the branching ratio being age-independent.

The Bellman-Harris process is formulated as follows: Let $X(t)$ be an integer-valued random variable representing the number of particles at thickness t; and define $p(x,t)=Pr(X(t)=x)$, $x\geq 0$. Let

$$\pi(s,t)=\sum_{x=0}^{\infty} p(x,t)s^x, \quad |s|<1 \tag{1}$$

be the generating function for the probabilities $p(x,t)$ starting with one particle at thickness zero. $[\pi(s,t)]^n$ is the generating function if the process starts with $n>1$ particles at thickness zero. In treating both cases the assumption is made that the particles do not interact with one another. The generating function (1) has been shown to satisfy the nonlinear Stieltjes functional equation

$$\pi(s,t)=\int_0^t h[\pi(s,t-\tau)]dG(\tau)+s[1-G(t)], \tag{2}$$

where

$$h(s)=\sum_{n=0}^{\infty} q_n s^n, \tag{3}$$

that is, $h(s)$ is the generating function for the transformation probabilities q_n. The equation for the gener-

* Work sponsored by the Office of Scientific Research of the Air Force.

[1] W. H. Furry, Phys. Rev. **52**, 569 (1937).
[2] D. Hawkins and S. Ulam, Los Alamos Scientific Laboratory Report LADC 265, 1944 (unpublished).
[3] N. Arley, *On the Theory of Stochastic Processes and Their Applications to the Theory of Cosmic Radiation* (John Wiley and Sons, Inc., New York, 1949).
[4] L. Jánossy, Proc. Roy. Soc. (London) **A63**, 241 (1950).
[5] F. G. Foster, Proc. Cambridge Phil. Soc. **47**, 77 (1951).
[6] A. Ramakrishnan, J. Roy. Stat. Soc. **B13**, 131 (1951).
[7] R. Bellman and T. E. Harris, Ann. Math. **55**, 280 (1953).

ating function can be derived as follows. By definition,

$$p(x,t)=Pr(X(t)=x)=\int_0^t Pr(X(t)=x|\tau)dG(\tau),$$

where $Pr(X(t)=x|\tau)$ is the probability of x particles at thickness t from a single particle at thickness zero which is known to have branched at $t=\tau$. Now

$$Pr(X(t)=x|\tau)$$

$$=\sum_{n=0}^{\infty} q_n\{\sum_{i_1+\cdots+i_n=x} p(i_1,t-\tau)\cdots p(i_n,t-\tau)\},$$

where the term in braces is the coefficient of s^x in the expansion of

$$[\sum_{x=0}^{\infty} p(x,t-\tau)s^x]^n=\pi^n(s,t-\tau).$$

(The reasoning used above is the same as that used in the theory of compound probability distributions.) Multiplying $p(x,t)$ by s^x and summing over x we obtain, after adding the term for $p(1,t)=1-G(t)$, Eq. (2). If $G(t)$ has a density function $g(\tau)$ of bounded total variation, we can write (2) as

$$\pi(s,t)=\int_0^t h[\pi(s,t-\tau)]g(\tau)d\tau+s[1-G(t)].$$

Differentiation of (2) with respect to s yields intergal equations of the renewal type for the moments of $X(t)$, the properties of which can be studied using well-known methods.[8] For example, the expected value of $X(t)$ is

$$EX(t)=m(t)=K\int_0^t m(t-\tau)g(\tau)d\tau+1-G(t), \quad (4)$$

where

$$K=\sum_{n=0}^{\infty} nq_n=\left(\frac{dh}{ds}\right)_{s=1}.$$

In a forthcoming publication we plan to treat models of cascade phenomena which involve more than one type of particle, and in which energy considerations are taken into account. We plan also to discuss the diffusion equations associated with age-dependent branching processes and their physical applications.

AN AGE-DEPENDENT MODEL

Consider a single particle of the soft component of cosmic radiation falling on a material slab (e.g., lead). and its effect being multiplied to form a cascade shower, The model we consider assumes (i) $G(t)=1-e^{-\lambda t}$, and (ii) $h(s)=q_0+q_1s+q_2s^2$. With $G(t)$ thus defined the state of the cascade at any thickness t depends only upon the number of particles at that thickness and is independent of their previous paths; hence, the stochastic process we consider is a Markov process with an enumerable number of states. If we disregard the photons in the electron-photon cascade the probability that an electron will be transformed between t and $t+\delta t$ is $\lambda\delta t+o(\delta t)$, where λ is defined as the birth constant or birth-rate. From the definition of $h(s)$, (ii) states that an electron after travelling a distance of random length τ has probability q_0 of being absorbed, probability q_1 of being absorbed and producing one new electron, and probability q_2 of being absorbed and producing two new electrons. Each new electron then has probability $G(\tau)$ of travelling a distance τ before being transformed again.

The generating function in this case satisfies the equation,

$$\pi(s,t)=\int_0^t\{\sum_{n=0}^{2} q_n\pi^n(s,t-\tau)\}\lambda e^{-\lambda\tau}d\tau+se^{-\lambda t}. \quad (5)$$

This integral equation can be written as the differential equation,

$$(1/\lambda)\partial\pi/\partial t=q_2\pi^2+(q_1-1)\pi+q_0,$$

or

$$(1/\lambda)\partial\pi/\partial t=q_2\pi^2-(q_0+q_2)\pi+q_0. \quad (6)$$

If we put $q_0=q_1=0$, Eq. (6) becomes the generating function of the Furry distribution.[1] The solution to (6) with initial condition $\pi(s,0)=s$ is

$$\pi(s,t)=\frac{q_0-q_2[(q_2s-q_0)/(q_2s-q_2)]e^{\lambda(q_0-q_2)t}}{q_2\{1-[(q_2s-q_0)/(q_2s-q_2)]e^{\lambda(q_0-q_2)t}\}}. \quad (7)$$

By (1), the probabilities $p(x,t)$ can now be found by taking the coefficient of s^x in the powers series expansion of $\pi(s,t)$. We first rewrite (7) as

$$\pi(s,t)=\frac{A+Bs}{C-Ds}=\frac{1}{C}(A+Bs)\sum_{x=0}^{\infty}\left[\frac{D}{C}\right]^x s^x, \quad (8)$$

where

$$A=q_0q_2e^{\lambda(q_0-q_2)t}-q_0q_2,$$

$$B=q_0q_2-q_2^2e^{\lambda(q_0-q_2)t},$$

$$C=q_0q_2e^{\lambda(q_0-q_2)t}-q_2^2,$$

$$D=q_2^2e^{\lambda(q_0-q_2)t}-q_2^2.$$

Therefore,

$$p(x,t)=\left[\frac{A}{C}+\frac{B}{D}\right]\left[\frac{D}{C}\right]^x, \quad x\geqslant 1. \quad (9)$$

Using Eq. (4) we can write the integral equation for the expected, or mean, value of $X(t)$. We have

$$EX(t)=m(t)=(1-q_0+q_2)$$

$$\times\int_0^t m(t-\tau)\lambda e^{-\lambda\tau}d\tau+e^{-\lambda t}. \quad (10)$$

[8] W. Feller, Ann. Math. Stat. 12, 243 (1941).

Equation (10) reduces to the differential equation

$$\partial m(t)/\partial t=\lambda(q_2-q_0)m(t), \tag{11}$$

whose solution, when $X(0)=1$, is

$$m(t)=\exp\{\lambda(q_2-q_0)t\}. \tag{12}$$

It is clear that the behavior of $EX(t)$ will depend on the values of q_0 and q_2. As t approaches infinity we have

$$\lim_{t\to\infty} EX(t)=\begin{cases}0, & q_0>q_2\\ \infty, & q_2>q_0\\ 1, & q_0=q_2.\end{cases} \tag{13}$$

Whenever the probability of absorption is introduced into a model of cascade phenomena it is of interest to determine the probability $p(0,t)$ that the cascade will die out, that is that all particles will for some thickness t be absorbed. From (1) and (8) we see that this probability is given by

$$p(0,t)=\frac{A}{C}=\frac{q_0e^{\lambda(q_0-q_2)t}-q_0}{q_0e^{\lambda(q_0-q_2)t}-q_2}. \tag{14}$$

The probability that all electrons will eventually be absorbed is given by

$$\lim_{t\to\infty} p(0,t)=\begin{cases}1, & q_0>q_2\\ q_0/q_2, & q_0<q_2.\end{cases} \tag{15}$$

Should the cascade start with $n>1$ electrons at thickness zero, the expected number of electrons in the cascade can be obtained by multiplying (12) by n. Since independence is assumed, this is equivalent to considering n independent processes with associated random variables $X_1(t), X_2(t), \cdots, X_n(t)$, and since

$$E\Big(\sum_{i=1}^{n} X_i(t)\Big)=\sum_{i=1}^{n} EX_i(t)$$

the above result follows. An explicit expression for $p(x,t)$ can be obtained by expanding $\pi^n(s,t)$ as a power series in s and proceeding as before. Hence

$$\pi^n(s,t)=\left(\frac{A+Bs}{C}\right)^n\left(1-\frac{D}{C}s\right)^{-n}$$

$$=\left(\frac{A+Bs}{C}\right)^n\sum_{x=0}^{\infty}\binom{-n}{x}\left[-\frac{D}{C}\right]^x s^x. \tag{16}$$

We have, therefore,

$$p(x,t)=\left\{\sum_{i=0}^{n}\binom{n}{i}\left[\frac{A}{C}\right]^{n-i}\left[\frac{B}{D}\right]^i\right\}\times\binom{-n}{x}\left[-\frac{D}{C}\right]^{x-i}, \quad x\geq n. \tag{17}$$

This distribution is of the negative binomial type. The asymptotic behavior of the mean is the same as before, except that now $EX(t)=n$ when $q_0=q_2$. In addition, we have

$$p(0,t)=(A/C)^n, \tag{18}$$

and

$$\lim_{t\to\infty} p(0,t)=\begin{cases}1, & q_0>q_2\\ (q_0/q_2)^n, & q_0<q_2.\end{cases} \tag{19}$$

Ionization Energy Loss of Mesons in a Sodium Iodide Scintillation Crystal*

THEODORE BOWEN†
Department of Physics, University of Chicago, Chicago, Illinois
(Received June 21, 1954)

The response of a thallium-activated sodium iodide crystal to high-energy charged particles passing through the scintillator has been investigated. Pions and muons produced by the Chicago 450-Mev cyclotron have been used to cover energies ranging from 61 Mev (pions) to 245 Mev (muons). Sea-level cosmic-ray muons have been used to cover energies from 200 Mev to greater than 2 Bev. At each energy, the most probable energy loss is determined from the pulse-height distribution, making use of Po-Be 4.44-Mev γ rays for an energy calibration. The distributions from cyclotron data are found from the density variations on photographs of the superposition of many pulses appearing on an oscilloscope. Because the cosmic-ray counting rate is low, each pulse is individually photographed and measured. The results for energies below the occurrence of the minimum in ionization indicate good agreement with the probable energy loss as given by the Bethe-Bloch formula. Beyond the minimum the probable loss is in fair agreement with Sternheimer's calculations for sodium iodide, rising slightly more rapidly than predicted to the Fermi plateau.

INTRODUCTION

AN exact understanding of energy losses by high energy charged particles has long been the object for much theoretical and experimental work. An accurate knowledge of the behavior of ionization energy loss not only helps us to select the best theoretical model for the phenomena, but also makes it possible to use ionization loss along the path of a particle as a quantitative tool in the carrying out of experiments on the properties of high-energy particles. The comparatively recent development of scintillation-counting techniques provides an attractive method of measuring the specific ionization of fast particles, and thus offers the possibility of making new and more accurate comparisons with ionization loss theory.

The first theory of ionization energy loss was developed by Bohr[1] along essentially classical lines. The theory was improved by the quantum mechanical calculations of Bethe and Bloch,[2] and the formula derived by them for the specific energy loss as a function of the velocity of the charged particles has come to be known as the Bethe-Bloch formula. By suitably adjusting the one parameter, the average ionization potential of the absorber, excellent agreement between theory and experiment can be obtained for non-relativistic particle energies.[3] When the Bethe-Bloch formula is extrapolated to the region of relativistic energy losses, one is led to expect the specific energy loss to increase logarithmically with the energy, with no upper limit to the loss which can be reached.

Swann[4] first suggested that polarization of the medium by the fields surrounding the moving charged particle might reduce the energy loss to be expected at high energies. This polarization or density effect was first calculated quantitatively by Fermi,[5] who showed that for extreme relativistic particles the rate of energy loss depends only upon the electron density of the absorber. If, as in most experimental conditions, the occasional energy losses to single electrons larger than some arbitrary energy, T, are ignored, then the energy loss per unit of path length is expected to reach a constant plateau at extreme relativistic energies. Fermi also showed that part of the loss at relativistic energies was in the form of Čerenkov radiation.

The theory of the density effect was then extended by Halpern and Hall[6] and Wick[7] by introducing multifrequency models of a dispersive medium into the calculations. Further studies of the energy loss of relativistic particles have been made by A. Bohr, Schönberg, Messel and Ritson, Huybrechts and Schönberg, Sternheimer, Budini and Poiani, and Fowler and Jones.[8–11] From the earlier work[8] based on the Lorentz dispersion model it appeared that the relativistic rise in the energy loss escaped in the form of Čerenkov radiation, and hence, would not be expected to contribute to the ionization observed close to the path of the particle. However, it has been shown[10,11] that when the dispersion model of the Kramers-Kallmann-Mark theory based on x-ray work is used, very little energy is lost in the form of Čerenkov radiation, and the relativistic rise appears in the form of ionization close to the path of the particle. The

* Supported in part by a joint program of the Office of Naval Research and the U. S. Atomic Energy Commission.
† U. S. Atomic Energy Commission Predoctoral Fellow during part of this work.
[1] N. Bohr, Phil. Mag. **25**, 10 (1913); **30**, 581 (1915).
[2] H. Bethe, Ann. Physik **5**, 325 (1930); Z. Physik **76**, 293 (1932); F. Bloch, Ann. Physik **16**, 285 (1933); Z. Physik **81**, 363 (1933).
[3] S. K. Allison and S. D. Warshaw, Revs. Modern Phys. **25**, 779 (1953).
[4] W. F. G. Swann, J. Franklin Inst. **226**, 598 (1938).
[5] E. Fermi, Phys. Rev. **56**, 1242 (1939); **57**, 485 (1940).
[6] O. Halpern and H. Hall, Phys. Rev. **57**, 459 (1940); **73**, 477 (1948).
[7] G. C. Wick, Ricerca sci. **11**, 273 (1940); **12**, 858 (1941); Nuovo cimento **1**, 302 (1943).
[8] A. Bohr, Kgl. Danske Videnskab. Selskab. Mat.-fys. Medd. **24**, No. 19 (1948); M. Schönberg, Nuovo cimento **8**, 159 (1951); H. Messel and D. Ritson, Phil. Mag. **41**, 1129 (1950).
[9] M. Huybrechts and M. Schönberg, Nuovo cimento **9**, 764 (1952).
[10] R. M. Sternheimer, Phys. Rev. **88**, 851 (1952); **91**, 256 (1953).
[11] P. Budini and G. Poiani, Nuovo cimento **9**, 199 (1952); P. Budini, Phys. Rev. **89**, 1147 (1953); G. N. Fowler and G. M. D. B. Jones, Proc. Phys. Soc. (London) **A66**, 597 (1953).

results of this work will be compared mainly with the calculations of Sternheimer,[10] since he has made explicit numerical computations for sodium iodide.

In order to make measurements of the rate of energy loss of a fast particle, it is generally necessary to determine the energy lost along a small, fixed length of its path. Unfortunately, this loss is subject to large fluctuations or straggling due to the occasional production of high-energy δ rays or knock-on electrons. The energy loss straggling in thin absorbers was first calculated by Williams[12] and later more accurately by Landau.[13] Symon[14] extended the theory to the intermediate case between a thin absorber which gives rise to a Landau distribution and a thick absorber which gives rise to a Gaussian distribution of energy losses. Blunck and Leisegang[15] have computed the effect of resonances in the energy loss process which cause a broadening of the Landau distribution for very thin absorbers where the loss is of the same order of magnitude as the atomic ionization potential of the absorber. Thus, in comparing energy loss theories with experiment, it is not only necessary to correct the average energy loss as computed from the Bethe-Bloch formula for the density effect, but also for the effect of straggling.

Recent measurements[16] of the ionization in gases using cloud chambers, proportional counters, inefficient counters, and ion chambers show a definite relativistic increase and appear to be in good agreement with the most recent theoretical calculations.[10,11] However, over the range of energies and gas pressures studied in most of this work, the energy loss is given by the Bethe-Bloch formula, so very little information has been gained in the region where the density effect becomes important.

Whittemore and Street,[17] by comparing the pulse distributions from an AgCl crystal counter for two meson-energy ranges, were among the first to find convincing experimental evidence of the density effect. The energy loss of 9.6- and 15.7-Mev electrons from a betatron in a number of solids has been measured using a magnetic analyzer by Goldwasser, Mills, and Hanson.[18] They find good agreement with the theory using the density effect correction, except for the heaviest elements. More recently, Goldwasser, Mills, and Rubillard[19] have directly observed the density effect by observing the energy loss in the same chemical compound in the gaseous and solid states and find good agreement with the theory. While these data check the position of the Fermi plateau, they do not yield information about the shape of the energy loss curve before reaching the plateau.

Measurements of grain density in photographic emulsions show a definite relativistic increase.[20] However, the various workers do not agree too well on the exact magnitude and energy dependence of the relativistic rise. Part of the discrepancy may be due to the inaccuracy of momentum measurements in the region where the relativistic rise takes place. In addition, as has been pointed out by Brown,[21] the observed grain densities may not always be proportional to the total energy loss because an energy threshold must be exceeded in order to cause a grain to develop. Therefore, it may be premature to draw definite conclusions from the agreement or lack of agreement of grain density measurements with theory.

The ionization energy loss of high-energy particles can be studied as a function of particle energy by means of the pulse height distributions produced in scintillation counters. This has been demonstrated using cosmic-ray muons by the work of Bowen and Roser,[22] Meshkovskii and Shebanov,[23] and Baskin and Winckler[24] on the organic scintillators anthracene, stilbene, and terphenyl in xylene, respectively. All find good agreement with the theory when the density effect is taken into account. Hudson and Hofstadter[25] find that the pulse height distribution in sodium iodide due to sea level cosmic-ray mesons is only consistent with the theory when a density effect is included. However, since the mesons were not separated into energy groups, they could not study the detailed behavior of the energy loss as a function of the meson energy.

On the basis of the work cited above, energy loss as a function of the particle energy seems well established in gases and in condensed media of low atomic number. However, more data on condensed media of relatively high atomic number are needed to establish the energy loss curve in the region of minimum ionization and

[12] E. J. Williams, Proc. Roy. Soc. (London) **125**, 420 (1929).
[13] L. Landau, J. Phys. (U.S.S.R.) **8**, 201 (1944).
[14] K. R. Symon, Harvard University thesis, 1948 (unpublished). Most of the results are published in *High Energy Particles* by B. Rossi (Prentice-Hall Inc., New York, 1952).
[15] O. Blunk and S. Leisegang, Z. Physik **128**, 500 (1950).
[16] M. H. Shamos and I. Hudes, Phys. Rev. **84**, 1056 (1951); Gosh, Jones, and Wilson, Proc. Phys. Soc. (London) **A65**, 68 (1952); R. S. Carter and W. L. Whittemore, Phys. Rev. **87**, 494 (1952); G. W. McClure, Phys. Rev. **87**, 680 (1952); Price, West, Becker, Chanson, Nageotte, and Treille, Proc. Phys. Soc. (London) **A66**, 167 (1953); Perry, Rathgeber, and Rouse, Proc. Phys. Soc. (London) **A66**, 541 (1953); R. H. Frost and C. E. Nielson, Phys. Rev. **91**, 864 (1953); J. E. Kupperian, Jr., and E. D. Palmatier Phys. Rev. **91**, 1186 (1953); H. R. Snodgrass, Phys. Rev. **92**, 1089 (1953).
[17] W. L. Whittemore and J. C. Street, Phys. Rev. **76**, 1786 (1949).
[18] Goldwasser, Mills, and Hanson, Phys. Rev. **88**, 1137 (1952); C. Warner, III, and F. Rohrlich, Phys. Rev. **93**, 406 (1954).
[19] Goldwasser, Mills, and Rubillard, Phys. Rev. **90**, 378 (1953).
[20] E. Pickup and L. Voyvodic, Phys. Rev. **80**, 89 (1950); I. B. McDiarmid, Phys. Rev. **84**, 851 (1951); A. H. Morrish, Phil. Mag. **43**, 533 (1952); Daniel, Davies, Mulvey, and Perkins, Phil. Mag. **43**, 753 (1952); L. Jauneau and F. Hug-Bousser, J. Phys. et radium **13**, 465 (1952); M. M. Shapiro and B. Stiller, Phys. Rev. **87**, 682 (1952); R. P. Michaelis and C. E. Violet, Phys. Rev. **90**, 723 (1953); A. H. Morrish, Phys. Rev. **91**, 423 (1953); J. R. Fleming and J. J. Lord, Phys. Rev. **92**, 511 (1953); B. Stiller and M. M. Shapiro, Phys. Rev. **92**, 735 (1953).
[21] L. M. Brown, Phys. Rev. **90**, 95 (1953).
[22] T. Bowen and F. X. Roser, Phys. Rev. **85**, 992 (1952).
[23] A. G. Meshkovskii and V. A. Shebanov, Doklady Akad. Nauk. S.S.S.R. **82**, 233 (1952).
[24] R. Baskin and J. R. Winckler, Phys. Rev. **92**, 464 (1953).
[25] A. Hudson and R. Hofstadter, Phys. Rev. **88**, 589 (1952).

beyond where the relativistic rise to the Fermi plateau takes place. An accurate knowledge of the rate of energy loss in this region should help to extend the energy region in which mass measurements and particle identifications can be made.

The work of Hofstadter[26,27] and others has shown that the thallium-activated sodium iodide scintillation crystal has many properties which make it ideally suited for investigating ionization energy loss. The high content of iodine ($Z=53$) gives it a relatively high mean atomic number, comparable to that of AgBr in emulsion; hence, the results from sodium iodide scintillators and emulsion should be similar. The high atomic number also makes possible precise absolute energy calibrations from photoelectrons and pairs produced by γ rays of known energy.[27] Taylor *et al.* [28] have shown that except for slow α particles, where the ionization is of the order of two hundred times minimum ionization, the light output of a sodium iodide crystal is proportional to the energy lost by the charged particle.

In order to investigate the specific energy loss in a scintillating material, particles of known energy must be allowed to pass through a fixed thickness of scintillator in which they lose only a small fraction of their initial energy. Because of straggling of the energy losses, the pulses from the scintillation counter will be distributed in pulse height. The distribution is very skew, with a long tail in the direction of large energy losses. The problem of determining the energy loss is, then, essentially the problem of determining the position of the pulse height distribution. Because of the nature of the distribution, the average pulse height is a very poor estimate of the position of the distribution, since it is subject to large fluctuations caused by occasional very large losses. It is much better to characterize the position of the distribution by the position of the maximum, i.e., by the most probable pulse height. Even though the width at half maximum of the distribution is greater than 20 percent, the most probable value can be obtained to any desired accuracy by obtaining a sufficient number of events. The experimental work was planned to give an accuracy of 1 percent or better in the determination of each probable energy loss.

If a complete investigation of energy loss in sodium iodide were to be undertaken, it seemed desirable to examine the shape of the ionization *versus* energy curve on both the nonrelativistic and relativistic side of the minimum. Mesons provide ideal particles for this energy range, since energy losses due to radiation are negligible. For nonrelativistic energies, mesons produced by the 450-Mev Chicago cyclotron are very suitable, since monoenergetic high intensity beams were available for pion energies up to 227 Mev. For higher energies, one can use muons up to 250 Mev, which is close to the energy for minimum ionization. For still higher energies in the relativistic range, one can use muons from the sea level cosmic radiation. The energy spectrum of muons at sea level has a broad maximum between 100 and 1000 Mev so that most of the mesons lie in the energy region of the relativistic increase in energy loss. The highest energy to which it is practical to go is determined partially by the decrease in meson intensities with higher energies and partially by the increasing difficulty of measuring high energies. The latter limitation was most important in this work where range was used, the largest range measurement corresponding to about 2 Bev. Because of the difference in experimental techniques, the study of energy losses is divided into two parts corresponding to work at energies up to the energy corresponding to minimum ionization using cyclotron-produced mesons and the work at relativistic energies using cosmic-ray mesons.

CYCLOTRON ARRANGEMENT

The arrangement using the 227-Mev π^- beam from the cyclotron is shown in Fig. 1. Protons of 450-Mev energy striking an internal beryllium target produce pions, which are first magnetically analyzed by the

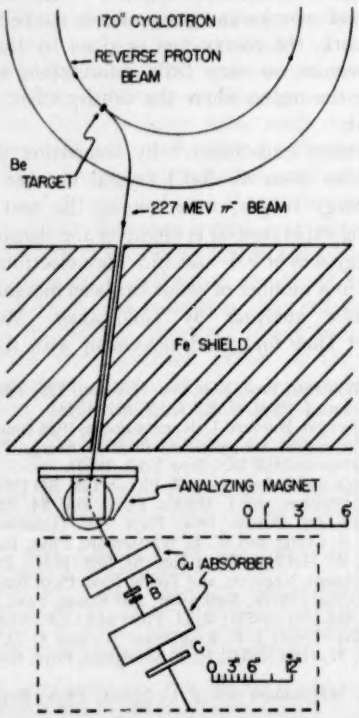

FIG. 1. Cyclotron arrangement for the 227-Mev π^- beam. The counter arrangement is shown in an enlarged scale.

[26] R. Hofstadter, Phys. Rev. 75, 796 (1949).
[27] R. Hofstadter and J. A. McIntyre, Phys. Rev. 80, 631 (1950).
[28] Taylor, Jentchke, Remley, Eby, and Kruger, Phys. Rev. 84, 1034 (1951).

cyclotron's magnetic field. A channel through the shield wall is used which selects negative particles of 340 Mev/c momentum coming from the target. After passing through the shield wall, the particles are magnetically analyzed a second time by a deflection through 35°, giving a beam consisting of 97 percent 227-Mev negative pions and about 3 percent negative muons.[29] Since the muons mainly originate from the decay of pions close to the target and pass through two analyzing magnetic fields, they also have a momentum of 340 Mev/c, which corresponds to an energy of 250 Mev. Some data was also taken using the 122-Mev beam, the setup being similar except for the use of a different channel through the shield and different target and analyzing magnet settings.

The average energy of the 227-Mev beam has been determined by range measurements to within ±3 Mev with a total spread in energies of less than 4 Mev. In the 122-Mev beam the energy is known to ±2 Mev and the total spread in energies is less than 3 Mev. Other lower energies were obtained with each beam by introducing copper absorbers in front of counter A (Fig. 1). This introduces a small additional fluctuation in energy of the order of 3 percent due to energy loss straggling, as well as reducing the beam intensity by nuclear absorption and by nuclear and Coulomb scattering out of the beam.

A view of the counter arrangement is shown in Fig. 1 in an expanded scale. Scintillator A is the thallium-activated sodium iodide crystal[30] in which the energy loss was to be studied. It was 1.51×3.47×5.97 cm³ and was positioned so the 5819 photomultiplier tube viewed one end. The crystal was wrapped with an aluminum foil reflector and was hermetically sealed in an aluminum can with a Lucite window. The light collection was uniform to within ±6 percent.

Counters B and C formed a coincidence telescope to select the mesons for which a measurement of the energy loss was to be made in the sodium iodide. Counter B was a 1.0×2.5×5.0-cm³ plastic scintillator[31] viewed at one end by a 5819 photomultiplier tube. The large counter C consisted of two 2×6×17 cm³ plastic scintillators, each viewed by a separate photomultiplier tube, and located side by side so that an effective area of 12×17 cm² was covered. The sensitive area was made large so that losses would be reduced due to small angle Coulomb and diffraction scattering in counters A and B and in any copper absorber which might be between B and C. With this arrangement, almost all the mesons selected by the coincidence BC have passed through the sodium iodide crystal A.

When it was desired to measure the energy loss of pions, no absorber was used between B and C. To measure the effect of the 250-Mev muons only, 126 g/cm² of copper absorber was inserted between counters B and C. The range of pions of 340-Mev/c momentum is 122 g/cm² Cu, whereas muons of the same momentum have a range of 144 g/cm² Cu. Since the total amount of material ahead of counter C was equivalent to 134 g/cm² Cu, the pions were unable to reach C and cause coincidences. However, the muons could still reach C and give coincidences. In this way it was possible to measure the energy losses due to muons.

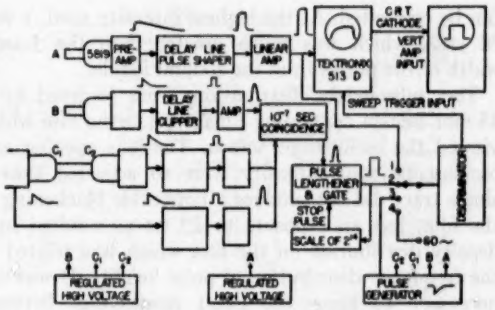

FIG. 2. Block diagram of the electronics for cyclotron produced mesons.

A block diagram of the electronics for cyclotron produced mesons is shown in Fig. 2. Counter B is in a 10^{-7}-second coincidence with the combined output of C_1 and C_2. This coincidence pulse, after passing through a gate circuit and discriminator, is used to trigger the sweep of a Tektronix 513D oscilloscope. The output of the sodium iodide scintillation counter A is shaped into a rectangular pulse 1.0 μsec wide by means of delay line. This pulse enters the vertical input of the oscilloscope. Since each meson which passes through B and C also has passed through A, each oscilloscope trace presents a pulse whose height is proportional to the energy lost by a meson in the sodium iodide A. A scale of 2^{14} circuit is also operated by the coincidence pulses. This circuit closes the gate circuit after $2^{14}=16\,384$ events, thus stopping the recording until manually restarted. The input of the discriminator which triggers the oscilloscope sweep may be switched to other trigger sources for the purpose of recording the distribution due to the calibration γ-ray source (position 1), observing artificial test pulses from a mercury switch pulse generator (position 3), and recording a zero reference base line (position 4).

In the 227-Mev pion beam, typical counting rates were 9600 counts per minute for 227-Mev pions, 4100 counts per minute for pions slowed down to 167 Mev, 2100 counts per minute for pions slowed down to 121 Mev, and 360 counts per minute for 250-Mev muons. Although much higher rates were possible in the 122-Mev pion beam, the beam intensity was adjusted for similar rates to avoid any possibility of pulse pileup. When the duty cycle of the cyclotron is taken into account, the average spacing τ between counter pulses

[29] Anderson, Fermi, Martin, and Nagle, Phys. Rev. **91**, 155 (1953); M. Glicksman, Phys. Rev. **95**, 1045 (1954).

[30] Obtained from Harshaw Chemical Company, Cleveland, Ohio.

[31] C. N. Chou, Phys. Rev. **87**, 903 (1952). The author wishes to thank Dr. Chou for kindly supplying the scintillating plastic.

can be computed. At the highest intensity used, τ was 78 μsec, which was much greater than the 1-μsec. width of the pulses from the sodium iodide.

The pulse-height distributions were recorded by a 35-mm camera containing Linagraph Ortho film which viewed the oscilloscope screen. The lens opening and oscilloscope spot intensity were so adjusted that a single trace did not produce a noticeable blackening of the film, but an exposure to 2^{14} traces resulted in a density distribution on the film which was related to the frequency distribution of pulse heights. It was not necessary to know the exact relationship between density on the film and frequency since it was only necessary to find the most probable pulse height, which corresponds to the location of the region of greatest optical density on the film.

A calibration of the scale of pulse heights in Mev of energy loss was made possible by recording the pulse height distribution produced by a 2.5-millicurie polonium-beryllium neutron source. The main γ-ray produced by this source is one of 4.44 Mev from the decay of the first excited state of C^{12}.[22] This γ-ray produces a pair peak at 3.42 Mev which is used for energy calibration. Comparison of the pulse height of this pair peak with the 0.662-Mev Cs^{137} photopeak showed the response to be linear.

Before and after making each exposure to a pulse-height distribution, a zero reference line was recorded by exposing to about 300 blank traces. This was done at the beginning and end of each exposure to provide a check against possible drift of the oscilloscope image, since some of the exposures lasted longer than 30 minutes.

To eliminate the possibility of a slow drift of the sensitivity of the equipment while the measurements were being carried out, the distribution from pions of the full beam energy was repeated between each exposure to a different energy and between each γ-ray calibration. As the light intensity required for optimum exposure was rather critical, three exposures at each energy were taken differing by factors of two in light intensity. To obtain reproducible oscilloscope beam intensities, a second oscilloscope was used to observe the pulse across a small cathode resistor caused by the beam current.

In order to make more accurate estimates of the most probable pulse height, microphotometer tracings of the density distributions were made. The linearity between pulse height at the output of the photomultiplier and the measurement on the microphotometer tracing was checked by introducing artificial pulses of known amplitude ratios and was found to be within 1 percent over the region used.

COSMIC-RAY ARRANGEMENT

An apparatus was designed which would select cosmic-ray muons passing through a small area and solid angle where scintillation materials could be placed. In order to study the dependence upon meson energy of the scintillation responses, provision was made for classifying the selected mesons into four range intervals. Means were also provided to eliminate events due to electrons and showers. For each event, the responses of up to four separate scintillators could be simultaneously recorded. By providing an arrangement where the data over all the energy ranges for several scintillators could be collected simultaneously, not only was a large saving in operating time made possible, but accurate comparisons of the results from different energies and scintillators were made possible which are not subject to the errors of calibrations and slow drifts with time. The design follows very closely that of Bowen and Roser.[22]

The arrangement of counters and absorbers is shown in Fig. 3. Charged particles are selected by the side-by-side telescopes AB_1C_1D and AB_2C_2D. Either of these coincidences provides a master pulse which allows the recording of the pulse heights from the four scintillation counters and the recording of whether or

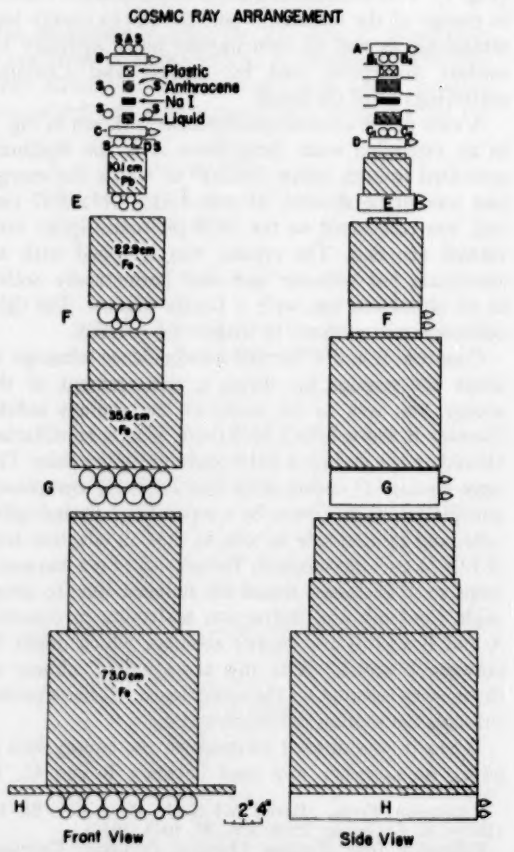

FIG. 3. Arrangement of counters and absorbers for cosmic-ray mesons. The dimension shown on each absorber refers to its vertical thickness.

[22] R. G. Thomas and T. Lauritsen, Phys. Rev. 88, 969 (1952).

not GM trays E, F, G, and H and shower counters S are in coincidence with the master pulse. The E, F, G, and H trays determine to which range interval the meson belongs. The S counters prove highly efficient in detecting when two or more particles are present, as judged from the observation that almost all anomalously large or small scintillation counter pulses are accompanied by S.

A block diagram of the electronics is shown in Fig. 4. A 10^{-5}-sec coincidence of AB_1C_1D or AB_2C_2D triggers the camera drive and dead-time circuit. If 12 seconds or more have elapsed since the preceding event so that the camera is ready, then a pulse is promptly sent on to trigger the sweep of the Tektronix 514D oscilloscope. The pulses from the scintillation counters are delay-line-shaped to a width of 1.5 μsec; they are then delayed by 0, 3, 6, and 9 μsec and mixed together. After a further 4-μsec delay, the group of pulses enters the vertical amplifier of the oscilloscope. In this way, each pulse is individually displayed. Pulses delayed 48, 42, 34, 27, and 20 μsec from counter trays S, E, F, G, and H, respectively, also appear on the oscilloscope sweep. These delayed pulses are obtained from the trailing edges of pulses from one shot multivibrators. Delayed pulses are also used to indicate which of the two possible master coincidences triggered the sweep.

The recording of the oscilloscope traces was made on Linagraph Ortho 35-mm film. Each time the oscilloscope sweep was triggered, the camera drive circuit started the camera motor to move the film in position for the next event. At the same time a mechanical register was also operated whose numbers could be correlated with the events on the film. Auxiliary feedback-type circuits had to be added to the oscilloscope to improve the stability of the vertical positioning and spot intensity, making the recordings of more uniformly good quality.

The four scintillators used were from top to bottom, anthracene in polystyrene plastic,[31] an anthracene crystal, a thallium-activated sodium iodide crystal, and terphenyl plus diphenylhexatriene in phenylcyclohexane liquid.[32] The final results from the three organic scintillators will be presented in a later publication. The sodium iodide crystal was the same one used with cyclotron-produced mesons with dimensions $1.51\times3.47\times5.97$ cm.[3] The crystal was viewed from one end as in the cyclotron arrangement by an RCA 5819 photomultiplier tube. Since the mesons selected by telescopes AB_1C_1D and AB_2C_2D passed through the crystal at different average distances from the photocathode, some information about the uniformity of the light collection efficiency could be gained.

The events could be classified into four meson energy ranges corresponding to the master coincidence being accompanied by E, EF, EFG, or EFGH. It was also required that there be no pulse from counters S and

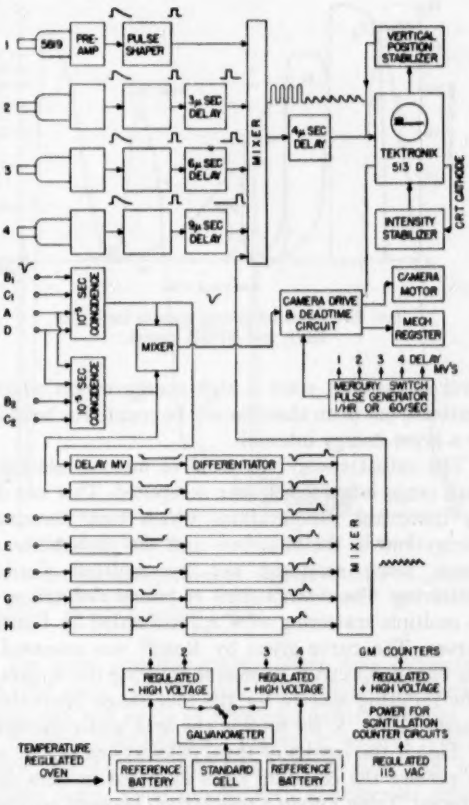

FIG. 4. Block diagram of the electronics for cosmic-ray mesons.

that all four scintillator pulses be present and at least one-half the most probable height. From an analysis of events which were otherwise acceptable, but which had one tray missing, such as FGH, or EFH, the efficiency of counter trays E, F, and G were found to be greater than 99 percent. Tray H could not be checked in the same way, but a comparison of single counting rates shows that its efficiency should be about 99 percent.

The energy spectrum of mesons selected by a particular coincidence is determined not only by the energy loss of the mesons in the absorbers between counter trays, but also by the amount of scattering which the mesons suffer. The first absorber is 10.1 cm of lead. Although mesons which have more than 193 Mev at the center of the sodium iodide crystal can pass through this lead, most electrons found at sea level will be stopped. The remaining absorbers, however, consist of iron, in which, for equal thicknesses, the rate of ionization energy loss is only about 9 percent less than that for lead, yet the rms multiple Coulomb scattering is less by a factor of about 1.88 because of the lower atomic number of iron. It is important in this application to reduce the multiple Coulomb scattering to as low a

[32] H. Kallmann and M. Furst, Nucleonics **8**, No. 3, 32 (1951).

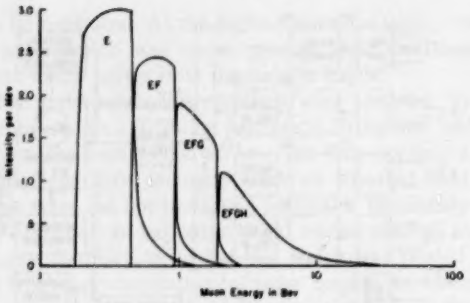

FIG. 5. Calculated energy spectra for E, EF, EFG, and EFGH events.

level as possible, since a high energy meson which is scattered out of an absorber will be counted as belonging to a lower energy interval.

The actual energy spectrum of mesons selected by each range interval has been computed. This was done by numerical computations which took account of energy loss in the absorbers and the probability of a muon being scattered out by multiple Coulomb scattering. The distributions of lateral deflections due to multiple scattering were approximated by Gaussian curves. The curve given by Rossi[34] was assumed for the energy spectrum of muons entering the apparatus. The resulting spectra for the four range intervals are shown in Fig. 5. By finding the area under the curves of Fig. 5, the results of these calculations can be used to predict the counting rates expected in each range interval. Table I gives a comparison between computed and actual counting rates. The agreement appears satisfactory in view of the approximations made in the calculations and the uncertainties in the meson spectrum.

Since the cosmic-ray apparatus had to be operated over a period of more than three months, it was necessary to provide for a high degree of stability. It was especially important to provide a very stable high voltage to the photomultiplier tubes, since a change of 1 percent in the high voltage would result in a 10 percent change in photomultiplier gain. Consequently, the electronically regulated supplies for the photomultipliers used batteries as voltage references. These reference batteries were enclosed along with a standard cell in an oven whose temperature was regulated at (30.5±0.5)°C. The high voltage from either supply could be checked against the standard cell by means of a voltage divider using precision wire wound resistances and a null indicating galvanometer. With the above arrangement, the high voltage supplied to the photomultiplier tubes was kept well within ±0.1 percent.

Outputs from a mercury-switch pulse generator went to all scintillator and counter inputs. During normal operation of the equipment, this generator gave one pulse each hour which was recorded in the same way as a normal event. This not only provided an hourly time marker, but also provided a calibration for the pulse-height scale, since the heights of the pulses from the generator were held constant to within ±0.5 percent throughout the experiment. Each calibration pulse also provided a check of the operation of the delay multivibrator circuits.

Approximately once a week an energy calibration of the pulses from the sodium iodide counter was made using the 4.44-Mev γ rays from a Po-Be source. The pulse-height distribution due to the γ rays was recorded and measured in the same way as in the cyclotron arrangement. The results of these calibrations showed that the gain of the photomultiplier remained constant within ±1 percent during the course of the experiment.

The recorded oscilloscope traces were projected onto a horizontal screen on a table-top with an enlargement such that the images were five times the size of the original trace on the face of the cathode-ray tube. Full scale deflection corresponded to about 20 cm on the screen, and the most probable pulse height to about 7 cm. The height of each scintillation counter pulse was measured with an error of ±0.01 cm and recorded, along with the information provided by the counter tray pulses. The artificial calibration pulses were also measured along with the genuine events. Each measurement of an event was converted to an energy loss in Mev by dividing by the average size of the calibration pulses at the time of the event and multiplying by the Mev equivalent of a calibration pulse as determined from the Po-Be calibrations.

RESULTS

The relation between the probable energy loss of a singly charged particle, ϵ_{prob}, in a thickness of t cm of material is expected to be given by the equation

$$\epsilon_{\text{prob}}=\frac{2\pi ne^4t}{mv^2}\left[\ln\frac{2mv^2(2\pi ne^4t/mv^2)}{I^2(1-\beta^2)}-\beta^2+j-\delta\right],$$

where n is the electron density, e is the electronic charge, m is the mass of the electron, I is the average ionization potential of the material, and v is the velocity of the charged particle. The term j is a small correction term calculated from straggling theory[14] which depends upon the absorber thickness and the particle velocity and which approaches 0.37 when

$$2\pi ne^4t/mv^2\ll 2mv^2/(1-\beta^2).$$

TABLE I. Calculated and observed counting rates.

Type of event	Calculated rate/hour	Observed rate/hour
E	0.518	0.586±0.041
EF	0.645	0.640±0.043
EFG	0.925	1.093±0.056
EFGH	2.31	2.12 ±0.077

[34] B. Rossi, Revs. Modern Phys. 20, 538 (1948).

δ represents the density effect correction, which arises because the polarization of the medium reduces the energy loss. Numerical values of δ have been calculated by Sternheimer[10] for sodium iodide, which is the material used in this experiment. If $x=\log_{10}[\beta/(1-\beta^2)^{\frac{1}{2}}]$, then δ is given approximately by

$$\delta=0 \qquad x<0.09;$$
$$\delta=4.606x-5.77+0.278(3-x)^{3.77}, \quad 0.09<x<3.00;$$
$$\delta=4.606x-5.77, \qquad x>3.00.$$

Following Sternheimer, the mean ionization potential I was taken from an interpolation of the values given by Bakker and Segrè[35] to be 392 ev. In the cyclotron arrangement the correction for the lengthening of the average path length of the mesons in the sodium iodide due to scattering ranged from 0.66 percent at the lowest energy to 0.07 percent at the highest energy. In the cosmic-ray arrangement, the counter geometry (Fig. 3) was such that the average path length was increased by only 0.2 percent of the actual scintillator thickness of 1.51 cm. The theoretical values to be compared with the experimental results were all computed from the above relations.

While ionization loss is the only process which contributes significantly to energy loss by muons, this is not true for pions. In addition to ionization energy loss, pions may also lose energy by nuclear interaction. On the basis of emulsion, cloud chamber, and counter studies of pion interactions,[36] five percent of the pions are expected to undergo nuclear interactions and another five percent to be diffraction scattered in the 1.51 cm of sodium iodide. Less than five percent of the nuclear interactions will be counted, since a pion with $E>35$ Mev or a proton with $E>70$ Mev within 30° of the beam direction is required to actuate the coincidence counters (B and C in Fig. 1). The lengthening of the average path length in the sodium iodide due to the diffraction scattering of pions is less than 0.1 percent. For the one percent accuracy required in this experiment the effects of nuclear interactions and diffraction scattering can be neglected. Pions and muons also differ in spin, pions having spin zero and muons probably having spin $\frac{1}{2}$. However, the effect of the magnetic moment probably associated with the muon is completely negligible over the range of energies used in this work.[37] Therefore, since the energy loss equation for singly charged particles heavier than the electron involves only the velocity of the particle, pions and muons are expected to give equally valid results on the energy loss in sodium iodide.

Before stating the results, it is important to explain how the most probable energy losses were estimated from the data. In the case of cyclotron-produced mesons, use was made of microphotometer tracings of the density distributions. Figure 6 shows typical density distributions for 4.44-Mev γ rays and for 122-Mev pions. Even though each distribution represents about 1.6×10^4 mesons, there are still small fluctuations in the curve. The position of the highest point of such a distribution curve clearly is not the best estimate of the position of the distribution. One can do better by also making use of the steeply rising and falling regions of the distribution curve.

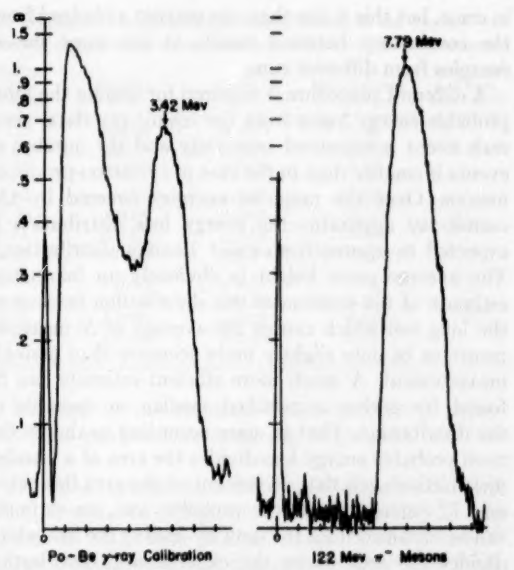

FIG. 6. Sample microphotometer tracings of the photographic density distributions due to (left) Po-Be γ-rays and (right) 122-Mev π^- mesons in sodium iodide.

In the procedure adopted for the cyclotron data, the most probable pulse height was determined with the help of a standard curve which was an average of a number of the observed distributions. The peak of this curve was marked. The standard curve was then superimposed on each pulse-height distribution to give the best fit possible by visual observation. The position of the peak of the standard curve was taken as the location of the most probable pulse height. By making use of the γ-ray calibration and assuming that the pulse height was proportional to the energy lost in the crystal, the distance from the zero reference line to the most probable pulse height could be used to calculate the most probable energy loss in the scintillator. The accuracy of a probable pulse-height measurement made in this way of an individual distribution was ±1.3 percent as determined from the consistency of all the results from a single energy. In using the above method there is the possibility of introducing a systematic error if the peak of the standard curve is

[35] C. J. Bakker and E. Segrè, Phys. Rev. **81**, 489 (1951).
[36] Bernardini, Booth, and Lederman, Phys. Rev. **83**, 1075 (1951); R. L. Martin, Phys. Rev. **87**, 1052 (1952); J. O. Kessler and L. M. Lederman, Phys. Rev. **94**, 689 (1954).
[37] H. J. Bhabha, Proc. Roy. Soc. (London) **A164**, 257 (1938); H. S. W. Massey and H. C. Corben, Proc. Cambridge Phil. Soc. **35**, 463 (1939).

in error, but this is less than one percent as judged from the consistency between results at the same meson energies from different runs.

A different procedure is required for finding the most probable energy losses from the cosmic-ray data, since each event is measured separately and the number of events is smaller than in the case of cyclotron-produced mesons. Over the range of energies covered by the cosmic-ray apparatus the energy loss distribution is expected to approach an exact Landau distribution.[18] The average pulse height is obviously an inaccurate estimate of the position of this distribution because of the long tail which causes the average of N measurements to be only slightly more accurate than a single measurement. A much more efficient estimate can be found by taking a modified median or quantile of the distribution. That is, since according to theory the most probable energy loss divides the area of a Landau distribution such that 28 percent of the area lies below and 72 percent above the probable loss, an estimate can be obtained from the data by finding the loss which divides the area under the experimental distribution curve in the ratio of 28 to 72. For the Landau distribution, the error in the probable loss obtained from this quantile method is about 1.5 times the error of the best possible estimate theoretically attainable.

A further difficulty arose when it was found that the actual energy loss distributions did not exactly fit the expected Landau distributions. The experimental energy loss distributions are shown in Fig. 7. With increasing meson energy, more large energy losses were found than were expected. This was attributed to knock-on electrons produced in the scintillators and counter walls in the path of the mesons directly above the sodium iodide crystal. The energy distribution of knock-ons striking the sodium iodide crystal was calculated for several muon energies. The theoretical cross section for the production of knock-on electrons by muons (spin ½) was used.[37] Since knock-on electrons produced with energies less than 1 Mev have very little chance of striking the sodium iodide crystal because of their large angle of emission and large multiple scattering, only electrons produced with energies greater than 1 Mev were considered, which made it possible to assume a constant rate of ionization energy loss in the calculation. These distributions were then folded into the Landau distributions. The resulting distributions had tails which agreed much better with the data, the number of large energy losses being more frequent at higher muon energies. The positions of the peaks of the original Landau distributions were not shifted by more than 0.5 percent, but quantile estimates of the probable losses would be shifted to larger values, the shift being dependent upon muon energy.

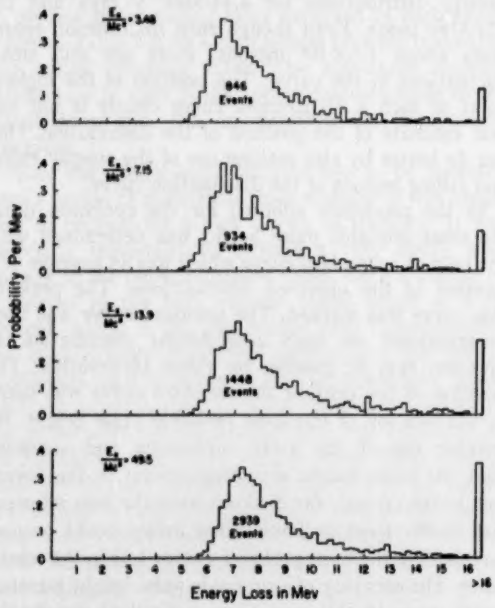

FIG. 7. Histograms of the cosmic-ray muon energy losses. The distributions from top to bottom represent E, EF, EFG, and EFGH events. The effective value of the muon kinetic energy in units of its rest energy (E_k/Mc^2) is given for each distribution. The shift of the histograms to larger losses for the higher energies can be seen clearly.

It was also observed that the peaks of the observed distributions were significantly broader than for those of pure Landau distributions. The theory of Blunck and Leisegang[15] predicts some broadening due to resonance losses in the neighborhood of the ionization potentials which for the sodium iodide crystal means that an additional fluctuation obeying a Gaussian distribution with a standard deviation of 0.10 Mev must be combined with the Landau distribution. Good agreement with the observed distributions requires assuming a standard deviation of 0.4 Mev. It is then most likely that the additional fluctuations arise from small nonuniformities in the light collection efficiency, statistical fluctuations in the number of photoelectrons and variations in gain of the photomultiplier.

Theoretical distribution curves, which included the effects of knock-on electrons and the Gaussian ($\sigma=0.4$ Mev) errors, were calculated. It appeared from these curves that a further improvement in estimating the probable energy loss could be obtained by cutting off the tail of the energy loss distribution. The cut-off was arbitrarily taken to be the position on a pure Landau distribution which divides the area so that 20 percent is in the cut-off tail. This cut-off was found to be 2.2 Mev above the probable energy loss. 35 percent of the remaining 80 percent of the area was found to lie below the probable loss and 65 percent above. The probable loss of an experimental distribution was obtained by starting with a crude estimate of the probable loss and placing the cut-off 2.2 Mev higher. An improved estimate of the probable loss was obtained from the quantile which divided the remaining area

TABLE II. Summary of results for the probable energy loss in 1.51 cm NaI. E_k is the average kinetic energy of the mesons.

Group	E_k/Mc^2	E_k (Mev)	Type	Energy spread (Mev)	Probable energy loss (Mev)	Relative error	Absolute error	Sternheimer's theory	Probability of least squares fit
122-Mev π^-	0.436	61	π	5	10.32	±0.08	±0.13	10.28	
Cyclotron	0.607	85	π	4	8.66	±0.06	±0.11	8.76	0.19
beam	0.843	118	π	3	7.77	±0.04	±0.09	7.83	
227-Mev π^-	0.857	120	π	7	7.84	±0.05	±0.09	7.82	
Cyclotron	1.164	163	π	6	7.19	±0.04	±0.08	7.23	0.55
beam	1.588	222	π	4	6.81	±0.03	±0.08	6.85	
	2.29	245	μ	5	6.50	±0.06	±0.09	6.59	
Cosmic	3.48	368	μ		6.48	±0.06	±0.09	6.53	
rays	7.15	755	μ		6.51	±0.06	±0.09	6.55	0.064
	13.9	1470	μ		6.78	±0.05	±0.08	6.72	
	49.5	5230	μ		7.13	±0.04	±0.08	7.02	

in the ratio of 35 to 65. The cut-off was then placed 2.2 Mev above the new probable loss estimate, the process of successive approximations going on until no further improvement was obtained. The modified quantile estimates obtained in this manner from the theoretical distribution curves were found to agree within 0.5 percent with the most probable losses given by the original Landau distributions. This method of arriving at the value of the probable loss has the distinct advantage of being unaffected by the presence of knock-on electrons or small Gaussian fluctuations in the distribution.

Table II gives the results from both the cyclotron and cosmic-ray data for the most probable energy loss at various energies. The cyclotron meson energies given are the average energies at the center of the sodium iodide (A in Fig. 1). Each cosmic-ray meson energy is that energy which would give the same probable loss as that expected from the actual spectrum of energies. This energy is very closely equal to the median of the respective energy band. The last row in the cosmic-ray group represents all muons with an energy greater than 2 Bev.

The relative errors of the probable energy losses are for use in making comparisons within one of the three groups into which the data has been divided. They refer to the errors in estimating the peaks of the pulse-height distributions, but do not include errors in the absolute energy calibration. The relative errors of the cyclotron results are estimated from the internal consistency of the data. The relative errors of the cosmic-ray data are computed assuming that the fractions of the data lying on either side of the true probable energy loss obey a binomial probability distribution. The error in the calibration needed to make absolute comparisons with the theory is estimated to be ±1.0 percent, to which ±0.6 percent is contributed by the uncertainty in the calibration γ-ray energy, ±0.5 percent by the error in locating the position of the distribution due to the γ rays, and ±0.3 percent by the uncertainty in the thickness of the sodium iodide crystal. An error in the calibration will affect all the losses in a group by the same factor, and is included in the estimate of absolute error, which should be used in comparing any single point with the theory.

The two master coincidences, $AB_1C_1D=M_1$ and $AB_2C_2D=M_2$ (see Fig. 3) allowed the data to be separated into two groups which passed through different regions of the sodium iodide crystal. The M_1 mesons passed through a region which was one inch closer to the photomultiplier than the M_2 group. The M_1 pulse-height distributions were located at 6.7 percent higher pulse heights than those of M_2. In the pulse-height histograms shown in Fig. 7, the M_1 distributions have been shifted down by this amount to coincide with the M_2 distributions. Except for this shift, the two sets of data agreed and showed the same relativistic rise within statistical errors. Use was made of this difference in light collection efficiency between the M_1 and M_2 groups in making comparisons with the calibration γ-ray distributions, which involve the whole volume of the crystal.

The results are also shown plotted in Fig. 8 along with a curve calculated from the theory of Sternheimer. For energies below the minimum of ionization, the

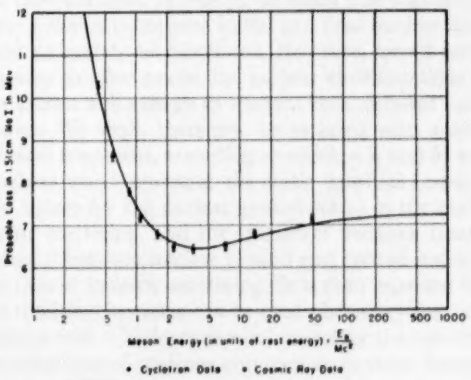

FIG. 8. The probable energy loss of mesons in 1.51 cm of sodium iodide is shown as a function of meson energy in units of its rest energy. The curve is calculated from the theory of Sternheimer. The solid circles represent cyclotron data using pions, except for the highest point at $E_k/Mc^2=2.3$, using muons. The open circles show the cosmic-ray muon results.

agreement between theory and experiment is perfectly satisfactory. Beyond the minimum the experimental data shows an indication of a somewhat more rapid rise, as can be seen in Fig. 8, where the errors indicated are the absolute errors of Table II. It is possible to test the agreement between theory and experiment in another way by making use of the relative errors, which are appreciably smaller than the absolute errors. The results from any one of the three groups in Table II can be normalized to the theoretical curve by a weighted least-squares fit. The exactness of this fit can then be tested by well known statistical methods. In the last column of Table II the probability due to statistical fluctuations of deviations as large or larger than those found is given for each group. The groups of data from the cyclotron give reasonably high probabilities (0.19 and 0.55), showing that the relative losses from theory and from experiment agree. The low probability of 0.064 for the points from the cosmic-ray data at energies in the region of the relativistic rise indicates a discrepancy between theory and experiment which may be significant.

To be more certain that the relativistic rise found in sodium iodide was not due to any instrumental errors, a preliminary check was made of part of the data from the liquid scintillator (terphenyl plus diphenylhexatriene in phenylcyclohexane) which was taken concurrently with the sodium iodide data. The probable pulse heights from all four range intervals agree and show that the relativistic increase could not exceed 2 percent, in contrast to the 10.9±1.0 percent increase found in sodium iodide. This result for phenylcyclohexane agrees with previous results on similar organic materials[22–24] and with theory.[10]

CONCLUSIONS

The results of this work demonstrate the possibility of exact determinations of the ionization energy loss of high-energy charged particles by the use of scintillation counters. Excellent agreement is found between theory and experiment for the probable energy loss of pions and muons at energies below the minimum of ionization where the density effect is not important. The experimental data for muons with energies beyond the minimum of ionization give conclusive evidence for the existence of the density effect in sodium iodide. In addition, the experimental results show a definite relativistic increase in the probable energy loss, the increase being 10.9±1.0 percent in going from the minimum to an energy of $50Mc^2$ ($M=207m_e$).[38] This compares with the prediction of 8.2 percent rise at $50Mc^2$ from the calculations of Sternheimer. The theory predicts a total rise in going from the minimum to the plateau at infinite energy of 11.4 percent, which is perfectly consistent with the results obtained here (10.9±1.0 percent) if it is assumed that the energy loss reaches the plateau more rapidly than expected.

It is a pleasure to acknowledge the advice and encouragement given by Professor Marcel Schein throughout the course of this work. The author also wishes to thank Professor H. L. Anderson and Mr. L. Kornblith for the use of the cyclotron and Dr. O. Joensuu of the Geology Department for the use of the microphotometer. Thanks are also due to members of the Cosmic Ray Group who have assisted in various phases of the work.

[38] Smith, Birnbaum, and Barkas, Phys. Rev. 91, 765 (1953).

Nuclear Multipole Transitions in Inelastic Electron Scattering*

L. I. SCHIFF
Stanford University, Stanford, California
(Received July 26, 1954)

Expressions are obtained for the differential cross sections for inelastic scattering of fast electrons with excitation of various nuclear multipole transitions. The most probable transitions are those that involve collective motion of many nucleons, and in this case the term arising from the transition charge density dominates those that come from the current and magnetization densities. There is then a close relation between the probability for inelastic electron scattering and the probability for the corresponding radiative electric multipole transition, although an assumption must be made as to the shape of the transition charge density. This is illustrated with a detailed discussion of the collective electric quadrupole transitions, using the model of Bohr and Mottelson. When the transition is produced by one or a small number of nucleons, or when it is of magnetic multipole type, there is likely to be little relation between inelastic scattering and radiation probabilities. The electric monopole transition (0+→0+) is also discussed. It is shown how the elastic scattering can be corrected for unresolved inelastic scattering as well as elastic quadrupole scattering before an analysis is made in terms of the spherically symmetric part of the static nuclear charge density, and also how the strength as well as the shape of the transition charge density can be determined experimentally when only relative measurements of inelastic scattering are available.

I. INTRODUCTION

RECENT experimental work of Hofstadter and collaborators[1,2] has demonstrated the possibility of obtaining precise distributions in energy and angle for electrons of very high initial energy scattered by nuclei, and has yielded specific results in a number of cases. Analysis of the angle distributions of such elastically scattered electrons[3] has already provided information on the radial dependence of the static charge density in various nuclei. There are two main reasons why a similar analysis must be made for the inelastically scattered electrons. First, with imperfect energy resolution, some inelastically scattered electrons corresponding to excitation of low-lying nuclear states will be included in the measurement of elastic scattering, and may affect the charge density inferred from these measurements. Second, when inelastically scattered electrons can be resolved in energy, it is anticipated that their distribution in angle can often be used to determine the strength and multipole character of the corresponding nuclear transition.

The information concerning nuclear transitions that can be obtained from inelastic electron scattering is very similar to that which can be obtained from Coulomb excitation by heavy charged particles that are slow enough so that they do not penetrate the nuclear Coulomb barrier appreciably.[4] In both cases, the interaction between incident particle and nucleus is essentially all electromagnetic and is calculable. Thus far, Coulomb excitation experiments have yielded total excitation probabilities as a function of the charge, mass, and velocity of the incident particle, which can be used to determine the strength and multipolarity of nuclear electric multiple transitions. Accurate measurements of the angle dependence of inelastically scattered electrons can determine these quantities independently and can, in addition, give the radial dependence of the transition charge density. In principle, such experiments can also provide similar information concerning magnetic multipole transitions; it will be shown, however, that such transitions are likely to be less probable than electric multipole transitions, and that they are more difficult to interpret.

In the present paper, the nucleus is described by charge, current, and magnetization densities ρ, $\mathbf{j}$, and $\mathbf{M}$, which are treated as classical quantities. Actually, they should be regarded as quantum-mechanical operators of the type discussed by Foldy,[5] in which case appropriate matrix elements between initial and final nuclear states must ultimately be calculated. However, for all except the very simplest nuclei, the nuclear wave functions are not known well enough to warrant such detailed calculations. We shall, therefore, be satisfied with a semiclassical treatment, according to which ρ, $\mathbf{j}$, and $\mathbf{M}$ are c numbers which represent the static densities (expectation values for the nuclear ground state) in the case of elastic scattering, and the transition densities (matrix elements between nuclear ground and excited states) in the case of inelastic scattering. It is then expected that the resulting formulas can be used phenomenologically, perhaps with a hydrodynamical model for the combined contributions of nucleons and mesons to these densities (see Sec. VIII).

It is inherent in the present work that the dynamic interaction between electron and nucleus is treated by

* Supported in part by the Office of Scientific Research, Air Research and Development Command.

[1] Hofstadter, Fechter, and McIntyre, Phys. Rev. **92**, 978 (1953); Hofstadter, Hahn, Knudsen, and McIntyre, Phys. Rev. **95**, 512 (1954).

[2] McIntyre, Hahn, and Hofstadter, Phys. Rev. **94**, 1084 (1954).

[3] Yennie, Ravenhall, and Wilson, Phys. Rev. **95**, 500 (1954), and private communication.

[4] T. Huus and Č. Zupančič, Kgl. Danske Videnskab. Selskab, Mat.-fys. Medd. **28**, 1 (1953); C. L. McClelland and C. Goodman, Phys. Rev. **91**, 760 (1953); N. P. Heydenburg and G. M. Temmer, Phys. Rev. **93**, 906 (1954); K. Alder and A. Winther, Phys. Rev. **91**, 1578 (1953).

[5] L. L. Foldy, Phys. Rev. **92**, 178 (1953).

first-order perturbation theory, and this seems to be a reasonable approximation.[6] In addition to this, we shall assume that the static interaction is also small, and use plane wave functions for the incident and scattered electrons; this is justified only for light elements, and is equivalent to the use of the Møller potentials and fields.[7] This latter approximation can be improved by using Coulomb wave functions for the electron like those calculated numerically in connection with elastic scattering,[8] and such calculations are now under way.

The work reported here differs from other recent calculations of radiative transitions[8,9] and of inelastic electron scattering[10] in one or both of two respects: the reduced wavelength $1/q$ associated with the change of momentum $\hbar\mathbf{q}$ of the electron is not necessarily large in comparison with nuclear dimensions, and this wavelength is usually much smaller than $\hbar c$ divided by the energy loss of the electron.[11] The first point means that there may be retardation within the nucleus, so that the radial dependences of the transition densities may be significant. Also, the transition probabilities do not necessarily decrease as the multipole order increases; the expansion in multipoles is nevertheless useful since nuclear selection rules often limit possible transitions to one or two multipole types. The second point means that the probability for inelastic electron scattering is fundamentally different from that for radiation, since in the latter case the reduced wavelength of the photon is equal to $\hbar c$ divided by the energy of the photon. It turns out that there is a close relation between the leading terms in the probabilities for the two processes in the case of electric, but not in the case of magnetic multipole transitions.

II. GENERAL FORMULATION AND MAGNETIC MULTIPOLE CALCULATION

We start from the interaction energy H' between the nuclear densities ρ, $\mathbf{j}$, $\mathbf{M}$, and an arbitrary external electromagnetic field that is described by the potentials φ, $\mathbf{A}$ or the field strengths $\mathfrak{E}$, $\mathfrak{H}$:

$$H'=\int(\rho\varphi-c^{-1}\mathbf{j}\cdot\mathbf{A}-\mathbf{M}\cdot\mathfrak{H})d\tau. \tag{1}$$

In order that H' result in a transition that conserves the energy, the time variations of the nuclear and field quantities must cancel, so we assume that the nuclear quantities vary like $e^{i\omega t}$ and the field quantities like $e^{-i\omega t}$, where $\hbar\omega$ is the energy of the transition. The electric field strength may be expressed in terms of the potentials in either of the forms

$$\mathfrak{E}=-\partial\mathbf{A}/\partial ct-\mathbf{grad}\,\varphi=(i\omega/c)\mathbf{A}-\mathbf{grad}\,\varphi,$$

and the equation of continuity is

$$\mathrm{div}\mathbf{j}=-\partial\rho/\partial t=-i\omega\rho.$$

Substitution into Eq. (1) and integration by parts leads to

$$H'=\int[(i/\omega)\mathbf{j}\cdot\mathfrak{E}-\mathbf{M}\cdot\mathfrak{H}]d\tau; \tag{2}$$

the partial integration assumes that the nuclear densities have a finite extension in space, so that boundary terms at infinity vanish.

We wish to decompose H' into parts that correspond to electric and magnetic multipole transitions of all possible orders. Since the treatment of the magnetic transitions is the same whether the external field is a free radiation field (emission or absorption of photons) or arises from external sources (inelastic electron excitation), we start with this case. For magnetic multipole radiation of order l, the electric field is transverse and has the parity $(-1)^l$. We therefore substitute for $\mathfrak{H}$ in Eq. (2) from one of Maxwell's equations which is valid whether or not there is an external charge and current density,

$$\mathbf{curl}\,\mathfrak{E}=-\partial\mathfrak{H}/\partial ct=(i\omega/c)\mathfrak{H}, \tag{3}$$

to obtain

$$H'=\int[(i/\omega)\mathbf{j}\cdot\mathfrak{E}+(ic/\omega)\mathbf{M}\cdot\mathbf{curl}\,\mathfrak{E}]d\tau$$
$$=(i/\omega)\int(\mathbf{j}+c\,\mathbf{curl}\,\mathbf{M})\cdot\mathfrak{E}d\tau. \tag{4}$$

Now as discussed by Blatt and Weisskopf,[8] any vector function of the polar angles θ, ϕ can be expanded in terms of three kinds of vector spherical harmonics. The first kind, of total angular momentum l, is

$$\mathbf{X}_{lm}(\theta,\phi)=-i[l(l+1)]^{-\frac{1}{2}}(\mathbf{r}\times\nabla)Y_{lm}(\theta,\phi), \tag{5}$$

where Y_{lm} is the ordinary scalar spherical harmonic, $\mathbf{X}_{lm}$ is transverse and has the parity $(-1)^l$; the other two kinds of the same total angular momentum have the parity $(-1)^{l+1}$. The three kinds together, for all l, constitute a complete orthonormal set of vector functions with respect to integration of θ and ϕ over the sphere. We can therefore write for the part of H' that

[6] An order of magnitude estimate of the second-order dynamic interaction (nuclear dispersion) indicates that it is relatively small.

[7] C. Møller, Z. Physik **70**, 786 (1931).

[8] J. M. Blatt and V. F. Weisskopf, *Theoretical Nuclear Physics* (John Wiley and Sons, Inc., New York, 1952), Appendix B.

[9] W. Franz, Z. Physik **127**, 363 (1950); P. R. Wallace, Can. J. Phys. **29**, 393 (1951).

[10] Amaldi, Fidecaro, and Mariani, Nuovo cimento **7**, 553, 757 (1950); Thie, Mullin, and Guth, Phys. Rev. **87**, 962 (1952); R. Gatto, Nuovo cimento **10**, 1559 (1953); J. H. Smith, Phys. Rev. **95**, 271 (1954).

[11] The importance of the difference between the short wavelength associated with the electron momentum transfer and the long wavelength associated with the nuclear excitation energy, in the case of high-energy electrons, was pointed out by J. S. Blair in a letter to Richard Wilson, July 1952.

gives rise to magnetic l-pole transitions:

$$H'_{lm}{}^{(M)}=(i/\omega)\int(\mathbf{j}+c\,\mathbf{curl}\,\mathbf{M})\cdot\mathbf{X}_{lm}{}^{*}(\theta,\phi)\times\left[\int\mathbf{X}_{lm}(\theta',\phi')\cdot\mathfrak{E}(r,\theta',\phi')d\Omega'\right]d\tau. \quad (6)$$

Summation of Eq. (6) over l and m, with inclusion of the corresponding terms that come from the other two kinds of vector spherical harmonics will, because of the completeness of these functions, yield Eq. (4). These other two classes of terms give rise to electric multipole transitions, and are more conveniently expressed in terms of an integral that involves $\mathbf{X}_{lm}$ and a different combination of nuclear densities (see Sec. III).

We now evaluate the square-bracketed integral in Eq. (6), assuming that the electric field has the form

$$\mathfrak{E}=\mathbf{e}e^{i\mathbf{q}\cdot\mathbf{r}}=\mathbf{e}\sum_{l}[4\pi(2l+1)]^{\frac{1}{2}}i^{l}j_{l}(qr)Y_{l0}(\theta',\phi'). \quad (7)$$

The vector $\hbar\mathbf{q}$ is the photon momentum in the radiation case, or the momentum change of the electron in the electron scattering case; the way in which Eq. (7) is written assumes that the direction of $\mathbf{q}$ is the polar or z axis with respect to which the spherical harmonics are defined. Substitution of Eqs. (5) and (7) into the square-bracketed integral of Eq. (6) yields, after a partial integration,

$$\int\mathbf{X}_{lm}(\theta',\phi')\cdot\mathfrak{E}(r,\theta',\phi')d\Omega'=[\pi(2l+1)]^{\frac{1}{2}}i^{l}(e_x\pm ie_y)j_l(qr),$$

if $m=\pm1$, and zero otherwise. Equation (6) now becomes, after use of Eq. (5) and integration by parts,

$$H'_{l,\pm1}{}^{(M)}=(i^{l}/\omega)[\pi(2l+1)/l(l+1)]^{\frac{1}{2}}(e_x\pm ie_y)\times\int j_l(qr)Y_{l,\pm1}{}^{*}\mathbf{r}\cdot\mathbf{curl}(\mathbf{j}+c\,\mathbf{curl}\,\mathbf{M})d\tau. \quad (8)$$

III. ELECTRIC MULTIPOLE TRANSITIONS

For electric multipole radiation of order l, the magnetic field is transverse and has the parity $(-1)^{l}$. We therefore substitute for $\mathfrak{E}$ in Eq. (2) from another of Maxwell's equations,

$$\mathbf{curl}\,\mathfrak{H}=\partial\mathfrak{E}/\partial ct+4\pi\mathbf{j}_e/c=(-i\omega/c)\mathfrak{E}+4\pi\mathbf{j}_e/c,$$

to obtain

$$H'=-\int[(c/\omega^2)\,\mathbf{curl}\,\mathbf{j}+\mathbf{M}]\cdot\mathfrak{H}d\tau+(4\pi/\omega^2)\int\mathbf{j}\cdot\mathbf{j}_e d\tau. \quad (9)$$

Here, $\mathbf{j}_e$ is the transition current density that arises from the change in state of the electron; it is zero for a radiative transition and is given by

$$\mathbf{j}_e=ec\mathbf{a}e^{i\mathbf{q}\cdot\mathbf{r}} \quad (10)$$

in the case of electron scattering, where $\mathbf{a}$ is the matrix element of the Dirac $\boldsymbol{\alpha}$ operator between initial and final electron plane wave states of momenta $\mathbf{p}_0$ and $\mathbf{p}$, and $\hbar\mathbf{q}=\mathbf{p}_0-\mathbf{p}$.

The first integral in Eq. (9) can be reduced in precisely the same way as Eq. (4). We put $\mathfrak{H}=\mathbf{h}e^{i\mathbf{q}\cdot\mathbf{r}}$, and obtain for the electric l-pole part of this integral, which is the entire interaction energy for a radiative transition:[12]

$$H''_{l,\pm1}{}^{(E)}=i^{l+1}[\pi(2l+1)/l(l+1)]^{\frac{1}{2}}(h_x\pm ih_y)\times\int j_l(qr)Y_{l,\pm1}{}^{*}\mathbf{r}\cdot\mathbf{curl}[\mathbf{M}+(c/\omega^2)\,\mathbf{curl}\,\mathbf{j}]d\tau \quad (11a)$$

$$=-i^{l+1}[\pi(2l+1)/l(l+1)]^{\frac{1}{2}}(h_x\pm ih_y)\times\left\{\int j_lY_{l,\pm1}{}^{*}\,\mathrm{div}(\mathbf{r}\times\mathbf{M})d\tau-(ic/\omega)\int(j_l+rdj_l/dr)Y_{l,\pm1}{}^{*}\rho d\tau-(cq^2/\omega^2)\int j_lY_{l,\pm1}{}^{*}(\mathbf{r}\cdot\mathbf{j})d\tau\right\}. \quad (11b)$$

In the latter form, use has been made of the equation of continuity to replace $\mathrm{div}\mathbf{j}$ by $-i\omega\rho$.

In the electron excitation case, we must also decompose the second integral of Eq. (9) into electric multipole contributions. We cannot now use the symmetry of the magnetic field as a guide, and must rely on the symmetry of the nuclear charge-current density instead. Inspection of the first integral of Eq. (9) and the second integral of Eq. (11b) shows that the $\mathbf{X}_{lm}$ part of $\mathbf{curl}\,\mathbf{j}$ and the Y_{lm} part of ρ give rise to electric l-pole transitions. We therefore transform the second integral of Eq. (9) so that only these combinations of nuclear densities appear. The electron current density can be written as the sum of the gradient of a scalar (irrotational part) and the curl of a divergenceless vector (solenoidal part):

$$\mathbf{j}_e=\mathbf{grad}\,\chi+\mathbf{curl}\,\psi,\quad \mathrm{div}\psi=0.$$

From this

$$\mathrm{div}\mathbf{j}_e=\nabla^2\chi,\quad \mathbf{curl}\,\mathbf{j}_e=-\nabla^2\psi.$$

With the form (10) for $\mathbf{j}_e$, we find that

$$\chi=-(i/q^2)(\mathbf{q}\cdot\mathbf{j}_e),\quad \psi=(i/q^2)(\mathbf{q}\times\mathbf{j}_e).$$

[12] Some relations given in reference 8 are useful in deriving Eq. (11b) from (11a).

Thus with the help of some partial integrations and the equation of continuity, we obtain

$$\int \mathbf{j}\cdot\mathbf{j}_e d\tau = (\omega/q^2)\int \rho(\mathbf{q}\cdot\mathbf{j}_e)d\tau + (i/q^2)\int \mathbf{curl}\,\mathbf{j}\cdot(\mathbf{q}\times\mathbf{j}_e)d\tau. \quad (12)$$

Equation (12) can now be broken down into multipole parts in analogy with the decomposition of Eq. (4) into terms of the type (6). The result for the contribution of the second integral of (9) to the electric l-pole transition is

$$H'''_{l,m}{}^{(E)} = (4\pi/\omega q^2)\int \rho Y_{lm}{}^*(\theta,\phi) \times\left[\int Y_{lm}(\theta'\phi')(\mathbf{q}\cdot\mathbf{j}_e)d\Omega'\right]d\tau + (4\pi i/\omega^2 q^2)\int \mathbf{curl}\,\mathbf{j}\cdot\mathbf{X}_{lm}{}^*(\theta,\phi) \times\left[\int \mathbf{X}_{lm}(\theta',\phi')(\mathbf{q}\times\mathbf{j}_e)d\Omega'\right]d\tau.$$

Since the z axis is along $\mathbf{q}$, the first square-bracketed integral vanishes unless $m=0$, and the second square-bracketed integral vanishes unless $m=\pm 1$. Use of the form (10) for $\mathbf{j}_e$ leads to the following results:

$$H'''_{l,0}{}^{(E)} = (8\pi i^l e c a_z/\omega q)[\pi(2l+1)]^{\frac{1}{2}} \times\int j_l(qr)Y_{l,0}\rho d\tau, \quad (13)$$

$$H'''_{l,\pm 1}{}^{(E)} = -(4\pi i^{l+1} e c/\omega^2 q)(a_y \mp i a_x)[\pi(2l+1)]^{\frac{1}{2}} \times\int j_l \mathbf{X}_{l,\pm 1}{}^*\cdot(\mathbf{curl}\,\mathbf{j})d\tau. \quad (14)$$

The external fields $\mathfrak{E}$ and $\mathfrak{H}$ may be found from solution of Maxwell's equations with the electron current (10). The results are the Møller fields,[7] which have the forms used above, with

$$\mathbf{e} = 4\pi i e(k\mathbf{a}+\mathbf{q}a_0)/(q^2-k^2),$$
$$e_x \pm i e_y = 4\pi i e k(a_x \pm i a_y)/(q^2-k^2),$$
$$\mathbf{h} = 4\pi i e(\mathbf{q}\times\mathbf{a})/(q^2-k^2),$$
$$h_x \pm i h_y = -4\pi i e q(a_y \mp i a_x)/(q^2-k^2),$$

where $k=\omega/c$ and a_0 is the matrix element of the Dirac unit operator between initial and final electron states. It can now be shown without difficulty that Eq. (14) is just equal to $-(q^2-k^2)/q^2$ times the lm part of the **curl j** term in the first integral of Eq. (9). Thus when Eqs. (11) and (14) are added together, the result is to leave the **M** integral in (11a) or (11b) unchanged, and multiply the other integrals by a factor k^2/q^2.

We give here the interaction energies for electric and magnetic l-pole transitions in the electron excitation case. Equation (13) has been changed slightly by making use of the Dirac equation to write $\mathbf{q}\cdot\mathbf{a}+(\omega a_0/c)=0$, or $a_z=-(ka_0/q)$, and a substitution has been made for $e_x \pm i e_y$ in Eq. (8).

$$H'_{l,0}{}^{(E)} = -(4\pi i^l e a_0/q^2)[4\pi(2l+1)]^{\frac{1}{2}} \times\int j_l(qr)Y_{l,0}\rho d\tau; \quad (15)$$

$$H'_{l,\pm 1}{}^{(E)} = [4\pi i^l e q(a_y \mp i a_x)/(q^2-k^2)] \times[\pi(2l+1)/l(l+1)]^{\frac{1}{2}}\int j_l(qr)Y_{l,\pm 1}{}^* \mathbf{r}\cdot\mathbf{curl}\,[\mathbf{M}+(cq^2)^{-1}\,\mathbf{curl}\,\mathbf{j}]d\tau; \quad (16)$$

$$H'_{l,\pm 1}{}^{(M)} = [4\pi i^{l+1} e(a_x \pm i a_y)/c(q^2-k^2)] \times[\pi(2l+1)/l(l+1)]^{\frac{1}{2}}\int j_l(qr)Y_{l,\pm 1}{}^* \mathbf{r}\cdot\mathbf{curl}\,[\mathbf{j}+c\,\mathbf{curl}\,\mathbf{M}]d\tau. \quad (17)$$

Equations (16) and (17) can of course be further transformed in analogy with the change from Eq. (11a) to (11b).

IV. ORDERS OF MAGNITUDE

We now estimate the relative orders of magnitude of the various terms in the above three equations. For this purpose, we note that a_0, a_z and a_y are of order unity and that $k \ll q$ for situations of current interest, and assume that all integrals over nuclear densities can be represented by a common form factor F. Then Eq. (15) is of order eFQ/q^2, where Q is the total charge involved in the transition.

The first (magnetization) term in Eq. (16) involves a derivative operator which, by partial integration, is seen to introduce a factor of order q. The vector $\mathbf{r}$ introduces a factor R, which is an average radial distance from the center of the nucleus for the main contributions to the integral; for large q, R is expected to be somewhat larger than $1/q$ and somewhat smaller than the nuclear radius. Then the order of magnitude of this term is $(eF/q)(qR)(Q'\hbar/Mc)$, where $Q'\hbar/Mc$ is the total magnetization involved in the transition, and M is the nucleonic mass. In the second (current) term of Eq. (16), the two derivative operators introduce a factor q^2, and there is again a factor R. Thus its order of magnitude is $(eF/q)(R/c)Q''v$, where $Q''v$ is the total current involved in the transition, and v is the nuclear convection velocity associated with motion of the charge Q''.

In similar fashion, we find that the current and magnetization terms in Eq. (17) have the orders of magnitude $(eF/cq^2)qRQ''v$ and $(eF/cq^2)(cq^2R)(Q'\hbar/Mc)$, respectively.

If now we call the order of magnitude of Eq. (15) unity, then the relative orders of magnitude of the magnetization and current terms in Eq. (16) are, respectively,

$$(qR)(q\hbar/Mc)(Q'/Q), \quad (qR)(v/c)(Q''/Q),$$

and the orders of magnitude of the current and magnetization terms in Eq. (17) are, respectively,

$$(qR)(v/c)(Q''/Q), \quad (qR)(q\hbar/Mc)(Q'/Q).$$

For large-angle scattering of electrons with about 200-Mev energy, $q\hbar/Mc\sim\frac{1}{3}$ and $qR\sim 3$. For single-particle excitation of a nucleus, Q, Q', and Q'' are all expected to be of order unity, and $v/c\sim\frac{1}{3}$. For a collective mode of excitation, Q' should still be of order unity, Q and Q'' should have the same order of magnitude and be much larger than unity, and v/c should be much less than $\frac{1}{3}$.

We conclude, therefore, that for single-particle excitation in this energy range, all terms of Eqs. (15), (16), and (17) can be of the same order of magnitude. For excitation of collective modes, on the other hand, it is likely that Eq. (15) is not only the leading term for the electric multipole transitions, but is significantly larger than either of the magnetic multipole terms, which are comparable with each other. Further, if we assume that the current density associated with a collective mode is irrotational,[13] then **curl j**$=0$ and the current terms in Eqs. (16) and (17) are zero.

It may be noted at this point that summation of Eq. (15) over l yields, with the help of Eq. (7),

$$\sum_l H'_{l,0}{}^{(E)} = -(4\pi e a_0/q^2)\int e^{i\mathbf{q}\cdot\mathbf{r}}\rho d\tau. \qquad (18)$$

This is just what would have been obtained if only the first factor in Eq. (1) had been retained, and the static, nonretarded, Coulomb interaction had been used in calculating φ. Thus the present paper provides a justification for the use of this term by itself, at least so far as excitation of collective nuclear oscillations is concerned.[14]

V. DIFFERENTIAL SCATTERING CROSS SECTION

Each of the interaction energies (15) through (18) is of the form AV, where A is one of the quantities a_0, $a_x\pm ia_y$, $a_y\mp ia_x$, which involves only the electron spin functions, and V involves only integrals over nuclear quantities. In order to obtain a differential scattering cross section, it is necessary to sum $|AV|^2$ over final electron spin states, average over initial spin states, multiply by $2\pi/\hbar$ times the energy density of final electron states, and divide by the incident electron flux.

In the extreme relativistic region, the spin sum operation on $|A|^2$ yields $\cos^2\frac{1}{2}\theta$ when $A=a_0$, where θ is the angle between $\mathbf{p}_0$ and $\mathbf{p}$. When $A=a_x\pm ia_y$ or $A=a_y\mp ia_x$, the spin sum leads to

$$[(p_0+p)^2(1-\cos\theta)-p_0p\sin^2\theta]/\hbar^2q^2$$
$$=[1+\sin^2(\tfrac{1}{2}\theta)]\left[1+\frac{\hbar^2k^2}{2p_0p[1+\sin^2(\tfrac{1}{2}\theta)]}\right]$$
$$\times\left[1+\frac{\hbar^2k^2}{4p_0p\sin^2(\tfrac{1}{2}\theta)}\right]^{-1};$$

except for very small scattering angles, this is very nearly equal to $[1+\sin^2(\frac{1}{2}\theta)]$ when the nuclear excitation is moderate. The last group of multiplicative factors involving the incident flux and the density of final states is, in the extreme relativistic region, $(p/2\pi\hbar^2c)^2$. Thus the differential scattering cross section per unit solid angle is equal to $[p\cos(\frac{1}{2}\theta)/2\pi\hbar^2c]^2|V|^2$ when either (15) or (18) is used for V, and is approximately equal to $(p/2\pi\hbar^2c)^2[1+\sin^2(\frac{1}{2}\theta)]|V|^2$ when either (16) or (17) is used for V.

VI. COMPARISON WITH RADIATIVE TRANSITIONS

It may be desirable in some cases to relate the inelastic electron scattering cross section to the radiation probability for the same nuclear transition. We therefore examine the expressions for the electric and magnetic l-pole moments, which are respectively[8]

$$\int r^lY_{lm}{}^*\rho d\tau - ik(l+1)^{-1}\int r^lY_{lm}{}^*\,\mathrm{div}(\mathbf{r}\times\mathbf{M})d\tau, \qquad (19)$$

$$-[c(l+1)]^{-1}\int r^lY_{lm}{}^*\,\mathrm{div}(\mathbf{r}\times\mathbf{j})d\tau$$
$$-\int r^lY_{lm}{}^*\,\mathrm{div}\mathbf{M}d\tau. \qquad (20)$$

Estimates like those of Sec. IV show that the relative orders of magnitude of the two terms of (19) and the two terms of (20) are

$$1, \quad (k\hbar/Mc)(Q'/Q);$$
$$(v/c)(Q''/Q), \quad (\hbar/McR)(Q'/Q).$$

Here, R is the nuclear radius. Since $k\hbar/Mc\ll 1$, the first term of Eq. (19) dominates the electric l-pole moment, whether the nucleus undergoes a single-particle or collective transition. Likewise, the first term of Eq. (20) is the larger in the single-particle case, while the two terms are more nearly comparable for a collective transition.

It follows that there is a close relation between the leading terms for electric multipole transitions in the radiative case [first term of Eq. (19)] and in the electron excitation case [Eq. (15)]. The same quantity ρ appears in both terms, and indeed the former is simply

[13] A. Bohr, *Rotational States of Atomic Nuclei* (Ejnar Munksgaards Forlag, Copenhagen, 1954), Appendix.

[14] Equation (18) has been used in much of the earlier work on inelastic electron scattering (see reference 10).

the first term in the expansion of the latter in powers of q. A similar relation obtains between the first (current) terms of Eqs. (17) and (20) in the magnetic multipole case, since $\mathbf{r}\cdot\mathbf{curl}\,\mathbf{j}=-\mathrm{div}(\mathbf{r}\times\mathbf{j})$. However, the second (magnetization) terms are much less closely related to each other, and this term is more important in the electron excitation than in the radiative case. Thus it is much easier to connect the probabilities for the two types of transitions in the electric than in the magnetic multipole case; an assumption must of course be made concerning the radial dependence of ρ (see for example Sec. VIII).

VII. ELECTRIC MONOPOLE TRANSITIONS

The electric monopole interaction energy $H'_{0,0}{}^{(E)}$ is responsible for the elastic scattering from a static spherically symmetric charge density, which is the expectation value for the nuclear ground state. In this case, either Eq. (15) or Eq. (18) can be used.

The transition between nuclear states with total angular momentum $I=0$ and the same parity (which is even in all known cases), is of considerable interest. It is essential to realize here that the orthogonality of the initial and final nuclear states makes $\int\rho d\tau$ vanish. Thus for small q, the apparently leading terms in Eqs. (15) and (18) are actually zero. As a reminder that this occurs, one should replace the spherical Bessel function in Eq. (15) by $j_0(qr)-1$, and the exponential in Eq. (18) by $\exp(i\mathbf{q}\cdot\mathbf{r})-1$. Thus for small q, the electric monopole and electric quadrupole transitions have the same q dependence.

The difference in behavior between the elastic and inelastic monopole transitions corresponds to the fact that a static spherically symmetric charge density has a field that extends to large distances, whereas a radially oscillating charge density has no time-dependent field external to itself. Therefore interaction with the spherically symmetric part of the electron potential can occur only through its variation over the nucleus, and the leading term, which is independent of r, results in no interaction.

VIII. COLLECTIVE ELECTRIC QUADRUPOLE TRANSITIONS

There is a close relation between the contribution of the static nuclear electric quadrupole moment to the elastic scattering[15] and the contribution of the transition quadrupole moment to the inelastic scattering. This is because the collective model relates both the static and the transition moments to an intrinsic quadrupole moment.[15,16] The relation is worth exploring, since with imperfect energy resolution the two effects may be experimentally indistinguishable.

[15] L. I. Schiff, Phys. Rev. **92**, 988 (1953).
[16] A. Bohr and B. R. Mottelson, Kgl. Danske Videnskab. Selskab, Mat.-fys. Medd. **27**, 16 (1953).

In both cases we use Eq. (15), and neglect the difference between the two values of q for the same incident electron energy and angle of scattering. We consider first the case of a uniformly charged nucleus of radius R, for which the quadrupole parts of the static and transition charge densities both have the approximate form $\delta(r-R)$.[15,16] Then the integral in Eq. (15) in the static case is equal to that in the transition case for all values of q, except for a multiplicative constant. For small q, the integral is proportional to the static quadrupole moment Q in the elastic case, and to the transition quadrupole moment in the inelastic case, both of which can be expressed in terms of the intrinsic quadrupole moment Q_0. The two integrals can then be expressed in terms of Q_0 for small q, and hence also for all q.

It seems plausible to assume that the situation is similar when the nucleus is not a uniformly charged sphere;[3] this situation is now under study. We assume that the static and transition quadrupole charge densities have the same radial dependence, so that the elastic and inelastic form factors are constant multiples of each other for all q. They can then be related to Q_0 for small q, and hence found for all q if some radial dependence is assumed.

From Eq. (15) and Sec. V, the differential cross section for elastic scattering is given by [compare with Eqs. (2) and (14) of reference 15]

$$\sigma_e(\theta)=[e^2\cos^2(\tfrac{1}{2}\theta)/4E^2\sin^4(\tfrac{1}{2}\theta)]\,|F_e|^2,$$

$$|F_e|^2=(2I+1)^{-1}\sum_{m_i}\sum_{m_f}\left|(4\pi)^{\frac{1}{2}}\int[j_0(qr)Y_{00}-5^{\frac{1}{2}}j_2(qr)Y_{20}]\rho_e(m_i,m_f)d\tau\right|^2, \tag{21}$$

where $\rho_e(m_i,m_f)$ is the matrix element of the static charge density between initial and final magnetic substates of the nuclear ground state of total angular momentum I.[17] We choose the axis with respect to which the magnetic substates are defined as $\mathbf{q}$, which is the axis of Y_{l0}, in which case the integrals fail to vanish only if $m_f=m_i$. We call this common value m, and note that the Y_{00} part of the integral is independent of m, while the Y_{20} part of the integral depends on m through the factor[18]

$$f_m=[3m^2-I(I+1)]/I(2I-1)$$

[17] Alternatively, $\rho_e(\mathbf{r})$ may be regarded as an operator (see reference 5), and the matrix element taken after the integration is performed over $\mathbf{r}$; all results are the same.
[18] Reference 8, p. 28. The numerator of f_m is the quantum-mechanical transcription of $P_2(\cos\theta)$, and the denominator merely normalizes it so that $f_I=1$. Thus the fact that f_m is indeterminate when $I=0$ or $\frac{1}{2}$ is not significant; in these cases f_m should be regarded as zero since the numerator vanishes. Equation (24) is consistent with this interpretation.

in the following way:

$$|F_e|^2=[4\pi/(2I+1)]\sum_m\Big\{\Big|\int j_0Y_{00}\rho_e(I,I)d\tau\Big|^2 - (20)^{\frac{1}{2}}f_m Re\int j_0Y_{00}\rho_e(I,I)d\tau\int j_2Y_{20}\rho_e(I,I)d\tau +5f_m^2\Big|\int j_2Y_{20}\rho_e(I,I)d\tau\Big|^2\Big\}.$$

Now $\sum_m f_m=0$, so that the interference term vanishes. Also,

$$\sum_m f_m^2=(2I+1)/5A_I^2 =(I+1)(2I+1)(2I+3)/5I(2I-1),$$

where A_I is the quantity defined in reference 15. We thus obtain

$$|F_e|^2=4\pi\Big\{\Big|\int j_0Y_{00}\rho_e(I,I)d\tau\Big|^2 +[(I+1)(2I+3)/I(2I-1)]\times\Big|\int j_2Y_{20}\rho_e(I,I)d\tau\Big|^2\Big\}. \quad (22)$$

The first term of Eq. (22) gives the scattering from the spherically symmetric part of the nuclear charge density, and the second term we call the quadrupole part of the elastic scattering.

In order to relate the second term of Eq. (22) to the intrinsic quadrupole moment Q_0, we note that for small q,

$$\int j_2Y_{20}\rho_e(I,I)d\tau\rightarrow(q^2/15)\times\int r^2Y_{20}\rho_e(I,I)d\tau=(q^2/15)(5/16\pi)^{\frac{1}{2}}eQ,$$

where the observed quadrupole moment Q is given in terms of Q_0 by Eq. (V.6) of reference 16:

$$Q=[I(2I-1)/(I+1)(2I+3)]Q_0.$$

Q_0 is calculated in the same way as Q, except that the axis of Y_{20} is the nuclear symmetry axis rather than I. Thus if we fix the magnitude of ρ_e by the equation

$$eQ_0=(16\pi/5)^{\frac{1}{2}}\int r^2Y_{20}\rho_e d\tau, \quad (23)$$

and infer its shape in some other way, then the quadrupole part of $|F_e|^2$ is

$$|F_{eq}|^2=4\pi[I(2I-1)/(I+1)(2I+3)]\times\Big|\int j_2(qr)Y_{20}\rho_e d\tau\Big|^2. \quad (24)$$

It must be remembered that in Eqs. (23) and (24), the axis of Y_{20} is the symmetry axis of the nuclear charge distribution ρ_e.[19] Note that there is no elastic quadrupole scattering if $I=0$ or $\frac{1}{2}$, just as there is no observed quadrupole moment; the charge distribution as viewed by the incident electron is spherically symmetric in this case, even though Q_0 may not be zero.

The differential cross section for inelastic scattering is given by the first of Eqs. (21), with F_e replaced by the quantity F_i:

$$|F_i|^2=(2I_i+1)^{-1}\sum_{m_i}\sum_{m_f}|F_i(m_i,m_f,0)|^2, \quad (25)$$

where

$$F_i(m_i,m_f,m)=-(20\pi)^{\frac{1}{2}}\int j_2(qr)Y_{2m}\rho_i(m_i,m_f)d\tau,$$

and $\rho_i(m_i,m_f)$ is the transition charge density between the initial state I_i, m_i and the final state I_f, m_f. Since the summations in Eq. (25) are carried over all m_i and m_f, the result is independent of the axis chosen for Y_{20}, and hence has the same value if $F_i(m_i,m_f,0)$ is replaced by $F_i(m_i,m_f,m)$ where m is not necessarily equal to zero. Then

$$|F_i|^2=[5(2I_i+1)]^{-1}\sum_m\sum_{m_i}\sum_{m_f}|F_i(m_i,m_f,m)|^2 =(1/5)\sum_m\sum_{m_f}|F_i(m_i,m_f,m)|^2;$$

the second equality holds because the summations over all m and m_f make the result independent of the value of m_i.

For small q,

$$F_i(m_i,m_f,m)\rightarrow-(20\pi)^{\frac{1}{2}}(q^2/15)\int r^2Y_{2m}\rho_i(m_i,m_f)d\tau.$$

The reduced radiative transition probability is defined in Eq. (VII.2) of reference 16 as

$$B(E2)=\sum_m\sum_{m_f}\Big|\int r^2Y_{2m}\rho_i(m_i,m_f)d\tau\Big|^2,$$

so that for small q,

$$|F_i|^2\rightarrow4\pi(q^2/15)^2B(E2).$$

There are in general two possible quadrupole transitions from the ground state I: to the first excited state $I+1$, and to the second excited state $I+2$.[20] From Eqs. (33) and (36) of reference 13, the reduced transition proba-

[19] The averaging over nuclear orientations was not performed correctly in reference 15; the charge density defined by Eq. (17) of that reference is the same as the quantity ρ_e of the present paper except for a normalization factor Ze, but in Eqs. (20) and (21), ρ_2 should be replaced by $A_I\rho_2$. This does not affect the estimate of the quadrupole scattering below Eq. (22), since only the ratio of (21) to (20) enters there.

[20] If the ground state I is zero, the first excited state has $I=2$, and if the ground state I is $\frac{1}{2}$, the results below may be altered (see references 13 and 16).

bility in the first case is

$$B_1(E2)=(15/16\pi)(eQ_0)^2[I/(I+1)(I+2)],$$

and from Eqs. (34) and (36) of reference 13, this quantity in the second case is

$$B_2(E2)=(15/16\pi)(eQ_0)^2[2/(I+2)(2I+3)].$$

We thus find for the transition $I\rightarrow I+1$ and small q

$$|F_{c1}|^2\rightarrow(5/4)(eQ_0)^2(q^2/15)^2[3I/(I+1)(I+2)], \quad (26)$$

and for the transition $I\rightarrow I+2$

$$|F_{c2}|^2\rightarrow(5/4)(eQ_0)^2(q^2/15)^2[6/(I+2)(2I+3)]. \quad (27)$$

We now assume that the extrapolation from small to large q can be made as in Eq. (24). We then find that the inelastic scattering is also described by Eq. (24), except that the square bracket there must be replaced by the square bracket in Eq. (26) or (27). Some numerical values are given in Table I. It must be remembered that these results may not apply when the ground state I is equal to $\frac{1}{2}$, and that Eq. (27) represents the transition to the first (not the second) excited state when $I=0$.[20]

It is interesting to note that there is a kind of sum rule for the three kinds of quadrupole scattering, which are the only possible kinds

$$[I(2I-1)/(I+1)(2I+3)]+[3I/(I+1)(I+2)]+[6/(I+2)(2I+3)]=1.$$

TABLE I. Values of the square bracket factors in Eqs. (24), (26), and (27), for a few values of I.

I	Elastic $I\rightarrow I$, Eq. (24)	Inelastic $I\rightarrow I+1$, Eq. (26)	Inelastic $I\rightarrow I+2$, Eq. (27)
0	0	0	1
3/2	1/5	18/35	2/7
5/2	5/14	10/21	1/6
7/2	7/15	14/33	6/55

IX. CONCLUSIONS

Excitation of nuclear multipole transitions by inelastic electron scattering occurs along with the elastic scattering of high-energy electrons. If sufficiently accurate measurements of the distribution of the scattered electrons in energy and angle can be made, the elastically scattered electrons give information concerning the static nuclear charge distribution, and the inelastically scattered electrons give information concerning both the strength and shape of the transition charge density. The static quadrupole scattering must be allowed for when interpreting the angle distribution of the elastically scattered electrons in terms of a radial distribution of nuclear charge. If the energy resolution is not good enough to separate the inelastic from the elastic scattering, then it must also be allowed for before the elastic scattering is analyzed.

It is important to note that absolute measurements of the inelastic scattering are not necessary in order to determine the strength of the transition charge density. Analysis of the relative elastic scattering, even if no absolute cross sections are available, yields a shape for the static charge density. The magnitude of the nuclear charge is of course known, so that an absolute elastic cross section can be computed. Then comparison of the relative magnitudes of inelastic and elastic scattering at each angle gives absolute values for the former, from which the strength as well as the shape of the transition charge density can be determined.

The order of magnitude estimates given in Sec. IV are of course not completely reliable, and simply indicate that Eq. (15) or Eq. (18) is likely to be the dominant term, especially for collective transitions, which appear to be much the strongest in any event. For single-particle transitions, where detailed nuclear wave functions are more likely to be available, it would be worth while to make more careful estimates of the relative importance of Eqs. (16) and (17).

Short-Lived Radio-Nuclides Produced by a Synchrocyclotron

H. TYRÉN AND P.-A. TOVE
The Gustaf Werner Institute for Nuclear Chemistry, University of Uppsala, Uppsala, Sweden
(Received June 25, 1954)

A method of studying short-lived radio-nuclides produced by the internal beam in a synchrocyclotron is described. Preliminary results on a number of proton-produced activities in the mass range below 70 are given.

SHORT-LIVED activities induced in a target by the circulating beam of a 200-Mev proton synchrocyclotron have been studied by use of detector close to the target and an electronic "time analyzer" for registering the detector pulses.

The target is irradiated during a short time interval, of the order of the half-life of the activity under investigation. After the beam has been shut off by pulsing the oscillator, the detector placed below the target starts detecting radiation. In order to determine the time distribution of the detector pulses, the latter are fed to a time analyzer with ten channels which are successively opened and closed. The pulses stored in a certain channel thus measure the radiation from the target at a certain time after the beam has been shut off. The time interval a channel is open is controlled by a pulse generator; it can be the same for all channels or it can be increased 2, 4, or 8 times for any desired channels. After this "count period," which is of the order of a few half-lives, a recovery period begins, which allows more long-lived activities produced during the irradiation to decay. A new period of bombardment then follows and the whole cycle is repeated automatically. By thus adding the pulses from many repetitions of the cycle one can gain information about nuclei of fairly small production cross sections. Typical experiments involve 10 to 1000 repetition cycles.

The range of half-lives which can be analyzed by the time analyzer extends from a few microseconds to seconds or minutes. At present there is no synchronization between the cyclotron "on" and "off" pulses and the modulation cycle. The lower limit is then about 1 millisecond.

The detector consists of a plastic scintillation phosphor placed in a heavy lead shield below the target and a Plexiglas light guide with a photomultiplier outside the magnetic field of the cyclotron. β rays are collimated into a vertical ray by the magnetic field. In some early experiments a pair of proportional counters in coincidence were used. The pulses were fed to 6*AK*5 cathode followers. There was some trouble in making these work satisfactorily in the strong magnetic field.

Most of the experiments were done with a single scintillation counter. It was found that nearly all of the activity came from the target. During the cyclotron pulse a burst of scattered particles hits the phosphor and gives rise to many pulses. There is no gating of the amplifier. The counting, however, is started 2 milliseconds after the cyclotron pulse and the amplifier employed is capable of heavy overloading with short recovery time. Some of the scattered particles give rise to nuclear reactions in the phosphor and the 13-millisecond N^{12} β^+ activity [$C^{12}(p,n)N^{12}$] is found as a weak background in some cases when using a plastic phosphor.

Some preliminary experiments on a number of

TABLE I. Elements irradiated and activities found. Bombardments were normally made at proton energies of 23, 50, 80 or 100, 130, and 180 Mev. The listed figure is the lowest energy at which the activity appears in appreciable amount. The purity of elements marked† was only about 99 percent.

Element irradiated	Activities sec	Proton energy Mev	Suggested origin	Reference
Li†	0.85	23	He^6	e
	≈0.4	50	Be^6 or Li^8	a, b
Be†	0.85	23	Li^8	e
	0.4	50	Be^6 or Li^8	a, b
Mg	0.13	23	Al^{29} or Mg^{29}	
	2.3	23	Al^{31}	e
	7	23	Al^{34} or Al^{35}	e
	0.4	50		
	4.5	80		
Al	1.7	23	Si^{28}	
	≈5	23	Si^{27}	e
	≈0.2	80		
Si†	0.27	20	P^{28}	c
	≈2.5	20		
	≈4.8	20	Si^{27} or P^{29}	e
	≈1	50		
S	0.28	23	Cl^{32}	c
	≈1.7	23	Cl^{33}	e
Ca†	≈0.35	23	Sc^{40}	
	≈1.2	23	Ca^{39} or K^{37}	e
Ti	0.40	23	V^{46}	d
	0.58	80	Ti^{45}	e
	≈0.2	80		
V	1.1	57	Cr^{48}	
	0.4	57	V^{46} or Cr^{47}	
Cr†	0.26	45	Mn^{50}	d
	0.43	100	Mn^{49} or Cr^{47}	
	1.1	165	Cr^{48}	
Mn	0.28	95	Mn^{50}	d
	0.77	95		
Fe	0.20	23	Co^{54}	d
	0.55	50		
Ni	3	23	Cu^{58}	e
	0.18	50	Co^{54} or Cu^{57}	
Cu	0.3	130		
	1.3	130		
Zn	0.15	100		
	0.8	100		

[a] See reference 1.
[b] See reference 2.
[c] See reference 3.
[d] See reference 4.
[e] See reference 5.

elements have been made. Table I shows the element irradiated and the activities found. Some of the activities have been investigated or discussed earlier.[1-5] Experiments are under way to study short-lived isomeric states in some heavier elements, and also to detect short-lived α-decaying nuclides. In the latter case a thin layer of ZnS phosphor coated on Plexiglas has been used to discriminate α from β and γ pulses.

Experiments will be carried out with more channels in the analyzer to facilitate resolution of the decay curves and also perhaps with scintillation counters in coincidence.

Mass assignments will be made mainly by the study of excitation curves. Properties of the radiation will be studied by pulse-height analysis of the crystal pulses at different times after the cyclotron pulse.

The suggested assignments in Table I are from a simple consideration of preferred reaction types and estimates of thresholds, with some mass values obtained from the table of Metropolis and Reitwiesner.[6] It is probable that several corrections will have to be made as experiments proceed.

[1] R. K. Sheline, Phys. Rev. **87**, 557 (1952).
[2] T. Lauritsen, Ann. Revs. Nuclear Sci. **1**, 85 (1952).
[3] Glass, Jensen, and Richardson, Phys. Rev. **90**, 320 (1953).
[4] W. M. Martin and S. W. Breckon, Can. J. Phys. **30**, 643 (1952).
[5] Hollander, Perlman, and Seaborg, Revs. Modern Phys. **25**, 469 (1953).
[6] N. Metropolis and G. Reitwiesner, Report NP-1980 (unpublished).

PHYSICAL REVIEW VOLUME 96, NUMBER 3 NOVEMBER 1, 1954

Energy Level Displacements in Pi-Mesonic Atoms

S. DESER, *Institute for Advanced Study, Princeton, New Jersey,*
M. L. GOLDBERGER, *Institute for Nuclear Studies, and Department of Physics, University of Chicago, Chicago, Illinois,*
K. BAUMANN, *Physikalisches Institut, Universität Wien, Austria,*
AND
W. THIRRING, *Physikalisches Institut, Bern, Switzerland*
(Received July 26, 1954)

The energy level shifts and level widths of the s states of the π-mesonic atoms are discussed. The discussion is limited to fairly light nuclei. On the basis of Orear's determination of the scattering lengths for meson-nucleon scattering, semiquantitative predictions are made. It is pointed out that even a knowledge of the algebraic sign of the level shift would be of value.

I. INTRODUCTION

SEVERAL years ago[1] the low-energy properties of the π^--p, π^0-n system were discussed on the basis of a formalism closely related to that of Wigner and Eisenbud.[2] The system was treated as a two-channel nuclear reaction (taking into account only s state interaction, which we shall also do here) with the boundary conditions at the surface of a sphere of a radius, the meson Compton wavelength being specified in terms of three real energy-dependent parameters. The only unusual feature in the calculation is the treatment of the capture of a negative pion from a bound K orbit.[3] There appear quite naturally in the calculation the shift of the Bohr level associated with the pion-proton interaction and the width of the level due to the capture process. It is the purpose of the present note to deduce the level shift and level width in mesonic atoms in a more elementary and to a certain extent a less phenomenological manner than was done previously[1] and further to discuss briefly the possibilities of comparison with experiment.

II. DERIVATION OF THE LEVEL SHIFT AND LEVEL WIDTH

Before taking up the details of the calculation it is expedient to discuss the rather peculiar role played by the Coulomb field in the mesonic atom problem as well as in the ordinary low-energy scattering. The Coulomb force is of course essential for the very existence of mesonic atoms and its influence on the low-energy scattering is quite marked in so far as the interpretation of the data is concerned. On the other hand, provided that the nuclear charge is low (exactly how low will appear later) the Coulomb field may be treated very

[1] E. Fermi and M. L. Goldberger (unpublished); a short account of the work appears in Phys. Rev. **83**, 239(A) (1951). An essentially equivalent derivation has recently been independently given by G. C. Wick (private communication). We are indebted to Prof. Wick for informing us of his results.
[2] E. P. Wigner and L. Eisenbud, Phys. Rev. **72**, 29 (1947).
[3] The usual formulation of reaction theory deals with scattering rather than bound states. The necessary formal extension of the theory was later given independently by J. B. Ehrmann, Phys. Rev. **81**, 412 (1951). Our problem is much simpler in that the small level shift and level width enables us to approximate the Coulomb functions in a simple way.

simply, and in the scattering problem may be almost ignored since it scarcely influences even the zero energy scattering lengths, in contradistinction to the familiar proton-proton situation. There are two reasons for this: (1) The relevant parameter in the expansion of the reciprocal of the scattering length in terms of zero-charge quantities is the ratio of the range of the meson-nucleon interaction divided by one-half of the mesonic Bohr radius[4] and this is a number of the order of $2Z/137$ as compared to the nuclear case where it is about 1/10; and (2) the meson nucleon scattering lengths are small compared to the force range and one is not faced with a near resonance at zero energy which greatly magnifies the Coulomb corrections to 1/(scattering length) in the p-p problem. Because of the second circumstance we can tolerate quite large values of Z, say up to about 30. The capture rate for elements heavier than about oxygen is so rapid (from s states) that this restriction is unimportant.

We now proceed to the actual calculation. We write the Schrödinger equation for the complete system as

$$(K+C+V)\Psi=E\Psi, \tag{1}$$

where K is the kinetic energy operator which is taken to include the n-p and π^--π^0 mass differences, C is the Coulomb interaction, and V is the pion-nucleon interaction. (We consider first the π^--p system and will later generalize to the case of a nucleus.) We do not imply that V is anything like a point potential in configuration space; it is necessary to assume only that it is effectively a short-range interaction. We choose as the zero of energy the energy of a negative pion and a proton infinitely far apart. Thus, because of the mass differences, even negative energies down to $-[M_p-M_n+M_{\pi^-}-M_{\pi^0}]\approx-3.6$ Mev are not stationary states. We ask now for the energy level shift due to V of a negative pion bound in a K orbit of energy E_0. If Ψ is the complete wave function and Ψ_0 that of the stationary Bohr orbit which exists if V is zero, we may write

$$\Psi=\Psi_0+(1-P_0)\Psi$$
$$=\left[1+\frac{1}{E-K-C-(1-P_0)V}(1-P_0)V\right]\Psi_0, \tag{2}$$

where P_0 is the projection operator onto the state Ψ_0 and we have chosen the normalization so that $(\Psi_0,\Psi)=1$. (We imagine the system to be enclosed in a large box, as usual.) From Eq. (1) and the equation satisfied by Ψ_0 it follows immediately that

$$\delta E=E-E_0=\left(\Psi_0,\left[V+V\frac{1}{E-K-C-(1-P_0)V}\times(1-P_0)V\right]\Psi_0\right). \tag{3}$$

[4] G. F. Chew and M. L. Goldberger, Phys. Rev. **75**, 1637 (1949).

This expression, which is exact, is to be compared to the matrix element describing the forward scattering of positive energy pions by protons (neglecting Coulomb effects), namely,

$$R_{00}\equiv(\chi_0,R(E_+)\chi_0)$$
$$=\left(\chi_0,\left[V+V\frac{1}{E_+-K-V+i\epsilon}V\right]\chi_0\right), \tag{4}$$

where χ_0 represents a plane wave state corresponding to the relative motion of a negative pion and a proton with the positive energy E_+, normalized to unity in a box of volume Ω. We wish to see to what extent the energy shift, Eq. (3), may be expressed in terms of R_{00}. If we were to neglect the Coulomb field inside the square brackets of Eq. (3), which means setting C and P_0 equal to zero, we would have very nearly the expectation value of the operator R occurring in Eq. (4). There are two differences, namely, the numerical value of the energies, and the presence of the outgoing wave instruction, "$i\epsilon$," in Eq. (4). As to the first we shall set $E_+=0$ so as to deal eventually with conventional zero energy scattering lengths and then assume that the energy variation of the operator in going from zero to about -3200 ev (in the case of H, and about $Z^2\times3700$ ev for a nucleus) is unimportant. If what is essentially the real part of the operator R is chosen by using a principal value rather than the "$i\epsilon$," the second of the above differences disappears, since in our quasi-continuum situation (which becomes a true continuum as $\Omega\to\infty$) such principal values are implied in Eq. (3). More precisely, the real part of R_{00} is obtained by using principal values instead of the "$i\epsilon$" conditions. This feature is not changed by the presence of Ψ_0 in Eq. (4) rather than χ_0. We may write then finally

$$\delta E\simeq\mathrm{Re}(\Psi_0,R(0)\Psi_0). \tag{5}$$

If we now make use of the assumed short range of V to replace the wave function by their values at the origin, we may write

$$\delta E\simeq\mathrm{Re}|\Psi_0(0)|^2\Omega(\chi_0,R(0)\chi_0). \tag{6}$$

If we were to simply insert $R(0)$ with the "$i\epsilon$" included in place of the bracket in Eq. (3), we would obtain Eq. (6) without the instruction to take the real part, and we obtain an imaginary contribution to the level shift which is, of course, interpreted as the level width. To save writing we shall use such complex energy shifts. We may relate $(\chi_0,R(0)\chi_0)$ to the zero energy scattering length, $a(\pi^-)$, for ordinary (non-exchange) scattering of negative pions by protons according to

$$\Omega(\chi_0,R(0)\chi_0)=-(2\pi/\bar{\mu})a(\pi^-), \tag{7}$$

where $\bar{\mu}$ is the reduced mass of the pion-proton system. The total level shift (real and imaginary parts) is

given by

$$\delta E = -(2\pi/\bar{\mu})|\Psi_0(0)|^2 a(\pi^-). \tag{8}$$

In the next section we shall compare these predictions with experiment.

III. COMPARISON WITH EXPERIMENT

To the zeroth order in the mass differences, $a(\pi^-)$ may be expressed directly in terms of the scattering lengths for states of isotopic spin $\frac{1}{2}$ and $\frac{3}{2}$ which we shall call a_1 and a_3 respectively. We have

$$a(\pi^-) = \tfrac{1}{3}(2a_1 + a_3). \tag{9}$$

In this approximation $a(\pi^-)$ is real, since there is no decay if the mass difference vanishes. Inserting the value of $|\Psi_0(0)|^2$, namely $1/\pi r_B^3$ with r_B the mesonic Bohr radius $(1/\bar{\mu}e^2)$, we obtain for the level shift in hydrogen

$$\delta E/E_0 = -4(2a_1 + a_3)/3r_B, \tag{10}$$

where E_0 is the Bohr energy, $e^2/2r_B$. For a nucleus of charge Z, assuming the effects of the various nucleons are simply additive, and recalling that the π^--n scattering length is a_3, we find

$$\frac{\delta E}{E_Z} = -\frac{4Z}{r_B}\left[\frac{2}{3}Za_1 + \frac{3N+Z}{3}a_3\right]. \tag{11}$$

E_Z is in Eq. (11) the Bohr energy appropriate to a nucleus of charge Z. Taking the values of a_1 and a_3 given by Orear,[5] namely $a_1 = 0.16/\mu$, $a_3 = -0.11/\mu$, we find for hydrogen $\delta E/E_0 \sim -1.8\times 10^{-3}$ and $\delta E \sim -6$ ev. For a nucleus with $N = Z$, $\delta E/E_Z \sim +Z^2/850$. We must expect our approximations on the Coulomb field to fail when $\delta E/E_Z \sim 1$ so that we restrict our attention to $Z \ll 30$. A particular case of interest is Be^9, for which we obtain $\delta E \sim +1850$ ev. The corrections due to finite mass differences cannot be calculated without a specific model, but the considerations of the capture process to be treated immediately below indicate that they are small. There is of course also a level shift due to the extended electric charge in a nucleus other than hydrogen but this is very small compared to those considered here, for light nuclei.

The imaginary part of the level shift, i.e., the level width, involves a knowledge of the imaginary part of $a(\pi^-)$ at zero energy. This quantity may be computed directly from the unitarity condition on the R matrix,[6] namely

$$-\mathrm{Im}R_{aa} = \pi \sum_b |R_{ba}|^2 \delta(E_b - E_a), \tag{12}$$

applied to a state a representing a zero kinetic energy pion and proton. The only states b that make a non-vanishing contribution are those associated with the capture process and we find from Eq. (12), using Eq. (7),

$$\mathrm{Im}a(\pi^-) = q_c\sigma_c/(4\pi) = q\,|a(\pi^0 \leftarrow \pi^-)|^2, \tag{13}$$

where q is the relative momentum of the π^0-n system, related to the mass difference by $q^2/2\bar{\mu} = \delta M$, and $q_c\sigma_c$ is the product of the (zero) momentum of the incident pion and the charge exchange cross section at zero energy; $a(\pi^0 \leftarrow \pi^-)$ is the charge exchange scattering length. From Eq. (8), then, we find an imaginary contribution to the level shift, namely,

$$\mathrm{Im}(\delta E/E_0) = -4(qr_B)\,|a(\pi^0 \leftarrow \pi^-)/r_B|^2. \tag{14}$$

To zero order in q, $a(\pi^0 \leftarrow \pi^-)$ is given by

$$a(\pi^0 \leftarrow \pi^-) = \tfrac{1}{3}(2)^{\frac{1}{2}}(a_1 - a_3), \tag{15}$$

and thus we find from Eq. (14) a level width Γ $(\Gamma = -\mathrm{Im}\delta E)$,

$$\Gamma/E_0 = (8/9)(qr_B)\,|(a_1 - a_3)/r_B|^2. \tag{16}$$

For a nucleus of charge Z (since only the protons contribute to the capture process considered here),

$$\Gamma/E_Z = (8/9)Z^2(qr_B)\,|(a_1 - a_3)/r_B|^2. \tag{17}$$

In hydrogen, $\Gamma \sim 0.3$ ev, whereas in Be it is about 77 ev. Thus in both cases the level width is much smaller than the level shift and consequently the expansion in powers of qr_B which we have used should be quite accurate. This parameter is about $\frac{1}{4}$ and the correction terms to both the level shift and the width are proportional to $(qr_B)^2$.

IV. CONCLUSIONS

We shall not enter into an exhaustive discussion of the various effects which can contribute to the level width and level shift which have not been considered here. For light elements the effect we have been discussing would appear to be the most important. There may be significant contributions to the width due to star formation, but the level shift is probably not greatly affected. The only measurements of the level shift carried out to date are some very preliminary ones at Carnegie Tech[7] on Be^9 which show effects of the same order of magnitude as those considered here.

It would be of considerable interest to know even the algebraic sign of the level shift in several elements, for this alone would enable us to draw some conclusions about the signs of the scattering lengths. For example, Orear's assignment yields always a positive δE (i.e., less binding, a repulsive interaction) whereas any assignment which makes a_1 and a_3 both positive leads to tighter binding, negative δE's.

[5] Jay Orear, Phys. Rev. **96**, 176 (1954).
[6] B. Lippmann and J. Schwinger, Phys. Rev. **79**, 469 (1950).
[7] Private communication from Professor de Benedetti to Professor Fermi.

Bursts in NaI(Tl) near Sea Level*

S. STANDIL
Department of Physics, University of Manitoba, Winnipeg, Canada
(Received June 29, 1954)

The spectrum of cosmic-ray events induced in a NaI(Tl) scintillation spectrometer has been observed near sea level. The high-energy bursts so observed are interpreted as due mainly to nuclear interactions in the crystal with an energy distribution given by the power law $N(E)dE \propto E^{-3.6}dE$. The attenuation length for the star-producing component in concrete is found to be 200±25 g/cm².

THE differential distribution of energy releases or bursts due to cosmic radiation in an unshielded NaI(Tl) crystal near sea level (elevation 775 feet) has been observed during a period of 3000 hours. The experiment is similar to burst studies with ionization chambers,[1] differing in that a medium-Z solid detector is employed. The use of NaI has an advantage in that its density and constituent atomic numbers are close to that of photographic emulsions, hence comparison of results by the two methods is made easier.

Two scintaillation spectrometers were employed, each consisting of NaI crystals (diameter 3½ inches, thickness 2 inches) mounted on DuMont K1198 photomultipliers. The amplified spectrometer pulses were lengthened and displayed by pen recorders. Energy calibration was in terms of a 2.6-Mev gamma ray, assuming linearity.

The observed distribution is given in Fig. 1. The feature A is due to singly charged relativistic particles, mainly μ mesons, passing right through the crystal.[2] Beyond about 100 Mev the distribution can be represented by a power law $N(E)dE \propto E^{-\gamma}dE$, with $\gamma = 3.6 \pm 0.2$. There is some deviation from this at very high energies, possibly due to extensive air showers. For reasons outlined below it is thought that almost all of the events >100 Mev are due to stars or nuclear interactions initiated in the crystal by the N component.

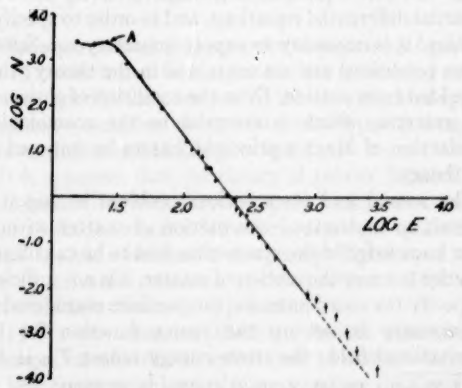

FIG. 1. N represents the hourly rate per 10-Mev interval and E is the energy in Mev. Standard deviations are indicated where they are appreciable.

Preliminary coincidence measurements indicate that less than 3 percent of the events greater than 100 Mev in one counter are accompanied by events of at least 20 Mev in the second counter when they are placed close together. Thus the contribution of events >100 Mev by showers originating outside the detectors is small. Further, charged cosmic ray particles just coming to rest in this size of crystal would not liberate sufficient energy to seriously alter the above interpretation. For example, protons just coming to rest in this detector would give pulses of energy from about 120 to 150 Mev.

George and Evans[3] give the frequency of stars with 3 or more prongs in emulsion to be 1.46±0.07/cc day. For such 3-pronged stars Tidman and Hodgson[4] determined the mean total energy of the low- and medium-energy particles (ionization >1.5 minimum ionization) as 196±18 Mev of which about 55 percent is taken by neutrons. Translating the above frequency figure to the NaI detector used here, one would then expect about 23 such events per hour. A frequency of this magnitude is found for events >140 Mev, indicating that this detector captures a large fraction of the energy liberated in such stars.

With the assumption that over a limited energy range the NaI detector captures a fixed fraction of the total star energy the distribution of star energies is then given by the power law above. This is not in agreement with the results of Barton *et al.*[5] who, using emulsions, also find a power law distribution with $\gamma = 2.6 \pm 0.1$. The reason for this discrepancy is not clear. It should be noted, however, that the present method gives a direct measurement of energy loss in the detector. The results of Barton *et al.* are obtained indirectly by determining the prong number distribution and using corrected data for total star energy *vs* prong number.

The above experiment has also been performed in a basement laboratory, the total thickness of concrete above the detectors being about 3 feet. The distribution is attenuated but similar to that in Fig. 1. Comparison of integral counting rates above 100 Mev gives an attenuation length of 200±25 g/cm² for the star-producing component in concrete.

* Supported by the National Research Council of Canada.
[1] See for example, C. N. Chou, Phys. Rev. **74**, 1659 (1948); H. Carmichael and J. F. Steltjes, Phys. Rev. **93**, 913 (1954).
[2] A. Hudson and R. Hofstadter, Phys. Rev. **88**, 589 (1952).
[3] E. P. George and J. Evans, Proc. Roy. Soc. (London) **A63**, 1248 (1950).
[4] D. A. Tidman and P. E. Hodgson, Phil. Mag. **43**, 992 (1952).
[5] Barton, George, and Jason, Proc. Roy. Soc. (London) **A64**, 175 (1951).

Mach's Principle and Unified Field Theory

JOSEPH CALLAWAY*
Palmer Physical Laboratory, Princeton University, Princeton, New Jersey†
(Received May 13, 1954)

An argument based on the impossibility of satisfying Mach's principle within general relativity is given which leads to the idea of unified field theory. A possible alternative is discussed.

IT is interesting to discuss whether there is an argument, based on classical physics, which would suggest that a unified field theory of some sort is desirable. By unified field theory is meant a theory in which "matter" or the sources of the space-time field are absorbed into the field itself, so that one has a set of homogeneous partial differential equations. I have tried to examine this question from the point of view of Mach's principle, which can be stated: The local inertial frame (the coordinate system in which Newton's laws are obeyed) is determined by the matter in the universe. Mach's principle is a statement concerning the relation between space-time and matter which asserts the subordination of space-time to matter. It is important to determine the status of Mach's principle, because if Mach's principle is either contained in general relativity, or can be satisfied in it; there is no classical argument for the radical approach of unified field theory which usually asserts the identity of space-time and matter. In other words, if Mach's principle holds, we can retain the apparently observed distinction between space-time and matter and at the same time eliminate the absolutes of Newtonian physics. However, if it is impossible to conform to the principle in general relativity, then we can no longer preserve the separation between matter and space-time once the field-theoretic approach of general relativity has been adopted. If matter cannot be consistently regarded as the source of the field, we must treat it as part of the field. In this case, once one has accepted general relativity, one is impelled to go all the way to unified field theory.

It seems apparent that general relativity does not contain Mach's principle in the sense that solutions of the field equations can be found which are inconsistent with the principle. One example of this is the Schwarzschild solution for a centrally symmetric field. In this, space is flat—Minkowski space—at large distances from the gravitating particle, and therefore is a space of definite properties uninfluenced by matter. Also, Taub has found solutions of the field equations which do not represent flat space and yet contain no matter.[1]

The question remains: can one find solutions of the field equations of general relativity which conform to Mach's principle? Another form of this question is: Given arbitrary bodies in motion, can one calculate what will be the local inertial frame and so verify the theory? (The calculation of the local inertial frame can be tested by experiment, for in it the plane of vibration of the Foucault pendulum will be stationary.) That this question should be answered affirmatively is suggested by two results: (1) The calculations of Thirring[2] show that a particle which is placed at the center of a massive, rotating, spherical shell (rotating with respect to the distant matter in the universe) should experience Coriolis and centrifugal forces caused by the rotating shell. (2) Similarly, one can show[3] that the inertia of a test particle is increased by the presence of massive bodies, and that a test body will experience a parallel acceleration when neighboring masses are accelerated.

There is, however, a basic difficulty. The calculations mentioned above are carried out for a situation in which the properties of space-time are largely known in advance, and all we have to do is to determine the effect of a small perturbation. Analysis of these calculations reveals that it is impossible to generalize them so that we can determine the inertial properties of a particle by considering the effect of all other bodies, unless some fundamental assumption is made in advance (which is not contained in general relativity) about the properties of space-time.

The first problem is the question of boundary conditions. The field equations of general relativity are a set of partial differential equations, and in order to specify a solution[4] it is necessary to supply boundary conditions. These conditions are not contained in the theory; they are added from outside. Even the condition of closure of the universe, which is essential to the cosmological satisfaction of Mach's principle, has to be imposed on the theory.[5]

The second and more serious problem is that it is difficult to understand the motion of matter without prior knowledge of the space-time field to be calculated. In order to know the motion of matter, it is not sufficient to specify the coordinates for the particles considered; it is necessary to set up the source function for the gravitational field; the stress energy tensor T_{ik} in the

* National Science Foundation Predoctoral Fellow.
† Present address: Department of Physics, University of Miami, Coral Gables, Florida.
[1] A. H. Taub, Ann. Math. 53, 472 (1951).
[2] H. Thirring, Physik. Z. 19, 33 (1918); 22, 29 (1921).
[3] A. Einstein, *The Meaning of Relativity* (Princeton University Press, Princeton, 1953), fourth edition, p. 100.
[4] This can, of course, only be done up to a coordinate transformation.
[5] One may consider adopting a system consisting of differential equations plus boundary conditions. This requires the explicit introduction of an extra hypothesis about space-time.

equation

$$R_{ik}-\tfrac{1}{2}g_{ik}R=kT_{ik}. \tag{1}$$

In order to determine the stress-energy tensor it is necessary to know the laws governing the behavior of matter. Because of the existence of nongravitational forces, these have to be added to general relativity from outside. When these laws are written in a covariant form, they will contain the components of the metric tensor or related quantities. Consequently we will not be able to understand matter apart from space-time. This is in accord with the previously mentioned result that the inertia of a body is increased by the presence of other bodies. For example, consider the case of free particles: The contravariant stress-energy tensor can be written (if pressure is neglected):

$$T^{ik}=\rho\frac{dx^i}{ds}\frac{dx^k}{ds}. \tag{2}$$

Not only do the velocities dx^i/ds depend on the field, but we must in the general case supply a rule by which the particle density ρ may be calculated, and include in this the effect of the gravitational field on the masses of the particles.

The example of the cosmological solutions of general relativity will serve to illustrare some of these problems. In order to begin, it is necessary to impose the cosmological principle or its equivalent: the universe appears homogeneous and isotropic to any (fundamental) observer. This is an extremely powerful assumption as Milne has demonstrated, and is consistent with general relativity but certainly not required by it. From the cosmological principle it follows that the metric of space-time can be put in the form

$$ds^2=dt^2-\frac{R^2(t)}{1+\frac{1}{4}kr^2}[(dx^1)^2+(dx^2)^2+(dx^3)^2]. \tag{3}$$

The equations of general relativity give an equation for $R(t)$ which can be integrated, but it remains necessary to specify the constant k, the curvature of space, as positive, negative, or zero. The case of positive curvature conforms to Mach's principle.

It is apparent that the theory of general relativity is incomplete: it is necessary to supply additional assumptions about the relation between matter and space-time which are not contained in the theory. There seem to be two conceivable solutions to this problem which preserve the field-theoretic approach:

(1) We can abandon Mach's principle and with it attempts to subordinate space-time to matter. Instead, we look for general laws of the space-time field and try to derive from these laws the behavior of matter, which is to be constructed from the space-time field. This is the approach of unified field theory. It is supported by the beautiful result of general relativity, that if we regard gravitating particles as singularities in the field, then the equations of motion of these particles can be obtained from the field equations.

(2) The second approach, suggested by Professor J. A. Wheeler, is less radical. If we knew additional relations between matter and space-time, we could supplement general relativity and hope to obtain a self-consistent scheme. There is at least one situation in which this can be done: the case in which matter consists of an electromagnetic field. The energy tensor is

$$T_{ik}=\frac{1}{4\pi}(F_{i\alpha}F^{\alpha}{}_{k}-\tfrac{1}{4}F_{\alpha\beta}F^{\alpha\beta}g_{ik}). \tag{4}$$

The laws governing the electromagnetic field are just Maxwell's equations

$$\frac{\partial F_{ik}}{\partial x^l}+\frac{\partial F_{kl}}{\partial x^i}+\frac{\partial F_{li}}{\partial x^k}=0 \tag{5}$$

and

$$\frac{\partial}{\partial x^{\alpha}}(\sqrt{(-g)}\,F^{i\alpha})=0. \tag{6}$$

We can hope to be able to construct such a system in any case where the laws of matter are sufficiently well known. Such a theory possesses at least one of the characteristics of a unified field theory; for it is no longer possible to distinguish source from field; matter and space-time enter on an equal basis.[6] Consequently, Mach's principle is not observed. The difficulty with boundary conditions is not surmounted in this kind of a theory. The boundary conditions have to be added explicitly as an extra hypotheses. This is legitimate since Mach's principle has been abandoned. (The situation as regards boundary conditions in unified field theories is still unclear, because nothing is known about allowable solutions.) It may be that a more conservative theory of this sort is preferable at the present stage of science because one is more certain of the component parts.

The conclusions of this argument are the following: It is impossible to satisfy Mach's principle within general relativity because matter cannot be understood apart from knowledge of space-time. If the approach of field theory is accepted, it is necessary to construct a theory in which matter and space-time enter as equals. There are at least two possibilities of doing this.

I wish to thank Professor J. A. Wheeler and Professor A. Einstein for valuable discussions. This note was stimulated by the conflict of their views. I also wish to thank Mr. J. R. H. Dempster for his criticisms and suggestions which have contributed greatly to the clarification of my ideas.

[6] J. A. Wheeler, Phys. Rev. **94**, 773 (1954). The system of Maxwell's equations and the field equations of general relativity is being integrated by Professor Wheeler for a special case.

APPENDIX

Professor Einstein has proposed unified field theory as an alternative to quantum theory because he believes that quantum theory, based essentially on probabilities, cannot give a complete description of nature. Many physicists who are skeptical of the ability of unified field theory to yield all the verified results of quantum theory, do not share this attitude. It is too early to pass judgment on this attempt. However, it may be observed that his theory will either be able to handle quantum phenomena or it will fail completely. I refer in particular to the existence of a sharp value for the elementary electric charge. It has been shown[7] that if solutions of Einstein's unified field theory are admitted which depend continuously on a parameter (i.e., a spread in value for the electronic charge), then the Coulomb law can never be satisfied. It may be concluded from this and other work that the theory is either extremely powerful or useless.

[7] C. P. Johnson, Phys. Rev. **89**, 320 (1953). See also A. Einstein, Phys. Rev. **89**, 321 (1953).

PHYSICAL REVIEW VOLUME 96, NUMBER 3 NOVEMBER 1, 1954

Direct Proof of the Covariance of Gupta's Indefinite Metric in Quantum Electrodynamics

FREDERIK J. BELINFANTE
Department of Physics, Purdue University, Lafayette, Indiana

(Received March 26, 1954)

Gupta's method of the indefinite metric is at this time for many purposes the most satisfactory method of formulating the principles of quantum electrodynamics. Gupta's indefinite metric, however, depends on the number of scalar photons. This number is no invariant. Yet, the covariance of Gupta's indefinite metric has been proved before. This seems at first surprising. In the present paper we show why the lack of invariance of the number of scalar photons does not matter and how a certain covariance of the occupation numbers together with "repolarization operators" insures the covariance of Gupta's method. In particular, if the norms of the eigenfunctions of occupation numbers are chosen in accordance with Gupta's prescription in one Lorentz frame, they are automatically in accordance with this prescription in a different Lorentz frame.

1. INTRODUCTION

AT the time this is written, Gupta's form of quantum electrodynamics is the most satisfactory formulation of quantum electrodynamics for most field-theoretical considerations. The advantages of Gupta's treatment of the problem of longitudinal and "scalar" (or "time-like") photons[1-4] are the following: (1) It avoids state vectors which cannot be normalized.[5] (2) It does not give the photon a small mass.[6] (3) It does not introduce more "redundant" field variables than the longitudinal and "scalar" potentials and their four-dimensional divergence.[7] (4) By its manifest covariance it enables us to perform renormalizations unambiguously in a covariant way.[8] Gupta's theory is at present the only theory combining these four advantages.

It is true that the problem of longitudinal and scalar photons can also be solved by avoiding to introduce it in the first place. For a Maxwell field interacting with a finite number of Dirac particles this was first shown by Pauli.[9] Later, this "gauge-independent" method was further developed and was adapted to positon theory by Belinfante.[10-11] While the covariance of this method can be proved,[9-10] the complicated form of the Lorentz transformation of the field components in this theory has thus far largely obstructed its applicability. In particular, nobody as yet seems to have succeeded in developing a clearly formulated renormalization technique using exclusively gauge-independent methods. True enough, French and Weisskopf based their calculation of the Lamb shift on this type of description of nature.[12] However, a look at their Eq. (13) and at the symmetry in their subsequent treatment of the k occurring in the various terms of this equation shows that they brought in through the back door the Coulomb-interaction-by-way-of-longitudinal-and-scalar-photons which they had thrown out through the front door. Also, their argument for explaining why their treatment is covariant had to be much more complicated and less

[1] S. N. Gupta, Proc. Phys. Soc. (London) **A63**, 681 (1950).
[2] K. Bleuler, Helv. Phys. Acta **23**, 567 (1950).
[3] S. N. Gupta, Proc. Phys. Soc. (London) **A66**, 129 (1953).
[4] S. N. Gupta (to be published).
[5] F. J. Belinfante, Phys. Rev. **76**, 226 (1949).
[6] F. J. Belinfante, Progr. Theoret. Phys. (Japan) **4**, 165 (1949).
[7] J. C. Valatin, Kgl. Danske Videnskab. Selskab, Mat.-fys. Medd. **26**, No. 13 (1951).
[8] S. N. Gupta, Proc. Phys. Soc. (London) **A64**, 426 (1951). Also reference 3 and references given there.
[9] W. Pauli, in H. Geiger and H. Scheel, *Handbuch der Physik* (Springer, Berlin, 1933), second edition, Vol. 24, Part I, Chap. 2, Sec. B8, p. 269. (Reprinted by Edwards Brothers, Ann Arbor.)
[10] F. J. Belinfante and J. S. Lomont, Phys. Rev. **84**, 541 (1951).
[11] F. J. Belinfante, Phys. Rev. **84**, 644 (1951).
[12] J. B. French and V. F. Weisskopf, Phys. Rev. **75**, 1240 (1949).

direct than in the manifestly covariant theory, where this covariance is seen by inspection.

No doubt exists that the gauge-independent treatment comes closer to the way many physicists think about phenomena involving electromagnetic radiation besides Coulomb interaction. The advantage of the gauge-independent method lies not only in the fact that it avoids redundant field variables altogether, but also in the fact that in many applications one *wants* to treat Coulomb interaction as a first-order, preferably even zeroth-order effect. Yet, to this date, the manifestly covariant method remains the single mathematical tool by which the theoretician has successfully attacked the more complicated problems of quantum electrodynamics and arrived at results comparable with experiment.[13] Therefore, it is important to find a consistent interpretation of this covariant method.

This has not been possible within the framework of a quantum theory operating in a Hilbert space of positive definite metric. The many published attempts at such interpretation all contain either errors or inconsistencies, or other unsatisfactory features.[14] Therefore, for a justification of modern quantum electrodynamics without eliminating the part of Hilbert space describing the states of longitudinal and scalar photons, one must replace Hilbert space by what I may call *Gupta space*, that is, the more general type of Hilbert space in which the condition of a positive definite metric has been dropped.[4]

2. THE PROBLEM OF COVARIANCE OF GUPTA'S "RULE OF NORMS"

As the gauge-independent theory, thus also at first Gupta's theory gives to the unsuspecting reader the impression of being noncovariant. This is due to the choice of the metric in Gupta space. It is convenient to choose the eigenfunctions of the incident-photon occupation numbers[15–17] as basic vectors in Gupta space. Gupta has shown, then, that the metric in Gupta space must be such that the norm of these basic vectors is -1 $(+1)$, as the number of incident "scalar" photons is odd (even).[1] We shall call this Gupta's "rule of norms." Now, everybody knows that the number of incident "scalar" photons is not invariant under Lorentz transformation. Therefore, the average reader will at first be skeptical about the possibility of covariance of such rule of normals. However, here as for gauge-independent quantum electrodynamics, the covariance of the theory has been proved nevertheless.

By a proof of covariance, of course, we mean that two physicists, moving with respect to each other and each using the same rule of norms in his own different coordinate system, will both ascribe the same norm to the same basic vector in Gupta space. This may be expressed differently as follows. Physicist A may draw his attention for instance to a state,[18] in which from his point of view there is one scalar photon besides, perhaps, several vector photons. He gives it the norm -1. This same basic vector, according to physicist B, describes a mixture of states, in which there are $0, 1, 2, \cdots$, scalar photons present. Anyhow, the norm of this mixed state from A's observation was already known to be -1, and B cannot change that. Similarly, there is an infinite number of other states, which look like mixed states to B, but for which the norms are known, because for A these states happen to have a simpler aspect allowing A the application of the rule of norms. The norms of this complete set of mixed states, then, already will determine completely the metric of Gupta space for B. In particular, it will also fix the norms of states which look simple to B, and to which he would have liked to apply the rule of norms himself. The question then, is whether, for the latter cases, the metric thus by A already fixed for B will automatically guarantee or will automatically contradict the validity of the rule of norms for B.

This is not just a question of "elegance" of the theory. This is a question of necessity for the covariance of the theory. For it is not sufficient that field equations and commutation relations are consistent and covariant. In the first place, it is also necessary that expectation values of observables will transform in exactly the same way as the corresponding q numbers do. Therefore, no difference in expectation value should be caused by differences in methods for obtaining expectation values from q numbers in different Lorentz systems. The calculation of expectation values involves use of the metric. The same metric should, therefore, be used by different observers. This is the reason why we said above that the metric for observer B is completely determined by the metric for observer A, and that B cannot change that.

In the second place, if the special relativity principle is to hold, the laws of nature for B should be the same

[13] R. Karplus and N. M. Kroll, Phys. Rev. **77**, 536 (1950).

[14] In my own attempt [F. J. Belinfante, Physica **12**, 17 (1946)], the asymmetry between the treatment of the products of F into Ψ and into $\Psi^\dagger$ in expressions like $(\Psi^\dagger F \Psi)$ was an unsatisfactory feature which can be remedied. In that attempt, a basic idea of the gauge-independent theory was smuggled half-heartedly into the manifestly covariant theory, by defining Ψ in a subspace of Hilbert space only. While such a "half-hearted" theory possibly could be further developed, this has never been done.

[15] By "incident-photon" occupation numbers we understand the occupation numbers which are derived from the Fourier components of the potentials given in an interaction representation coinciding with the Heisenberg representation at the "time of incidence" (usually $t = -\infty$). See references 16, 17, and 11.

[16] G. Källén, Arkiv Fysik **2**, 187, 371 (1951).

[17] C. N. Yang and D. Feldman, Phys. Rev. **79**, 972 (1950).

[18] This remark needs clarification. By "state" we do not mean here a physical state satisfying the Schrödinger equation and auxiliary condition, but we mean only some eigenfunction of the incident-photon occupation numbers and, therefore, of the free-photon energy in interaction representation. By the "value" of this free-photon energy we will then understand the corresponding eigenvalue. As the norm of the eigenfunction may be negative, this eigenvalue may be opposite in sign to the corresponding contribution to the expectation value in a physical state containing admixture of this eigenfunction.

as for A. Now, the rule of norms is a law of nature, important because it determines the expectation values of observables. Therefore, Gupta's rule of norms is acceptable only if it can be proved that, once it is valid for A, it will be valid for B automatically.

A somewhat complicated and not entirely complete proof of the covariance of this rule of norms was given by Bleuler.[3] He proved the following general theorem, which we shall purposely somewhat reformulate, in order to facilitate for us the completion of the proof we are asking for.[19]

Let A be, for instance, the x component of the potential four-vector operator. Let χ be an eigenfunction of A belonging to some given eigenvalue a. There is an operator S, such that $A'=S^{-1}AS$ is now the x' component of the potential four-vector operator in a second (primed) Lorentz frame. Then, obviously, $\chi'=S^{-1}\chi$ is the "corresponding" eigenfunction of A' belonging to that same eigenvalue a. "Covariance of norms" now requires that χ' shall have the same norm as χ had. This was shown by Bleuler to be so.

In order to complete the proof that the rule of norms remains valid for the primed Lorentz frame in the way we formulated it for the unprimed Lorentz frame, it is now sufficient to generalize Bleuler's theorem[19] to the case where A in the above is not just a component of the potential itself, but is some functional of it, such as an occupation number for a "scalar" photon. In this way one finds a proof, although a rather complicated one, of the covariance of Gupta's method. In the following, we shall find a much shorter and more direct proof of the covariance of Gupta's rule of norms. (See Chap. 4.)

Recently, Gupta himself has reformulated the definition of the metric in Gupta space in such way that its covariance becomes more or less evident. The general idea of this reformulated theory is approximately the following.[20]

We first postulate in one Lorentz frame that there shall be a state of nonvanishing norm, in which the incident-photon energy takes a minimum value.[15,18] It is then shown that this automatically leads to the validity of Gupta's rule of norms in this particular Lorentz frame. But it is also shown that this lowest energy state must then be the zero-energy zero-momentum state of the photon vacuum, and that all other states automatically have a time-like energy-momentum four-vector pointed into the positive energy direction. The latter property is invariant. Therefore, now also in any other Lorentz frame all energies are positive except the zero energy of the vacuum state. This, then, guarantees the automatic validity of Gupta's rule of norms in every Lorentz frame.

This new proof of Gupta is brief and elegant. However, it somewhat bypasses the question which we originally asked. For, while Gupta's new brief proof of covariance, of course, *implies* that the metric for B must satisfy the same rule of norms as for A, yet it does so without *explicitly calculating* the norm of a state which by B contains n scalar photons, in terms of the norms defined according to the rule of norms as postulated by A. If by a direct calculation of this type it could be demonstrated that the rule of norms then will hold automatically for B as well, this would be the most direct and therefore the most convincing proof of the covariance of Gupta's method.

The purpose of the present paper is to give this proof in a brief and simple form.

3. GUPTA'S REPRESENTATION OF EMISSION AND ABSORPTION MATRICES

We are here interested in the norms of the eigenfunctions of the occupation number operators N_μ used by Gupta in his rule of norms.[1] These N_μ are to be taken in interaction representation, not only in the definition of the Gupta norm in interaction representation, but also[21] in the definition of the Gupta norm in Heisenberg representation.[22]

These occupation-number operators can be introduced in a covariant way.[23] They form the diagonal components of mixed tensors,

$$N_\mu{}^\nu(K)=a_\mu{}^\dagger(K)\,a^\nu(K), \tag{1}$$

where K denotes a small domain on the positive-energy cone $k^0=+|\mathbf{k}|$ in momentum space. This so-called $+k$ cone[23] is assumed to be subdivided into many such domains; for each of these, there are four occupation-number operators, *viz.*,

$$N_0=-a_0{}^\dagger a_0, \quad N_j=+a_j{}^\dagger a_j \quad (j=1,2,3). \tag{2}$$

[19] In fact, Bleuler explicitly proved something slightly different from the theorem as we formulate it. For him, our χ' (called ψ by him) denoted a certain state, in which, for instance, the x component of the potential four-vector in the unprimed frame of reference has the expectation value A, while the x' component in the primed frame of reference has the expectation value A'. For him, our χ (his ψ') represents a state, in which then the x component in the unprimed Lorentz frame has the expectation value A'. The different interpretation of Bleuler's formulas found in the text above makes it easier to pass from Bleuler's "proof of covariance of Gupta's method of quantization" to the more specific question of the covariance of the rule of norms, in which we are interested here.

[20] I thank Dr. Gupta for private communication of this reformulation of his theory. A full discussion of this treatment of the theory of the indefinite metric will appear in a forthcoming book *Quantum Theory of Fields* by S. N. Gupta [North Holland Publishing Company, Amsterdam (to be published)]. It uses the simplified formulation of quantum theory in Gupta space found in reference 4.

[21] This is most easily seen using Gupta's new formulation (see references 4 and 20). With the old formulation of Gupta's theory (see reference 1), it follows from the fact that the transformation between interaction and Heisenberg representation is unitary in the sense that its inverse is equal to its adjoint, not its Hermitian conjugate. Such unitary transformation of a state vector leaves its norm invariant.

[22] This fact will not complicate the use of Heisenberg representation in those problems, in which one can characterize the physical state of specifying the numbers of "incident" photons (see references 15–17).

[23] See the Appendix.

The operators $a_\mu(K)$ and $a_\mu^\dagger(K')$ are absorption and emission operators for the momentum regions K and K'. They are commutative for $K \neq K'$, while for $K=K'$ they satisfy the commutation relations,[23]

$$a_\lambda a_\mu^\dagger - a_\mu^\dagger a_\lambda = g_{\lambda\mu} (= \delta_{\lambda\mu} - 2\delta_{\lambda 0}\delta_{\mu 0}). \tag{3}$$

Let χ be the normalized simultaneous eigenfunction of all occupation-number operators, which belongs to the eigenvalues $\eta_{K\mu}$:

$$N_\mu(K)\chi = n_{K\mu}\chi; \quad \chi^\dagger\chi = \pm 1. \tag{4a-b}$$

By $\chi(n_{K\mu}\pm 1)$ we shall denote the simultaneous eigenfunction belonging to this same set of eigenvalues except $(n_{K\mu}\pm 1)$ replacing $n_{K\mu}$; by $\chi(n_{K\mu}\pm 1, n_{K\nu}\mp 1)$ for $\mu \neq \nu$ we shall denote one belonging to the same eigenvalues as $\chi(n_{K\mu}\pm 1)$ except $(n_{K\nu}\mp 1)$ replacing $n_{K\nu}$; etc. Further, we shall omit the subscript or argument K wherever this does not cause confusion.

Gupta[24] then has found the following representation of the operators $a_\mu^\dagger$ and a_μ:

$$a_0\chi = n_0^{\frac{1}{2}}\chi(n_0-1), \tag{5a}$$

$$a_0^\dagger\chi = -[n_0+1]^{\frac{1}{2}}\chi(n_0+1), \tag{5b}$$

$$a_j\chi = n_j^{\frac{1}{2}}\chi(n_j-1), \quad (j=1,2,3), \tag{5c}$$

$$a_j^\dagger\chi = [n_j+1]^{\frac{1}{2}}\chi(n_j+1). \tag{5d}$$

Indeed, it is easily seen that Eqs. (5) ensure the validity of Eq. (3), and by (2) also the validity of (4a). In fact, the solution (5) of Eqs. (2)–(4) is unique but for the possible effect of a more arbitrary choice of the complex relative phase factors of the various eigenfunctions χ. Thus, (5) determines a fixed and convenient choice for these phases.

As for Eq. (4b): Eq. (5) also determines the signs of the norms of the eigenfunctions χ, if we choose the norm of the vacuum state to be $+1$. This is so because the meaning of the symbol † in Eqs. (5b) and (5d) involves that

$$\{\chi^\dagger a_\mu(K)\psi\}^* = \psi^\dagger a_\mu^\dagger(K)\chi, \tag{6}$$

if the asterisk $(^*)$ denotes ordinary complex conjugation. Now, introduce the notation η for the norm of χ, that is,

$$\eta = \chi^\dagger\chi, \quad \eta(n_\mu\pm 1) = \chi(n_\mu\pm 1)^\dagger\chi(n_\mu\pm 1), \quad \text{etc.} \tag{7}$$

Then, in Eq. (6) once take $\mu=0$ and $\psi=\chi(n_{K0}+1)$ and apply (5a–b), and once take $\mu=j(=1,2,3)$ and $\psi=\chi(n_{Kj}+1)$ and apply (5c–d). The two results thus obtained can be written by (7) as

$$\eta = -\eta(n_{K0}+1) = +\eta(n_{Kj}+1).$$

Thence, choosing $\eta=+1$ for the vacuum state, Gupta finally finds

$$\chi^\dagger\chi = \eta = \prod_K (-1)^{n_{K0}} = (-1)^{\sum_K n_{K0}} \tag{8}$$

for his rule of norms.[1] Finally, it is easily seen that the eigenfunctions χ satisfy the orthogonality relations[1,4]

$$\chi^\dagger\psi = \eta \prod_\mu \prod_K \delta(n_{K\mu}, m_{K\mu}), \tag{9}$$

if ψ is an eigenfunction like χ, but for a completely independent set of eigenvalues $m_{K\mu}$, so that $N_\mu(K)\psi = m_{K\mu}\psi$. In (9), we wrote $\delta(n,m)$ for the Kronecker symbol δ_{nm}.

4. PROOF OF THE LORENTZ COVARIANCE OF GUPTA'S RULE OF NORMS

Suppose that the eigenfunctions χ of the occupation numbers $N_\mu(K)$ in our original (unprimed) coordinate system have been orthonormalized according to (8)–(9), and that the phases have been chosen according to Eqs. (5). This fixes the Gupta metric in the unprimed Lorentz system.

We are interested in the covariance of these formulas, so we want to show that in a new (primed) frame of reference the new eigenfunctions χ' of the new occupation-number operators $N_\mu'(K)$ can be chosen in such a way as to satisfy Eqs. (5′), (8′), and (9′); that is, Eqs. (5), (8), and (9) with primes.

It is sufficient to prove this covariance for infinitesimal Lorentz transformations only. For finite Lorentz transformations it then follows by integration.

For the sake of simplicity, we choose our x axis in the direction of the infinitesimal velocity v of the new (primed) Lorentz frame with respect to the old one. Let $b=v/c$, and $x^0=-x_0=ct$. Since the annihilation operators form a four-vector,[23] we then must have

$$\begin{aligned} a_0' &= a_0 + b\,a_1, \quad a_1' = a_1 + b\,a_0, \\ a_2' &= a_2, \quad a_3' = a_3\,. \end{aligned} \tag{10}$$

By (2) and (10), or by the tensor character of $N_{\mu\nu} = a_\mu^\dagger a_\nu$, it then follows, always for infinitesimal b, that

$$\begin{aligned} N_0' &= -a_0^\dagger a_0 - b(a_0^\dagger a_1 + a_1^\dagger a_0), \\ N_1' &= +a_1^\dagger a_1 + b(a_0^\dagger a_1 + a_1^\dagger a_0), \\ N_2' &= N_2, \quad N_3' = N_3, \end{aligned} \tag{11}$$

are the occupation-number operators in the primed Lorentz frame.[25]

The new simultaneous eigenfunctions χ' should now satisfy

$$N_\mu'(K)\,\chi' = n_{K\mu}\chi'\,. \tag{4a'}$$

We shall at once write down the solutions of (4a′) which fulfill our requirements. Expressed in terms of the old eigenfunctions χ of the operators $N_\mu(K)$, they are

$$\begin{aligned} \chi' = \chi &- b\textstyle\sum_k n_{k0}^{\frac{1}{2}}[n_{k1}+1]^{\frac{1}{2}}\chi(n_{k0}-1, n_{k1}+1) \\ &- b\textstyle\sum_k [n_{k0}+1]^{\frac{1}{2}} n_{k1}^{\frac{1}{2}}\chi(n_{k0}+1, n_{k1}-1), \end{aligned} \tag{12}$$

[24] See reference 1, Eqs. (16) and (20). Our $a_0 = -a^0$ corresponds to Gupta's $-C_0$.

[25] Here, N_μ' and N_μ are abbreviations for $N_\mu'(K)$ and $N_\mu(K)$ with the same invariant argument K. A four-vector f_λ inside the invariant region K, of course, changes its components to f_λ', as it transforms like a four-vector.

where the dummy index k stands for K (therefore $\sum_k$ for an "integration" over the $+k$-cone) with the small letter k used merely for avoiding some primes in the following.

Next, it must be proved that the functions (12) satisfy our requirements indeed. First, we shall show that they satisfy the relations (5a′–d′), that is, the relations (5) with primes on the χ and the a, where a_μ' is given by (10).

Starting with (5a′), we first compare its right-hand member $n_{K0}^{\frac{1}{2}}\chi'(n_{K0}-1)$ with $a_0(K)\,\chi'$. In each term of (12), operation of the unprimed $a_0(K)$ will lower by 1 the argument n_{K0} of the featured unprimed eigenfunction, at the same time multiplying the term by the square root of the original number of $K0$ photons (=photons "scalar" with respect to the old frame of reference and with the proper wave vectors inside K). This yields a factor $n_{K0}^{\frac{1}{2}}$ for most terms of the expansions (12). The only exceptions are the terms with $k=K$ in the two sums. These terms become

$$-b\,n_{K0}^{\frac{1}{2}}[n_{K0}-1]^{\frac{1}{2}}[n_{K1}+1]^{\frac{1}{2}}\chi(n_{K0}-2,\,n_{K1}+1) - b\,[n_{K0}+1]\,n_{K1}^{\frac{1}{2}}\chi(n_{K0},\,n_{K1}-1).$$

In $n_{K0}^{\frac{1}{2}}\chi'(n_{K0}-1)$, on the other hand, we find similar terms, except

$$-b\,n_{K0}^{\frac{1}{2}}[n_{K0}-1]^{\frac{1}{2}}[n_{K1}+1]^{\frac{1}{2}}\chi(n_{K0}-2,\,n_{K1}+1) - b\,n_{K0}\,n_{K1}^{\frac{1}{2}}\chi(n_{K0},\,n_{K1}-1)$$

for the terms with $k=K$ in the two sums. Thence,

$$n_{K0}^{\frac{1}{2}}\chi'(n_{K0}-1)=a_0(K)\,\chi' + b\,n_{K1}^{\frac{1}{2}}\chi(n_{K0},\,n_{K1}-1). \tag{13}$$

The last term here is just $b\,a_1(K)\,\chi$. Since the difference between this and $b\,a_1(K)\,\chi'$ is quadratic in the infinitesimal b and therefore is to be neglected, Eq. (13) by Eq. (10) just gives the desired Eq. (5a′).

The other primed equations (5b′), (5c′), (5d′) can be verified similarly. The minus sign in Eq. (5b) causes no trouble at all, but combines in just the right way with the other signs in Eqs. (5d), (10), and (12).

Thus, the functions χ' given by (12) will for an observer in the primed frame of reference take the place which the functions χ take for an observer in the unprimed frame of reference. Just as (4a) by (2) followed from the Eqs. (5a–d), now (4a′) will follow from the validity of Eqs. (5a′–d′) by the relation (2′), or its equivalent (11).

This completes most of our task. The only thing yet to be verified is the automatic validity of the rule of norms in the primed Lorentz frame. That is, we should verify that $\chi'^{\dagger}\psi'$ satisfies Eqs. (8′)–(9′) as in Eq. (14) below, if $\chi'^{\dagger}$ is given by the adjoint (12†) of Eq. (12), while ψ' is given by an equation (12ψ) obtained from (12) by changing χ into ψ and $n_{K\mu}$ into $m_{K\mu}$.

The proof is easy. The expression (12) was written as a sum of three terms, say, $(12)_1+(12)_2+(12)_3$, so

$$\chi'^{\dagger}\psi'=[(12^{\dagger})_1+(12^{\dagger})_2+(12^{\dagger})_3]\cdot[(12\psi)_1+(12\psi)_2+(12\psi)_3].$$

Now, $[(12^{\dagger})_2+(12^{\dagger})_3][(12\psi)_2+(12\psi)_3]$ is infinitesimal of second order and can be omitted. Further,

$$(12^{\dagger})_2(12\psi)_1+(12^{\dagger})_1(12\psi)_3 = [-b\sum_k n_{k0}^{\frac{1}{2}}[n_{k1}+1]^{\frac{1}{2}}\{\chi^{\dagger}(n_{k0}-1,\,n_{k1}+1)\cdot\psi\} - b\sum_k\{\chi^{\dagger}\cdot\psi(m_{k0}+1,\,m_{k1}-1)\}[m_{k0}+1]^{\frac{1}{2}}m_{k1}^{\frac{1}{2}}]=0,$$

as by (9) the two expressions { } are nonvanishing for $n_{k0}=m_{k0}+1$, $n_{k1}+1=m_{k1}$ only, and then these expressions have opposite signs on account of (8). Similarly, $(12^{\dagger})_3(12\psi)_1+(12^{\dagger})_1(12\psi)_2=0$. Thus, we are left with $(12^{\dagger})_1(12\psi)_1$ only; that is,

$$\chi'^{\dagger}\psi'=\chi^{\dagger}\psi=(-1)^{\sum_K n_{K0}}\prod_\mu\prod_K\delta(n_{K\mu},m_{K\mu}), \tag{14}$$

where we have finally used Eqs. (8)–(9) without primes.

Equation (14) then shows the validity of the rule of norms in the primed Lorentz frame, so that this completes our proof.

We thus find that the minus signs in Gupta's metric do not cause any difficulty in the demonstration of the covariance of his theory, but always combine with each other in such a way that this covariance is maintained.

APPENDIX

We shall show here the covariance of the occupation numbers for a photon field in interaction representation. In particular, we shall show that they form tensors together with the repolarization operators given by Eq. (1).

For an electromagnetic field in interaction representation, expand the positive-energy part $A_\mu^{+}(x)$ of the potential four-vector as a Fourier integral in four dimensions:

$$A_\mu^{+}(x) = (2\pi)^{-2}(2hc)^{\frac{1}{2}}C\int_{(k^0>0)}d^{(4)}k \times\delta(k_\lambda k^\lambda)A_\mu(k)\exp(ik_\sigma x^\sigma). \tag{A1}$$

The factor $\delta(k_\lambda k^\lambda)$ here ensures vanishing of the Fourier components except on the half-cone $k^0=+|\mathbf{k}|$, which we shall call the "$+k$-cone." Similarly, we shall call $k^0=-|\mathbf{k}|$ the "$-k$-cone." Our Greek indices take the values 0, 1, 2, 3; never 4. The electrostatic potential is $A^0=-A_0$, and $x^0=-x_0=ct$. The numerical constants have been chosen for future convenience; $C=(4\pi)^{\frac{1}{2}}$ in the Gaussian system, and $C=1$ in the Heaviside-Lorentz system. By $\int_{(k^0>0)}d^{(4)}k$ we understand integration over any four-dimensional region which contains all of the $+k$-cone but nothing of the $-k$-cone. The total potential $A_\mu=A_\mu^{+}+A_\mu^{-}=A_\mu^{+}+(A_\mu^{+})^{\dagger}$ is "self-adjoint" in the sense that its components have real expectation values.[1]

Four-vectors on the $+k$ cone we shall denote by $\mathfrak{k}$. Three parameters suffice to determine such a four-vector; for instance, the three components of its spatial part $\mathbf{k}$. Use of $\mathbf{k}$ for denoting $\mathfrak{k}$ does not destroy the covariance of our notation. While $\mathbf{k}$ is not invariant under Lorentz transformation, as space part of $\mathfrak{k}$ it is perfectly covariant, that is, its Lorentz transformations as the space part of a four-vector with

$$k^0=(k_x^2+k_y^2+k_z^2)^{\frac{1}{2}}$$

are well-defined (although not linear).

We define covariant integration over the $+k$-cone as follows. Let $K4$ denote an arbitrary four-dimensional volume in k space not intersecting the $-k$-cone, but intersecting the $+k$-cone by K. Let $F(\mathfrak{k})$ be a function of $\mathfrak{k}$ to be covariantly integrated over K. Then, let $F(k)$ be a function of the four-vector k, arbitrary except for its identity with $F(\mathfrak{k})$ on the $+k$-cone. Integration of $F(\mathfrak{k})$ over K shall then be defined Lorentz-covariantly by

$$\int_K F(\mathfrak{k})\,dV(\mathfrak{k})=2\int_{K4}F(k)\,\delta(k_\lambda k^\lambda)\,d^{(4)}k. \quad \text{(A2)}$$

Because of the delta-function, the shape of $K4$ outside the $+k$-cone and the values of $F(k)$ off the $+k$-cone do not matter. The factor 2 is for convenience: by

$$\delta(k_\lambda k^\lambda)=\delta(\mathbf{k}^2-k_0^2)=[\delta(|\mathbf{k}|-k^0)]/|2\mathbf{k}|$$

around the $+k$-cone, it enables us to write (A2) as

$$\int_K F(\mathfrak{k})\,dV(\mathfrak{k})=\int_{\mathbf{K}}F(\mathfrak{k})\,d^{(3)}\mathbf{k}/|\mathbf{k}|, \quad \text{(A3)}$$

where $\mathbf{K}$ is the projection of K on the $k_xk_yk_z$ hyperplane. Thence,

$$dV(\mathfrak{k})=d^{(3)}\mathbf{k}/|\mathbf{k}| \quad \text{(A4)}$$

can be regarded as the invariant "volume element on the $+k$-cone" corresponding to the definition (A2). (Never mind its dimensions!) The invariant "volume" of a finite domain K on the $+k$-cone is

$$V(K)=\int_K dV(\mathfrak{k})=\int_{\mathbf{K}}d^{(3)}\mathbf{k}/|\mathbf{k}|. \quad \text{(A5)}$$

We define the "German-$\mathfrak{d}$ function" on the $+k$-cone by

$$\int_K F(\mathfrak{k})\,\mathfrak{d}(\mathfrak{k}-\mathfrak{k}')\,dV(\mathfrak{k})=F(\mathfrak{k}')\,\delta(\mathfrak{k}',K), \quad \text{(A6)}$$

where

$$\mathfrak{d}(\mathfrak{k}',K)=\int_K\mathfrak{d}(\mathfrak{k}-\mathfrak{k}')\,dV(\mathfrak{k})=\begin{cases}=1, \text{ if } \mathfrak{k}' \text{ inside } K,\\ =0, \text{ if } \mathfrak{k}' \text{ outside } K.\end{cases} \quad \text{(A7)}$$

From (A3) with (A6) we easily see that, in any Lorentz frame, the invariant German-$\mathfrak{d}$ function may be written as

$$\mathfrak{d}(\mathfrak{k}-\mathfrak{k}')=|\mathbf{k}|\,\delta^{(3)}(\mathbf{k}-\mathbf{k}'). \quad \text{(A8)}$$

With this notation we may write (A1) and its adjoint as

$$\begin{aligned}A_\nu^+(x)&=\tfrac{1}{4}\hbar^{\frac{1}{2}}c^{\frac{1}{2}}\pi^{-3/2}C\int_\infty A_\nu(\mathfrak{k})\exp(i\mathfrak{k}_\sigma x^\sigma)dV(\mathfrak{k}),\\ A_\mu^-(x)&=\tfrac{1}{4}\hbar^{\frac{1}{2}}c^{\frac{1}{2}}\pi^{-3/2}C\int_\infty A_\mu^\dagger(\mathfrak{k}')\\ &\qquad\times\exp(-i\mathfrak{k}_\sigma' x^\sigma)\,dV(\mathfrak{k}').\end{aligned} \quad \text{(A9)}$$

Here, $\int_\infty$ denotes integration over the entire $+k$-cone. Using Schwinger's notation of the D^+ function,[26] which in our notation may be written as

$$D^+(x)=(16\pi^3 i)^{-1}\int_\infty\exp(i\mathfrak{k}_\sigma x^\sigma)\,dV(\mathfrak{k}), \quad \text{(A10)}$$

the commutation rules for $A_\mu=A_\mu^+ + A_\mu^-$ can be expressed by

$$\begin{aligned}[A_\nu^+(x)\,;A_\mu^-(x')]&=i\hbar C^2 g_{\nu\mu}D^+(x-x'),\\ [A_\nu^+(x)\,;A_\mu^+(x')]&=[A_\nu^-(x)\,;A_\mu^-(x')]=0,\end{aligned} \quad \text{(A11)}$$

with $g_{00}=-1$, $g_{11}=g_{22}=g_{33}=+1$, and $[A\,;B]=AB-BA$. They can also be expressed covariantly, on account of Eqs. (A9), (A6), (A10), and $A_\nu=g_{\nu\lambda}A^\lambda$, by

$$\left.\begin{aligned}[A^\lambda(\mathfrak{k})\,;A_\mu^\dagger(\mathfrak{k}')]&=\delta_\mu^{\ \lambda}\,\mathfrak{d}(\mathfrak{k}-\mathfrak{k}'),\\ [A^\lambda(\mathfrak{k})\,;A^\nu(\mathfrak{k}')]&=[A_\mu^\dagger(\mathfrak{k})\,;A_\nu^\dagger(\mathfrak{k}')]=0.\end{aligned}\right\} \quad \text{(A12)}$$

Now consider the free-photon energy and momentum four-vector G^λ. Performing the necessary[27] subtraction of the meaningless infinite vacuum energy, we find[28]

$$G^\lambda=\int_\infty\hbar c\mathfrak{k}^\lambda\,A_\mu^\dagger(\mathfrak{k})A^\mu(\mathfrak{k})\,dV(\mathfrak{k}). \quad \text{(A13)}$$

This result suggests that

$$N_\mu(K)=\int_K A_\mu^\dagger(\mathfrak{k})A^\mu(\mathfrak{k})\,dV(\mathfrak{k}) \text{ (no sum over } \mu) \quad \text{(A14)}$$

should be regarded as the number of "incident" photons[11,15–17] of polarization μ and with energy-momentum four-vectors given by wave vectors $\mathfrak{k}$ inside the region K on the $+k$-cone. Evidently the $N_\mu(K)$ are the diagonal components of a mixed tensor

$$N_\mu^{\ \nu}(K)=\int_K A_\mu^\dagger(\mathfrak{k})A^\nu(\mathfrak{k})\,dV(\mathfrak{k}). \quad \text{(A15)}$$

The $N_\mu^{\ \nu}(K)$ for $\mu\neq\nu$ one might call the "repolarization operators," as they describe a change in polarization direction of a photon.

If K is an infinitesimal domain dK on the $+k$-cone, $N_\mu^{\ \nu}(K)$ may be denoted by $dN_\mu^{\ \nu}$:

$$dN_\mu^{\ \nu}=A_\mu^\dagger(\mathfrak{k})\,A^\nu(\mathfrak{k})\,dV(\mathfrak{k}). \quad \text{(A16)}$$

From (A13) and (A16) we obtain

$$G^\lambda=\int_\infty\hbar c\mathfrak{k}^\lambda\,dN_\mu^{\ \mu}. \quad \text{(A17)}$$

Our interpretation of $N_\mu(K)$ as an occupation number, and an interpretation of $A^\lambda(\mathfrak{k})$ and $A_\lambda^\dagger(\mathfrak{k})$ as

[26] J. Schwinger, Phys. Rev. **75**, 651 (1949).
[27] F. J. Belinfante, Phys. Rev. **76**, 461 (1949).
[28] J. L. Lopes, Anais acad. brasil. cienc. **23**, 39 (1951), Eq. (22).

absorption (=annihilation) and emission (=creation) operators for an incident photon of momentum $\hbar\mathbf{k}$, are justified by the following relations, which follow from Eqs. (A15), (A12), and (A7). First,

$$[A^\lambda(\mathbf{f})\,;N_\mu{}^\nu(K)]=\delta_\mu{}^\lambda\,\delta(\mathbf{f},K)\,A^\nu(\mathbf{f}),$$
$$[A_\lambda{}^\dagger(\mathbf{f})\,;N_\mu{}^\nu(K)]=-\delta_\lambda{}^\nu\,\delta(\mathbf{f},K)\,A_\mu{}^\dagger(\mathbf{f}). \tag{A18}$$

Thence, if $N_\mu(K)\chi_n=n\chi_n$,

$$N_\mu(K)\{A^\lambda(\mathbf{f})\chi_n\}=[n-\delta_\mu{}^\lambda\delta(\mathbf{f},K)]\{A^\lambda(\mathbf{f})\chi_n\},$$
$$N_\mu(K)\{A_\lambda{}^\dagger(\mathbf{f})\chi_n\}=[n+\delta_\lambda{}^\mu\delta(\mathbf{f},K)]\{A_\lambda{}^\dagger(\mathbf{f})\chi_n\}. \tag{A19}$$

Therefore, if we start from the eigenfunction χ_n belonging to the eigenvalue n of $N_\mu(K)$, application of the operator $A^\mu(\mathbf{f})$ with $\mathbf{f}$ inside K makes an eigenfunction belonging to $(n-1)$, and $A_\mu{}^\dagger$ makes an eigenfunction belonging to the eigenvalue $(n+1)$. By successive applications of these operators one can construct eigenfunctions corresponding to "stepladders" of eigenvalues $n\pm1$, $n\pm2$, $n\pm3$, $\cdots$. Now, using Eq. (A17) in Gupta's new definition of the indefinite metric,[29] we find that not only $dN_j=A_j{}^\dagger A_j\,dV(\mathbf{f})$ with $j=1, 2, 3$, but also $dN_0=-A_0{}^\dagger A_0\,dV(\mathbf{f})$ cannot have bottomless stepladders of eigenvalues, so that obviously the stepladders for dN_μ downwards must break off. However, they can break off, say beneath a bottom step m, only if for all attempts to go down below m by applying another time $A^\mu(\mathbf{f})$ with $\mathbf{f}$ inside K one always finds $A^\mu(\mathbf{f})\chi_m=0$. Then, however, by (A14), also $N_\mu(K)\chi_m=0$; that is, $m=0$ must be the bottom of every "stepladder" of eigenvalues. From here upwards, by successive applications of $A_\mu{}^\dagger(\mathbf{f})$ with $\mathbf{f}$ inside K, one then finds eigenfunctions belonging to the eigenvalues 1, 2, 3, $\cdots$. This fact, combined with the Eqs. (A19) furnishes the justifications we wanted.

Now, state vectors describing photon fields may be expanded in terms of the simultaneous eigenfunctions of the occupation numbers $N_\mu(K)$ for the various regions K on the $+k$-cone. For this purpose, the $+k$-cone is subdivided into a large number of very small regions K, each so small that we cannot measure differences of $\mathbf{f}$ inside such a region. Therefore, the only absorption and emission operators that correspond to observably distinct changes of the state of the photon field, are obtained by bunching together all operators $A_\mu(\mathbf{f})$ inside each such small finite region. Let us therefore define covariantly

$$\mathfrak{A}^\mu(K)=\int_K A^\mu(\mathbf{f})\,dV(\mathbf{f}),$$
$$\mathfrak{A}_\mu{}^\dagger(K)=\int_K A_\mu{}^\dagger(\mathbf{f})\,dV(\mathbf{f}). \tag{A20}$$

Now, if two regions K and K' would have a part in common, which we shall denote by $K\bigcap K'$, then the "volume" of this common region, given by (A5), can be written by (A7) as

$$V(K\bigcap K')=\int_K\delta(\mathbf{f},K')\,dV(\mathbf{f})$$
$$=\int_K dV(\mathbf{f})\int_{K'}dV(\mathbf{f}')\,\delta(\mathbf{f}-\mathbf{f}'). \tag{A21}$$

From (A20), (A12), and (A21) we then find

$$[\mathfrak{A}^\lambda(K)\,;\mathfrak{A}_\mu{}^\dagger(K')]=\delta_\mu{}^\lambda\,V(K\bigcap K'). \tag{A22}$$

Similarly, from (A20) and (A18),

$$[\mathfrak{A}^\lambda(K)\,;N_\mu{}^\nu(K')]=\delta_\mu{}^\lambda\,\mathfrak{A}^\nu(K\bigcap K'),$$
$$[\mathfrak{A}_\lambda{}^\dagger(K)\,;N_\mu{}^\nu(K')]=-\delta_\lambda{}^\nu\,\mathfrak{A}_\mu{}^\dagger(K\bigcap K'). \tag{A23}$$

By putting $\nu=\mu$ (no sum over μ!) we obtain from (A23) commutation relations between $\mathfrak{A}_\lambda$ and N_μ.

In practice, subdivisions of the $+k$-cone are made in such a way that the different regions K and K' either completely coincide, or are completely separate. Therefore we may introduce Kronecker symbols $\delta_{KK'}$, which are $=1$ and $=0$, respectively, for these two possibilities. We also introduce new four-vector operators a_λ and $a_\lambda{}^\dagger$, by

$$a_\lambda(K)=V(K)^{-\frac{1}{2}}\,\mathfrak{A}_\lambda(K). \tag{A24}$$

Thus, the commutation relations (A22)–(A23) become

$$[a^\lambda(K)\,;a_\mu{}^\dagger(K')]=\delta_\mu{}^\lambda\,\delta_{KK'}; \tag{A25}$$

$$[a^\lambda(K)\,;N_\mu{}^\nu(K')]=\delta_\mu{}^\lambda\,\delta_{KK'}\,a^\nu(K),$$
$$[a_\lambda{}^\dagger(K)\,;N_\mu{}^\nu(K')]=-\delta_\lambda{}^\nu\,\delta_{KK'}\,a_\mu{}^\dagger(K). \tag{A26}$$

By a reasoning similar to that applied to Eqs. (A18) in and below Eqs. (A19), we conclude from Eqs. (A26) that $a^\mu(K)$ and $a_\mu{}^\dagger(K)$ are annihilation and creation operators for the occupation numbers $N_\mu(K)$. In order to find the matrix elements of the operators $a^\mu(K)$ between normalized eigenfunctions of the operators $N_\mu(K)$, however, we would need one more relation, *viz.*, the analog of Eq. (A16).

While the above equations are valid for any subdivision of the $+k$-cone into regions K, whatever large these are taken, we will not be able to express $N_\mu(K)$ in terms of $a_\mu{}^\dagger(K)$ and $a^\mu(K)$ for arbitrarily large domains K. One might think of by-passing this difficulty by defining new operators

$$N_\mu{}^\nu(K)=a_\mu{}^\dagger(K)a^\nu(K);\quad N_\mu\equiv N_\mu{}^\mu\ (\text{no sum!}). \tag{A27}$$

Truly enough, the operators $N_\mu(K)$ have eigenvalues 0, 1, 2, $\cdots$, and the $a_\mu(K)$ and $a_\mu{}^\dagger(K)$ are absorption and emission operators for them. The catch, however, is that for arbitrarily large regions K the operators $N_\mu(K)$ do not represent the true occupation numbers in which the physicist is interested. This interest stems from the possibility of expressing the energy and momentum in the form of Eq. (A17). From (A17) we see that dN_μ is the occupation number for an infinitesimal region dK. The physicist then wants to define the occupation number for finite K as the integral of dN_μ. By (A14), this integral is $N_\mu(K)$, not $N_\mu(K)$.

[29] See the text above footnote 20.

In fact, while $N_\mu(K)$ by (A14) has the desirable property $N_\mu(K_1+K_2)=N_\mu(K_1)+N_\mu(K_2)$, the operators $N_\mu(K)$ by (A27) with (A24) and (A20) do not even have this additive property, and therefore cannot be interpreted as the proper occupation number for any finite K which meaningfully may be cut up into smaller parts.

The way out of this difficulty is by taking the size of the regions K as small as we suggested above the Eqs. (A20). We might call these regions then "physically infinitesimal."[30] In this case, our various covariant definitions may be simplified. Equations (A15), (A20), and (A24) may then, by (A5), be re-written as

$$N_\mu{}^\nu(K) \approx A_\mu{}^\dagger(\mathbf{f})\, A^\nu(\mathbf{f})\, V(K), \qquad \text{(A15a)}$$

$$\mathfrak{A}_\mu(K) \approx A_\mu(\mathbf{f})\, V(K), \qquad \text{(A20a)}$$

$$a_\mu(K)=V(K)^{-\frac{1}{2}}\,\mathfrak{A}_\mu(K) \approx V(K)^{\frac{1}{2}}\,A_\mu(\mathbf{f}), \qquad \text{(A24a)}$$

where $\mathbf{f}$ may have any value inside K, and where $\approx$ denotes experimental indistinguishability. From (A15a) and (A24a), then, we find for such small K

$$N_\mu{}^\nu(K) \approx a_\mu{}^\dagger(K)\, a^\nu(K)=N_\mu{}^\nu(K). \qquad \text{(A28)}$$

Equations (A25), (A26), and (A28) then determine in the usual way[1] the matrix elements of the emission and absorption operators $a_\mu{}^\dagger(K)$ and $a_\mu(K)$ between states characterized by the occupation numbers $N_\mu(K) \approx N_\mu(K)$. [Compare Eqs. (5a–d).]

Finally, replacing the integrals in (A9) by sums over the arbitrarily but invariantly chosen cells K on the $+k$-cone, we may write the potential four-vector $A_\mu(x)$ in terms of the matrices $a_\mu(K)$ and $a_\mu{}^\dagger(K)$, as

$$A_\mu(x)=\tfrac{1}{4}\hbar^{\frac{1}{2}}c^{\frac{1}{2}}\pi^{-3/2}C\sum_K V(K)^{\frac{1}{2}}\times \{a_\mu(K)\exp(i\mathbf{f}_\sigma x^\sigma)+a_\mu{}^\dagger(K)\exp(-i\mathbf{f}_\sigma x^\sigma)\}. \qquad \text{(A29)}$$

This covariant expression contains as a special case the familiar expression

$$A_\mu(x)=\tfrac{1}{4}\hbar^{\frac{1}{2}}c^{\frac{1}{2}}\mathcal{V}^{-\frac{1}{2}}\sum_{\mathbf{k}}(2|\mathbf{k}|)^{-\frac{1}{2}}\times \{a_\mu(K)\exp(i\mathbf{f}_\sigma x^\sigma)+a_\mu{}^\dagger(K)\exp(-i\mathbf{f}_\sigma x^\sigma)\}, \qquad \text{(A30)}$$

in which one sums over a discrete set of $\mathbf{k}$ values forming a cubic lattice in such a way that there is one "allowed" $\mathbf{k}$ value for each cubic volume element $\mathbf{K}$ of size

$$d^{(3)}\mathbf{k}=(2\pi)^3\mathcal{V}^{-1} \qquad \text{(A31)}$$

in three-dimensional $\mathbf{k}$ space. Here, $\mathbf{f}_\sigma$ has the components $\mathbf{k}$ and $k_0=-k^0=-|\mathbf{k}|$.

In order to see the equivalence of (A30) to (A29), we make for the latter a special subdivision of the $+k$-cone into cells K in such a way that the projection of each cell K onto the $k_xk_yk_z$ hyperplane will coincide with one cubic cell $\mathbf{K}$ of volume (A31) containing just one of the $\mathbf{k}$ values, over which we sum in (A30). But then, by (A4), the corresponding "invariant volume on the $+k$-cone" of such a cell K will be equal to

$$V(K)=d^{(3)}\mathbf{k}/|\mathbf{k}|=(2\pi)^3\mathcal{V}^{-1}|\mathbf{k}|^{-1}. \qquad \text{(A32)}$$

If this is inserted in Eq. (A29), that equation takes the familiar form (A30) indeed.

This shows that Eq. (A30) is nothing more than Eq. (A29) written up for some special subdivision of the $+k$-cone, in which the constant $\mathcal{V}$ by (A31) simply tells how finely we are subdividing $\mathbf{k}$ space into cubes. There is no need, therefore, for the conventional interpretation of $\mathcal{V}$ as "the volume of a cubic world."

Under Lorentz transformations, then, the $a^\nu(K)$ and the $a_\mu{}^\dagger(K)$ transform like four vectors, and the $N_\mu{}^\nu(K)\approx N_\mu{}^\nu(K)$ for any "infinitesimal" region K on the $+k$-cone transform as a tensor. The region K itself is invariantly fixed on the $+k$-cone, and may be characterized by the four-vector(s) $\mathbf{f}_\sigma$ which it contains. The fact that someone in a particular Lorentz frame may have characterized it by the projection $\mathbf{k}$ of $\mathbf{f}$ onto $\mathbf{k}$ space—or may even have chosen this $\mathbf{k}$ as part of some cubic lattice, as in (A30)—does not effect the invariance of K or the covariance of the four-vector $\mathbf{f}$. Also, it does not matter that in a different Lorentz frame the projection of $\mathbf{f}$ onto the new $\mathbf{k}'$ space does not form part of any cubic lattice at all, since from (A29) it is clear that in subdividing the $+k$-cone into cells K it is *not necessary* to make the projections $\mathbf{k}$ form a cubic lattice, or even space them regularly as by (A31).

[30] Therefore, we could also denote them by dK. However, mathematically, these regions dK are finite. For, in the first place, there is no sense in making the subdivision into regions K much finer than what can be distinguished experimentally, as the state vector, expressed in terms of occupation numbers for these regions, should express our factual knowledge about the photon field, and not more than that. In the second place, we want them finite, as otherwise the definition (A24) would become meaningless.

Self-Energy Effects on Meson-Nucleon Scattering According to the Tamm-Dancoff Method*†

WILLIAM M. VISSCHER
University of Maryland, College Park, Maryland

(Received June 3, 1954)

The lowest-order Tamm-Dancoff equations for the meson-nucleon system are derived by the method of Cini, using the wave functions defined by Dyson. The contributions of the meson and nucleon self-energies to the kernel of the momentum-space integral equation are renormalized. Their effects are absorbed into the coupling G^2, making it momentum and energy dependent. The effective coupling turns out to exhibit an anomalous behavior, having a pole for a spacelike momentum, to which it is difficult to attach a sensible physical interpretation.

I. INTRODUCTION

CALCULATIONS of the meson-nucleon scattering phase shifts have recently been performed by the Tamm-Dancoff method.[1] This paper is essentially a continuation of one in which that undertaking is reported. The lowest-order Tamm-Dancoff equations were there derived and solved approximately by unmerical methods, with several of the terms in the kernel, namely, those which correspond to the nucleon, meson, and vacuum self-energies, and some which contribute to the interaction only in the $I=1/2, J=1/2$ state, simply dropped. It is the purpose of the present paper to ascertain the effects of the former omission on the scattering phase shifts; in other words, to find the renormalization corrections to the scattering in states in which either I or J, or both, are different from 1/2.

One of the omitted terms, the vacuum self-energy, may be eliminated by a simple redefinition of the Tamm-Dancoff amplitudes, as was shown by Dyson.[2] In addition, this redefinition makes possible a consistent relativistic renormalization of mass and charge.[3]

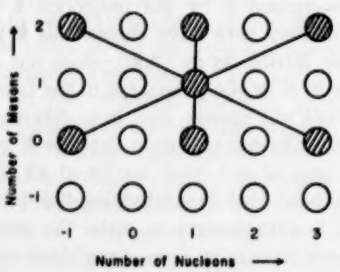

FIG. 1. Intermediate states of the meson-nucleon scattering system which are allowed in the Tamm-Dancoff approximation. Vertically is plotted the number of mesons present in the real state in excess of those present in the vacuum, horizontally the number of nucleons.

In order to perform a reliably unambiguous separation of the divergent parts of the self-energy integrals, it is essential to write them in a covariant form. For this purpose we use the method of Cini,[4] applied to the DTD theory.

In Part III we reduce the equations derived in Part II to a form similar to that obtained formerly.[1] They turn out to be, in fact, identical, except for some of the self-energy terms, and one of the terms that occurs only in the $I=1/2$, $J=1/2$ state. Thus the self-energy corrections which will be derived in Part IV may be applied to the phase shifts calculated previously.[1] The results are discussed in Part V.

II. THE CINI METHOD APPLIED TO THE DTD EQUATIONS

We define a two-particle amplitude,

$$\Phi_{\rho\alpha}(x, y; t)=(\Psi_0^*(t)\psi_\rho(x)\phi_\alpha(y)\Psi(t)), \qquad (1)$$

where $\Psi_0(t)$ is the interacting vacuum state in the interaction representation, $\Psi(t)$ is the real state vector in the interaction representation, and $\psi_\rho(x)$ and $\phi_\alpha(y)$ are interaction representation operators for the nucleon and meson fields, respectively. x and y need not be on the spacelike surface t. $\Psi(t)$ and $\Psi_0(t)$ satisfy the Schrödinger equation,

$$id\Psi(t)/dt=H_I(t)\Psi(t). \qquad (2)$$

It is a consequence of Eqs. (1) and (2) that

$$\Phi_{\rho\alpha}(x, y; t)-\Phi_{\rho\alpha}(x, y; -\infty)=-\int_{-\infty}^{t}dt'\int_{-\infty}^{t'}dt''$$

$$\times(\Psi_0^*(t'')[H_I(t''), [H_I(t'), \psi_\rho(x)\phi_\alpha(y)]]\Psi(t'')), \qquad (3)$$

if one requires that the initial state $\Psi(-\infty)$ be a state with one meson present.

We choose Eq. (3) as the fundamental equation for our system, because it will yield results in a simple way which are equivalent to the lowest-order Tamm-Dancoff approximation. The Tamm-Dancoff approximation as applied to Eq. (3) may be stated in the following manner. One arranges the operators occurring

* Part of this paper has been submitted to the Graduate School of Cornell University in partial fulfillment of its requirements for for Ph.D. degree.

† Supported in part by the Office of Naval Research.

[1] Bethe, Dyson, *et al.*, Phys. Rev. (to be published); M. Fubini, Nuovo cimento **10**, 564 (1953).

[2] F. J. Dyson, Phys. Rev. **90**, 994 (1953). We shall call Dyson's modification of the Tamm-Dancoff theory, the DTD theory.

[3] F. J. Dyson, Phys. Rev. **91**, 421, 1543 (1953).

[4] M. Cini, Nuovo cimento **10**, 526 (1953).

in the integrand in the normal order (absorption operators to the right of emission operators), yielding a sum of terms of the general form of $\Phi(x, y; t)$, possibly containing more than two field operators. We then drop all the terms except those having exactly the form of $\Phi(x, y; t)$. That this procedure is equivalent to the usual Tamm-Dancoff approximation may be seen in the following way. An array of states can be constructed (Fig. 1) which helps the enumeration of the nonzero matrix elements of the interaction Hamiltonian H_I. Since H_I contains two nucleon field operators and one meson operator, the nonzero elements are only those between states which differ by zero or two nucleons, and by one meson. The lines in Fig. 1 represent matrix elements which connect the "ground state" (1 meson, 1 nucleon in state Ψ in excess of those in Ψ_0) to other states. It is clear that our approximation is equivalent to the Tamm-Dancoff approximation which restricts the allowed states of the system to the cross-hatched circles in Fig. 1.

When the above procedure has been carried out, we shall be left with an integral equation for $\Phi_{\rho\alpha}(x, y; t)$ similar in appearance to the lowest-order Bethe-Salpeter equation for the meson-nucleon system, with the important difference that our field operators are in the interaction representation, and their time dependence is known.

Inserting

$$H_I(x_0)=\int d^3x H_I(x),$$

where

$$H_I(x)=iG\bar{\psi}(x)\gamma_5\tau_\alpha\phi_\alpha(x)\psi(x), \tag{4}$$

into Eq. (3), we obtain

$$\Phi_{\rho\alpha}(x, y; t)-\Phi_{\rho\alpha}(x, y; -\infty)=G^2\int_{-\infty}^{t}dz\int_{-\infty}^{z_0}dw$$
$$\times(\Psi_0^*(w_0)[\bar{\psi}(w)\gamma_5\tau_\beta\phi_\beta(w)\psi(w),$$
$$[\bar{\psi}(z)\gamma_5\tau_\delta\phi_\delta(z)\psi(z), \psi_\rho(x)\phi_\alpha(y)]]\Psi(w_0)), \tag{5}$$

where

$$\int_{-\infty}^{t}dz \text{ means } \int_{-\infty}^{t}dz_0\int d^3\mathbf{z}.$$

The double commutator in Eq. (5) may, without much difficulty, be put into normal order; if one retains only those terms which correspond to a one-meson, one-nucleon amplitude, it becomes

$$-3iS(x-z)\gamma_5[1+\epsilon(z-w)P][\langle\phi(w)\phi(z)\rangle_0$$
$$\times\langle\bar{\psi}(w)\psi(z)\rangle_0]\gamma_5\phi_\alpha(y)\psi(w) \tag{6a}$$
$$-2i\Delta(y-z)(1-P)\,\mathrm{Sp}[\gamma_5\langle\bar{\psi}(w)\psi(z)\rangle_0\gamma_5$$
$$\times\langle\psi(w)\bar{\psi}(z)\rangle_0]\phi_\alpha(w)\psi_\rho(x) \tag{6b}$$
$$+[\langle\phi(z)\phi(y)\rangle_0\langle\bar{\psi}(z)\psi(x)\rangle_0+\langle\phi(y)\phi(z)\rangle_0\langle\psi(x)\bar{\psi}(z)\rangle_0]$$
$$\times\gamma_5(1+\epsilon(z-w)P)\langle\bar{\psi}(w)\psi(z)\rangle_0\gamma_5\tau_\alpha\tau_\beta\phi_\beta(w)\psi(w) \tag{6c}$$
$$+i\Delta(y-z)[\langle\psi(w)\psi(z)\rangle_0\gamma_5\langle\psi(w)\bar{\psi}(z)\rangle_0$$
$$-\langle\psi(x)\bar{\psi}(w)\rangle_0\gamma_5\langle\bar{\psi}(z)\psi(w)\rangle_0]\gamma_5\tau_\beta\tau_\alpha\phi_\beta(w)\psi(z) \tag{6d}$$
$$-iS(x-z)[\langle\phi(w)\phi(y)\rangle_0\gamma_5\langle\bar{\psi}(w)\psi(z)\rangle_0$$
$$+\langle\phi(y)\phi(w)\rangle_0\gamma_5\langle\psi(z)\bar{\psi}(w)\rangle_0]\gamma_5\tau_\beta\tau_\alpha\phi_\beta(z)\psi(w). \tag{6e}$$

By application of the usual rules for drawing the Feynman diagram corresponding to a given S-matrix element, the terms (6a)–(6e) may be seen to correspond to the time-ordered graphs drawn in Fig. 2. It will be noticed that the graphs (a), (b), and (c) occur alone, without their negative-energy intermediate state analogs, and that the vacuum self-energy fails to appear at all, in contrast to what one finds with the old Tamm-Dancoff method.[2] The reason that these terms do not appear is that the structure of the commutator in Eq. (5) is such that any Feynman diagram representing parts of it must have a line connecting z with x or y, or both.

If we next insert the propagation functions defined by[5]

$$\begin{aligned}
P\langle\phi(x)\phi(y)\rangle_0&=\tfrac{1}{2}\Delta_F(x-y),\\
\epsilon(x-y)P\langle\psi(x)\bar{\psi}(y)\rangle_0&=-\tfrac{1}{2}S_F(x-y),\\
\langle\psi(z)\bar{\psi}(y)\rangle_0&=-iS^+(z-y)\\
&=-iS_A{}^+(z-y)\quad z_0<y_0\\
&=+iS_R{}^+(z-y)\quad z_0>y_0,\\
\langle\bar{\psi}(y)\psi(z)\rangle_0&=-iS_A{}^-(z-y)\quad z_0<y_0\\
&=+iS_R{}^-(z-y)\quad z_0>y_0,\\
\langle\phi(z)\phi(y)\rangle_0&=+i\Delta_A{}^+(z-y)\quad z_0<y_0\\
&=-i\Delta_R{}^+(z-y)\quad z_0>y_0,\\
\langle\phi(y)\phi(z)\rangle_0&=-i\Delta_A{}^-(z-y)\quad z_0<y_0\\
&=+i\Delta_R{}^-(z-y)\quad z_0>y_0
\end{aligned} \tag{7}$$

for the vacuum expectation values in (6d) and (6e) which depend on field operators at w and z, we may extend the integration over w in (5) to all space-time, because (6a), (6b), and (6c) are already zero when $z_0<w_0$. The result of this substitution is that (5)

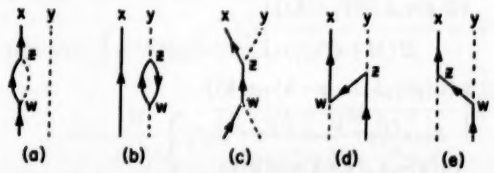

FIG. 2. Feynman diagrams corresponding to the terms of Eq. (6). Time increases vertically.

[5] F. J. Dyson, Phys. Rev. **75**, 1736 (1949).

becomes

$$\Phi_\alpha(x,y;t)-\Phi_\alpha(x,y;-\infty)=iG^2\int_{-\infty}^{t}dz\int_{-\infty}^{\infty}dw$$
$$\times\{[3S(x-z)\gamma_5\Delta^-(z-w)S^-(z-w)$$
$$+\tfrac{3}{4}S(x-z)\gamma_5\Delta_F(z-w)S_F(z-w)\gamma_5]\Phi_\alpha(w,y;w_0)$$
$$+\Delta(y-z)\,\mathrm{Sp}[2\gamma_5S^-(z-w)\gamma_5S^+(w-z)$$
$$+\tfrac{1}{2}\gamma_5S_F(z-w)\gamma_5S_F(w-z)]\Phi_\alpha(x,w;w_0)$$
$$+\tfrac{1}{2}i[-\Delta^-(y-z)S^-(x-z)+\Delta^+(y-z)S^+(x-z)]\gamma_5$$
$$\times[2iS^-(z-w)+S_F(z-w)]\gamma_5\tau_\alpha\tau_\beta\Phi_\beta(w,w;w_0)$$
$$+\Delta(y-z)[-S^-(x-w)\gamma_5S_A{}^+(w-z)$$
$$+S^+(x-w)\gamma_5S_A{}^-(w-z)]\gamma_5\tau_\beta\tau_\alpha\Phi_\beta(z,w;w_0)$$
$$+S(x-z)[-\Delta^-(y-w)\gamma_5S_R{}^-(z-w)$$
$$+\Delta^+(y-w)\gamma_5S_R{}^+(z-w)]\gamma_5\tau_\beta\tau_\alpha\Phi_\beta(w,z,w_0)\}. \quad (8)$$

III. REDUCTION TO THE NONCOVARIANT FORM

It will be noticed from the form of $\Phi(x,y;t)$ that it is nonzero in four different physical situations.[3] Specifically, decomposing ψ and ϕ into their positive and negative energy parts, one may write

$$\Phi(x,y;t)=\Phi^{++}+\Phi^{+-}+\Phi^{-+}+\Phi^{--}(x,y;t), \quad (9)$$

where, for example,

$$\Phi_{\rho\alpha}{}^{-+}(x,y;t)=(\Psi_0{}^*(t)\phi_\alpha{}^-(x)\psi_\rho{}^+(y)\Psi(t)).$$

This decomposition may be done explicitly here because the time dependence of the interaction representation operators ϕ and ψ is known. A nonzero Φ^{++} corresponds to having a meson and a nucleon in the state Ψ in excess of those in Ψ_0; Φ^{-+} to one more nucleon and one less meson, Φ^{+-} to one more meson and one less nucleon, Φ^{--} to one less meson and one less nucleon in Ψ than in Ψ_0. We will now operate from the left on Eq. (9) with a positive energy projection operator for both nucleons and mesons, yielding a somewhat simplified equation:

$$\Phi_\alpha{}^{++}(x,y;t)-\Phi_\alpha{}^{++}(x,y;-\infty)=iG^2\int_{-\infty}^{t}dz\int d\xi$$
$$\times\{[3S^+(x-z)\gamma_5\Delta^-(\xi)S^-(\xi)\gamma_5$$
$$+\tfrac{3}{4}S^+(x-z)\Delta_F(\xi)\gamma_5S_F(\xi)\gamma_5][\Phi_\alpha{}^{++}+\Phi_\alpha{}^{-+}]$$
$$\times(z-\xi,y;z_0-\xi_0)+\Delta^+(y-z)\,\mathrm{Sp}\{2\gamma_5S^-(\xi)\gamma_5S^+(-\xi)$$
$$-\tfrac{1}{2}\gamma_5S_F(\xi)\gamma_5S_F(-\xi)\}[\Phi_\alpha{}^{++}+\Phi_\alpha{}^{+-}](x,z-\xi;z_0-\xi_0)$$
$$+\tfrac{1}{2}i\Delta^+(y-z)S^+(x-z)\gamma_5[2iS^-(\xi)+S_F(\xi)]$$
$$\times\gamma_5\tau_\alpha\tau_\beta\Phi_\beta(z-\xi,z-\xi;z_0-\xi_0)+\Delta^+(y-z)S^+$$
$$\times(x-z+\xi)\gamma_5S_A{}^-(-\xi)\gamma_5\tau_\beta\tau_\alpha\Phi_\beta(z,z-\xi;z_0-\xi_0)$$
$$+S^+(x-z)\Delta^+(y-z+\xi)\gamma_5S_R{}^+(\xi)$$
$$\times\gamma_5\tau_\beta\tau_\alpha\Phi_\beta(z-\xi,z;z_0-\xi_0)\}. \quad (10)$$

This is exactly the equation which would have been obtained if we had started with Φ^{++} in Eq. (3). We will next drop all terms on the right-hand side of Eq. (10) which contain either meson or nucleon negative-energy amplitudes. This is consistent with the Tamm-Dancoff approximation; these components of the wave function are not among those connected on Fig. 1 to the ground state.

The terms in Eq. (10) containing $\Delta^-(\xi)S^-(\xi)$, $S^-(\xi)S^+(-\xi)$, and $S^-(\xi)$ will vanish in the integration over ξ_0. After dropping the negative-energy amplitudes, we take the Fourier transform of Eq. (10). The expansion of Φ^{++} is found to be

$$\Phi_\alpha{}^{++}(x,y;t)=\int d^3\mathbf{q}\int d^3\mathbf{r}(\omega_qE_r)^{-\frac{1}{2}}$$
$$\times e^{i(r\cdot x+q\cdot y)}u(\mathbf{r})a(\mathbf{r}u,\mathbf{q}\alpha;t), \quad (11)$$

where a sum is implied over positive-energy nucleon spinors $u(\mathbf{r})$ (normalized so that $\bar{u}u=u^*\gamma_4u=1$), $r\cdot x=\mathbf{r}\cdot\mathbf{x}-r_0x_0$, $E_r=(M^2+\mathbf{r}^2)$, $\omega_q=(\mu^2+\mathbf{q}^2)$ (M and μ are the masses of the nucleon and meson), and

$$a(\mathbf{r}u,\mathbf{q}\alpha;t)=(\Psi_0{}^*(t)b_{ru}a_{q\alpha}\Psi(t)). \quad (12)$$

Annihilation operators for the nucleon and meson, respectively, are b_{ru} and $a_{q\alpha}$. By inserting the time dependence of the state vectors,

$$\Psi(t)=e^{-i(E-H_0)t}\Psi(0),$$
$$\Psi_0(t)=e^{-i(E_0-H_0)t}\Psi_0(0), \quad (13)$$

where H_0 is the noninteraction Hamiltonian, E is the total energy of the system, and E_0 is the vacuum state energy, Eq. (12) becomes ($\epsilon=E-E_0$):

$$a(\mathbf{r}u,\mathbf{q}\alpha;t)=e^{-i(\epsilon-E_r-\omega_q)t}a(\mathbf{r}u,\mathbf{q}\alpha), \quad (14)$$

where $a(\mathbf{r}u,\mathbf{q}\alpha)=(\Psi_0{}^*(0)b_{ru}a_{q\alpha}\Psi(0))$. With this notation, Eq. (10) written in momentum space in the center-of-mass system becomes ($\mathbf{p}$=momentum of nucleon; $\Delta=\epsilon-E_p-\omega_p$):

$$a(\mathbf{p}u,-\mathbf{p}\alpha)=-\tfrac{3}{4}iG^2\frac{M}{E_p}\int d\xi(\bar{u}(\mathbf{p})\gamma_5S_F(\xi)\gamma_5u(\mathbf{p}))\Delta_F(\xi)$$
$$\times e^{-ip\cdot\xi+i(\Delta+E_p)\xi_0}a(\mathbf{p}u,-\mathbf{p}\alpha)-\tfrac{1}{4}iG^2\frac{1}{\omega_p}\int d\xi$$
$$\times\mathrm{Sp}[\gamma_5S_F(\xi)\gamma_5S_F(-\xi)]e^{ip\cdot\xi+i(\Delta+\omega_p)\xi_0}a(\mathbf{p}u,-\mathbf{p}\alpha)$$
$$+\frac{M^2G^2}{16\pi^3}\int\frac{d^3\mathbf{k}}{(E_p\omega_pE_k\omega_k)^{\frac{1}{2}}}\Bigg\{\Bigg[\frac{(\bar{u}(\mathbf{p})\gamma_5\Lambda_+(0)\gamma_5v(\mathbf{k}))}{M(M-\epsilon)}$$
$$+\frac{(\bar{u}(\mathbf{p})\gamma_5\Lambda_-(0)\gamma_5v(\mathbf{k}))}{M(M+\epsilon)}\Bigg]\tau_\alpha\tau_\beta$$
$$+\Bigg[\frac{(\bar{u}(\mathbf{p})\gamma_5\Lambda_-(-\mathbf{p}-\mathbf{k})\gamma_5v(\mathbf{k}))}{E_{p+k}(E_p+E_{p+k}+E_k-\epsilon)}$$
$$+\frac{(\bar{u}(\mathbf{p})\gamma_5\Lambda_+(\mathbf{p}+\mathbf{k})\gamma_5v(\mathbf{k}))}{E_{p+k}(E_{p+k}+\omega_k+\omega_q-\epsilon)}\Bigg]\tau_\beta\tau_\alpha\Bigg\}a(\mathbf{k}\nu,-\mathbf{k}\beta). \quad (15)$$

Here, for convenience in the next section, we have left the self-energy parts in terms of invariant functions. Except for these terms, and for the terms involving the energy denominator $1/(M+\epsilon)$, which contributes only to the states for which $I=J=1/2$, this equation is identical to that derived by the old Tamm-Dancoff method.[1] We may therefore evaluate these self-energy parts, and use them to find corrections to the phase shifts previously calculated, except for the $I=J=1/2$ states.

IV. RENORMALIZATION

Let $\Omega(\xi)=\gamma_b S_F(\xi)\gamma_b\Delta_F(\xi)$, and

$$\Sigma(\xi)=\mathrm{Spur}\{\gamma_b S_F(\xi)\gamma_b S_F(-\xi)\}. \tag{16}$$

There are the well-known nucleon and meson self-energy propagation factors from second-order perturbation theory, whose strong singularity at $\xi=0$ causes the divergence of their momentum-space integrals. We shall follow the usual relativistic subtraction procedures to extract their finite parts. First take the 4-dimensional Fourier transform of Ω and Σ,

$$\Omega(\rho)=\int e^{-i\rho\cdot\xi}\Omega(\xi)d^4\xi,$$
$$\Sigma(\kappa)=\int e^{-i\kappa\cdot\xi}\Sigma(\xi)d^4\xi. \tag{17}$$

These are now relativistically invariant functions of the 4-vector momenta ρ and κ. More specifically, $\Omega(\rho)$ is a function of $\rho\cdot\gamma$ only, since $\rho\cdot\gamma$ is the simplest invariant matrix function of ρ. Similarly $\Sigma(\kappa)$ is a function of κ^2 only. These facts may be easily verified by explicit calculation.

In the usual way,[6] we set the observable (renormalized) parts of the self-energy operators equal to the following expressions:

$$\Omega_R(\rho\cdot\gamma)=\Omega(\rho\cdot\gamma)-\Omega(iM)-(\rho\cdot\gamma-iM)\left[\frac{\partial\Omega}{\partial(\rho\cdot\gamma)}\right]_{\rho\cdot\gamma=iM}, \tag{18}$$

$$\Sigma_R(\kappa^2)=\Sigma(\kappa^2)-\Sigma(-\mu^2)-(\kappa^2+\mu^2)\left[\frac{\partial\Sigma}{\partial\kappa^2}\right]_{\kappa^2=-\mu^2}. \tag{19}$$

Nucleon Self-Energy Renormalization

The subtractions indicated in (18) may be carried out by following exactly the procedure that Karplus and Kroll[7] used for the electron self-energy,

$$\Omega(\rho\cdot\gamma)=\int e^{-i\rho\cdot\xi}\gamma_b S_F(\xi)\gamma_b\Delta_F(\xi)d^4\xi$$
$$=-\frac{4i}{(2\pi)^4}\int d^4s\gamma_5\frac{s\cdot\gamma+\rho\cdot\gamma+iM}{(\rho+s)^2+M^2}\gamma_5\frac{1}{s^2+\mu^2}. \tag{20}$$

We apply the formula

$$\frac{1}{ab}=\int_0^1\frac{du}{[au+b(1-u)]^2} \tag{21}$$

to (20) to obtain

$$\Omega(\rho\cdot\gamma)=\frac{4i}{(2\pi)^4}\int d^4s\int_0^1 du \times\frac{s\cdot\gamma+\rho\cdot\gamma-iM}{\{[(\rho+s)^2+M^2]u+[s^2+\mu^2](1-u)\}^2}. \tag{22}$$

The denominator of the integrand of (22) may be written $[(s+\rho u)^2+\Delta^2]^2$, where $\Delta^2=\rho^2(u-u^2)+M^2u+\mu^2(1-u)$. We expand the integrand in a power series in pu; keeping only the first two terms, because the higher ones may be transformed into vanishing surface integrals. This casts (22) into the form

$$\Omega(\rho\cdot\gamma)=\frac{4i}{(2\pi)^4}\int d^4s\int_0^1 du\left\{\frac{s\cdot\gamma+\rho\cdot\gamma(1-u)-iM}{[s^2+\Delta^2]^2}+\rho u\cdot\frac{\partial}{\partial s}\frac{s\cdot\gamma}{[s^2-\Delta^2]^2}\right\}. \tag{23}$$

Upon carrying out the differentiation in (23), and making use of the facts that

$$\int f(l^2)l\cdot\gamma d^4l=0,$$
$$\int f(l^2)(a\cdot l)(b\cdot l)d^4l=\tfrac{1}{4}(a\cdot b)\int f(l^2)l^2d^4l, \tag{24}$$

we find the following form for Ω:

$$\Omega(\rho\cdot\gamma)=\frac{4i}{(2\pi)^4}\int d^4l\int_0^1 du\left(\frac{\rho\cdot\gamma-iM}{(l^2+\Delta^2)^2}-\frac{ul^2}{(l^2+\Delta^2)^3}\right). \tag{25}$$

The subtraction procedures (18) may be applied to this equation, and, making use of[8]

$$\int d^4l\left(\frac{1}{(l^2+\Delta^2)^2}-\frac{1}{(l^2+\Delta_0^2)^2}\right)=-i\pi^2\log\left|\frac{\Delta^2}{\Delta_0^2}\right|$$
$$=-i\pi^2\int_0^1 dv\frac{\Delta^2-\Delta_0^2}{\Delta_0^2+(\Delta^2-\Delta_0^2)v}, \tag{26}$$

[6] P. T. Matthews, Phil. Mag. 41, 185 (1950).
[7] R. Karplus and N. M. Kroll, Phys. Rev. 77, 536 (1950).
[8] R. P. Feynman, Phys. Rev. 76, 769 (1949).

one obtains

$$\Omega_R(\rho\cdot\gamma)=\frac{1}{(2\pi)^2}(\rho\cdot\gamma-iM)^2\int_0^1 du\int_0^1 dv \times\frac{u-u^2}{\Lambda_0^2+(\rho^2+M^2)(u-u^2)v} \times\left[(\rho\cdot\gamma+iM)\left(1-u-\frac{2M^2u^2(1-u)v}{\Lambda_0^2}\right)-iMu\right], \quad (27)$$

where $\Lambda_0^2=M^2u^2+\mu^2(1-u)$.

It is worth-while noting that, although it would greatly simplify the approximate evaluation of (27) to put $\mu^2=0$, it may not be done, because Ω_R is not an analytic function of μ^2 at $\mu^2=0$.

Meson Self-Energy Renormalization

$$\Sigma(\kappa)=\int e^{-i\kappa\cdot\xi}\,\mathrm{Sp}\{\gamma_5 S_F(\xi)\gamma_5 S_F(-\xi)\}d^4\xi =\frac{1}{4\pi^4}\int d^4p\,\mathrm{Sp}\left\{\gamma_5\frac{p\cdot\gamma+iM}{p^2+M^2}\gamma_5\frac{(p-\kappa)\cdot\gamma+iM}{(p-\kappa)^2+M^2}\right\}. \quad (28)$$

By evaluating the spur in (28) one may write

$$\Sigma(\kappa)=-\frac{1}{8\pi^4}\int\frac{d^4p}{(p-\kappa)^2+M^2}-\frac{1}{8\pi^4}\int\frac{d^4p}{p^2+M^2} +\frac{\kappa^2}{8\pi^4}\int\frac{d^4p}{[(p-\kappa)^2+M^2][p^2+M^2]}. \quad (29)$$

The second term of (29) clearly gives no contribution to Σ_R, since it will drop out in the first subtraction in (19). This is also true of the first term, as may be seen by expanding the integrand, as was done in (23). We find

$$\int\frac{d^4p}{(p-\kappa)^2+M^2}=\int\frac{d^4p}{p^2+M^2}-\kappa^2M^2\int\frac{d^4p}{(p^2+M^2)^3},$$

which will completely drop out in the subtraction (19). Therefore the observable parts of Σ are all contained in the third term of (29), Σ_3.

Application of (21) to Σ_3 yields

$$\Sigma_3=\frac{\kappa^2}{8\pi^4}\int_0^1 du\int d^4s\frac{1}{[s^2+u(1-u)\kappa^2+M^2]^2}, \quad (30)$$

after a change of variable $s=p-u\kappa$. We define

$$J(\lambda)=\frac{\kappa^2}{8\pi^4}\int_0^1 du\int d^4s\left(\frac{1}{[s^2+u(1-u)\kappa^2+M^2]^2} -\frac{1}{[s^2+u(1-u)\kappa^2+\lambda^2]^2}\right), \quad (31)$$

where λ is a very large mass. By using (26), (31) becomes

$$J(\lambda)=-\frac{i}{8\pi^2}\kappa^2(M^2-\lambda^2)\int_0^1 du\int_0^1 dw \times\frac{1}{\lambda^2+\kappa^2(1-u)u+(M^2-\lambda^2)w}. \quad (32)$$

The subtractions of (19) may be conveniently performed on this expression. When one does them, and lets $\lambda^2\to\infty$, (32) is transformed to

$$\Sigma_R(\kappa^2)=\frac{1}{8\pi^2}(\kappa^2+\mu^2)^2\int_0^1 du\int_0^1 dw\frac{u(1-u)}{M^2-u(1-u)\mu^2} \times\left(\frac{\kappa^2u(1-u)w}{u(1-u)w(\kappa^2+\mu^2)+M^2-u(1-u)\mu^2}-1\right), \quad (33)$$

which may be quite accurately approximated by letting $\mu^2=0$ under the integral sign. Equation (33) then reduces to

$$\Sigma_R=-\frac{i}{8\pi^2}(\kappa^2+\mu^2)^2\int_0^1 du\frac{1}{\kappa^2}\log\left|1+u(1-u)\frac{\kappa^2}{M^2}\right|. \quad (34)$$

V. CONCLUSION

The integrals in (27), (34) are elementary, and may be carried out without difficulty. The four-vector arguments ρ and κ of Ω and Σ are replaced by the quantities which occur in the integral Eq. (15), namely $(\mathbf{p}, \Delta+E_p)$ and $(-\mathbf{p}, \Delta+\omega_p)$, respectively. Since Ω is surrounded in (15) by $\bar{u}(\mathbf{p})$ and $u(\mathbf{p})$ and $(\mathbf{p}\cdot\gamma+i\gamma_4E_p-iM)u(\mathbf{p})=0$, the Dirac matrices $(\rho\cdot\gamma-iM)^2$ and $(\rho\cdot\gamma-iM)^2\times(\rho\cdot\gamma+iM)$, which occur in (27), become $-\Delta^2$ and $-i\Delta E_p(\Delta+2E_p)/M$.

By collecting terms which multiply $a(\mathbf{p}u, -\mathbf{p}\alpha)$, Eq. (15) may be rewritten in the form

$$a(\mathbf{p}u, -\mathbf{p}\alpha)=(F^2/4\pi)\times(\text{interaction terms}), \quad (35)$$

where the "interaction terms" are all those on the right side of (15), except the first two (self-energy terms), divided by $G^2/4\pi$; and

$$\frac{F^2}{4\pi}=\frac{G^2}{4\pi}\left(1+\frac{3iG^2}{4}\frac{M}{E_p}\Omega+\frac{iG^2}{4\omega_p}\Sigma\right)^{-1}. \quad (36)$$

Equation (35), therefore, absorbs the self-energy effects into the coupling "constant" $F^2/4\pi$, which now depends on $|\mathbf{p}|$ and ϵ.

The asymptotic expressions for Ω and Σ for $|\mathbf{p}|/M\to\infty$ may be easily derived. When they are inserted into (36) it becomes

$$\frac{F^2}{4\pi}=\frac{G^2}{4\pi}\left(1-\frac{3G^2}{32\pi^2}\log\left|\frac{\mathbf{p}}{M}\right|-\frac{G^2}{32\pi^2}\frac{\epsilon}{|p|}\log\left|\frac{\mathbf{p}}{M}\right|\right)^{-1}. \quad (37)$$

The first term within the bracket arises from the nucleon self-energy, and dominates for large $\mathbf{p}$. $F^2/4\pi$ is clearly negative for $\mathbf{p}$ large enough.[9] For $\Delta=0$ it is by definition positive and equal to $G^2/4\pi$. Therefore, for some $\mathbf{p}=\mathbf{k}$ for which $\Delta<0$ $F^2/4\pi$ has a pole. A pole in $F^2/4\pi$ implies a pole in the wave function $a(\mathbf{p}u, -\mathbf{p}\alpha)$ or, in other words, an incoming or outgoing wave of momentum $\mathbf{k}$ in the coordinate-space wave function. It would be possible to interpret the pole as an inelastic scattering if $2|\mathbf{k}|<\epsilon$, but a rough numerical calculation shows this condition not to be fulfilled for laboratory energies (values of ϵ from M to $2M$). If $?|\mathbf{k}|>\epsilon$ an interpretation as inelastic scattering is not possible, because there is too much momentum for the fixed amount of energy in the system, and at least one of the scattered particles would have a spacelike energy-momentum four vector, or an imaginary mass. No reconciliation oft his nonsensical prediction with reality has yet been made, and at present it must be considered as raising serious doubt about the consistency of the Tamm-Dancoff approximation.

The author would like to express his gratitude to F. J. Dyson for suggesting this problem, for essential guidance, and for helpful discussions.

[9] R. H. Dalitz (private communication) has pointed out an error made by the author in the evaluation of these terms which radically altered their behavior. His information has prevented the possible publication of qualitatively wrong results, and is greatly appreciated.

PHYSICAL REVIEW VOLUME 96, NUMBER 3 NOVEMBER 1, 1954

Mesonic Corrections to the Quadrupole Moment of the Deuteron*

A. M. SESSLER†
Laboratory of Nuclear Studies, Cornell University, Ithaca, New York
(Received June 10, 1954)

Mesonic corrections to the quadrupole moment of the deuteron are calculated by means of the method of Tamm and Dancoff. Only the two-nucleon and two-nucleon—one-meson amplitudes are included. The first is associated with a phenomenological wave function for the deuteron, the second yielding a correction to the quadrupole moment. A correction exists even in neutral scalar theory, and for pseudoscalar (pseudoscalar) symmetric theory the result in adiabatic approximation to second order is $\Delta Q=3.1$ percent or $\Delta Q=-0.7$ percent, depending on choice of wave functions (assuming $g^2/4\pi=10$). Contributions from multiple meson amplitudes are examined, and for a hard-core deuteron function they are shown to contribute only slightly.

I. INTRODUCTION

A PHENOMENOLOGICAL theory of the deuteron consists of choosing an arbitrary potential which is to act between two nucleons and only depends explicitly on nucleon variables, and then calculating the binding energy of the deuteron, the quadrupole moment, the n-p triplet scattering length, and the n-p triplet effective range. These quantities are then compared with experiment, and if they all agree, within experimental error, then the potential is an acceptable one.

The phenomenological theory is not complete in that it ignores the coordinates of the mesons associated with the two-nucleon system. It does not, however, completely ignore the mesons, in so far as they contribute to the potential acting between nucleons. The question arises as to how valid the phenomenological theory is, or, equivalently, how much of a correction will the inclusion of meson coordinates make in which potentials are considered acceptable.

It is not known how to obtain from meson theory a quantitatively correct answer to this question. However, as we shall see, the only one of the above mentioned quantities we need calculate with meson theory is the quadrupole moment of the deuteron. Because this is an outside quantity one should be able to obtain a very reasonable estimate of the magnitude of the effect, and in view of the rather large estimates which appear in the literature,[1,2] it was felt that a re-examination of the problem was necessary.

The results of a field-theoretic calculation of the two-nucleon system may be expressed in terms of a wave functional in Fock space. The method of Tamm[3] and Dancoff,[4] in lowest approximation, consists of equating to zero all amplitudes of the functional other than the two-nucleon (2,0), and two-nucleon—one-meson (2,1) amplitudes. We shall make this lowest approximation first, and examine its validity in Sec. IV.

We may associate the (2,0) amplitude with a phenomenological wave function. It satisfies a Schroedinger equation in which the potential term arises from the amplitudes involving mesons, but does not contain meson coordinates. Furthermore, the binding energy of the deuteron, and the n-p scattering length, and the n-p effective range may be obtained from the (2,0) amplitude alone. The quadrupole moment differs in that it

* Supported in part by the U. S. Office of Naval Research.
† National Science Foundation Post-Doctoral Fellow.

[1] F. Villars, Phys. Rev. **86**, 476 (1952).
[2] S. Deser, Phys. Rev. **92**, 1542 (1953).
[3] I. Tamm, J. Phys. (U.S.S.R.) **9**, 449 (1945).
[4] S. M. Dancoff, Phys. Rev. **78**, 382 (1950).

receives a direct contribution from the charge density of the (2,1) amplitude, and in that it depends on the normalization of the (2,0) amplitude. This normalization does not otherwise enter in the identification of the (2,0) amplitude with the phenomenological wave function.

We shall calculate the contribution arising from the (2,1) amplitude taking into account its effect on the normalization of the (2,0) amplitude. This contribution must be regarded as a correction which should be applied to the experimental quadrupole moment before it is used as input data in a phenomenological theory. The resulting phenomenological theory may then be considered as associated with the (2,0) amplitude in a Fock space representation of the field-theoretic solution of the two-nucleon problem.

II. NEUTRAL SCALAR THEORY

We shall first, for the purpose of giving a simple exposition, carry through the calculation using neutral scalar theory. The notation is the same as that of Lévy,[5] and $\hbar=c=M=1$. The (2,1) amplitude can be obtained from the (2,0) amplitude by the following equation:

$$[E-E_{p1}-E_{p2}-\omega(k)]a(\mathbf{p}_1,\mathbf{p}_2;\mathbf{k})$$
$$=g(2\pi)^{-\frac{1}{2}}[2\omega(k)]^{-\frac{1}{2}}[a(\mathbf{p}_1+\mathbf{k},\mathbf{p}_2)+a(\mathbf{p}_1,\mathbf{p}_2+\mathbf{k})]. \quad (1)$$

The program is to associate $a(\mathbf{p}_1,\mathbf{p}_2)$ with the Fourier transform of a phenomenological wave function $\psi(\mathbf{x}_1,\mathbf{x}_2)$ and believe meson theory only to the extent of Eq. (1), which gives $a(\mathbf{p}_1,\mathbf{p}_2;\mathbf{k})$ in terms of $a(\mathbf{p}_1,\mathbf{p}_2)$. Let $a(\mathbf{x}_1,\mathbf{x}_2;\mathbf{s})$ be the Fourier transform of $a(\mathbf{p}_1,\mathbf{p}_2;\mathbf{k})$. Then $|a(\mathbf{x}_1,\mathbf{x}_2;\mathbf{s})|^2$ is the probability of locating a meson at $\mathbf{s}$, and nucleons at $\mathbf{x}_1$ and $\mathbf{x}_2$. Since we are calculating in a neutral theory, the only contribution to the quadrupole moment comes from

$$\rho(\mathbf{x}_2)=\int|a(\mathbf{x}_1,\mathbf{x}_2;\mathbf{s})|^2d\mathbf{x}_1d\mathbf{s}, \quad (2)$$

which is the charge density in the state in which there are two nucleons and one meson.

We make the adiabatic approximation of setting $E-E_{p1}-E_{p2}=0$. This yields

$$\rho(\mathbf{x}_2)=\frac{g^2}{2(2\pi)^6}[\rho_1+\rho_2+\rho_3+\rho_4], \quad (3)$$

FIG. 1. Graphs contributing to the charge density in the (2,1) state.

[5] M. M. Lévy, Phys. Rev. 88, 72 (1952).

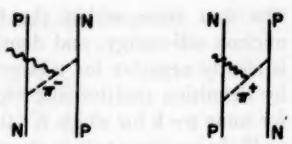

FIG. 2. Meson current contributions to the quadrupole moment.

where

$$\rho_i(\mathbf{x}_2)=\int d\mathbf{p}_1d\mathbf{p}_2d\mathbf{p}_2'd\mathbf{k}\frac{e^{i(\mathbf{p}_2-\mathbf{p}_2')\cdot\mathbf{x}_2}}{\omega^3(k)}K_i,$$
$$K_1=a(\mathbf{p}_1+\mathbf{k},\mathbf{p}_2)a^*(\mathbf{p}_1+\mathbf{k},\mathbf{p}_2'),$$
$$K_2=a(\mathbf{p}_1+\mathbf{k},\mathbf{p}_2)a^*(\mathbf{p}_1,\mathbf{p}_2'+\mathbf{k}), \quad (4)$$
$$K_3=a(\mathbf{p}_1,\mathbf{p}_2+\mathbf{k})a^*(\mathbf{p}_1+\mathbf{k},\mathbf{p}_2'),$$
$$K_4=a(\mathbf{p}_1,\mathbf{p}_2+\mathbf{k})a^*(\mathbf{p}_1,\mathbf{p}_2'+\mathbf{k}).$$

Graphs may be drawn corresponding to ρ_1, ρ_2, ρ_3, and ρ_4. They appear in Fig. 1, from which it is clear that the logarithmically divergent terms ρ_1 and ρ_4 are self-terms and must in the spirit of noncovariant renormalization be dropped. They correspond to a meson cloud associated with each nucleon, and the finite contribution of these terms may be estimated phenomenologically.[6]

Combining the above we obtain

$$\rho(\mathbf{x}_2)=g^2(2\pi)^{-3}\int d\mathbf{y}|\psi(\mathbf{y},\mathbf{x}_2)|^2I(|\mathbf{x}_2-\mathbf{y}|), \quad (5)$$

where

$$I(|\mathbf{x}_2-\mathbf{y}|)=\int d\mathbf{k}\omega^{-3}(\mathbf{k})e^{i\mathbf{k}\cdot(\mathbf{x}_2-\mathbf{y})}. \quad (6)$$

Transforming to the center of mass, and relative coordinates $\mathbf{r}$, and evaluating $I(|\mathbf{x}_2-\mathbf{y}|)$ by the method of Lévy,[7] we obtain

$$\rho(\mathbf{r})=g^2(2\pi^2)^{-1}|\Phi(r)|^2K_0(\mu r), \quad (7)$$

where $\Phi(r)$ is the deuteron wave function in relative coordinates.

The contribution to the quadrupole moment is given by

$$\Delta Q=\Delta Q'-NQ_{\text{phen}}, \quad (8)$$

where

$$\Delta Q'=\tfrac{1}{2}\int\rho(\mathbf{r})r^2P_2(\cos\theta)d\mathbf{r}, \quad N=\int\rho(\mathbf{r})d\mathbf{r}. \quad (9)$$

The first term being a direct contribution from the (2,1) state, the second term coming from a change in normalization of the (2,0) state. The two terms tend to cancel,

[6] The electron-neutron interaction measures $I=\int r^2\rho(r)$, where $\rho(r)$ is the charge density of a neutron, and can be expressed as $I<e(\hbar/\mu c)^2(\mu/M)^2$. This leads to a correction to the quadrupole moment of the order of

$$\left[\frac{\hbar}{Mc}\frac{1}{R}\right]^2,$$

where R is the radius of the deuteron. This is less than 0.3 percent, and negligible.

[7] M. M. Lévy, Phys. Rev. 88, 738 (1952), see Appendix.

TABLE I. Contributions to ΔQ for two-deuteron functions. In pseudoscalar theory $g^2/4\pi$ has been chosen equal to 10.

		Yukawa-Yukawa			Hard core		
		$\Delta Q'$	$-NQ_{\text{phen}}$	ΔQ	$\Delta Q'$	$-NQ_{\text{phen}}$	ΔQ
Scalar (2,1)		$0.467(g^2/2\pi^2)$	$-1.54(g^2/2\pi^2)$	$-1.07(g^2/2\pi^2)$ $-1.9\%\ Q_{\text{exp}}$			
Pseudo-scalar (2,1)	$s-s$	$0.03114(g^2/4\pi)$	$0.01578(g^2/4\pi)$		$0.02953(g^2/4\pi)$	$0.00183(g^2/4\pi)$	
	$s-d$	-0.01002	-0.02387		-0.01255	-0.03230	
	$d-d$	0.00245	0.00359		0.00431	0.00478	
Total				$0.0191(g^2/4\pi)$ $3.1\%\ Q_{\text{exp}}$			$-0.0044(g^2/4\pi)$ $-0.7\%\ Q_{\text{exp}}$
Pseudo-scalar (2,2)		$2.56\times10^{-4}(g^2/4\pi)^2$	$-67.7\times10^{-4}(g^2/4\pi)^2$	$-10.5\%\ Q_{\text{exp}}$	$2.82\times10^{-4}(g^2/4\pi)^2$	$-9.80\times10^{-4}(g^2/4\pi)^2$	$-1.1\%\ Q_{\text{exp}}$

and would give zero if the K_0 function were absent. Since the K_0 function weights small r, the normalization term dominates and ΔQ is negative. Simply for comparison purposes, a numerical calculation was performed, the results for a reasonable value of $(g^2/4\pi)$ being listed in Table I.

III. SYMMETRIC PSEUDOSCALAR THEORY

The calculation proceeds exactly as in scalar theory, except for a few minor changes, Eq. (1) becomes

$$[E-E_{p1}-E_{p2}-\omega(k)]a(\mathbf{p}_1,\mathbf{p}_2;\mathbf{k})$$
$$=g\Lambda_a{}^+\Lambda_b{}^+(2\pi)^{-\frac{1}{2}}[2\omega(k)]^{-\frac{1}{2}}$$
$$\times[\tau_i{}^a\gamma_5{}^a a(\mathbf{p}_1+\mathbf{k},\mathbf{p}_2)+\tau_i{}^b\gamma_5{}^b a(\mathbf{p}_1,\mathbf{p}_2+\mathbf{k})]. \quad (10)$$

We need still calculate only $\rho(\mathbf{k}_2)$ since the contribution of meson currents vanishes[8] (see Fig. 2). The adiabatic approximation $E-E_{p1}-E_{p2}=0$ is again made, and because of the presence of γ_5 we must use a two component reduction approximation for the deuteron function. This is equivalent to calculating with a pseudovector theory, since pair terms do not contribute to this order. We obtain

$$\rho(\mathbf{r})=-\frac{g^2}{2\pi^2}\frac{\boldsymbol{\tau}^a\cdot\boldsymbol{\tau}^b}{(2M)^2}|\Phi(\mathbf{r})|^2(\boldsymbol{\sigma}^a\cdot\boldsymbol{\nabla})(\boldsymbol{\sigma}^b\cdot\boldsymbol{\nabla})K_0(\mu r). \quad (11)$$

The deuteron function $\Phi(\mathbf{r})$ for $m=1$, may be written as

$$\Phi(\mathbf{r})=\frac{1}{\sqrt{(4\pi)}}\varphi(r)X_1+\psi(r)Y_D, \quad (12)$$

where φ and ψ are radially normalized and

$$Y_0=\left(\frac{2}{20}\right)^{\frac{1}{2}}X_1Y_{20}+\left(\frac{6}{20}\right)^{\frac{1}{2}}X_0Y_{21}+\left(\frac{12}{20}\right)^{\frac{1}{2}}X_{-1}Y_{22}. \quad (13)$$

The quadrupole moment correction is given by Eq. (8), the evaluation of which is rather involved due to the more complicated nature of $\rho(\mathbf{r})$. Separating terms corresponding to the S and D states of the deuteron, we obtain

$$\Delta Q_S'=\frac{g^2}{8\pi^2M^2\mu^3}\left(\frac{1}{5}\right)\times\int_0^\infty\varphi^2(x/\mu)x^4dx\left[K_0(x)+\frac{2K_1(x)}{x}\right],$$

$$\Delta Q_{SD}'=-\frac{g^2}{8\pi^2M^2\mu^3}\left(\frac{1}{5\sqrt{2}}\right)\int_0^\infty\varphi(x/\mu)\times\psi(x/\mu)x^4dx\left[K_0(x)+\frac{5K_1(x)}{x}\right],$$

$$\Delta Q_D'=\frac{g^2}{8\pi^2M^2\mu^3}\left(\frac{1}{20}\right)\times\int_0^\infty\psi^2(x/\mu)x^4dx\left[5K_0(x)+\frac{13K_1(x)}{x}\right], \quad (14)$$

$$N_S=\frac{g^2}{8\pi^2M^2\mu}\int_0^\infty\varphi^2(x/\mu)x^2dx\left[K_0(x)-\frac{K_1(x)}{x}\right],$$

$$N_{SD}=\frac{g^2}{8\pi^2M^2\mu}(4\sqrt{2})\int_0^\infty\varphi(x/\mu)\times\psi(x/\mu)x^2dx\left[K_0(x)+\frac{2K_1(x)}{x}\right],$$

$$N_D=-\frac{g^2}{8\pi^2M^2\mu}\times\int_0^\infty\psi^2(x/\mu)x^2dx\left[K_0(x)+\frac{5K_1(x)}{x}\right].$$

The evaluation may not be performed using zero-range functions due to the singularity in N_S. Any function corresponding to a nonzero-range force gives a finite result. We have carried through the numerical work

[8] H. Miyazawa, Progr. Theoret. Phys. (Japan) 7, 207 (1952).

FIG. 3. Typical diagrams in g^4 order.

using two functions.[9] The first is a solution of a central and tensor Yukawa well potential, and the second is from a similar potential with a hard core at $r=0.375\hbar/\mu c$. Both functions fit the triplet data. The results are given in Table I.

We have not calculated the self-terms by means of a renormalization program. It seems probable that these terms may be sufficiently accurately estimated phenomenologically.[6]

IV. TWO-MESON AMPLITUDE TERMS

In pseudoscalar theory one might think the fourth-order terms are much larger than the previously calculated terms. Because the quadrupole moment is an outside effect and the multiple-meson effects are concentrated at small distances, this is not so. The leading terms are the two-pair terms,[7] and we shall calculate the charge density associated with the (2,2) amplitude. A straightforward calculation yields

$$\rho(\mathbf{r})=g^4(4M)^{-2}(2\pi)^{-6}\tau_\lambda{}^a\tau_\mu{}^a[\tau_\lambda{}^b\tau_\mu{}^b+\tau_\mu{}^b\tau_\lambda{}^b]|\Phi(r)|^2J(r), \quad (15)$$

where

$$J(r)=\int\int\frac{d\mathbf{k}d\mathbf{q}e^{i(\mathbf{k}+\mathbf{q})\cdot\mathbf{r}}}{\omega(k)\omega(q)[\omega(k)+\omega(q)]^2}. \quad (16)$$

$J(r)$ may be easily evaluated,[7] and the results are to be found in Table I. Because of the short range and the singularity of the operators, the results are very sensitive to the inner regions of the wave function. Very little is known about the deuteron function in this region, but a hard core type of behavior seems probable. If we assume a hard core, none of the other multiple-meson amplitudes contribute appreciably.

[9] Dr. M. Kalos has been kind enough to supply us with these functions.

V. CONCLUSIONS

Using pseudoscalar theory, and including the (2,0) and (2,1) amplitudes, we find the nonphenomenologic contribution to the quadrupole moment is 3.1 percent and -0.7 percent for Yukawa well and hard-core functions, respectively (this assumes $g^2/4\pi=10$). The plus sign is such as to imply a decrease in the percentage of D state of a phenomenological function. With a hard-core function, modification due to multiple-meson amplitudes is small, and one is led to believe that the whole effect is probably of the order of one percent. With Yukawa functions, which is a rather extreme case, multiple-meson amplitudes contribute appreciably, and a definite statement cannot be made.

One should compare this with the four-dimensional calculations of Villars[1] and Deser.[2] Deser breaks the interaction between the nucleons into an instantaneous and a retarded part. He associates the solution obtained with only the instantaneous interaction, with a phenomenological theory. He then calculates the effect of the retarded part and considers this as the correction to the quadrupole moment. Actually most of this is included in a phenomenological theory, for if we take the one four-dimensional diagram Fig. 3A and break it up into time-ordered diagrams, then clearly diagrams where no meson is in flight during the interaction with the photon, like Fig. 3B, are included in the phenomenological theory, while only Fig. 3C should be considered a true correction to the quadrupole moment. In addition to this, differences in the numbers are due to Deser's use of zero-range functions which, being singular at the origin, give a much larger contribution. Neither Deser nor Villars has included the change in normalization of the wave function, which tends to decrease the effect.

I wish to thank Professor H. A. Bethe, Dr. N. Austern, Dr. A. Klein, and Dr. R. H. Dalitz for many enlightening conversations.

Letters to the Editor

PUBLICATION of brief reports of important discoveries in physics may be secured by addressing them to this department. The closing date for this department is five weeks prior to the date of issue. No proof will be sent to the authors. The Board of Editors does not hold itself responsible for the opinions expressed by the correspondents. Communications should not exceed 600 words in length and should be submitted in duplicate.

Effect of Precipitation Hardening on the Superconducting Transition of an Aluminum Alloy*

R. E. MOULD† AND D. E. MAPOTHER
Physics Department, University of Illinois, Urbana, Illinois
(Received July 19, 1954)

THIS letter reports the preliminary results of an experimental investigation of the changes in superconducting properties which accompany the precipitation hardening of an alloy. It was necessary to choose a precipitation hardening system whose major constituent was a superconductor and preferably a system whose mechanical and metallurgical properties had been reasonably well investigated. For these reasons the aluminum alloy Alcoa 63*S* was chosen. Its composition is 0.7 percent Mg, 0.4 percent Si, more than 98 percent Al, and traces of other elements. The precipitation hardening in this alloy is associated with the precipitation of the Mg and Si from a supersaturated solid solution in the form of the compound Mg_2Si. The heat treatment of the alloy first requires a soaking at 575°C to disperse the Mg and Si in solid solution followed by a water quench to room temperature. In the quenched alloy the Mg and Si are in supersaturated solution and the specimen is quite soft, being only slightly harder than pure aluminum. The alloy is hardened by reheating it to an intermediate temperature (in our case 175°C) so that precipitation can proceed by diffusion. For a given intermediate temperature

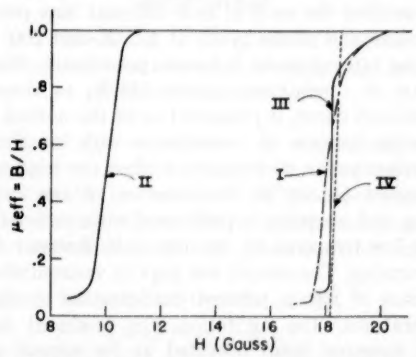

FIG. 1. Superconducting transitions for the aluminum alloy 63*S* showing the effect of heat treatment. All transitions shown above were measured at $T=1.049$°K. (I) quenched alloy; (II) fully hardened alloy; (III) annealed alloy; (IV) pure aluminum.

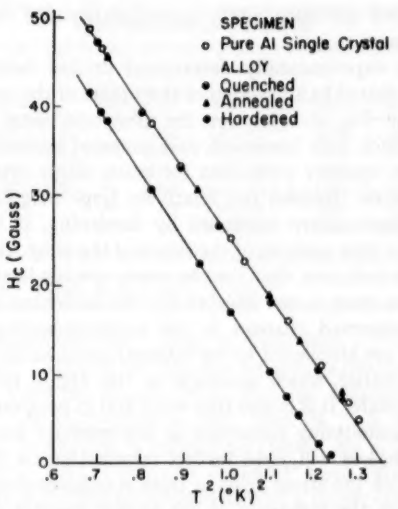

FIG. 2. Temperature dependence of critical field for aluminum alloy 63*S* for different heat treatments. Data for pure aluminum are included for comparison.

the hardness, tensile strength, etc., increase with time to a maximum value (after about 24 hours) and then decline slowly with continued heating. If the precipitation of Mg_2Si is allowed to proceed until substantially complete, the specimen becomes soft again and this is designated as the annealed condition. The specimens used in this study were machined into the shape of ellipsoids of revolution from lengths of commercial bar stock.[1] Efforts to recrystallize the ellipsoids as single crystals removed the magnesium from the alloy and so the present measurements were made on polycrystalline material.

The superconducting measurements were made by a sensitive ballistic induction technique which measures the flux change in the specimen when the external magnetic field is changed by uniform stepwise increments. The measuring method makes it possible to follow the flux changes in the specimen as it goes from the superconducting to the normal state or visa versa. We have found it convenient to represent the transition in terms of the "effective" permeability of the specimen as a function of the applied magnetic field. A plot of this type is shown in Fig. 1 on which are represented the superconducting transitions for an alloy specimen in several conditions of hardness. The abscissa of Fig. 1 is a considerably expanded scale and it will be noted that the alloy transitions are relatively narrow. The measuring method employed makes it possible to compare the transition of an alloy specimen with a pure single crystal of aluminum of identical shape on the same experimental run. As can be seen in Fig. 1, the transition for the alloy in the quenched condition closely approximates that of pure aluminum. The maximum displacement of the transition corresponds to maximum hardness of the alloy specimen, and the transition for an

annealed specimen again approximates that for pure aluminum.

The experimentally determined critical fields have been plotted as a function of the square of the temperature in Fig. 2. Data for the alloy specimens in the quenched, fully hardened, and annealed conditions are shown together with data for pure, single crystalline aluminum. Besides the relatively large magnitude of the displacement produced by hardening, it is noteworthy that analysis of the slopes of the alloy transition curves indicates that the electronic specific heat in the normal state is not affected by the hardening process. The observed changes in the superconducting properties are attributed to the internal strain in the aluminum lattice which develops as the Mg_2Si begins to precipitate. It is hoped that work still in progress on the superconducting properties in intermediate conditions of hardness will yield further information on the way in which the stress fields in these specimens develop.

From the viewpoint of the atomic theories recently advanced by Fröhlich[2] and by Bardeen,[3] the substantial displacement of the critical field curve can be interpreted as due to a change in the vibration spectrum of the lattice. The validity of this interpretation can be examined by experiments on the effect of precipitation hardening upon the Debye temperature. From a simple argument based on the Fröhlich-Bardeen concept it can be shown that the Debye temperature for a superconductor should vary inversely with its critical temperature when the changes are induced by lattice strains. The magnitude of the changes in critical temperature observed in the present work are believed to be sufficiently large to correspond to measurable changes in the Debye temperature of this alloy if the above proportionality is correct. An investigation of this possibility is now being carried out.

* This work has received partial support from the Office of Ordnance Research.

† On leave from Preston Laboratories, Butler, Pennsylvania.

[1] Kindly supplied to us by the Aluminum Company of America.

[2] H. Fröhlich, Phys. Rev. **79**, 845 (1950).

[3] J. Bardeen, Revs. Modern Phys. **23**, 261 (1951).

Distribution of Trapping Levels in Cadmium Selenide

HARALD C. JENSEN* AND ROBERT J. CASHMAN
Northwestern University, Evanston, Illinois

(Received September 13, 1954)

TRAP distributions in phosphors have been investigated with the glow curve technique by many workers including Randall and Wilkins,[1] Klasens,[2] Bude,[3] Gillson,[4] and Johnson and Williams.[5] The technique involves cooling the phosphor in the dark, irradiating, and then warming again in the dark after the original phosphorescence has decayed to equilibrium. During the warming process the phosphor glows as

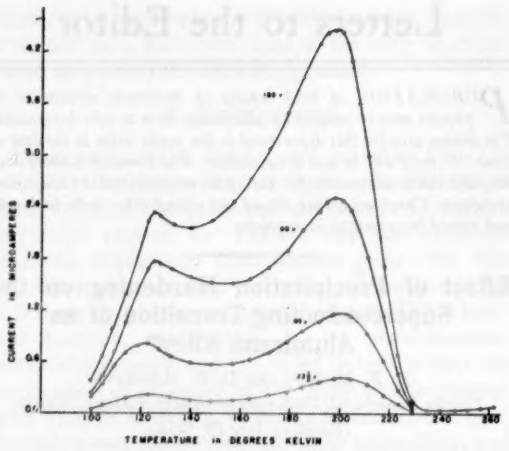

FIG. 1. "Electrical glow curves" taken in CdSe with various bias potential differences.

traps are emptied by thermal activation and the intensity of glow is measured as a function of the temperature. The temperature at which the glow peak occurs is proportional to the energy depth of the traps and the height of the peak is proportional to the number of traps at that temperature.[1]

An analogous procedure for the investigation of trap distributions in photoconductors is suggested by the work of Herman and Hofstadter[6] with willemite reported in 1940 and that of Frerichs[7] with cadmium sulfide in 1949 where current pulses, instead of light pulses, occur during the warming of photoconducting materials, in the dark. Measurements of this nature were made by Dutton and Maurer[8] in 1953 on KCl and KBr who also measured absorption after irradiation, but both before and after warming, that gave definite correlation between absorption peaks and current peaks. Herman and Hofstadter used ultraviolet, Frerichs gamma rays, and Dutton and Maurer x-rays.

Figure 1 exhibits "electrical glow curves" for a crystal of cadmium selenide (4 mm long by 1-mm^2 cross section) for each of four different bias potential differences and shows peaks at 125°K and 200°K for warming rates of about 2 degrees per minute. The slow increase of conductance above 235°K, as shown on the 180-volt curve, is presumed to be the normal semiconductor increase of conductance with temperature. No further peaks were observed when the temperature was raised to 360°K. Furthermore, if the cycle of cooling and warming is performed without irradiation at the low temperature, no current is observed during the warming. The sample was kept in vacuum of about 10^{-6} mm of Hg to prevent condensation at the low temperatures. The excitation was produced with a small tungsten lamp operated at its normal power rating of six watts.

Although the curves in Fig. 1 were all taken from the same sample of CdSe, other samples were investi-

gated and they also showed current peaks differing only in detail. It is to be noted that the currents involved here are many orders of magnitude larger than those mentioned by other workers. Frerichs reports a total charge of 10^{-7} coulomb in CdS and Dutton and Maurer report only 10^{-11} coulomb, while the charge involved in the 22½ volt curves for CdSe was 10^{-3} coulomb. The large currents and charges reported here may be attributed to several factors: (1) higher original excitation, (2) high photosensitivity of CdSe to light in the visible portion of the spectrum, (3) larger bias potential differences used in this work, and (4) a possibility of higher trap densities in CdSe.

The photosensitivity and the time required for photocurrent decay in cadmium selenide are both very much greater at the low temperatures where the traps are active than at room temperatures where they cannot be active. Work involving this aspect of photoconductivity in cadmium selenide is in progress and will be reported later.

The writers wish to thank Dr. Rudolf Frerichs for helpful discussions during the progress of this work and also to acknowledge partial support of the work by a grant from the Research Corporation of New York. They are also indebted to Dr. John E. Jacobs of the General Electric x-ray department at Milwaukee, Wisconsin for furnishing the samples of cadmium selenide which were made there by improvements of methods devised by Frerichs.[9]

* On leave from Lake Forest College, Lake Forest, Illinois.
[1] J. T. Randall and M. H. F. Wilkins, Proc. Roy. Soc. (London) **A184**, 365 (1945).
[2] H. A. Klasens, J. Electrochem. Soc. **100**, 72 (1953).
[3] R. H. Bude, J. Phys. Chem. **57**, 785 (1953).
[4] J. L. Gillson, J. Opt. Soc. Am. **44**, 341 (1954).
[5] J. S. Johnson and F. E. Williams, J. Opt. Soc. Am. **39**, 709 (1949).
[6] R. C. Herman and R. Hofstadter, Phys. Rev. **57**, 936 (1940).
[7] Rudolf Frerichs, Phys. Rev. **76**, 1873 (1949).
[8] D. Dutton and R. J. Maurer, Phys. Rev. **90**, 126 (1953).
[9] Rudolf Frerichs, Naturwiss. **33**, 281 (1946).

Voltage Dependence of Electroluminescent Brightness

B. T. Howard, H. F. Ivey, and W. Lehmann
Westinghouse Electric Corporation, Bloomfield, New Jersey
(Received September 3, 1954)

THE voltage dependence of electroluminescent brightness is of considerable interest since it may provide valuable indications of the processes involved, and also since any theory which is proposed to explain the phenomena must be able to account for this dependence.

Destriau[1] has proposed the relationship,

$$L=aV^n \exp(-b/V), \qquad (1)$$

where a and b are constants and n, in general, lies between 1 and 3. Weymouth and Bitter[2] have stated, for a single phosphor particle, that the relationship between brightness and voltage is linear with a "voltage threshold." Thorington[3] has also reported a relationship of this type for phosphors in vacuum. Halsted and Koller,[4] using transparent thin films of ZnS, report that the brightness is related to voltage by a simple power law. Also, Piper and Williams[5] have explained the form of the voltage dependence by a rather complex equation involving the distribution of electron traps in the phosphor. However, since they used an experimental arrangement in which a ZnS single crystal was in contact with metallic electrodes, their data are not, strictly, applicable to the case which we are considering, namely that of a conventional plaque cell, in which the phosphor is embedded in a dielectric medium between two planar electrodes.

TABLE I. Fit of Eq. (2) to several representative electroluminescent phosphors.

Material	Reference	Frequency (cps)	a (arb. units)	b (volts)	V_0 (volts)	b/V_0
ZnS:Ag(*WL*.132)	a	1000	7.0×10^{-10}	1200	67	18
ZnS:Cu(*WL*.100)	a	1000	1.0×10^{-6}	1050	39	26
ZnS:Cu(*WL*.168)	a	1000	2.1×10^{-7}	970	30	32
ZnO:Zn(*WH*.200)	a	1000	6.0×10^{-9}	1150	82	14
ZnS: ?	b	60	2.0×10^{-7}	600	27	22
ZnS: ?	c	60	9.5×10^{-7}	2500	113	22

a These phosphors were made in this laboratory.
b E. Lowry, Physics Today **6**, No. 7, 4 (1953).
c Waymouth, Jerome, and Gungle, Sylvania Technologist (July, 1952).

However, none of these relationships provides good fit to all of the available experimental data over a large voltage range. Thus, we have tried to find an equation which, although having no more constants than that proposed by Destriau, could be universally applied. As a result, we have found that an equation of the form

$$L=aV \exp[-b/(V+V_0)] \qquad (2)$$

satisfactorily fits the voltage dependence of the electroluminescent output from a conventional plaque cell.

The general form of Eq. (2) is similar to that of Eq. (1) in that it gives zero brightness at zero voltage and

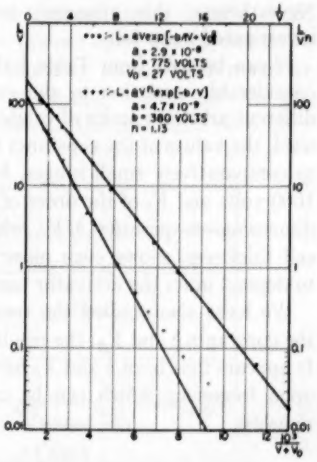

FIG. 1. Comparison between the fit for Eqs. (1) and (2) for a typical electroluminescent phosphor (ZnS:Cu).

infinite brightness at infinite voltage. However, Eq. (1) predicts a point of inflection under certain conditions while Eq. (2) does not. Also, Eq. (1) predicts a power-law dependence at high voltages while Eq. (2) gives a linear dependence.

This equation has been tested on results reported from several published sources and we have also carried out more exhaustive comparisons with experimental results obtained in this laboratory. The results are shown in summarized form in Table I. In all cases the fit of the curve, given by Eq. (2), to the experimental results was as good as, or better than, that of the other relationships proposed. A typical example is shown in Fig. 1 for a ZnS:Cu phosphor prepared in this laboratory. It can be seen that, while the Destriau relationship gives considerable deviation at low voltages, Eq. (2) provides good agreement over the whole voltage range. The deviation at very high voltages, shown in this figure, has been observed in only a few cases and generally lies within the limits of experimental accuracy. Nevertheless, this apparent inconsistency is being investigated more fully.

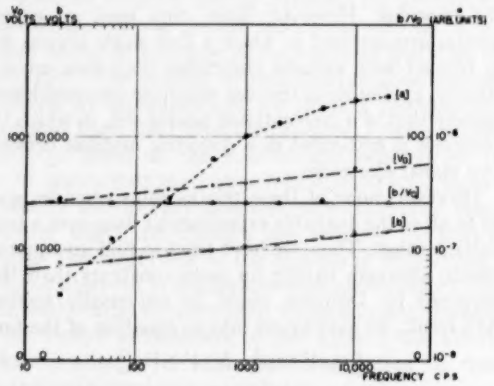

FIG. 2. Variation of the constants a, b, and V_0 of Eq. (2) with frequency of applied electric field (ZnS:Cu).

It can be seen from Table I that, although there is considerable variation in the constant a due to the different arbitrary units of brightness which have been used, the values of the constants b and V_0 are restricted to comparatively small ranges, b being of the order of 1000 volts and V_0 of the order of 50 volts. Further, the dimensionless quantity b/V_0, which is independent of cell thickness, shows even more constancy and seems to depend upon the activator used in the phosphor.

We have also studied the frequency dependence of the constants b and V_0; the results are shown in Fig. 2. It appears that both b and V_0 have a slight dependence upon frequency which can be expressed by the relationship,

$$b=b'f^n, \tag{3}$$

$$V_0=V_0'f^n, \tag{4}$$

where the exponent n is the same in both cases. This results from the fact that the ratio b/V_0 remains constant over the whole frequency range, as we have shown in the diagram. The frequency dependence of the constant a, also shown in Fig. 2, appears to be somewhat more complex; this is not too surprising since it would appear that this constant is the most sensitive to external influences.

No attempt has been made, in this Letter, to interpret the implications of Eq. (2) but a more complete account of this work will be published at a later date.

[1] G. Destriau, Phil. Mag. **38**, 700 (1947).
[2] J. Waymouth and F. Bitter, Phys. Rev. **95**, 941 (1954).
[3] L. Thorington, Spring Meeting, Electrochemical Society, Philadelphia, May 4–8, 1952 (unpublished).
[4] R. Halsted and L. Koller, Phys. Rev. **93**, 349 (1954).
[5] W. Piper and F. Williams, Conference on Luminescence, Cambridge, April 7–10, 1954 (unpublished).

Magnetic Anisotropy Constants of Ferromagnetic Spinels

R. S. WEISZ
David Sarnoff Research Center, RCA Laboratories, Princeton, New Jersey
(Received September 15, 1954)

IN calculations involving magnetization processes, it is necessary to know the magnetic anisotropy constant of the material in question. Unfortunately, this information is lacking for most ferromagnetic spinels. Single crystals of $NiFe_2O_4$ and $CoFe_2O_4$ made by the flame-fusion method apparently always have some ferrous iron present[1] and are, therefore, in reality mixed crystals with magnetite, Fe_3O_4. Magnetite, however, has been made in single crystals of good purity[2] and K_1, the first order magnetic anisotropy constant, measured[3,4] as -1.1×10^5 ergs/cm^3.

One can calculate anisotropy constants for the ferromagnetic spinels as follows. Went and Wijn[5] have presented strong evidence that, unlike metals, the *initial permeability*, μ_0, of sintered, polycrystalline ferromagnetic spinels is predominantly due to spin rotation. We then have

$$\mu_0-1=kM_s^2/K_1,$$

where M_s is the saturation magnetization and k is a constant variously given[6–8] as π, $4\pi/3$, and $8\pi/3$. From the known data for magnetite ($\mu_0=45$ for sintered material and $M_s=480$, both at room temperature) we find $k=21$. Now taking this value for k we find K_1 for the other ferromagnetic spinels. Initial permeability of dense, polycrystalline materials was obtained by the author for carefully prepared samples. These were

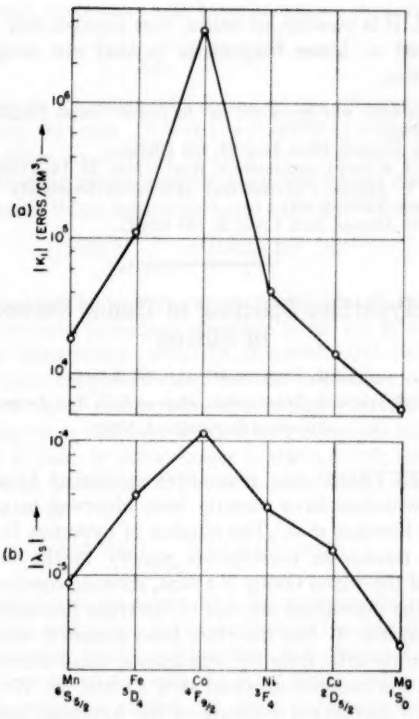

FIG. 1(a). Calculated anisotropy constant, K_1, (b) observed average magnetostriction constant, λ_s, plotted against M, for the ferromagnetic spinels, MFe$_2$O$_4$. Below each M is the ground-state term of M^{++}.

cooled slowly and are presumably nearly strain-free, with the exception of $CuFe_2O_4$ which had to be quenched. Values of M_s at room temperature were obtained in these laboratories and from other appropriate sources.[9]

The calculated values of $|K_1|$ for MFe_2O_4 are plotted in Fig. 1(a) *versus* the ground-state term of M^{++}. One will note there the direct correspondence between K_1 and J, the inner quantum number of M^{++}. Such a relationship is expected in view of the dependence of magnetic anisotropy on spin-orbit coupling. Van Vleck[10] has discussed a similar behavior in the paramagnetic bivalent salts of the iron series.

We find by our calculations, $K_1=-4.0\times10^4$ ergs/cm^3 for $NiFe_2O_4$ and $K_1=-3.4\times10^6$ for $CoFe_2O_4$. Experimental values are, respectively,[11,1] -5.1×10^4 and -1.7×10^6. Since these experimental values were obtained on crystals containing some magnetite in solid-solution,[1] it seems reasonable that K_1 for $NiFe_2O_4$ is higher and K_1 for $CoFe_2O_4$, lower, respectively than what we calculated for pure materials.

Figure 1(b) is a plot of $|\lambda_s|$, the average value of the saturation magnetostriction for sintered, polycrystalline ferromagnetic spinels. (We have ignored the fact that λ_s is positive for Fe_3O_4 and negative for the others). The values for λ_s were obtained here (with the exception of $CoFe_2O_4$)[12] and are believed to be accurate to ±25 percent. One will note again the same type of dependence on J.

[1] R. M. Bozorth and J. G. Walker, Phys. Rev. **88**, 1209 (1952).
[2] J. Smiltens, J. Chem. Phys. **20**, 990 (1952).
[3] L. R. Bickford, Jr., Phys. Rev. **78**, 449 (1950).
[4] H. Danan, Compt. rend. **238**, 1304 (1954).
[5] J. J. Went and H. P. J. Wijn, Phys. Rev. **82**, 269 (1951); see also F. Brown and C. Gravel, Phys. Rev. **95**, 652 (1954).
[6] R. M. Bozorth, *Ferromagnetism* (D. Van Nostrand Company, Inc., New York, 1951), pp. 821–2.
[7] C. Kittel, J. phys. et radium **12**, 291 (1951).
[8] H. P. J. Wijn, dissertation, Leiden, 1953 (unpublished), p. 37.
[9] R. Pauthenet and L. Bochirol, J. phys. et radium **12**, 249 (1951); references to earlier work may be found here.
[10] J. H. Van Vleck, Phys. Rev. **41**, 208 (1932).
[11] D. W. Healy, Jr., Phys. Rev. **86**, 1009 (1952).
[12] R. Vautier, Compt. rend. **235**, 356 (1952).

Infrared Spectrum of Barium Titanate*

R. T. MARA, G. B. B. M. SUTHERLAND, AND H. V. TYRELL
Randall Physics Laboratory, University of Michigan, Ann Arbor, Michigan

(Received September 16, 1954)

THE infrared absorption of barium titanate ($BaTiO_3$) has been studied between 2μ and 33μ. The spectrum obtained (Fig. 1) consists of two broad bands, one centered near 550 cm^{-1}, the other starting near 450 cm^{-1} and reaching a maximum beyond 300 cm^{-1}. The low transmission in the high-frequency end of the spectrum is due to scattering since the barium titanate was examined as a fine powder deposited on a KBr (or NaCl) plate from a suspension in isopropyl alcohol.

Several specimens of barium titanate were examined. The majority showed additional bands at 6.95, 9.45, and 11.65μ, which were proved to be due to carbonate ion impurities. Other impurity bands were noted at 7.1, 10.3, 11.05, 11.4, 11.85, and 12.85μ, but the impurities were not identified. The spectrum of a very

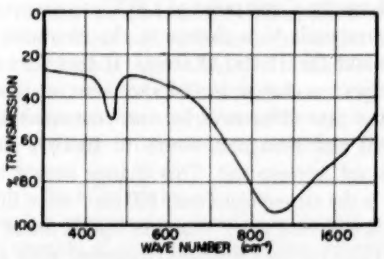

FIG. 1. The infrared absorption spectrum of $BaTiO_3$.

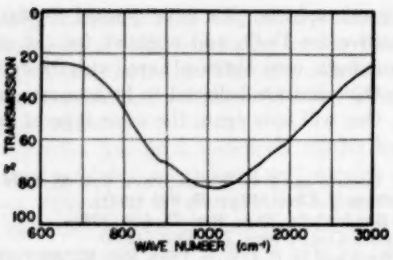

FIG. 2. The infrared absorption spectrum of $SrTiO_3$.

pure specimen of powdered strontium titanate ($SrTiO_3$) was observed between 2μ and 15μ (Fig. 2). It is identical with that of barium titanate obtained under similar conditions over that region of the spectrum. Noland[1] has recently reported the spectrum of a single crystal of strontium titanate between 1μ and 10.5μ, at which wavelength the extinction coefficient is greater than 100 cm^{-1} and is still increasing. He finds two weak bands near 5.5μ and 7.5μ. These could easily have been missed by us since our effective thickness was much less than the thickness he used. We might add that the spectrum of a single crystal of barium titanate just run in this laboratory by M. Haas shows a weak band at 8μ and a "cutoff" near 11.2μ. The spectrum of ilmenite ($FeTiO_3$) has been recorded by Hunt and others.[2] With the exception of a weak band at 1000 cm^{-1}, it is also very similar to that of barium titanate.

Apart from impurity bands, there appears to be no difference between the spectrum of barium titanate in the hexagonal and in the tetragonal form over the range 2μ to 15μ. No change was observed in the spectrum of barium titanate (ceramic) when heated to 150°C.

The foregoing observations may be considered in the light of recent theories about the ferroelectric character of barium titanate.

Jaynes[3] has predicted from an electronic theory that there should be an infrared absorption at 1000 cm^{-1}. There is definitely no *strong* absorption band in the neighborhood of 1000 cm^{-1}. Although a few specimens have shown a very weak absorption near 1000 cm^{-1}, this is most probably due to BaO impurity.

Megaw[4] has proposed that the change from the cubic form (above the Curie point of 120°C) to the tetragonal form corresponds to a change in the character of the bonds round the Ti and O atoms. If this were so, one might expect a change in the spectrum on heating to 150°C and also differences between the spectra of the tetragonal and hexagonal forms of $BaTiO_3$ since the latter is not ferroelectric. This change should be very marked in the strong band near 600 cm^{-1} since this band [which is common to all titanates and is found also in rutile (TiO_2)] is undoubtedly connected with a vibration of the TiO_4 tetrahedra. No such change was observed. It is possible, of course, that changes may have occurred at lower frequencies beyond our range of detection.

* This work was sponsored by the Signal Corps. Engineering Laboratory.

[1] J. A. Noland, Phys. Rev. **94**, 724 (1954).
[2] Hunt, Wisherd, and Bonham, Anal. Chem. **22**, 1478 (1950).
[3] E. T. Jaynes, *Ferroelectricity* (Princeton University Press, Princeton, 1953), p. 69.
[4] H. D. Megaw, Acta Cryst. **5**, 739 (1952).

Hyperfine Splitting of Donor States in Silicon

J. M. LUTTINGER* AND W. KOHN†
Bell Telephone Laboratories, Murray Hill, New Jersey
(Received September 3, 1954)

ELECTRON spin resonances exhibiting hyperfine structure have recently been observed in *n*-type Si by Fletcher *et al.*[1] The number of hyperfine lines of these resonances corresponds exactly to the nuclear spin of the added Group V atoms, showing conclusively that the resonances are due to electrons localized near such atoms. It has therefore been assumed[1] that the resonances arise from the well-known donor states with ionization energies of about 0.04 to 0.05 ev. We have made a theoretical estimate of the hyperfine splitting of phosphorus donor states to be expected on this assumption and find agreement with experiment within a factor of ~ 2.5. (We estimate the uncertainty of our theoretical result as about a factor of 5.)

Following is a brief summary of our calculations; a detailed report will be published shortly. The conduction band of Si has 6 minima on the (1,0,0) and equivalent axes.[2] The effective masses at one of these minima are $0.19m$ (twice) and $0.99m$.[3] Let $\psi(\mathbf{k}^{(i)},\mathbf{r})$ be the Bloch function corresponding to the energy minimum at $\mathbf{k}^{(i)}$, so normalized that

$$\int_{\text{cell}} |\psi(\mathbf{k}^{(i)},\mathbf{r})|^2 d\tau = \text{volume of unit cell}, \qquad (1)$$

and phased so as to be real at $\mathbf{r}=0$. It may then be shown that in the so-called effective mass approximation, the normalized ground-state wave function of the donor electron has the following form:

$$\psi(\mathbf{r}) = \frac{1}{(6)^{\frac{1}{2}}} \sum_{i=1}^{6} F^{(i)}(\mathbf{r}) \psi(\mathbf{k}^{(i)},\mathbf{r}). \qquad (2)$$

The $F^{(i)}(\mathbf{r})$ satisfy effective mass equations with the above masses and the potential $-e^2/\kappa r$ (κ=dielectric constant). They are taken as real and are normalized to unity over all space. The hyperfine splitting is then determined by the value of

$$|\psi(0)|^2 = 6|F^{(i)}(0)|^2 |\psi(\mathbf{k}^{(i)},0)|^2. \qquad (3)$$

To obtain agreement with experiment one requires

$$|\psi(0)|^2_{\text{exptl}} = 0.44\times10^{24}\ \text{cm}^{-3}. \quad (4)$$

From an approximate solution of the effective mass equation we find $|F^{(1)}(0)|^2 = (0.000037\pm10\%)\times10^{24}$ cm^{-3}, while an estimate of $|\psi(\mathbf{k}^{(i)},0)|^2$, if we use the tight-binding approximation, gives 370 within a factor of about 2. When substituted into (3), these values give

$$(|\psi(0)|^2)_{\text{eff. mass}} \approx 0.082\times10^{24}\ \text{cm}^{-3}. \quad (5)$$

When the ionization energy is calculated by the effective mass formalism one finds 0.028 ev, in rather serious disagreement with the observed 0.044 ev.[4] We have made rough allowance for the breakdown of the effective mass theory near the impurity atom. The resulting wave function, when the experimental binding energy is used, is rather larger in the last cell, and results in an increase of (5) by a factor of about 13. The final value is

$$(|\psi(0)|^2)_{\text{theor}} \approx 1.1\times10^{24}\ \text{cm}^{-3}. \quad (6)$$

The fact that (6) agrees with the experimental value [Eq. (4)], well within the uncertainty of the calculation, lends support to the picture that the observed resonances are associated with the usual donor states.

This work was carried out while we were guests of the Bell Telephone Laboratories, and we would like to thank the staff for their cooperation and friendliness.

* Permanent address: University of Michigan, Ann Arbor, Michigan.
† Permanent address: Carnegie Institute of Technology, Pittsburgh, Pennsylvania.

[1] R. C. Fletcher *et al.*, Phys. Rev. **94**, 1392 (1954); **95**, 844 (1954).
[2] C. Smith, Phys. Rev. **94**, 42 (1954); B. Lax and co-workers (private communication).
[3] B. Lax and co-workers (private communication).
[4] F. J. Morin *et al.*, Phys. Rev. **96**, 833 (1954).

Elastoresistance in *p*-Type Ge and Si*

E. N. Adams
Chicago Midway Laboratories, Chicago, Illinois
(Received September 10, 1954)

SMITH has reported[1] a large elastoresistance effect in Ge and Si of both *n*- and *p*-type. In *n*-type material there is an accumulation of evidence to support the explanation that the large elastoresistance is brought about by a strain-induced transfer of electrons between nonequivalent anisotropic energy minima in the conduction band.[2] However, no such electron transfer mechanism seems capable of explaining the large elastoresistance of *p*-type material, since the spin-orbit coupling model[3] now seems firmly established, and this model predicts that the two nearly degenerate surfaces in the valence band have cubic symmetry individually.

We believe that the large elastoresistance of *p*-type specimens originates in a strain-induced mixing of the nearly degenerate bands and a consequent strong warping of the energy surfaces. We have carried through a formal theory of this process using the methods of Fuchs and Peng,[4] McClure,[5] and Shockley,[6] and assuming the spin-orbit coupling model. Our result is that to first order in the strain the energy states in the strained lattice are given by

$$E(\mathbf{p}) = (A+2B)p^2/3 \pm R + \mathbf{p}\cdot\boldsymbol{\epsilon}\cdot\mathbf{p}/m - \mathbf{p}\cdot\boldsymbol{\epsilon}\cdot\nabla_{\mathbf{p}}E(\mathbf{p}) + (E_{11}+2E_{12})\epsilon/3 \pm \Delta R, \quad (1)$$

with

$$R^2 \equiv (A-B)^2p^4/9 + [C^2-(A-B)^2][p_x^2p_y^2+p_y^2p_z^2+p_z^2p_x^2]/3, \quad (2)$$

$$\Delta R = (1/R)\{CE_{44}[p_xp_y\epsilon_{xy}+p_yp_z\epsilon_{yz}+p_zp_x\epsilon_{zx}]/3 + (A-B)(E_{11}-E_{12})[(3p_x^2-p^2)(3\epsilon_{xx}-\epsilon)+(3p_y^2-p^2) \times(3\epsilon_{yy}-\epsilon)+(3p_z^2-p^2)(3\epsilon_{zz}-\epsilon)]/27\}. \quad (3)$$

The + and − signs refer to the energy surfaces for the carriers of small and large mass, respectively. In the above equations $\boldsymbol{\epsilon}$ denotes the tensor of strain, ϵ its trace. The constants E_{11}, E_{12}, and E_{44} are three unknown matrix elements which enter the theory. Their designations are chosen to emphasize that they transform like the components of a fourth rank tensor under cubic symmetry operations. The E_{ij} are expected to have the order of magnitude of electron volts, so the terms in (1) proportional to the E_{ij} are by far the largest for the states responsible for semiconduction properties.

A theory of the elastoresistance based on the above expressions for the energy levels shows that in the notation of reference 1, the volume elastoresistance coefficient $(M_{11}+2M_{12})/3$ is small compared to M_{44}, in agreement with experiment. Of the other two principal coefficients, M_{44} is proportional to CE_{44}/kT and $(M_{11}+M_{12}/2)$ is proportional to $(A-B)(E_{11}-E_{12})/2kT$ as might be expected. Experimentally, $(M_{11}-M_{12})/2$ is small compared to M_{44}. This we must interpret as implying that $(E_{11}-E_{12})/2$ is small compared to E_{44}, since the parameters $(A-B)$ and C as determined from the cyclotron resonance experiment have the same order of magnitude.

Our formal theory does not suggest why E_{44} is relatively so large. However, we believe the physical reason is not difficult to conjecture. Essentially E_{44} is a matrix element of the strain-induced incremental electron potential for a shear which changes the angles between the cubic axes while $(E_{11}-E_{12})/2$ is a matrix element of the potential for a strain which does not change the angle. To first order in $\boldsymbol{\epsilon}$ only the former type of strain can cause a change in the nearest neighbor distances, and we suspect that that is the underlying physical reason why E_{44} is relatively so large.

We think it encouraging that the spin-orbit coupling model is capable of giving a satisfactory account of the large elastoresistance in *p*-type material without the

introduction of separate energy minima, since so many other data seem to be satisfactorily accounted for on that model. The principal fact of observation remaining to be understood is the strange temperature dependence of mobilities in p-type materials. We have under way a calculation which attempts to explain this temperature dependence on the basis of the theory referred to above.

* Details of the calculations described herein are contained in CML Technical Note No. CML-TN-P8, and are available on request from the Chicago Midway Laboratories, 6040 S. Greenwood Ave., Chicago 37, Illinois. This research was supported in whole by the U. S. Air Force.

[1] C. S. Smith, Phys. Rev. **94**, 42 (1954).

[2] F. Herman and J. Callaway, Phys. Rev. **89**, 518 (1953); B. Abeles and S. Meiboom, Phys. Rev. **95**, 31 (1954); Dresselhaus, Kip, and Kittel, Phys. Rev. **92**, 547 (1953); Lax, Zeiger, Dexter, and Rosenblum, Phys. Rev. **93**, 1418 (1954).

[3] Dresselhaus, Kip, and Kittel, Phys. Rev. **95**, 568 (1954); Dexter, Zeiger, and Lax, Phys. Rev. **95**, 557 (1954); Dexter and Lax (on p–Si), (to be published); A. Kahn, thesis, University of California, 1954 (unpublished).

[4] K. Fuchs and H. W. Peng, Proc. Roy. Soc. (London) **A180**, 451 (1942).

[5] Joel W. McClure, thesis, University of Chicago, 1954 (unpublished).

[6] W. Shockley, Phys. Rev. **78**, 173 (1950).

Energies of π^- Mesonic X-Ray K Lines*

M. B. Stearns, M. Stearns, S. DeBenedetti, and L. Leipuner
Carnegie Institute of Technology, Pittsburgh, Pennsylvania
(Received September 13, 1954)

As reported in a previous Letter,[1] we have studied the energies of the $2p \rightarrow 1s$ transitions of the π^- mesonic x-rays using the method of critical absorption. The main purpose of this study is to search for possible shifts caused by a specifically nuclear interaction of the meson. A description of the experimental technique and of the method of calculation can be found in reference 1. The results are given below.

Lithium.—This is the lightest element whose mesonic x-rays can be detected with our equipment. Its $2p \rightarrow 1s$ line (Table I) should fall between the K edges of Pd ($Z=46$, edge energy 24.35 kev)[2] and Ag ($Z=47$, edge energy 25.51 kev). Metallic foils of $Z=42$, 45, 46, 47, 48, 49, and 50 were used in the absorption experiments. The thickness of the foils corresponded to a transmission of 50 percent for x-rays just below the K-absorption edge. The resulting pulse-height distribution

Table I. Lithium and beryllium π-mesonic x-ray energies.

	Lithium $2p \rightarrow 1s$	Beryllium $2p \rightarrow 1s$
Klein-Gordon energy for $m_\pi = 272.5 m_e$ (kev)	24.520	43.82
Vacuum polarization[a] (kev)	+0.096	+0.20
Finite nuclear size (for $r_0 = 1.2 \times 10^{-13}$ cm) (kev)	−0.033	−0.12
Computed energy (kev)	24.58	43.90
Experimental determination (kev)	$23.22 < E < 24.35$	$42.00 < E < 43.57$

[a] H. C. Corben and A. Mickelwait (private communication).

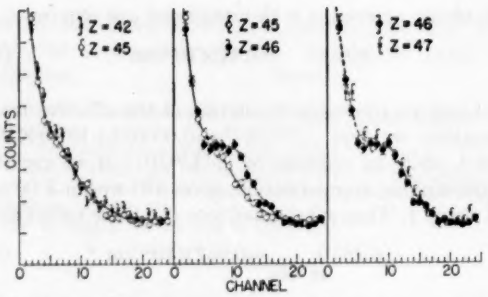

Fig. 1. Pulse-height distribution showing the transmission of the lithium $2p \rightarrow 1s$ π-mesonic line through absorbers $Z=42$, 45, 46, and 47. The errors indicated are standard statistical errors.

curves for absorbers close to the transmission discontinuity are plotted in Fig. 1 and show that the line under study lies between the edges of Rh ($Z=45$, edge energy 23.22 kev) and Pd. This corresponds to a shift of at least 230 ev and no more than 1360 ev toward lower energy.

Beryllium.—The absorbers used were thin-walled Lucite cells, 1 cm thick, containing an aqueous solution of a salt of the absorbing element. The concentration was such as to give a factor 4 in transmission above and below the K edge. The $2p \rightarrow 1s$ line of Be (Table I) should fall between the edges of elements 60 (Nd, 43.57 kev) and 61 (Pm, 45.2 kev).

The curves obtained for elements 57, 58, 59, 60, and 62 are shown in Fig. 2. From this series and many other

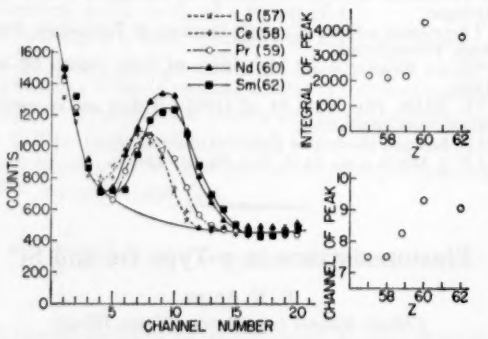

Fig. 2. Pulse-height distribution showing the transmission of the Be $2p \rightarrow 1s$ π-mesonic line through absorbers $Z=57$, 58, 59, 60, and 62. Also shown as a function of Z are the transmitted intensities and the positions of the peaks. This figure should be compared with Fig. 1 of reference 1.

similar runs it appears that the Be $2p \rightarrow 1s$ transition definitely lies below the edge of Nd ($Z=60$) and above the edge of Pr ($Z=59$, 42.00 kev). This corresponds to an energy shift of at least 330 ev, and not more than 1900 ev toward lower energy. However, the line seems to lie closer to Pr than to Nd indicating a shift nearer to the larger value. Measurements of peak positions relative to known lines indicate a similar negative shift (see Fig. 3).

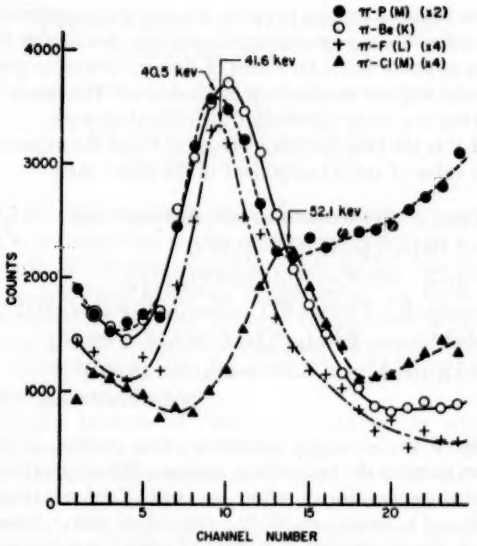

FIG. 3. Pulse-height distribution showing peak position for the Be $2p \rightarrow 1s$ π-mesonic line compared with other mesonic lines of known energy [P (M), 40.5 kev; F (L), 41.6 kev; Cl (M), 52.1 kev]. As a result of the comparison the Be energy is 42.9±0.5 kev corresponding to a negative shift of about 1.0±0.5 kev.

Boron.—The results obtained to date are not fully understood. Further studies with the separated isotopes will be made before reporting on this element.

Carbon, nitrogen, oxygen, and fluorine.—The K-mesonic lines of these elements cannot be studied with the critical absorption technique. We have measured their energies using the pulse-height selector and have found negative shifts varying roughly from 7 percent for carbon to about 13 percent for fluorine. The results of these measurements will be described in a later communication.

In conclusion we have observed that the $2p \rightarrow 1s$ lines in the elements lithium to oxygen are shifted to lower energies with the possible exception of boron. This indicates an effective repulsive potential between the meson in the $1s$ state and the nucleus.

* Supported in part by the U. S. Atomic Energy Commission.

[1] Stearns, Stearns, DeBenedetti, and Leipuner, Phys. Rev. **95**, 1353 (1954); Stearns, Stearns, Leipuner, and DeBenedetti, Phys. Rev. **95**, 625(A) (1954).

[2] The K-absorption edge values were taken from a recent compilation of Lewis Slack, Naval Research Laboratory.

Formula for Polarization in Nucleon-Nucleon Scattering*

G. BREIT AND J. B. EHRMAN
Yale University, New Haven, Connecticut

(Received September 7, 1954)

THE importance assumed by experiments[1] on the polarization of nucleons makes it desirable to have available a general formula for the calculation of polarization effects. The quantity under consideration is that usually denoted by P which is related to δ_y, the mean spin component normal to scattering plane in a single scattering experiment with unpolarized particles, by $P=2\delta_y$. An explicit formula in terms of the scattering matrix referred to weak-field spin states is available in several theoretical papers,[2] for example in Eq. (15) of Goldfarb and Feldman.[3] In principle, these formulas solve the problem but the work involved in the transition to special forms containing phase shifts is large at times. It appeared desirable therefore to reduce the general expressions to a point representing a compromise between compactness and explicitness. For $p-p$ scattering,

$$k^2(P\sigma)_{p-p}=2\sin\theta\cos\varphi\,\mathrm{Im}\{\alpha_1(\alpha_2+\alpha_c)^* -(1-\mu^2)\alpha_1\alpha_3^*+\alpha_4^*(\alpha_5+\alpha_c)\}, \quad (1)$$

where the colatitude and azimuthal angles θ, φ are as in Swanson's paper, $k=2\pi$ times reciprocal of wavelength, Im indicates the imaginary part of expression in braces. The six quantities $\alpha_1, \alpha_2, \cdots, \alpha_c$ are as follows:

$$\alpha_1=-\Sigma[L(L+2)Q_{L+1}(L)-(2L+1)Q_L(L) -(L^2-1)Q_{L-1}(L)][P_L'/L(L+1)]e_{L0} -2B[(l+1)P_{l+2}'-(l+2)P_l'], \quad (2)$$

$$\alpha_2=\Sigma\tfrac{1}{2}e_{L0}[(L+2)Q_{L+1}(L) +(2L+1)Q_L(L)+(L-1)Q_{L-1}(L)]P_L -(l+1)(l+2)B(P_{l+2}+P_l), \quad (3)$$

$$\alpha_3=\Sigma\tfrac{1}{2}e_{L0}[LQ_{L+1}(L)-(2L+1)Q_L(L) +(L+1)Q_{L-1}(L)][P_L''/L(L+1)] -B(P_{l+2}''+P_l''), \quad (4)$$

$$\alpha_4=\Sigma e_{L0}[Q_{L+1}(L)-Q_{L-1}(L)]P_L' -2B[(l+1)P_{l+2}'-(l+2)P_l'], \quad (5)$$

$$\alpha_5=\Sigma e_{L0}[(L+1)Q_{L+1}(L)+LQ_{L-1}(L)]P_L +2B(l+1)(l+2)(P_{l+2}+P_l), \quad (6)$$

$$\alpha_c=\tfrac{1}{4}\eta[-\mathbf{s}^{-2}\exp(-i\eta\ln\mathbf{s}^2)+\mathbf{c}^{-2}\exp(-i\eta\ln\mathbf{c}^2)], \quad (7)$$

where

$$Q_J(L)=[-1+\exp(2i\delta_J^L)]/(2i), \quad (8)$$

$$e_{L0}=\exp(2i\sigma_{L0})=\exp[2i(\tan^{-1}(\eta/L) +\tan^{-1}(\eta/(L-1))+\cdots+\tan^{-1}\eta)]. \quad (9)$$

δ_J^L is the phase shift for total angular momentum $J\hbar$ and orbital angular momentum $L\hbar$, while the other symbols have the following meaning: $\eta=e^2/\hbar v$, v=relative velocity; $\mathbf{s}=\sin\theta/2$, $\mathbf{c}=\cos\theta/2$, θ=scattering angle in center of mass system; $\mu=\cos\theta$, $P_L=P_L(\mu)$, $P_L'=dP_L/d\mu$, $P_L''=d^2P_L/d\mu^2$. If there is no coupling between states of different L for the same J the constant $B=0$. If states with $J=l+1$ having values $L=l$ and $L=l+2$ are coupled to each other, then

$$B=\tfrac{1}{2}C_{L\,l+2}(l+1)^{-1}(l+2)^{-1}\exp[i\sigma_{L0}+i\sigma_{l+2,0}], \quad (10)$$

where $C_{l,l+2}$ is as in Thaler, Bengston, and Breit and $Q_{l+1}(l)$, $Q_{l+1}(l+2)$ are modified by replacing them by $Q_{l+1}(l)+C_{ll}$, $Q_{l+1}(l+2)+C_{l+2,l+2}$. The matrix

$$(\mathrm{T})=\begin{pmatrix} Q_-+C_{--} & C_{-+} \\ C_{+-} & Q_++C_{++} \end{pmatrix}, \tag{11}$$

can then be related to (S) by

$$(\mathrm{T})=[(S)-1]/(2i), \tag{12}$$

and (S) is a general unitary symmetric matrix expressible by means of 3 parameters. The subscripts $-$ and $+$ are used to indicate the smaller and larger of the two L. The Q as used in Thaler, Bengston, and Breit have a generic meaning in connection with the special model used by them. In calculations, however, the diagonal elements of (T) enter instead in the equations for $\alpha_1, \cdots, \alpha_5$.

Substitution of Eqs. (2), (3)$\cdots$, (7) into Eq. (1) enables one to collect coefficients of a product involving two Q's such as Q_1, Q_2^*. These combine with terms in $Q_2Q_1^*$ which can be converted under the Im sign to the order $Q_1Q_2^*$ by taking the complex conjugate and changing the sign. For uncoupled terms,

$$\mathrm{Im}(Q_2Q_1^*)=\sin\delta_2\sin\delta_1\sin(\delta_2-\delta_1)$$

then gives readily the forms needed for numerical work.

In Eq. (1) the sums over L are supposed to be taken over odd values only. The formula can be used for the calculation of $(P\sigma)_{p-n}$ provided a coefficient $\frac{1}{4}$ is inserted on the right side, thus changing the 2 in front of $\sin\theta$ to $\frac{1}{2}$ and provided the sum is made to extend over odd and even L employing all triplet states. In both cases the singlet states do not enter.

* Assisted by the Office of Ordnance Research, U. S. Army.

[1] Oxley, Cartwright, Rouvina, Baskir, Klein, Ring, and Skillman, Phys. Rev. **91**, 419 (1953); L. F. Wouters, Phys. Rev. **84**, 1069 (1951); Marshall, Marshall, Nagle, and de Carvalho, Phys. Rev. **93**, 1431 (1954); Chamberlain, Donaldson, Segrè, Tripp, Wiegand, and Ypsilantis, Phys. Rev. **95**, 850 (1954); Kane, Stallwood, Sutton, Fields, and Fox, Atomic Energy Commission Report NYO-6569, July 6, 1954 (unpublished), to cite some of the many recent papers.

[2] J. Schwinger, Phys. Rev. **69**, 681 (1946); **73**, 407 (1948); L. Wolfenstein, Phys. Rev. **75**, 1664 (1949); **76**, 541 (1949); L. J. B. Goldfarb and D. Feldman, Phys. Rev. **88**, 1099 (1952); D. R. Swanson, Phys. Rev. **89**, 749 (1953); R. H. Dalitz, Proc. Phys. Soc. (London) **A65**, 175 (1952); A. Simon and T. A. Welton, Phys. Rev. **90**, 1036 (1953).

Formula for Polarization in p-p Scattering for P and F Waves*

M. H. Hull, Jr., and A. M. Saperstein
Yale University, New Haven, Connecticut
(Received September 7, 1954)

An expression for the calculation of polarization of protons produced by single scattering taking into account P and F waves has been worked out and is given below. Coupling between $^3P_2$ and $^3F_2$ is neglected, but otherwise the most general condition describable by a set of phase shifts for states of definite orbital as well as total angular momentum is considered. The result is written in a form convenient for numerical work.

If P is the polarization, defined as twice the expectation value of the y component of the spin,[1] then

$$\begin{aligned} k^2(P\sigma)_{p-p}=&(a+b\cos^2\theta+c\cos^4\theta)\sin\theta\cos\theta\cos\varphi \\ &-2\,\mathrm{Im}\{\alpha_c^*[\tfrac{3}{2}e_{10}(Q_2(P)-Q_1(P)) \\ &-\tfrac{1}{8}e_{30}(-8Q_2(F)-7Q_3(F)+15Q_4(F))] \\ &-\alpha_c[e_{10}(Q_2(P)-Q_0(P))^*-\tfrac{3}{2}e_{30}(Q_4(F)-Q_2(F))^*]\} \\ &\times\sin\theta\cos\varphi-2\,\mathrm{Im}\{\alpha_c^*[\tfrac{5}{8}e_{30}(-8Q_2(F)-7Q_3(F) \\ &+15Q_4(F))]-\alpha_c[(15/2)e_{30}(Q_4(F)-Q_2(F))^*]\} \\ &\times\sin\theta\cos^2\theta\cos\varphi, \end{aligned} \tag{1}$$

where σ is the single scattering cross section, k the wave number of the incident protons. Other quantities are: $e_{LO}=\exp(2i\sigma_{LO})$, where σ_L is the Coulomb phase shift and $\sigma_{LO}=\sigma_L-\sigma_O$; $Q_J(L)=\exp(i\delta_J{}^L)\sin\delta_J{}^L$, where $\delta_J{}^L$ is the phase shift in a state of orbital angular momentum Lh and total angular momentum Jh;

$$\begin{aligned} \alpha_c=(\eta/4)[&-\mathbf{s}^{-2}\exp(-i\eta\ln\mathbf{s}^2) \\ &+\mathbf{c}^{-2}\exp(-i\eta\ln\mathbf{c}^2)], \end{aligned} \tag{2}$$

where $\eta=e^2/\hbar v$, $\mathbf{s}=\sin(\theta/2)$, $\mathbf{c}=\cos(\theta/2)$, θ is the scattering angle in the center-of-mass system, v the relative velocity;

$$\begin{aligned} a=9\{&(P_1,P_2)+\tfrac{2}{3}(P_0,P_2)+(7/12)(F_3,F_2) \\ &-(77/12)(F_4,F_2)-(35/24)(F_4,F_3)+(F_2,P_1,31) \\ &+\tfrac{2}{3}(F_2,P_0,31)-(10/3)(F_2,P_2,31)-(7/12)(F_3,P_2,31) \\ &+(5/3)(F_4,P_0,31)+(5/2)(F_4,P_1,31) \\ &-(23/12)(F_4,P_2,31)\}; \end{aligned} \tag{3}$$

$$\begin{aligned} b=(1/16)\{&-420(F_2,F_2)+6020(F_4,F_2)+1540(F_4,F_3) \\ &+1200(F_2,P_2,31)-840(F_4,P_1,31)+420(F_3,P_2,31) \\ &-220(F_4,P_2,31)-560(F_4,P_0,31)]\}; \end{aligned} \tag{4}$$

$$c=(25/8)\{140(F_2,F_4)+49(F_3,F_4)\}, \tag{5}$$

where

$$\begin{aligned} &(L_J,L_{J'})=\sin\delta_J{}^L\sin\delta_{J'}{}^{L'}\sin(\delta_J{}^L-\delta_{J'}{}^{L'}), \\ &(L_J,L_{J'},31)=\sin\delta_J{}^L\sin\delta_{J'}{}^{L'}\sin(\delta_J{}^L-\delta_{J'}{}^{L'}+2\sigma_{31}), \end{aligned} \tag{6}$$

and

$$\sigma_{LL'}=\sigma_L-\sigma_{L'}, \quad \text{with} \quad \sigma_L-\sigma_{L-1}=\tan^{-1}(\eta/L).$$

This result agrees with that of Goldfarb and Feldman[1] up to second order in $\cos\theta$ if coupling is neglected in their work and Coulomb terms are neglected in Eq. (1). It has been checked throughout with the zero-coupling limit of the result of Breit and Ehrman.[2]

* Assisted by the Office of Ordnance Research, U. S. Army.

[1] L. J. B. Goldfarb and D. Feldman, Phys. Rev. **88**, 1099 (1952).

[2] G. Breit and J. B. Ehrman, preceding Letter [Phys. Rev. **96**, 805 (1954)].

Phase Shifts for Nucleon-Nucleon Scattering at 280 Mev*

G. Breit, J. B. Ehrman, A. M. Saperstein, and M. H. Hull, Jr.
Yale University, New Haven, Connecticut
(Received September 7, 1954)

RECENT results on the polarization of nucleons as measured by double scattering have given more specific indications regarding phase shifts[1] than have been previously available. In particular, the more recent data[2] at 280 Mev indicate[3] the presence of phase shifts for orbital angular momenta $L>1$ at this energy. A closer examination shows that even more specific conclusions can be drawn.

If the analysis of $(P\sigma)_{p-p}$ is confined to orbital angular momenta $L<4$, it may be shown that even if one assumes the presence of coupling between $^3P_2$ and $^3F_2$, the terms in $\sin\theta\cos\varphi\cos^5\theta$ can be present only if there is a $^3F_4$ phase shift $\delta_4{}^F$. The presence of terms of above type in $(P\sigma)_{p-p}$ indicates, therefore, that there are effects caused by F-wave phase shifts δ^F originating directly rather than through coupling to states of lower orbital angular momenta. The conclusion regarding the presence of direct δ^F effects rests heavily on the presence of the term $0.116(\sin 6\theta)$ mb/sterad in the analysis of $(P\sigma)_{p-p}$. According to the authors,[2] the presence of this term is not quite certain since the data can be represented reasonably well without it. Considering the Fourier analysis of the experimental curve by means of Fourier's formula, the coefficient 0.116 is a sum of two positive integrals in the intervals from (0°,30°) and (60°,90°) and one negative integral over (30°,60°). Each of the positive integrals is ~3 times the sum of the three so that the accuracy of the result is rather poor. The most uncertain of the three is the integral over (0°,30°). The knowledge of the curve in this region would admit an error of 10 percent in the integral over it corresponding to an error of perhaps 30 percent in the number 0.116. A qualitatively incorrect value of this coefficient thus appears unlikely but is not altogether excluded since both for $p-p$ and $p-n$ the experimental points at $\theta\cong 18°$ are systematically off the curves. If the data could be made more accurate in this respect, clarification regarding F waves would result.

Since there is little doubt regarding the presence of noncentral forces at low energies, as indicated by the quadrupole moment of the deuteron, it appears likely that there are differences between different δ^D and between different δ^F. The coupling of $^3S_1$ to $^3D_1$ is very likely for the same reason. Calculation shows that if $\delta_2{}^D=\delta_3{}^D=0$ and if all phase shifts but δ^D, δ^S are neglected then $(P\sigma)_{p-n}$ contains no term in $\sin\theta\cos\theta P_2(\cos\theta)$ the only dependence being on $\sin\theta\cos\theta$. While it is probable that the differences in the δ^D and the coupling of $^3S_1$ to $^3D_1$ are connected through the interaction energy, one can separate phenomenologically the coupling from the direct occurrence of $\delta_2{}^D$ and $\delta_3{}^D$. In this sense the $^3D_1$ state caused by $^3S_1$ does not produce $\sin\theta\cos\theta P_2(\cos\theta)$ terms, without the aid of cross products involving the pairs *S-G*, *D-D*, *P-F*, etc., the sum of the L's in a product being even if an odd power of $\cos\theta$ multiplying the factor $\sin\theta$ is desired.

Among the *D-D* combinations the $^3D_1-{}^3D_2$ term does not occur with $\sin\theta\cos^3\theta$ similarly to the absence of $^3F_3-{}^3F_2$ combinations with $\sin\theta\cos^5\theta$. Presence of coupling between $^3D_1$ and $^3S_1$ or between $^3F_2$ and $^3P_2$ does not interfere with this rule. The conclusion regarding the role of $^3S_1-{}^3D_1$ coupling differs only in emphasis from that of Fried, the possibility of $^3D_2={}^3D_3=0$ in the presence of the coupling being specifically considered here.

The ^3F phase shifts required by the data are of the order of 15°, an amount sufficiently smaller than the ^3P phase shifts to make it conceivable that phase shifts for $L>3$ are not important in the analysis of $p-p$ data at this energy. The repulsive character of potentials expected for triplets with odd L in $p-p$ scattering on the symmetric theory may be expected to contribute to the smallness of these phase shifts.

* Assisted by the Office of Ordnance Research, U. S. Army.
[1] A. Garren, Phys. Rev. **92**, 213 (1953); de Carvalho, Heiberg, Marshall, and Marshall, Phys. Rev. **94**, 1796 (1954).
[2] Chamberlain, Donaldson, Segrè, Tripp, Wiegand, and Ypsilantis, Phys. Rev. **95**, 850 (1954).
[3] B. D. Fried, Phys. Rev. **95**, 851 (1954). In the paper by Thaler, Bengston, and Breit, Phys. Rev. **94**, 683 (1954) quoted by Fried, Eq. (9) contains a misprint, < appearing for >, in contradiction to the text immediately to the right of Eq. (9).

Polarization of High-Energy Protons in Elastic Scattering on Helium and Carbon*

O. Chamberlain, E. Segrè, R. Tripp, C. Wiegand, and T. Ypsilantis
Radiation Laboratory, Department of Physics, University of California, Berkeley, California
(Received September 14, 1954)

WE have previously reported[1] results of experiments concerning polarization of proton beams by scattering from complex nuclei. Other authors[2] have also dealt with this problem. Particular interest has been attached to polarization by elastic scattering and several publications[3-5] have treated the theory for this case.

As previously, we have attempted to isolate elastic scattering by insertion of an absorber into the counter telescope used to detect the scattered protons. Owing to range straggling in the absorber and to inhomogeneity of the beam, it is impossible to exclude with certainty all protons resulting from inelastic scattering. For example, we mention the scattering by carbon in which the lowest excited state is at 4.4 Mev, while our counting arrangement could be guaranteed to reject scatter-

ing events only if at least 20 Mev were lost to the scattering nucleus.

At small angles of scattering from any target the elastic scattering is easily determined simply because it is strongly predominant over inelastic scattering. However, at angles larger than about 20° the so-called elastic scattering is contaminated with an appreciable fraction of protons from inelastic scattering.

Helium is of special interest in this regard because there are no excited or unbound states at energies lower than 20 Mev. Therefore, our existing method of detection is adequate to exclude all protons inelastically scattered by helium at any angle.

We have measured the elastic-scattering cross sections of helium for 315-Mev 74 percent-polarized protons, and of carbon for 290-Mev 64 percent-polarized protons. Our second targets were 1.7 g/cm² of liquid helium and 3.2 g/cm² of graphite respectively. The polarized beams were obtained by scattering 340-Mev protons to the left at 15° and 18° respectively, from a beryllium first target inside the cyclotron as previously described.[1] The beam polarizations were determined in separate experiments by external scattering from beryllium at 15° and 18°.

The results for both left and right scattering from helium are shown in Fig. 1(a), in which the differential-scattering cross sections have been corrected for nuclear attenuation in the absorber. Figure 1(b) shows the polarization $P(\Theta)$ in the elastic scattering by helium as computed from the points shown in Fig. 1(a) and the known beam polarization. The relation used is

$$e(\Theta)=P_B P(\Theta) \tag{1}$$

in which

$$e(\Theta)=[\sigma_{\text{left}}(\Theta)-\sigma_{\text{right}}(\Theta)]/[\sigma_{\text{left}}(\Theta)+\sigma_{\text{right}}(\Theta)],$$

P_B is the polarization of the beam, and $P(\Theta)$ is the polarization that would be produced by scattering an unpolarized beam at angle Θ on the substance in question (in the present experiment, helium or carbon). Figure 2 shows the corresponding results for a carbon second target.

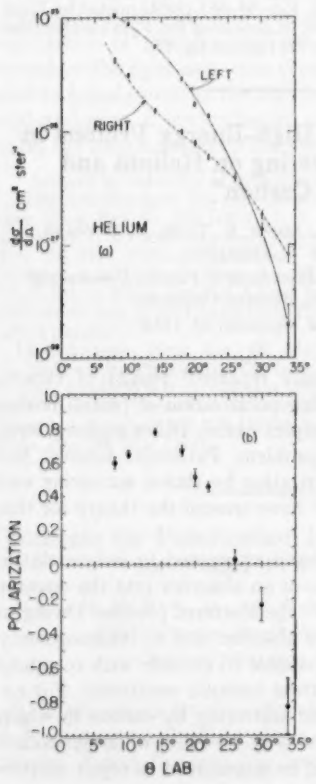

FIG. 1(a). Differential-scattering cross sections *versus* left and right scattering angles for 74 percent-polarized 315-Mev protons scattered elastically by helium. (b) Polarization $P(\Theta)$ of protons elastically scattered by helium *versus* scattering angle.

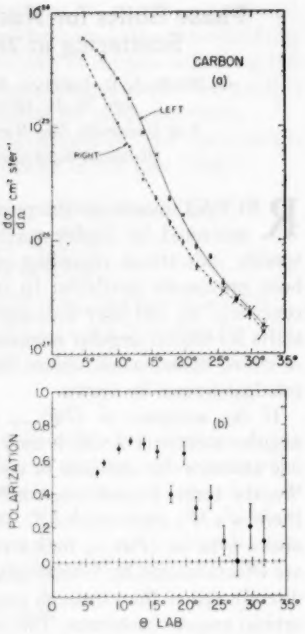

FIG. 2(a). Differential-scattering cross sections *versus* left and right scattering angles for 64 percent-polarized 290-Mev protons scattered elastically by carbon. (b) Polarization $P(\Theta)$ of protons elastically scattered by carbon *versus* scattering angle. At angles greater than 20° the so-called elastic scattering from carbon is contaminated by inclusion of some inelastically scattered protons.

An interesting feature of the helium results is that they show a definite change in sign of the polarization. Changes in sign near minima of the diffraction scattering curve of carbon have been predicted by Fermi, by Malenka, and by Snow, Sternheimer, and Yang.[3] However, it is not clear that the observed change in sign should be attributed to the mechanism implied by these theoretical considerations. On the other hand Tamor[5] assumed the validity of the impulse approximation for light nuclei, and on that basis predicted that the polarization of carbon and helium should be the same. That they are the same seems fairly well borne out for angles small enough (up to 20°) that the carbon experiment can be deemed to represent purely elastic scattering. In the framework of Tamor's theory

either helium or carbon polarization data should be viewed as exemplifications of that part of the nucleon-nucleon scattering that involves no change in spin state of the target nucleons.

The authors have relied heavily on discussions with Dr. B. D. Fried, Dr. J. V. Lepore, Dr. W. Heckrotte, and Dr. S. Tamor.

* This work was performed under the auspices of the U. S. Atomic Energy Commission.

[1] Chamberlain, Segrè, Tripp, Wiegand, and Ypsilantis, Phys. Rev. **93**, 1430 (1954), and **95**, 1105 (1954).
[2] Oxley, Cartwright, and Rouvina, Phys. Rev. **93**, 806 (1954); Marshall, Marshall, and de Carvalho, Phys. Rev. **93**, 1431 (1954); also J. M. Dickson and D. C. Salter, Nature **173**, 946 (1954).
[3] E. Fermi, Nuovo cimento **11**, 407 (1954) and private communication; Snow, Sternheimer, and Yang, Phys. Rev. **94**, 1073 (1954); B. J. Malenka, Phys. Rev. **95**, 522 (1954).
[4] W. Heckrotte and J. V. Lepore, Phys. Rev. **94**, 500 (1954); W. Heckrotte, Phys. Rev. **94**, 1797 (1954); R. M. Sternheimer, Phys. Rev. **95**, 587 (1954).
[5] S. Tamor, Phys. Rev. **94**, 1087 (1954).

Energetic Disintegration of a Heavy Nuclear Fragment*

W. F. Fry and M. S. Swami
Department of Physics, University of Wisconsin, Madison, Wisconsin
(Received September 7, 1954)

SEVERAL events[1–11] have been observed in photographic emulsion where a nuclear fragment stopped and subsequently disintegrated. In some of these events a π meson was emitted, while in other events, only nuclear particles were observed. The energy release from the disintegration of the nuclear fragment has been measured quite accurately in a few cases[6,7,9] and found to be consistent with the assumption that a Λ^0 particle was loosely bound in the nuclear fragment.

An energetic disintegration of a nuclear fragment was found in a 1000-micron glass-backed plate which had been exposed to cosmic rays in a sky-hook balloon flight. A photograph of the event is shown in Fig. 1. The primary star is of the type $(22+9p)$. The track of the nuclear fragment F, is 192 microns long. The thindown along the track F and the multiple scattering near the end of the track show that the fragment stopped before producing the secondary star. From a comparison of the thindown characteristics along track F with other tracks of known Z, the charge of the fragment is found to be greater than $2e$ and definitely less than $5e$. The secondary star has four prongs. The characteristics of the tracks from the secondary star are given in Table I.

If track 4 is assumed to be a π meson, the residual momentum of the charged particles from the secondary star is 342 Mev/c; if track 4 is assumed to be a proton, the residual momentum is 680 Mev/c. If the residual momentum is carried away by two neutrons traveling together in the direction to conserve the residual momentum, the energy of the two neutrons is found to be 28 Mev if track 4 is assumed to be a π meson, and 116 Mev if track 4 is assumed to be a proton. If track 4 is ascribed to a π meson, the minimum energy release from the secondary star is $2.7+14+20+(45-18)+28 \cong 92$ Mev. If track 4 is due to a proton, the minimum

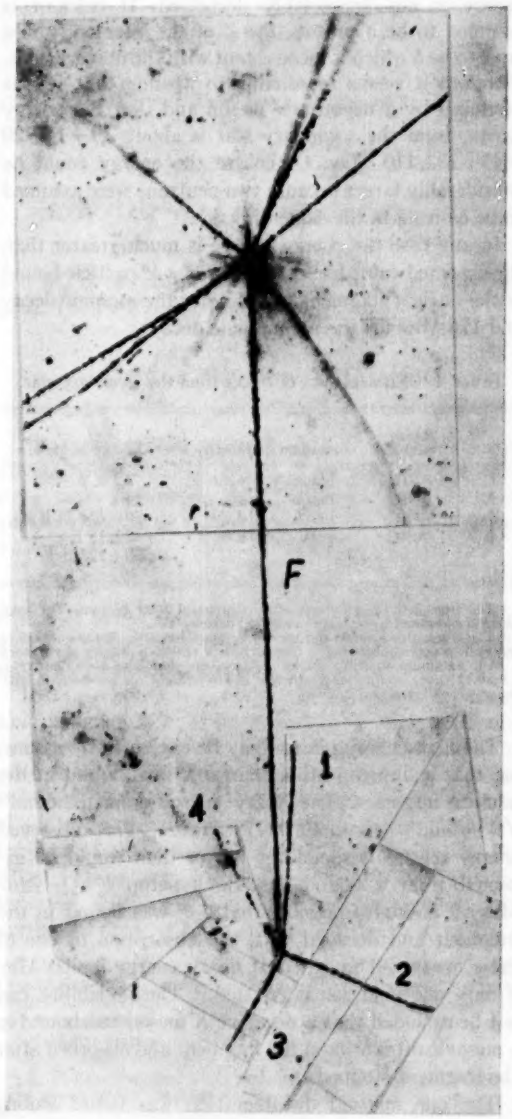

FIG. 1. A nuclear fragment F from a cosmic-ray star stops in the emulsion and produces a secondary star which has four prongs. Tracks 1 and 3 were produced by a proton or deuteron or triton; and track 2 by an α particle. Track 4 is most likely due to a negative π meson. (Observer: J. Slowey.)

energy release is $2.7+14+20+(300-125)+116\cong 328$ Mev. If only one neutron was emitted from the star, the total energy of the secondary star would be greater than the above estimates. If it is assumed that more than two neutrons were ejected, the total estimated energy is not appreciably decreased. If track 4 is assumed to be a proton, the Z of the fragment would have to be 5 which is inconsistent with the observations, therefore it seems reasonable to assume that it was produced by a negative π meson and that the energy release from the secondary star is about $2.7+14+20+45+28\cong 110$ Mev. Of course the energy could be considerably larger because two neutrons were assumed to be emitted in the same direction.

In any case the energy release is much greater than the expected value from the decay of a Λ^0 particle bound in the nuclear fragment (37 Mev for the mesonic decay and 176 Mev for the nonmesonic decay).

TABLE I. Characteristics of tracks from the secondary star.

Track	Range microns	Ionization	Identity	Energy in Mev
1	62	black	p,d,t	2.7 if p
2	109	black	α	14
3	>2000[a]	black	p,d,t	$20<E<24$ if p
4	>300[b]	gray	π or p	45 ± 18 if π 300 ± 125 if p

[a] The track left the emulsion after a range of 2000 microns. The total range is estimated to be less than 2500 microns.
[b] The track dips steeply and leaves the emulsion after 300 microns. The energy was determined from a comparison of the blob density along track 4 with minimum ionizing tracks of the same dip. The blob density is 1.5 ± 0.12 times minimum. The track is too straight for an electron with the observed ionization.

The high-energy release may be explained by assuming that a hyperon other than a Λ^0 was bound in the nuclear fragment. The decay energy from a bound[12] Y^+ would be about 117 Mev.[13] The observed energy release is somewhat higher than would be expected from a bound cascade hyperon $Y^-(Q_Y\cong 67$ Mev).[14] It is also possible that a θ^0 was bound in the fragment and decayed with the absorption of one of the π mesons. The expected decay energy is 360 Mev if only one π meson is emitted.[15] The possibility can not be excluded that a negative K meson was bound in a mesonic orbit around the fragment and absorbed after the fragment stopped.

The one unusual disintegration was found among 7000 cosmic-ray stars and 15 000 stars produced by 3-Bev protons. Among these stars 15 additional cases of the disintegration of a nuclear fragment have been observed which are consistent with the interpretation of a bound Λ^0 particle.

The authors are very grateful to Major David Simons, USAF, for exposing the plates. Many discussions with Dr. M. Gell-Mann, Dr. M. Goldhaber, and Mr. W. Holladay were helpful and stimulating. A portion of the plates was scanned by Mr. J. Slowey and Mr. R. Benson.

* Supported in part by the Graduate School from funds supplied by the Wisconsin Alumni Research Foundation.

[1] M. Danysz and J. Pniewski, Phil. Mag. **44**, 348 (1953).
[2] Tidman, Davis, Hertz, and Tennant, Phil. Mag. **44**, 350 (1953).
[3] J. Crussard and D. Morellet, Compt. rend. **236**, 64 (1953).
[4] Lovera, Barbanti Silva, Bonacini, De Pietri, Perilli Fedeli, and Roveri, Nuovo cimento **10**, 986 (1953).
[5] Freier, Anderson, and Naugle, Phys. Rev. **94**, 677 (1954).
[6] Hill, Salant, Widgoff, Osborne, Pevsner, Ritson, Crussard, and Walker, Phys. Rev. **94**, 797(A) (1954).
[7] Bonetti, Levi Setti, Panetti, Scarsi, and Tomasini, Nuovo cimento **11**, 210 (1954) also Nuovo cimento **11**, 330 (1954).
[8] Ciok, Danysz, and Gierula, Nuovo cimento **11**, 436 (1954).
[9] W. F. Fry and G. R. White, Nuovo cimento **11**, 551 (1954).
[10] P. H. Barrett, Phys. Rev. **94**, 1328 (1954).
[11] Naugle, Freier, and Ney, Phys. Rev. **96**, 829 (1954).
[12] M. Gell-Mann, Phys. Rev. **92**, 833 (1953) and private communications. According to the isotopic spin assignments of Gell-Mann, this positively charged hyperon, which decays by the reaction $Y^+\rightarrow p+\pi^0$, has $T_Z=+1$. This Y^+ particle should not remain in a nucleus because the reaction $Y^++n\rightarrow\Lambda^0+p$ should occur rapidly. Similarly the cascade Y^- particle, which decays by the reaction $Y^-\rightarrow\Lambda^0+\pi^-$ and has $T_Z=-\frac{1}{2}$, should also not remain in a nucleus because of the fast reaction $Y^-+p\rightarrow\Lambda^0+\Lambda^0$. However, the $\theta^0(T_Z=-\frac{1}{2})$ could be stable in a nucleus, from isotopic spin considerations, in a way similar to the Λ^0 particle.
[13] Genoa-Milan and Padua groups, Report of the Padua Conference (unpublished). W. F. Fry and M. S. Swami, Phys. Rev. **96**, 333 (1954).
[14] E. W. Cowan, Phys. Rev. **94**, 161 (1954).
[15] Thompson, Buskirk, Etter, Karzmark, and Rediker, Phys. Rev. **90**, 1122 (1953).

Neutron-Proton Mass Difference*

W. G. HOLLADAY† AND R. G. SACHS
University of Wisconsin, Madison, Wisconsin
(Received August 5, 1954; revised manuscript received September 15, 1954)

IT has recently been suggested[1] that the nucleon may be treated as a structured system having varying numbers of pions in bound states centered on a core particle of spin and isotopic spin $\frac{1}{2}$. An interesting question concerning this model is whether or not it is capable of accounting for the sign and order of magnitude of the neutron-proton mass difference on the basis of electromagnetic interactions alone.[2] The purpose of this note is to point out that the model does indeed account for the mass difference. Furthermore, its success in this respect depends directly on those peculiar features of the nucleon wave function that were found necessary[1] to account for the nucleon magnetic moments. The peculiarities are as follows:

(1) The total probability that pions occur with a total orbital angular momentum $L=1$ is small, of the order of 10 percent.

(2) The probability that a pair of pions occurs in the $L=1$ state is rather large, comparable to or possibly greater than the probability for the occurrence of a single pion (which must have $L=1$).

In order to isolate the effects that may contribute to the mass difference, we assume that the charged and uncharged core particles have the same mass.[2] It will also be assumed that the motion of the core may be neglected. On the basis of the charge independence hypothesis, neither the mass difference between the charged and neutral pions nor the electromagnetic interactions between the pions enters into the neutron-proton mass difference. The difference in the electromagnetic energies of the two systems then consists of two parts, the electrostatic interaction between the pions and charged core, and the interaction of the magnetic moment of the charged core with the magnetic field produced by the pion currents. It is assumed that the neutral core has no magnetic moment.

As is well known, the electrostatic terms have the wrong sign; the neutron may divide into a positive core associated with a π^- or associated with a (π^-, π^0) pair while the corresponding state of the proton has a neutral core, hence no electrostatic energy of this kind. This effect alone would lead to a neutron mass smaller than the proton mass, but the effect is a small one because the probability for the occurrence of the pions is small according to condition (1) above. Even if the radius of the pion orbit is assumed to be as small as twice the nucleon Compton wavelength, the electrostatic energy amounts to about -250 kev as compared to the 1.3-Mev mass difference.

On the other hand, the magnetic coupling with the core moment leads to a large positive contribution. The reason for its being large is that the pion current operator involves a pion pair creation and a pair annihilation term.[3] Hence, according to condition (2), there is an important contribution to the average current due to a cross term between the two pion state and the zero pion state. This contribution is proportional to the *amplitude* of the two pion state whereas the other terms are proportional to the square of the amplitude which is relatively small. The same cross term in the current is responsible for the greater part of the magnetic moment anomaly.[1] The cross term always involves a (π^+, π^-) pair, so for the neutron (the core is neutral) there is no magnetic energy of this kind. On the other hand, in the proton the current loop formed by the pair must have such a direction as to add to the magnetic moment of the core. Then the magnetic field at the core due to the loop is parallel to the core moment, and the magnetic energy is negative. Hence the proton mass is reduced.

It is interesting to note that the calculation of this effect is quite analogous to the calculation of atomic hyperfine structure and that the sign of the effect is fixed just as in the hyperfine splitting.

The magnetic energy of the proton due to this cross term between the zero and two pion state is given by

$$\Delta E_p = -6\mu_c \Delta\mu_p \rho^{-3}, \tag{1}$$

where μ_c is the magnetic moment of the charged core, $\Delta\mu_p$ is the contribution to the proton moment due to the cross term between the zero and two pion states and ρ is a distance depending on the extent of the pion wave function. If the wave function of the two pions has the form $f(\mathbf{r}_1,\mathbf{r}_2)\mathbf{r}_1\times\mathbf{r}_2$, the quantity ρ is defined in terms of the function $G(r)$ given by

$$r^{-2}\mathbf{r}G(r) = \frac{1}{2}\int d^3r_1 \int d^3r_2 K(\mathbf{r}-\mathbf{r}_1)K(\mathbf{r}-\mathbf{r}_2) \times f(\mathbf{r}_1,\mathbf{r}_2)(\mathbf{r}_1+\mathbf{r}_2), \tag{2}$$

where

$$K(\mathbf{r}) = (2\pi)^{-3} m_\pi^{\frac{1}{2}} \int d^3k (k^2+m_\pi^2)^{-1} \exp(i\mathbf{k}\cdot\mathbf{r}), \tag{3}$$

and m_π is the reciprocal Compton wavelength of the pion. Then ρ is defined by

$$\rho^{-3} = \int_0^\infty r^{-3} G(r) r^2 dr \Big/ \int_0^\infty G(r) r^2 dr.$$

An experimental estimate of ρ may be obtained directly from Eq. (1). If ΔE_p is set equal to the total $n-p$ mass difference, $\Delta\mu_p$ to the magnetic moment anomaly and μ_c is taken to be one nuclear magneton, we find

$$\rho = 2.4\hbar/Mc, \tag{4}$$

where M is the nucleon mass. The electrostatic effect and the other contributions to the moment anomaly will lead to a slight reduction in the value of ρ.

It is interesting that the result, Eq. (4), is in reasonable agreement with the estimate of the cutoff momentum for the bound pion function obtained from the pion-nucleon scattering.[4] It was found there that the cutoff in the bound p function occurs at a momentum of $0.6Mc$ corresponding to a cutoff radius $1.6\hbar/Mc$. In view of the spreading effect of the kernels in Eq. (2) and the reduction in the coefficient in Eq. (4) to be expected when all the small effects are included, the agreement appears to be satisfactory.

* This work was supported in part by the U. S. Atomic Energy Commission and in part by the University of Wisconsin Research Committee with funds provided by the Wisconsin Alumni Research Foundation.

† National Science Foundation Predoctoral Fellow.

[1] R. G. Sachs, Phys. Rev. **87**, 1100 (1952).

[2] R. P. Feynman and G. Speisman, Phys. Rev. **94**, 500 (1954), have given an account of the mass difference by computing a difference in electromagnetic self energies between nucleons which are essentially structureless. We are concerned here only with electromagnetic interactions between particles in a structured nucleon. That is the reason for ignoring, below, the difference in mass between the charged and neutral cores. A difference in core mass can be compensated by a small change in the dimensions (ρ) of the pion cloud.

[3] The occurrence of these operators in the expression for the current is also responsible for pion pair creation or annihilation with the absorption or emission of gamma radiation. The contribution to the proton mass may be described in terms of the emission of virtual radiation by pair annihilation followed by absorption of the radiation by the charged core.

[4] R. G. Sachs, Phys. Rev. **95**, 1065 (1954).

Reaction $p+p\rightarrow\pi^{+}+d$ with Polarized Protons*†

T. H. Fields, J. G. Fox, J. A. Kane, R. A. Stallwood, and R. B. Sutton
Carnegie Institute of Technology, Pittsburgh, Pennsylvania
(Received September 9, 1954)

THE 45 percent polarized proton beam[1] of the Carnegie synchrocyclotron has been used to measure the azimuthal asymmetries of the above reaction at π^{+} c.m. angles of 90° and 50°. The polarized external beam of 415±5 Mev protons impinged upon liquid hydrogen, and the resulting pions were detected in fast coincidence with their associated deuterons. We define the asymmetry $\epsilon(\theta)$ to be $[I(\theta)-I(-\theta)]/[I(\theta)+I(-\theta)]$ with $I(\theta)$ the intensity at a c.m. angle of θ. θ is in the same plane as the first scattering which produces the polarized beam and positive θ is in the same sense as the first scattering. We find $\epsilon(90°)=-0.20\pm0.03$ and $\epsilon(50°)=-0.023\pm0.015$, where these refer to the asymmetries in the sense defined by the meson. These values are the average of four separate runs at 90° and three at 50°, with each run taken on a different day and of about 15 hours duration.

To exclude the reaction $p+p\rightarrow\pi^{+}+p+n$, which would otherwise constitute about 10 percent of the counting rate in the geometry we used, sufficient absorber was placed in front of the deuteron counter to absorb the slow protons resulting from this reaction. The beam direction was determined from a beam profile obtained by using the meson counter as the defining counter. The beam polarization and energy were checked before each run as described in reference 1. By using the normal unpolarized proton beam, degraded to 415 Mev, an asymmetry measurement at 90° c.m. yielded $\epsilon=-0.01\pm0.04$.

As shown by Marshak and Messiah,[2] an azimuthal asymmetry in the reaction $p+p\rightarrow\pi^{+}+d$ can arise through the interference of meson S and P states (but from neither alone), and the resulting asymmetry will be given by $\epsilon(\theta)=PQA\sin\theta/(A+\cos^{2}\theta)$, with P the beam polarization, Q a parameter of their theory, and $A+\cos^{2}\theta$ the unpolarized angular distribution. A recent experiment[3] by Crawford and Stevenson yields $Q=0.39\pm0.05$ at $(\text{K.E.}_{\pi})_{\text{c.m.}}=11.3$ Mev. The present experiment gives $Q=0.45\pm0.08$ for $(\text{K.E.}_{\pi})_{\text{c.m.}}=55$ Mev.

According to the above equation, $\epsilon(50°)$ should be given by[4] $\epsilon(90°)/(4.0\pm0.4)$, which is -0.050 ± 0.009. The difference between this and our experimental value is 0.027 ± 0.018. In this connection, it should be stated that the quoted errors are statistical only; systematic errors are probably smaller than these. It was pointed out to us by Professor L. Wolfenstein that a $P-D$ interference term will make a maximal contribution to ϵ at 50°. The fact that this difference is scarcely nonzero outside of statistics and does not include the unknown systematic error means that it cannot be interpreted as more than a possible indication of such a D-state effect.

* This research supported in part by the U. S. Atomic Energy Commission.
† To be submitted by T. H. Fields in partial fulfillment of the requirements for the degree of Doctor of Philosophy at Carnegie Institute of Technology.
[1] Kane, Stallwood, Sutton, Fields, and Fox, Phys. Rev. **95**, 1694 (1954).
[2] R. E. Marshak and A. M. L. Messiah, Nuovo cimento **11**, 337 (1954).
[3] F. S. Crawford, Jr., and M. L. Stevenson, Phys. Rev. **95**, 1112 (1954).
[4] We have here used $A=0.20\pm0.02$ as measured at an incident proton energy of 437 Mev. Fields, Fox, Kane, Stallwood, and Sutton, Phys. Rev. **95**, 638 (1954).

Search for 15-Mev Gamma Radiation from $N^{14}+d$ and $Be^{9}+\alpha$†

V. K. Rasmussen, John R. Rees, M. B. Sampson, and N. S. Wall
Department of Physics, Indiana University, Bloomington, Indiana
(Received August 5, 1954)

COHEN, Moyer, Shaw, and Waddell[1] have recently reported 15.2-Mev γ radiation from the bombardment of carbon with protons and of B^{11} with deuterons, but not from the bombardment of beryllium with alphas. They suggest that the state in C^{12} involved is the isotopic spin $T=1$ analog of the ground states of B^{12} and N^{12}. The isotopic spin selection rules would then forbid the production of this state in the $N^{14}(d,\alpha)$ reaction. We have attempted to verify this.

A 1-inch Harshaw canned NaI(Tl) crystal viewed by a DuMont 6291 photomultiplier was available for the detection of γ rays. The crystal was surrounded by $2\frac{1}{2}$ inches or more of lead except for a 0.52-inch diameter aperture filled with Lucite which was directed towards the target. A $\frac{3}{4}$-inch long Bakelite plug was placed between the front face of the crystal and the lead.

This arrangement was not, of course, the best possible for detecting 15-Mev γ radiation. Its most important defect was that lower-energy pulses from other γ rays required the use of very low ($\sim0.005\mu$a) deuteron beams to avoid excessive total counting rates. Figure 1 shows the pulse spectrum obtained when a thick B_4C target is bombarded with 10.8-Mev deuterons. Although no detailed analysis of the shape of the spectrum was made, its form is not unexpected because of the small crystal size. By taking the break point in the curve as equal to $(E_{\gamma}-1.02)$ Mev and using the pair peak of the 4.43-Mev γ ray from C^{12} for calibration we get 15.1 ± 0.4 Mev for the highest-energy γ ray. If, as a very rough estimate, it is assumed that 15 percent of the 15-Mev quanta that enter the 0.52-inch aperture produce pulses >11.6 Mev, then our yield for this γ ray is $\sim3\times10^{-5}$ per deuteron.

With a thick Melmac 404 $(N_6C_3H_6)^2$ target, we obtained a small number of counts corresponding to γ

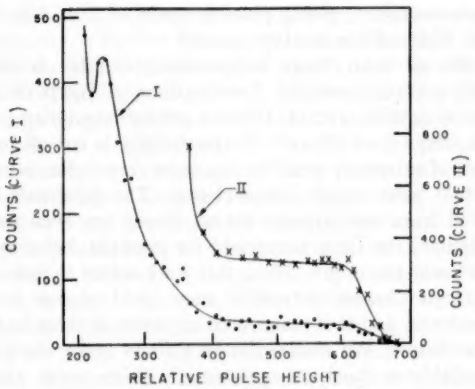

FIG. 1. Scintillation spectrum of the γ radiation from the bombardment of thick B_4C by 10.8-Mev deuterons. For Curve II more deuterons were incident on the target per point, and the discriminator was set to accept a wider range of pulse heights. A relative pulse height of 610 on Curve II was assumed to correspond to $(E_\gamma - 1.02)$ Mev. There is no significance in the apparent pulse-height shift in the two curves. The data were taken at different times and in each case a spectrum of the 4.43-Mev γ ray from C^{12*} was also taken for an energy calibration (see text).

radiation >12.5 Mev. Land Camera pictures of an oscilloscope screen indicated that this was probably the same γ ray as observed with the boron target. Comparison of integral counting rates from the Melmac and B_4C targets, after subtraction of background, gave an intensity ratio of ~ 0.03.

We have also looked for this radiation from a thick beryllium target bombarded by 21.7-Mev α particles. Gamma radiation of the same energy (± 0.5 Mev) and ~ 6 percent of the intensity of that from B_4C was observed. Examination of the original data of McMinn *et al.*[3] indicates that this yield is consistent, within an order of magnitude, with that for $Be^9(\alpha,p)B^{12}$.

Our results do not seem to have any immediate bearing on the isotopic spin assignment for this state in C^{12}. The possible small yield from $N^{14}(d,\alpha)C^{12*}$ can be explained by the approximate nature of the isotopic spin selection rules. On the other hand, it does not seem proper to say that its smallness proves that a $T=1$ state is involved, since there is no reason to expect the uninhibited (d,α) and (d,n) cross sections to be equal. However, we see no reason to doubt the $T=1$ assignment of Cohen *et al.*[1] Assuming this, we can infer that the α width of this level is small. This follows from the requirement of the charge-independence hypothesis that the $Be^9(\alpha,p)$ and $Be^9(\alpha,n)$ cross sections differ only by a factor of two[4] and from the approximate equality of the proton and γ-ray yields from $Be^9+\alpha$. After allowance for error in the yields involved, we conclude that Γ_γ is certainly less than 100 Γ_α and is probably less than 10 Γ_γ. Since 7.8 Mev is available for α emission, a strong selection rule is indicated. For this purpose, we note that as the analog of B^{12} and N^{12}, this C^{12} state might be assumed to have spin $J=1^+$, thus forbidding decay to the 0^+ ground state of Be^8 and requiring d-wave α emission to the 2^+ first excited state. Isotopic spin rules would further inhibit decay to the first excited state.

Another possible origin of the γ ray, in the cascade $C^{12} \rightarrow Be^{8*} + He^4$; $Be^{8*} \rightarrow Be^8 + h\nu$, may be ruled out, since it should have been easily observed in previous work on the $Li^7(d,n)Be^8$ reaction[5] and since a 15-Mev state in Be^8 is not energetically accessible in the bombardment of Be^9 with 21.7-Mev alpha particles.

† This work was supported by the joint program of the Office of Naval Research and the U. S. Atomic Energy Commission.

[1] Cohen, Moyer, Shaw, and Waddell, Phys. Rev. **95**, 664(A) (1954); this issue [Phys. Rev. **96**, 714 (1954)]. We are indebted to Professor Moyer for sending us a copy of this paper before publication.
[2] F. Ajzenberg and W. Franzen, Phys. Rev. **94**, 409 (1954).
[3] McMinn, Sampson, and Rasmussen, Phys. Rev. **84**, 963 (1951).
[4] R. K. Adair, Phys. Rev. **87**, 1041 (1952).
[5] F. Ajzenberg and T. Lauritsen, Revs. Modern Phys. **24**, 321 (1952).

Calculations on Charge Independence with Repulsive Core Potentials

M. A. PRESTON, *Hamilton College, McMaster University, Hamilton, Ontario, Canada*
AND
J. SHAPIRO,* *Physics Department, University of Toronto, Toronto, Ontario, Canada*
(Received September 3, 1954)

BECAUSE of the current interest in two-body static potentials with repulsive cores,[1] calculations have been carried out to see whether such a potential can explain both the np and pp low energy scattering in the ^1S state, i.e., the experimental values of the scattering lengths $a_s(n-p)$ and $a_s(p-p)$ and the effective ranges $r_{0s}(n-p)$ and $r_{0s}(p-p)$. According to the effective range theory,[2] these four constants may be obtained from the solutions of the wave equation at zero energy for (a) the $n-p$ system and (b) the $p-p$ system. These two problems were coded for FERUT, the digital computer at the University of Toronto, for potentials of the form[3]

$$V = \infty \quad \text{for} \quad r < r_c,$$
$$= -V_0 f(r/r_s) \quad \text{for} \quad r > r_c.$$

The equations were solved by numerical integrations, starting with the asymptotic solutions and integrating inwards until the solutions became zero, thereby determining the core radius r_c. The integrals giving the effective ranges were evaluated using these solutions. In order to improve the accuracy of the solutions, the substitution $y = \ln(r/r_s)$ was made in the differential equations.[4] Because of this substitution, there was a

TABLE I. Charge-independent potentials and corresponding effective ranges. The potential is $V=\infty$, for $r<r_c$, $V=-V_0e^{-r/r_s}/(r/r_s)^2$, for $r>r_c$.

r_c (10^{-13} cm)	r_s (10^{-13} cm)	V_0 (Mev)	$r_{0s}(n-p)$ (10^{-13} cm)	$r_{0s}(p-p)$ (10^{-13} cm)
2.60	0.014	3.50	2.33	2.60
2.70	0.007	3.07	2.35	2.65
2.80	0.000	2.70	2.37	2.70

minimum core radius which the program could handle. The method of integrating inwards has the advantage that only solutions corresponding to the experimental values of the scattering lengths are obtained, since the asymptotic solutions depend only on the scattering lengths. For a given pair V_0, r_s, the criteria for charge independence used were: (a) the same cutoff r_c should be obtained for both $n-p$ and $p-p$ and (b) the effective ranges should satisfy $1.9<r_{0s}(n-p)<2.9$, $2.54<r_{0s}\times(p-p)<2.74$ (units 10^{-13} cm). Runs were done for scattering lengths corresponding to the best experimental value and to the experimental limits in order to determine how closely the two values of r_c had to agree.

The values used for the scattering lengths were $a_s(n-p)=-23.69\pm0.06\times10^{-13}$ cm,[5] $a_s(p-p)=-7.68\pm0.04\times10^{-13}$ cm.[6] Calculations were made for the following attractive wells outside the core: (1) exponential,[7] (2) Yukawa, (3) Gaussian, (4) $f(x)=e^{-x}/x^2$. About 200 pairs of values V_0, r_s were used for each shape. Only e^{-x}/x^2 gave charge independence, and this for very small core radii. Three choices of parameters giving charge independence are given in Table I, together with the corresponding effective ranges.[8] Because of the small core radii involved, extrapolations were necessary, giving possible errors of 2 or 3 in the last digits of the numbers quoted.

We see that charge independence can be obtained with a static potential. Two features of this potential are of significance: (1) it has a strong singularity near the origin ($\sim1/r^2$) and (2) this infinity is cut off by a core of extremely small radius (zero core radius is consistent with charge independence). The potentials derived from pseudoscalar meson theory are even more singular; the Lévy potential,[1] for example, behaves as $1/r^3$ near the origin. Thus, this work seems to indicate that the meson potentials may yield charge independence, and it is planned to try some of these in the near future. We would also be glad to make the code available to check other potentials (with cores) which other workers may obtain.

* Holder of National Research Council of Canada Studentship, 1951–52; National Research Council of Canada Fellowship, 1952–53. This work is to be submitted in partial fulfilment of the requirements for the degree of Doctor of Philosophy at the University of Toronto.

[1] R. Jastrow, Phys. Rev. **81**, 165 (1951); M. M. Lévy, Phys. Rev. **88**, 725 (1952); A. Klein, Phys. Rev. **90**, 1101 (1953); Phys. Rev. **94**, 195 (1954); J. M. Blatt and M. H. Kalos, Phys. Rev. **92**, 1563 (1953).

[2] H. A. Bethe, Phys. Rev. **76**, 38 (1949); J. D. Jackson and J. M. Blatt, Revs. Modern Phys. **22**, 77 (1950).

[4] The code is actually more general and can handle potentials of the form $Af(r/a)+Bg(r/b)+Ch(r/c)$ with very slight modifications.

[4] H. A. Bethe, Phys. Rev. **82**, 60 (1951).

[5] G. Snow, Phys. Rev. **87**, 21 (1952).

[6] M. C. Yovits *et al.*, Phys. Rev. **85**, 540 (1952). The value of $a_s(p-p)$ was taken from their shape-independent fit; the error was assigned so as to include their results for other shapes.

[7] The $n-p$ equation can be solved explicitly for the exponential potential. This was used as a check on the program. The cutoffs agreed to 6 figures, the effective ranges to 5 figures.

[8] The results of E. M. Hafner *et al.*, Phys. Rev. **89**, 204 (1953), and an estimate of the shape parameters, P, suggest $r_{0s}(n-p)=2.21\pm0.25$ for these potentials.

PHYSICAL REVIEW VOLUME 96, NUMBER 3 NOVEMBER 1, 1954

Proceedings of the American Physical Society

MINUTES OF THE 1954 SPRING MEETING OF THE OHIO SECTION AT OHIO UNIVERSITY, ATHENS, OHIO, APRIL 16 AND 17, 1954

THE regular spring meeting of the Ohio Section of the American Physical Society was held at Ohio University, Athens, Ohio, on Friday and Saturday, April 16 and 17, 1954. For Friday morning, no formal program was prepared save the showing of recently released educational films and time provided for viewing the exhibits of the High School projects prepared for the Junior Section of the Ohio Academy of Science. Approximately one-third of all the exhibits were related to the field of physics. Eight invited papers were presented having as the main theme the development of physics in the past century in the Northwest Territory. The subject was suggested by the Sesquicentennial of Ohio in 1953 and the present celebration of Ohio University which was the first college organized within the Territory; "Ohio University Celebrates its Sesquicentennial, 1804–1954," by John E. Edwards, Ohio University; "Remarks on the History of Astronomy in Cleveland," J. J. Nassau, Case Institute of Technology; "A New Analysis of the Interferometer Observations of Dayton C. Miller," by R. S. Shankland, S. W. McCuskey, and F. C. Leone, Case Institute of

Technology, (abstract included); "Physics in Industry," H. R. Nelson, Battelle Memorial Institute; "Ohio Machine Tools and Physical Science," M. E. Merchant, Cincinnati Milling Machine Tool Company; "The Past Half Century of Physics at University of Cincinnati," C. Harrison Dwight, University of Cincinnati; "Ohio's Contribution to Meteorology; Climatic Trends Since 1880," A. N. Dingle, The Ohio State University (abstract). The eighth invited paper was presented on Saturday morning, "Physics in American Universities: Its Growth and Influence," by Alpheus W. Smith, The Ohio State University.

This being the annual business meeting of the Ohio Section the following officers were chosen for the year 1954–1955: Chairman, William H. Gran, Miami University, Oxford, Ohio; Vice-Chairman, Richard N. Thayer, Lamp Development Laboratory, General Electric Company, Cleveland, Ohio; and Secretary-Treasurer, Leon E. Smith, Denison University, Granville, Ohio.

The nineteen contributed papers were presented in two sections so that the meeting could be completed by noon. There were three for which no abstracts appear: "Apparatus for Three Experiments Redesigned for General Physics," W. M. Pierce, Ohio University; "Undergraduate Research," J. W. McGrath, Kent State University; and "An Operational Definition of Inertial Mass Without the Use of Newton's Second Law of Motion," Thomas D. Phillips, Marietta College. The abstracts of the seventeen contributed papers and two invited papers follow.

LEON E. SMITH, *Secretary*,
The Ohio Section
American Physical Society
Granville, Ohio

Ohio's Contribution to Meteorology: Climatic Trends since 1880. A. N. DINGLE, *The Ohio State University.*—The temperature and precipitation records of selected stations in the United States are summarized graphically and presented. Study of the trend curves suggests a time-space continuity of prominent features of these curves from station to station. The synoptic study of the distribution of interdecadal changes of ten-year average precipitation values reveals some interesting indications of significant long term shifts of cyclonic activity and moist air currents. In the absence of casual relationships the secular changes of climate must be examined and explained statistically.

A New Analysis of the Interferometer Observations of Dayton C. Miller. R. S. SHANKLAND, S. W. MCCUSKEY, AND F. C. LEONE, *Case Institute of Technology.*—For nearly thirty years the results of the Michelson-Morley experiment obtained by Dayton C. Miller on Mount Wilson have stood at variance with all other trials of this experiment. As interest in Miller's results has continued to the present time, and since the original data sheets are available to the present writers, it has seemed appropriate that the observations be subjected to a new analysis by statistical methods. It is now concluded that the small periodic fringe displacements found by Miller are due in part to statistical fluctuations in the readings of the fringe positions in a very difficult experiment. The remaining systematic effects are so distributed in azimuth that it is concluded they are due to local physical causes, especially temperature effects. These were more troublesome at Mount Wilson than those encountered by other experimenters, including Miller himself in his work done at Case in Cleveland. As interpreted in the present study, Miller's extensive Mount Wilson researches are entirely consistent, within the accuracy of his readings, with a null result at all epochs throughout a year.

Color Shifts Produced by Use of Polaroid Photographic Filters. ALEX KISHA, *Bowling Green State University.*—When a polaroid filter was used with a color film in taking a certain photograph, it was found that a shift in color had occurred in the blue-green region. The problem that presents itself here is that if the light coming from the subject is polarized and then enters the camera through a filter, the filter acts as an analyzer, the resulting intensity being dependent upon the angle between the axis of the polarizer and analyzer. The work is confined to analyzing various polaroid filters as to the effect of the angle of polarization on the transmission of monochromatic filters. The Beckman DU Spectrophotometer is used. The polarization angle indicated an influence upon the transmission for wavelengths of 400 to 825 mu. For wavelengths up to 650 mu at 90° angle, all light was absorbed. In the blue-green region, as the polarizing angle increased, the green was being eliminated more rapidly. For wavelengths below 350 mu there was no transmission. For wavelengths greater than 700 mu, there was a tendency for the percent transmission to converge at one point in the high red region, regardless of the angle.

Theory of Reflection and Transmission Measurements on Thin Metallic Films. THURSTON E. MANNING, *Oberlin College.*—The work of Matossi[1] on the intensities of reflected and transmitted beams of light incident on backed thin metallic films will be applied in a form suitable for the usual experimental work. In addition, a discussion of the polarization predicted in the reflected and transmitted beams on the basis of classical electromagnetic theory will be given.

[1] Matossi, J. Opt. Soc. Am. **39**, 928 (1949).

Optical Reflection and Transmission of Thin Aluminum Films. WILLIAM A GAREE, *Oberlin College.*—The results of measurements on the reflected and transmitted intensities of nearly monochromatic light (5140A) on glass backed films of aluminum will be reported. The measurements give the influence of the thickness of the metal film on the reflection and transmission. The results of limited experiments on the polarization of the reflected and transmitted beams will be given.

Laboratory Problems in Introductory Electricity and Optics. ALBERT B. STEWART, *Antioch College.*—In a twenty-week course in electricity and optics for science majors the students have been encouraged to work toward the solution of experimental problems, the answers to which cannot easily be found in texts or periodicals. Most students spend about half of their time on these original problems and half on the usual type of organized experiments. In grading their work, the quality of their approach, the completeness of their laboratory records and the care with which they evaluate the experimental uncertainties are emphasized over their success in solving the problems. Some of the advantages of this laboratory procedure seem to be: the problems capture the students' enthusiasm and call forth their best efforts; they provide an effective

way to learn how to treat experimental uncertainties; they help make the laboratory a stimulating place for both students and instructor. Two disadvantages, some students become overly discouraged by failure to solve a problem, and it is difficult to have equipment ready in advance without unduly influencing the students' approach. A few of the laboratory problems will be described.

A Simple Recording Microphotometer. ROBERT LIEFELD, *Kent State University.*—The design and construction of a simple but adequate microphotometer using apparatus commonly available will be discussed. The microphotometer is presently being used for measurement of x-ray M edge spectra.

Design and Behavior of Two Acoustic Lenses. JAMES V. SANDERS, *Kent State University.*—The design of a path delay lens and an obstacle array lens will be discussed. Experimental results on their behavior will be indicated. These lenses will be demonstrated after the session if time and facilities permit.

Electric Field in an Oscillating Discharge.* R. E. WARNER, G. E. OWEN, AND A. B. STEWART, *Antioch College.*—The time average electric field strength in an argon dc glow discharge with spontaneous oscillations has been studied by measuring the potential difference between two plane probes 1.1 cm apart placed in the positive column at fixed distances from the cathodes. With a discharge current of 17 ma, a pressure of 12.4 mm of Hg, an external series resistance of 30 000 ohms, and cylindrical iron electrodes (anode moveable) the oscillations were stable with a frequency of 2700–2940 cps over the range of electrode separations studied (10 to 30 cm). The electric field between the probes varied between 2.3 and 7.5 volts/cm as the electrode separation was changed, repeating approximately its variation with each 4 cm increase in length of the discharge. An abrupt change of 2–4 volts/cm coincided with the creation of an additional wavelength of the positive striations in the positive column. From the probe data a curve of the time average potential difference as a function of distance from the anode has been constructed for the positive column. The voltage across the tube increases linearly with increasing separation.

* Supported by the Frederick Gardner Cottrell Fund of the Research Corporation.

Cloud-Chamber Program at Kent State University.* A. A. SILVIDI AND J. GLENN MAXWELL, *Kent State University.*—Since the advent of continuous cloud chambers, several qualitative uses of the instrument have been reported[1-3]. The Kent State program is investigating the quantitative features of this instrument by obtaining a beta spectrum and comparing it with the spectrum obtained by other instruments. Construction details of the chamber will be presented; field characteristics of the magnetic coils will be discussed; and preliminary photographs of beta tracks taken with and without magnetic field will be shown.

* Research supported by National Science Foundation.
[1] A. Langsdorf, Rev. Sci. Instr. 10, 91 (1939).
[2] E. W. Cowan, Rev. Sci. Instr. 21, 991 (1950).
[3] T. S. Needels and C. E. Nielsen, Rev. Sci. Instr. 21, 976 (1950).

Neutron Slowing Down Time.* C. E. FOREMAN AND M. F. CROUCH, *Case Institute of Technology.*—A study is in progress of the slowing down time of fast neutrons produced in the reaction $He^4+Be^9\rightarrow C^{12*}+n$ and detected by a BF_3 counter in a paraffin moderator. The photon emitted by the excited C^{12} nucleus signals the time of production of the neutron. Measurements are made of the time delay between production of the neutrons and their capture in the BF_3 proportional counter. 7200 events were recorded with delays less than 25 microseconds, and an integral distribution of delay times was plotted. This curve, after correcting for accidental coincidences and for the effect of competing capture processes, was found to reach a constant slope at 9.6 microseconds, which was taken to indicate that virtually all neutrons were thermalized by this time. Assuming a roughly symmetrical distribution of slowing down times, this gives a mean slowing down time of about 5 microseconds. The curve was observed to rise almost immediately with a slop not much less than the final constant value, indicating that the greater distance traveled per microsecond by the faster neutrons offsets, to a large extent, the $1/v$ law detector response.

* Work supported by the U. S. Atomic Energy Commission.

Theory of the Photodisintegration of Li^6, I.* E. F. CAROME, *Case Institute of Technology.*—As part of a general program of investigating gamma-ray processes in light nuclei, calculations of cross sections for the photodisintegration of Li^6 from threshold to about 30 Mev have been made on the basis of two assumed nuclear models. The present investigation is based on a deuteron-alpha particle model for the ground state of Li^6. The neutron and proton are described by plane waves in the final state and the alpha particle is assumed unchanged throughout the process. Utilizing approximate wave functions for the initial and final states of the system it has been possible to obtain expressions for the electric and magnetic dipole contributions to the $Li^6(\gamma,np)He^4$ reaction. Because three particles emerge in the final state the expressions for the differential cross section are rather complex and numerical integrations were necessary to obtain the total cross section. The result of these calculations will be presented. The reaction $Li^6(\gamma,d)He^4$ has also been investigated. It is easily demonstrated that this reaction does not occur in the dipole approximation. Calculations of the electric quadrupole contribution to the cross section indicate that it is quite small consistent with recent experimental results.[1,2]

* Work supported by U. S. Atomic Energy Commission.
[1] E. W. Titterton and T. A. Brinkley, Proc. Phys. Soc. London **A65**, 1052 (1952).
[2] P. Jensen and K. Gis, Z. Naturforsch. **8a**, 137 (1953).

Auxiliary Condition in Generalized Quantum Electrodynamics.* GEORGE R. PITMAN, JR., *University of Cincinnati.*—In Podolsky's generalized electrodynamics[1] one obtains the wave equation of the form $(1-a^2\Box)\Box A_\mu(x)=0$ from the generalized Maxwell-Lorentz equations if one assumes either of the following auxiliary conditions:

$$(1-a^2\Box)A_{\mu,\mu}(x)=0; \quad A_{\mu,\mu}(x)=0.$$

Defining the ordinary and extraordinary potentials, respectivly, as $\bar{A}_\mu(x)=(1-a^2\Box)A_\mu(x)$ and $\bar{\bar{A}}_\mu(x)=a^2\Box A_\mu(x)$ so that $A_\mu(x)=\bar{A}_\mu(x)+\bar{\bar{A}}_\mu(x)$, the first of these conditions demands the vanishing of only the four divergence of the ordinary field potentials whereas the second demands the vanishing to the divergence of both the ordinary and extraordinary potentials. The energy eigenvalues of the extraordinary field are:

$$\bar{\bar{H}}=-c\hbar k_0(\bar{\bar{n}}_1+\bar{\bar{n}}_2+\bar{\bar{n}}_3-\bar{\bar{n}}_0).$$

Imposing the second condition demands that $\bar{\bar{n}}_0\leq\bar{\bar{n}}_1+\bar{\bar{n}}_2+\bar{\bar{n}}_3$ which means that the energy of this field will be negative definite whereas the use of the first condition imposes no restriction on the relative magnitude of the occupation numbers and the energy may be positive. The author is indebted to Professor Boris Podolsky for his help and guidance during the course of this investigation.

* Because of printing limitations, a bar has been substituted for the author's tilde over A, H, n, and k in this abstract.
[1] B. Podolsky, Phys. Rev. 62, 68 (1942); B. Podolsky and P. Schewd, Rev. Modern Phys. 20, 40 (1948).

Theory of the Photodisintegration of Li^6, II.* G. F. BING, *Case Institute of Technology.*—The present investigation assumes a Li^6 ground-state model consisting of an alpha particle

with orbital neutron and proton. Using this model calculations of the cross sections for the reactions $Li^6(\gamma,n)Li^5$ and $Li^6(\gamma,p)He^5$ have been made. It is assumed that the residual Li^5 or He^5 nucleus may be treated as stable for purposes of this calculation. The contributions of the electric and magnetic dipole matrix elements to the cross sections have been calculated using suitable approximate wave functions for initial and final states. The alpha particle is assumed unchanged in the energy range of interest, that is from threshold to about 30 Mev. It is hoped that comparison of experimental results with the predictions based on the deuteron-alpha model and the present model will yield some information about the actual Li^6 ground state.

* Work supported by U. S. Atomic Energy Commission.

Half-Life Determinations of Radium-223 and Thorium-227. G. R. HAGEE, M. L. CURTIS, AND G. R. GROVE, *Mound Laboratory,** *Monsanto Chemical Company.*—Half-life values for radium-223 and thorium-227 have been determined by analyzing data obtained from samples of each element by alpha counting in a proportional counter over a period of 116 days. The samples contained small amounts of other members of the actinium chain. The growth and decay equation of the principal activity and its daughters plus contaminants was derived in terms of the decay constants of radium-223 and thorium-227 and the amounts of each activity present. The decay constants and the disintegration rates of the activities were each set equal to an approximate value plus a correction term. Taylor's expansion was applied to the general equation to yield an expression which was linear in the correction terms. A least-squares treatment was used to derive the correction terms most representative of the data. The half-life values obtained from these analyses were 18.169 ± 0.084 days for thorium-227 and 11.685 ± 0.056 days for radium-223.

* Operated under U. S. Atomic Energy Commission contract.

Half-Lives of Al^{25} and Al^{26}.* D. W. GREEN, J. C. HARRIS, AND J. N. COOPER, *Ohio State University.*—The half-lives of Al^{25} and Al^{26} have been determined by a method previously reported.[1] The Al^{25} was produced by exciting the $Mg^{24}(p,\gamma)Al^{25}$ reaction with 825-kev protons from a Van de Graaff generator in targets of isotopic Mg^{24}, which was obtained from Carbide and Carbon Chemicals Corporation, Oak Ridge, Tennessee. The value measured for Al^{25} was 7.20 seconds, which is in good agreement with the 7.3 seconds reported by Bradner and Gow.[2] The half-life of Al^{26} was measured both at the 563- and the 720-kev resonances in the $Mg^{25}(p,\gamma)Al^{26}$ reaction. The values obtained were 6.47 and 6.40 seconds, respectively, which agree well with the 6.3 seconds of Bradner and Gow[2] and with the 6.5 seconds found by Katz and Cameron.[3]

* Supported in part by the U. S. Atomic Energy Commission through a contract with The Ohio State University Research Foundation.
[1] Green, Harris, and Cooper, Phys. Rev. **90**, 1132 (1953).
[2] H. Bradner and J. D. Gow, Phys. Rev. **74**, 1559 (1948).
[3] L. Katz and A. G. W. Cameron, Phys. Rev. **84**, 1115 (1951).

X-Ray Absorption in a Curved Crystal at the Bragg Angle. ROBERT G. SAUER AND JOHN E. EDWARDS, *Ohio University.*—Primary extinction generally decreases the transmitted x-ray beam intensity when Laue type diffraction occurs in a single crystal. However, Borrmann[1] and others[2] have observed an increase in the transmitted intensity in "thick" crystals at the Bragg angle. An attempt has been made to observe this absorption anomaly in a curved crystal. A double Gauchois type spectrograph was used, the first crystal serving as a monochromator with the speciman crystal placed back of the focal circle. Thus, only x-rays from a very small point on the target were diffracted from the specimen crystal giving sharp lines slightly greater than the natural width. Characteristic lines and the transmitted beams were photographed with a 0.2-mm quartz crystal for wavelengths ranging from 0.469 A to 2.289 A. A 0.81-mm quartz crystal and a 0.56-mm mica crystal were used with 1.54 A lines. A pronounced decrease in intensity of the transmitted beam was observed in every case. The "deficiency" lines were nearly the same width as the diffracted lines.

[1] G. Borrmann, Physik. Z. **42**, 157 (1941).
[2] N. Campbell, J. Appl. Phys. **22**, 1139 (1951); R. L. Rogosa and G. Schwarz, Phys. Rev. **87**, 995 (1952).

Collective Model in the Analysis of Gamma Rays. D. N. KUNDU, *The Ohio State University.*—Nuclear gamma energies are studied from a combined point of view of the independent particle model and the collective model. The former provides the broad pattern of the nuclear energy states on which is superimposed additional states arising from the collective motion of the nucleons within the nucleus. The Coulomb excitation data, whenever available, have been utilized to identify rotational lines near the ground state. The success and also the limitations of the models are examined, among others, with Se^{75}, Lu^{176}, Hf^{181}, Au^{195}, and Hg^{197}, as examples. The gamma rays of Np^{238} have been used to illustrate the possibility of rotational levels associated with the ground state and also the particle-excited state of Pu^{238}. Some tentative decay schemes involving the collective model will be suggested.

MINUTES OF THE 1954 JUNE MEETING HELD AT MINNEAPOLIS, MINNESOTA, JUNE 28–30, 1954

(Corresponding to *Bulletin of the American Physical Society*, Volume 29, No. 5)

THE 1954 June meeting of the American Physical Society was held at Minneapolis on Monday, Tuesday, and Wednesday, June 28, 29, and 30. The unusual choice of days of the week was dictated by the fact that a total eclipse of the sun occurred at 5:07 A.M. on June 30, although preliminary announcements of the meeting stated that the local committee had kindly arranged for the eclipse as an added attraction to the meeting. Be that as it may, the local committee certainly provided ideal weather for the eclipse. After several hot and high-humidity days, interspersed with thunderstorms, the sun rose on Wednesday in a clear and cloudless sky, which remained that way during the entire duration of the eclipse. But within an hour after the eclipse the sky was again half covered with clouds. The great bulk of our members saw the eclipse, as well as the "Skyhook" balloon launching, from the Old University airport, under perfect seeing conditions. A very few were so fortunate as to see it from one of the two special planes provided by the airplane companies.

The American Association of Physics Teachers held concurrent sessions with the American Physical

Society, and there was a common registration and much intermingling of attendance. The total registration was 484, considerably below that (741) at the March Detroit-Ann Arbor meeting. But over 240 attended the banquet on Tuesday evening, a slightly larger number than at the Detroit-Ann Arbor banquet. If half the registrants should attend the banquet at one of the large Atlantic Coast meetings, it would certainly create a problem. The after-dinner speakers were E. W. Davis of the University of Minnesota, speaking on the processing of taconite iron ore, and R. M. Sutton of Haverford College, who by personally devised slides and actual demonstrations illustrated clearly the theory and detailed features of the impending total eclipse. The banquet ended at 10:00 P.M., giving opportunity for a full three to four hours of sleep for those who later viewed the eclipse.

The four lecture rooms of the Physics Building, plus one lecture room in the closely adjacent Murphy Hall, provided more than adequate accommodations for the sessions of both organizations. The largest single attendance, some 350, occurred at the joint session on Monday afternoon, when four invited papers on astronomical subjects were presented. During the middle of Tuesday morning the total attendance at the three physics sections was about 240 and that at the AAPT section was 165. Strange to relate, the total attendance Wednesday morning, in spite of the early morning exertions incident to the eclipse, was equally large, with 160 at the session of invited papers on nuclear accelerators. There were 32 invited papers and 112 contributed papers (plus three post-deadline papers), although how many were read by title only is not known to the undersigned.

The local arrangements were ably handled by a local committee headed by John Winckler, and the ladies were royally entertained by a committee, headed by Mrs. C. N. Wall, which also arranged an enjoyable tea for Monday afternoon. The entire meeting proceeded with great smoothness in spite of the highly unusual but unavoidable absence of Dr. Darrow.

RAYMOND T. BIRGE, *Vice-President*
American Physical Society

Council Meeting of June 18, 1954

The Council of the American Physical Society met in New York City on June 18, 1954, for the purpose of acting on candidates to Fellowship and to Membership. It elected four candidates to Fellowship and 151 to Membership: the names follow.

Elected to Fellowship: W. L. Brown, D. N. Kundu, J. D. Kurbatov, R. D. Spence.

Elected to Membership: *Roger Harris Anderson, Frank Asaro, *John Joseph Bartulovich, Edward Arthur Baum, Richard Charles Beitz, Paul Belgodere, *William Ralph Bennett, Jr., Harold Berger, *Eugene M. Bernstein, Eugene P. Bertin, Avadh Behari Bhatia, *David Theobald Blackstock, John Dieterle Blades, Eliot Z. Block, *Charles R. Bruce, Harry Bryant, *James Warland Burgess, *Jay Burns, III, *Nina Byers, Robert Swain Caird, Jr., Willie Russell Callahan, George Weirich Callendine, Jr., *Richard Andrew Campbell, *Murray Cantwell, *Joan Robinson Clark, Kenneth Leon Clum, James W. Cobble, Royal Eugene Collins, Joseph M. Conley, Frederick Pitkin Cranston, Jr., Robert Wallace Crowe, *Robert Emil Danielson, John Edmund Davey, Jefferson Deveaux Davis, Jr., Robert Benjamin Davis, Donald Paul Devor, *Bertram Gale Dick, Jr., Pierre Donzelot, Gloria Lee Dority, E. Doser, Albert Charles Doskocil, Jr., *Ross Alan Douglas, *George C. Dousmanis, *James Holahan Doyle, *Gene F. Dresselhaus, Richard John Eden, Nicholas E. Efremov, *Stanton Lea Eilenberg, John Robert Eklund, Winfield W. Evans, Norman J. Field, Val L. Fitch, *Joseph Newton Fritz, Edward Joseph Furno, Wolfgang Gärtner, Andre Gauvenet, *Joseph Giordano, Harvey Louis Glick, *Irwin Goldberg, *James Power Gordon, *Kazuo Gotow, *Alexander Louis Harvey, Russell LaVerne Heath, Carl Christian Hein, *Leon Heller, *Charles D. Hendricks, Jr., David Franklin Herring, Casselman Ben Hess, *John Harold Hoffman, *John P. Hurley, Merle M. Irvine, John Edward Ivory, Jay Andrew Horton Jacobs, Richard Victor Jones, Walter E. Jordan, *Robert Michael Kalbach, Shu-koo Kao, Robert Franklin Keith, Donald W. Kent, Yutaka Kohasi, *Earl Leonard Koller, John Nelson Kriebel, *Robert Krotkov, *Theodore Jugo Kruse, Donald Lee Lafferty, W. Laskar, Kent D. Lawson, Robert Briggs Leachman, Graham Edward Lee-Whiting, Lutz Leopold, *Alfred U. MacRae, Lawrence Bersell Magnusson, *Willard Edward Matheson, Sanford Aaron Meltzer, *Bruce Howard McCormick, Forrest S. Mozer, Raj Pratap Misra, Akira Miyahara, Joseph Jackson Murray, Jr., Edward S. Naidus, *Edward Hagi Nicollian, Tetsuji Nishikawa, John Torrey Norton, Felix E. Obenshain, Reinhard Oehme, Thomas Otten Paine, James Henry Parker, Jr., *William J. Pervin, *Richard J. Plock, Kenneth Stanley Preschel, *Allen Bishop Robbins, *Paul C. Robison, Donald Stanley Rodbell, James Edward Roderick, Roop Chand Sahns, *Alvin Martin Saperstein, Muneo Sasaki, Seibun Sasaki, Cameron B. Satterwaite, *Heinz Scharfstein, *Leon Joseph Schkolnick, *Stanley Schneider, Robert T. Schumacher, Herman P. Schwan, *Bernice G. Segal, William Eno Semple, *Rodman Alton Sharp, *James Leonard Shilts, Rachel Stahl, Clare Perry Stanford, Alden Stevenson, *James Carr Suits, George K. Tajima, Phrixos J. Theodorides, John Wright Thomas, Ho Yet Tom, Jay Todd, Jr., *Arnold Martin Toxen, Robert Allen Tracy, Henry Snowden Valk, Johann Siegfried Wagener, *Richard John Wagner, Stephen Waldron, William Charles Walker, Jack Dussel Warthman, *Donald Arthur Wiegand, David Jean Winslow, *Robert William Wright, Michael Koichi Yonemitsu, John Sheldon Youtcheff, John Southey Wise, and Solomon Zwerdling.

* Student.

KARL K. DARROW, *Secretary*
American Physical Society

Errata Pertaining to Papers B1, D1, and H11

B1, by Richard Schlegel. In line 10, the comma between $S=S'$ and $\beta=1/kT$ should be a semicolon.

D1, by Milan D. Fiske. The following should be added to the by-line: Metallurgy Research Department, General Electric Research Laboratory, Schenectady, New York.

H11, by B. E. Simmons, D. M. Van Patter, D. F. Famularo, and R. V. Stuart. In line 5, 136 kev should read 131 kev.

PROGRAMME

MONDAY MORNING AT 10:00

Murphy 105

(D. ALPERT presiding)

Surface Physics and Domain Formation

Invited Papers

(A1 and A2 after A5, and A3 after A7)

A1. Recent Results in Sputtering by Ion Bombardment. G. K. WEHNER, *Wright-Patterson Air Force Base.* (25 min.)

A2. Domains and Their Formation in Barium Titanate Single Crystals. W. J. MERZ, *Bell Telephone Laboratories.* (25 min.)

A3. Surface-Barrier Determination by Periodic Deviations from the Schottky Effect. E. A. COOMES, *University of Notre Dame.* (35 min.)

Contributed Papers

A4. Low-Frequency Dielectric Loss Peaks in KCl Containing Divalent Cation Impurities. E. BURSTEIN, J. W. DAVISSON, AND N. SCLAR, *Naval Research Laboratory.*—Low-frequency dielectric loss measurements have been carried out as a function of temperature, over the range from 25°C to 200°C, for KCl containing divalent cation impurities. KCl containing Sr^{++} exhibits a single peak at 117°C in the dielectric loss *vs* temperature curve for 10 000 cps. On going to lower frequencies, the peak shifts to lower temperatures. A plot of the log of the frequency against the reciprocal temperature at which the peak occurs yields a straight line curve so that the data can be represented by the equation $\nu=\nu_0 \exp(-U/kT)$; with $\nu_0=1.9\times10^{12}$/sec and $U=0.64$ ev. Similar peaks are also observed in KCl crystals containing Pb^{++}. The data for these crystals are, however, still incomplete. The low-frequency loss peaks, first pointed out by Breckenridge, are presumably due to relaxation processes involving "ghost" dipoles in the form of divalent cation—positive ion vacancy pairs. The inability to observe loss peaks due to positive ion vacancy—negative ion vacancy pairs in pure alkali halides is attributed to the fact that the concentration of the ion vacancy pairs is very low.

A5. Thin Films of $BaTiO_3$. CHARLES FELDMAN, *Naval Research Laboratory.*—Ferroelectric films of $BaTiO_3$, about 1–2 microns thick, have been formed on platinum substrates by evaporation in a vacuum and a subsequent heat treatment in air. X-ray diffraction examination of the films shows that the structure is mainly perovskite with the hexagonal phase as a minor constituent. Dielectric and hysteresis measurements show the Curie temperature at about 120°C. The room temperature dielectric constant is of the order of 100. Because of their small thickness, the films are almost completely polarized by the voltages used in the dielectric measurements. The measured value accordingly compares favorably with the dielectric constant bulk ceramic.

A6. A Simple Interpretation of Wehner's Sputtering Law. WALTER WESSEL, *Wright-Patterson Air Force Base.*—The law, which states[1] that for the threshold of low voltage sputtering the momentum M, transferred upon a metal atom by the impinging ion, multiplied by the bulk velocity of sound v_s, is proportional to the heat of sublimation S of the metal:

$$Mv_s=C\cdot S \qquad (1)$$

seems to demand an explanation on very general terms, because the constant C (≈11.2) in (1) is so markedly the same for a great number of metals. We have tried to do this, assuming the propagation of a real sound wave along the surface of the metal and applying only the theorems of conservation of momentum and energy. As a result we find the above formula replaced by

$$Mv_t=S(2+2(R/S)^{\frac{1}{2}}+4R/S), \qquad (2)$$

where $R=mv_t^2/2$, m = mass of the metal ions and v_t = surface velocity of sound. The agreement with the experiments is not as good as in the empirical formula (1), being the bracket in (2) variable between 9.3 and 15.9; but its average value 12.2 for 26 metals comes rather close to the value of C in (1).

[1] G. K. Wehner, Phys. Rev. **93**, 633 (1954).

A7. Gettering of a Vacuum Vessel by Titanium Metal. VIRGIL L. STOUT AND MARTIN D. GIBBONS, *General Electric Research Laboratory.*—Data has been obtained for the gettering of gases by titanium metal. The getter was formed of an iodide titanium ring which was heated by a radio-frequency induction heater. Gases that were gettered included oxygen, nitrogen, carbon dioxide, hydrogen, water vapor, methane, and room air. Gettering information was obtained using the closed vessel sorption technique, which has yielded values of gettering rates and quantities of gas that can be sorbed. Residual gases have been identified using the mass spectrometer and reaction products have been analyzed by x-ray diffraction.

A8. Contact Electrification Effects in a Metal-Metal System. I. General Theory. ARTHUR PASKIN, *Sylvania Electric Products, Inc.**—When two dissimilar metals are placed in contact and subsequently separated, an electrostatic charge develops on the two metals. It is found that an application of current ideas on what happens at a metal-metal contact will adequately explain the sign of the charge and give an upper limit to the magnitude of the charge observed in contact electrification. A quantitative understanding of contact charging can be obtained by examining the reduction of charge through field emission as the two metals are separated. Calculations have been carried out which take into account the effect of field emission. The details of these calculations depend on the particular geometry of the metal contacts.

A formula has been developed for the charge to be expected when the two metals are of spherical and planar geometry, respectively. This relationship is found to be in good agreement with preliminary contact electrification experiments carried out in this laboratory.

* Work supported by the U. S. Naval Ordnance Laboratory.

A9. Contact Electrification in a Metal-Metal System. II. Results for Mercury-Steel. PAUL E. CARROLL, *Sylvania Electric Products, Inc.**—Contact electrification measurements have been performed with mercury and steel being used as the contact metals. The measurements were performed in such a way that both contact potential difference and contact electrification could be determined with the same physical arrangement. The two measurements on the same contact surfaces were needed to correlate these measurements with the theory presented in the preceding paper. The use of a liquid metal for one of the contacts reduced the effects of any frictional electrification to the point where they were not detected. The measurements were in agreement with the theory within experimental error.

* Work supported by the U. S. Naval Ordnance Laboratory.

MONDAY MORNING AT 10:30

Physics 170

(E. L. HILL presiding)

Theoretical Physics

B1. Relativistic Statistical Mechanics of an Ideal Gas. RICHARD SCHLEGEL, *Michigan State College.*—For an ideal monatomic gas at equilibrium in system K, $n_i=\exp(-\alpha-\beta\epsilon_i)$; α and β are constants, n_i and ϵ_i are, respectively, the number of atoms and relativistic kinetic energy per atom in the ith phase-space cell. In system K', with velocity $v=v_x$ relative to K, $n_i'=\exp(-\alpha'-\beta'\epsilon_i')$. $n_i=n_i'$. Relativistic transformations on x and momentum p_x lead to $\Delta\tau=\Delta\tau'$, where $\Delta\tau$ is phase-space cell volume. Association of entropy S with statistical probability gives $S=S'$, $\beta=1/kT$ and $\beta'=1/kT'$, where k is Boltzmann's constant and T is temperature, are obtained from customary thermodynamic arguments; $\alpha=\alpha'$ follows from $T=T'$ for $v=0$. The use of the relativistic energy transformation, $\epsilon_i'=[\epsilon_i-vp_x(i)]/\gamma$, where $\gamma=(1-v^2/c^2)^{\frac{1}{2}}$, gives $T_i'=(T/\gamma)/[1-vp_x(i)/\epsilon_i]$, and, on averaging, $T'=T/\gamma$. Radiation from the gas is found by the energy transformation to have frequency $\nu'=\nu\gamma/(1-v/c\cos\theta')$, the usual relativistic Doppler equation, where θ' is the angle in K' between the observed radiation path and velocity vector of K. Relation to thermodynamic results for transformation of T and possible physical meaning of relativistic transformation of thermodynamic quantities will be discussed.

B2. Virial Expansion of the Ideal Bose-Einstein Gas.* B. WIDOM, *University of North Carolina.*—The ideal Bose-Einstein gas can be looked upon as an imperfect gas, imperfection being due to quantum effects and giving rise to a condensation phenomenon. The virial expansion is obtained in terms of the dimensionless density $x_1=h^3(2\pi mkT)^{-\frac{3}{2}}\rho$ and the dimensionless pressure $x_2=(h^3/kT)(2\pi mkT)^{-\frac{3}{2}}p$, by eliminating y from the equations $x_1=\Sigma_1^\infty n^{-\frac{1}{2}}y^n$ and $x_2=\Sigma_1^\infty n^{-5/2}y^n$. The result is

$$x_2=x_1\left\{1+\sum_1^\infty(-1)^n\frac{D_n}{(n+1)!}x_1^n\right\}, \qquad (1)$$

where D_n is a determinant of order n, the elements a_{ij} of which are given by $[(i-j+1)n+j-1](i-j+2)^{-1}$ when $j\leq i+1$, and by 0 when $j>i+1$. The Einstein condensation occurs at $x_1=\zeta(3/2)=2.612\cdots$. The radius of convergence, R, of (1), can be estimated in several ways. Starting with the series in y, and applying a theorem of Landau, gives $R\geq\zeta(3/2)[\zeta(3/2)-[\zeta(3/2)^2-1]^{\frac{1}{2}}]^{\frac{1}{2}}=0.103\cdots$. A rough estimate of the magnitude of D_n yields $R\geq 1/2e^{\frac{1}{2}}=0.184\cdots$. A better estimate of D_n yields $R\geq 1/2e^{\frac{1}{2}}=0.257\cdots$.

* Work supported by U. S. Office of Naval Research.

B3. Universal Curves for Dispersion and Scattering of X-Rays.* L. G. PARRATT AND C. F. HEMPSTEAD, *Cornell University.*—The theoretical expression for the dispersion (or atomic scattering factor) of x-rays has been integrated for any value of p_q in a λ^{p_q} term in the distribution of dispersion-oscillators for each q shell of electrons. The dispersion-oscillator distribution may be written generally as the sum of n terms $\Sigma_n C_{q_n}\lambda^{p_{q_n}}$ or, as is commonly done, as a single $C_q\lambda^{p_q}$ term. Damping has been retained, its effect evaluated and shown to be negligible except for λ extremely close to the wavelength of an absorption discontinuity. Universal dispersion curves (with damping neglected) are presented. From the universal curves, if p_q and g_q (the oscillator strength) are known, the refractive index (or the atomic scattering factor) for each q shell of any atom, and hence the sum of all q shells, can be readily and very conveniently deduced. Comparison of these more exact theoretical values with experiment shows less satisfactory agreement than before.

* This research was supported by the United States Air Force through the Office of Scientific Research of the Air Research and Development Command.

B4. Comparison of Several Approximations to Scattering of High-Energy Electrons. J. MAYO GREENBERG, *Rensselaer Polytechnic Institute.*—Several exact calculations of the scattering of high-energy electrons by nuclei have been completed[1] or are in the process of being computed. It is, therefore, now possible to determine the suitability of the various available approximations with the view to finding more convenient methods of analyzing the experimental data.[2] At the least it seems probable that accurate extrapolations from exact calculations can be obtained. Calculations using the soft sphere[3] method show good agreement with those of Yennie *et al.* in the positions of the minima of the diffraction pattern but are in poor agreement otherwise. Further calculations are being made using a method[4] based on the W. K. B. treatment of the incident plane wave.

[1] Yennie, Wilson, and Ravenhall (to be published).
[2] Hofstadter, Fechter and McIntyre, Phys. Rev. 92, 978 (1953).
[3] E. W. Montroll and J. M. Greenberg, Phys. Rev. 86, 889 (1952).
[4] R. J. Glauber, Phys. Rev. 91, 459 (1953); G. Molière, Z. Naturforsch. 2a, 133 (1947).

B5. Numerical Solution of the Diffusion Equation in Cylindrical Geometries, G. M. ROE AND R. H. STARK. *Knolls Atomic Power Laboratory.**—The equation, $\nabla\cdot D\nabla\psi+A\psi=S$, with D, A, and S functions of position in (r,s) space, was

replaced by a set of simultaneous second order difference equations applicable to an NxM mesh. The difference equivalents of the gradient, divergence, and integral operators were chosen to be consistent in the sense that Green's theorem holds exactly. The difference equations were set up for solution on the UNIVAC, using an extrapolated Liebmann iteration scheme. Young's formula[1] for the extrapolation factor, valid for symmetric matrix operators, can be shown to hold also for the nonsymmetric matrix in this problem; and the optimum extrapolation factor can be estimated by a variational method. The convergence rate can frequently be improved by renormalizing the approximate solution at each stage of the iteration.

* Operated by the General Electric Company for the United States Atomic Energy Commission.

[1] D. M. Young, Jr., "Iterative Methods for Solving Partial Differential Equations of Elliptic Type," Ph.D. thesis, Harvard University, 1950.

B6. Classical Field Theory in the Hamilton-Jacobi Formalism. HANS FREISTADT, *Newark College of Engineering.*—The Hamilton-Jacobi formalism referred to[1] in connection with an attempt to describe quantum effects by a classical relativistic field theory is developed further. Both "time-independent" and "time-dependent" formulations are given, and the relation between them is discussed. In the former, the constants of the motion are identified with the "new" field variables, whereas in the latter they are the values of the fields on a suitable space-like surface. As an illustration of the respective procedures, the classical Dirac and Klein-Gordon free fields are solved explicitly. A perturbation method is formulated for the case of fields in interaction. The metric tensor is not treated as a field quantity.

[1] H. Freistadt, Phys. Rev. **B94**, 746 (1954).

B7. On the Correlation Function in Burgers' Model of Turbulence.* MORTON A. HYMAN, *Westinghouse Electric Corporation* (introduced by F. N. FRENKIEL).—Burgers has derived[1] from his well-known model the following equation for the 2nd-order velocity correlation function $R(\eta,t)$ in homogeneous turbulence (η is distance between points correlated, t is time):

$$\frac{\partial^2 R}{\partial t^2}-(2+\beta)\frac{\partial^2 R}{\partial t\partial\eta^2}+2\beta\nu^2\frac{\partial^4 R}{\partial\eta^4}=-\frac{\partial^2}{\partial\eta^2}(\bar{R}-R)^2; \qquad (1)$$

ν is the kinematic viscosity, β is an unspecified pure number, and $\bar{R}(t)\equiv R(0,t)$. It is shown here that $\beta=0$. The resulting 3rd-order differential equation is integrated first qualitatively and then by an accurate numerical scheme. The calculated results are consistent with experiment, indicating that the assumptions made by Burgers in his derivation of (1) are reasonable and that this new approach might be profitably pursued. The problem simplifies if one restricts attention to the cases $\eta\to 0$ and $|\eta|\to\infty$.

* This research was carried out while the author was a Fulbright Scholar at the Technical University, Delft, Holland.

[1] J. M. Burgers, *Proc. 7th Intern. Congr. Theoret. Appl. Mech.*, Istanbul, 1952 (to appear).

MONDAY MORNING AT 10:30

Physics 150

(J. M. BLAIR presiding)

Invited Papers on Nuclear Radii

C1. Determination of Nuclear Radii by Electron Scattering. R. W. PIDD, *University of Michigan.* (30 min.)

C2. Nuclear Radii from Beta Transition-Energies between Mirror Pairs. D. J. ZAFFARANO, *Iowa State College.* (30 min.)

MONDAY MORNING AT 10:30

Physics 133

(E. P. T. TYNDALL presiding)

Solid-State Physics

D1. Effects of Elastic Dilatation and Shear on the Superconducting Transition of Tin. MILAN D. FISKE.—The earlier[1] measurements on the depression of the superconducting magnetic threshold of tin by hydrostatic pressure have been improved by new apparatus using the same differential technique as previously. The isothermal difference between the critical field of one crystal under pressure and that of a similar one under atmospheric pressure has been measured to a precision of $\pm 1\times 10^{-4}$ gauss/atmosphere above 3.4°K. The critical field dependence on pressure varies from -6.8×10^{-3} gauss atmos^{-1} at 3.65°K to -6.5×10^{-3} gauss atmos^{-1} at 3.0°K. These values are in good agreement with those of previous investigators and with the recent results (in press) of Garber and Mapother near 3.6°K. The speculation that shear stresses have a negligible effect on the superconducting transition in tin has been checked by a method analogous to that of the hydrostatic experiment. A thin-walled tubular polycrystal of tin was strained in torsion to provide a nearly uniform pure shear. No effect whatsoever was detectable within the elastic range. From the constants of the apparatus it follows that the effect of shear stress on the magnetic transition is less than 4×10^{-4} gauss/atmos. A similar result with a solid tin cylinder has been obtained by Maxwell and Lutes.

[1] M. D. Fiske, Phys. Rev. (to be published). This contains a summary of results of previous studies.

D2. Temperature Dependence of the Periodic Hall Effect in Bismuth.* J. M. REYNOLDS AND D. D. TRIANTOS, *Louisiana State University.*—At 1.4°K the Hall effect in bismuth shows oscillations which are periodic in $1/H$, and whose amplitude increases with increasing magnetic field.[1] We have measured the Hall effect in a single crystal of bismuth in fields up to 8 kilogauss and at seven temperatures ranging from 1.38°K to 4.21°K. The magnetic field was parallel to the trigonal axis of the crystal and the current was along one of the binary axes. The period and phase of the oscillations were found to be independent of temperature while the amplitude decreased rapidly with increasing temperature. From these data estimates are made of the values of the effective Bohr magneton and of the Fermi energy of the electrons responsible for the effect. For this orientation β^* is 2.2×10^{-19} erg/gauss and E_0 is 1.5×10^{-14} erg $=0.009$ ev.

* Supported by the National Science Foundation.
[1] Reynolds, Leinhardt, and Hemstreet, Phys. Rev. **93**, 247 (1954).

D3. Oscillatory Thermal Conductivity of Bismuth in Magnetic Fields at Liquid Helium Temperatures. J. BABISKIN AND M. C. STEELE, *United States Naval Research Laboratory.*—An oscillatory dependence of the thermal conductivity upon magnetic fields has been observed in a bismuth single crystal at 1.60°K in fields up to 12 600 gauss. The magnetic field was perpendicular to the trigonal axis and parallel to a binary axis, while the heat current was parallel to the trigonal axis. For this orientation the thermal conductivity oscillations were periodic in H^{-1} with β/E_0 equal to 7.2×10^{-5} gauss^{-1}. This value is in good agreement with the results of the measurements of the magnetothermoelectric oscillations[1] and the calculated value from the de Haas-van Alphen effect[2] for the same orientation. The amplitude of the oscillating component amounted to 0.83 percent of the total thermal conductivity at 8300 gauss. The mean value of the thermal conductivity decreased 3.7 percent in going from zero field to 12 600 gauss.

[1] M. C. Steele and J. Babiskin, Phys. Rev. (to be published).
[2] D. Shoenberg, Trans. Roy. Soc. (London) **A245**, 1 (1952).

D4. Order-Disorder Problem for a Cubic Lattice. F. J. MURRAY, *Department of Mathematics, Columbia University.*—A new formulation for the van der Waerden probability approach to the statistics of a cubic lattice is based mathematically on the principle that the order in which flaws are introduced is immaterial. Also a precise treatment of the interference relations between polyhedra is given. This leads to a summation problem involving the matrix A previously considered by the author. For the three-dimensional case, methods are developed for evaluating the A sum which yield the internal energy and specific heat over the full temperature range without mathematical singularity. In two dimensions, A does not have the completely continuous character (when regarded as an infinite matrix) upon which these methods are based. The three-dimensional computation does require large-scale automatic sequence calculation even when certain judicious approximations are made. Agreement with other theoretical evaluations is as good as one could expect in the range over which these are valid, but comparison with the experimental results of Sykes shows definite qualitative differences. However, it may be worth noting that if interference is ignored, good agreement over a specified range is possible. Funds were provided by the Office of Naval Research for this investigation and the Florida Automatic Digital Computer was made available at Patrick Air Force Base.

D5. Effect of Surface Friction on High-Speed Penetration. JOSEPH M. KRAFFT, *Naval Research Laboratory.*—The frictional adhesion between projectile and target during a ballistic penetration has been measured with a torsional Hopkinson bar. The apparatus allows measurement of the torsional adhesion of a spinning projectile during its penetration of the bar end. Both the axial and torsional forces are measured as strain waves in a long bar, separation of the two occurring by virtue of the lower propagation velocity of the torsional wave. By assuming the friction resisting rotation to be equal to that resisting axial penetration, the energy loss due to friction was computed. It was found that friction accounts for at most three percent of the striking energy of the projectile; common surface contaminants, not necessarily special lubricants, reduce this loss to less than one percent. The torque-time pattern during penetration can be closely predicted with the assumption of a frictional energy loss just sufficient to keep the sliding surfaces at the melting temperature of the metal.

D6. Diffusion of Impurities in Silicon. W. C. DUNLAP, JR., H. V. BOHM, AND H. P. MAHON, JR., *General Electric Research Laboratory.*—Measurements of the diffusion of several impurities into silicon have been made using the following methods: (a) the p-n junction method,[1] for antimony and boron; (b) the radioactive tracer method, for antimony and gold; and (c) capacity measurements, for gold. The capacity method is based upon the high ionization energy of gold in silicon;[2] when gold diffuses into p-type silicon, there is created a layer which becomes highly insulating at liquid nitrogen temperature. By measurement of the capacity of the sample, coated with aluminum-gallium electrodes, the thickness of the insulating layer was measured. Measurements were made on the aforementioned impurities between 900°C and 1300°C. Antimony and boron diffuse relatively slowly. Their diffusion coefficients at 1100°C are about 10^{-13} and 10^{-12} cm^2/sec, respectively. The activation energy for diffusion is about 3.5 ev. Both these elements are probably substitutional in silicon. Gold, on the other hand, diffuses relatively rapidly and has a diffusion coefficient at 1100°C of about 10^{-7} cm^2/sec. The apparent temperature dependence of diffusion is, however, greater than for antimony and boron. Because of the donor action of gold in silicon and the large diffusion coefficient at 1100°C, it is postulated that gold is interstitial in silicon.

[1] W. C. Dunlap, Jr., Phys. Rev. **87**, 615 (1952).
[2] E. A. Taft and F. H. Horn, Phys. Rev. **93**, 64 (1954).

D7. Oxidation of Thin Films of Ge and Si. W. C. DASH, *General Electric Research Laboratory.*—A thin film of varying thickness of amorphous Ge or Si is evaporated onto one wall of a glass tube. Optical transmission studies are made as a function of position along the film using 5461A light for Ge and 3650A for Si. Exposure to silver-diffused oxygen or to room air immediately increases the transmission, and it continues to increase over a period of several days. Using absorption constants reported in the literature, an "apparent" oxide thickness can be computed. This apparent oxide thickness is found to vary approximately linearly with thickness of the film, consistent with the idea that the film is porous or granular. A Ge film which has been recrystallized by annealing for an hour at 400°C[1] oxidizes much more slowly than an unannealed film. It is not possible to decide from these results how thick an oxide layer is formed, but the experiments do establish that at least a monolayer of oxide and probably more is formed very quickly on an amorphous or crystalline film of Ge and on an amorphous film of Si upon exposure to pure silver-diffused oxygen as well as to the atmosphere.

[1] G. H. Haas and N. W. Scott, J. phys. radium **11**, 394–402 (1950).

MONDAY AFTERNOON AT 2:00

Murphy 105

(W. G. SHEPHERD presiding)

Ion and Electron Dynamics, Luminescence

Invited Papers

(F1 at beginning, F2 after F4, and F3 after F8)

F1. Low-Energy-Loss Interaction of Electrons with Solids. L. B. LEDER, *National Bureau of Standards.* (25 min.)

F2. Recent Developments in the Design of High-Energy Synchrotrons. J. P. BLEWETT, *Brookhaven National Laboratory.* (25 min.)

F3. Post-War Developments in Amplifiers Involving Energy-Exchange Processes between Electron Beams and Microwave Electric Fields. L. M. FIELD, *California Institute of Technology.* (25 min.)

Contributed Papers

F4. Investigations of Intensity Anomalies in Electron Diffraction from Crystals.* HENRY E. BREED AND J. MAYO GREENBERG, *Rensselaer Polytechnic Institute.*—The expected intensities of reflections occurring in electron diffraction are generally calculated using the first Born approximation. Errors in this approximation may appear in interpretation of molecular gas diffraction (where atomic numbers differ greatly) and in crystals (where atomic numbers differ by a smaller amount).[1] This experimental investigation has been designed to evaluate anomalous intensities in diffraction of crystals of medium atomic weights, in terms of errors inherent in the approximation. Experimental results on cubic AgBr and hexagonal AgI show that for the former the 111 and 311, and for the latter the 004 reflections are considerably stronger than the Born approximation predicts. Geometrically, destructive interference occurs between silver and halide atoms in these reflections. Incomplete interference is attributed to relative internal phase shift between atoms of different atomic number. A small phase difference is sufficient to account for the anomalies. Approximate calculations of the phase difference, based on the Thomas Fermi model, are in qualitative agreement with the experimental observations.

* Supported in part by the Research Grants Committee of Rensselaer Polytechnic Institute.
[1] Glauber and Shomaker, Phys. Rev. **89**, 667–671 (1953).

F5. Mass Doublet Measurements Using a Modulated Magnetic Field.* CLAYTON F. GIESE AND T. L. COLLINS, *University of Minnesota.*—A double-focusing mass spectrometer previously described[1] now employs a modulated magnetic field for sweeping of mass peaks. A supplementary coil wound directly on the spectrometer tube within the magnet gap supplies the modulating field and permits, in conjunction with an electron multiplier and fast electrometer amplifier, the display of a portion of the mass spectrum on the oscilloscope. A system of high-speed commercially available (millisec) relays provides for incremental changes in the ion accelerating voltage and electrostatic analyzer deflection voltage on alternate sweeps. Adjustment of this increment until the two peaks of a mass doublet are superimposed on the oscilloscope screen is then equivalent to finding the relative change in energy required to give the two ions of different mass the same trajectory. Calculation of the mass difference follows from this relative change in energy, measured in terms of resistance by a precision voltage divider. The advantages of this technique are: (1) instantaneous observation of the mass peaks facilitates adjustment of the spectrometer, and (2) the fast sweeping eliminates the problem of drifts.

* This research sponsored in part by the joint programme of the U. S. Office of Naval Research and U. S. Atomic Energy Commission.
[1] A. O. Nier and T. R. Roberts, Phys. Rev. **81**, 507 (1951).

F6. Applications of Rapid Sweeping to a Single-Focusing Mass Spectrometer. C. ROBERT LAGERGREN, *University of Minnesota.*—A method of rapid sweeping and alternate selecting of ion beams in an ordinary 60° mass spectrometer permits the investigation of initial kinetic energy distributions of fragment ions formed by electron impact. A deflection coil placed in the gap of the analyzer magnet sweeps the ion beam over a single mass peak. Two ion accelerating voltages, accurately determined by the ratio of the masses of the ions involved, are alternately applied by means of a high-speed commercially available (millisec) relay and a precision voltage divider network. The relative positions and shapes of the two ion peaks appearing simultaneously on an oscilloscope reflect their relative initial kinetic energy distributions. Choosing for one of the peaks that of a molecular ion whose shape is assumed to represent the "zero" initial kinetic energy distribution; one can obtain information about the initial energy distribution of the other. The superposition of ion peaks also facilitates the rapid measurement of the relative abundances of ions. This is accomplished by a selective attenuation of the input signals to the oscilloscope so that the alternate peaks are matched in height.

F7. Stabilization of Potentials in a Precision Double-Focusing Mass Spectrometer.* K. S. QUISENBERRY, T. T. SCOLMAN AND T. L. COLLINS, *University of Minnesota.*—Preliminary tests and measurements have been completed on a large double-focusing mass spectrometer.[1] To realize the advantages of the high resolution, which is approximately 1 in 40 000, extreme stability is required. This is accomplished by using two sensing and stabilizing circuits. The first of these, which stabilizes the potential supplied to the electrostatic analyzer and compensates for any changes in the magnetic field, employs a second smaller spectrometer with a modulated ion beam. This system utilizes a synchronous detection technique. The second circuit regulates the accelerating potential in the large spectrometer tube by sensing the position of the ion beam after leaving the 90° electrostatic analyzer. These systems employ both electronic feedback and

mechanical servomechanisms so that the error signals are maintained essentially zero.

* Supported by a grant from the National Science Foundation.
[1] Collins, Scolman, and Nier, Bull. Am. Phys. Soc. **29**, No. 4, 27 (1954).

F8. A Model of Solar Proton Streams. WILLARD H. BENNETT, *Naval Research Laboratory.*—A laboratory tube has been developed which provides a true scale model of the paths of solar proton streams in the earth's magnetic field. This model shows that proton streams approaching the earth in a stream whose diameter is of the order of 1000 kilometers is mostly turned back by the earth's field before reaching the earth, while only a small part of the stream reaches the earth at the auroral zone of magnetic latitude in a spiral which tightens as the stream nears the earth. Streams can also pass the earth and be turned back towards the earth forming a ring current about the earth near the equatorial plane. The magnetic effects of the ring currents and of the tight spirals between them account at least qualitatively for magnetic storms, and the patterns in the laboratory model agree at least qualitatively with the timing of the sequence of events in sun spots, first auroral displays and magnetic disturbances.

F9. Luminescence from NaCl.* W. E. SPICER, *University of Missouri.*—The low intensity, x-ray induced luminescence from single NaCl crystals has been studied in the range 240 mμ to 580 mμ using photon-counting techniques. The spectra obtained depend strongly on the past history of the sample. With no heat treatment and small x-ray dosages, bands centering about 550, 400, and 250 mμ were observed. Heating the crystals to temperatures between 200°C and 550°C for a few minutes causes new, more intense bands at 350 mμ and 505 mμ to replace (or mask) the two long wavelength bands. The 250 mμ band is increased by a factor of about 20. This spectrum changes with time under constant x-ray irradiation. After 5½ hours of irradiation, the 350 mμ band becomes rudimentary, the 250 band is greatly reduced, the band at 505 mμ disappears, leaving the 550 mμ band and a new band at 430 mμ. Repeating the heat treatment restores the high intensity of the 505, 350, and 250 mμ bands. The luminescence was also studied as a function of time after stopping the irradiation. It was found that after a decay in intensity of three orders of magnitude had taken place, almost all of the original intensity could be regained by shining white light on the crystal.

* Supported in part by the United States Office of Naval Research.

F10. Long Life Luminescence and Diffusion in Magnesium Oxide.* B. GOODMAN, *University of Missouri.*—An ionic (vacancy) diffusion model is considered for the very long life phosphorescence ($\sim 10^7$ seconds) observed by Eisenstein[1] in x-ray irradiated MgO crystals. It is assumed that: (1) the x-rays release vacancies at dislocation lines,[2] some of which diffuse away from the region of influence of the stress field of dislocation; (2) the vacancy mobility is enhanced during the irradiation;[3] (3) luminescence results in some unspecified way when the vacancies reunite with dislocations. Calculated decay curves are similar to those observed which follow t^{-n} ($n \sim 0.3$–0.7) for a number of decades and then fall off rapidly but the theoretical curves do not fall off as rapidly. If the diffusion coefficient is written as $D = D_I + (T)$ where D_I is the x-ray induced part (assumed proportional to the x-ray intensity) and $D(T) \alpha e^{-E/kT}$ is the normal coefficient, the ratio $D_I/D(T)$ can be estimated by using different x-ray intensities and different temperatures. Both estimates give $D_I/D(T) \sim 40$ for the room temperature irradiations. A rather low activation energy, $E \sim 0.6$ ev, is obtained from a fit of the decay curves at different temperatures to the calculated curves.

* Supported by the U. S. Office of Naval Research.
[1] A. S. Eisenstein, Bull. Am. Phys. Soc. **29**, No. 1, 39 (1954).
[2] J. J. Markham, Phys. Rev. **77**, 500 (1952).
[3] F. Seitz, Phys. Rev. **89**, 1299 (1953).

F11. Optical Absorption Spectra of Stoichiometric Single Crystals of MgO.* W. T. PERIA, *University of Minnesota.*—Magnesium oxide single crystals, believed to be of stoichiometric composition, have in the ultraviolet region of the spectrum an absorption commonly believed to be the tail of the fundamental absorption band. However, in experiments on the coloration of these crystals with excess magnesium, changes in this "background" absorption have been observed quite apart from the large absorption changes caused by the addition of the excess magnesium. This has led to attempts to correlate the background absorption with the densities of the various types of lattice defects present in the crystal. To this end background absorption spectra are being studied as a function of the time and temperature of heat treatment in vacuum.

* Supported by United States Signal Corps.

F12. Excitation of Zinc Oxide Phosphors by Low-Energy Electrons. ROSS E. SHRADER, *RCA Laboratories Division.*—The phenomenon of excitation of ZnO phosphors by electrons when the applied voltages are equal to or less than the equivalent ev of the observed photons has been investigated. The results suggest that in ZnO phosphors the energy level distribution is such that any electron accepted by the crystal lattice, regardless of how small was its velocity in vacuum, has the ability to produce luminescence.

MONDAY AFTERNOON AT 2:00

Physics 150

(R. T. BIRGE presiding)

Joint Session of American Physical Society and AAPT

Invited Papers on Astronomical Subjects

G1. Galactic Magnetic Fields. W. A. HILTNER, *Yerkes Observatory.* (30 min.)
G2. White Dwarfs and Degenerate Stars. W. J. LUYTEN, *University of Minnesota.* (30 min.)
G3. The Probable Age of the Earth. T. L. COLLINS, *University of Minnesota.* (30 min.)
G4. Galactic and Extra-Galactic Sources of Radio Waves. F. GRAHAM SMITH, *Cambridge University.* (30 min.)

MONDAY AFTERNOON AT 2:00

Physics 170

(G. FREIER presiding)

Mainly Reactions of Transmutation

H1. Gamma Rays from Proton Capture in Li^7 and F^{19}.* E. B. NELSON, W. LAWRENCE, AND R. R. CARLSON, *State University of Iowa.*—Sodium iodide scintillation detectors and a 10-channel pulse-height analyzer were used to search for cascade gamma-ray transitions following the capture of 440-kev protons by Li^7. The number of coincidences between a gamma ray of energy greater than 6 mev and one of energy greater than 2.6 Mev is less than 1 percent of the total gamma transitions. A three-crystal scintillation pair spectrometer was used to search for gammas in the energy region of 10–12 Mev. Their intensity is less than 10 percent of the 17.6-Mev intensity. The 13.08-Mev state in Ne^{20}, formed by the capture of 224-kev protons by F^{19}, was found to decay by alpha emission to the 6.13-Mev state in O^{16}. The angular distribution of the 6-Mev radiation is strongly anisotropic. Alpha emission to the ground state of O^{16} is inhibited by at least a factor 2 compared to the short-range alpha. These results limit the l value of the captured proton and the spin and parity of the capture state.

* Supported in part by the U. S. Atomic Energy Commission.

H2. Gamma Rays from (p,γ) Reactions in B^{11} and Mg^{24}. D. S. CRAIG, W. G. CROSS, AND R. G. JARVIS, *Chalk River Laboratories.*—The yield of 16-Mev radiation from $B^{11}(p,\gamma)C^{12}$ has been found to exhibit a resonance at 163 kev with an intensity 1/40 that of the 12-Mev radiation in agreement with Moak and Robinson.[1] The angular distribution of the 16-Mev radiation at this resonance has been determined from measurements at 0, 60, 90, and 120° to be of the form $1-A\cos\theta+B\cos^2\theta$ with $B=A\pm0.03$ and $A=0.22\pm0.06$. The presence of the odd power cosine term can be interpreted as interference with a level of opposite parity. The gamma spectrum from the 222-kev resonance in $Mg^{24}(p,\gamma)Al^{25}$ shows a line of 2.03 ± 0.02 Mev coincident with one of 0.47 ± 0.02. In disagreement with measurements of Casson[2] no 2.5-Mev transitions to the ground state with an intensity greater than 2 percent of the 2.03 component has been fund. The angular distribution of the 2.03-Mev radiation is isotropic to within a few percent. Assuming this transition is to the first excited state then the spin and parity of the 2.5-Mev level in Al^{25} is $1/2\pm$, or possibly $3/2+$.

[1] Oak Ridge National Laboratory 1005 (unpublished).
[2] H. Casson, Phys. Rev. **89**, 809 (1953).

H3. The Reaction $C^{14}(p\gamma)N^{15}$ Above the (pn) Threshold. H. E. GOVE, G. A. BARTHOLOMEW, E. B. PAUL, AND A. E. LITHERLAND, *Chalk River Laboratories.*—The yield of the proton capture gamma ray leading to the ground state of N^{15} has been measured at three angles 0°, 90°, and 142° from $Ep=0.90$ to 2.2 Mev. The angular distribution and partial width of this gamma ray were measured at resonances at 1.17 and 1.32 Mev and, in addition, the partial width was measured at 1.46 Mev. The results are summarized in the table. The values for Γn and Γp will be discussed in the following abstract. The spin and parity assignments are based on angular distributions, interference effects, and single particle limit arguments. The previously unreported broad s-wave state at 1.46 Mev whose total width and partial width for ground-state gamma emission are both about 0.2 of the single particle limit may account for the thermal neutron-capture cross section and gamma-ray spectrum. Some previous measurements have been reported.[1]

Ep	Γkev	Γnkev	Γpkev	$\omega\gamma$ev	J	$\Gamma\gamma$ev	Radiation
1.17	7.5	1.3	6.2	0.17	$\frac{1}{2}-$	0.21	$M1$
1.32	43	34	9.4	0.48	$\frac{1}{2}+$	2.2	$E1$
1.46	500	~5	~500	29	$\frac{1}{2}+$	29	$E1$

[1] Spearman, Hudspeth, and Morgan, Bull. Am. Phys. Soc. **29**, 10 (1954).

H4. Neutrons from the Reaction $C^{14}(pn)N^{14}$. A. E. LITHERLAND, E. B. PAUL, G. A. BARTHOLOMEW, AND H. E. GOVE, *Chalk River Laboratories.*—The $C^{14}(pn)N^{14}$ reaction has been studied with protons in the energy range from the threshold to 2.2 Mev. The angular distribution of the neutrons has been measured at the resonances previously reported[1] using a long BF_3 counter as detector. All distributions but one showed odd terms in $\cos\theta$ indicating interference between states of opposite parity. The 1.17 and 1.32-Mev resonances seem to interfere with the broad level at 1.46 which is more clearly seen in the γ-ray yield curve. The angular distributions are consistent with assignments of $\frac{1}{2}-$ and $\frac{1}{2}+$ respectively for the former resonances and $\frac{1}{2}+$ for the broad state. The neutron and proton partial widths have been calculated using the known $(np)^3$ and $(nn)^3$ cross sections and our (pn) yield measurements. The assignments of higher resonances from width and angular distribution measurements will be discussed.

[1] Roseborough, McCue, Preston, and Goodman, Phys. Rev. **83**, 1133 (1951).
[2] C. H. Johnson and H. H. Barschall, Phys. Rev. **70**, 818 (1950).
[3] Hinchey, Stelson, and Preston, Phys. Rev. **86**, 483 (1952).

H5. An Excited State of Oxygen-19.* T. F. STRATTON, K. F. FAMULARO, H. D. HOLMGREN, AND R. V. STUART, *University of Minnesota.*—Foils of 0.04-mil nickel were oxidized with oxygen enriched to 23 percent O^{18}[1] to form self-supporting NiO targets containing approximately 10^{19} oxygen atoms per square centimeter. Comparison of the yield of reaction products with deuterons incident on normal and enriched targets showed one new proton group due to the O^{18} target. The experimentally determined Q for the reaction was 0.3 ± 0.3 Mev. Assuming a mass defect of 8.65 Mev[2] for O^{19} places the excited state in O^{19} at about 1.6 Mev. The differential cross section for the reaction was measured for 3.01 Mev deuterons at twenty center-of-mass angles ranging from 5° to 161°. The distribution was of the character of a typical $1_n=0$ type stripping distribution with a cross section of 213 mb at 5° falling to a minimum of 11 mb at 48° and rising to a secondary maximum of 27 mb at 84°. Attempts to resolve the ground-state protons from $O^{18}(d,p)O^{19}$ and $O^{16}(d,p)O^{17}$ failed, indicating that the Q's for these reactions are the same within the resolution of our detectors, 0.4 Mev.

* Assisted in part by the joint program of the U. S. Office of Naval Research and the U. S. Atomic Energy Commission.
[1] Courtesy of Professor A. O. Nier.
[2] E. Bleuler and W. Zünti, Helv. Phys. Acta **20**, 195A (1947).

H6. Angular Distribution of the $O^{16}(d,p)O^{17}$ Reaction.* D. M. VAN PATTER, B. E. SIMMONS, T. F. STRATTON, AND D. M. ZIPOY, *University of Minnesota.*—Nickelous oxide foil targets as described in the preceding abstract were bombarded with incident deuterons of laboratory energies 2.3 Mev to 3.9 Mev. The absolute yield of the $O^{16}(d,p)O^{17}$ ground-state

reaction was measured at $\theta_{cm}=53°$ in 35-kv steps over the indicated energy range. A resonant type yield was obtained with differential cross sections at $\theta_{cm}=53°$ of 17 mb at 2.65 Mev, 33 mb at 3.01 Mev, 19 mb at 3.25 Mev, and 31 mb at 3.43 Mev. Angular distributions[1] obtained over twenty-two center-of-mass angles from 5° to 161° at these four deuteron energies showed a forward maximum at 53° falling to a minimum of 13 mb in the neighborhood of 90° and rising gradually to 16 mb in the back angles. Fluctuations of intensity at the forward maximum provided the major contribution to maxima in the total yield at 3.0 Mev and 3.4 Mev. The differential cross section for the $O^{16}(d,p)O^{17*}$ reaction (0.875-Mev level) was measured at 3.01 Mev and 3.43 Mev. The distribution obtained was of the typical stripping type with $l_n=0$.

* Assisted in part by the joint program of the U. S. Office of Naval Research and the U. S. Atomic Energy Commission.
[1] N. P. Heydenburg and D. R. Inglis, Phys. Rev. **73**, 230 (1948).

H7. Angular Distributions in (d,p) Reactions with Ti^{47} and Ti^{49}.* F. B. Shull and M. M. Bretscher, *Washington University.*—Thin targets of TiO_2 (one with Ti^{47} enriched to 82 percent, another with Ti^{49} enriched to 99 percent) were bombarded with 10.2-Mev deuterons. Proton angular distributions were determined by a photographic method. Aluminum foils in front of nuclear emulsion plates served as energy selectors, so that proton groups from various excited states could be studied separately. Comparison with Butler's[1] theoretical curves establishes the angular momentum $l_n\hbar$ for the captured neutron, from which spin and parity of the final nuclear level may be determined. Our results are tabulated:

Reaction	Q value (Mev)*	l_n	Final Spin	Final Parity
$Ti^{47}(d,p)Ti^{48}$	8.14	3	0	even
	6.81	1,(3?)	1,2,3,4	even
	5.83	1	1,2,3,4	even
	4.83	1	1,2,3,4	even
$Ti^{49}(d,p)Ti^{50}$	5.81	3	5/2,7/2	odd
	4.46	1	1/2,3/2	odd
	4.11	1	1/2,3/2	odd

* G. F. Pieper, Phys. Rev. **88**, 1299 (1952).
* Supported by the U. S. Air Force through the Office of Scientific Research of the Air Force Research and Development Command.
[1] S. T. Butler, Proc. Roy. Soc. (London) **A208**, 559 (1951).

H8. Phase-Shift Analysis of the Elastic Scattering of Protons by He^3. R. W. Lowen, *University of Minnesota* (introduced by C. Critchfield).—A phase-shift analysis of the differential cross sections for the elastic scattering of protons by He^3 in the region from 1.01 to 3.52 Mev[1] has been made. It is found that the data can be fitted within the probable errors of approximately 5 percent by a single S-wave and a single P-wave phase shift, without any spin dependence. The S-wave phase shift is very nearly that of a charged hard sphere of radius 3.6×10^{-13} cm, while the P-wave phase shift is positive and increases from about 4° at 1.01 Mev to 25° at 3.52 Mev. The best value for the D-wave phase shift at the highest energy is zero.

[1] Famularo, Brown, Holmgren, and Stratton, reported at the Thanksgiving meeting of the American Physical Society, 1953 (to be published).

H9. Energy Levels of Li^6.* A. Galonsky and M. T. McEllistrem, *University of Wisconsin.*—A phase-shift analysis of deuteron-helium elastic scattering[1] has been performed. The single-particle level at 2.187 Mev in Li^6 has been verified at 3^+. The broad anomaly extending from 3 Mev to the limit of observation, 4.62 Mev, cannot be analyzed in terms of a single level. Instead, it has been fitted with two single-particle levels, a 2^+ level at $E_R=4.53$-Mev excitation in Li^6 and a 1^+ level at 5.4 ± 0.5 Mev. The 1^+ level cannot be located more accurately because only the tail is visible at the bombarding energies available. Of all the other two-level combinations only (3^+, 1^+) has not yet been ruled out. The assignments (3^+, 2^+, 1^+) and locations of the levels agree with an intermediate coupling[2] which is close to the $L-S$ extreme. In fitting the 3^+ resonance, it was necessary to use a small positive P-wave phase shift, whereas the usual hard-sphere phases are negative. Neither inclusion of G-wave excitation of the 3^+ level nor variation of the interaction distance can change the sign of the P-wave phase shift.

* Work supported by the Wisconsin Alumni Research Foundation and the U. S. Atomic Energy Commission.
[1] Galonsky, Douglas, Haeberli, McEllistrem, and Richards, Phys. Rev. **93**, 928 (1954).
[2] D. R. Inglis, Revs. Modern Phys. **25**, 390 (1953).

H10. Cloud-Chamber Investigation of High-Energy Photonuclear Reactions.* W. E. Matheson,† C. R. Carlson,‡ F. S. Mathews, R. O. Haxby, and R. M. Whaley, *Purdue University.*—A 14-inch Wilson cloud chamber with associated timing and control equipment designed for use with the Purdue 300-Mev electron synchrotron has been constructed and put into operation with the accelerator. While the 13 000-gauss magnetic-field equipment is being completed, experiments have been carried out by irradiating internal and external chamber targets with a 285-Mev photon beam. Photodisintegrations in carbon, argon, and helium have been observed inside the chamber. Photoprotons from carbon with energies ranging from 45 Mev to 105 Mev have been observed at 90° to the photon beam. The proton differential spectrum as determined from 236 protons recorded in approximately 6800 photographs compares well with the results obtained by other workers using scintillation-counter techniques. Nuclear cross sections obtained in units of $d\sigma/Qd\Omega$ microbarn-effective quantum^{-1}-steradian^{-1} are: 37.5 ± 4.5 in the proton-energy interval 45 Mev–80 Mev and 13.0 ± 1.5 in the interval 80 Mev–105 Mev.

* Supported in part by the U. S. Atomic Energy Commission.
† Now at Linde Air Products Company.
‡ Now at Sandia Corporation.

H11. Coulomb Excitation of Neodymium.* B. E. Simmons, D. M. Van Patter, K. F. Famularo, and R. V. Stuart, *University of Minnesota.*—A NaI-Tl scintillation spectrometer with 9° angular resolution was employed in conjunction with the Minnesota electrostatic generator to study the 136-kev gamma[1] resulting from the proton bombardment of neodymium metal.[2] A target "thick" to protons and "thin" to the gammas was prepared by evaporating Nd onto a 0.1-mil nickel backing. Electronic circuits designed to prevent overloading and a 10-channel pulse analyzer provided stable operation for obtaining an angular distribution of this gamma ray, of the form $1+0.2\cos^2\theta$ for a proton energy of 2.25 Mev. At this energy the yield at 90° is 0.20 that of the Ta 137-kev gamma ray, whose angular distribution was measured, as a check, to be isotropic to ±2 per cent. Measurements of the excitation function and the absolute cross section for production of the Nd gamma ray, as well as theoretical calculations concerning its angular distribution, are in progress.

* Assisted in part by the joint program of the U. S. Office of Naval Research and the U. S. Atomic Energy Commission.
[1] This gamma has been previously reported by N. P. Heydenburg and G. M. Temmer, Phys. Rev. **93**, 906 (1954).
[2] We are indebted to Professor F. H. Spedding for making available the neodymium.

H12. Comparative Study of Gamma Spectrum of I^{131} with Scintillation and Thick Lens Spectrometer. M. Sakai, B. Murray, and J. D. Kurbatov, *The Ohio State University.*—Gamma-ray spectrum of highly chemically pure I^{131}* was first obtained with an ordinary single-channel scintillation spectrometer. This spectrum was resolved for the well-known 364-kev, 634-kev, and the 720-kev gamma rays by comparison with the gamma rays emitted by Hg^{203} and Be^7 using a procedure which will be described. A new "peak" of 514 ± 25 kev ap-

peared in the spectrum of I^{131}. The Compton spectrum was also measured independently with a pure aluminum radiator. In addition to the three previously noted gamma rays, analysis of the Compton spectrum produced evidence for a new gamma ray of approximately 514 kev. The intensity of the gamma ray is estimated at 1.2 to 2.0 percent of the intensity of the 364-kev gamma ray. Since disintegration of the 514-kev gamma ray in all observations followed the eight day half-life, it is conditionally assigned to I^{131}.

* I^{131} was obtained from Oak Ridge National Laboratory and further purified chemically.

H13. Radiations of Pa^{232}.* C. I. BROWNE, D. C. HOFFMAN, H. L. SMITH, M. E. BUNKER, J. P. MIZE, J. W. STARNER, R. L. MOORE, AND J. P. BALAGNA, *Los Alamos Scientific Laboratory.*—The nuclide Pa^{232} has been prepared by thermal neutron irradiation of Pa^{231} in the Materials Testing Reactor and the Los Alamos "water boiler" and its radiations have been studied with a magnetic lens beta-ray spectrometer and several types of NaI(Tl) scintillation spectrometers. Coincidence and delayed coincidence techniques were utilized in the scintillation studies. The beta-ray spectrometer data indicate three negatron groups of end-point energies 1.27, 0.502, and 0.304 Mev with relative abundance of 2, 8, and 90 percent, respectively. At least fifteen gamma rays have been found to accompany the decay of this isotope. The decay of Pa^{232} was followed over eight half-lives, giving a value of 1.31 days for the half-life. This is in good agreement with the value of 1.32 days previously reported.[1] Gamma-ray energies, K/L ratios, and conversion coefficients will be given and a decay scheme presented.

* Work performed under the auspices of the U. S. Atomic Energy Commission.

[1] A. H. Jaffey and E. K. Hyde, Phys. Rev. **79**, 280 (1950).

TUESDAY MORNING AT 9:30

Murphy 105

(G. WANNIER presiding)

Electronic Conduction in Solids

Invited Papers

(K1 at beginning of session and K2 after K5)

K1. Photoelectric Emission and the Electronic Energy Structure of Some Amorphous Semiconductors. L. APKER, *General Electric Company.* (25 min.)

K2. The Role of Crystal Imperfections in Photoconductivity. R. H. BUBE, *Radio Corporation of America.* (25 min.)

Contributed Papers

K3. On the Fermi Level in Semiconducting Amorphous Antimony Films. E. TAFT AND L. APKER, *General Electric Research Laboratory.*—Thin layers of Sb were evaporated onto substrates of single-crystal Ge held slightly above 300°K. They were included as interchangeable emitters in a concentric-sphere retarding-potential phototube in the usual way.[1] Results showed that the Sb had the electronic energy structure of a semiconductor. The Fermi level lay about 0.1 ev above the top of an occupied band. When the films were heated to 100 or 200°C, they converted irreversibly to ordinary crystalline semimetallic Sb.[1] One concludes that the semiconducting layers were amorphous, a form of Sb previously observed only at considerably lower temperatures.[2] The Fermi level as determined here is consistent with resistivity-temperature data of Moss and of Suhrmann and Berndt.[2] The behavior of evaporated Sb is thus analogous in character to that of As,[1] and the electronic energy structure changes in the same general way when the amorphous material is crystallized.

[1] E. Taft and L. Apker, Phys. Rev. **75**, 1181 (1949); **76**, 270 (1949).
[2] F. S. Moss, Proc. Phys. Soc. (London) **A65**, 147 (1952) and cited references.

K4. Photoelectric Emission from BaO.† H. R. PHILIPP,* *University of Missouri.*—The energy distribution of photoelectrons from sprayed coatings of BaO indicates two sets of energy levels located photoelectrically about 2.0 and 2.7 ev below the vacuum level as well as an exciton-induced distribution appearing for wavelengths below 3500 A. Yield curves from two deactivated cathodes showed no exciton-induced emission nor any yield in the 2-ev region indicating that exciton-induced photoelectrons probably have their origin in the 2-ev level. Measurements were made of the temperature dependence of photoelectric emission. The yield was found to increase with temperature in the region of the threshold and decrease with temperature for wavelengths below 4000 A. Semilog plots of exciton-induced emission *vs* $1/T$ give straight lines corresponding to an activation energy of 0.15 ev for the thermal destruction of excitons. Irradiating the cathode with red light had no effect on the exciton-induced emission. Measurements were made of the photoelectric enhancement of thermionic emission. The enhancement increases rapidly for enhancing wavelengths below 4500 A. Photoelectric emission was found to saturate with voltage for all incident wavelengths.

† Supported in part by the U. S. Office of Naval Research.
* Minneapolis-Honeywell Research Fellow.

K5. Surface "Channel" Detection Method for Semiconductors. H. CHRISTENSEN, *Bell Telephone Laboratories, Inc.*—Electrical "channel" conduction phenomena[1,2] occurring on germanium and silicon surfaces have been advantageously studied for a considerable time by a chopped light spot method similar to that used for minority carrier diffusion and lifetime measurements.[3] The observed phenomena can be illustrated by consideration of the photoresponse that is obtained for a reverse biased n-p grown junction bar of germanium when the chopped light spot is moved parallel to the axis of the bar.

If no channel is present, the ac photocurrent through the bar drops off approximately logarithmically with distance from the n-p junction. When a "channel" is present on the surface, the photoresponse to chopped light remains the same as at the n-p junction when the chopped light spot is moved a considerable distance away from the junction into the channel region. This constant response distance is a function of reverse bias voltage and specific conductivity of the channel conduction skin. The method can separate "channel" conduction and surface ionic leakage effects.

[1] W. H. Brattain and J. Bardeen, Phys. Rev. **75**, 1208 (1949); Bul. System Tech. J. **32**, 1 (1953).
[2] W. L. Brown, Phys. Rev. **91**, 518 (1953).
[3] F. S. Goucher, Phys. Rev. **81**, 475 (1951).

K6. Computation of the Mobility Ratio in Pure p-Type Semiconductors.* ALLEN NUSSBAUM, *Honeywell Research Center.*—Pure p-type semiconductors will show a reversal in the Hall coefficient as their temperature rises into the intrinsic range. The ratio c of electron to hole mobility for such materials can be computed from resistivity *vs* temperature and Hall coefficient *vs* temperature data by the formula $(10^3/T_r) - (10^3/T_s) = (0.397/E_G) \log|c/c-1|$, where E_G is the forbidden band width in ev, T_r is the Hall reversal temperature, and T_s is the temperature at which the extrapolated intrinsic and impurity sections of the resistivity curve intersect. In the case of pure Te, where it is impossible to determine c by direct measurement, the formula gives a value which agrees fairly well with that obtained by indirect measurement.[1,2] Similarly, for Te–Se alloys, the computed values increase with Se concentration, agreeing with the predicted theoretical trend.[3] Direct verification has been obtained for one sample of single-crystal Ge, with a measured value[4] of 1.47 and a computed value of 1.41.

* Work supported by U. S. Air Force while at the University of Pennsylvania.
[1] Fukoroi, Tanuma, and Tobisawa, Science Repts. Research Insts., Tôhoku Univ. Ser. **A1**, 373 (1949).
[2] A. Nussbaum, Phys. Rev. (to be published).
[3] H. B. Callen, J. Chem. Phys. **22**, 518 (1954).
[4] R. M. Baum and D. C. Eckhardt, Sylvania Electric Products, Inc. (unpublished).

K7. Grain Boundary Conduction in Gold-Doped Ge. A. G. TWEET, *General Electric Research Laboratory.*—Bicrystals of n and p-type gold-doped germanium have been drawn from the melt using (100) seeds bound symmetrically on either side of a Mo wedge. The wedge angle β was 5° to 15° and lay in a (110) plane common to the two seeds. Wafers were cut from the bicrystals perpendicular to the axis of growth and ohmic contacts fused to either face. The resistance at 80°K between these contacts was in the megohm range for bulk germanium,[1] but was found to be from 2×10^3 to 10^5 ohm if the contacts were on the grain boundary. Hall effect measurements show that the grain boundary current is p type for the case of either n or p-type bulk germanium. Measurements of the conductivity between 20°K and 80°K show that it varies approximately as $\exp(-\varphi/kT)$, with φ between 0.01 and 0.07 ev. φ seems to be dependent upon β and γ, where γ is the angle which the perpendicular to the plane of the grain boundary makes with the common (110) planes of the bicrystal halves. Twin boundaries do not conduct.

[1] W. C. Dunlap, Jr., Phys. Rev. **91**, 1282 (1953).

K8. Ultraviolet Transmission and Alpha Bombardment Conduction Inhomogeneities in Diamond. A. J. AHEARN, *Bell Telephone Laboratories.*—Most diamonds showed some alpha-particle bombardment conduction but its magnitude varied widely. Experiments with a beam of alpha particles revealed extensive inhomogeneities[1] within given specimens. Contradictory results were obtained in tests with gamma rays[2] *vs* alpha particles[1] to see if this counting property could be related to the optical transmission in the ultraviolet. This suggested that the diamonds were mixtures of opaque and transparent types. Contact print transmission photographs were taken at 2540–2570 A.U. which showed that many specimens were mixtures of opaque and transparent regions. With certain diamonds in the form of thin slabs, the same variations in alpha counting were observed on both sides, and the opaque and transparent regions were larger than the alpha beam. On a given diamond meeting these two qualifications, the high alpha-count regions agreed well with the transparent areas and the low alpha-count regions agreed well with the opaque areas. This confirms the conclusion[3] drawn from similar comparisons between small diamonds under beta- and alpha-particle bombardment.

[1] A. J. Ahearn, Phys. Rev. **73**, 1113 (1948); **84**, 798 (1951).
[2] Friedman, Birks, and Ganvin, Phys. Rev. **73**, 186 (1948).
[3] F. C. Champion, Proc. Phys. Soc. (London) **B65**, 465, (1952).

TUESDAY MORNING AT 10:00

Physics 150

(PHYLLIS FREIER presiding)

Cosmic Rays and Mesons

L1. Search for Departures of Cosmic Rays from Poisson's Law at Low Counting Rates. I. T. E. BAKER, JR.,* N. C. BLAIS,† C. L. HEMENWAY, V. ROJANSKY, M. S. WEBSTER,‡ AND M. S. WERMAN,§ *Union College.*—A small GM tube was triggered by cosmic rays on the average about once per second. Each pulse originating in this tube was counted by a scaler A, and every 64th pulse was recorded by an Esterline-Angus recorder. A pulse separated from the preceding pulse by more than about 20 milliseconds opened after a short delay a 20-millsecond electronic gate. A pulse that arrived while the gate was open triggered not only A but also a second scaler A', and moved a second pen of the recorder. We found that the number of pulses passing through the gate was about 3 percent larger than that computed on the basis of Poisson's law from the readings of A. The probability that this discrepancy occurred in our experiment by chance was about one in twenty.

* Now at the University of Illinois.
† Now at Yale University.
‡ Now at Washington University.
§ Now at New York University.

L2. Search for Departures of Cosmic Rays from Poisson's Law at Low Counting Rates. II. W. M. CEGELSKI, A. T. GOBLE, C. L. HEMENWAY, K. REINITZ, V. ROJANSKY, AND F. A. RUSHWORTH,* *Union College.*—Our apparatus is a modification of that described in the preceding abstract. A pulse originating in the GM tube is counted by the scaler A, as before, and also by a scaler B, which is reset 50 times

per minute by a synchronous motor. The "on" time of B is about 0.7 second, the "off" time about 0.5 second. If (and only if) B accumulates four or more counts during an "on" interval, it triggers, when reset, a second pen of the recorder. We find that the number of sets of four or more pulses occurring during the "on" intervals of B is somewhat larger than that computed on the basis of Poisson's law from the readings of the scaler A; numerical results will be presented at the meeting. Measurements were also made with B modified to count sets of eight or more pulses. A two-tube coincidence circuit, activated by a radon source, is being constructed in order to permit us to feed random pulses into the apparatus and thus to obtain a comparison with cosmic rays.

* On leave from St. Andrews University, Scotland.

L3. Heavy Cosmic-Ray Nuclei.* JOHN LINSLEY, *University of Minnesota.*—Analysis has been completed of data obtained with a Čerenkov counter-cloud chamber apparatus during two balloon flights at 40° geomagnetic latitude and atmospheric depths 15 and 19 g/cm². Pulses from the Čerenkov counter, gated by a Geiger counter telescope, were recorded continuously during the 13 hours at high altitude, and cloud-chamber photographs were obtained of 394 of the events that caused pulses. The primary purpose of the experiment was to measure the flux of fast alpha-particles, and 175 photographs show the track of such an object, but in addition some 40 show the track of a heavier nucleus. The pulse height record, which exhibits peaks corresponding to charge 6, 7, 8, and a group of pulses ($Z \geqslant 9$) that saturated the amplifier, served to identify the nuclei whose tracks were photographed. On the other hand, the cloud-chamber data made it possible to evaluate the counter background, which proves to be small, especially in the region $Z \geqslant 6$. Values will be reported for the flux of helium; that of Li, Be, B; that of C, N, O; and that of nuclei with $Z \geqslant 9$.

* The research was supported in part by the joint program of the U. S. Atomic Energy Commission and the U. S. Office of Naval Research.

L4. Cosmic-Ray Studies with a Čerenkov Detector at $\lambda = 10°$ and 55°.* K. A. ANDERSON, *University of Minnesota.*—Absolute flux measurements of the cosmic-ray albedo obtained at balloon altitude by means of a Čerenkov detector have now been made at $\lambda = 10°$ and 55°N, supplementing the data already reported for 40°.[1] The apparatus incidentally performs a simultaneous range and velocity determination on the cosmic-ray particle.[2] The slow portion intensities thus obtained are in agreement with those from other methods. Using the experimental value of the splash albedo flux and also taking into account the dependence of multiple meson production on energy, an approximate calculation shows that the E−W asymmetry predicted by geomagnetic theory on the basis of all positive primaries can be brought into agreement with the measured value[3] at $\lambda = 10°$. This would indicate (1) that the "distant" albedo is not large compared with the splash flux, at least for $\lambda = 10°$, and (2) it is not necessary to require that 20 percent of the primaries are negatively charged as Bhowmik[4] has done.

* This research was supported in part by the joint program of the U. S. Office of Naval Research and the U. S. Atomic Energy Commission.
[1] J. R. Winckler and K. Anderson, Phys. Rev. **93**, 596 (1954).
[2] J. R. Winckler, Phys. Rev. **85**, 1053 (1952).
[3] J. R. Winckler *et al.*, Phys. Rev. **79**, 656 (1950).
[4] B. Bhowmik, Phys. Rev. **89**, 327 (1953).

L5. Flux and Azimuthal Asymmetry of Primary Cosmic-Ray Nuclei at the Equator.* R. E. DANIELSON, P. S. FREIER, J. S. NAUGLE, AND E. P. NEY, *University of Minnesota.*—Nuclear emulsions were flown for a period of six hours at an average atmospheric depth of 15.2 g/cm² and at a geomagnetic lattitude of 9–10°. This flight was part of Project Churchy, sponsored by the U. S. Office of Naval Research. Six 4 in. × 10 in. stacks were exposed, each stack consisting of two 600 μ Ilford G-5 emulsions and one 600 μ Ilford G0–G5 emulsion. The stacks were flown horizontally and were oriented with respect to the earth's magnetic field for approximately 70 percent of the time at altitude. A preliminary value† of the flux for $z \geqslant 10$ has already been given as $0.36 \pm 0.05/m^2$ sec sterad. A better value for the flux based on about 1000 particles will be reported as well as the azimuthal asymmetries of these particles.

* Supported by the joint program of the U. S. Office of Naval Research and the U. S. Atomic Energy Commission.
† Reported at Duke Conference on Cosmic Rays.

L6. Densitometric Measurement of Emulsion Tracks.* E. P. NEY, JOHN NAUGLE, PHYLLIS FREIER, *University of Minnesota.*—A track densitometer of the general type described by von Friesen† has been designed and used to measure the area of developed grains on tracks of heavy particles as a function of their residual range. The method is useful for determining the charges of stopping particles. It has been found that the method is more reproducible than δ-ray counting. The uses and limitations of the device will be discussed and compared with the results obtained by δ-ray counting.

* Assisted by the joint program of the U. S. Office of Naval Research and the U. S. Atomic Energy Commission.
† Sten von Friesen, Arkiv Fysik **4** (1952).

L7. An Example of an Unstable Nuclear Fragment Being Emitted from a Heavy Meson Induced Star.* J. E. NAUGLE, P. S. FREIER, AND E. P. NEY, *University of Minnesota.*—A very unusual event has been observed in an emulsion exposed at 15.2 g/cm² at the equator during the Churchy expedition sponsored by the U. S. Office of Naval Research. A charged particle travels 1.6 cm in a G-5 emulsion before coming to rest. At the end of its range is a star, similar to an ordinary sigma star. However, one of the fragments of this star travels 78 microns before coming to rest in the emulsion. At the end of its range is a second star consisting of a short nuclear fragment, a 9.0 ± 0.2 Mev proton and 23.5 ± 0.5 Mev pion, which travels 1.1 cm before coming to rest. The tentative explanation of this event is that a negative heavy meson is captured by a nucleus of the emulsion, this nucleus disintegrates into several fragments, one of which contains a "bound V^0 particle" and which suffers a mesonic decay after coming to rest in the emulsion. The energetics, masses of the particles involved, and possible decay schemes will be discussed.

* Supported by the joint program of the U. S. Office of Naval Research and the U. S. Atomic Energy Commission.

L8. Nuclear Collisions at Extreme Relativistic Energies.* MARCEL SCHEIN, D. M. HASKIN, AND R. G. GLASSER, *University of Chicago.*—Two unusually large stars have been observed which may further contribute to our understanding of the processes which occur in nucleon-nucleus collisions at very high energies. The N star is of type 32+137 (n) and the P star is of type 25+76 (p). The stars are practically identical in laboratory angular distribution showing a strong forward collimation. The total charge of the outgoing slow fragments in the N star is estimated at 40–45, so that the target nucleus must have been silver. Of the 137 shower particles in the N star, at least 130 must be created particles; π mesons, K mesons, proton-antiproton pairs, and hyperons. Thus, counting neutral radiation a total of about 200 particles are being created in a collision of one nucleon with only a few nucleons. It is most difficult indeed to see how any modification of an

essentially plural theory can explain this fact. Preliminary estimates indicate that the primary energy for both these stars should be over 10^{13} ev. The *N* star and the *P* star represent conclusive evidence that in interactions with a heavy nucleus multiple meson production must occur in processes involving more than one nucleon.

* Supported in part by a joint program of the U. S. Office of Naval Research and the U. S. Atomic Energy Commission.

L9. Comparison of Proton and Meson Produced Stars of Comparable Excitation Energy.* A. D. SPRAGUE, *DePauw University*, AND D. M. HASKIN, R. G. GLASSER, AND MARCEL SCHEIN, *University of Chicago.*—An analysis is carried out of star formation in nuclear photoplates of 405-Mev protons and 222-Mev negative pions produced in the University of Chicago 250-Mev synchrocyclotron. A comparison of the angular distribution of the charged particles in proton stars with a Monte Carlo calculation is made. The results show that the cascade mechanism is an important factor in proton produced stars at these energies. In addition, the number of charged particles arising from excitation and subsequent evaporation of the heavy nucleus were determined and found to be in disagreement by a factor of 5 with predictions of evaporation theory. Pion produced stars yield an angular distribution of charged particles which is much flatter than that of proton produced stars.

* Supported in part by a joint program of The U. S. Office of Naval Research and The U. S. Atomic Energy Commission.

L10. Studies of Penetrating and Cascade Showers of Cosmic Rays with Plastic Scintillators at an Elevation of 11 500 Feet.* C. N. CHOU, *University of Chicago.*—An apparatus consisting of G-M counters and four $18\times18\times1$ cm^3 plastic scintillation counters interposed with lead plates of various thicknesses was used to investigate the penetrating showers produced in carbon by cosmic rays at an altitude of 11 500 feet. The frequency *versus* energy relation of γ rays produced from the decay of neutral pions in penetrating showers and also the multiplicity spectrum of the charged pions were obtained. In addition, the frequency *versus* energy relation of cascade showers produced by the bremsstrahlung accompanying high-energy μ mesons was determined. The same apparatus was also used to measure the energy spectra of high-energy photons and electrons of cosmic rays at 11 500 feet.

* Supported in part by a joint program of The U. S. Office of Naval Research and the U. S. Atomic Energy Commission.

L11. Coulomb Effect on the Photoproduction of Low-Energy Charged Mesons.* J. R. VOSS, T. R. PALFREY, AND R. O. HAXBY, *Purdue University.*—Following the method of White,[1] the Purdue 300-Mev electron synchrotron has been used to expose some Ilford 600 micron G-5 plates. Thin targets were placed in the γ-ray beam and reaction products at 120° from the beam were captured in the emulsion. The π^- and π^+ mesons that stopped in the emulsion were counted. The Coulomb field of the nucleus might be expected to shift the energy of charged mesons as they leave the vicinity of the nucleus. Since the photoproduction cross section of π mesons strongly increases with energy at low energies, the Coulomb shift would manifest itself in an increase in the π^-/π^+ ratio as the energy decreases. Experimentally this change has been found in the energy range 0–20 Mev for the elements *C*, Cu, Sn, and Pb. The effect is strong, especially for the higher *Z* materials.

* Work supported in part by contract with U. S. Atomic Energy Commission.

[1] R. H. White, University of California Radiation Laboratory Report 1319 (1951).

L12. Ionization Energy Loss of Mesons in a Sodium Iodide Scintillation Crystal.* THEODORE BOWEN, *University of Chicago.*—The response of a thallium activated sodium iodide crystal to high-energy charged particles passing through the scintillator has been investigated. π and μ mesons produced by the Chicago 450 Mev cyclotron have been used to cover energies ranging from 61 Mev π mesons to 245 Mev μ mesons. Sea level cosmic ray μ mesons have been used to cover energies from 200 Mev to greater than 2 Bev. At each energy, the most probable energy loss is determined from the pulse height distribution, making use of Po–Be 4.44 Mev γ rays for an energy calibration. The distributions from cyclotron data are found from the density variations on photographs of the superposition of many pulses appearing on an oscilloscope. Because the cosmic ray counting rate is low, each pulse is individually photographed and measured. The results for energies below the occurrence of the minimum in ionization indicate good agreement with the probable energy loss as given by the Bethe-Bloch formula. Beyond the minimum the probable loss is in fair agreement with Sternheimer's calculations[1] for sodium iodide, rising slightly more rapidly than predicted to the Fermi plateau.

* Supported in part by a joint program of The U. S. Office of Naval Research and The U. S. Atomic Energy Commission.

[1] R. M. Sternheimer, Phys. Rev. **88**, 851 (1952); **91**, 256 (1953).

TUESDAY MORNING AT 10:00

Physics 170

(C. L. CRITCHFIELD presiding)

Invited Papers in Theoretical Physics

M1. Various Comments on Deuteron-Induced Reactions. W. B. CHESTON, *University of Minnesota.* (30 min.)

M2. The *S*-Operator in Quantum Electrodynamics. J. M. JAUCH, *State University of Iowa.* (30 min.)

M3. Formal and Methodological Aspects of Present Quantum Electrodynamics. F. ROHRLICH, *State University of Iowa.* (30 min.)

TUESDAY AFTERNOON AT 1:45

Murphy 105

(H. REISS presiding)

Gaseous Electronics

Invited Papers

(Q1 at beginning of session, Q2 after Q6, Q3 after Q8)

Q1. Drift Velocities and Mobilities. R. N. VARNEY, *Washington University.* (25 min.)

Q2. Microwave Discharges. W. P. ALLIS, *M.I.T.* (25 min.)

Q3. Atomic Collision Processes in Ionized Gases. M. A. BIONDI, *Westinghouse Research Laboratories.* (25 min.)

Contributed Papers

Q4. Drift Velocities of Argon Ions in Argon at Various Temperatures.* E. BEATY AND R. VARNEY, *Washington University.*—A microsecond pulsed Townsend type of parallel-plate discharge tube has been designed and constructed for submerged operation in a regulated temperature bath. The leads to the electrodes and a quartz window for admission of ultraviolet radiation remain out of the bath during operation but are mounted to provide a tube surface area which is not at the equilibrium temperature. Limited results have been obtained fitting qualitatively with theoretical predictions. Extension to a greater range of temperature and of E/p, the field-strength-to-pressure ratio will be described.

* Supported in part by the U. S. Office of Naval Research and by a grant from Research Corporation.

Q5. Mobilities of Various Ions in the Noble Gases. LORNE M. CHANIN AND MANFRED A. BIONDI, *Westinghouse Research Laboratories.*—The recently developed techniques[1] for measuring the mobilities of near-thermal ions in gases have been extended to studies of ions moving in gas mixtures. The measurements provide an experimental test of the validity of Blanc's Law, which states that the mobility μ_{AB} of an ion moving in a mixture of gases A and B is given by $1/\mu_{AB} = (f_A/\mu_A)+(f_B/\mu_B)$, where μ_A and μ_B are the mobilities of the ion in the pure gases, and f_A and f_B are the fractional concentrations of the gases. Systematic deviations from Blanc's Law have been observed for Ne^+ moving in helium and neon. In addition, measurements have been made of the mobility as a function of E/p of such systems as He^+ in neon and Ne^+ in helium. In these cases the resonance interaction of charge transfer between ion and atom is absent, and the polarization interaction is of importance. It is found that in some cases, e.g., He^+ in neon, the experimental values differ widely from the predictions of Langevin's theory.[2]

[1] M. A. Biondi and L. M. Chanin, Phys. Rev. **94**, 910 (1954).
[2] P. Langevin, Ann. Chim. phys. **5**, 245 (1905); H. R. Hasse and W. R. Cook, Phil. Mag. **12**, 554 (1931).

Q6. Corrected Values for the Charge Transfer Cross Section in the Noble Gases. GREGORY H. WANNIER, *Bell Telephone Laboratories.*—Ziegler published recently[1] values for the ion-atom charge transfer cross section which he had obtained by direct measurement. Such cross sections were also published by some of us at Bell Laboratories as deduced from ion mobility studies. These latter appear high by about 50 percent. An even bigger discrepancy appears in the predictions of Sena.[2] However, Ziegler's observations show that the physical assumption of Sena's theory is closer to the truth than the one of the author: namely little or no momentum is transferred in most charge transfer collisions. Perusal of Sena's work and correction of an error in the derivation yields the usual square root law for the drift velocity with a factor $(2/\pi)^{\frac{1}{2}}$ instead of 1.147 as published previously by the author.[3] This yields the following values for the charge transfer cross sections of helium, neon, argon, krypton, xenon: 38, 45, 93, 109, 134×10^{-16} cm^2. The new values are in close numerical agreement with the ones of Ziegler in three out of five cases. The cause for the remaining discrepancies is not clear.

[1] B. Ziegler, Z. Physik. **136**, 108 (1953).
[2] L. Sena, J. Phys. U.S.S.R. **10**, 179 (1946).
[3] G. H. Wannier, Bell System Tech. J. **32**, 170 (1953), Eq. (100).

Q7. Mechanism of the Termination of the Geiger-Plateau Region.* HERBERT L. WISER AND A. D. KRUMBEIN, *University of Maryland.*—Experimental investigation of counting rate and number of positive ions per pulse *versus* voltage for Geiger counters at the high-voltage end of the plateau leads to the belief that spurious counts, and therefore the termination of the plateau, can be accounted for by secondary electrons created by positive ion bombardment of the cathode and metastable atom collisions in the gas. Studies were made on counters of different cathode diameters and partial pressures of the main gas and of the quenching vapor. The rate of spurious counts caused by positive ion bombardment is found to be proportional to the rate of positive ions striking the cathode, and therefore, to the voltage. The rate of spurious counts caused by metastable collisions depends on the number of metastables existing after the deadtime of the Geiger tube, and therefore is an exponential function of the ratio of the deadtime to the metastable half life. Since the deadtime decreases with increasing voltage, the rate of spurious counts caused by metastable collisions is an exponential function of voltage.

* This work is supported by the Bureau of Ships, U. S. Navy Department.

Q8. Corona Discharge Current from Aircraft.* SEVILLE CHAPMAN, *Cornell Aeronautical Laboratory.*—In a system for maintaining zero electrostatic charge on aircraft where electric field meters on the surfaces of the wings control a high-voltage corona discharge point behind the tail of the aircraft, the primary factors influencing the magnitude of blow-away discharge current i are point potential V, aircraft speed v, point geometry, and space charge from the already discharged current. The fundamental physical effects are that V must be large enough to create an electric field vector toward the rear to drive the discharge current into the space charge behind the point, but since this same V creates a field vector forward toward the aircraft skin, the point must be disposed so that the wind past the point prevents return current to the aircraft. The problem is approached mathematically from several points of view, to evaluate constants F, G, and H in $i=\epsilon_0(FkV^2/l+GvV+Hlv^2/k)$ where k is the mobility and l a length. Currents of a few hundred micro-

amperes can be expected when $V=100$ kilovolts and $v=200$ knots. Some data are presented.

* Supported by the Air Force Cambridge Research Center.

Q9. Absorption Studies of the Helium Metastable Molecule. A. V. PHELPS, *Westinghouse Research Laboratories.*—Measurements of the lifetime of helium atoms in the triplet metastable state (2^3S) as a function of the pressure of the helium gas[1] have shown that these metastable atoms are destroyed as a result of collisions with the wall of the absorption cell and by three-body collisions with neutral helium atoms. In order to test the proposal[1] that these three-body collisions result in the formation of a helium molecule in the metastable state ($2s^3\Sigma_u^+$), arrangements were made to measure absorption of the 4650A band during the afterglow of a pulsed discharge.[2] The observed absorption shows that metastable molecules are formed as predicted and that the natural lifetime of the $2^3\Sigma_u^+$ state is at least 0.005 second. These experiments also show that the lifetime of the triplet metastable molecule is very sensitive to small concentrations of neon (~one part in 10^6) present in commercial reagent grade helium.

[1] A. V. Phelps and J. P. Molnar, Phys. Rev. **89**, 1202 (1953).
[2] The 4650 Å band is the O→O band of the $3p^3\Pi \rightarrow 2s^3\Sigma$ system; see e.g., G. H. Dieke and E. S. Robinson, Phys. Rev. **80**, 1 (1950).

Q10. Diffusion of Metastable Mercury Molecules. A. O. MCCOUBREY AND C. G. MATLAND, *Westinghouse Research Laboratories.*—In studies on the band fluorescence of mercury vapor,[1] diffusion data obtained for metastable diatomic mercury molecules, $Hg_2(^3O_u^-)$, suggested that the molecules may be partially reflected by glass walls; this circumstance complicated the evaluation of the diffusion coefficient. In the present work, metal walls were substituted for the glass walls. The experimental method is that used in previous work, in which $Hg_2(^3O_u^-)$ molecules are created as a consequence of the absorption of 2537A resonance radiation. The time variation of the concentration of the molecules is obtained during the afterglow by measuring the intensity of band radiation. The data obtained with a vessel having nickel walls is consistent with the hypothesis that the $Hg_2(^3O_u^-)$ molecules are completely destroyed upon diffusing to the boundaries. The product of the diffusion coefficient and the mercury vapor density obtained from this work is $ND=63\times10^{-16}$(atoms cm^3/cc sec). These experiments, which extend over a wider density range than heretofore, have also yielded a more accurate value for the three-body collision induced radiation rate for the $Hg_2(^3O_u^-)$ molecules, i.e., $29\times10^{-32}\times$(atom/cc)$^{-2}$ sec^{-1}. Further work is in progress to more accurately determine the reflection coefficient of the molecules at a glass surface.

[1] A. O. McCoubrey, Phys. Rev. **93**, 1249 (1954).

Q11. Excitation by Electron Impact of the Optically Forbidden Transition $1^1S\rightarrow2^1S$ in Helium.* E. N. LASSETTRE, M. E. KRASNOW, AND S. SILVERMAN, *The Ohio State University.*—The electron spectrometer described previously[1] has been used for the study of the transitions $1^1S\rightarrow2^1P$ and $1^1S\rightarrow2^1S$ in helium. These transitions are separated in energy (0.6 ev) by slightly more than the resolution of the apparatus. Incident electrons with kinetic energies of about 500 volts were used. Electron impact energy spectra have been obtained for scattering angles from 3.8 to 15.3 degrees. Over this angular range the relative electronic collision cross sections of the two transitions vary in such a way that the optically forbidden transition $1^1S\rightarrow2^1S$, which is undetectable at the smallest angle, becomes almost equal in intensity to the $1^1S\rightarrow2^1P$ transition at 15.3 degrees. Electron impact energy spectra showing this variation will be presented. Electronic collision cross sections have also been calculated from the data over this angular range. At the smaller angles these cross sections are subject to considerable error because of the indirect method which must be used to separate the contribution of the $1^1S\rightarrow2^1S$ transition from the $1^1S\rightarrow2^1P$ transition.

* The research reported in this paper has been sponsored by the Geophysics Research Directorate of the Air Force Cambridge Research Center, Air Research and Development Command.
[1] Lassettre, Berman, Silverman, and Krasnow, Bull. Am. Phys. Soc. **29** No. 4, 47 (1954).

Q12. The Quenching of Sodium Iodide Fluorescence by Various Gases and Vapors.* HOWARD G. HANSON, *University of Minnesota, Duluth Branch.*—Experimental data has been taken on the quenching of the sodium D line arising from the optical dissociation of NaI molecules by ultraviolet light in the 2000A to 2500A range. The gases and vapors used were hydrogen, carbon dioxide, hydrogen chloride, and water vapor. Water vapor shows little quenching action. The quenching action of hydrogen and cargon dioxide show slight experimental dependence on the velocity of the excited sodium atoms. The quenching action of hydrogen chloride is the greatest and shows an experimental dependence on the relative velocity of the excited sodium atoms and the HCl molecules. The intensity of the sodium D line as a function of wavelength of exciting ultraviolet light has been measured. The wavelength for maximum excitation of the sodium D line shifts to higher ultraviolet wavelengths with increasing temperature of the NaI salt. A grating monochromator was used to isolate narrow regions of ultraviolet light from a hydrogen discharge lamp. A photomultiplier tube circuit measured the intensity of fluorescence. A device to record intensity of fluorescence as a function of exciting wavelength is described together with other experimental detail.

* Supported by the U. S. Office of Ordnance Research.

TUESDAY AFTERNOON AT 2:00

Physics 170

(A. VAN DER ZIEL presiding)

Mainly Semiconductors

R1. Magnetic Susceptibility of Residual Bisulfate Compounds of Carbon. H. T. PINNICK, *University of Buffalo.*—The introduction of bisulfate ions between the graphitic layers in carbons and graphite results in the formation of excess holes in the π band. The magnetic susceptibility of a series of bisulfate residue compounds of carbons has been studied at room temperature. Compounds with residual ion concentrations varying from 5×10^{-4} ion/atom to 15×10^{-4} ion/atom were prepared from rods of soft carbon heat-treated (H.T.) to temperatures ranging from 1600°C to 2800°C. The decrease in susceptibility with increasing ion concentration was found to be greater for carbons heat-treated to higher temperatures. The decrease per 1×10^{-3} ion/atom is about 23 percent for 2800°C H.T., 18 percent for 2400°C H.T., 14 percent for

2000°C H.T., and approximately zero for 1700°C H.T. Since the susceptibility of pure carbons reaches the maximum value at heat-treatment temperatures of about 2000°C and remains constant for higher H.T.[1] the susceptibility of the bisulfate compounds with a given ion concentration reaches a maximum at about 2000°C heat-treatment and decreases for higher heat-treatment temperatures, leading to the rather unexpected result above 2000°C H.T. of a decreasing diamagnetic susceptibility for carbon compounds with increase of crystallite diameters.

[1] H. T. Pinnick, Phys. Rev. **94**, 319 (1954).

R2. Magnetoresistance and Planar Hall Effects in *N*-Type Germanium. R. E. Davis and Colman Goldberg, *Westinghouse Research Laboratories.*—The magnetoresistance and planar Hall[1] effects have been measured from 77°K to 300°K for oriented samples of 13 ohm-cm *n*-type germanium. The magnetoresistance measurements permit calculation of the planar Hall effect, and this calculation agrees with actual measurement of the latter effect. The data are in qualitative agreement with calculations[2] based upon the assumption that the energy surfaces are ellipsoids of revolution about the (111) directions in *k* space.[3]

[1] C. Goldberg, Phys. Rev. **93**, 913 (1954); R. E. Davis and C. Goldberg, Phys. Rev. **93**, 913 (1954); C. Goldberg and R. E. Davis, Phys. Rev. **94**, 1121 (1954).
[2] S. Meiboom and B. Abeles, Phys. Rev. **93**, 1121 (1954).
[3] Lax, Zeiger, Dexter, and Rosenblum, Phys. Rev. **93**, 1418 (1954).

R3. Resistivity Changes in Silicon Induced by Heat Treatment. C. S. Fuller, J. A. Ditzenberger, N. B. Hannay, and E. Buehler, *Bell Telephone Laboratories.*—Room temperature resistivity measurements on a variety of single crystals of silicon grown by the Teal-Little method show that large changes in resistivity may be induced by heat treatment. These appear to be independent of surface impurities and occur throughout the volume of the material. At temperatures between about 300–700°C many crystal show an increase in electron content with time. The rate and magnitude of these changes are a maximum at 430–450°C and require between 1–48 hours for completion. Changes as great as 5×10^{16} electrons cm^{-3} are observed. Smaller increases occur above and below this temperature. By heating to temperatures above about 500°C these changes are reversed, the original resistivity being rapidly obtained above 800°C. The changes in carrier content are intimately associated with the crystal growing variables. A discussion of these and possible origins of the observed effects will be given.

R4. The Interaction of Traps and Heat Treatments in Silicon. N. B. Hannay, J. R. Haynes, and R. G. Shulman, *Bell Telephone Laboratories.*—Shallow and deep trapping levels in both *n*- and *p*-type silicon have previously been observed[1] at room temperature. Densities of these four traps have been measured in crystalline regions which had been pulled from the melt under different growth conditions. Reproducible measurements of many crystals indicate that the trap concentrations after growth are related to the crystal growing variables. Trap densities are high in those crystals which change resistivity upon heat treatment as discussed in the preceding paper. They are one to two orders of magnitude lower in crystals whose resistivities are not affected by heat treatments. Typical values of effective trap concentrations are 10^{13}/cc in the former regions and 10^{11}/cc in the latter. After the crystals have been grown different time-temperature cycles drastically alter trap densities. As a result of the measurements it is seen that the same conditions which give high trap concentrations also give large resistivity changes at 450°C. In order to identify the traps the effects of different temperature cycles, high-energy electron bombardment, dislocations and chemical impurities have been studied.

[1] J. R. Haynes and J. A. Hornbeck, Phys. Rev. **90**, 152 (1953).

R5. Impurity Levels in Silicon. F. J. Morin, J. P. Maita, R. G. Shulman, and N. B. Hannay, *Bell Telephone Laboratories.*—Electron energy levels associated with nine different impurities and several annealing conditions have been found in the forbidden gap of silicon. The levels were located with respect to the conduction band edge in *n*-type silicon and the valence band edge in *p*-type silicon by analysis of carrier concentration data determined from measurement of the Hall coefficient as a function of temperature. Energies measured in electron volts are as follows: *p*-type silicon; B, 0.045[1]; Al, 0.057; Ga[1], 0.065; In, 0.16; Au[2], 0.39. For *n*-type silicon; P, 0.039; As[1], 0.049; Sb, 0.039; Li, 0.033; annealed at 475°C 100 hours,[3] 0.033; annealed at 475°C 10 minutes,[3] 0.133 and 0.3. The differences in ionization energies of the Group III elements were not expected on the basis of the hole on a neutral acceptor moving in a hydrogen-like orbit. Changes of lifetime due to these and other chemical impurities will be discussed.

[1] E. Burstein *et al.*, J. Phys. Chem. **57**, 849 (1953) and private communication report similar values from optical absorption.
[2] E. A. Taft and F. H. Horn, Phys. Rev. **93**, 64 (1954).
[3] Prepared by C. S. Fuller (see preceding paper).

R6. Hole Trapping Due to Lattice Defects in Germanium. R. G. Shulman, W. L. Brown, and R. C. Fletcher, *Bell Telephone Laboratories.*—An investigation of *n*-type germanium indicates that hole traps are created by high-energy electron bombardment at room temperature. Using a technique similar to that of Haynes and Hornbeck,[1] one observes the rise and fall of photoconductivity associated with chopped light falling on the sample. Trap concentrations were studied in several samples having different bombardments. The measured concentrations ($\sim10^{13}$/cc) agreed with the density of bombardment centers to ±25 percent. Decay times did not change when the surfaces were alternately etched and sandblasted. In control samples trap densities were negligible. Measurements made from 160°K to 240°K were consistent with a capture cross section of $\sim2\times10^{-16}$ cm^2. Decay curves were simple exponentials with time constants of 300 μsec at 200°K. The energy of the traps above the valence band can be determined from both the temperature dependence and the absolute value at any temperature of the decay time constants.

[1] J. R. Haynes and J. A. Hornbeck, Phys. Rev. **90**, 152 (1953).

R7. The Absence of Bombardment Annealing in the Electron Bombardment of Germanium. R. C. Fletcher and W. L. Brown, *Bell Telephone Laboratories*, and K. A. Wright, *M.I.T.*—In the bombardment of *n*-type germanium with electrons the rate of change in conductivity with bombardment has been found to decrease as the bombardment proceeds. Investigation indicates that this nonlinearity cannot be caused entirely by thermal annealing nor by the proximity of the Fermi level to a bombardment induced energy level. Two other possible causes are (1) annealing induced by the presence of the high-energy electrons and (2) a nonuniform distribution of impurities. We have been able to show experimentally that the former is an unlikely explanation. First, if, as we would suppose, the rate of annealing is much less dependent on the bombardment energy than the rate of creating damage, damage created at 3 Mev should anneal out by bombardment at 1.5 Mev. No such annealing was observed. Second, with enough bombardment a steady state should be reached, limiting the maximum amount of damage possible. No such saturation was found; nonlinearity was observed at densities of bombardment centers as low as 10^{15} cm^{-3} in a 1 ohm-cm sample, but densities as high as 10^{18} cm^{-3} were achieved

without saturation in a 0.003 ohm-cm sample. The most plausible source of this nonlinearity seems to be a microscopically nonuniform distribution of impurities.

R8. Traps Produced by Electron Bombardment of Germanium at Low Temperature. W. L. BROWN AND R. C. FLETCHER, *Bell Telephone Laboratories*, AND K. A. WRIGHT, *M.I.T.*—Minority carrier traps[1] have been produced in both *n*- and *p*-type germanium by electron bombardment at 78°K. Hole traps are responsible for approximately 3 percent of the total change in conductivity produced by 1.5- and 3-Mev bombardments of *n*-type samples (1.4 mho/cm at 300°K). At 1.5 Mev in *p*-type samples (1.6 mho/cm at 300°K) the conductivity changes are very small and no traps have been observed, but at 2.5 and 3 Mev when the equilibrium conductivity changes are comparable to those in *n*-type, 70–80 percent of the change is associated with two classes of electron traps characterized by different electron capture cross sections. The larger cross section is $\sim 10^{-19}$ cm^2 at 78°K. The release time for electrons for this class of traps is about a minute at 140°K. A preliminary investigation of its temperature dependence indicates a trap depth of about 0.2 ev below the conduction band. While minority carrier lifetime is not limited by recombination in these traps, the lifetime is markedly reduced as the traps are filled with electrons. The defects responsible for both classes of electron traps anneal out at about 185°K or below. The hole traps in *n*-type disappear with annealing at about 140°K.

[1] J. R. Haynes and J. A. Hornbeck, Phys. Rev. **90**, 152 (1953).

R9. Plastic Deformation of Gold-Doped Germanium. C. J. GALLAGHER AND A. G. TWEET, *General Electric Research Laboratory*.—The center sections of $\frac{1}{16}$ in.$\times\frac{1}{8}$ in.$\times$2 in. rods of Ge doped with 2×10^{14} gold atoms/cm^3 have been bent[1] to a prescribed radius of curvature on a quartz form at temperatures between 400°C and 700°C. The rods, which were etched and then rinsed in KCN to remove Cu, were supported at the ends in an atmosphere of forming gas during bending. The resistance at 80°K of the unbent section of a typical rod was in the megohm range,[2] while the average resistance in the bent portion was found to be from 10 to 10^4 times smaller. Higher conductivity was associated with sharper bending. The resistivity of all samples showed considerable variation with position, as did the density of slip lines on the surface. Since the unbent gold-doped Ge was *p*-type, the data suggest that bending introduces an acceptor level somewhere between the valence band and the lower gold level, which lies 0.15 ev above the valence band.

[1] C. J. Gallagher, Phys. Rev. **88**, 721 (1952).
[2] W. C. Dunlap, Jr., Phys. Rev. **91**, 1282 (1953).

R10. Action Spectra for the Photoconductivity of Dye Films. JOHN W. WEIGL, *The Ohio State University*.*—Electrons or holes responsible for photoconduction in films of basic dyes[1,2] may be optically excited by visible light,[3] absorbed at any wavelength in the main absorption bands of the dyes. Since the bands in the solid films appear to correspond to the normal singlet-singlet bands of the "isolated" molecules in solution, one may identify the optical transitions leading to carrier excitation with those of the component molecules—a situation peculiar to organic photoconductors. This makes it possible to apply existing information concerning the spectroscopy and photochemistry of the "isolated" dye molecules to phenomena characteristic of the solid state. Action spectra of examples of xanthene, acridine, cyanine, and triphenylmethane dyes will be presented.

* Work supported by the Charles F. Kettering Foundation.
[1] A. Vartanian, Acta Physicochimica U.R.S.S. **22**, 201 (1947).
[2] R. C. Nelson, J. Chem. Phys. **19**, 798 (1951); **20**, 1327 (1952).
[3] A. Vartanian, J. Phys. Chem. U.R.S.S. **24**, 1361 (1950).

R11. Electron Energy Levels in Ionic Crystals.* E. L. JOSSEM AND L. G. PARRATT, *Cornell University*.—Information on the electron energy levels in solids is provided by the energy positions, intensities, and shapes of component lines in x-ray emission and absorption spectra. The x-ray $K\beta$ emission spectra of chlorine in the alkali chlorides and in cuprous chloride have been recorded with a curved crystal focusing vacuum spectrometer using a proportional counter detector. These lines involve transitions from levels in or near the valence band to an inner (K shell) vacancy. The principal features of the spectra are: (a) the chlorine $K\beta_1$ line, commonly ascribed to the transition valence-band-to-K-vacancy, is uniformly too narrow to permit such assignment; (b) the intensity of the chlorine β_2 and β_3 lines relative to the β_1 line varies with the compound. Interpretation of these features in terms of the band structure of the crystal and the sharp "impurity-type" levels[1] introduced by the inner shell vacancy will be discussed.

* This research was supported by the United States Air Force through the Office of Scientific Research of the Air Research and Development Command.
[1] L. G. Parratt and E. L. Jossem, Phys. Rev. **84**, 362 (1951) and **85**, 729 (1952).

TUESDAY AFTERNOON AT 2:00

Physics 150

(E. P. NEY presiding)

Invited Papers in Cosmic-Ray Physics

S1. High-Energy Nuclear and Electromagnetic Interactions. PHYLLIS FREIER, *University of Minnesota*. (30 min.)

S2. Alpha-Particles in Primary Cosmic Rays. NAHMIN HORWITZ, *University of Minnesota*. (30 min.)

S3. The Light Elements in Cosmic Rays. LELAND BOHL, *University of Minnesota*. 30 min.)

S4. Recent Results with *S*-Particles. H. S. BRIDGE, *MIT*. (30 min.)

TUESDAY AFTERNOON AT 2:00

Physics 133

(R. G. HERB presiding)

Various Topics in Nuclear Physics

T1. Measurement of Phase Noise in a Pre-Excited Oscillator System.* LAWRENCE H. JOHNSTON, NORTON M. HINTZ, AND HARRY J. SCHULTE, *University of Minnesota.*—If multiple, independent linear accelerator cavities are driven by free-running oscillators, can they be phased within a few degrees by a small, coherent pre-exciting signal? This case is of interest for linacs designed for 100 Mev and higher energy. Slater† reports ±10° probable phase fluctuations from pulse to pulse for the MIT electron linac, due to magnetron noise. A unique opportunity was recently afforded for such a measurement when the first cavity of the Minnesota Linac was driven by an interim system of oscillators to give 10-Mev protons. (Two more cavities will eventually give 68 Mev.) Phase of rf in the cavity was compared to that of a crystal CW pre-exciting source (5 percent voltage), the relative phase being displayed on an oscilloscope. While relative phase drifts (~30°) were observed during a 450-microsecond rf pulse, these repeated on 100 successive pulses within ±5°, and this "jitter" was found to be largely instrumental. We conclude that the oscillators built up in constant phase relationship to the pre-exciter within less than ±5°.

* Partially supported by the U. S. Atomic Energy Commission.
† Demos, Kip, and Slater, J. Appl. Phys. **23**, 53–65 (1952).

T2. A 200 Mc Phase Detector.* EDMUND B. TUCKER, LAWRENCE H. JOHNSTON, AND DONALD E. YOUNG,† *University of Minnesota.*—The inter-cavity phasing problem for an accelerator consisting of a number of independent high Q cavities requires accurate tuning of the individual cavities even when amplifiers are used to power the machine. For the case of a cavity with a Q of 70 000 a phasing tolerance of ±8° requires a tuning accuracy of 1 part in 10^6. The automatic frequency control designed for use with the Minnesota linear accelerator is similar in principle to that used by Rideout,[1] Pound,[2] and others for stabilization of microwave oscillators. The phase detector used in this system operates at the accelerator frequency of 202.5 Ms and consists of distributed constant circuits. During stability tests the phase detector has shown a drift of less than 1° over a period of 10 hours. The complete system including integrators, amplifiers, servos, and tuners has been tested at low power in the first cavity of the accelerator with a resulting tuning accuracy of 1 part in 4×10^6.

* Partially supported by the U. S. Atomic Energy Commission.
† Now at General Mills Research Laboratories, Minneapolis, Minnesota.
[1] V. C. Rideout, Proc. Inst. Radio Engrs. **35**, 767 (1947).
[2] R. V. Pound, Proc. Inst. Radio Engrs. **35**, 1405 (1947).

T3. A "Zipper" Scattering Chamber.* C. J. COOK, *University of Nebraska.*—A continuously variable vacuum port has been developed. This apparatus is similar to a zipper in that it consists of two rubber diaphragms under pressure that form a vacuum tight seal along a slot in the wall of a vacuum chamber, and a port, or "zipper foot," that slides between the rubber diaphragms without destroying the vacuum inside the chamber. By utilizing this vacuum "zipper" it was possible to construct a plane scattering chamber suitable for studying the energy and angular spectrum of the secondary electrons resulting from ionizing collision of a 20- to 400-kev proton and a gas molecule. With this type of scattering chamber it is possible to observe the scattered beam continuously through a laboratory angle of 0 to 150 degrees symmetrically about the incident beam. Another major advantage of this type of scattering chamber is that all of the necessary detecting apparatus for the scattered particles is conveniently placed outside of the small active portion of the scattering cell. A detailed description will be given, with slides, of the construction and operation of this specific "zipper" scattering chamber.

* This work is being carried out under contract with the U. S. Atomic Energy Commission.

T4. Mass Measurement by Multiple Coulomb Scattering on Stopped Particles.* R. G. GLASSER, *University of Chicago.*—Measurements have been made on 100 stopping protons and on 20 positive pions produced in the 450-Mev synchrocyclotron of the University of Chicago in order to determine the relation between range and scattering. The particles could be unambiguously identified. The relationship can be represented by a power law

$$\langle|N|\rangle_{Av}=(18.9\pm0.1)R^{-(0.807\pm0.005)}\left(\frac{M}{M_P}\right)^{-(0.393\pm0.003)}\left(\frac{t}{50}\right)^{1}$$

where $\langle|N|\rangle_{Av}$ is the absolute average sagitta of successive chords, R is the range at the midpoint, M and M_P are, respectively, the mass of the particle and of the proton, and t is the cell length; all lengths are in microns. The formula given enables one to compute a constant sagitta (varying cell length) measurement scheme for any particle. The use of this method allows dependable scattering measurements of mass to be made. The mass of an artificially produced negative K meson, which Dr. Salant and Dr. Hornbostel of Brookhaven National Laboratories kindly provided, was measured as 1300±150 times the electron mass.

* Supported in part by a joint program of the U. S. Office of Naval Research and the U. S. Atomic Energy Commission.

T5. Comparison of Proton Energy Loss by Integral and Differential Experiments. THEODORE JORGENSEN, JR., *University of Nebraska.*—The apparatus for range determinations of protons in gases[1] has been modified to determine the ratio of $(\Delta E/\Delta X)_D$ (differential experiment) to $(\Delta E/\Delta X)_R$ (obtained from range measurements) by inserting an additional diaphragm at about 10 percent of the range from the entrance diaphragm. The two diaphragms act to form a differential stopping cell and the range measurements serve to determine the energy lost in the cell. The result of this experiment shows that $(\Delta E/\Delta X)_D$ and $(\Delta E/\Delta X)_R$ are essentially equal. This checks the agreement between our results and those of the differential experiments.[2] Results for protons in argon show that $(\Delta E/\Delta X)_D<(\Delta E/\Delta X)_R$ and that $\Delta E/\Delta X$ by the two methods cannot be expected to agree for gases in which proton scattering is excessive. Details of the experiment and results will be presented.

[1] Cook, Jones, and Jorgensen, Phys. Rev. **91**, 1417 (1953).
[2] S. K. Allison and S. D. Harshaw, Revs. Modern Phys. **25**, 798 (1953)

T6. Low-Energy Pair Production Cross Sections in Scintillators. HARRY I. WEST, JR.,* *Stanford University.*—Using the center crystal of a three-crystal scintillation pair spectrometer[1] as the pair convertor, we have measured both absolute and relative pair cross sections in NaI(Tl) and anthracene for Co^{60} γ rays (1.173 Mev and 1.333 Mev) and relative pair cross sections in NaI(Tl) for the γ rays of Na^{24} (1.38 Mev and 2.76 Mev). The detection efficiency of the spectrometer for pairs was measured by coincidence methods using the decay properties of Na^{22} (β^+ followed by a single γ ray). The cross

sections obtained for carbon (from anthracene) are $\sigma p(1.33)/\sigma p(1.17) = 5.20 \pm 0.17$ and $\sigma p(1.33) = 6.03 \pm 0.17 \times 10^{-28}$ cm². From the Born approximation theory of Hough[3] we find 6.16 and 5.97×10^{-28} cm², respectively. The cross sections obtained for iodine (from NaI(Tl)) are $\sigma p(2.76/\sigma p(1.38) = 15.0 \pm 0.8$, $\sigma p(1.33)/\sigma p(1.17) = 5.00 \pm 0.15$ and $\sigma p(1.33) = 6.82 \pm 0.15 \times 10^{-26}$ cm². From the Born approximation theory of Hough, we get 18.7, 6.16, and 4.68×10^{-26} cm², respectively. Experimental techniques, treatment of data including the bremsstrahlung and electron escape problem from the pair convertor, and comparison of results with theory will be discussed.

* Now at the Army Chemical Center.
[1] Harry I. West, jr., and L. G. Mann, Rev. Sci Instr. **25**, 129 (1954).
[3] P. V. C. Hough, Phys. Rev. **73**, 266 (1948).

T7. Neutron Cross Sections of Light Nuclei.* CHARLES E. PORTER, *Brookhaven National Laboratory.*—Examination of data[1,2] on the neutron total cross sections of light nuclei indicates that much of the variation of these cross sections can be accounted for by the complex-potential model[3] proposed for heavy nuclei. An attempt is being made to see to what extent this is so and will be reported on.

* Work carried out under contract with the U. S. Atomic Energy Commission.
[1] N. Nereson (private communication).
[2] Neutron Cross-Section Compilation, U. S. Atomic Energy Commission Report AECU-2040, 1952 and three supplements (unpublished).
[3] Feshbach, Porter, and Weisskopf, Phys. Rev. **90**, 166 (1953).

T8. (Abstract withdrawn.)

T9. Small Angle Scattering of 1-Mev Neutrons by Intermediate and Heavy Nuclei. S. E. DARDEN, W. HAEBERLI, AND R. B. WALTON, *University of Wisconsin.**—Previous measurements[1] on the angular distributions of elastically scattered neutrons show qualitative agreement with the complex-well scattering model,[2] but suggest that the predicted values are too large at small scattering angles. In an attempt to provide a more sensitive check, the previous measurements have been extended to smaller angles. Using a ring geometry, differential scattering cross sections for 1-Mev neutrons were measured at five angles between 8° and 30° for ten elements. The observed cross sections are about ten percent higher than values found by extrapolating the previous measurements[1] to smaller angles, but appreciably lower than the predicted values[2] for heavy elements.

* Work supported by the U. S. Atomic Energy Commission and the Wisconsin Alumni Research Foundation.
[1] M. Walt and H. H. Barschall, Phys. Rev. **93**, 1062 (1954).
[2] Feshbach, Porter, and Weisskopf, Phys. Rev. **90**, 166 (1953).
[3] Feshbach, Porter, and Weisskopf, Massachusetts Institute of Technology Technical Report No. 62 (1953).

T10. Scattering of Polarized Neutrons from Heavy Nuclei. A. OKAZAKI, R. L. BECKER, AND H. H. BARSCHALL, *University of Wisconsin.**—Experiments to determine the polarization of neutrons scattered by intermediate and heavy elements have been continued. As in previous measurements[1] 380-kev neutrons from the $Li^7(p,n)$ reaction emitted at 50° in the laboratory system were scattered through 90° from cylindrical samples, and the left-right asymmetry was observed. Seventeen elements from Cu to U were investigated. Elements between Nb and Sn showed appreciable asymmetries in one direction, while a slight asymmetry in the opposite direction was found for the heaviest elements in qualitative agreement with previous measurements.[1] An attempt was made to deduce the polarizations produced in the scattering from the intermediate and heavy elements by measuring the polarization of the incident $Li(p,n)$ neutrons. For this purpose the 435-kev neutron resonance in oxygen was used. The results are so far not entirely consistent with the assumed parameters of the O^{17} level so that polarizations cannot be deduced with certainty.

* Work supported by the U. S. Atomic Energy Commission and the Wisconsin Alumni Research Foundation.
[1] Darden, Fields, and Adair, Phys. Rev. **93**, 931 (1954).

T11. Gas Recoil Fast Neutron Spectrometer.* R. E. BENENSON, M. B. SHURMAN, AND W. HAEBERLI, *University of Wisconsin.*—A gas recoil neutron spectrometer similar in operation and geometry to that described by Giles[1] has been constructed and tested with monoenergetic neutrons from 0.68 to 5.1 Mev, using fillings of palladium-filtered H_2 and 99.9 percent pure tank propane. The number of wires in the transparent cathode and anticoincidence anodes has been increased over the number used by Giles; end effect anticoincidences are employed; and clean vacuum techniques to eliminate electron capture by electronegative impurities have been used. The width of the peak and peak-to-background ratio are markedly dependent on the proton recoil range chosen. Widths of the peak at half-maximum of 10 percent have been attained. Efficiencies of the order of 10^{-4} are obtained for the pressures and ranges employed. In the most favorable case the average background was reduced to 5 percent of the peak height; 10 percent is considered to be compatible with good efficiency. The anticoincidence voltage is independently variable; multiplications of the order of 10^4 are required in the anticoincidence counters for good gating. Nuclear reactions are being studied.

* Work supported by the Wisconsin Alumni Research Foundation and the U. S. Atomic Energy Commission.
[1] R. Giles, Rev. Sci. Instr. **24**, 986 (1953).

TUESDAY EVENING AT 7:00

Junior Ballroom, Coffman Memorial Union

(MARSH W. WHITE presiding)

Banquet of the AAPT and the American Physical Society

After-dinner speakers: R. M. SUTTON and E. W. DAVIS.

WEDNESDAY MORNING COMMENCING AT 4:30

Total Eclipse of the Sun

WEDNESDAY MORNING AT 10:30

Murphy 105

(R. L. SPROULL presiding)

Electron Emission and Ejection Phenomena, I.

Invited Paper

U1. On the Escape Mechanism for Secondary Electrons. A. J. DEKKER, *University of Minnesota.* (25 min.)

Contributed Papers

U2. Methods of Preparing Thin Film MgO Secondary Emission Surfaces on Ag-Mg Alloys.* PETER WARGO, *University of Minnesota.*—Many procedures have been described for the preparation of thin film secondary emission surfaces of MgO. Variations in these procedures give rise to widely varying results. Two simple procedures will be described which result in consistent maximum values of δ of approximately 12 at a primary energy near 500 volts. The simpler method using a low pressure of oxygen is particularly suited to cases where the targets are prepared in one vessel and transferred to a second for application. Some of the problems encountered in this transfer process will be discussed. The second method using a CO_2 atmosphere is particularly suited to situations where the targets can be processed in the final site.

* Supported by the U. S. Signal Corps.

U3. Inelastic Scattering of Medium-Fast Electrons in Alkali Metals.* E. M. BARODY, *Battelle Memorial Institute.*—Earlier calculations[1] concerning the excitation of valence electrons to the next Brillouin zone by medium-fast primaries have been extended. Using the approximation of nearly free electrons, explicit expressions for the number of interzonal transitions per unit primary path and for the distribution in energy of the transitions have been obtained and applied to several alkalis. For these metals, a similar method has been used in the past to account for the absorption of visible and ultraviolet light; and for sodium, potassium, and rubidium, Butcher[2] has chosen Fourier coefficients of the lattice potential which give adequate agreement with the limited experimental data. When Butcher's coefficients are introduced into our equations, interzonal transitions are found to be infrequent, only two or three being predicted per 1000A when the primary energy is 1000 ev. This supports the view that the interzonal transitions emphasized in the Fröhlich-Wooldridge theory of secondary emission from metals are actually of minor importance.

* Sponsored by the U. S. Army Signal Corps and the U. S. Air Force.
[1] E. M. Baroody, Phys. Rev. **89**, 910 (1953).
[2] P. N. Butcher, Proc. Phys. Soc. (London) **A64**, 765 (1951).

U4. Work Functions of Tungsten Single Crystal Planes.* ERWIN W. MÜLLER, *Pennsylvania State University.*—Electron emission from the 110 plane has been measured as a spurious effect only.[1,2] The method of a field emission microscope with a probe hole in the screen and behind it a suppressor and a collector[3] has been improved. The current density in the 110 plane was found to be 4 to 5 orders of magnitude smaller than in the strongly emitting planes. Applying the Fowler-Nordheim theory and assuming $\phi_{111}=4.38$ *ev* according to,[1] one finds ϕ_{110} between 5.80 and 6.15 ev, depending on the temperature at which the crystal has been annealed previously (2500°K and 1200°K, respectively, vacuum 10^{-12} mm). The same effect at the 112 plane yields work functions between 4.80 and 5.05 ev. It is caused by freezing in the thermal imperfections. The data of all strongly emitting planes agree with those obtained by thermionic methods.

* Work supported by U. S. Office of Scientific Research, U. S. Air Research and Development Command, Baltimore, Maryland.
[1] M. H. Nichols and G. F. Smith: U. S. Office of Naval Research Report No. 24433 (1952).
[2] W. P. Dyke and co-workers: J. Appl. Phys. **25**, 106 (1954).
[3] E. W. Müller, Z. Physik **120**, 261 (1943).

U5. Noise Mechanisms in Oxide-Coated Cathodes.* A. VAN DER ZIEL, *University of Minnesota.*—Order of magnitude considerations will be applied to discriminate between various noise mechanisms that might be proposed to explain flicker noise in vacuum tubes. It will be shown that noise due to fluctuations in number of adsorbed atoms or noise due to fluctuations in the number of donor atoms in the coating cannot account for the observed noise, but that either Schottky's emission center theory or the spontaneous fluctuations in the number of carriers in the surface layer may explain the experimental results.

* Work supported by the U. S. Signal Corps.

U6. Influence of Different Activating Agents on Flicker Noise in Oxide-Coated Cathodes.* W. W. LINDEMANN, *University of Minnesota.*—A series of experiments to determine the differences in the flicker noise characteristics of tubes with different types of cathode nickel alloys will be discussed. Of the alloys used (Inco 220, Inco 225, 0.1 percent Al, 0.4 percent W, and 499 nickel). 0.1 percent Al nickel consistently gave the least noisy tubes. Some observations of other characteristics of the various cathode nickel alloys which might suggest an explanation of these results will also be given.

* Supported by U. S. Signal Corps Contract.

U7. Influence of Tube Structure and Tube Operating Conditions Upon Flicker Noise.* H. J. HANNAM, *University of Minnesota.*—To show how the amount of flicker noise generated in vacuum tubes depends upon the tube structure, a comparison will be made of the noise generated in a triode and the noise generated in the same tube in diode connection. To show the influence of operating conditions, measurement will be presented of flicker noise in triodes and pentodes as a function of the applied voltages. A discussion of possible causes of effects will be given.

* Work supported by the U. S. Signal Corps.

WEDNESDAY MORNING AT 10:00

Physics 150

(J. H. WILLIAMS presiding)

Invited Papers on Nuclear Accelerators

V1. Recent Cyclotron Experiments at Harvard University. N. F. RAMSEY, *Harvard University.* (30 min.)

V2. Recent Progress in Electrostatic-Generator Techniques. R. G. HERB, *University of Wisconsin.* (30 min.)

V3. Preliminary Operation of the Bevatron. E. J. LOFGREN, *University of California, Berkeley.* (30 min.)

V4. Research with the Cosmotron. LYLE W. SMITH, *Brookhaven National Laboratory.* (30 min.)

WEDNESDAY MORNING AT 10:00

Physics 170

(J. VALASEK presiding)

General Physics

W1. Preliminary Description and Analysis of the Spectrum of Polonium. G. W. CHARLES, D. J. HUNT, G. PISH, AND D. L. TIMMA, *Mound Laboratory.**—Purified polonium has been excited by both high-frequency electrodeless discharges of 10, 30, and 400 megacycles/sec at temperatures ranging from 200° to 800°C, and in an enclosed spark source. One hundred forty-seven lines have been found in the spectrum from the electrodeless discharge and thirteen additional lines have been observed in the spectrum of the spark discharge. Forty-eight lines have been classified as transitions involving twenty-four energy levels of PoI. Four levels of the fundamental configuration $6p^4$ have been identified. The observations have been compared with theoretical predictions for this configuration. Separations are well represented by theory with the parameter $F_2 = 1112$ cm^{-1} and $\zeta = 12393$ cm^{-1}. The absolute value of the lowest level $6p^4\,{}^3P_2^1$ has been estimated from the first two members of the series $6p^3(^4S^0)ns$ using the method of Russell. An estimate of 67 990 cm^{-1} is obtained. This corresponds to an ionization potential of 8.43 volts.

* Operated by Monsanto Chemical Company for the United States Atomic Energy Commission.

W2. Thomas-Fermi Calculation of the C−H Bond Moment in Methane.* H. GLAZER AND H. REISS,† *Boston University.*—The pyramids formed by the planes bisecting the H−C−H bond angles were taken as elements of symmetry. Each pyramid encloses a carbon-hydrogen bond and the four close pack to form the methane molecule. To simplify the problem, the pyramid was replaced by a cone of equal volume. The Fermi-Thomas equation was solved for the potential within this cone subject to the appropriate boundary conditions, on the IBM 701 Electronic Data Processing Machines, using the extrapolated Liebmann method. Boundaries were chosen about each nucleus on which the superposition solution was used. The equation was solved for carbon alone and then for carbon-hydrogen within the cone. The dipole moment was taken as the difference[1] between the two and found to be 2.8 D C^+H^-. The large magnitude is attributed to the poor description of hydrogen by the statistical theory.

* Supported by the Geophysics Research Directorate, Air Force Cambridge Research Center.

† Present address: Bell Telephone Laboratories.

[1] C. A. Coulson, Conference on Quantum Mechanical Methods in Valence Theory, Long Island, New York, September, 1951, p. 19.

W3. The Shape of the Coexistence Curve of Two-Phase Systems Near the Critical Point.* O. K. RICE, *University of North Carolina.*—The data of Atack and Rice[1] on the coexistence curve of the cyclohexane-aniline system and on the densities of the coexisting phases have been correlated, and the conclusion confirmed that the coexistence curve has a flat top (i.e., a *range* of critical compositions). The data on the liquid-vapor equilibrium in two one-component systems, xenon[2] and carbon dioxide,[3] have also been examined. Although the authors of these papers believe that the coexistence curves are rounded on top, it is shown that the data are not conclusive on this point. In the case of carbon dioxide, in particular, the evidence may indicate a flat horizontal portion at the top of the coexistence curve. Certain thermodynamic relations between the shape of the coexistence curve and the shape of the critical isotherm have been worked out and applied to the available data.

* Supported by U. S. Office of Naval Research.

[1] D. Attack and O. K. Rice, J. Chem. Phys. **22**, 382 (1954).

[2] H. W. Habgood and W. G. Schneider, Can. J. Chem. **32**, 98 (1954).

[3] H. L. Lorentzen, Acta Chem. Scand. **7**, 1335 (1953).

W4. Kinetics of Phase Transitions for Systems Undergoing Association: Monomer-Dimer Equilibrium. HOWARD SALTSBURG, *Air Force Cambridge Research Center,* AND HOWARD REISS, *Bell Telephone Laboratories.*—The kinetics of nucleation of a system in which the metastable phase contains an equilibrium mixture of monomer and dimer has been formulated in terms of the vector model of Reiss.[1] The results will be contrasted with the result of the recent formulation of Frisch and Willis[2] and, in particular, the distinction between the perturbing effects of collisions between embryos of size two and nucleation in a system in which dimers are present will be made. Numerical results will be presented for ethanol vapor nucleation assuming various ratios of

monomer to dimer in the vapor phase. In contrast to the result predicted by Frisch and Willis, the nucleation rate falls off quite sharply with increasing amounts of dimer. The failure of the simple Becker-Doring theory to predict the observed critical supersaturation for methanol vapor will be considered in the light of this analysis.

[1] H. Reiss, J. Chem. Phys. **18**, 840 (1950).
[2] H. Frisch and C. Willis, J. Chem. Phys. **22**, 243 (1954).

W5. The Excitation of Molecular Vibrations in Halogen-Substituted Methanes. THOMAS ROSSING AND SAM LEGVOLD, *Iowa State College.**—The relaxation times for the excitation of molecular vibrations in CH_3ClF, $CHCl_2F$, $CHClF_2$, CBr_2F_2, $CBrClF_2$, CCl_3F, CCl_2F_2, $CClF_3$, CH_2F_2, CH_3Br, and CH_3Cl have been measured with an acoustic interferometer. All the gases studied were found to have a single relaxation time, indicating that intermodal coupling in these gases is strong. The average probabilities for the excitation of molecular vibrations have been calculated from the relaxation data and examined on the basis of existing theory. Preliminary calculations show that an energy barrier type of theory recently suggested[1] describes the probability better than the theory of Bethe and Teller.[2] The height of the barrier is found to depend upon the energy of the lowest mode and upon the number of hydrogen atoms replaced.

* Work supported by the National Advisory Committee for Aeronautics.
[1] Fogg, Hanks, and Lambert, Proc. Roy. Soc. (London) **A210**, 490 (1953).
[2] Bethe and Teller, Report X-117, Aberdeen Proving Grounds.

W6. Evaporation of Small Drops at Low Pressures. LOUIS MONCHICK, *Boston University*, AND HOWARD REISS, *Bell Telephone Laboratories.*—The rates of evaporation of small drops of diamyl sebacate (average radius, approximately one micron) were measured in a Millikan oil-drop chamber and observed to obey a law of the form $dR/dt=a/(1+bRp)$ which has been predicted by the theories of Fuchs and Frisch and Collins. Using a nonequilibrium distribution function of velocities, the relation has been rederived in a more rigorous fashion (over a limited range of conditions). Certain corrections in the constants a and b are introduced, and the validity of the Fuchs theory in this range of conditions is demonstrated. Using the formulation of Frisch and Collins, the law may be derived in the same form, subject to certain conditions.

Post-Deadline Papers, if Any

WEDNESDAY AFTERNOON AT 1:30

Murphy 105

(G. E. MOORE presiding)

Electron Emission and Ejection Phenomena, II

Invited Papers

X1. Experiments Bearing on the Mobile-Donor Hypothesis in Oxide Cathodes. L. S. NERGAARD, *Radio Corporation of America.* (25 min.)

X2. Elementary Processes in Semiconductor Emitters. J. A. KRUMHANSL, JR., *Cornell University.* (25 min.)

Contributed Papers

X3. Electronic Structure of Magnesium Oxide.* J. R. STEVENSON,† *University of Missouri.*—Measurements are reported on the thermionic emission, photoelectric emission, and optical absorption of MgO in different physical forms. Samples include single crystals, powders, and thin films. For six powdered samples studied in the temperature range 1300°K to 900°K the true work function ϕ was 3.3 ± 0.2 ev and $d\phi/dT$ was about 10^{-4} ev/°K. For a single crystal the value of ϕ of 3.5 ev was obtained in the same temperature range. $d\phi/dT$ was also about 10^{-4} ev/°K. The thresholds for photoelectric emission, as determined by linear extrapolation to zero current, were approximately 3.5 ev for powdered samples and single crystals. However, the quantum efficiencies of the powdered samples at 4.9 ev were a factor of 10^6 larger than for the single crystal. Photoelectric emission from metals into single crystals of MgO indicate an electron affinity for MgO of 1.8 ± 0.5 ev. Two new optical absorption bands have been detected at 1.2 and 1.8 ev. These bands are enhanced by oxygen doping and x-ray irradiation.

* Supported in part by the U. S. Office of Naval Research.
† Sylvania Fellow (1951–1953).

X4. Measurement and Theoretical Study of the Conductivity and Hall Effect in the Oxide Cathode. R. FORMAN, *National Bureau of Standards, University of Maryland.*—Conductivity, Hall effect, and magnetoresistive measurements have been made on oxide cathodes having varying degrees of porosity. Anomalous effects at high temperatures, previously reported,[1,2] have been confirmed. These are (1) large Hall coefficients, (2) large values for mobility, and (3) large magnetoresistive effects. The temperature at which these measurements were made has been extended down to 500°K by the use of an electrometer instead of the usual potentiometric techniques. In the temperature range below 700°K the mobility was found to decrease rapidly with decreasing temperature. The variation of resistance with magnetic field was found to be dependent on the degree of porosity of the cathodes. These experimental results and others, which will be discussed, are consistent with the model originally suggested by Loosjes and Vink[3] to explain the electrical properties of the oxide cathode. A theory has been developed, based on the high-temperature pore conductivity model, which is in qualitative and quantitative agreement with the data.

[1] D. A. Wright, Brit. J. Appl. Phys. **1**, 150 (1950).
[2] Ishikawa, Sata, Okumura, and Sasaki, Phys. Rev. **84**, 371 (1951).
[3] R. Loosjes, and H. J. Vink, Philips Research Repts. **4**, 449 (1949).

X5. Reaction between BaO and C and BaO and Si. MICHAEL HOCH, ANTHONY J. LAMANTIA, AND HERRICK L. JOHNSTON, *The Ohio State University.*—The reactions $BaO+C\rightarrow Ba$

+CO(1) and $4BaO+Si \rightarrow BaSiO_4+2Ba$(2) were studied by the Knudsen effusion method between 1290°–1390°K and 1280°–1600°K, respectively. In reaction (1) the measured partial pressure of CO agrees well with calculated values, whereas the Ba pressure is much lower. In reaction (2), the partial pressure of Ba corresponded to the calculated value. These measurements indicate a strong adsorption of Ba on BaO, which, however, is not enough to explain the long life of the oxide cathode.

X6. Measurement of Excess Ba in Emitting Oxide-Coated Cathodes. L. A. WOOTEN,* GEORGE E. MOORE, AND W. G. GULDNER.—More than 300 cathodes of various structures were tested thermionically throughout lifetimes up to 50 000 hr and submitted to a destructive chemical analysis which exposed the cathode to water vapor and measured the H_2 liberated by reoxidation of excess Ba. Measurable sensitivity was 0.02 microgram. We discuss typical tests illustrating potentialities and limitations of the analytical method. Relatively large quantities of readily available Ba (as on glass surfaces) react completely within 15 min at ambient. Because nearly all Ba produced leaves the oxide coating in practical cathodes, measurements significant for correlation with thermionic emission require isolation of the cathode. Both nickel itself and its impurities can, under suitable circumstances, react with water to produce H_2, but the rates of these side reactions become insignificant through interfaces formed in the processing of practical cathodes. For an isolated cathode, H_2 forms in amounts approximately linear in the logarithm of exposure time. To avoid side reactions, the H_2 evolved upon 16 hours' exposure to water vapor is taken to measure Ba content; relative Ba content of different cathodes is usually not altered significantly by using any exposure time from 1 min to 65 hr.

* Deceased.

X7. Excess Ba Content of Emitting Oxide-Coated Cathodes. GEORGE E. MOORE, L. A. WOOTEN,* AND JAMES MORRISON.—Measurements were made of excess Ba content and emission for 125 coated equipotential cathodes, and 15 coated filaments, each isolated from its experimental tube. Similar measurements of equivalent Ba were made for 19 uncoated cathode sleeves. Support metals were grade A nickel, relatively pure Ni, and purified platinum. Coating composition was usually 35 mole percent BaO, 65 mole percent SrO, but pure BaO and pure SrO were also examined. Results cover 5 orders of magnitude in both Ba content and emission. Throughout this range, there was no indication of increased emission with increase in Ba content. Deposited Ba in excess of 0.05 layer decreased emission and re-evaporated above 600°K within 5 min; production of Ba by exposure to methane usually decreased emission but such Ba was stable even above 1100°K. Median Ba content for demounted filaments prepared commercially was 0.90×10^{17} atoms per cc, equivalent to only 0.005 monolayer on the true oxide surface but sufficient for emission according to the semiconductor model for oxide cathodes. However, absence of correlation between emission and Ba content indicates that other factors are decisive. For example, emission observed from coated platinum was significantly less than from coated nickel, regardless of Ba content.

* Deceased.

X8. Applications of Radioactive Tracer Techniques to the Study of Thermionic Emission of Oxide-Coated Cathodes.* R. W. PETERSON, D. E. ANDERSON, AND W. G. SHEPHERD, *University of Minnesota.*—Studies of the evolution of Sr and Ba from oxide-coated cathodes using radioactive isotopes have indicated that for the normal range of operating temperatures the rate of Ba evolution differs only slightly from that to be expected from the evaporation of BaO. On the other hand, the evolution of Sr is orders of magnitude larger than would be expected from the simple evaporation of SrO, suggesting that the Sr is evolved principally by the reduction of SrO. This suggests that the evolution of Sr should serve as a measure of the reduction rate of the oxide coating. Studies will be reported which have been concerned with determining whether a correlation exists between the thermionic emission and the rate of reduction of the oxide coating.

* Supported by the U. S. Navy.

X9. Solute Diffusion in Nickel.* R. A. SWALIN AND A. E. MARTIN, *University of Minnesota.*—Diffusion studies of manganese, aluminum, and titanium in nickel have been made as part of a general program of investigation of solute diffusion in nickel. A diffusion couple method embodying low concentration changes was used and diffusion coefficients were calculated by the Grube method. Special spectrophotometric methods of analysis were adapted for each element. Diffusion coefficient measurements were made in the temperature range of 1100 to 1300°C with the following results:

Solute	D_0(cm²/sec)	ΔH (kcal/g-atom)
Mn	7.50	67.1
Al	1.87	64.0
Ti	0.86	61.4

The values of the activation enthalpies approximate that for self-diffusion of nickel in agreement with Nowick's hypothesis.[1]

* Supported by U. S. Navy.
[1] A. S. Nowick, J. Appl. Phys. **22**, 1182 (1951).

X10. Diffusion of Tungsten in Nickel. H. W. ALLISON AND GEORGE E. MOORE, *Bell Telephone Laboratories, Inc.*—Diffusion of radioactive tungsten in nickel has been measured over a temperature range 1100°C to 1400°C by using a sectioning technique. The couples used were of three types, (1) radioactive tungsten powder in contact with nickel, (2) tungsten deposited by evaporation onto nickel, (3) 4.9 percent W−Ni alloy in contact with nickel. Values of D, computed assuming D independent of concentration, agree within experimental error for all three types of couples. These D values fit an equation $D=Ae^{-Q/RT}$, and are representative of combined volume and grain boundary diffusion through nickel with grain size ranging from 0.2 mm to 7 mm. Radioautographs indicate that grain boundary diffusion may be appreciable in polycrystalline nickel. Rates of reaction of SrO coating with tungsten diffusion to the surface of a 4.9 percent W−Ni alloy were determined for a temperature range 1200°–1540°K by use of the hydrogen evolution technique. The measured rates indicate that the reaction of the initial 10 percent of the coating is not limited by diffusion of the tungsten through the nickel.

X11. An Oxide Impregnated Nickel Matrix Cathode. W. BALAS, J. DEMPSEY, AND E. F. REXER, *Honeywell Research Center.*—A new cathode is described consisting of an oxide-impregnated nickel matrix. A sintered nickel matrix of controllable porosity is prepared and impregnated with solutions, which precipitates a mixed carbonate within the matrix. The resulting cathode is a dispenser type with a minimum of surface coating. The cathodes can be activated by schedules which approximate those of a normal oxide-coated. Pulse-emission tests of these cathodes show properties intermediate between the oxide-coated cathode and the L cathode, and of the same order as the molded cathode described by McNair, Lynch, and Hannay.

Author Index to Papers Presented at the Minneapolis Meeting

Ahearn, A. J.—K8
Allis, W. P.—Q2
Allison, H. W. and George E. Moore—X10
Anderson, K. A.—L4
Apker, L.—K1
Babiskin, J. and M. C. Steele—D3
Baker, T. E., Jr., N. C. Blais, C. L. Hemenway, V. Rojansky, M. S. Webster, and M. S. Werman—L1
Balas, W., J. Dempsey, and E. F. Rexer—X11
Baroody, E. M.—U3
Beaty, E. and R. Varney—Q4
Benenson, R. E., M. B. Shurman, and W. Haeberli—T11
Bennett, Willard H.—F8
Biondi, M. A.—Q3
Blewett, J. P.—F2
Bohl, Leland—S3
Bowen, Theodore—L12
Breed, Henry E. and J. Mayo Greenberg—F4
Bridge, H. S.—S4
Brown, W. L., R. C. Fletcher, and K. A. Wright—R8
Browne, C. I., D. C. Hoffman, H. L. Smith, M. E. Bunker, J. P. Mize, J. W. Starner, R. L. Moore, and J. P. Balagna—H13
Bube, R. H.—K2
Burstein, E., J. W. Davisson, and N. Sclar—A4
Carroll, Paul E.—A9
Cegelski, W. M., A. T. Goble, C. L. Hemenway, K. Reinitz, V. Rojansky, and F. A. Rushworth—L2
Chanin, Lorne M. and Manfred A. Biondi—Q5
Chapman, Seville—Q8
Charles, G. W., D. J. Hunt, G. Pish, and D. L. Timma—W1
Cheston, W. B.—M1
Chou, C. N.—L10
Christensen, H.—K5
Collins, T. L.—G3
Cook, C. J.—T3
Coomes, E. A.—A3
Craig, D. S., W. G. Cross, and R. G. Jarvis—H2
Danielson, R. E., P. S. Freier, J. S. Naugle, and E. P. Ney—L5
Darden, S. E., W. Haeberli, and R. B. Walton—T9
Dash, W. C.—D7
Davis, R. E. and Colman Goldberg—R2
Dekker, A. J.—U1
Dunlap, W. C., Jr., H. V. Bohm, and H. P. Mahon, Jr.—D6
Feldman, Charles—A5
Field, L. M.—F3
Fiske, Milan D.—D1
Fletcher, R. C., Brown, W. L., and K. A. Wright—R7
Forman, R.—X4
Freier, Phyllis—S1
Freistadt, Hans—B6
Fuller, C. S., J. A. Ditzenberger, N. B. Hannay, and E. Buehler—R3
Galonsky, A. and M. T. McEllistrem—H9
Gallagher, C. G. and A. G. Tweet—R9
Glasser, R. G.—T4
Glazer, H. and H. Reiss—W2
Giese, Clayton F. and T. L. Collins—F5
Goodman, B.—F10
Gove, H. E., G. A. Bartholomew, E. B. Paul, and A. E. Litherland—H3
Greenberg, J. Mayo—B4
Hannam, H. J.—U7
Hannay, N. B., J. R. Haynes, and R. G. Shulman—R4
Hanson, Howard G.—Q12
Herb, R. G.—V2
Hiltner, W. A.—G1
Hoch, Michael, Anthony J. Lamantia, and Herrick L. Johnston—X5
Horwitz, Nahmin—S2
Hyman, Morton A.—B7
Jauch, J. M.—M2
Johnston, Lawrence H., Norton M. Hintz, and Harry J. Schulte—T1
Jorgensen, Theodore, Jr.—T5
Jossem, E. L. and L. G. Parratt—R11
Krafft, Joseph M.—D5
Krumhansl, J. A., Jr.—X2
Lagergren, C. Robert—F6
Lassettre, E. N., M. E. Krasnow, and S. Silverman—Q11
Leder, L. B.—F1
Lindemann, W. W.—U6
Linsley, John—L3
Litherland, A. E., E. B. Paul, G. A. Bartholomew, and H. E. Gove—H4
Lofgren, E. J.—V3
Lowen, R. W.—H8
Luyten, W. J.—G2
McCoubrey, A. O. and C. G. Matland—Q10
Matheson, W. E., C. R. Carlson, F. S. Mathews, R. O. Haxby, and R. M. Whaley—H10
Merz, W. J.—A2
Monchick, Louis and Howard Reiss—W6
Moore, George E., L. A. Wooten, and James Morrison—X7
Morin, F. J., J. P. Maita, R. G. Shulman, and N. B. Hannay—R5
Müller, Erwin W.—U4
Murray, F. J.—D4
Naugle, J. E., P. S. Freier, and E. P. Ney—L7
Nelson, E. B., W. Lawrence, and R. R. Carlson—H1
Nergaard, L. S.—X1
Ney, E. P., John Naugle, and Phyllis Freier—L6
Nussbaum, Allen—K6
Okazaki, A., R. L. Becker, and H. H. Barschall—T10
Parratt, L. G. and C. F. Hempstead—B3
Paskin, Arthur—A8
Peria, W. T.—F11
Peterson, R. W., D. E. Anderson, and W. G. Shepherd—X8
Phelps, A. V.—Q9
Philipp, H. R.—K4
Pidd, R. W.—C1
Pinnick, H. T.—R1
Porter, Charles E.—T7
Quisenberry, K. S., T. T. Scolman, and T. L. Collins—F7
Ramsey, N. F.—V1
Reynolds, J. M. and D. D. Triantos—D2
Rice, O. K.—W3
Roe, G. M. and R. H. Stark—B5
Rohrlich, F.—M3
Rossing, Thomas and Sam Legvold—W5
Sakai, M., B. Murray, and J. D. Kurbatov—H12
Saltsburg, Howard and Howard Reiss—W4
Schein, Marcel, D. M. Haskin, and R. G. Glasser—L8
Schlegel, Richard—B1
Shrader, Ross E.—F12
Shull, F. B. and M. M. Bretscher—H7
Shulman, R. G., W. L. Brown, and R. C. Fletcher—R6
Simmons, B. E., D. M. Van Patter, K. F. Famularo, and R. V. Stuart—H11
Smith, F. Graham—G4
Smith, Lyle W.—V4
Spicer, W. E.—F9
Sprague, A. D., D. M. Haskin, R. G. Glasser, and Marcel Schein—L9

Stevenson, J. R.—X3
Stout, Virgil L. and Martin D. Gibbons—A7
Stratton, T. F., K. F. Famularo, H. D. Holmgren, and R. V. Stuart—H5
Swalin, R. A. and A. E. Martin—X9
Taft, E. and L. Apker—K3
Tucker, Edmund B., Lawrence H. Johnston, and Donald E. Young—T2
Tweet, A. G.—K7
van der Ziel, A.—U5
Van Patter, D. M., B. E. Simmons, T. F. Stratton, and D. M. Zipoy—H6
Varney, R. N.—Q1
Voss, J. R., T. R. Palfrey, and R. O. Haxby—L11
Wannier, Gregory H.—Q6
Wargo, Peter—U2
Wehner, G. K.—A1
Weigl, John W.—R10
Wessel, Walter—A6
West, Harry I., Jr.—T6
Widom, B.—B2
Wiser, Herbert L. and A. D. Krumbein—Q7
Wooten, L. A., George E. Moore, and W. G. Guldner—X6
Zaffarano, D. J.—C2

Minutes of the Pacific Northwest Meeting, Held at Seattle, Washington, and on Mount Painter, July 7, 8, 9, and 10, 1954

(Corresponding to *Bulletin of the American Physical Society*, Volume 29, No. 6)

THE 1954 Summer Meeting of the American Physical Society was held at Seattle on the Campus of the University of Washington, on Wednesday, Thursday, and Friday, July 7, 8, and 9, and on Mount Rainier on Saturday, July 10. The meeting was very well attended and the local arrangements were excellent. The Secretary wishes to thank Professor E. A. Uehling and his local committee for their part in the planning of the meeting and in making these fine arrangements. The sessions arranged by our Division of Fluid Dynamics were its first in the Pacific Northwest, and they were excellent and well-attended sessions. Post-deadline papers were given by K. Krishnamurty of the California Institute of Technology on "Production of Sound at Cut-Outs on an Aerodynamic Surface"; by E. Segrè, R. Tripp, C. Wiegard, and T. Ypsilantis of the University of California, Berkeley, on "Depolarization on Scattering of Polarized Protons from Hydrogen"; and by M. Schein, D. M. Haskin, and R. G. Glasser of the University of Chicago on "Narrow Beam of Pure Photons Probably Arising from the Annihilation of a High Energy Cosmic Ray Particle Close to the Top of the Atmosphere." Papers F14 and L14 were ready by title.

The demonstration cruise of the *HMCS Cedarwood*, the research ship of the Royal Canadian Navy, an outdoor salmon barbecue, and the luncheon of the Society, combined with the relatively leisurely tempo of the meeting, made this one of the most enjoyable ones of recent years.

J. Kaplan, *Local Secretary for the Pacific Coast*

Errata Pertaining to Papers I12 and N3

I12, by S. A. Heiberg. In the next to the last line, 30 millibarns should read 10 millibarns.

N3, by B. H. Muller and Myer Bloom. In line 9, 4.3 A should read 4.2 A. In line 10, 2.27 A should read 2.19 A.

PROGRAMME

WEDNESDAY MORNING AT 9:30

Guggenheim Hall

(R. T. ELLICKSON presiding)

Contributed Papers

A1. Adiabatic Theorems in Field Theory. S. DESER,* *Institute for Advanced Study.*—The effect of a particle in the limit of infinite mass is investigated field theoretically. Using a technique expressing the relevant exact propagation functions as functional integrals, the desired limiting process need only be performed on a simple propagator for one particle in an external field to get the result for the exact functions. By comparing the resultant propagator for n particles of which m become infinitely heavy with that for n-m particles in an external field, it is shown that the heavy particles act as point sources of static fields determined by the nature of the intermediate particles (maxwell, scalar meson, etc.) and the usual vacuum polarization effects due to virtual pairs of any lighter fields. In the case of mesons with no nonrelativistic limit, as $ps(ps)$, the situation is more complicated. By means of a Foldy transformation and absorption of the mass into the coupling constant, a nonzero resultant potential may be obtained. Weak and strong coupling limits thereof will be discussed. Further applications of the functional technique are in progress.

* On summer leave at University of California, Berkeley.

A2. Critical Flow Rate and Zero Entropy of Helium Superfluid. WILLIAM BAND, *State College of Washington.*—A Bose-Einstein assembly with nondegenerate energy spectrum has only one symmetrized wave function for any distribution-in-energy: the entropy is therefore absolutely zero at all temperatures. The Heisenberg uncertainty relation may blur the energy levels until they overlap each other, validate the usual approximations, and produce entropy. This mechanism may fail in liquid helium superfluid. B. E. statistical fluctuations into the lowest states may be localized with linear dimensions L, energy levels spaced roughly $\hbar^2/8\pi m^* L^2$, where m^* is effective mass required to give the observed lambda transition temperature: $m^* = 1.55 m_{He}$. The fluctuation life time τ is long enough to keep the levels distinct and destroy entropy if $\tau\hbar/8\pi m^* L^2 > 1$. Assuming τ given by thermal conductivity relaxation times,[1] $\tau u_s^2 = 0.05$ cm²/sec at 2°K, where u_s is the speed of transport of superfluid. Substitution yields $u_s L = 10^{-3}$ cm²/sec. The fluctuations can therefore be fed into a capillary of width 3×10^{-5} cm at a speed 30 cm/sec, all entropy filtered out. A higher speed would force shorter relaxation time, broaden the energy levels and restore normal entropy in the capillary.

[1] L. Meyer and W. Band, Phys. Rev. **74**, 394 (1948).

A3. Electrohydrodynamics. I. Equilibrium of a Charged Gas in a Container. JOSEPH B. KELLER, *Mathematics Branch, Department of the Navy, Washington 25, D. C.*—Since phenomena involving the equilibrium or motion of fluids in which magnetic forces are important are called magnetohydrodynamic phenomena, it seems appropriate to designate as electrohydrodynamics that class of phenomena in which the equilibrium or motion of a fluid is involved and in which electric forces are important. A typical phenomenon of this type is the equilibrium of a charged gas within a container. In this example, equilibrium is achieved when electrostatic and pressure forces balance each other. It is, therefore, necessary to determine the pressure p, the electric field E, and the electric charge density ρ, in order to solve this problem. These quantities satisfy the equilibrium equation and Poisson's equation which are $\nabla p = \rho E$, $\nabla \cdot E = 4\pi\rho$. Furthermore, according to the equation of state, p is a function of the mass density which is assumed to be $(m/e)\rho$, where m/e is the mass-charge ratio of the charged particles constituting the gas. Thus, $p = p[(m/e)\rho]$. For a perfect gas in which p is proporitonal to ρ, both p and E can be eliminated from the preceding equations leading to the following equation for q which is essentially $\log\rho$: $\nabla^2 q = e^q$. In addition to the preceding equations, the total charge within the container must be specified, and if the container is a perfect conductor, the tangential component of electric field must be required to vanish on its surface. It is shown that for every value of the total charge there is one and only one solution of the preceding equations, satisfying the conditions just stated. The density and pressure are both constant on the surface of the container for each value of the total charge and $|\rho|$ assumes its maximum value on this surface. Furthermore, at each point of the container ρ increases as the total charge does.

A4. Oscillation and Stability in Certain Nonlinear Systems. WILLIAM M. WHYBURN, *University of North Carolina and U. S. Naval Ordnance Test Station* (introduced by J. Kaplan).—A simple pendulum is an elementary example of a nonlinear system which oscillates and is stable in the sense that amplitudes remain bounded for all time. This system is a special case of a class of nonlinear systems discussed in the present paper. Conditions are given under which solutions of such systems oscillate and are stable. Under other conditions, the solutions are shown to be unstable. Special consideration is given to the second order differential system $y' = K(t,y,z)z$, $z' = G(t,y,z)y$ and principal results are stated for this system. Some reference is made to nth order systems where conditions of uniqueness fail and solutions of critical types exist.

A5. A Semiautomatic Apparatus for Thermocouple Comparison and Calibration. T. M. DAUPHINEE, *National Research Council, Ottawa.*—Several thermocouples are continuously intercompared with a standard couple of the same type over a wide temperature range. A permanent record of the total emf of the standard thermocouple and the emf difference between the standard and each of the other thermocouples appears on a recorder strip chart, the accuracy of the difference measurement being better than $\pm 1\mu v$. If desired, comparison between the corresponding individual elements of the standard and test thermocouples may be obtained at the same time. Temperature is varied at any required rate by means of a motor controlled variac. The hot junctions of the thermocouples are welded together to ensure identity of temperature in spite of the nonequilibruim conditions in the furnace. An isolating potential comparator[1] allows the emf difference measurements to be made in spite of this electrical connection at the junction.

[1] T. M. Dauphinee, Can. J. Phys. **31**, 577 (1953).

A6. The Creep of Aluminum Under Cyclotron Irradiation.* A. ANDREW,† M. R. JEPPSON,‡ R. L. MATHER,§ AND H. P. YOCKEY.‖—The effect of cyclotron irradiation on the steady-state creep rate of aluminum has been measured at beam densities up to 1.2×10^{13} alpha particles per cm² per second. The

data show a slight decrease in rate (up to 19 percent) during irradiation. Since the effect is small, apparently independent of beam density, and is comparable to the usual deviations in the absence of radiation, it can be considered a null result. A description of the apparatus and techniques used will also be given.

* This work was based on studies conducted for the U. S. Atomic Energy Commission.
† North American Aviation, Inc., Atomic Energy Research Department, Downey, California.
‡ Now at Applied Radiation Corporation, Walnut Creek, California.
§ Now at NRDL, San Francisco, California.
|| Now at ORNL, Oak Ridge, Tennessee.

A7. Reversibility of the Additive Coloring Reaction in KCl.* D. R. WESTERVELT, *Atomic Energy Research Department, North American Aviation, Inc.*—Shamovsky, Rybakova, and Gosteva[1] recently have reported experiments which suggest that the additive coloring process is irreversible. This conclusion was based on observations that the *F*-center concentration obtained was independent of the metal used in coloring, hence, on the atomic concentration in the vapor; and that after coloring at one temperature further heating at a lower temperature did not result in a decrease in the *F*-center concentration. Because of the importance of these assertions, which tend to invalidate the present theory of additive coloring, some of the Russian experiments have been repeated. It was found that crystals of KCl colored in saturated K vapor at 575°C contained 3.0 times the *F*-center density of crystals colored at 520°C, but those colored first at 575°C and subsequently heated in the vapor at 520°C did not differ in concentration from those heated only at 520°C by more than 10 percent. Equilibrium was verified at each temperature. KCl colored in saturated K and Na vapors at 725°C agreed in *F*-center density within 50 percent, whereas the atomic concentrations in the vapor differ by a factor of 5. An explanation for this result is given within the framework of an extension of the equilibrium theory of the reaction between alkali metal vapor and alkali halides.[2] The results obtained thus do not confirm the reported irreversibility of the additive coloring reaction.

* This report is based on studies conducted for the U. S. Atomic Energy Commission.
[1] Shamovsky, Rybakova, and Gosteva, Doklady Akad. Nauk SSSR, **91**, 67 (1953).
[2] D. R. Westervelt, "Theory of the reaction between alkali metal and alkali halides," NAA-SR report (to be published).

A8. Application of the Engravement Method to the Study of Particle Velocity Distribution in Explosively Loaded Cylinders. JOHN PEARSON AND JOHN S. RINEHART, *Michelson Laboratory, U. S. Naval Ordnance Test Station.*—The engravement method for measuring high-intensity transient stress wave particle velocities in impulsively loaded bodies[1] has been used to study the particle velocity distribution in the walls of modified thick-walled metal cylinders internally loaded with explosive charges. Particle velocity measurements have been obtained to within ½ inch from the metal-explosive interface. Even though each of the modified cylinders broke into a number of fragments, the engravements were well enough preserved to furnish considerable data. Temporal and spatial particle velocity distribution curves have been obtained for cylinders of annealed low-carbon steel and brass.

[1] J. S. Rinehart and J. Pearson, J. Appl. Phys. **24**, 462 (1953).

A9. A Critical Angle Associated with High Speed Impact of a Sphere on a Thin Plate. WILLIAM A. ALLEN, JOE M. MAPES, AND WESLEY G. WILSON, *Michalson Laboratory, U. S. Naval Ordnance Test Station.*—Steel spheres ½ in. in diameter have been fired at velocities in excess of 3000 ft/sec through thin steel plates. The recovered projectile is marked by a series of concentric circular rings caused by lateral plastic deformation. All rings are characterized by radii $r > r_0(v)$, where r_0 is a critical radius that depends upon the velocity v of the sphere. Spacing of a given ring from its neighbor can be approximated by a term of an infinite geometrical series. The sum of the infinite series is used to determine the critical radius. This radius bears a relation to the critical angle obtained by a Los Alamos Scientific Laboratory group from another kind of experiment.[1] The phenomenon of the critical radius is explained by means of hydrodynamical concepts of compressible flow of steel treated as a fluid without viscosity or heat conduction. The experimental evidence has been compared with predictions from two published[1,2] theoretical equations of state for iron.

[1] Walsh, Shreffler, and Willig, J. Appl. Phys. **24**, 349 (1953).
[2] Pack, Evans, and James, Proc. Phys. Soc. (London) **60**, 1 (1948).

A10. Ablation from Ultra-Speed Pellets. WILLIAM C. WHITE, *Michelson Laboratory, U. S. Naval Ordnance Test Station.*—It has been observed on continuous motion picture photographs of ultra-speed pellets[1] that some of the ablated material appears as luminous streaks. These streaks were measured to determine the velocities of the ablated particles. From aerodynamic considerations, particle radii and masses were determined. A count of the number of streaks per unit path length yields ablated mass per unit length and rate of ablation.

[1] Allen, Rinehart, and White, J. Appl. Phys. **23**, 132 (1952).

A11. The Rittinger's Number for Several Minerals. M. E. BACKMAN AND H. L. MORRISON, *Michelson Laboratory, U. S. Naval Ordnance Test Station.*—Rittinger's number[1] is known for many common materials but is still undetermined for some minerals and ores. The values for five materials have been obtained using the method of Gross and Zimmerly[2] for determining the energy of fracture and a flow permeability method for obtaining the surface created during fracture. These values are as follows: volcanic breccia 15.2 cm²/kg cm, limestone 16.5 cm²/kg cm, an iron ore 6.0 cm²/kg cm, pyrophyllite 33.2 cm²/kg cm, and quartzite 11.2 cm²/kg cm. The method of measurement is reviewed, changes in equipment and details of the procedure are discussed.

[1] von Rittinger, *Lehrbuch der Aufbereitungskunde* (Berlin, 1867).
[2] J. Gross and S. R. Zimmerly, Am. Inst. Mining Met. Engrs. Tech Pub No. 126 (1928).

WEDNESDAY MORNING AT 9:30

Physics 320

(G. M. SHRUM, presiding)

Contributed Papers

B1. The Spectra of Indium. R. A. NODWELL AND A. M. CROOKER, *University of British Columbia.*—Approximately 350 indium lines have been measured in the spectral region from 1200A to 6900A. Many lines previously reported in indium I and indium II have been confirmed, and several lines not previously reported have been classified in indium II. Most of the lines measured are high excitation and attempts are being made to classify them in the indium III spectrum. An electrodeless discharge has been used as a source, and the light analyzed by means of a vacuum grating spectrograph in which the test sample is exposed through a slit with an angle of incidence at 80° and a comparison source is exposed simultaneously through a slit with angle of incidence at 21°, thus making it possible to compare the wavelength in the vacuum ultravoilet region directly with known wavelengths in the visible or near visible region.

B2. Spectra of Arsenic. R. E. BEDFORD AND A. M. CROOKER, *University of British Columbia.*—The spectra of arsenic in the visible and ultraviolet regions have been photographed with a 21-foot grating and a Littrow prism spectrograph using an electrodeless discharge. The wavelengths of approximately 1000 lines ranging from 2300–6500 A have been measured relative to iron standards. Many of these have previously been classified by A. S. Rao[1] and several others have been assigned to transitions in AsII, AsIII, and AsIV. From preliminary investigations it appears that the following new terms have been located in AsIII.

$4s^25g\ ^2G$	39.00 cm^{-1}
$6g\ ^2G$	27.535
$7g\ ^2G$	20.253
$6d\ ^2D_2$	37.223 (called $5g\ ^2G$ by K. R. Rao).[2]

In AsIV the multiplet $4s5d\ ^3D-4s6p\ ^3P$ has been identified leading to the new terms

$4s6p\ ^3P$	87.574 cm^{-1}
$^1P^0$	87.478
$^3P_2$	87.296.

Further analysis is currently in progress, including the photography of the spectra in the infrared and vacuum ultraviolet regions.

[1] A. S. Rao, Ind. J. Phys. **16**, 561 (1932).
[2] K. R. Rao, Proc. Phys. Soc. (London) **43**, 68 (1931).

B3. The g Factors of the ^3P Terms of Atomic Oxygen. K. KAMBE AND J. H. VAN VLECK, *Harvard University.*—Abragam and Van Vleck[1] have calculated the deviations of the g factors of the $2p^4\ ^3P$ terms of atomic oxygen from the simple Lande formula which arise from a variety of causes, *viz.*, relativity, spin-orbit interaction, diamagnetic screening, the motion of the nucleus, and the Schwinger quantum-electrodynamical correction. However, for simplicity they nelgected exchange and assumed that the charge distribution in which any $2p$ electron moves in centro-symmetric despite the fact that the three other $2p$ electrons do not really form a closed shell. The present paper refines the calculations by no longer making these two simplifying assumptions. The procedure consists in expanding the correction terms in the Hamiltonian in a finite series of spherical harmonics in a fashion very similar to that in the standard Slater expansion of $1/r_{ij}$. The diagonal matrix elements in the $1s^lm^lm_s$ system are first calculated, and those in the LSJM scheme obtained from the invariance of the diagonal sum. The most important integrals have already been computed for a Hartree-Fock self-consistent field by Hartree, Hartree, and Swirles,[2] while the remaining integrals have been estimated by employing modified Slater-type wave functions. We find $g(^3P_1)=1.500974$, $g(^3P_2)=1.500913$ to be compared with the experimental[3] values $g(^3P_1)=1.500971$, $g(^3P_2)=1.500905$.

[1] A. Abragam and J. H. Van Vleck, Phys. Rev. **92**, 1448 (1953).
[2] Hartree, Hartree, and Swirles, Trans. Roy. Soc. (London) **A238**, 229 (1939).
[3] E. B. Rawson and R. Beringer, Phys. Rev. **88**, 677 (1952).

B4. Magnetic Interactions in $^2\Sigma$ Molecules.* ROBERT L. WHITE,† *Columbia University.*—In a second-order approximation the electronic angular momentum of a rotating $^2\Sigma$ molecule is not zero. The associated magnetic field is on the same order of magnitude as the field arising from the rotation of the positively charged nuclear frame. The total resultant field interacts with the magnetic moments of the nuclei of the molecule to produce an interaction of the form $W_{mag}=[c_1+(c_2-c_1)K^2J^{-1}(J+1)^{-1}]\mathbf{I}\cdot\mathbf{J}$ for a nucleus on the symmetry axis of a symmetric top molecule. The c_i may be of either sign, depending upon both nuclear and molecular parameters. The algebraic values of c_i for the molecules $O^{17}CS$, OCS^{33}, $OCSe^{79}$, $Cl^{35}CN^{14}$, $Cl^{35}CN^{15}$, CH_3Cl, SiH_3Cl, and GeH_3Cl have been measured on a high resolution bridge-type microwave spectrometer. A correlation between measured and theoretical c_i for these molecules and for a number of others for which c_i is known (primarily from molecular beams data) will be given. The molecular parameters thus obtained will be compared with those inferred from molecular g factors and diamagnetic susceptibilities.

* This research supported jointly by the U. S. Army, U. S. Navy, and U. S. Air Force under contract with Columbia University.
† Present address, Hughes Research and Development Laboratories, Culver City, California.

B5. Ground-State Potential Constants of ClO_2.† J. K. WARD, *Agricultural and Mechanical College of Texas** (introduced by J. B. Coon).—Sufficient information is available to compute the four harmonic potential constants of the ground state of ClO_2. Coon's[1] ultraviolet rotational structure analysis furnishes $2\bar{B}''=0.612\pm0.003$, $2(\bar{B}'-\bar{B}'')=-0.0615\pm0.001$, and $2(A'-A'')=-1.250\pm0.006$ cm^{-1}; a least-square treatment of Nielsen and Woltz's[2] infrared rotational structure data yields $2(A''-\bar{B}'')=2.831\pm0.01$ cm^{-1}. From this data one obtains $2\theta''=117.4\pm0.2°$, $r_0''=1.472\pm0.005$A, $2\theta'=107.4\pm0.4°$, $r_0'=1.620\pm0.015$A. By using $2\theta''$ in conjunction with $\omega_1''=964.8$, $\omega_2''=451.8$, and $\omega_3''=1127.3$ cm^{-1} given by Coon and Ortiz,[3] and one isotope shift $\Delta\omega_1''=-6.41$ cm^{-1},[4] the ground-state valence potential constants are determined: $k=6.990$, $k_\theta=0.649$, $k_1=-0.191$, $k_2=-0.035\times(10)^5$ dyne-cm^{-1}. Poor agreement exists with potential constants determined using three ground-state frequencies and the criterion of Glockler and Tung:[5] $k=7.411$, $k_\theta=0.803$, $k_1=0.230$, $k_2=0.930\times(10)^5$ dyne-cm^{-1}. Disagreement also exists with the prediction of Duchesne and Nielsen[6] that k_1 and k_2 should be positive.

† This research was supported by the U. S. Air Force through the Office of Scientific Research of the Air Research and Development Command.
* Now at Boeing Airplane Company, Seattle, Washington.
[1] J. B. Coon, J. Chem. Phys. **14**, 665 (1946).
[2] A. H. Nielsen and J. H. Woltz, J. Chem. Phys. **20**, 1878 (1952).
[3] J. B. Coon and E. Ortiz, Phys. Rev. **82**, 766 (1951).
[4] J. B. Coon (to be published).
[5] G. Glockler and J.-Y. Tung, J. Chem. Phys. **13**, 388 (1945).
[6] J. Duchesne and A. H. Nielsen, J. Chem. Phys. **20**, 1968 (1952).

B6. Polarized Infrared Absorption Spectrum of Gypsum. D. S. WEBBER, *University of California, Los Angeles.*—The absorption spectrum of gypsum, $CaSO_4 \cdot 2H_2O$, has been obtained in the region from 3000 cm^{-1} to 9000 cm^{-1} using polarized radiation. A detailed analysis of the structure observed in the broad water band in the 3000 cm^{-1} to 4000 cm^{-1} region is reported in this paper. The high-resolution prism grating spectrometer described by Lyon and Kinsey[1] was used in this work. Polarization was achieved with a pile of selenium films placed in front of the exit slit of the spectrometer. The samples were placed just behind the exit slit. This arrangement of polarizer and sample eliminates spurious polarization effects. Samples were prepared with faces parallel to the perfect cleavage plane in the gypsum. Components of the band have been identified with the fundamentals of the symmetric and asymmetric stretching modes and the first overtone of the bending mode of water. Other components have been interpreted as bands caused by the couplings of three hindered translations and two hindered rotations with the molecular vibrations of the water molecule.

[1] W. K. Lyon and E. L. Kinsey, Phys. Rev. **61**, 482 (1942).

B7. Energy Parameters of Two-Dimensional Graphite. G. S. COLLADAY, *Michelson Laboratory, U. S. Naval Ordnance Test Station.*—In the theoretical study of the 2-dimensional model of graphite[1,2] certain energy parameters, E_0, γ_0, γ_0', occur which cannot be explicitly evaluated due to a lack of knowledge concerning the lattice potential function. These parameters are evaluated by combining the energy expression $E(\mathbf{K})$ for the valence π electrons with experimental data, e.g., work function of graphite, soft x-ray emission spectrum, thermochemical data. In calculating $E(\mathbf{K})$, first and second nearest neighbors have been included in the overlap and resonance integrals.

[1] P. R. Wallace, Phys. Rev. **71**, 622 (1947).
[2] C. A. Coulson and R. Taylor, Proc. Phys. Soc. (London) **A65**, 815 (1952).

B8. Thermal Conductivity of Single Crystalline Silicon. G. W. HULL AND T. H. GEBALLE, *Bell Telephone Laboratories.*—Measurements of the thermal conductivity k of single crystal silicon have been made from liquid hydrogen temperatures to room temperature on a filament cut from a crystal pulled in the (100) direction. Analysis of Hall data for this crystal indicates a total impurity concentration of 10^{-4} atom percent. A room temperature value of $k = 1.48$ watt units for this sample is to be compared with the current literature value of 0.84 watt units. k rises to a value of 9 at 80°K and 19.5 at 30°K with no sign of reaching its maximum value. The relative thermal conductivities of a series of samples in which arsenic atoms have been added up to 0.05 atom percent as determined by Hall measurements have also been observed. Isotherms of k decrease rapidly in the concentration range above 10^{-4} atom percent, while there seems to be little variation in k at lower concentrations even at 30°K. The room temperature value of k for the 0.05 atom percent sample is down to 0.90 watt unit; at 75°K it is less by a factor of 5 than k for the 10^{-4} atom percent sample.

B9. Seebeck Effect in Single Crystal Silicon. T. H. GEBALLE AND G. W. HULL, *Bell Telephone Laboratories.*—The Seebeck effect has been investigated in single crystal silicon as a function of excess concentration of charge carriers produced by addition of arsenic atoms. Measurements have been made from liquid hydrogen temperatures to above room temperature and compared with Hall data for the same samples. The results show a very large rise in Q, the Seebeck voltage per degree difference between junctions, as the temperature decreases. This is the same behavior previously observed in germanium.[1] The large values of Q are attributed to the type of phonon-electron interaction postulated for germanium. A sample of large dimension in which boundary scattering effects are reduced reaches a value of 59 millivolts per degree at 30°K and varies as $T^{-2.1}$. Consideration of the Hall data indicates that the $T^{-2.1}$ behavior is approximately characteristic of the phonon-electron interaction all the way to room temperature. Q passes through zero and becomes positive below 13°K for a sample with 2.2×10^{18} arsenic atoms per cc. This together with an abnormal drop in Hall mobility at 16°K previously observed by Morin and Maita[2] for the same sample suggests impurity band conduction.

[1] T. H. Geballe and G. W. Hull, Phys. Rev. (to be published).
[2] F. J. Morin and J. P. Maita, Phys. Rev. (to be published).

B10. Dependence of Signal-to-Noise Ratio in Photoconductive PbSe Layers on the Temperature of the Black-Body Source.* A. M. CROOKER AND E. B. DORLING, *University of British Columbia.*—We have prepared sensitive PbSe photoconductive cells and measured the signal/noise ratio obtained with a black body source at 200°C and 500°K. This experiment has been done with the cell at room temperature and at liquid air temperature. The results are compared with what one calculates assuming that the long wave cutoff of the cell is linear and that this cutoff shifts as reported by Moss.[1]

* This work is supported by the Defence Research Board, Ottawa.
[1] T. S. Moss, Proc. Phys. Soc. (London) **B62**, 741 (1949); **B63**, 167 (1950).

B11. Microwave Properties of Manganese-Ferrite Single Crystal.* P. E. TANNENWALD, *M.I.T.*—Resonance absorption and anisotropy measurements have been carried out on a single crystal of Mn-ferrite (~10 ohm-cm resistivity) between room temperature and 4.2°K. A 0.42-mm sphere was rotated in an X-band waveguide-type cavity in such a way that the dc magnetic field always lay in a (110) plane of the crystal but along different crystallographic axes. At room temperature the dispersion has also been measured, and the Kramers-Krönig relations are found to be satisfied. Comparison of the real and imaginary parts of the susceptibility with the Bloch-Bloembergen theory gives fair agreement. ΔH, the full width at half-power absorption, decreases from 260 oersteds at 20°C to 130 oersteds at 4.2°K and is the same in the three principal crystal directions at each temperature. The anisotropy increases sharply as the temperature is lowered but decreases again slightly below 77°K. The g factor is practically constant at a value of 2.00. A secondary peak has been observed at low temperatures and in certain crystal directions. Details of this peak will be presented and its possible origin will be discussed.

* Supported jointly by the U. S. Army, Navy, and Air Force under contract with the Massachusetts Institute of Technology.

B12. Fermi-Dirac Degeneracy in Liquid He^3 below 1°K.* W. M. FAIRBANK, W. B. ARD, G. K. WALTERS, *Duke University.*—The temperature dependence of the nuclear magnetic susceptibility of liquid He^3 has been measured directly down to 0.2°K. by observing the strength of the nuclear magnetic resonance absorption signal. These measurements give an answer to the much discussed question of the extent to which liquid He^3 behaves as an ideal Fermi-Dirac gas. At sufficiently low temperatures the spins of the particles of an ideal Fermi-Dirac gas would be expected to line up antiparallel and this would cause the spin magnetic susceptibility to deviate from the classical $1/T$ law and finally to become temperature-independent. Previous measurements by us[1] indicated than no measureable degeneracy occurs in liquid He^3 down to 1.2°K, although the calculated degeneracy temperature for an ideal Fermi-Dirac gas of the same atomic mass and density as liquid He^3 is 4.7°K. The present measurements indicate that below 1°K the nuclear spins of the liquid He^3 begin to line up antiparallel with the same temperature dependence as an ideal Fermi-Dirac gas with a degeneracy temperature of 0.45°K. At 0.25°K the He^3 nuclei are approximately 40 percent antiparallel aligned. The temperature was independently checked by the nuclear resonance signal from protons in a salt in contact with the He^3.

* Work supported by a contract with the Office of Ordinance Research, U. S. Army.
[1] Fairbank, Ard, Dehmelt, Gordy, and Williams, Phys. Rev. **92**, 208 (1953).

WEDNESDAY MORNING AT 9:30

Physics 334

(F. N. FRENKIEL, presiding)

Contributed Papers

C1. Hot-Wire Measurements of Turbulence in the Ocean. R. W. STEWART, *Pacific Naval Laboratory.*—Ordinary constant temperature hot-wire anemometry techniques have been adapted to measure oceanic turbulence. Two channels have been built so that cross correlation studies are possible and Pacific Naval Laboratory's very large playback/record speed ratio tape recorder has been employed for measurements of spectra. Some preliminary results have been obtained in inshort waters.

C2. Metastable Jet-Tone States of Jets from Sharp-Edged, Circular, Pipe-Like Orifices. A. B. C. ANDERSON, *Naval Ordnance Test Station.*—Characteristics of spectra from relatively thick orifices differ from those from relatively thin. In a given range of Reynolds number, the jet may often exist in any one of several reproducible jet-tone states (metastable states) characteristic of the orifice. The dependence of the component frequencies of the jet-tone spectra (expressed in terms of the orifice-number $fd/(\Delta p/\rho)^{\frac{1}{2}}$ on Reynolds number $[\rho d/(\Delta p/\rho)^{\frac{1}{2}}]/\mu$ is shown, where d is diameter of orifice; f, frequency; Δp, pressure difference across orifice; ρ, density; and μ, viscosity of gas. The orifice numbers of the components of the jet-tone spectra generally tend to fall on the orifice-number levels of a single array of equally spaced orifice-number levels. Jet tones from the same orifice plates, characteristic of both thin as well as thick orifice plates, are found to coexist over a small transition range of orifice thickness-diameter ratio. If the orifice number of the head of the most probable mode for a given orifice thickness-diameter ratio is noted, the same will be found again for the head of the most probable mode at approximate orifice thicknesses $t \pm nd$, where n is a small integer.

C3. The Transition Through a Contact Region. J. G. HALL, *Institute of Aerophysics, University of Toronto* (introduced by G. N. Patterson).—An approximate treatment is given of temperature and density transition through the one-dimensional contact region of shock tube flows. The simple model considered is a homogeneous gas having step change in density and temperature but constant pressure at time zero. Behavior for subsequent time is determined from the three conservation equations for a viscous, compressible, heat-conducting gas. Simplifying assumptions are ideal gas, zero body forces, linear viscosity-temperature relation, and negligible pressure change. For very weak transitions, complete linearization of the differential equations gives spacially monotonic and antisymmetric temperature and desnity change with the transition region spreading as the square root of time. For stronger transitions, a von Mises transformation followed by linearization in the transformed plane leads to closed solutions exhibiting nonlinear effects in the physical plane. Nonlinearities give asymmetric temperature and density change; the square root of time growth becomes dependent on the initial discontinuity. Experimental shock-tube results are noted for two types of contact regions. Piezocrystal pressure recordings indicate pressure effects as slight. Experimental density transitions from interferometry are compared to theory where possible. Agreement is qualitatively good for the weak transitions studied.

C4. The Incompressible Laminar Boundary Layer on a Spinning Cylinder at Small Angles of Attack. HOWARD R. KELLY, *U. S. Naval Ordnance Test Station.*—An approximate solution is found for the Navier-Stokes equations for the boundary-layer flow along a cylinder spinning slowly on its axis, including the case where the free stream is inclined at a small angle α to the cylinder axis. By a perturbation method, the velocity profiles and displacement effects are evaluated to second order in α and in the spin ω. The effects of wall curvature are treated in much the same manner as was done by Seban and Bond.[1] The velocity profiles are described in terms of a dimensionless parameter η, analogous to that used by Blasius.[2] The results of this study are basic to a better understanding of the aerodynamics of bodies of revolution.

[1] Seban and Bond, J. Aeronaut. Sci. **18**, No. 10, 671 (1951).
[2] Blasius, Math. Phys. Bd. **56**, 1 (1908).

C5. The Displacement Effect of a Three-Dimensional Boundary Layer of Moderate Thickness. ELDON L. DUNN AND HOWARD R. KELLY, *U. S. Naval Ordnance Test Station.*—A method is developed for determining the "displacement surface" of a known three-dimensional compressible boundary layer flow in terms of the mass-flow defects associated with the profiles of the two velocity components parallel to the body surface. The results are given in a form for use in any coordinate system, and are applicable for boundary layers of moderate thickness. The development parallels that of Moore,[1] whose results are given in Cartesian coordinates and are applicable only in the case of an extremely thin boundary layer. Using generalized orthogonal coordinates x_1, x_2, x_3 with scale factors e_1, e_2, e_3, the general relation between the displacement surface and the mass-flow defects is given by

$$\frac{\partial}{\partial x_1}\left[\int^{\Delta} \rho_1 e_2 e_3 u_1 dx_2 - \delta x_1\right] + \frac{\partial}{\partial x_3}\left[\int^{\Delta} \rho_1 e_1 e_2 w_1 dx_2 - \delta x_3\right] = 0,$$

where δx_1 and δx_3 are quantities characterizing the mass-flow defects, $x_2 = \Delta$ is the displacement surface, u and w are velocity components in the x_1 and x_3 directions, respectively, ρ is density, and $x_2 = 0$ is the equation of the body surface. The subscript 1 refers to conditions of inviscid flow. Applications of the method are considered for shapes of interest in aerodynamic theory.

[1] Franklin K. Moore, Natl. Advisory Comm. Aeronaut. NACA Report 1124 (1953).

C6. Response of Pressure Gauges to Dust-Laden Shock Waves. J. R. BANISTER AND C. D. BROYLES, *Sandia Corporation.*—A series of shock tube studies demonstrate that two types of pressure gauges respond to dust carried with shock waves by indicating an increase in dynamic pressure. This contribution to the dynamic pressure is approximately the product of the dust density and the square of the dust velocity under the experimental conditions. Besides this information the studies give insight into the interaction of a square shock wave with dust when that dust is placed in a plane before and parallel to the shock front. It is found that the shape of the pressure wave is little changed except for a rounding of the front. The dust, after accelerating, is carried as a pulse with the mass flow velocity of the air.

C7. The Shape of a Shock Wave Derived from a Spherical Shock Wave Incident on a Concave Wedge. JAY TODD, JR., AND RALPH SCHELLENBAUM, *Sandia Corporation.*—A 13.5-gram charge is detonated above a rigid plane which is

bounded by a second plane making an angle of 5.7° with the first. This forms a concave wedge with an interior angle of 174.3°. Successive shadowgraph pictures of the shock were obtained near the intersection of the two planes. The shape of the diffracted wave differs slightly from that found in the similar case for plane shocks,[1] in that the Mach stem is less highly concave. This is accentuated as the wave progresses up the plane until the curvature is reversed. The data are sufficiently accurate to permit a determination of shock strength as a function height above the inclined plane.

[1] D. R. White, "An experimental survey of the Mach reflection of shock waves," Princeton Department of Physics, Tech. Report II-10, August 21, 1951.

C8. Two-Fluid Flow with Application to Dust-Laden Air. M. L. MERRITT AND J. R. BANISTER, *Sandia Corporation.*—We wish to consider the flow of two mutually interfering and interpenetrating fluids of different equations of state and different heat contents. Such a two-fluid flow might be that of air carrying a dust burden. If the two are constantly in thermal equilibrium and move with the same velocity (this implies that the dust is of small size, and that one does not examine too small intervals of time) it is possible to write equations expressing their joint equation of state, hydrodynamic flow, shock flow, etc. The effective γ of the combination is reduced, the density increased, the heat content per volume increased, and the resultant velocity of sound decreased. If the two fluids are not in thermal and momentum equilibrium. they will interact with each other so as to approach that equilibrium. The hydrodynamic equations of the combination are twice as many in number. The velocity of sound in the mixture is but little reduced. The effect on the shock conditions is similar to those of the relaxation effects of CO_2 and of hydrocarbon gases, that is, the pressure first jumps as if the noncontributing fluid were not there then adjusts flow to the presence of the other. The most direct check of these ideas will be the experimental study of the velocity of sound in a two-fluid situation and a study of shocks passing through them.

C9. Path of Triple Point for Spherical Shocks Above a Rigid Plane. RALPH SCHELLENBAUM AND JAY TODD, JR., *Sandia Corporation.*—Lincoln Smith[1] has shown that similarity solutions are valid in the case of plane shocks incident on a wedge. As a consequence the path of the triple point is a straight line. The angle between this line and the surface of the wedge (X) is a function of the shock strength and the angle of incidence. During the course of experiments at Sandia Corporation the path of the triple point for spherical waves incident on a flat plane has been measured. Comparisons are made between the slope of this trajectory and X as determined by Lincoln Smith for plane waves.

[1] OSRD-6271.

C10. On the Stability of the Spherical Shape of a Vapor Cavity in a Liquid.* M. S. PLESSET AND T. P. MITCHELL, *California Institute of Technology.*—The stability of the spherical shape of a gas bubble in a liquid is investigated for the case in which the difference between the pressure in the bubble p_i and the pressure in the liquid p_0 is constant. These conditions apply approximately to a vapor bubble growing ($p_i > p_0$) or collapsing ($p_i < p_0$) in a liquid at constant external pressure. The general solution for the behavior of a small deformation in the spherical shape of the cavity is readily obtained when surface tension is neglected. For a growing bubble, the deformation increases slowly and monotonically; for a collapsing bubble, the deformation oscillates with small amplitude until the mean radius of the bubble approaches zero when the magnitude of the deformation increases rapidly. The consistency and applicability of the small amplitude theory for a significant range of bubble radius change is demonstrated. A solution may also be obtained which includes the effect of surface tension. In this case the distortion amplitude decreases monotonically for the expanding bubble; the singularity in the distortion amplitude for the collapsing bubble for small radius persists.

* This study was supported by the U. S. Office of Naval Research.

C11. Free Molecule Flow of a Nonuniform Gas. S. BELL AND S. A. SCHAAF, *University of California.*—Heat transfer and aerodynamic force characteristics of a cylinder are calculated for the case of free molecule flow of a nonuniform monatomic gas, i.e., a gas which is not in Maxwellian equilibrium but which has viscous stresses and heat flux present. It is shown that a shear stress will induce an aerodynamic lift and that a heat flux produces a force (the "radiometer" force) in the direction of the heat flux. These nonuniformities also affect the heat transfer to the cylinder and its equilibrium temperature. Applications to the use of small wires for supersonic wind tunnel probes are discussed. This work was sponsored by the U. S. Office of Naval Research and the U. S. Office of Scientific Research.

WEDNESDAY AFTERNOON AT 2:00

Health Sciences Auditorium

(S. H. NEDDERMEYER, presiding)

Cosmic Rays and High Energy Physics

Invited Papers

D1. Experimental Findings at the Brookhaven National Laboratory. C. N. YANG, *Institute for Advanced Study, Princeton.* (30 min.)

D2. The Identification of Heavy Mesons. W. B. FRETTER, *University of California, Berkeley.* (30 min.)

D3. Recent Results on *V*-Particles. R. W. THOMPSON, *Indiana University.* (30 min.)

D4. *V*-Particles with Neutral Secondaries. E. W. COWAN, *California Institute of Technology.* (30 min.)

THURSDAY MORNING AT 9:00

Guggenheim Hall

(R. F. CHRISTY, presiding)

Medium Energy Nuclear Physics

Invited Papers

E1. Investigations with the University of Washington Cyclotron. F. H. SCHMIDT, *University of Washington.* (30 min.)

E2. Deuteron Reaction Studies with the Pittsburgh Cyclotron. R. S. BENDER, *University of Pittsburgh.* (30 min.)

E3. Elastic Scattering of Protons by Medium and Heavy Nuclei. P. C. GUGELOT, *Princeton University.* (30 min.)

E4. Cross-Section Measurements with 29-Mev Nitrogen Ions. ALEXANDER ZUCKER, *Oak Ridge National Laboratory.* (30 min.)

THURSDAY MORNING AT 9:00

Physics 320

(C. L. UTTERBACK, presiding)

Contributed Papers

F1. Hf and Zr Total Cross-Section Measurements.* E. G. JOKI AND J. E. EVANS, *Atomic Energy Division, Phillips Petroleum Company.*—The MTR crystal spectrometer has been used to measure σ_t from 0.04 to 10 ev with a Hf metal sample. Our measurements give 92.4b at 0.4 ev and 64.4b at 0.1 ev which are lower than corresponding Harwell data.[1] A possible explanation for the discrepancy will be discussed. The new data are consistent with the tabulated thermal value of 123±15b in U. S. Atomic Energy Commission AECU-2040. The energies of the first two resonances have been measured to be 1.095±0.005 and 2.378±0.016 ev, consistent with the recent work of Bollinger *et al.*[2] Single level Breit-Wigner parameters, corrected for Doppler broadening and instrument resolution, will be given. σ_t for Zr is essentially flat at 6.2b from 0.02 to 60 ev. These results are lower than Harwell results[1] but agree with recent Argonne fast chopper results.[3] The sample used was 18.9 g/cm² of Zr metal which contained 400 ppm by weight of Hf.

* Work carried out under the auspices of the United States Atomic Energy Commission.

[1] Egelstaff and Taylor, Nature **167**, 896 (1951).
[2] Bollinger *et al.*, Phys. Rev. **92**, 1527 (1953).
[3] Progress Report, Argonne National Laboratory Report ANL-5140, November 1953.

F2. Contour Diagrams of Thermal Neutron Absorption Cross Sections*. J. E. EVANS, *Atomic Energy Division, Phillips Petroleum Company.*—Separate contour diagrams showing lines of equal thermal neutron absorption cross sections have been drawn for nuclei having even-even, even-odd, odd-even, and odd-odd numbers of protons and neutrons. In general, the higher neutron cross sections are found to occur for the neutron-poor and proton-rich nuclei. A striking feature of the study is that in nearly all cases there is a gradual change of cross section values from one nucleus to an adjacent nucleus of the same type. The most outstanding exception is the Xe^{135} nucleus, which lacks one neutron of having a magic number (or closed shell) of neutrons. The diagrams should prove helpful in estimating cross sections of nuclei for which no measurements exist if the cross sections for some of its neighbors are known. Some possible implications of the study to nuclear theory are discussed.

* Work carried out under the auspices of the U. S. Atomic Energy Commission.

F3. MTR Crystal Spectrometer Data Printing System.* G. L. SMITH AND L. G. MILLER, *Atomic Energy Division, Phillips Petroleum Company.*—Operating automatically, the MTR Crystal Spectrometer can accumulate up to 1500 separate counting meausrements with 0.3 percent statistics in a week-end period. This imposes a serious data handling problem. A data printing system using glow-transfer counters and an electric typewriter has been installed to replace the commercial scaler and traffic counter system. The 1-microsecond scaler has scales of 1 to 16 preceding the 6 glow-transfer counters. After a count, a motor driven scanning switch connects the 10 points of each glow-transfer tube simultaneously through triode-operated relays to the solenoid actuators of the 10 numbers on the typewriter. Only the point having the glow discharge will record. The system will handle up to 10^6 cpm and print 6 digits without the attendant short lifetimes of electric reset registers and traffic counters. In addition, the scaling factor, time, crystal position, arm angle, and sample wheel position are printed on folded and perforated teletype sheets which are later bound to form a permanent record. A special spacing is used which permits calculations to be made on the data sheets without data transfer.

* Work done under the auspices of the U. S. Atomic Energy Commission.

F4. The Photoproduction of Charged Mesons from Deuterium.* M. SANDS, J. G. TEASDALE, AND R. L. WALKER, *California Institute of Technology.*—The yield of charged mesons of each sign produced in a high-pressure deuterium target by the x-ray beam of a 500-Mev synchrotron has been measured at 73°, laboratory angle, for several meson energies. Mesons were selected by the magnetic spectrometer used previously in this laboratory.[1] The preliminary results for the ratio of the yield of negative mesons to that of positive mesons

are given in the table. The mesons observed are those which would be produced at an angle of 90° in the center-of-momentum system of a photon of energy "k" and a single nucleon initially at rest.

T_π(Mev, lab)	43	71	103	147	200
N_-/N_+	1.25 ±0.03	1.15 ±0.03	1.09 ±0.02	1.13 ±0.03	1.16 ±0.07
"k" (Mev)	207	247	293	363	451

Ratios measured at laboratory angles of 29° and 140° will also be reported.

* Supported in part by the U. S. Atomic Energy Commission.
[1] Walker, Teasdale, and Peterson, Phys. Rev. 92, 1090 (1953).

F5. Photostar Production Up to 500 Mev.* VINCENT PETERSON, *California Institute of Technology.*—The production of stars in G-5 nuclear emulsions by high-energy bremmstrahlung photons is being studied for various maximum synchrotron energies (k max) up to 503 Mev. The beam was monitored by a thick wall Cornell-type ionization chamber whose energy sensitivity varies slowly with k(max). The total star yield was counted and corrected for measured scan efficiency and pre-exposure background. Results obtained from several runs give for the integral cross section for producing stars of 3 or more prongs (errors are standard deviations):

k max in Mev	σ (mb per equiv. quantum)
309	2.85 ±0.30
376	4.60 ±0.34
420	5.11 ±0.30
503	5.95 ±0.35

The excitation function per photon *vs* photon energy may be derived from the integral curve. The data are consistent with, but do not necessarily prove that, the photostar cross section exhibits the resonance shown by the free nucleon photomeson production cross sections.

* This work was supported in part by the U. S. Atomic Energy Commission.

F6. Photoproduction of Mesons from Hydrogen Near Threshold.* VINCENT PETERSON AND I. GEORGE HENRY, *California Institute of Technology.*—Mesons produced by 500-Mev bremsstrahlung photons incident upon a high-pressure hydrogen gas target were observed at laboratory angles of 30°, 51°, 73°, 104°, and 140°. Tungsten slits defined the target volume, and the low-energy mesons were detected at the end of their range in C-2 nuclear emulsions. Corrections for decay, nuclear absorption, slit penetration, and scattering from collimator walls are small. Duplicate scanning reduced efficiency corrections below 5 percent. Measured meson background was 1½ percent. Minimum detectable target meson energy is 11.3 Mev at 73°. The absolute cross section at this angle, measured continuously between 167- and 233-Mev photon energy with ~10 percent statistics per point, is in good agreement with the CIT counter data[1] taken above 200 Mev. Below 200 Mev the data furnishes additional evidence[2] for preponderance of S-wave interaction, as does the angular distribution at 187 Mev. The yield of negative (i.e., star producing) mesons at 73° is 11±2 percent of the positives, with negligible background. Analyzed gas impurities appear to account for less than 1 percent. The negative mesons energies are dynamically allowed by pion-pair production.

* This work was supported in part by the U. S. Atomic Energy Commission.
[1] Walker, Teasdale, and Peterson, Phys. Rev. 92, 1090(A) (1953).
[2] G. Bernardini and E. L. Goldwasser, Phys. Rev. 94, 729 (1954).

F7. The High-Energy Photodisintegration of the Deuteron. Procedure.* A. V. TOLLESTRUP, J. C. KECK, and W. R. SMYTHE, II, *California Institute of Technology.*—The reaction $\gamma+D\rightarrow p+n$ is being investigated in the energy region from 100 to 450 Mev at laboratory angles from 38 to 160 degrees. A high-pressure low-temperature deuterium gas target is irradiated by 500-Mev synchrotron x-rays, and the emitted protons are identified by their ionization and range in a scintillation counter telescope. The proton energy, as determined by its range in copper, and the angle of emission fix the energy of the interacting photon. Energy momentum considerations serve to exclude the disintegrations in which free mesons are produced. Care must be taken to exclude those protons produced by other particles in the material of the telescope and also a correction for nuclear absorption of the protons in the wall of the target and in the telescope must be made. Backgrounds obtained with the target evacuated were in general ess than 5 percent.

* This work was supported in part by the U. S. Atomic Energy Commission.

F8. The High-Energy Photodisintegration of the Deuteron. Results.* J. C. KECK, A. V. TOLLESTRUP, AND W. R. SMYTHE, II, *California Institute of Technology.*—The photodissociation of the deuteron is being investigated by the technique described in the preceding paper. Measurements of the differential cross section in the center-of-mass system have been made for angles of 170, 150, 130, 110 degrees for photon energies in the laboratory system from 100 to 450 Mev. The energy distributions at a given angle are characterized by a weak minimum at 150 Mev followed by a maximum at 250 Mev. At 450 Mev the cross section is a factor of 5 smaller than at the maximum. The cross section decreases from 110° to 170° at all energies. The magnitude of the cross section at 250 Mev and 110 degrees is 5 ub/ster in agreement with results of workers at Cornell. The results suggest a connection with the process of photomeson production which may be interpreted in terms of the idea of an excited state of the nucleon which can decay either by meson production or collision with the second nucleon in the deuteron.

* This work was supported in part by the U. S. Atomic Energy Commission.

F9. Magnetic Analysis of the $O^{18}(d,p)O^{19}$ and $N^{15}(d,p)N^{16}$ Reactions.* JACQUES THIRION, RENÉ COHEN, AND WARD WHALING, *Kellogg Radiation Laboratory, California Institute of Technology.*—Enriched isotopic targets have been used with a double focusing magnetic spectrometer to measure the energy of the protons emitted from the (d,p) reactions with O^{18} and N^{15}.[1] At $\theta=140°$ and deuteron bombarding energy 2.18 Mev, three groups of protons were observed from the $O^{18}(d,p)O^{19}$ reaction with Q values 1.732±0.008, 1.632±0.008, and 0.263±0.010 Mev. More energetic proton groups were not observed, and we attribute these Q values to the ground state and excited states at 0.100 and 1.469 Mev in O^{19}. The proton spectrum shows no other states in O^{19} with excitation energy $\lesssim$2.4 Mev. At $\theta=60°$ and deuteron bombarding energy 2.0 Mev three proton groups were observed from the $N^{15}(d,p)N^{16}$ reaction with preliminary Q values 0.158, −0.022, and −0.118 Mev. These Q values indicate a level spacing in N^{16} similar to that found by Ahnlund and Meleikowsky[2] for the first, second, and third excited states of N^{16}. Further work is in progress to observe more energetic protons accompanying the ground-state transition in the presence of an interfering group of protons from the $N^{14}(d,p)N^{15}$ reaction.

* Assisted by the joint program of the U. S. Office of Naval Research and the U. S. Atomic Energy Commission.
[1] We are indebted to A. O. C. Nier for furnishing the enriched O^{18}.
[2] Curt Meleikowsky (private communication).

F10. An Easily Reproducible Thermal Neutron Density Standard. RENÉ COHEN,* *Centre d'Etudes Nucléaires de Saclay.*—The use of a copper foil whose thickness is greater than the range of the ^{64}Cu β particles with a 4π beta counter enables one to have a very reproducible (±1.5 percent) standard of thermal neutron density. The standard thermal density we

use is such that once established in a copper disk of 15.00-mm diameter and 500 mg cm^{-2} thick[1] it produces a saturated β activity (^{64}Cu) which produces 1 pulse per second when measured in a 4π counter. This standard density as measured in absolute value at Saclay is equal to $(5.70\pm0.19)\cdot10^{-3}$ n. cm^{-3}. The use of this standard facilitates the intercalibration of absolute measurements.[2]

* Present address: Kellogg Radiation Laboratory, California Institute of Technology, Pasadena, California.
[1] The activity increases by less than 1 percent for an increase of 50 ug cm^{-2}.
[2] D. J. Hughes, Pile Neutron Research (Addison-Wesley, Cambridge, 1953); A. Wattenberg, Ann. Rev. Nuclear Sci. 3, 119 (1953).

F11. Hole Configurations in Light Nuclei.* R. F. CHRISTY AND W. A. FOWLER, *Kellogg Radiation Laboratory, California Institute of Technology.*—The low-energy (114 kev) negative parity ($\frac{1}{2}^-$) excited state[1] in F^{19} points to a need to reexamine the shell model in this region. We consider this state as a proton hole in the $p_{\frac{1}{2}}$ shell with four (s,d) particles coupled to $T=J=0$ outside it. We estimate the energy of the $\frac{1}{2}^-$ state in F^{19} from the ground-state energy of Ne^{20} and the binding of the last $p_{\frac{1}{2}}$ proton given by the $N^{15}-O^{16}$ mass difference, so $M_{19}(\frac{1}{2}^-)=M_{20}-M_{16}+M_{15}$. This neglects the change in kinetic energy and the change in the $p-(s,d)$ interaction and gives a $\frac{1}{2}^-$ state $\frac{3}{4}$ Mev below the ground state of F^{19}, accounting for a low $\frac{1}{2}^-$ state. Similarly, the series of excited states, O^{16}(O^+ at 6.05 Mev), O^{17}($\frac{1}{2}^-$ at 3.07 Mev), F^{17}($\frac{1}{2}^-$ at 3.10 Mev), F^{19}($\frac{1}{2}^-$ at 0.114 Mev) and Ne^{20}(O^+ ground state) may be considered as the addition of four (s,d) particles to the ground states of C^{12}, C^{13}, N^{13}, N^{15}, O^{16}, respectively. There results a series of numbers for the binding of the four particles which increases by only 3.5 Mev from C^{12} to O^{16}.

* Assisted by the joint program of the U. S. Office of Naval Research and the U. S. Atomic Energy Commission.
[1] Peterson, Thirion, Sherr, and Christy, Phys. Rev. **94** (to be published).

F12. Elastic Scattering of Protons by F^{19}.† T. S. WEBB, F. B. HAGEDORN, W. A. FOWLER, AND C. C. LAURITSEN, *Kellogg Radiation Laboratory, California Institute of Technology.*—The differential cross section for the elastic scattering of protons by F^{19} has recently been measured using magnetic analysis of the protons scattered by thick targets of LiF. Measurements have been made for proton energies from 0.55 to 1.8 Mev at scattering angles of 90°; 125°18′ and 159°46′ in the center-of-mass system. Marked anomalies have been observed at proton energies corresponding to known gamma-ray resonances at $E_p=0.669$; 0.831; 0.874; 0.935; 1.355; 1.381; 1.431; and 1.69 Mev. The behavior of the cross section off resonance is approximately in agreement with the calculated Rutherford cross section. Further experimental work is planned to cover forward scattering angles and a more detailed investigation of these regions where known gamma-ray resonances occur which did not give sufficient scattering anomalies to be conclusively identified. In addition, theoretical analysis of the data has been started.

† Assisted by the joint program of the U. S. Office of Naval Research and the U. S. Atomic Energy Commission.

F13. Inelastic Proton Scattering Cross Section of F^{19}.† C. A. BARNES, W. A. FOWLER, C. C. LAURITSEN, AND R. W. PETERSON, *Kellogg Radiation Laboratory, California Institute of Technology.*—The excitation functions of the 114 kev and 200 kev gamma rays, resulting from inelastic scattering of protons by fluorine,[1] have been studied with NaI scintillation counters from 330-kev to 1750-kev bombarding energy. Most of the well known high-energy gamma ray, nuclear pair, and long-range alpha particle resonances appear as resonances for one or both of the low-energy gamma rays. Cross sections for some of the prominent resonances are given in the table, superseding the approximate values given in reference 1. The cross sections for the other observed resonances will be reported. Observation of the inelastically scattered protons yields $\sigma_{114}=(1.9\pm0.2)\times10^{-25}$ cm^2 at 1431 kev, and $\sigma_{200}=(4.3\pm0.4)\times10^{-28}$ cm^2 at 1381 kev, in good agreement with the gamma-ray results.

Proton Energy	(kev)	873	935	1381	1431
$\sigma_{114\ kev}$	(cm^2)	$<10^{-27}$	$(1.3\pm0.3)\times10^{-25}$	$(2.4\pm0.5)\times10^{-25}$	$(1.7\pm0.3)\times10^{-25}$
$\sigma_{200\ kev}$	(cm^2)	$(9\pm2)\times10^{-26}$	$(1.1\pm0.4)\times10^{-27}$	$(3.8\pm0.8)\times10^{-28}$	$(9\pm3)\times10^{-27}$

† Assisted by the joint program of the U. S. Office of Naval Research and the U. S. Atomic Energy Commission.
[1] Peterson, Barnes, Fowler, and Lauritsen, Phys. Rev. (to be published).

F14. Measurement of π^- Mass with Mesonic X-Rays.* M. STEARNS, M. B. STEARNS, L. LEIPUNER, S. DEBENEDETTI, *Carnegie Institute of Technology.*—The critical absorption technique is being used for precise measurements of upper and lower limits of mesonic x-ray lines of L and M series. Thin absorbers are inserted in front of the NaI crystal,[1] and the transmission of the x-rays is studied as a function of the Z of the absorber. We find the energy of the $4f\rightarrow3d$ line of π^- mesons captured by phosphorus above the K edge of $_{58}$Ce (40.40 kev).[2] This corresponds to $m_\pi\geq272.5m_e$ as calculated from the Klein-Gordon equation using a point charge Coulomb potential. Similarly the π^- Potassium $4f\rightarrow3d$ line is lower than the Hf K edge (65.08 kev) corresponding to $m_{\pi^-}\leq273.3m_e$. Many other lines (e.g., Al, Fl, and Mg $3d\rightarrow2p$) have also been studied and have verified the technique. From these measurements it follows $272.5m_e\leq m_{\pi^-}\leq273.3m_e$. When these values have been corrected for vacuum polarization effects the main error will be due to the uncertainty in the K edges of Ce and Hf. Experiments are in progress for determining closer limits and will be reported.

* Supported by U. S. Atomic Energy Commission.
[1] Stearns, DeBenedetti, Stearns, and Leipuner, Phys. Rev. **93**, 1123 (1954).
[2] Landolt-Börnstein (Springer-Verlag, Berlin, 1952).

F15. The Reaction $D(T,\alpha)n$ at 1.5 Mev.* H. V. ARGO AND A. HEMMENDINGER, *Los Alamos Scientific Laboratory.*—The differential cross sections at 1.5-Mev triton energy, and for laboratory angles of 10, 20, 30, ⋯, 140, have been measured. A reaction chamber 14 inches in diameter with a movable and a fixed proportional alpha particle counter was used. The Pyrex entrance foil to the deuterium gas target was 10.5 kev thick for 1.5-Mev tritons. The argon filling in the movable counter was separated from the target gas by a glass foil of about 2.5-mm air equivalent. Preliminary results for differential cross sections in the center-of-mass system at the angles 14.4°, 28.7°, 42.8°, 56.5°, 69.8°, 82.5°, 94.6°, 105.8°, 116.2°, 125.8°, 134.6°, 142.5°, 149.8°, 156.5° are 23.8, 23.5, 23.7, 23.4, 23.3, 22.7, 22.4, 21.7, 21.3, 20.3, 19.6, 19.0, 18.5, 18.6 mv/ster, with probable errors of 2 percent. The total cross section, from integration of the above data, is 0.275 ±0.005 barn.

* Work done under the auspices of the U. S. Atomic Energy Commission.

THURSDAY MORNING AT 9:00

Physics 334

(S. A. SCHAAF, presiding)

Invited Paper

G1. On the Interactions of Shock Waves. OTTO LAPORTE, *University of Michigan.* (30 min.)

Division of Fluid Dynamics

Symposium on Hypersonic Flow

G2. Review of Experimental Methods in Hypersonic Research. P. P. WEGENER, *Jet Propulsion Laboratory, California Institute of Technology.* (45 min.)

G3. A Low Density Wind Tunnel Study of Shock-Wave Structure and Relaxation Phenomena in Gases. F. S. SHERMAN, *University of California, Berkeley.* (45 min.)

G4. Boundary Layer Problems in Hypersonic Flow. F. K. HILL, *Applied Physics Laboratory, The Johns Hopkins University.* (45 min.)

THURSDAY AFTERNOON AT 2:00

Guggenheim Hall

(R. T. BIRGE, presiding)

Invited Paper

H1. The Bevatron at the University of California. E. J. LOFGREN, *University of California, Berkeley.* (30 min.)

Contributed Papers

H2. Grain Density and Ionization Loss in Nuclear Track Emulsions.* JOHN R. FLEMING AND J. J. LORD, *University of Washington.*—Grain density measurements in Ilford G5 plates of accelerated particles have been extended.[1,2] Now, over 400 000 grains have been counted for pion energies of 224, 121, 83, and 28 Mev. Measurements with plates exposed to the Cosmotron pion beams are now in progress and will be reported. Preliminary results for 500-Mev pions give good agreement with the Sternheimer theory.

* Assisted by the joint program of the U. S. Office of Naval Research and the U. S. Atomic Energy Commission.

[1] We are indebted to Professor Marcel Schein for plates from the Chicago Cyclotron and Dr. R. K. Adair for plates from the Cosmotron.

[2] J. R. Fleming and J. J. Lord, Phys. Rev. **92**, 511 (1953).

H3. Direct Creation of Electron Pairs by Electrons of Great Energy. I. Experimental Observations. D. T. KING, W. WADA, AND M. M. BLOCK,* *Naval Research Laboratory.*—Data on the direct creation of electron pairs by cosmic-ray electrons has been collected in nuclear emulsions by a track following method. The plates, Ilford G5 400 microns thick, were flown at altitudes exceeding 95 000 feet for 6 hours at geomagnetic latitude 55°N. The search was confined to flat tracks of low grain density. Sixty-one tridents with primary energies between 0.1 and 10 Bev, as determined from the sum of the three secondary energies, were found. The electron trident mean free path was evaluated through a comparison of the number of tridents (14 our of the 61) which occurred on arms of pairs, with the total track length of pair particles originating in the emulsion within our energy interval. This insured that the path length considered in the m.f.p. (mean free path) determination was electronic. After consideration of substantial corrections for the estimation of path length, and for the inclusion of pseudotridents,[1] a maximum likelihood estimate of 134 ± 42 cm was found for the m.f.p. This corresponds to a cross section of $0.93\pm0.29\times10^{-25}$ cm^2 in G5 emulsion.

* On military leave of absence from Duke University, Durham, North Carolina.

[1] D. T. King and M. M. Block, Bull. Am. Phys. Soc. **29**, No. 4, S13, 14 (1954).

H4. Direct Creation of Electron Pairs by Electrons of Great Energy. II. Theoretical Considerations. W. WADA, M. M. BLOCK,* AND D. T. KING, *Naval Research Laboratory.*—Predictions of cross section for direct pair production by fast electrons given by Bhabha[1] and Racah[2] have been evaluated. In the energy range 0.1–10 Bev it is found that there is a disagreement by a factor of ~2 between the total cross sections of these authors. A more detailed integration of the differential cross section given by Bhabha was made, and the result was in substantial agreement with Racah's prediction. The modified cross section was averaged over an assumed spectrum of the form $E^{-1.6}dE$ for the incident electrons within our energy interval. The result was 0.82×10^{-25} cm^2 for G5 emulsion, in good agreement with the determination in (I). The effect of screening for these energies is small. A study has also been made of the distribution of the primary energy among the secondary particles by the introduction of the variables, $R=E_{\text{pair}}/E_{\text{primary}}$ and $r=E_+/E_{\text{pair}}$, into the differential cross section. Experimental comparison is discussed in III.

* On military leave of absence from Duke University, Durham, North Carolina.

[1] H. J. Bhabha, Proc. Roy. Soc. (London) **A152**, 559 (1935).

[2] G. Racah, Nuovo cimento **14**, 93 (1937).

H5. Direct Creation of Electron Pairs by Electrons of Great Energy. III. Internal Energy Distributions. M. M. BLOCK,* D. T. KING, AND W. WADA, *Naval Research Laboratory.*—The differential cross section, expressed in terms of either R or r defined in II, has been evaluated as a function of primary energy. A simple comparison of theory with our experiment is possible when the differential distributions in R and r are normalized to the total cross section and averaged over primary energies between 0.1 and 10 Bev. This procedure allows us to utilize all 61 tridents for energy partition studies. Energies of the three secondaries of each trident were measured by multiple scattering. In the determination of the experimental values of R and r, we employed the convention that the two secondary particles of lowest energy represented the created pair. The experimental probability distributions in R and r were compared with the averaged theoretical distributions modified to take account of the convention. Reasonable agreement was obtained. Our collected results on total cross section, its variation with primary energy, and the internal energy partitions lead us to conclude that the theory gives a satisfactory prediction of trident processes in our energy interval.

* On military leave of absence from Duke University, Durham, North Carolina.

H6. Electromagnetic Events of High-Energy Particles at Sea Level. S. H. NEDDERMEYER AND ERLE HOWELL, JR., *University of Washington.*—A cloud chamber with a magnetic field in the middle part and with one aluminum and two lead plates 1 cm thick has been used with a triple coincidence counter system including one discriminated group which triggers on 3 or more particles. The system accepts both nuclear and *EM* events, and for the latter has a strong discrimination against low-energy "primary" mu's. Thus, about half the primaries of the *EM* events of energy above 0.5 Bev have momenta above 20 Bev, according to the magnetic deflections. The observed momentum distribution for the primaries is, in the low momentum region, much lower than that calculated from the theoretical cross sections for bremsstrahlung and secondaries, assuming a detection efficiency of one, but is in rough agreement at momenta above 15 Bev. On the other hand the absolute number of events observed (above 0.5 Bev) is in agreement for the aluminum but low for the Pb by a factor 2–3. Statistical uncertainties are still large; however both discrepancies are partially explainable by geometrical factors and energy loss and scattering in the Pb, which have the effect of decreasing the detection efficiency at low energy.

H7. Sidereal Time Variations in Cosmic Ray Intensities Produced by Fermi's Acceleration Mechanism. LEVERETT DAVIS, JR., *California Institute of Technology.*—If $\mathbf{B}_g$, the galactic magnetic field in the earth's neighborhood, is roughly uniform and if cosmic rays are accelerated by Fermi's[1] mechanism, then any anisotropy should be correlated with $\mathbf{B}_g$ rather than with stellar distributions. Assume that for very high-energy particles (unaffected by the earth's field) the flux per steradian in the direction $\mathbf{A}$ is $N-D\cos 2\theta$, where θ is the angle between $\mathbf{A}$ and $\mathbf{B}_g$. Suppose $\mathbf{A}$ is now fixed in apparatus and rotates with the earth. Let $(\pi/2)-\phi$ be the angle between $\mathbf{A}$ and $\mathbf{E}$, the earth's axis. (For measurements of vertical intensity, ϕ is the latitude.) Let $(\pi/2)-\beta$ be the angle between $\mathbf{E}$ and $\mathbf{B}_g$. If D is not too small, the observed intensity should show Fourier components of amplitudes $D\sin 2\phi \sin 2\beta$ (period 1 sidereal day), and $D\cos^2\phi\cos^2\beta$ (period ½ sidereal day), both minima coinciding. If $\mathbf{B}_g$ lies parallel to the nearest spiral arm (oscillations of 10° or more would not be surprising), $\beta=35°$ and, for $D>0$, the minimum would come at 20^h local sidereal time in the northern hemisphere and at 8^h in the southern.

[1] E. Fermi, Astrophys. J. **119**, 1 (1954).

H8. Unstable Cosmic-Ray Particles Observed in a Double Cloud Chamber Arrangement.* W. H. ARNOLD, J. BALLAM, H. GURSKY, A. L. HODSON, R. RONALD RAU, GEORGE T. REYNOLDS, AND S. B. TREIMAN, *Princeton University.*—A double cloud-chamber arrangement similar to that of the Ecole Polytechnique group,[1] consisting of one cloud chamber in a magnetic field of 5500 gauss placed above a second multiplate cloud chamber having seven one-half inch Pb plates, has been in operation at 10 600 feet (Inter-University High Altitude Laboratory, Echo Lake, Colorado) for several weeks. During this period approximately 60 unstable V^0 and $V^\pm$ particles have been observed. Several of the more interesting cases will be discussed.

* Supported by U. S. Office of Naval Research and U. S. Atomic Energy Commission.
[1] Report of the *Congres International sur le Rayonnement Cosmique* held at Bagnères-de-Bigorre, July, 1953, p. 101.

H9. Cascade Decay of a Negative Hyperon.* W. B. FRETTER AND E. W. FRIESEN, *University of California, Berkeley.*—The cascade decay of a negative hyperon into a meson and a Λ^0 particle, previously reported by the Manchester[1] and C.I.T.[2] groups, has been observed in which the meson has been identified by momentum and ionization measurements as a negative π meson with a mass of $(268\pm15)m_e$. The ionization measurements were made by droplet counts along the track of the particle in a cloudchamber filled with helium. The measured ionization was I/I min $=1.66\pm0.07$ and the measured momentum was (132 ± 4) Mev/c. The Λ^0 was identified by measurements of angles and ionization, since the tracks were too short for momentum measurements. Both decay events were coplanar within the error of coplanarity angle determination of $\pm2°$. The Q value for the reaction $Y^-\rightarrow\pi^\mp\Lambda^0+Q$ was 66 ± 6 Mev, in agreement with results reported by the C.I.T. group.

* Assisted by the joint program of the U. S. Office of Naval Research and the U. S. Atomic Energy Commission.
[1] Armenteros, Barker, Butler, Cachon, and York, Phil. Mag. **43**, 597 (1952).
[2] E. W. Cowan, Phys. Rev. **94**, 161 (1954).

H10. Long Term Studies of the Neutron and Ionizing Cosmic Ray Intensities.* E. L. CHUPP,† *University of California, Berkeley.*—Intensity monitors have been developed at Berkeley for the study of time variations by various cosmic-ray components. The neutron component is monitored by BF_3 counters surrounded by Pb which acts as a local star producing medium thereby increasing the neutron counting rate. Simpson found that the low-energy primary cosmic radiation is the principal source of the sea level neutron component; thus measurements of the variations in this component permit one to study the fluctuations in the low-energy primaries. We have demonstrated the existence of a long term variation in the neutron component (barometer corrected) similar to the 27-day periodicity reported by Simpson. This variation is typified by several series of intensity minima (separated by ~30 days), which may be associated with periods of maximum geomagnetic activity. We have also monitored the total and hard ionizing intensities with conventional GM counter telescopes. An example of the magnetic storm effect shows a decrease in the neutron intensity approximately three times larger than a simultaneous decrease in the hard intensity.

* Assisted by the joint program of the U. S. Office of Naval Research and the U. S. Atomic Energy Commission.
† Now at the University of California Radiation Laboratory, Livermore, California.

H11. Absolute Differential Range Spectrum of Low-Energy Cosmic-Ray μ-Mesons.* N. T. SEATON, *University of California, Berkeley.*—An absolute differential range spectrum in the region from 1 to 150 g/cm² has been obtained for cosmic-ray μ mesons at sea level. The apparatus consisted of a tray

A, 30×30 cm, of Geiger counters above a liquid scintillation counter B, of 10-cm diameter and 6-cm depth, with the intervening space of 30 cm occupied by varying amounts of lead absorber. The photomultiplier pulses were fed to a four-channel delay discriminator covering the total interval 0.2 to 10 μsec. The results were checked for evidence of spurious counts from photomultiplier after-pulsing and amplifier overloading. The events recorded were $A+B+(B$ delayed) and $B+(B$ delayed); the latter to provide an estimate of the required zenith angle correction. The results were found to agree very well with the spectrum estimated by Rossi.[1] This work was evidently somewhat similar to that recently reported by Fafarman and Shamos.[2]

* Assisted by the joint program of the U. S. Office of Naval Research and the U. S. Atomic Energy Commission.
[1] B. Rossi, Revs. Modern Phys. **20**, 537 (1948).
[2] A. Fafarman and M. H. Shamos, Bull. Am. Phys. Soc. **29**, No. 4, S12 (1954).

H12. Identification of Primary Cosmic-Ray Heavy Nuclei.* R. F. HOARD, J. R. FLEMING, AND J. J. LORD, *Department of Physics, University of Washington.*—Primary cosmic-ray heavy nuclei tracks in Ilford G5 emulsions have been identified by the photoelectric method of measurement. Results utilizing this measuring technique will be compared with grain, gap length, and delta-ray intensities of the tracks. Results will also be given on the application of this technique to the problem of the primary flux of cosmic-ray heavy nuclei at magnetic, latitude 10° North.

* Assisted by the joint program of the U. S. Office of Naval Research and the U. S. Atomic Energy Commission.

H13. Geiger-Mueller Counter Tube Age Characteristics.* W. C. ROESCH AND J. S. REDDIE, *General Electric Company.*—Three age characteristics of Geiger counters were investigated. The curve of maximum pulse height from a Geiger counter on exposure to a beta-ray source was observed as a function of counter voltage after various total counts; in the Geiger region these curves were found to shift fairly regularly to higher voltages as the counter aged. The Geiger threshold voltage was found to vary logarithmically with the counting rate. The change in threshold voltage per factor of ten increase in counting rate, the "threshold coefficient," varied linearly with the total number of counts. It was found that the pulse height at a fixed counter voltage varied approximately as a power of the counting rate, and that the logarithm of the ratio of the pulse heights corresponding to counting rates differing by a factor of ten, the "amplitude coefficient," varied linearly with the total number of counts.

* This paper describes in part work conducted under contract between the General Electric Company and the U. S. Atomic Energy Commission.

THURSDAY AFTERNOON AT 2:00

Physics 320

(S. T. STEPHENSON, presiding)

Contributed Papers

I1. Electron Scattering from Hydrogen, Deuterium, and Carbon at 190 Mev.* J. A. MCINTYRE AND R. HOFSTADTER, *Department of Physics, and W. W. Hansen, Laboratories of Physics, Stanford University.*—The recoil of the proton or deuteron permits solid targets of light and heavy polyethylene to be used in studying the elastic scattering of high energy electrons from the nuclei of hydrogen and deuterium, as distinguished from the elastic scattering from carbon nuclei. Inelastic electron scattering peaks have been observed in carbon at 4.5 Mev and 9.7 Mev and add a background below the carbon elastic peak which must be subtracted from the hydrogen and deuterium peaks. Angular distributions of the elastic electron scattering have been observed in hydrogen between 35° and 100° at 190 Mev in the laboratory frame. The proton appears to be a point charge since the experimental points fit the Mott formula. The deuteron definitely appears as not a point charge. Its finite size is exhibited by a fivefold reduction from the Mott formula at 105° in the center-of-mass system. The rms radius of the observed charge distribution is $1.5\pm0.2\times10^{-13}$ cm. This "radius" is a measure of the rms distance between the center of mass of the deuteron structure and the position of the proton.

* This research was supported jointly by the U. S. Navy (Office of Naval Research) and the U. S. Atomic Energy Commission, and by the U. S. Air Force through the Office of Scientific Research of the Air Research and Development Command. It was also aided by a grant from the Research Corporation.

I2. Electron Scattering in Hydrogen and Helium.* R. HOFSTADTER, R. MCALLISTER, AND E. WIENER,† *Department of Physics, and W. W. Hansen, Laboratories of Physics, Stanford University.*—To investigate the elastic scattering of high-energy electrons from hydrogen, helium, and other gases we have constructed a stainless steel scattering chamber containing gas at high pressure. The target is a right cylinder of length 2½ inches, diameter ¾ inch with walls 15 mils thick and end windows of thickness 5 to 10 mils. Operation at 1000 psi has proved quite convenient. The end effects are easily subtracted out by emptying the gaseous contents and are not important except at small angles (~35°). Studies of the angular distribution in hydrogen and helium have been carried out at 190 Mev in the laboratory frame of coordinates and show agreement with the Mott point-charge formula for hydrogen but distinct deviations from the Mott formula for helium. These studies thus demonstrate the finite size of the helium nucleus (the alpha particle). A preliminary estimate of the size of the alpha particle gives $1.40\pm0.2\times10^{-13}$ cm for the rms radius of the alpha particle. The rms radius is taken with respect to charge.

* This research was supported jointly by the U. S. Navy (Office of Naval Research) and the U. S. Atomic Energy Commission, and by the U. S. Air Force through the Office of Scientific Research of the Air Research and Development Command. It was also aided by a grant from the Research Corporation.
† Miss Eva Wiener met a tragic death in an automobile accident in 1953.

I3. The K-Capture/Positron Ratio of Na^{22}. W. E. KREGER AND C. SHARP COOK, *U. S. Naval Radiological Defense Laboratory.*—Using a gamma-ray scintillation spectrometer, the annihilation radiation and 1.3 Mev gamma ray from Na^{22} have been studied with a view toward determining the K-capture/positron ratio for this isotope. The ratios of photopeak have been studied with a view toward determining the K-capture/positron ratio for this isotope. The ratios of photopeak to total areas for a 4-in. diameter, 4-in. high NaI(Tl) crystal have been measured using collimated monoenergetic gamma rays from six sources.[1] Using these data and experimental measurements of the photopeak areas associated with the annihilation radiation and the 1.3-Mev gamma quanta from Na^{22}, the relative intensities of these two radiations

have been compared and indicate a K-capture/positron ratio of approximately 11 percent in agreement with Sherr and Miller.[2]

[1] W. E. Kreger and L. McIsaac, Phys. Rev. **93**, 943 (1954).
[2] R. Sherr and R. H. Miller, Phys. Rev. **93**, 1076 (1954).

I4. The Gamma Radiation Following the Decay of Pr^{144}. C. Sharp Cook and W. E. Kreger, *U. S. Naval Radiological Defense Laboratory.*—The gamma radiation following the decay of Pr^{144} has been studied using a 4-in. diameter, 4-in. high cylindrical NaI(Tl) crystal, and single-channel pulse-height analyzer. With the aid of photopeak to total ratios as determined for this crystal[1] from collimated monoenergetic gamma rays from six sources, the relative intensities of the three gamma rays following the decay of Pr^{144} have been determined in terms of the 0.134-Mev gamma ray of Ce^{144}. If we assume the 0.134-Mev transition to occur during 22 percent of the Ce^{144} disintegrations[2] and that six percent of these transitions appear in the form of internal conversion,[3] the relative abundance of the 0.696-Mev gamma ray is 1.8 percent of the total number of Pr^{144} transitions; that of the 1.49-Mev gamma ray is 0.32 percent; and that of the 2.185-Mev gamma ray is 0.83 percent.

[1] W. E. Kreger and L. McIsaac, Phys. Rev. **93**, 943 (1954).
[2] Auth, Emmerich, and Kurbatov, Phys. Rev. **94**, 794 (1954).
[3] F. T. Porter and C. S. Cook, Phys. Rev. **87**, 464 (1952).

I5. Spin-Orbit Interactions in Many-Body Nuclear Shell Theory.* Ingram Bloch and Yü-Chang Hsieh, *Vanderbilt University.*—A nuclear model with Hooke's-law forces between the nucleons has the same shell structure as if the nucleons all moved without interacting in a common harmonic-oscillator central field. Therefore a study has been made of some effects of spin-orbit interactions of the form $(a_pM_p+a_nM_n)\cdot(b_pS_p+b_nS_n)$, where the subscripts p and n refer, respectively, to the protons and the neutrons, M and S are, respectively, orbital and spin angular momenta, and the a's and b's are constants. The latest available results on these interactions will be reported.

* Assisted by the Office of Ordnance Research, U. S. Army.

I6. Internal Conversion Coefficients in Decay of Mn^{52}, Co^{60}, and Sc^{46}.* Glenn L. Keister,† *University of Washington.*—Conversion coefficients of the Cr^{52} gamma rays have been measured using sources of Mn^{52} produced in the University's 60-inch cyclotron. In addition, the coefficients of the well-known gamma rays of Ni^{60} and Ti^{46} were remeasured using very thin sources of high specific activity Co^{60} and Sc^{46} obtained from Oak Ridge. The measurements were made in a high resolution beta-ray spectrometer. The N_γ were determined from the known decay schemes[1] by integrating the beta spectra. Compton and external photoelectrons were negligible for Co^{60} and Sc^{46}; some error from these effects are present in Mn^{52}. The measured total coefficients (error±10 percent) are tabulated in Table I, together with theoretical K plus L coefficients for EQ radiations as determined from tables of Rose, Goertzel, and Swift:

Table I.

	E Mev	Total×10⁴	EQ_{K+L}×10⁴
Mn^{52}	0.74	2.95	3.60
	0.93	1.80	1.75
	1.46	0.72	0.69
Co^{60}	1.17	1.55	1.69
	1.33	1.18	1.29
Sc^{46}	0.89	1.55	1.61
	1.12	0.82	0.89

* Supported in part by the U. S. Atomic Energy Commission.
† Now at Boeing Airplane Company.
[1] Hollander, Perlman, and Seaborg, Revs. Modern Phys. **25**, 469 (1953).

I7. Elastic and Inelastic Scattering of 14-Mev Neutrons by Deuterons. John D. Seagrave, *Los Alamos Scientific Laboratory.*—A counter-telescope consisting of two proportional counters and a thin NaI scintillator in triple coincidence has been used to study the angular distribution of scattered deuterons and disintegration protons from the interaction of 14-Mev neutrons with deuterium. Simultaneous observation of particle energy E and dE/dx permitted unequivocal identification of charged reaction products. Thin radiators of deuterated and normal polyethylene were used, the latter to investigate the incident neutron spectrum and n-p scattering at 14 Mev. The absolute differential cross sections observed over the angular range 0 to 55 degrees in the laboratory system for elastic n-d and n-p scattering are in good agreement with recent measurements using nuclear emulsions.[1] Disintegration protons from the $D(n,2n)H$ process were observed over the (lab) angular range 0 to 80 degrees, with energies between the lower limit of detection (about 2 Mev) and the allowed maxima. The energy distribution over this range appears more nearly uniform than that estimated by Frank and Gammel,[2] and the forward-peaked differential cross section somewhat larger.

[1] Allred, Armstron, and Rosen, Phys. Rev. **91**, 90 (1953).
[2] Frank and Gammel, Phys. Rev. **93**, 463 (1954).

I8. The Decay of Rh^{102}.† D. B. Kochendorfer and Donald J. Farmer, *University of Washington.*—The radiations emitted by 210-day Rh^{102} have been examined using a solenoidal beta-ray spectrometer and a NaI(Tl) scintillation spectrometer. Rh^{102} was produced in the University's 60-inch cyclotron by both $Ru(p,n)$ and $Ru(d,xn)$ reactions, and the activity separated chemically. The decay of the rhodium fraction has been observed for a period of 190 days and exhibits a 220-day period. Gamma-ray transitions, arranged in order of decreasing intensity and having the following energies, are found: 0.474±0.001, 0.198±0.001, 0.127±0.001, 1.11±0.02, 1.07±0.02, 0.62±0.01, 0.76, 0.70, 158±0.02 Mev. The 0.127-Mev transition is highly internally converted. The presence of the weak 0.70- and 0.76-Mev transitions is inferred from the shape of the gamma-ray spectrum as observed with the scintillation spectrometer. Previous work[1] suggests the existence of only the 0.474-Mev transition. The positron and negatron spectra are both complex and have maximum endpoint energies of 1.27±0.01 and 1.12±0.01 Mev, respectively.

† Supported in part by the U. S. Atomic Energy Commission.
[1] Sullivan, Sleight, and Gladrow, *National Nuclear Energy Series*, (McGraw-Hill Book Company, Inc., New York, 1951), Division IV, Vol. 9, paper 330.

I9. One-Quantum Annihilation of Positrons. Donald J. Farmer and J. F. Streib, *University of Washington.*—5.0-mc C^{11}, carried by N_2 gas (145.0 cm³, 0.5 atmos), wherein it was produced by the (p,α) reaction in the cyclotron, is introduced, after a 25-minute "cool-off" period, into chambers lined with Pb, Ta, or Al. The resulting gamma-ray spectrum, presumably entirely the result of positron (0.99-Mev max) absorption, is filtered by 2.5 cm Pb and observed with a 5.0-cm thick NaI(Tl)-6292 spectrometer. Corrections for background and decay are made. Decay measurements show that the number of spurious high-energy counts due to pileup is small. Source intensities are determined by ordinary annihilation radiation; a calibration of the relative efficiency for detecting this radiation and higher-energy radiation is made with the positron-gamma (2.31-Mev) cascade of O^{14} produced by the $N(p,n)$ reaction, and carried by N_2 gas from which the C^{11} has been absorbed. Preliminary data for gamma-ray energies above 1.4 Mev indicate reasonable agreement with available theoretical results[1] for 1-quantum annihilation and 2-quanta annihilation in flight, which should have gamma ray energies up to 1.9 and 1.7 Mev, respectively.

[1] J. C. Jaeger and H. R. Hulme, Proc. Cambridge Phil. Soc. **32**, 158 (1936); H. Bethe, Proc. Roy. Soc. (London) **150**, 129 (1935).

I10. Elimination of the Pair Interaction in the Pseudoscalar Meson Theory. C. H. CHANG AND B. A. JACOBSOHN, *University of Washington.*—The pair interaction $\int d\tau \rho \varphi^{\alpha} \varphi^{\alpha}$ is eliminated from a Hamiltonian of pseudoscalar symmetric meson theory with an extended source (not extended interaction). The result is an equivalent Hamiltonian with pseudovector interaction only, but with a renormalized coupling constant and a modified source function. The scattering phase shifts are the sum of the shifts due to the core alone and those of the equivalent pseudovector interaction. The renormalized coupling constant and the modified source function is examined in detail in the case in which the original source is square. Some effects of the change in source shape will be briefly discussed. The foregoing result is applied to the classical calculation of nucleon isobar energy for several pair strengths and for a square source function of several sizes. In this particular calculation the effect of the change of the source shape is given approximately by a further renormalization of the coupling constant. The classical excitation energies of isobars in the moderate coupling region are in strong disagreement with the quantum-mechanical results.[1]

[1] F. H. Hawlow and B. A. Jacobsohn, Phys. Rev. **93**, 333 (1954).

I11. The Pulse Amplitude Distribution in a BF_3 Counter Irradiated with 4.87-Mev Neutrons. D. B. JAMES, W. KUBELKA, AND S. A. HEIBERG, *University of British Columbia.*—The amplitude distribution of pulses produced by 4.87-Mev neutrons in two BF_3 proportional counters has been studied; one counter contained normal boron and the other enriched boron with 96 percent B^{10}. In addition to the expected reaction $B^{10}(n,\alpha)Li^7$ ($Q=2.79$, 2.31). The reactions $F^{19}(n,\alpha)N^{16}$ and either or both of $B^{10}(n,t)Be^8$ and $B^{10}(n,p)Be^{10}$ were detected. The Q value for the F^{19} reaction was found to be -1.77 ± 0.13 Mev in agreement with the Q from mass values[1] if we assume the alpha emission to occur to the excited state of N^{16} at 0.3 Mev. For the B^{10} reaction $Q=0.51\pm0.15$ Mev, slightly higher than the Q from mass values for $B^{10}(n,t)Be^8$ and $B^{10}(n,p)Be^{10}$.

[1] F. Ajzenberg and T. Lauritsen, Revs. Modern Phys. **24**, 321 (1952).

I12. The Reaction $B^{11}(n,\alpha)Li^8$. S. A. HEIBERG, *University of British Columbia.*—Neutrons from a pulsed deuterium beam impinging on a tritium target were used to bombard a boron trifluoride proportional counter containing the normal ratio of B^{11} to B^{10}. The half-life of the activity and the energy of the particles indicated that they were due to the immediate breakup of Be^8 into two alphas after the 0.88-sec beta decay of the Li^8 formed by the $B^{11}(n,\alpha)Li^8$ reaction. The process was found to have a cross section of the order of 30 millibarns for 14-Mev neutrons.

I13. Beam Escape from Synchrocyclotrons. WARREN FENTON STUBBINS, *Radiation Laboratory, Department of Physics, University of California, Berkeley.*—A study of the large synchrocyclotrons reveals that only in three a small part, from one-half percent to ten percent, of the circulating beam is accelerated to the limit of radial stability and then spirals out of the cyclotron. The analysis of the conditions at the end of the acceleration cycle shows the following requirements for particles to escape: (a) a rapid rate of expansion of the synchronous orbit, (b) a small first harmonic in azimuthal variation of the magnetic field at the outer radii, and (c) a small amplitude of radial oscillation about the synchronous orbit. The dependence upon these factors is very strong as determined from experimental measurements, and the analysis of the equations of axial and radial oscillations which includes nonlinear terms in axial and radial amplitudes and their derivatives and the azimuthal variation in the magnetic field.

I14. Neutron-Proton Scattering at 90 Mev. CHUNG YING CHIH, *Radiation Laboratory, Department of Physics, University of California, Berkeley, California.*—An investigation of 90-Mev neutrons scattered by protons has been conducted with a cloud chamber filled with hydrogen and a mixture of methane and hydrogen, respectively, in a magnetic field of 22 000 gauss. The neutron energy spectrum has a full width at half-maximum of about 30 Mev. The neutron scatter angles range from 8° to 180° in the center-of-mass system. The differential scattering cross section is found to have a symmetry about 90° in the center-of-mass system. Detail results with a likely theoretical inference will be presented. This work was performed under the auspices of the U. S. Atomic Energy Commission.

I15. A Cerenkov Counter for Electron Detection. R. K. SQUIRE, B. J. MOYER, AND J. E. OSHER, *Radiation Laboratory, Department of Physics, University of California, Berkeley, California.*—A counter has been developed at this laboratory for the detection of electrons with energies from 20 Mev, up to a tested limit of 300 Mev, and which should be useful for much higher energies. It consists of a Lucite shaft 40 cm long and 25 cm in cross section. The radiation is divided at one end and viewed by 2 photomultipliers which operate a coincidence circuit which has a resolving time of 5×10^{-9} second. Tests show that electron energies from 20 to 80 Mev can be determined by pulse-height analysis, and above 90 Mev, simple detection with an almost constant efficiency of 80 percent is possible. 300-Mev electrons give a 0.5-volt pulse. The instrument is quite insensitive to heavy-particle background and was designed specifically for operation in regions of high neutron flux. Tests show that it has no response to the full intensity neutron beam of the 184-in. cyclotron. The counter can be expected to efficiently detect any charged particle which can traverse 10 cm or more of Lucite with a velocity of at least 0.8 c. This work was done under the auspices of the U. S. Atomic Energy Commission.

THURSDAY AFTERNOON AT 2:00

Physics 334

(H. W. LIEPMANN, presiding)

Invited Paper

J1. Turbulence and Atmospheric Pollution. F. N. FRENKIEL, *Applied Physics Laboratory, The Johns Hopkins University.* (30 min.)

Division of Fluid Dynamics

Symposium on Problems in Acoustics

Related to Fluid Dynamics

J2. Experiments on Sound Propagation in Rarefied Gases. MARTIN GREENSPAN, *National Bureau of Standards.* (45 min.)

J3. Attenuation of Very High Amplitude Sound Waves. I. RUDNICK, *University of California, Los Angeles.* (45 min.)

J4. Turbulent Boundary Layer Noise. O. K. MAWARDI, *Massachusetts Institute of Technology.* (45 min.)

FRIDAY MORNING AT 9:00

Guggenheim Hall

(J. H. VAN VLECK, presiding)

Electron Spin Relaxation

Invited Papers

K1. Some Dilemmas in Electron Spin Relaxation. J. H. VAN VLECK, *Harvavd University.* (30 min.)

K2. Electronic-Lattice Interaction in Paramagnetic Crystals. K. W. H. STEVENS, *Nottingham University, England.* (30 min.)

K3. Relaxation Processes in Ferromagnetic Resonance. FREDERIC KEFFER, *University of Pittsburgh.* (30 min.)

K4. Motion of Individual Ferromagnetic Domain Walls. JOHN K. GALT, *Bell Telephone Laboratories, Murray Hill.* (30 min.)

FRIDAY MORNING AT 9:00

Physics 320

(E. A. YUNKER, presiding)

Invited Paper

L1. Nuclear Spectroscopy. K. C. MANN, *University of British Columbia.* (30 min.)

Contributed Papers

L2. Gamma Radiation from the Proton Bombardment of Oxygen. J. B. WARREN, K. A. LAURIE, D. B. JAMES, AND K. L. ERDMAN, *University of British Columbia.*—The nuclear gamma radiation following the nonresonant capture of a proton in O^{16} has been studied with protons of energies from 800 kev to 2.1 Mev and found to consist of three components. The main transition goes, via a gamma ray of energy that varies with proton bombarding energy, to the $J=\frac{1}{2}+$ state of F^{17}. This state, 487 kev above the ground state, radiates directly to the ground state. In addition, there is a weaker direct radiative transition from the capture configuration to the ground state. At energies above $E_p=1.8$ Mev oxide targets bombarded with protons give rise to a radiation of 873 kev attributed to the presence of the O^{17} isotope via the reaction of $O^{17}(p,p')O^{17*}$, the radiation corresponding to the transition from the first excited state of O^{17} to the ground state.

L3. Gamma Rays from Li^7+p. K. L. ERDMAN, J. B. WARREN, D. B. JAMES, AND T. ALEXANDER, *University of British Columbia.*—We have studied the gamma rays emitted when a metallic Li^6 target on a backing of platinum is bombarded with protons of energy from 400 kev to 2.2 Mev. Gamma rays of various energies from 430 kev to 6 Mev were emitted. The gamma-ray decay scheme is quite complex, with a large percentage of the gamma rays cascading through the 430 kev first excited state of Be^7. The cross section at $Ep=400$ kev is in the neighborhood of 10^{-30} cm^2. Details of the decay scheme and excitation function will be given.

L4. Spins of Excited States of Some Odd A Nuclei According to the Collective Model.* RICHARD L. MOORE, *Los Alamos Scientific Laboratory, Los Alamos, New Mexico.*—The procedures used in recent papers[1] to estimate the spins of the excited states of Np^{237} and Np^{239} and the rotational energy $\hbar^2/2\Im$ have been applied to levels of other isotopes as observed in α decay. The levels and spins of Ac^{227} are as proposed by Moore.[2] The results which are consistent with the predictions follow:

Isotope	Level energy in kev and (spin)	$\hbar^2/2\Im$ (kev)
Po^{215}	0 (5/2) 270 (7/2) 622 (9/2)	38.7
Ac^{227}	0 (3/2) 38 (7/2) 97 (11/2)	3.1
	323 (7/2) 387 (11/2)	2.6
Th^{229}	0 (5/2) 42 (7/2) 96 (9/2)	6.0
Pu^{239}	277 (3/2) 321 (5/2) 382 (7/2)	8.8

Em^{219}, Ra^{225}, U^{235}, and Am^{241} are also considered.

* Work done under the auspices of the U. S. Atomic Energy Commission.
[1] J. O. Rasmussen, Jr., Arkiv Fysik **7**, 185, 1953. Frank Asaro and I. Perlman, Phys. Rev. **93**, 1423 (1954).
[2] Richard L. Moore, dissertation, The Ohio State University, 1953.

L5. Decay of Ta^{183}.† J. J. MURRAY, P. SNELGROVE, P. E. MARMIER, AND J. W. M. DUMOND, *California Institute of Technology.*—The β^- decay of $_{73}Ta_{110}^{183}$ into an excited state of $_{74}W_{109}^{183}$ has been observed, using the curved crystal gamma spectrometer, and the axial focusing homogeneous field β spectrometer. A unique energy level scheme for this mode of decay of W^{183} has been constructed on the basis of energies and conversion properties of 27 transitions. Spin and parity has been assigned to all levels. The γ energies in kev, decay fractions in percent, and multipolarities of the transitions are as follows: 40.97 (10.3) M1, 46.48 (61.4) M1, 52.59 (41.7) M1, 82.92 (2.5) M1, 84.70 (14) M1, 99.07 (31.9) E2, 101.94 (1.5) M1, 103.14 (0.5) E2, 107.93 (45.7) M1, 109.73 (2.9) M1, 120.38 (0.25) M1, 144.12 (6.4) M1, 160.53 (4.4) E2, 161.36 (18.2) M1, 162.33 (9.8) M1, 192.64 (0.4) M1, 203.27 (0.4) M1, 205.06 (1.4) M1, 208.81 (1.1) M1, 209.87 (5.4) E2, 244.26 (10) E2, 246.05 (35.6) M1, 291.71 (5.4) E2, 313.03 (8.8) M1, 354.04 (12) M1, 365.60 (0.8) M1, 406.58 (0.9) E2. The energy uncertainties are given by $\pm 0.15E^2\times 10^{-2}$ in volts or 10 ev, whichever is larger, where E is the energy in kev. The multipolarity assignments for the 82.92, 109.73, 365.60, 406.58, and 103.14 kev transitions were inferred from the decay scheme. All others were determined from conversion properties. The principal features of the scheme are no parity change throughout, frequent violation of single-particle selection rules, and several examples of competition between E2 and M1 transitions. The foregoing results provide an amplification of and corrections to preliminary results reported earlier.[1]

† Research worked supported by contract with Office of Ordnance Research, and U. S. Atomic Energy Commission.
[1] DuMond, Hoyt, Marmier, and Murray, Phys. Rev. **92**, 202 (1953).

L6. Rotational Levels in W^{183}.† R. F. CHRISTY, *Kellogg Radiation Laboratory, California Institute of Technology, Pasadena, California.*—Recent investigations by Murray, Marmier, Boehm, Snelgrove, and DuMond[1] of the decay of Ta^{183} reveal an energy-level diagram in W^{183} consisting of 8 excited states below 500 kev. The possibility of relating some of these levels to the rotational states discussed by A. Bohr[2] is being studied. Such an explanation requires alternating deviations of the form $(-1)^{I+\frac{1}{2}}\times(I+\frac{1}{2})\epsilon$ from the simple $I(I+1)$ scheme. However, the magnitude of ϵ requires a mixing of j values. It can be explained by a strong mixing of $p_{\frac{1}{2}}$ and $p_{\frac{3}{2}}$ particle states coupled to a distorted core so that the particle better approximates definite m_l, m_s than j, m_j. The magnitude of the ratio of spin orbit to orbit surface interaction is determined and is fairly small. Further features of the level scheme are being investigated.

† Assisted by the joint program of the U. S. Office of Naval Research and the U. S. Atomic Energy Commission.
[1] Abstract L5, this meeting, Murray, Snelgove, Marmier, and DuMond.
[2] A. Bohr, Kgl. Danske Videnskab. Selskab Mat.-fys. Medd. **26**, No. 14.

L7. Radiations from Some Odd-Odd $N=Z$ Nuclei.† DAVID GREEN AND J. REGINALD RICHARDSON, *University of California, Los Angeles.*—P^{30}, Cl^{34}, and K^{38} were produced by p,pn reactions on P_4S_3, NaCl, and KI, respectively, and were studied in a large double-lens magnetic spectrometer and in a NaI scintillation spectrometer. Data with higher precision than those previously published[1] are reported in this paper. Short half-lives encountered required beta-ray source preparation in final form before bombardment. These sources, evaporated on 3 mg/cm^2 aluminum foil backings, had an average areal density of about 10 mg/cm^2 and were about 3 mm in diameter. Data secured were: P^{30} half-life, 2.56±0.15 min; simple positron spectrum end point, 3.24±0.06 Mev; no gamma rays. Cl^{34*} half-life, 32.40±0.04 min; complex positron spectrum end points, 4.50±0.03 Mev, 2.48±0.07 Mev, 1.33±0.10 Mev. K^{38} half-life, 7.7±0.3 min; simple positron spectrum end point, 2.68±0.04 Mev; no conversion line present. Estimated maximum errors are quoted above. Evidence for the position of the $J=0$, $T=1$ level in K^{38} will be discussed. Magnetic spectrometer calibration included measurements on the photopeak of the thorium-converted 4.44-Mev gamma ray from C^{12}, available from a RaD-Be source.

† Supported in part by the joint program of the U. S. Office of Naval Research and the U. S. Atomic Energy Commission.
[1] Hollander, Perlman, and Seaborg, Revs. Modern Phys. **25**, 469 (1953).

L8. 15.2-Mev Gamma Emission from Carbon-12. CHARLES WADDELL, HARLAN SHAW, DAVID COHEN, AND B. J. MOYER, *Radiation Laboratory, Department of Physics, University of California, Berkeley.*—Pair spectrometer studies of photon emission from a carbon target bombarded by high-energy protons has revealed a 15.2±0.2 Mev gamma line. It has been observed for proton energies extending from 340 Mev down to 30 Mev, and in the energy region from 60 down to 30 Mev the yield rapidly increases. Proton energies below 30 Mev have not yet been available in this experiment. This gamma line is also seen in the deuteron bombardment of B^{11}, but not of B^{10}. This fact, together with energetics arguments, and with clear spectrometer separation from known gamma lines from excited Be^8, indicates strongly an excited C^{12} origin for the line. It is proposed tentatively that the excited C^{12} level here involved is a $T=1$ state for which isotopic spin selection rules forbid a disintegration into three alpha particles. Decay by neutron or proton emission is energetically forbidden. This work was done under the auspices of the U. S. Atomic Energy Commission.

L9. High-Energy Gamma Ray Studies with Nuclear Track Emulsions. HARRY H. HECKMAN, PETER C. GILES, AND WALTER H. BARKAS, *Radiation Laboratory, Department of Physics, University of California, Berkeley.*—A study of high-energy photons emitted from targets when bombarded by the 330 Mev proton and bremsstrahlung beams has been undertaken. The detection of the gamma rays is accomplished by observing electron pairs created by the photons in electron sensitive emulsions. When the gamma rays enter near grazing

incidence, the electron pairs have sufficiently long paths in the emulsion to enable one to estimate the electron pair energy by multiple scattering measurements. The experimental arrangements have been to place the emulsions at distances of 13 to 30 in. from the target in a straight or tapered channel at 90° to the beam direction. The channel is placed in a clearing magnetic field to eliminate the charged particle background originating in the target. Investigations have included observation of gamma rays, principally π^0 decays, emitted from the vicinity of targets bombarded by the 330-Mev proton beam and selective scattering of photons from the bremsstrahlung beam by carbon and lead nuclei. The energy resolution of this technique is also being determined experimentally, using the line spectrum of gamma rays obtained by bombarding LiF with 657-kev protons. This work was done under the auspices of the U. S. Atomic Energy Commission.

L10. Emulsion Tables. WALTER H. BARKAS AND GEORGE HAHN, *Radiation Laboratory, Department of Physics, University of California, Berkeley.*—Each measurable feature of a heavy charged particle track in emulsion may be normalized by functions of the particle mass and charge so as to become a function of the velocity alone. Since each is a known function of the velocity, a knowledge of one normalized quantity implies a knowledge of all others. This observation provides a basis for the systematic utilization of nuclear track emulsion as a quantitative instrument. An analysis of particle range, ionization, range, straggling, multiple scattering, delta-ray density, maximum delta-ray energy, grain density, residual time, momentum, magnetic curvature, kinetic energy, and total energy has been carried out. Tables and graphs have been constructed giving each quantity as a function of every other quantity. Supplementary information necessary for the correct and rapid utilization of the data has been tabulated. This work was done under the auspices of the U. S. Atomic Energy Commission.

L11. Production of Deuterons in High-Energy Nuclear Bombardment of Nuclei. W. N. HESS AND B. J. MOYER, *Radiation Laboratory, Department of Physics, University of California, Berkeley.*—The production of deuterons when various elements are bombarded with 300-Mev protons or 300-Mev neutrons has been studied at angles of 25° and 40° to the beam. The scattered particles have been identified by using either $H\rho$ and range or by using E and dE/dx. The dependence of the deuteron cross section on A and the shape of the deuteron energy spectra indicate that the production mechanism for forming these deuterons is the indirect pickup process of Bransden.* The A dependence of the deuteron cross section shows that the deuterons are formed on the surface of the nucleus. Because of this fact the cross sections for incident neutrons and for incident protons when compared can give information about the variety of nucleons found on the nuclear surface. The following values have been obtained for the fraction of surface nucleons that are neutrons:

Carbon $=0.47\pm0.09$,
Cadmium $=0.59\pm0.07$,
Lead $=0.78\pm0.12$,
Uranium $=0.75\pm0.10$.

For lead and uranium these values are significantly larger than the volume fraction of neutrons. This implies that at least for heavy elements there is a nuclear skin rich in neutrons. This work was done under the auspices of the U. S. Atomic Energy Commission.

* B. H. Bransden, Proc. Phys. Soc. (London) **A65**, 738 (1952).

L12. Elastic Scattering of 9.7-Mev Protons by Alpha Particles. BRUCE CORK AND WALTER HARTSOUGH, *Radiation Laboratory, Department of Physics, University of California, Berkeley.*—The differential cross section for the scattering of 9.7-Mev protons from helium has been measured over the range from 17° to 154° in the center-of-mass system. The new 9.8-Mev proton linear accelerator, which is now used as an injector for the Bevatron, was used as a source of incident protons. A scattering chamber has been used which has the solid angles at the various scattering angles determined by fixed slits. The scattered particles were detected with sodium iodide scintillators and RCA 6199 photomultiplier tubes. The detectors were conveniently arranged so that each scintillator could be well shielded, and background runs could be made easily. The counters were arranged so that they could be interchanged and three angles have been measured simultaneously, with a statistical accuracy in the forward direction of better than ±1 percent. The differential cross section measurements of the forward angles are in good agreement with published data in this energy region. However, the cross section for protons scattered in the background direction is approximately 75 percent of the published value. This work was done under the auspices of the U. S. Atomic Energy Commission.

L13. Radiative Capture of 300-Mev Neutrons in Hydrogen.* JOHN DEPANGHER,† *University of California, Berkeley.*—In the course of performing an n-p scattering experiment[1,2] at Berkeley with 300-Mev neutrons, six deuterons were observed starting in the collimated region of the cloud chamber.[1,3] Three possible reactions in which deuterons may appear in hydrogen are $n+d\rightarrow n+d$ (impurity scattering), $n+p\rightarrow\pi^0+d$ (neutral-meson production), and $n+p\rightarrow\gamma+d$ (radiative capture). One of these events clearly was an impurity-scattering event. A detailed analysis has been made in an attempt to distinguish the cases of neutral-meson production and of radiative capture from one another. An argument based on this analysis and on the shape of the neutron-energy spectrum will be presented to show that two of these deuterons were formed in the radiative-capture process while the remainder lies in the category of neutral-meson production. The present work, it is believed, is the first to demonstrate clearly[4] the radiative capture of neutrons by protons for neutron energies other than thermal.

* Work performed under the auspices of the U. S. Atomic Energy Commission.
† Now with the Hanford Atomic Products Operation, General Electric Company, Richland, Washington.
[1] University of California Radiation Laboratory Report UCRL-2153 (unpublished).
[2] J. DePangher, Phys. Rev. **92**, 1084 (1953).
[3] J. DePangher, Phys. Rev. **88**, 894 (1951).
[4] W. E. Crandall and B. J. Moyer, Phys. Rev. **92**, 749 (1953).

L14. Small-Angle n-p Scattering at 400 Mev.* R. T. SIEGEL, A. J. HARTZLER, AND W. OPITZ, *Carnegie Institute of Technology.*—The angular distribution of 400-Mev neutrons scattered at small angles from hydrogen has been studied for laboratory angles between 5.8° and 27.8°. A polythene converter and scintillation counter telescope were used as neutron detector, with a large anticoincidence counter preceding the array in order to screen out charged particles. Variable copper absorbers in the coincidence telescope provided a 365-Mev low-energy cutoff for the primary neutrons. Results show an essentially constant cross section between 12.7° and 50° (neutron scattering angle) in the center-of-mass system, (statistical standard deviation ~10 percent at each angle). This is quite different from the behavior at supplementary angles, where a cross section rising steeply towards 180° has been observed.[1]

* Supported in part by the U. S. Atomic Energy Commission.
[1] A. J. Hartzler and R. T. Siegel, Phys. Rev. **91**, 928 (1954); also Phys. Rev. (to be published).

FRIDAY MORNING AT 9:00

Physics 334

(R. GEBALLE, presiding)

Excitation and Ionization Phenomena

Invited Papers

M1. Mechanism of the Electric Spark. L. H. FISHER, *New York University.* (30 min.)

M2. Particle Induced Laboratory Auroral Phenomena. A. B. MEINEL, *Yerkes Observatory, Williams Bay, Wisconsin.* (30 min.)

M3. On the Morphology of Auroral Displays in Alaska. C. T. ELVEY, *Geophysical Institute, College, Alaska.* (30 min.)

Contributed Papers

M4. Solar X-Ray Emission. E. T. BYRAM, T. A. CHUBB, AND H. FRIEDMAN, *U. S. Naval Research Laboratory.*—Solar x-ray emission between 8 A and 60 A was measured with photon counters carried in 3 high altitude rockets flown at White Sands Proving Ground in November and December of 1953. Tubes equipped with Al foil windows were sensitive to 8 A–14 A x-rays. Windows of Mylar film (polyethylene terphthalate, 0.7 mg/cm²) were used for transmission of a relatively narrow band extending from the carbon K edge at 43 A to about 55 A. Thinner windows of Glyptal (0.2 mg/cm²) were used which were capable of transmitting a broader band from 10 to 80 A except for the region in the neighborhood of the carbon K absorption. Maximum solar x-ray emission was observed in the 43–50 A region. The intensity over the entire x-ray spectrum was of the order of 10^{-1} erg cm^{-2} sec^{-1}. A previous experiment[1] had indicated an order of magnitude greater intensity in the short wavelength portion of the spectrum. Both rocket measurements of solar x-rays appear to correlate with the intensity of the coronal green line as recorded at the Sacramento Peak and Climax observatories during the periods of the flights.

[1] Byram, Chubb, and Friedman, Phys. Rev. **92**, 1066–1067 (1953).

M5. Excitation of Air Glow by Electronic Impact.* C. Y. FAN, *Yerkes Observatory, University of Chicago.*—A spectrographic study has been made of the optical emission from a rarefied air sample under the bombardment of an electron beam of energy from 10 ev to 8000 ev. The spectral range covers 3800 A to 9000 A. It was found that the spectra are quite different from that excited by protons or heavier ions. In particular, the Meinel system of N_2^+ and the first negative system of O_2^+ are so distinctive in the former spectra for electron energy greater than 100 ev while they are *practically* missing in the later ones. This finding as related to the excitation mechanism of aurora borealis will be discussed.

* This investigation is supported in part by the Geophysical Research Directorate of the Air Force Cambridge Research Center under contract No. 19(122)-480.

M6. Electromagnetic Radiations from Hydrocarbon Flames.* SAMUEL C. LAWRENCE, JR., *Physical Research Unit, Boeing Airplane Company.*—Random radio-frequency noise generated in ramjet flame has been observed in the ultra-high-frequency spectrum. Some correlation of intensity of radiation and temperature exists. The effect, being several orders of magnitude greater than expected from Planck's distribution law, is attributed to electron plasma oscillations. Thermal disassociation of combustion products plus thermal radiation from combustion chamber walls produce sufficiently great electron densities to account for the frequencies observed. Part of the amplitude variations observed is believed due to attenuation effects of the flame. The Hamiltonian for the flame system is expressed in general form, from which it is believed that effects of temperature discontinuities due to shock waves and uneven burning can be evaluated.

* Work supported by U. S. Air Force Contract.

M7. Detection of Mercury Vapor by Resonance Ionization. K. C. CLARK AND L. KANAL, *University of Washington.*—It is known that mercury ions are produced on irradiation of mercury vapor by the resonance line 2537 A when an inert gas such as nitrogen is present at considerable pressure. The ions are derived from three-body collisions involving two excited atoms and at a rate proportional to the second power of the intensity at the core of the resonance line. This process of ionization by inelastic collision provides a sensitive monitor of the intensity of resonance radiation. Absorption of this line by mercury vapor in a sample of air is detected using this means in a balanced double path arrangement. Unfiltered light from commercial germicidal lamps can be used because of the selective wavelength response of the process. The detector contains mercury at room temperature, purified nitrogen at 50 mm, and molybdenum screen electrodes. The effect of Lorentz broadening in the absorption cell and in the detector is computed. Calibration with an absorption path of 10 in. shows that concentrations as low as 1 percent of the toxic limit of 0.1 mg/m³ can be measured.

SATURDAY MORNING AT 10:00

Community House, Longmire

Mt. Rainier National Park

(E. A. UEHLING, presiding)

Contributed Papers

N1. Relative Contributions of *K*-Shell and other Electrons to the Stopping Power of Light and Heavy Elements. EDWIN A. UEHLING, *University of Washington.*—The correction to the stopping power formulas caused by the binding of *K*-shell electrons has been calculated by Walske.[1] Walske has also estimated the effect of the *L* and higher shell electrons. Independent evidence of the importance of the higher shell electrons can be deduced from the Lindhard-Scharff[2] plot of stopping power data. Such a plot exhibits the deviations from logarithmic behavior of the stopping number. These deviations occur over a certain range of the parameter $\zeta = v^2/v_0^2 z$ and they are independent of the energy of the penetrating particle and of the atomic number regarded as independent parameters. The parameter ζ is related to Walske's parameter η_k. The *K*-shell corrections are determined by the values of η_k. There is a correspondence between the range of variation of η_k in which *K*-shell corrections are important and the range of variation of η in which the deviations from logarithmic behavior occur. These intervals overlap for the light elements but fail to do so for the heavy elements. An interpretation in terms of over-all corrections can be given.

[1] M. C. Walske, Phys. Rev. **88**, 1283 (1952).
[2] J. Lindhard and M. Scharff, Kgl. Danske Videnskab. Selskab. Mat.-fys. Medd. **27**, 15 (1953).

N2. Nuclear Electric Quadrupole Interactions of B^{11} in Kernite.* H. L. BLOOD AND W. G. PROCTOR, *University of Washington.*—Kernite, a monoclinic crystal of space group $P2/c$, has four molecules $Na_2B_4O_7 \cdot 4H_2O$ in a unit cell. Rotation of the crystal about the symmetry axis when perpendicular to a strong magnetic field H_0 reveals a pattern of 11 lines for the transitions between the magnetic energy levels of B^{11} ($I = 3/2$), strongly perturbed by the nuclear electric quadrupole interaction. Rotation about an axis perpendicular to the symmetry axis reveals a pattern of 21 lines, which, when related to the above, establish four nonequivalent sites for the boron nuclei in the unit cell. One rotation is sufficient to specify the electric field gradient tensor (except for signs) at a nuclear site if, as is the case for two of the sites, the transitions are such that second perturbation methods may be used in the analysis.[1] In this way we have obtained a tentative value for the quadrupole coupling constant at one site to be 1250 kc. Rotation about a third axis is now in progress.

* This research was supported by the U. S. Air Force, through the Office of Scientific Research of the Air Research and Development Command.
[1] G. M. Volkoff, Can. J. Research **31**, 820 (1953).

N3. Nuclear Spin Lattice Relaxation in Supercooled Menthol.* B. H. MULLER† AND MYER BLOOM,‡ *University of Illinois.*—The nuclear spin lattice relaxation time (T_1) of liquid and supercooled *l*-menthol has been measured between 33.8°C and 49.0°C within an accuracy of ±2 percent. The relaxation theory of Bloembergen, Purcell, and Pound has been applied to this case. This theory adequately predicts the magnitude of T_1 (about 0.2 sec) as well as the temperature dependence if 4.3 A is chosen as the "radius" of the menthol molecule and 2.27 A as the "average" interproton distance. An investigation of the structure of the menthol molecule and the amendment of the theory to take into account the CH_3 rotations within the molecule allows a prediction of 1.87 A for the "average" interproton distance. No unusual changes in T_1 or T_2 (the phase memory time) were observed as the temperature was changed through the normal freezing point (42.5°C). These measurements were done at too high a frequency (30 megacycles) to be able to determine whether or not the reported viscosity transition[1] is reflected in the magnetic resonance experiment.

* Research supported in part by the U. S. Office of Naval Research.
† Now at the University of Wyoming.
‡ Holder of a Province of Quebec Postgraduate Travelling Fellowship.
[1] E. N. da C. Andrade, Proc. Roy. Soc. (London) **A215**, 36 (1952).

N4. Temperature Dependence of the Nuclear Resonance in Metals.* W. D. KNIGHT, *University of California, Berkeley.*—The fractional frequency shift in cubic metals may be expressed[1] as $\Delta H/H = (8\pi/3)\chi_p P_f$, where χ_p is the Pauli spin susceptibility per atom, and P_f is the square of the electronic *s*-wave function averaged over the Fermi surface. Measurements of $\Delta H/H$ on Na, Al, Cu, V, and Nb between 1.2 and 300°K show small decreases with decreasing temperature. For Na, the value of $\Delta H/H$ drops (by about 10 percent of its 300° value) between 75° and 25°K. This behavior may be associated with a crystal structure change in this element.[2] No resonance is observed in Nb at 4°K, presumably because of superconducting domains. The temperature changes in $\Delta H/H$ for the other metals are much smaller than for Na. $\Delta H/H$ should be nearly independent of temperature, but χ_p, in a free electron approximation, will go as (volume)[1] (in rough agreement with the experiments), and P_f may be a weak function of atomic volume. Also, since both χ_p and the electronic heat are proportional to the density of electron states at the Fermi surface, one expects a correlation in the temperature dependencies of these quantities, and any positive peaks in density of states, as Frölich has proposed,[3] should show up in both. No evidence for an appreciable electron-lattice interaction, such as Frölich proposes, is found in these data.

* Supported in part by the U. S. Office of Naval Research.
[1] Townes, Herring, and Knight, Phys. Rev. **77**, 852 (1950).
[2] C. S. Barrett, Mineralogist **33**, 749 (1948).
[3] H. Fröhlich, Phys. Rev. **79**, 845 (1950); M. J. Buckingham, Nature **168**, 281 (1951).

N5. Nuclear Magnetic Resonance in CuAl Alloys.* D. R. TEETERS AND W. D. KNIGHT, *University of California, Berkeley.*—We have observed the nuclear resonances of Cu and Al in several quenched, unordered CuAl alloys. The following results are quoted for $\Delta H/H$: pure Cu, (0.23 percent), pure Al (0.17 percent), 10–90 Cu-Al (Cu 0.27 percent, Al 0.17 percent), 90–10 Cu-Al (Cu 0.23 percent, Al 0.11 percent). We see, first, that the resonance frequency of the solvent is relatively unaffected by a 5–15 percent solute concentration. Second, the solute frequency is changed appreciably. The Cu line shift is increased in an Al environment, while the reverse is true for Al in a Cu environment. By way of interpretation, we may say that small solute concentrations behave like impurities and leave the average electronic structure, as seen by the solvent, relatively unaffected.[1] On the other hand, both P_f and χ_p (see previous abstract) for the solute metal may be considerably altered. If we calculate, from experimentally derived susceptibilities, the expected change in $\Delta H/H$ for either Cu or Al in solution, we find that the direction of the effects is correct. However, to explain the magnitudes of the

effects, it is necessary to assume that changes in the volume per electron in the alloy alter the value of P_f. For example, we should expect P_f to be relatively larger in a half-filled zone, where the p-wave function admixtures are small. Data on alloys of Cu and Al in Ag and Au will be presented.

* Supported in part by the U. S. Office of Naval Research.
[1] J. Friedel, Phil. Mag. **43**, 153 (1952); N. Bloembergen and T. J. Rowland, Acta Metallurgica **1**, 732 (1953).

N6. Nuclear Magnetic Resonance in Kernite. H. WATERMAN, *University of British Columbia* (introduced by G. M. Volkoff).—The dependence of B^{11} nuclear resonance frequencies in a single crystal of kernite ($Na_2B_4O_7 \cdot 4H_2O$) on the angles of rotation of the monoclinic crystal about its b and c axes has been studied in a magnetic field of 7000 gauss perpendicular to the rotation axis. Eleven lines, some showing slight splitting, were observed in the b rotation. In the c rotation twenty-one lines were observed, which coalesced into eleven when the b axis was perpendicular to the magnetic field, suggesting that the slight doubling of some lines in the b rotation might be due to a slight misalignment of axes. An analysis of these results will be given which shows that they are consistent with the reported symmetry properties of kernite. Four independent sets of quadrupole coupling constants and asymmetry parameters, and four pairs of different orientations of the principal axes of the electric field gradient tensor at the boron sites are indicated. Of the four boron nuclei in a molecule two appear to be in regions of much more strongly inhomogeneous field than the other two.

N7. DC Prebreakdown Currents in Gases of High Dielectric Strength.* M. L. REEVES AND RONALD GEBALLE, *University of Washington*.—Measurements of dc prebreakdown currents[1] between plane parallel electrodes have been extended to the gases isopentane, SF_6, $SiCl_4$, and CCl_4. The first of these yields semilogarithmic graphs of current *vs* electrode separation which are linear, indicating that ionization by collision takes place without competition. Similar graphs for the other gases show curvature. In SF_6 and CCl_4 the curves actually saturate for a certain range of E/p, showing that electron attachment is the predominant reaction. Curves for $SiCl_4$ do not exhibit this feature over the range of E/p amenable to this method. Values of ionization and attachment coefficients are derived from the above data in SF_6 and CCl_4. In the latter gas each coefficient has a minimum when plotted against E/p. Evidence will be discussed that dissociation into ions, as well as ionization and attachment, is important in $SiCl_4$.

* Assisted by the U. S. Office of Ordnance Research.
[1] M. A. Harrison and R. Geballe, Phys. Rev. **93**, 1 (1953).

N8. Back Diffusion of Electrons to a Plane Emitting Surface. ROBERT P. STEIN, *U. S. Naval Ordnance Test Station, Inyokern, China Lake, California*.—A program has been set up for the 701 Computer wherein the current flux from a flat plate of infinite extent may be determined in terms of the electron liberation per unit area per unit time, the mean free path of the electron, and the impressed electric field. A description of this program and its results will be made.

N9. Some Experimental Facilities and Techniques Used at the Berkeley 60-in. Cyclotron for Irradiation Effects Studies.* W. S. GILBERT AND J. H. PEPPER, *North American Aviation, Inc.*—In the study of irradiation effects caused by high energy charged heavy particle bombardment of pure metals, alloys, and semiconductors, the electronic phenomena are of fundamental interest. Apparatus and procedures have been developed which enable us to measure electrical resistivity and thermoelectric power simultaneously while the target is in place at the cyclotron. These measurements can be rapidly made with relatively high precision under well-controlled temperature conditions. Excellent target cooling, coupled with control of the emergent proton beam shape permits us to bombard targets with beams of several microamperes/cm^2 while maintaining the targets within 5°C of a prescribed temperature. Details of the target configuration, the measuring equipment, the precision of data, and beam shape studies will be presented.

* This work was based on studies conducted for the U. S. Atomic Energy Commission.

N10. Disintegration of Arsenic-76. M. SAKAI, B. MURRAY, AND J. D. KURBATOV, *The Ohio State University*.—The disintegration scheme of arsenic-76 has been previously reported by many authors. While the main disintegration scheme is well established, the low-energy beta components and associated gamma rays are in doubt. A thick lens magnetic spectrometer, scintillation spectrometer, and coincidence scintillation spectrometer were used to clarify the disintegration scheme. Beta-ray spectrum, photoelectron spectrum, scintillation gamma-ray spectrum, gamma-gamma coincidence, and beta-gamma coincidence measurements were made. Gamma-ray energies of 549±4 kev, 643±6 kev, 1200±6 kev, 1402±15 kev, and 2053±18 kev, were obtained. The relative intensities of these gamma rays are 1/0.22/0.27/0.02/0.05, respectively. No gamma rays in the 1700–1800 kev region were obtained. By beta-gamma coincidence measurements the beta-ray endpoint energies associated with the 549 kev and 1200 kev gamma ray were clearly defined. The relative intensity and ft values for each beta component were obtained by subtraction of the Fermi plot using the beta-ray end point energy of the associated gamma ray. A disintegration scheme will be presented and energy levels discussed. All activities were obtained from Oak Ridge National Laboratories and were chemically purified.

N11. ZnS(Ag) Phosphor Mixtures for Neutron Detection. P. G. KOONTZ,* G. R. KEEPIN, AND J. E. ASHLEY, *University of California, Los Alamos Scientific Laboratory*.—In a search for a fast neutron detector with minimum gamma response, the scintillation characteristics of ZnS(Ag) were reexamined. The principal decay constant of ZnS(Ag) was measured as $\sim 0.04\mu$ sec with a fast scope (Tektronix 517) and short anode time constant ($\sim 5 \times 10^{-9}$). τ was found to be independent of the mode of excitation (alphas or electrons from gammas) and, as expected, measured values of τ increased with slower electronics. ZnS(Ag) thus appeared sufficiently promising to warrant a brief survey of various mixtures of this phosphor with boron, lithium, and fissionable compounds for neutron detection. Various atomic ratios and thicknesses were tested for each mixture. 100 mg/cm^2 of a mixture of finely ground boric acid powder and ZnS(Ag) powder (atomic ratio 1B/1.5 Zn) yielded the highest neutron counting efficiency, $\epsilon_n \sim 1$ percent, with a ratio of neutron-to-gamma counting efficiency $> 10^5$. Increased ϵ_n is obtained at the expense of $\epsilon_n/\epsilon_\gamma$ ratio. Various mixtures of boric acid and ZnS(Ag) were compression-molded into thin disks using a hydrogenless binding agent. Optimum counting efficiencies for these disks fell considerably below that of the powder mixtures.

* On leave from the College of Wooster, Wooster, Ohio.

Author Index to Papers Presented at the 1954 Pacific Northwest Meeting

Allen, William A., Joe M. Mapes, and Wesley G. Wilson—A9
Anderson, A. B. C.—C2
Andrew, A., M. R. Jeppson, R. L. Mather, and H. P. Yockey —A6
Argo, H. V. and A. Hemmendinger—F15
Arnold, W. H., J. Ballam, H. Gursky, A. L. Hodson, R. Ronald Rau, George T. Reynolds, and S. B. Treiman—H8
Backman, M. E. and H. L. Morrison—A11
Band, William—A2
Banister, J. R. and C. D. Broyles—C6
Barkas, Walter H. and George Hahn—L10
Barnes, C. A., W. A. Fowler, C. C. Lauritsen, and R. W. Peterson—F13
Bedford, R. E. and A. M. Crooker—B2
Bell, S. and S. A. Schaaf—C11
Bender, R. S.—E2
Block, Ingram and Yü-Chang Hsieh—I5
Block, M. M., D. T. King, and W. Wada—H5
Blood, H. L. and W. G. Proctor—N2
Byram, E. T., T. A. Chubb, and H. Friedman—M4
Chang, C. H. and B. A. Jacobsohn—I10
Chih, Chung Ying—I14
Christy, R. F.—L6
—— and W. A. Fowler—F11
Chupp, E. L.—H10
Clark, K. C. and L. Kanal—M7
Cohen, René—F10
Cook, C. Sharp and W. E. Kreger—I4
Cork, Bruce and Walter Hartsough—L12
Colladay, G. S.—B7
Cowan, E. W.—D4
Crooker, A. M. and E. B. Dorling—B10
Dauphinee, T. M.—A5
Davis, Leverett, Jr.—H7
Depangher, John—L13
Deser, S.—A1
Dunn, Eldon L. and Howard R. Kelly—C5
Elvey, C. T.—M3
Erdman, K. L., J. B. Warren, D. B. James, and T. Alexander —L3
Evans, J. E.—F2
Fairbank, W. M., W. B. Ard, and G. K. Walters—B12
Fan, C. Y.—M5
Farmer, Donald J. and J. F. Streib—I9
Fisher, L. H.—M1
Fleming, John R. and J. J. Lord—H2
Frenkiel, F. N.—J1
Fretter, W. B.—D2
—— and E. W. Friesen—H9
Galt, John K.—K4
Geballe, T. H. and G. W. Hull—B9
Gilbert, W. S. and J. H. Pepper—N9
Green, David and J. Reginald Richardson—L7
Greenspan, Martin—J2
Gugelot, P. C.—E3
Hall, J. G.—C3
Heckman, Harry H., Peter C. Giles, and Walter H. Barkas —L9
Heiberg, S. A.—I12
Hess, W. N. and B. J. Moyer—L11
Hill, F. K.—G4
Hoard, R. F., J. R. Fleming, and J. J. Lord—H12
Hofstadter, R., R. McAllister, and E. Wiener—I2
Hull, G. W. and T. H. Geballe—B8
James, D. B., W. Kubelka, and S. A. Heibert—I11
Joki, E. G. and J. E. Evans—F1
Kambe, K. and J. H. Van Vleck—B3
Keck, J. C., A. V. Tollestrup, and W. R. Smythe—F8
Keffer, Frederick—K3
Keister, Glenn L.—I6
Keller, Joseph B.—A3
Kelly, Howard R.—C4
King, D. T., W. Wada, and M. M. Block—H3
Knight, W. D.—N4
Kochendorfer, D. B. and Donald J. Farmer—I8
Koontz, P. G., G. R. Keepin, and J. E. Ashley—N11
Kreger, W. E. and C. Sharp Cook—I3
Laporte, Otto—G1
Lawrence, Samuel C., Jr.—M6
Lofgren, E. J.—H1
Mann, K. C.—L1
Mawardi, O. K.—J4
McIntyre, J. A. and R. Hofstadter—I1
Meinel, A. B.—M2
Merritt, M. L. and J. R. Banister—C8
Moore, Richard L.—L4
Muller, B. H. and Meyer Bloom—N3
Murray, J. J., P. Snelgrove, P. E. Marmier, and J. W. M. DuMond—L5
Neddermeyer, S. H. and Erle Howell, Jr.—H6
Nodwell, R. A. and A. M. Crooker—B1
Pearson, John and John S. Rinehart—A8
Peterson, Vincent—F5
—— and I. George Henry—F6
Plesset, M. S. and T. P. Mitchell—C10
Reeves, M. L. and Ronald Geballe—N7
Roesch, W. C. and J. S. Reddie—H13
Rudnick, I.—J3
Sands, M., J. G. Teasdale, and R. L. Walker—F4
Sakai, M., B. Murray, and J. D. Kurbatov—N10
Schellenbaum, R. and Jay Todd, Jr.—C9
Schmidt, F. H.—E1
Seagrave, John D.—I7
Seaton, N. T.—H11
Sherman, F. S.—G3
Siegel, R. T., A. J. Hartzler, and W. Opitz—L14
Smith, G. L. and L. G. Miller—F3
Squire, R. K., B. J. Moyer, and J. E. Osher—I15
Stein, Robert P.—N8
Stearns, M., M. B. Stearns, L. Leipuner, and S. DeBenedetti —F14
Stevens, K. W. H.—K2
Stewart, R. W.—C1
Stubbins, Warren Fenton—I13
Tannenwald, P. E.—B11
Teeters, D. R. and W. D. Knight—N5
Thirion, Jacques, René Cohen, and Ward Whaling—F9
Thompson, R. W.—D3
Todd, Jay, Jr. and Ralph Schellenbaum—C7
Tollestrup, A. V., J. C. Keck, and W. R. Smythe—F7
Uehling, Edwin A.—N1
Van Vleck, J. H.—K1
Wada, W., M. M. Block, and D. T. King—H4
Waddell, Charles, Harlan Shaw, David Cohen, and B. J. Moyer—L8
Ward, J. K.—B5
Warren, J. B., K. A. Laurie, D. B. James, and K. L. Erdman —L2
Waterman, H.—N6
Webb, T. S., F. B. Hagedorn, W. A. Fowler, and C. C. Lauritsen—F12
Webber, D. S.—B6
Wegener, P. P.—G2
Westervelt, D. R.—A7
Whyburn, William M.—A4
White, Robert L.—B4
White, William C.—A10
Yang, C. N.—D1
Zucker, Alexander—E4

CONTENTS—*Continued*

Letters to the Editor:

Effect of Precipitation Hardening on the Superconducting Transition of an Aluminum Alloy . . . R. E. Mould and D. E. Mapother 797

Distribution of Trapping Levels in Cadmium Selenide . . . Harold C. Jones and Robert J. Cashman 798

Voltage Dependence of Electroluminescent Brightness . . . E. T. Howard, H. F. Ivey, and W. Lehmann 799

Magnetic Anisotropy Constants of Ferromagnetic Spinels . . . R. S. Weber 800

Infrared Spectrum of Barium Titanate . . . H. T. Evans, G. B. B. M. Sutherland, and H. P. Tyrell 801

Hyperfine Splitting of Donor States in Silicon . . . J. M. Luttinger and W. Kohn 802

Magnetoresistance in p-Type Ge and Si . . . E. N. Adams 803

Energies of π^- Mesonic X-Ray *K* Lines . . . M. S. Sternheimer, M. Stearns, S. DeBenedetti, and L. Leipuner 804

Formula for Polarization in Nucleon-Nucleon Scattering . . . G. Breit and J. B. Ehrman 805

Formula for Polarization in p-p Scattering for *P* and *F* Waves . . . M. H. Hull, Jr., and A. M. Saperstein 806

Phase Shifts for Nucleon-Nucleon Scattering at 310 Mev . . . G. Breit, J. B. Ehrman, A. M. Saperstein, and M. H. Hull, Jr. 807

Polarization of High-Energy Protons in Elastic Scattering on Helium and Carbon . . . O. Chamberlain, E. Segrè, R. Tripp, C. Wiegand, and T. Ypsilantis 807

Energetic Disintegration of a Heavy Nuclear Fragment . . . W. F. Fry and M. S. Swami 809

Neutron-Proton Mass Difference . . . W. G. Holladay and R. G. Sachs 810

Reaction $p+p \rightarrow \pi^+ + d$ with Polarized Protons . . . T. H. Fields, J. G. Fox, J. A. Kane, R. A. Stallwood, and R. B. Sutton 813

Search for 15-Mev Gamma Radiation from $B^{11}+D$ and $Be^9+\alpha$ . . . V. K. Rasmussen, John R. Ross, M. B. Sampson, and N. S. Wall 812

Calculations on Charge Independence with Repulsive Core Potentials . . . M. A. Preston and J. Shapiro 813

Proceedings of the American Physical Society:

Minutes of the 1954 Spring Meeting of the Ohio Section at Ohio University, Athens, Ohio, April 16 and 17, 1954 . . . 814

Minutes of the 1954 June Meeting Held at Minneapolis, Minnesota, June 28–30, 1954 (Corresponding to *Bulletin of the American Physical Society*, Volume 29, No. 5) . . . 817

Minutes of the 1954 Pacific Northwest Meeting Held at Seattle, Washington and on Mount Rainier, July 7, 8, 9, and 10, 1954 (Corresponding to *Bulletin of the American Physical Society*, Volume 29, No. 6) . . . 842